Lecture Notes in Civil Engineering

P. V. Timbadiya
M. C. Deo
Vijay P. Singh *Editors*

Coastal, Harbour and Ocean Engineering

Proceedings of 26th International Conference on Hydraulics, Water Resources and Coastal Engineering (HYDRO 2021)

Springer

Lecture Notes in Civil Engineering

Volume 321

Lecture Notes in Civil Engineering (LNCE) publishes the latest developments in Civil Engineering—quickly, informally and in top quality. Though original research reported in proceedings and post-proceedings represents the core of LNCE, edited volumes of exceptionally high quality and interest may also be considered for publication. Volumes published in LNCE embrace all aspects and subfields of, as well as new challenges in, Civil Engineering. Topics in the series include:

- Construction and Structural Mechanics
- Building Materials
- Concrete, Steel and Timber Structures
- Geotechnical Engineering
- Earthquake Engineering
- Coastal Engineering
- Ocean and Offshore Engineering; Ships and Floating Structures
- Hydraulics, Hydrology and Water Resources Engineering
- Environmental Engineering and Sustainability
- Structural Health and Monitoring
- Surveying and Geographical Information Systems
- Indoor Environments
- Transportation and Traffic
- Risk Analysis
- Safety and Security

To submit a proposal or request further information, please contact the appropriate Springer Editor:

– Pierpaolo Riva at pierpaolo.riva@springer.com (Europe and Americas);
– Swati Meherishi at swati.meherishi@springer.com (Asia—except China, Australia, and New Zealand);
– Wayne Hu at wayne.hu@springer.com (China).

All books in the series now indexed by Scopus and EI Compendex database!

P. V. Timbadiya · M. C. Deo · Vijay P. Singh
Editors

Coastal, Harbour and Ocean Engineering

Proceedings of 26th International Conference on Hydraulics, Water Resources and Coastal Engineering (HYDRO 2021)

Springer

Editors
P. V. Timbadiya
Department of Civil Engineering
Sardar Vallabhbhai National Institute
of Technology
Surat, India

M. C. Deo
Department of Civil Engineering
Indian Institute of Technology Bombay
Mumbai, India

Vijay P. Singh
Department of Biological and Agricultural
Engineering, and Zachry Department
of Civil and Environmental Engineering
Texas A&M University
College Station, TX, USA

ISSN 2366-2557 ISSN 2366-2565 (electronic)
Lecture Notes in Civil Engineering
ISBN 978-981-19-9912-3 ISBN 978-981-19-9913-0 (eBook)
https://doi.org/10.1007/978-981-19-9913-0

Preface

We are glad to present a collection of 33 papers pertaining to various topics in coastal, harbor and ocean engineering.

A specialty of this collection is the dominance of various field-oriented works which should be of immediate use to the practicing engineers. Such studies include works on breakwater and fishing harbor restorations, harbor tranquility, submerged breakwater, reclamation effect on shorelines, determining fishing harbor layout, wave propagation, sedimentation in navigational channels and harbors, shoreline changes, feasibility of a jetty, impact of expansion of harbor facilities, mangrove sustainability, effects of cyclones, coastal vulnerability and groundwater discharge zones.

Apart from the above-mentioned field works, there are laboratory as well as numerical studies on wave runup, wave generation, coastal protection works, combined river flow and storm surge simulation, which should be of much use to researchers as well as designers.

The studies on field data collection and on development of a coastal management information system could be of general interest to readers of this volume.

Surat, India — P. V. Timbadiya
Mumbai, India — M. C. Deo
College Station, TX, USA — Vijay P. Singh

Acknowledgements

The editors are grateful for the support provided by the technical advisory committee and local organizing committee of the 26th International Conference on Hydraulics, Water Resources and Coastal Engineering (HYDRO 2021) held at Sardar Vallabhbhai National Institute of Technology (SVNIT), Surat, during December 23–25, 2021. The editors thank the Indian Society for Hydraulics (ISH), Pune, India, its office bearers and executive council members for their support in conducting the HYDRO 2021 International Conference. The editors wish to thank all the authors for their support and contribution to this book. The editors duly acknowledge the timely and sincere efforts of the reviewers in providing their valuable comments and suggestions to maintain the quality of the book. The editors would like to thank the keynote speakers, the session chairs and co-chairs, participants and student volunteers for their contribution to the successful conduct of the conference. The editors are also thankful to the administrators of Sardar Vallabhbhai National Institute of Technology, Surat (SVNIT), India, for supporting the HYDRO 2021 International Conference. Lastly, the editors are sincerely thankful to the publishing team of Springer Nature for their support and cooperation at various steps since the beginning of the book project.

P. V. Timbadiya
M. C. Deo
Vijay P. Singh

Contents

About the Editors

P. V. Timbadiya is an Associate Professor in the Water Resources Engineering section, Department of Civil Engineering, Sardar Vallabhbhai National Institute of Technology (SVNIT), Surat, India. He secured his doctoral degree and post-graduation in Water Resources Engineering from SVNIT Surat in 2012 and 2004, respectively. He did his under graduation in Civil Engineering from SVNIT. He has guided three doctoral thesis and 29 master's dissertations. He has more than 110 research papers to his credit, including 25 articles in peer-reviewed journals. He served as Dean (Alumni and Resources Generation), and currently serving as Sectional Head, Water Resources Engineering Section at SVNIT. He played an instrumental role in setting up infrastructure facilities in the Centre of Excellence on 'Water Resources and Flood Management' such as the Experimental Hydraulics Lab, Computational Hydraulics Lab, Water Circulation System, and others. He is appointed as 'National Consultant' for Kalpsar Project by Narmada, Water Resources, Water Supply and Kalpsar Department of Government of Gujarat, India. He received 'Prof. R. J. Garde Research Award' for the year 2020 by the Indian Society for Hydraulics. He has awarded DST-SERB Core Research Grant for the project on 'Local Scouring around tandem and staggered bridge piers on Non-uniform mobile bed' in 2021. He is active in various professional bodies and organized numerous conferences, workshops, and short-term training programmes in his academic career.

M. C. Deo currently works as Emeritus Fellow at Indian Institute of Technology (IIT) Bombay. He has been in the faculty of IIT Bombay since 1983. His main area of research interest is coastal and ocean engineering followed by studies in water resources and hydraulic engineering. Through a large number of application-oriented research, Prof. Deo demonstrated the power of various artificial intelligence tools to solve engineering problems related to hydrology and coastal engineering. Examples of such works include, enhancing accuracy levels of various design parameters and making real time prediction of river flows as well as that of waves, wind, currents and sediment transport. Additionally, region-specific impact of climate change on

waves, wind, wind power, sediment transport and shoreline changes has also been evaluated by him for various locations along the Indian coastline.

Vijay P. Singh is a University Distinguished Professor, a Regents Professor, and Caroline and William N. Lehrer Distinguished Chair in Water Engineering at Texas A&M University, USA. He received his B.S., M.S., Ph.D., and D.Sc. in engineering. He is a registered professional engineer, a registered professional hydrologist, and an Honorary Diplomate of ASCE-AAWRE. He is a Distinguished Member of ASCE, a Distinguished Fellow of AGGS, an Honorary Member of AWRA, and a Fellow of EWRI-ASCE, IAH, ISAE, IWRS, and IASWC. He has published extensively in the areas of hydrology, irrigation engineering, hydraulics, groundwater, water quality, and water resources (more than 1320 journal articles, 31 textbooks, 75 edited reference books, 110 book chapters, and 315 conference papers). He has received over 95 national and international awards, including three honorary doctorates. He is a member of 11 international science/engineering academies. He has served as President of the American Institute of Hydrology (AIH), Chair of the Watershed Council of the American Society of Civil Engineers and is currently President of the American Academy of Water Resources Engineers. He has served/serves as Editor-in-Chief of 3 journals and two book series and serves on editorial boards of more than 25 journals and three book series. His Google Scholar citations include 64073, h-index: 115, and I10-index: 903.

Experimental Studies of Wave Run-Up and Transmission Through Submerged Rigid and Flexible Vegetation

P. Kishore Kumar Reddy, M. G. Muni Reddy, and N. Prathap Kumar

Abstract Vegetation along a coastline could significantly protect the foreshore area from natural disasters such as storm surge and tsunami. In these circumstances, the flexibility of the vegetation stems in the green field belt is understood to play a predominant role in the dissipation of momentum of the approaching waves. Complication in modelling the rigidity of the plantations, both experimentally and numerically, is the leading cause of insufficient knowledge on vegetation modelling. Group of cylinders in vertical direction is expected to reiterate the typical characteristics of emergent vegetation. In the present study, characteristics of wave transmission with respect to relative water depth, wave run-up on slope, surf similarity parameter, and vegetal resistance under the action of regular waves were studied.

Keywords Wave transmission coefficient · Wave run-up · Submerged vegetation · Rigid and flexible vegetation

1 Introduction

Coastal zones are suffering from growing natural and human disturbances, such as sea-level rise, coastal erosion, and resource overexploitation, to mention a few. Natural coastal dangers like cyclones, storm surges, and tsunamis exert a terrible impact on coastal population and property. Conventional hard measures might generate environmental issues and are highly expensive, needing constant maintenance for its sustainability [1–3]. However, any mitigation should preferably be eco-friendly and should not produce further bad consequences to the coastal environment. The sustainability of geosynthetic material for tropical nations like India

P. Kishore Kumar Reddy (✉) · N. Prathap Kumar
Department of Civil Engineering, K.S.R.M College of Engineering Kadapa, Kadapa, Andhra Pradesh 516002, India
e-mail: pkkrnitc@gmail.com

M. G. Muni Reddy
Department of Civil Engineering, Andhra University College of Engineering, Visakhapatnam 530003, India

P. V. Timbadiya et al. (eds.), *Coastal, Harbour and Ocean Engineering*, Lecture Notes in Civil Engineering 321, https://doi.org/10.1007/978-981-19-9913-0_1

is currently being discussed. The notion of artificial beach nourishment has been successful only for a limited time, and its operation during harsh weather conditions is of major concern. The current coastal engineering ideas focus more on vegetation, for example, it is a non-intrusive kind of coast protection that maintains the shoreline while also providing a natural habitat for a range of creatures.

According to research, there is a definite correlation between serious coastal erosion problems across the region and the deterioration of coastal systems such as coastal forest and trees—notably mangrove forest. To understand how and under what conditions mangrove forests and other coastal plants effectively protect the shoreline from erosion, further scientific study and measurement of the physical processes and dynamic interaction of the system are necessary. The effects of the 2004 Indian Ocean tsunami demonstrated the importance of vegetation in reducing the height and distance between land and water [4]. Mascarenhas and Jayakumar [5] found that huge lengths of coastal Tamil Nadu (South East Indian Peninsula) with thick casuarinas, in addition to coconut, mangroves, and palm trees, served as effective wave attenuators. Investigation [6] on flow resistance of stiff and flexible vegetation through flume study results indicated that the varying velocities, depth of flow, and Reynolds number significantly affected the friction factor. These conditions are expected to increase the amount of wave attenuation due to the presence of plant stems. According to research and scientific discoveries, the presence of vegetation in coastal regions increases slope stability, consolidates sediment, and reduces wave energy going onshore, so safeguarding the coastline from erosion.

An extensive experimental programme was carried out to investigate in detail the interaction of emerged and submerged vegetation of different characteristics in steady uniform flow and in waves of high Uresell's parameter [7]. The wave height reduces between 10 and 35%, depending enormously on the plant characteristics, such as the submergence ratio and plant density N (stems/m^2) and the wave period,longer waves are mostly attenuated from submerged vegetation. The plants' stiffness is an important parameter for wave attenuation [8]. Shobhan Raj and Muni Reddy [9] conducted an experimental study for rigid emerged vegetation, and the model stems are made up of uPVC. The model was tested with different spacings and slopes (horizontal, 1:20 and 1:30). The wave attenuation is influenced by vegetation properties such as kind, height, density, and stiffness, as well as wave characteristics. Over the vegetative meadow, wave heights decrease exponentially [10].

Experiments have taken place in a wave flume to study the behaviour of the vegetation to have a preliminary idea as to how they influence the flow behaviour on vegetal parameter. The experimental investigation has been carried out in the present study with rigid vegetation simulating the mangroves and flexible vegetation simulating the marshy vegetation. Experiments have been conducted with regular waves of predefined amplitude and frequency on a horizontal and 1:20 bed slope with constant water depth.

2 Methodology

The interaction between the flow and vegetal stems was studied to represent coastal vegetation in a wave flume experiment. Furthermore, getting fundamental knowledge of the wave dissipation mechanism over vegetation in a scale-appropriate context under controlled conditions is crucial. To simulate coastal vegetation in the real world, a material suited for the model was identified. Young's modulus, E, is one of the guiding factors for this purpose. For the laboratory tests, the reference E value is taken as 0.35 GPa and the material with this E value is identified. uPVC pipes which has an E value of 0.35 GPa were used to make the vegetation models. uPVC pipes are relatively light. The present experimental investigation was carried out by conducting experiments on vegetation models with relative stem spacing (e_L/d) and the transmission and run-up of waves when encountering vegetation field in 2D wave flume.

The schematic diagrams of 2D wave flume are shown in Figs. 1, 2, and 3 for seabed slope of 1:20. Model tests were performed at Andhra University College of Engineering (A), Department of Civil Engineering Andhra University, Visakhapatnam, Andhra Pradesh. Figure 4 shows the pictures of the models placed in a wave flume (Tables 1 and 2).

A rigid vegetation model was created using a 22 mm-diameter uPVC pipe. These 22 mm pieces are inserted into the holes of a hardwood board with a length of 1.1 m and a width of 1.0 m. Along the width and length of a hardwood plank, the centre-to-centre spacing between the holes is 10 cm. eL is the relative stem spacing along

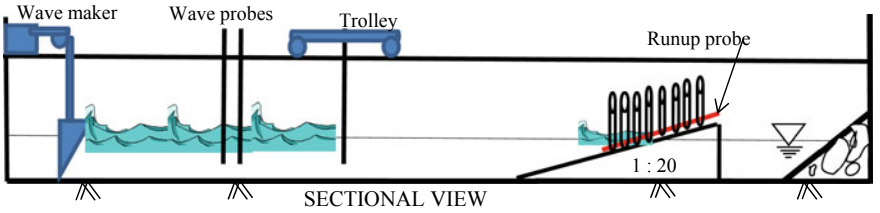

Fig. 1 Diagram of experimental set-up of rigid vegetation on a seabed slope of 1:20 in a wave flume (not to scale)

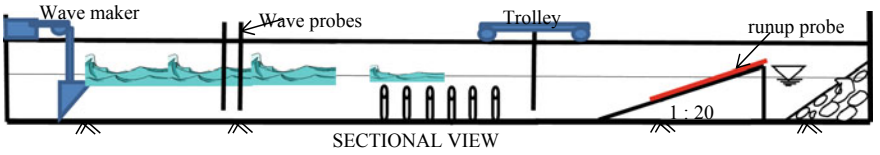

Fig. 2 Diagram of experimental set-up of rigid submerged vegetation on horizontal seabed in a wave flume (not to scale).

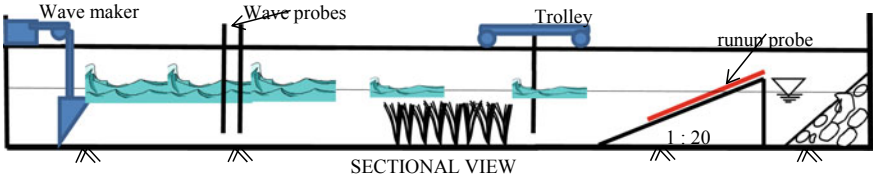

Fig. 3 Diagram of experimental set-up of submerged flexible vegetation on horizontal seabed in a wave flume (not to scale).

Fig. 4 Picture of the submerged rigid with roots and flexible models placed in a wave flume

Table 1 Dimensional parameters considered in the study

Dimensional variables	Definition	Unit
E	Young's modulus	GPa
e_L	Centre-to-centre spacing of stems in longitudinal (wave) direction	m
e_W	Centre-to-centre spacing of stems in normal to wave direction	m
D	Local water depth	m
H_i	Incident wave height	m
H_T	Transmitted wave height	m
g	Acceleration to gravity	m/s^2
H_f	Head loss due to friction	m

Table 2 Non-dimensional parameters considered in the study

Non-dimensional parameters	Definition
e_L/d	Relative stem spacing
D/Lo	Relative water depth
K_T	Wave transmission
H/lv	Wave height to the stem spacing
RU/Hi	Run-up coefficient
f	Darcy's friction factor
R_e	Reynolds number

Fig. 5 Models of flexible vegetation and rigid vegetation with roots

the direction of wave propagation which is explained as the ratio of the centre-to-centre distance between the pipes and diameter of the vegetation. Similarly, e_W is the relative stem spacing normal to the wave direction. In the present study, regular stem configuration is considered; hence, e_L and e_W are the same.

The flexible vegetation model is the second model developed in this study. The adaptable vegetation model was created with the help of self-locking cable ties. The width and length of the tie are 4.8 mm and 30 cm, respectively. The ties are bunched and placed into the holes of a wooden plank. In the present study, regular stem configuration is considered; hence, e_L and e_W are the same. The *third model* is rigid vegetation with banyan (Ficus benghalensis) roots as banyan tree roots are tied around the rigid pipes (Fig. 5).

A wavemaker is installed at one end of the wave flume, and a beach with rubble absorbers is installed at the other end to absorb incident wave energy and reduce wave reflection from the beach. The depth of the water ranged from 0.25 m to 0.80 m. The slope of 1:20 bed was adopted for the experiments. The water depth was maintained at 0.47 m throughout the experiments. The relative water depths (D/Lo) indicated that the results obtained apply to shallow water conditions.

Within the mechanical, geometrical, and hydraulic restrictions of the system, the wave generating system can generate many types of 2D regular wave sequences or sea states electric actuator system built for sine wave output for wave generation installed in the wave flume.

To measure the elevations of the water's surface, capacitance wave probes are employed. In the present investigation, three wave probes were utilized to assess the incident wave height, wave run-up, and wave reflection.

A 20 Hz low-pass filter was used to filter the wave gauge signals acquired by amplifiers. The personal computer was utilized to produce waves and acquire signals from the sensor pickups at the same time. The electrical signal was captured using a 12-bit A/D (analogue to digital) converter controlled by a quartz clock. This A/D converter was accompanied by software that managed the sample frequency of the DSO, the quantity of data points to be collected, the total time required for data

collection, and the storing of data on the personal computer. At a pace of forty samples per second, the data was gathered.

The raw data was analysed using the following calibration coefficients. In addition to obtaining frequency and time domain data by analysing the measured time histories of the wave surface height, frequency and time domain data was also collected. The threshold crossing choice corresponds to a standard zero-crossing analysis. It permits the computation of the time series value, duration, and peak–peak value of an event.

3 Results and Discussions

To obtain the transmission coefficient, the incident wave height H_i was calculated as the average of H_{imax} and H_{imin}, and transmitted wave height H_T was calculated as the difference between H_{Tmax} and H_{Tmin}.

3.1 Wave Transmission

Then the wave transmission (K_T) was estimated as the ratio of transmitted wave height H_T to incident wave height H_i.

Figure 6 explains the variation of transmission coefficient K_T with relative water depth D/Lo for close stem spacing of 4.5, bed slope of 1:20, H/l_v is 0.667, and water depth of 0.47 m. Flexible vegetation shows a decrease in transmission coefficient (K_T) with D/Lo. At the same time, K_T increases with D/Lo for rigid vegetation patches. At low relative water depths, i.e. up to D/Lo = 0.075, K_T is constant for three types of vegetation patches, and an average value is 0.135. For long-period waves, transmission coefficient is more as the wave energy penetrates through the stems in case of rigid vegetation patches. Fully grown flexible vegetation, blade-like ribbon-type leaf interacts with more flow path, thus becoming more complex.

3.2 Wave Run-Up

To obtain the run-up coefficient, the wave height of incident H_i calculated was taken as the average of H_{max} and H_{min}, and then the run-up height R_U was calculated as the crest height of the wave from mean water level. Then the run-up coefficient (R_U/H_i) is to be calculated as the ratio of run-up height to incident height H_i.

Vegetation's performance on energy dissipation is learned by studying the wave run-up (R_U/H_i). The wave run-up (R_U/H_i) is plotted against relative water depth D/Lo for rigid, flexible, and rigid vegetation with roots is shown in Fig. 7 and D/Lo for $H/l_v = 1.0$ and 0.667. It was observed that the (R_U/H_i) is more for flexible vegetation. Long-period waves result in less wave run-up (R_U/H_i) than the short-period waves.

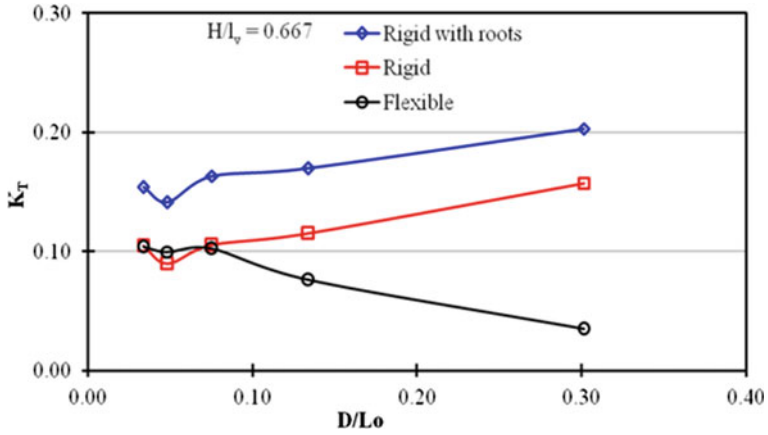

Fig. 6 Variation of transmission coefficient K_T with relative water depth (D/Lo) for H/l_v is 0.667 and three different vegetal patches

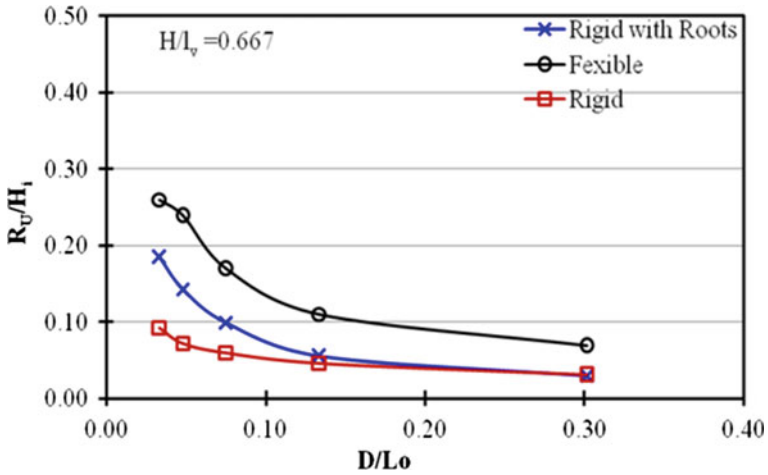

Fig. 7 Variation of run-up RU/Hi with relative water depth (D/Lo) for H/I_v is 0.667 and three different vegetal patches

The wave run-up (R_U/H_i) is plotted (Fig. 8) against surf similarity parameter ξ for different vegetation patches. Wave run-up (R_U/H_i) increases with ξ. Steeper or short-period waves carrying higher energy will break and dissipate energy rather than penetrating the vegetation.

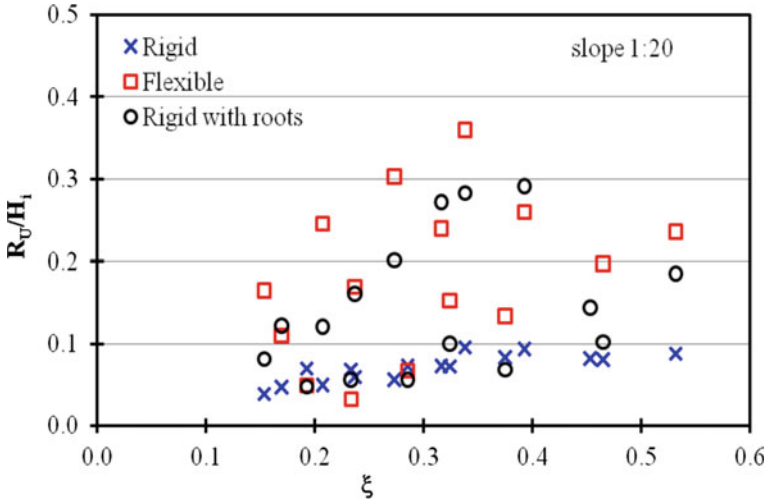

Fig. 8 Variation of wave run-up (R_U/H_i) with surf similarity parameter ξ

3.3 Resistance Due to Vegetation

The friction due to loss of head can be determined by using Bernoulli's equation

$$H_f = \frac{V_i^2 - V_T^2}{2g} \tag{3}$$

V_i and V_T are the incident and transmitted flow velocities and g acceleration due to gravity. However, H_f in Eq. (3) includes the addition of flume walls and the bed.

Open channel hydraulics research: The Froude model law is commonly used. The attachment off concerns $\mathbf{R_e}$, on the other hand, is thought to validate the results with those found in the literature. Jarvela [6] measured the f for sedges for a wide range of $\mathbf{R_e}$ at a flow depth of 0.2 m, and the findings are superposed in Fig. 9 with the current data for f, for flow depths ranging from 0.19 m to 0.2 m. This contrast supports Jarvela's measurements [6], Narayanan et al. [7], and Sobhan Raj [9] in the range of $\boldsymbol{R_e}$ considered. The present experiments were carried out of $\boldsymbol{R_e}$ in the range of 0 to 3×10^5, beyond the ranges covered by Jarvela [6], Narayanan et al. [7], and Sobhan Raj [9, 11].

It was observed from the results that Darcy's friction factor f reduces in the range of studied with Reynolds number in the range studied up to 3×10^5. The present study covers the range 0–5.0×10^4 and 1.5×10^4–3.0×10^5, comparing with previous results and covered beyond the ranges of earlier investigations.

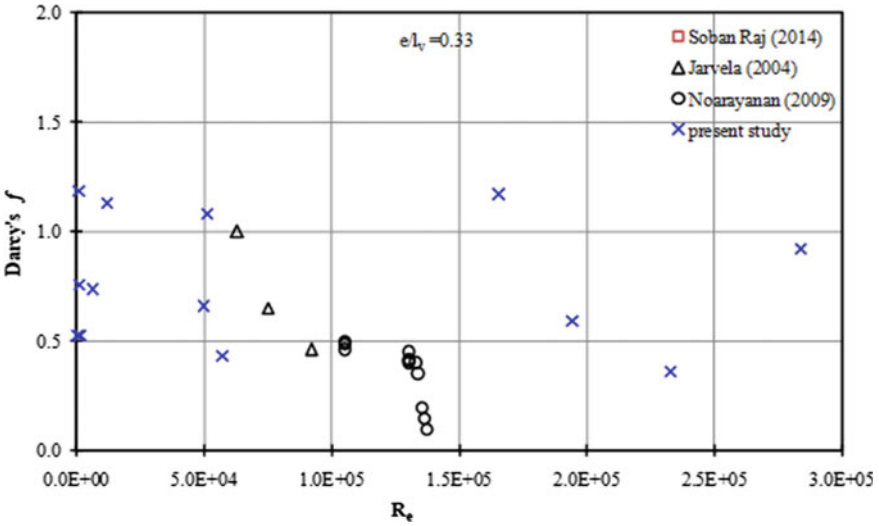

Fig. 9 Variation of Darcy's friction factor f with Reynolds number $\boldsymbol{R_e}$

4 Conclusions

Based on the study and analysis carried out on wave transmission, wave run-up, and friction factors, the following conclusions have been drawn:

Wave transmission and run-up are found to be decreasing with relative water depth for flexible vegetation. Conversely, transmission is increasing with relative water depth for rigid vegetation. Wave run-up increases with surf similarity parameter for the range of H/l_v studied in this investigation. Reynolds number will decrease Darcy's friction factor f in the range studied up to 3×10^5. The present study covers the range 0–5.0×10^4 and 1.5×10^4–3.0×10^5, comparing with previous results and covered beyond the ranges of earlier investigations. Munireddy et al. [11] conducted experimental and numerical studies wave attenuation characteristics over submerged breakwaters and rigid vegetation. Augusin et al. [12] were anlysed the laboratory data using linear wave theory to quantify bulk drag coefficients and with a nonlinear Boussinesq model to determine numerical friction factors to better represent wetland vegetation in engineering analysis.

References

1. Yılmaz N, Balas L, İnan A (2015) Coastal erosion problem, modelling and protection. Ocean Sci J 50:589–601
2. Balas L, Ozhan E (2000) An implicit three-dimensional numerical model to simulate transport processes in coastal water bodies. Int J Numer Meth Fluids 34:307–339. https://doi.org/10.1002/1097-0363(20001030)34:4%3c307::AID-FLD63%3e3.0.CO;2-T

3. Genc AN, Vural N, Balas L (2020) Modeling transport of microplastics in enclosed coastal waters: a case study in the Fethiye Inner Bay. Mar Pollut Bull 150:110747. https://doi.org/10.1016/j.marpolbul.2019.110747
4. Kathiresan K, Rajendran N (2005) Coastal mangrove forests mitigated tsunami. Estuar Coast Shelf Sci 65(3):601–606
5. Mascarenhas A, Jayakumar S (2008) An environmental perspective of the post- tsunami scenario along the coast of Tamil Nadu, India: role of sand dunes and forests. Jl Environ Manage 89(1):24–34
6. Jarvela J (2004) Determination of flow resistance caused by non-submerged woody vegetation. Int Jl River Basin Manage 2(1):61–70
7. Narayanan L, Murali K, Sundar V (2009) Wave attenuation by flexible vegetation on a mild slope. In: Proceedings of international conference in ocean engineering, IIT Madras, INDIA, pp 1157–1169
8. Koftas T, Prinos P (2011) Estimation of wave attenuation over Po-sidonia Oceanica. In: Proceedings of the 5th international conference on applied coastal research, pp 264–269. RWTH Aachen University, Germany
9. Raj S, Muni Reddy GM (2009) Hydrodynamic study of wave inter-action over rigid emerged vegetation. Andhra University, Thesis
10. Johna BM, Kiran GS, Rao S (2015) Effect of artificial vegetation on wave attenuation—an experimental investigation. In: International conference on water resources, coastal and ocean engineering (ICWRCOE 2015). Aquat Proc 4:221–226
11. Mutukuru MG, Kishorekumar Reddy P, Giridhar G (2021) Experimental and numerical modelling of wave transmission over submerged breakwater and rigid vegetation. Recent Adv Struct Eng Lect Notes Civ Eng 135:253–264. https://doi.org/10.1007/978-981-33-6389-2_1
12. Augustin LN, Irish JL, Lynett P (2009) Laboratory and numerical studies of wave damping by emergent and near-emergent wetland vegetation. Coastal Eng Jl 56:332–340

Wave Flume Studies for the Restoration of Existing Breakwater at Bhagwati Bunder Port, Ratnagiri, Maharashtra

Uday B. Patil, A. V. Mahalingaiah, and N. S. Ganesh

Abstract A breakwater structure is designed to absorb the energy of the waves. Design of flexible rubble mound structures is complex as it involves various aspects such as complex wave-structure interaction, interlocking characteristics of armour, friction between armour and secondary layer. Several empirical formulae such as Hudson formula and Van der Meer formula are available for preliminary or conceptual design of unit weight of armour. It is a universal practice to finalize the section of breakwater based on hydraulic model tests in wave flumes/wave basins to confirm the conceptual design evolved using empirical methods. The hydraulic model tests are essential to simulate the complex wave-structure interaction as well as correct prototype site conditions of seabed slope, water level, etc., can be simulated in the wave flume or wave basin. This paper outlines the approach to these studies and discusses the relative merits of the concepts considered for repairing or restoration of the damaged structures. In 1973, the Maharashtra Maritime Board (MMB) had constructed breakwater of 457 m length for development of Bhagwati Bunder Port, Ratnagiri and since then it has been serving the port by providing the tranquil conditions in the harbour area. However, due to action of hostile forces of waves over the years and being the flexible rubble mound structure, the breakwater has suffered considerable damage. In this context, the MMB has proposed to restore the existing breakwater and also extension of 200 m for prevailing wave tranquillity inside the harbour basin, approached Central Water and Power Research Station (CWPRS), Pune to conduct wave flume studies for design of restoration works. The conceptual design of breakwater was worked out using empirical methods. The wave flume was carried out for its hydraulic stability of restoration of existing breakwater and also for proposed extension of 200 m breakwater at various bed levels. The cross-section consists of 12 t tetrapod units in the armour layer from the root to (−) 9 m bed level for trunk portion. The section consists of 15 t tetrapods in the armour for roundhead portion of breakwater at (−) 9 m bed level have been suggested. The sections were found stable up to a significant wave height (H_s) of (+) 5.0 m and design maximum breaking wave height of (+) 6.35 m ($H_{1/10}$). The details of studies for the restoration of damaged breakwater at Bhagwati Bunder Port have been discussed in this paper.

U. B. Patil (✉) · A. V. Mahalingaiah · N. S. Ganesh
Central Water and Power Research Station, Khadakwasla, Pune 411 024, India
e-mail: patil.udayb@cwprs.gov.in

P. V. Timbadiya et al. (eds.), *Coastal, Harbour and Ocean Engineering*, Lecture Notes in Civil Engineering 321, https://doi.org/10.1007/978-981-19-9913-0_2

Keywords Armour unit · Breakwater · Breaking waves · Tetrapod · Wave flume

1 Introduction

The Maharashtra Maritime Board (MMB) had developed Bhagwati Bunder in order to induce and cater to the industrial development of the nearby area and fully utilize the export potential of the hinterland. The Bhagwati Bunder is situated in Mirya Bay, which is a small bay with width of about 3 km and depths of about 10 m, in Ratnagiri district of Maharashtra state at longitude 73°16′16″ E and latitude 16°59′51″ N shown in Fig. 1. A breakwater of 457 m length was constructed at Bhagwati Bunder Port, Ratnagiri in 1973 and since then it has been serving the port by providing the tranquil conditions in the harbour area. However, due to action of hostile forces of waves over the years and being the flexible rubble mound structure, the breakwater has suffered considerable damage. In this context, the MMB has proposed to restore the existing breakwater and also extension of 200 m for prevailing wave tranquillity inside the harbour basin. The Central Water and Power Research Station (CWPRS), Pune had conducted wave flume studies for design of restoration works [1]. The development area is exposed to incident waves during non-monsoon and monsoon seasons and diffracted waves from the existing breakwater reach the harbour. The layout of Bhagwati Bunder harbour basin with bathymetry is shown in Fig. 2. Presently, the crest level of the breakwater is at about (+)9.0 m and the armour and lee sides of the breakwater are partly damaged. The layout consists of a breakwater of length of 457 m extending up to −7.0 m contour and further extension of breakwater to additional length 200 m extending up to −9.0 m contour with roundhead protection to the breakwater as a whole as depicted in Fig. 2.

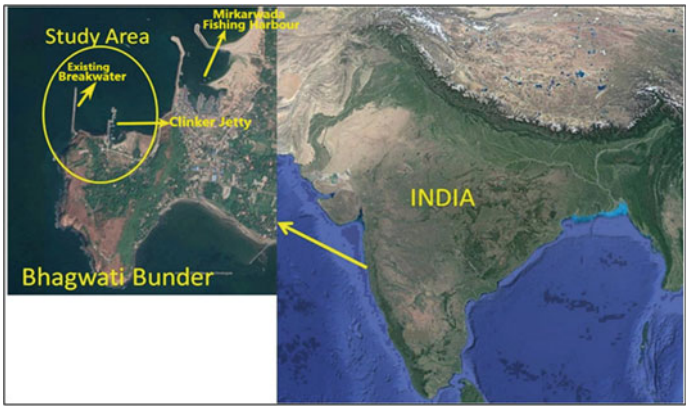

Fig. 1 Index map of study area

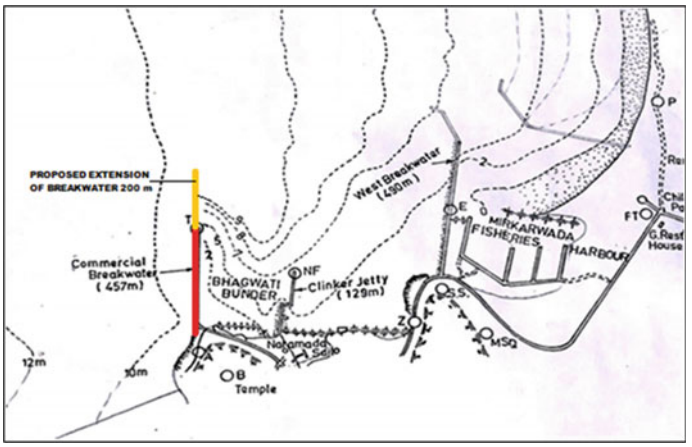

Fig. 2 Layout of Bhagwati Bunder Port

2 Prototype Data Used for Model Studies

2.1 Tidal Levels

The hydrographic chart for the area shows the following tidal levels w.r.t. chart datum (CD) at Bhagwati Bunder in Ratnagiri district of Maharashtra:

Highest high water level (HHWL)	+3.10 m
Mean higher high water (MHHW)	+2.30 m
Mean lower high water (MLHW)	+2.10 m
Mean sea level (MSL)	+1.50 m
Mean higher low water (MHLW)	+1.20 m
Mean lower low water (MLLW)	+0.50 m
Lower low water level (MLLW)	–0.08 m

The high water level (HWL) of +3.50 m including storm surge of 0.40 m was considered for the design of breakwater through wave flume studies.

2.2 Design Wave Conditions

The similar wave and tidal condition of the nearby Mirkarwada fishery harbour were considered. During the south-west monsoon, the waves approach predominantly from SW, NW and West directions with the design significant wave height (H_s) of 5.0 m to with wave periods of 8–12 s in the wave flume studies. The design significant

wave height (H_s) of 5.0 m and the maximum design breaking wave height ($H_{1/10}$) of 6.35 m at −9 m bed level have been considered for design of breakwater.

3 Design of Breakwater Cross-Sections

The layout consists of a breakwater of total length 657 m including the extension of 200 m length extending up to −9.00 m contour (Fig. 2). Desk studies have been conducted for evolving cross-sections at different bed levels based on empirical formulae, existing conditions at the site and previous in-house extensive wave flume studies conducted at CWPRS for hydraulic stability of breakwater [2]. A conceptual design of breakwater was evolved based on the desk studies. The design of cross-sections of breakwater at different bed levels with tetrapods in the armour layer was developed based on the site specific data such as bathymetry, wave conditions and tidal levels.

The weight of armour units is basically evaluated based on famous well-known Hudson's formula as given below:

$$W = \frac{w_r \cdot H^3}{K_D \times (S_r - 1)^3 \cot \theta}$$

where

H	wave height at the location of the proposed structure (m)
W	weight of armour unit (kg)
K_D	stability coefficient which varies with type of armour
W_r	unit weights of armour block (kg/m^3)
S_r	specific gravity of armour relative to water at the structure (W_r/W_w)
W_w	unit wt. of sea water (kg/m^3)
Cot θ	slope of breakwater armour measured with the horizontal.

A conceptual design of breakwater was evolved based on the desk studies. The design of cross-sections of breakwater at different bed levels with tetrapods in the armour as depicted in Figs. 3 and 4, considering the design wave condition at different bed levels. The cross-sections at different bed levels are marked along the alignment of the breakwater. The design cross-sections at different bed levels are described below:

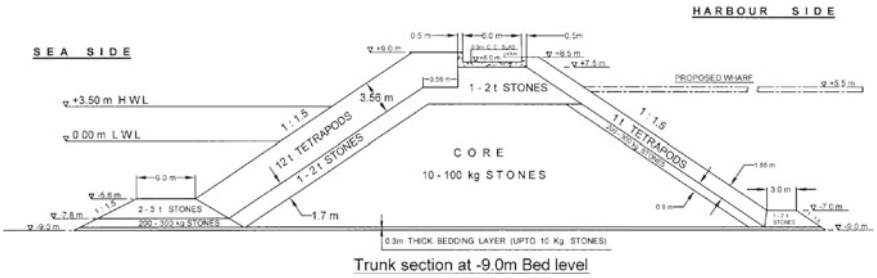

Fig. 3 Design trunk cross-section of breakwater for restoration using 1 t tetrapods on lee side from root to −9.00 m bed level at Bhagwati Bunder Port, Ratnagiri

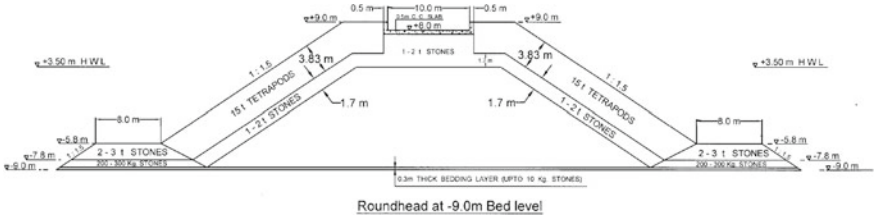

Fig. 4 Design cross-section of breakwater for roundhead at −9.00 m bed level

3.1 Design Cross-Section of Breakwater for Restoration Due Damage from Root to −9.00 m Bed Level with 1 t Tetrapods with 1:1.5 Slope on Lee Side

As suggested and desired by the project authority during the site visit held in months of February 2021, the lee side section was redesigned and modified for the breakwater from −0.0 to −9.0 m bed level as shown in Fig. 3b. This section consists of 12 t tetrapods in the armour with 1:1.5 slope on sea side and 1 t tetrapods with 1:1.5 slope on lee side. The secondary layer consists of 1 t to 2 t stones are provided below the toe-berm on sea side. Core consists of existing portion of previously laid of 10–100 kg stones, and a bedding layer of 0.3 m thick of stones up to 10 kg weight is proposed. A 0.5 m thick and 6.0 m wide crest slab is provided at el. +7.50 m with the top of its parapet is fixed at el. +9.00 m. A toe-berm is provided at el. −7.00 m on harbour side with side slope as 1:1.5 of 1 t tetrapods due to possibility of non-availability of quarry stones. This section may be superimposed on the existing breakwater, and the armour/secondary/bedding/core materials of the existing breakwater may be utilized for the restoration of damaged portion of the breakwater. The density of concrete and stones to be used for the construction of the breakwaters should be about 2.4 t/m^3 and 2.6 t/ m^3, respectively.

3.2 Design Cross-Section of Roundhead of Breakwater at −9.00 m Bed Level

The section is designed for the roundheads portion of breakwater at −9.00 m bed level as depicted in Fig. 4. This section consists of 15 t tetrapods in the armour on 1:1.5 slope on both the sides. The crest level of the toe is fixed at level −5.80 m with 6 m wide toe-berm consisting of 2 to 3 t stones on both the sides. The secondary layer consists of 1 t to 2 t stones provided on both the sides below the armour layer and toe. Core consists of 10–100 kg stones, and a bedding layer of stones up to 10 kg weight are proposed. A 0.5 m thick and 6.0 m wide crest slab is provided at el. + 7.5 m with the top of its parapet is fixed at el. +9.0 m.

The entire stretch of breakwater of length 457 m and extension of 200 m so that the entire section should behave as homogeneous section.

4 Hydraulic Model Studies

4.1 Model Scale

The model test for the design of breakwater was carried out in a wave flume by reproducing the section to a geometrically similar (GS) scale of 1:38. The model was based on Froude's criterion of similitude and as per Froude's criterion, and the various scales parameters were obtained as follows:

Model scale 1:38
• Length scale—L = 1:38
• Area scale—L^2 = 1:1,444
• Volume scale—L^3 = 1:54,872
• Time scale—$L^{1/2}$ = 1:6.1644
• Velocity scale—$L^{1/2}$ = 1:6.1644

4.2 Hydraulic Model Tests

4.2.1 Wave Flume Test Procedure

The section of the breakwater was tested under normal attack of waves in wave flume for its hydraulic stability of the structure. The sections were constructed to a geometrically similar model scale (1:38) in the flume. The number of tetrapods provided in double layer, on the seaside as armour and number of stones in the

toe were counted initially, before starting the test. After conducting the tests for a duration of one-hour, the number of tetrapods displaced from its original position was recorded and percentage of damage to the armour of breakwater was determined. During the test, extent of splashing/overtopping over the crest was also observed and recorded. The damage is expressed as percentage of number of stones displaced from their original position. The roundhead cross-section of breakwater is provided at end of extension at −9.00 m bed level and in between trunk cross-section should be provided.

4.2.2 Wave Flumes Test Conditions

The test conditions considered for the breakwater section are as follows:

1. Section was tested for the maximum breaking wave height ($H_{1/10}$) of 6.35 m and significant wave height (H_S) 5.0 m at high water level (HWL) of +3.5 m and water level at 0.0 m.
2. Tests were conducted for the different wave periods ranging from 8 to 12 seconds.
3. Trunk section was tested for normal attack of waves and the marginal splashing permitted during extreme climate conditions.
4. The bed slope of 1:100 was reproduced in front of the structure.

The trunk section at −9.0 m bed level is shown in Fig. 3 was constructed with a geometrically similar model scale of 1:38 in the wave flume. This section consists of 12 t tetrapods in the armour layer with 1:1.5 slope on sea side and 1 to 2 t stones in the secondary layer below armour with 1:1.5 slope. The sea side toe level is fixed at −5.8 m with 6 m wide toe-berm consisting of 1 to 2 t stones. The harbour side toe level is fixed at −7.00 m with 3 m wide toe-berm consisting of 1 to 2 t stones with armour layer of 1 t tetrapods with 1:1.5 slope on lee side. A secondary layer consists of 200–300 kg stones below the armour and toe-berm on sea side. A secondary layer consists of 100–200 kg stones below the armour on harbour side/lee side. Core consists of 10–100 kg stones, and a bedding layer of stones up to 10 kg weight is proposed. A 0.5 m thick and 6.0 m wide crest slab is provided at el. +7.50 m with the top of its parapet at el. 9.0 m on sea side.

The wave flume test was carried out for with design maximum breaking wave height ($H_{1/10}$) of 6.35 m at HWL of +3.5 m for one-hour duration (corresponding to 6.1664 h in prototype). It is observed that there was marginal splashing and no overtopping of the waves during the wave flume studies. It was observed that the highest wave run-up was just above +8.9 m and rundown was up to 0.00 m. It is observed during test that the waves were breaking on the armour causing no damage to armour and no damage to the toe-berm.

Another wave flume test was conducted with significant wave height (H_s) of 5.0 m at HWL of +3.5 m. There was marginal splashing and no overtopping of the waves. It was observed that the highest wave run-up was just above +8.5 m and rundown was up to +1.50 m. It is observed during test that the waves were breaking on the armour causing no damage to armour and no damage to the toe-berm.

Fig. 5 Wave action on armour layer of breakwater consisting of 12 t tetrapods and 1 t tetrapods on lee side at −9.0 m bed level with high water level of +3.50 m for wave height of 6.35 m and 5.0 m, respectively

The wave flume test was also conducted for stability of toe-berm considering maximum breaking wave height ($H_{1/10}$) of 6.35 m at water level of +0.0 m. There was marginal splashing and no overtopping of the waves. It was observed that the highest wave run-up was just above +4.0 m and rundown was up to −2.5 m. It was observed during test that the waves were breaking on the armour causing no damage to armour and no damage to the toe-berm.

Another wave flume test was conducted for stability of toe-berm significant wave height (Hs) of 5.0 m at water level of +0.0 m. There was marginal splashing and no overtopping of the waves. It was observed that the highest wave run-up was just above +4.0 m and rundown was up to −2.50 m. It was observed during test that the waves were breaking on the armour causing no damage to armour and no damage to the toe-berm (Fig. 5).

5 Discussions and Concluding Remarks

The layout consists of existing breakwater for 457 m and extension of breakwater of 200 m length at Bhagwati Bunder Port in Ratnagiri has been evolved through hydraulic model studies to facilitate the wave tranquillity in the harbour basin. The design cross-sections of breakwater have been confirmed through wave flume studies for the hydraulic stability of the structure as a whole. Based on desk and wave flumes studies, the design cross-sections of trunk and roundhead portions of the breakwater up to −9.0 m bed levels have been evolved. The breakwater cross-section for trunk portion consists of 12 t tetrapods in the armour layer and 15 t in the armour layer in the roundhead portion at −9 m bed level has been evolved. The maximum design significant wave height (Hs) of 5.0 m for maximum design water level at +3.5 m was considered for design of breakwater cross-sections. These sections are stable under the design wave conditions and safe from hydraulic point of view and may be adopted for the construction at the site. It is also proposed to provide 6 m wide crest slab with parapet wall with top level of +9.00 m. The proposed breakwater sections may be superimposed on the existing breakwater, and the armour/secondary/bedding/core

materials of the existing breakwater may be utilized for the restoration of damaged portion of the breakwater. The end portion of breakwater of about 100 m may be considered for roundhead of the breakwater.

Acknowledgements The authors are thankful to the Shri A.K. Agarwal, Director, CWPRS for providing direction to this work. The authors are also thankful to the project authorities for providing the prototype data.

References

1. CWPRS Technical Report No. 5895 (2021) Desk and Wave Flume Studies For the Restoration of Existing Breakwater at Bhagwati Bunder Port, Ratnagiri District, Maharashtra
2. US Army Corps of Engineers, Coastal Engineering Research Centre: Coastal Engineering Manual EC 1110–2–1100, Sept 2006

A Review on Directional Focusing Waves: Generation Methods Toward 3D Idealization of Rogue or Extreme Waves in Laboratory

R. Lakshman, V. Sriram, and V. Sundar

Abstract In the field of ocean engineering, rogue waves have been a critical phenomenon demanding attention over the past few decades, with their visible occurrence and their influence on the marine structure being repeated. The random isolated extreme events have posed a challenge in our ability to develop a well-defined description of such waves. There have been several studies in the past on the simulation of these events in 2D using experimental facilities and numerical tools with different theoretical approaches. However, completeness in the description of the extreme events is questionable owing to the non-consideration of their directionality. The three-dimensional studies are predominantly numerical in the literature, and 3D laboratory studies are scanty due to the challenges involved and thus, leading to an incomplete description of the rogue waves and their characteristics. A comprehensive theory should represent a physical representation of the scenario and simulate these events in numerical or experimental work. Based on this background, one could provide a wave field statistical distribution. However, we are yet to reach and gain an insight into the phenomenon. Nevertheless, it is imperative to understand where we are and the central questions to achieve the target. This paper is intended to give a comprehensive review of literature narrowing down to simulation challenges and the generation of these three-dimensional waves in laboratories. Furthermore, a simplified method used to generate the focused directional wave in deep water is briefly discussed. Also, the paper reports the preliminary results of the 3D directional focusing waves with different breaking scenarios for deep water conditions in the wave basin facility at the Department of Ocean Engineering, IIT Madras.

Keywords Rogue waves · Focused directional waves · Laboratory studies · Deepwater

R. Lakshman (✉) · V. Sriram · V. Sundar
Department of Ocean Engineering, Indian Institute of Technology Madras, Chennai 600036, India
e-mail: lakshman.clef92@gmail.com

V. Sriram
e-mail: vsriram@iitm.ac.in

V. Sundar
e-mail: vsundar@iitm.ac.in

P. V. Timbadiya et al. (eds.), *Coastal, Harbour and Ocean Engineering*, Lecture Notes in Civil Engineering 321, https://doi.org/10.1007/978-981-19-9913-0_3

1 Introduction

1.1 Definition of Rogue Waves

The concept of "rogue ocean waves" is practical and intellectually stimulating, considering its limited understanding of its nature and insufficient field data to have a statistical description of the sea state. According to established theory or hypothesis, wave being a rogue indicates being exceptionally high, steep, sudden, fleeing from one's surroundings, but also unlikely. Furthermore, no universally accepted definition of rogue waves exists. Every system has its own set of traits and statistical patterns. Even while a common feature of all rogue wave occurrences reveals significant deviations from the normal distribution, it is not characterized by one till now. Certainty in designating the severe events as rouge or an extreme wave event is still unclear.

Maritime observers have referred to the rogue wave as a "wall of water," a "sea cave," or a series of high waves. This sort of wave emerges in a calm atmosphere with no disturbances or any warning having deep troughs followed by the magnificent crests. They appear as an isolated massive wave of amplitude much greater than the typical wave tops in the surrounding area. As per [1], freak or rogue or giant wave are huge, steep, and asymmetric waves with heights exceeding 2.2 times the significant wave height. From our point of view, the standard definition of rogue waves, i.e., H = 2Hs or 2.2Hs where H is the wave height, and H_s being the significant wave height, which seems restrictive to characterize the corresponding extreme wave events. This comment is exemplified by [2]. They mentioned "an extreme wave event in the Mediterranean, off the coast of Catalonia, which struck at 14h15 TU a 207 m long ferry, the Louis Majesty, and killed two tourists. To be more precise, it consisted of three large waves (the three sisters). Their heights were estimated to be 8 m, whereas the significant height was 5 m. From the classical definition, this event is not a rogue wave event. Nevertheless, the waves were killer waves. Instead of a geometric definition, a definition based on wave energy might be more relevant to include the large population of different rogue waves appearing in the ocean." The rogue waves are also referred to as "holes in the sea" by [3].

Coming to the distribution of wave amplitudes in case of rogue waves, for a typical wavelength λ, crest peak to trough amplitude of the water waves is limited by a value $h_{lim} = (0.10 - 0.14)\lambda$ (proximal value to the limiting Stokes wave). A criterion for extreme waves is the maximum steepness of oceanic waves grows faster than their amplitude, becoming infinite before the breaking phenomenon. Hence, oceanic rogue waves are individual waves with very high steepness $h_{max} \geq 0.10\lambda$ compared to moderate waves with $h_o \leq 0.05\lambda$ representing smaller steepness waves. Above is essentially an exhaustive definition of oceanic rogue waves.

1.2 Background on the Description of Rogue Waves

Rogue waves have the following qualitative characteristics: (i) They have an extremely steep peak; (ii) they are highly asymmetric; and (iii) they arise out of nowhere and leave without a trace. A complete description of these waves requires a clear understanding of the phenomenon through physical principles formulated in mathematical terms. Further, based on the meaningful physical observations and parameters associated, they should help us understand and make useful predictions. Therefore, a complete theory for the description and mechanism of rogue waves requires mathematical physics and gives us statistical distribution for the whole wave field. The challenge is to satisfy both. If the first criterion is met, the mathematical answers will always agree with the observations. In this regard, Georg Lindgren mentions in [4] the current hypothesis based on the nonlinear Schrodinger (NLS) equation is highly successful among various domains of applications of rogue waves. Physics, mathematical theory, and experimentation all accord well. However, the second criteria are far from satisfied within the NLS equation framework, although various studies have demonstrated the relevance of directional seas.

1.3 Past Literature on Idealization of the Rogue Waves

Need for the idealization: Extreme events play a critical role in designing offshore and coastal structures, such as fixing the deck elevation and wave forces due to slamming. It is imperative to study and understand these violent directional waves ensuring the safe design of systems situated in such unpredictable environments. For the design, we need a precise understanding of the interaction of the extreme waves with the structures, for which a thorough knowledge of wave characteristics and kinematics is essential. In the past, through the attempts of field measurements of extreme waves, the number of such recorded events being insufficient, a complete statistical description of these sea states is difficult or questionable (Christou and Evans, 2014). The random occurrence of these events adds to the difficulty in field data acquisition. These isolated events have posed a challenge in our ability to develop a well-defined description of such extreme waves. Efforts in the idealization of the freak wave: The first attempt to derive the statistics of measured extreme waves was attempted by [5]. Simultaneously, the effects of finite bandwidth and nonlinearity were studied, reported later by [6]. There have been many experimental and numerical studies on 2D focusing waves in the past. However, the completeness in describing extreme events is somewhat questionable due to the non-consideration of its directionality. Efforts toward studying the directional focusing waves: [7] have attempted to investigate the generated directional extreme waves in the laboratory. The importance of directionality in the wave field and its impact on extreme waves' nonlinearity are discussed. Combining the steepness with the wave height, including other asymmetry parameters, gives a much better description and knowledge of the wave conditions

than either parameter alone. Realizing this importance, [8] reaffirmed the importance of wave steepness in many applications other than just considering the wave height alone. In laboratory studies, such extreme waves can be generated using wave focusing [9] or episoidal waves [10]. These focusing waves serve as an idealization of the freak waves.

The literature on the three-dimensional focused waves is still limited and is predominantly numerical [11–14] with few exceptions, such as in [7]; [15–17] having carried out experimental studies on the extreme waves in crossing seas. [18] analyze the possibility of extreme events due to currents. [15] considered the constant steepness spectrum for part of their study that focuses on energy loss during the propagation of a wave packet. However, the experiments were conducted with multiple directional spreading in shallow water depths. Difficulties in laboratory generation of the rogue waves: Although considerable work on extreme waves has been reported through numerical modeling, simulation of such waves in a laboratory has been scanty as it remains a challenge due to nonlinear interaction-induced complexities. Random wave tests, though they involve different wave components, seldom represent extreme events. Even if they do, the tests have to run for a long duration, and one needs adequate active and passive absorption control to have a possibility of an extreme event occurring in a random sea state, as discussed by [19]. In the following section, all the rogue wave's physical mechanisms are briefly mentioned, narrowing down to the generation process using wave-wave interaction and its types. Then, details of an attempt at the idealization of the 3D focusing waves experiment followed by the preliminary results of the investigation are presented.

2 Physical Mechanism of Rogue Waves

The existence of a dispersion relation and a coherent build-up of large amplitude pulses via collision/interference of solitons/wave packets traveling at distinct group velocities are required for rogue waves. Following are the main mechanisms followed by reference of the past attempt made, using the concerned mechanisms. For in-depth detail, refer to the studies mentioned to describe the occurrence of the rogue water wave as follows: interaction between water waves [20], three-dimensional (3D) directional wave focusing: [21], nonlinear focusing of transient frequency modulation wave group: [22], modulation instability [23], wave-current interaction wave packets with the dispersion amplification of transient wave groups and geometrical focusing on basins of varied depth, [4, 24, 25] and, solitary waves uniting randomly [2].

The purpose of this study was not to be thorough of all rogue wave events. All mechanisms concerned with the rogue waves, however, are discussed. For the present experimental study, it is limited to wave-wave interaction mechanisms in deep waters. Hence, a brief account of the wave-wave interaction mechanism followed by the description, the method adopted, and preliminary results of the laboratory experiment are presented. A summary of studies adopting the wave-wave interaction is presented. The extreme wave simulation method was initially proposed by [6], based

on the interplay of nonlinear waves. A given range of wave components (primary components) is created using this procedure. The phases of the waves are changed such that the various wave components are focused at a specific spot at a certain time. A substantial wave height emerges as a result of constructive interference. This nonlinear wave-wave interaction technique was used by [26] to explore the breaking wave process experimentally. Later, it was adopted by many researchers owing to its simplicity in its application. A detailed account can be obtained in [2, 27, 28].

2.1 A Brief on the Generation Methodology

We have three distinct generation approaches available for generation methodology, as reported in [29]. They are the reverse dispersion method, the group celerity method, and the phase speed method. Firstly, [10] proposed the reverse dispersion method concerning large episodic waves. This method systematically links individual wave singlets of specific frequency and amplitude to wave paddle displacements. The wave singlets generate a wave group that concentrates at a certain distance from the wave paddle. In the approach stated, all computations are done using linear wave theory. One of the most important requirements in the group celerity approach is to have instantaneous group celerity, which ensures that the wave energy is communicated to the focal point in the time remaining at all times. To determine the wave paddle displacements, the previously described thumb rule is used. This strategy proved successful for trials with big reflections, according to [29]. Many sinusoidal components are summed at distinct frequencies in the phase speed approach, with phases chosen to focus at a specific place in space and time. The present study adopts this method due to the simplicity of its application. The following section involves a brief about the simplified experimental setup, and its arrangements, test conditions. Further, a parameter is chosen for analysis, and the preliminary results are presented.

3 Experimental Setup and Arrangements

The tests were carried out at the wave basin facility at the Department of Ocean Engineering, Indian Institute of Technology, Madras. The wave basin is 30 m x 30 m x 3.8 m in size, with a maximum operating water depth of up to 3 m. As shown in Fig. 1a, the coordinate system has a y-component for the wave paddles, an x-component for the wave propagation direction, and a z-component for the free surface water level. The water depth was maintained at 2.98 m for all the experimental conditions. The sampling frequency and record time for each of the tests were 100 Hz and 60 s, respectively. The wave basin has 52 flap-type paddles with the artificial absorbing beach at the far end and on the side. The gantry carriage system has two degrees (X and Y) of translation freedom. The facility is used to capture the spatial surface elevation with a wave probe array (3nos x 3nos.). The 3×3 array is placed at

nine different locations with uniform distribution to form 81 data points covering an area of 1.6 m × 1.6 m, as discussed later to capture the wave profiles (Fig. 1b). The array center is placed at the predefined theoretical focusing point as the reference, which is 12.5 m from the wave paddle. In addition to the above arrangement, an additional wave probe was set up near the wave maker to register the incident wave profile at a distance of 1.56 m from the wave paddle. The purpose was to check the repeatability of the wave groups as the probe array is moved around nine different locations, as mentioned earlier, to form 81 grid points.

4 Test Conditions

The test cases involved the generation of focused waves of magnitude varied from small to large by increasing the gain parameter. The resulting wave height increases, and the crest elevation at the focusing point eventually breaks beyond the threshold. Five cases for each of the given input conditions, two corresponding to the non-breaking instances, one for mildly spilling breakers, and the remaining for the spilling breakers, were generated. Thus, overall, 10 test cases are presented, repeated nine times to capture the 81 points by moving the 3 × 3 array within the basin. Table 1 shows the details of the tested wave characteristics and the type of breaking based on visual observations.

A qualitative representation of the narrowband and broadband spectrum is shown in Fig. 2 [19]. For the present experiments, the central frequency, $f_c = 0.68$ Hz, and the bandwidths, $\Delta f/f_c = (0.5\ and\ 0.75)$, are used for a constant working water depth of 2.98 m (Table.1). The central frequency chosen corresponds to $k_c d = 5.55$ [30], subscript "c" refers to central frequency. The values indicate the wave groups are propagating in deep waters. Both narrowband and broadband spectra are covered. The total recording duration for each test case is roughly 1 min.

5 Parameter to Identify the Wave Characteristics

The plunging breaker is the limiting state for an asymmetric profile of the breaking waves. This tilt degree should directly affect the design of marine structures. [8] have carried out a wave-by-wave analysis to identify a wave and study its profile characteristics. A similar approach for the present study is chosen. An index to review these identified waves between zero crossings is the Atiltness parameter (ATP), as referred to in [31], to express the overall asymmetry in the wave profiles. Following are the Atiltness parameter inferences made from its numerical, i.e., values, for ATP = 0, represents a perfectly symmetric profile, ATP > 0, means the wave profiles show forward tilting as a whole, and for ATP < 0, wave profiles show backward tilting as a whole.

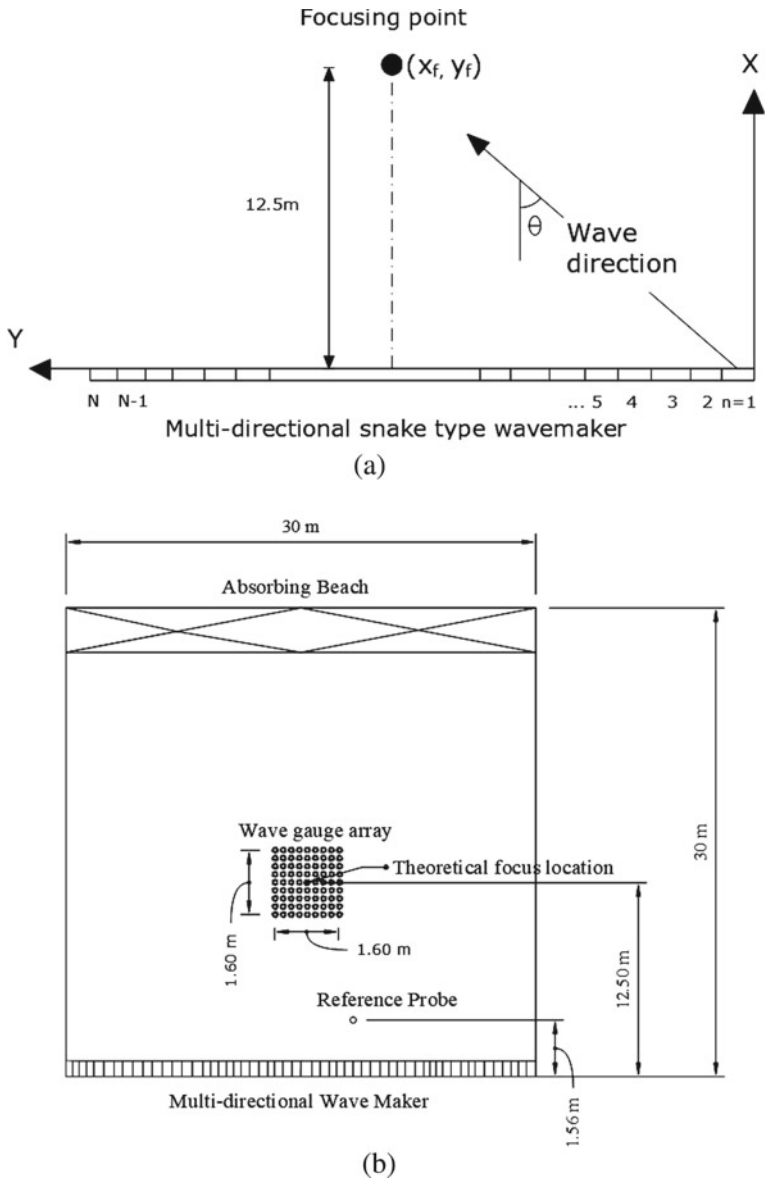

Fig. 1 **a** Multidirectional wavemaker arrangement along with the relationship between the wave direction and the wavemaker. Five principle wave directions {−250, −12.50, 00, 12.50, 250}, i.e., a directional range of 500 was employed for the experiments in the wave basin. The focus location (x_f, y_f) is predefined at 12.5 m. **b** Representation of top view of wave basin arrangement

Table 1 Test wave characteristics chosen for the experiments. Each test case was repeated nine times to capture all 81 data points, covering an area of 1.6 m × 1.6 m. For $f_c = 0.68$ Hz, the smaller increase in gain results in steeper crests. Hence, the smaller range of wave height across the test cases. The wave paddle displacements of the facility were used to the full limit for the broadband test cases

Test case	f_c (Hz)	Band width	f_1 (Hz)	f_N (Hz)	Wave height, H (cm)	Visual observation
1					45	Non-breaking
2					48	Non-breaking
3	0.68	Narrow	0.36	0.84	50	Mildly breaking
4					52	Breaking with spilling type breakers
5					55	Breaking with spilling type breakers
6					44	Non-breaking
7					46	Non-breaking
8	0.68	Broad	0.2	0.93	49	Mildly breaking
9					52	Breaking with spilling type breakers
10					54	Breaking with spilling type breakers

6 Results and Discussions

The significance of the interpretation through the Atiltness parameter (ATP) is similar to the third-order moment. However, it normalizes the skewness and provides a holistic picture of the data distribution [31]. The variations of ATP with nonlinearity parameter for fc = 0.68 Hz for both narrow and broadband spectrum are shown in Fig. 3a and b. The ATP is positive for all the data acquired for the narrowband spectrum suggest wave profiles showing a forward tilting as a whole. It also reinforces the well-defined crests dominate the narrowband spectrum. The ATP values vary from negative to positive for the broadband spectrum, suggesting the presence of crests and broader troughs. The existence of nonlinearity in the wave components indicates a deviation from the normal distribution, and nonlinear wave components suggest that certain phase angles are not independent but have a fixed relationship. Furthermore, component waves with dependent phase angles do not satisfy the dispersion relation [31]. The above observations with a spectral bandwidth, central frequencies, and Atiltness parameter are discussed with the nonlinearity parameter.

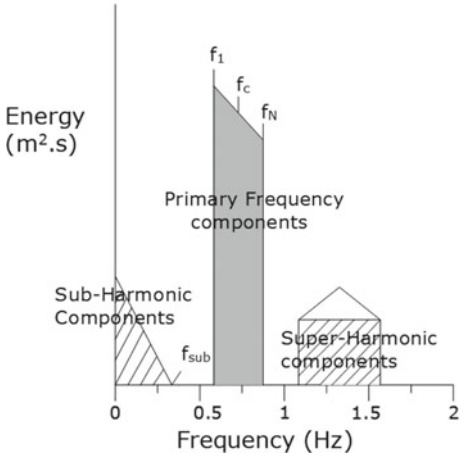

(a) Narrowband Spectrum

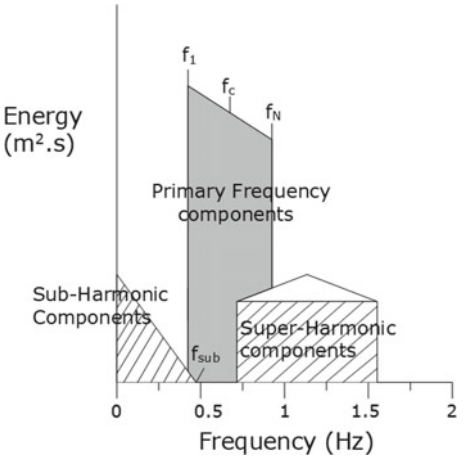

(b) Broadband Spectrum

Fig. 2 Qualitative representation of narrowband and broadband spectrum

7 Observations and Future Studies

A brief literature review on the varied perspectives on definition leads to an exhaustive definition of a rogue wave. Background on the description of the rogue waves attempts at its idealization in laboratories, difficulties in attempting these events at laboratory scale, and a collection of physical mechanisms and mechanisms adopted for the current experimental study are presented. Further, a detailed account of experimental setup and arrangements, the test conditions adopted, and the preliminary investigations conducted at IIT Madras are made available for the readers. This experiment was devised, and the idea was to recover the directional spreading back

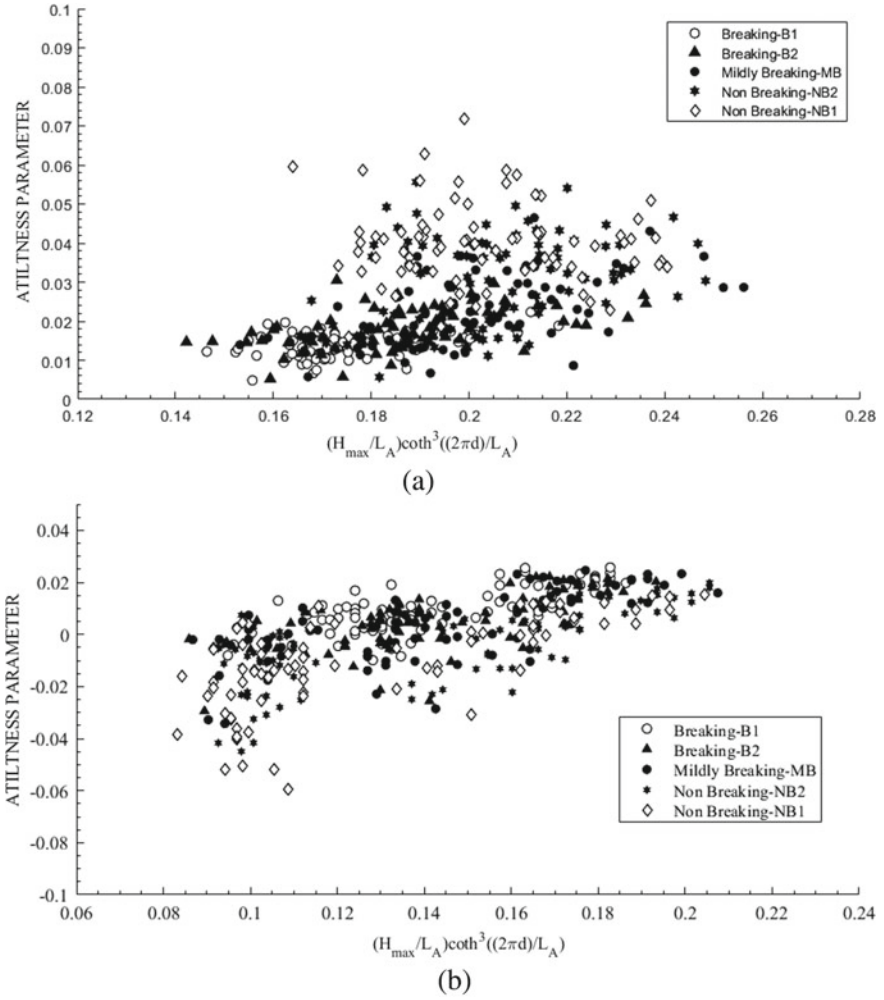

Fig. 3 **a** Atiltness parameter versus nonlinearity parameter, fc = 0.68 Hz, narrowband spectrum and **b** Atiltness parameter versus nonlinearity parameter, fc = 0.68 Hz, broadband spectrum

from the set of time series. Since a non-homogeneous and non-stationary wave group is adopted, it would require time and frequency characteristics. In this paper, the first part of the study wherein the investigated wave profile characteristics is carried out is partly presented for a group of test cases, as discussed earlier. It is intended to extend the study further to recover directional spreading and do a time-domain analysis in the future. Though it is hard to give a detailed account of a rogue wave and its mechanism in such a concise document, an attempt is made to provide a thorough brief and finally narrowing down to a simplified method to study directional focusing waves in laboratory conditions. Even though significant work has previously been completed,

comprehension is still relatively weak, numerically and experimentally. A lack of a robust deep water 3D wave model is seen, reported in [32]. Also, there is a lack of research studies in wave-wave interactions. Even if done, it is broadly for crossing seas, which does not give us a complete picture of the phenomenon. A constructive interference model is an old and accepted process for the occurrence of the rogue wave. At laboratory scale, understanding this particular aspect three-dimensionally is necessary, and a humble attempt is made here intending to broaden the horizon for these giant waves.

References

1. Dean RG, Dalrymple RA (1991) Water wave mechanics for engineers and scientists, vol 2. World Scientific Publishing Company
2. Kharif C, Pelinovsky E (2003) Physical mechanisms of the rogue wave phenomenon. Eur J Mech B/Fluids 22(6):603–634
3. Sand SE, Hansen NO, Klinting P, Gudmestad OT, Sterndorff MJ (1990) Freak wave kinematics. In: Water wave kinematics. Springer, Dordrecht, pp 535–549
4. Ruban V, Kodama Y, Ruderman M, Dudley J, Grimshaw R, McClintock PVE, Onorato M, Kharif C, Pelinovsky E, Soomere T, Lindgren G (2010) Rogue waves–towards a unifying concept?: Discussions and debates. Eur Phys J Spec Top 185(1):5–15
5. Longuet-Higgins MS (1956) Statistical properties of a moving wave-form. Math Proc Cambr Philos Soc 52(2):234–245. Cambridge University Press
6. Longuet-Higgins MS (1980) Modulation of the amplitude of steep wind waves. J Fluid Mech 99(4):705–713
7. Johannessen TB, Swan C (2001) A laboratory study of the focusing of transient and directionally spread surface water waves. Proc R Soc Lond Ser A Math Phys Eng Sci 457:971–1006 (2008)
8. Myrhaug D, Kjeldsen SP (1986) Steepness and asymmetry of extreme waves and the highest waves in deep water. Ocean Eng 13(6):549–568
9. Chan ES, Melville WK (1988) Deep-water plunging wave pressures on a vertical plane wall. Proc R Soc Lond A Math Phys Sci 417:95–131 (1852)
10. Funke ER, Mansard EPD (1979) SPLSH: a program for the synthesis of episodic waves. National Research Council Canada
11. Hong K, Meza E, Liu S (2004) Energy dissipation and transfer in breaking waves generated by directional and multi-frequency focusing in deep water. In: The fourteenth international offshore and polar engineering conference. OnePetro
12. Grilli ST, Dias F, Guyenne P, Fochesato C, Enet F (2010) Progress in fully nonlinear potential flow modeling of 3D extreme ocean waves. Advances in numerical simulation of nonlinear water waves, pp 75–128
13. Benetazzo A, Ardhuin F, Bergamasco F, Cavaleri L, Guimarães PV, Schwendeman M, Sclavo M, Thomson J, Torsello A (2017) On the shape and likelihood of oceanic rogue waves. Sci Rep 7(1):1–11
14. Zhang YH, Liang SX, Sun ZC (2019) Study on energy spectrum instability in the processes of propagating and breaking of focusing waves. China Ocean Eng 33(1):86–93
15. Liu S, Li J, Hong K, Meza E (2005) Experimental study on multi-directional wave focusing and breaking in shallow water. In: The fifteenth international offshore and polar engineering conference. OnePetro
16. McAllister ML, Draycott S, Adcock TAA, Taylor PH, Van Den Bremer TS (2019) Laboratory recreation of the Draupner wave and the role of breaking in crossing seas. J Fluid Mech 860:767–786

17. Luxmoore JF, Ilic S, Mori N (2019) On kurtosis and extreme waves in crossing directional seas: a laboratory experiment. J Fluid Mech 876:792–817
18. Wu CH, Yao A (2004) Laboratory measurements of limiting freak waves on currents. J Geophys Res Oceans 109(C12)
19. Sriram V, Schlurmann T, Schimmels S (2015) Focused wave evolution using linear and second order wavemaker theory. Appl Ocean Res 53:279–296
20. Peterson P, Soomere T, Engelbrecht J, Van Groesen E (2003) Soliton interaction as a possible model for extreme waves in shallow water. Nonlinear Process Geophys 10(6):503–510
21. Fochesato C, Grilli S, Dias F (2007) Numerical modeling of extreme rogue waves generated by directional energy focusing. Wave Motion 44(5):395–416
22. Pelinovsky E, Kharif C, Talipova T (2008) Large-amplitude long wave interaction with a vertical wall. Eur J Mech B/Fluids 27(4):409–418
23. Shats M, Punzmann H, Xia H (2010) Capillary rogue waves. Phys Rev Lett 104(10):104503
24. Pelinovsky E, Shurgalina E, Chaikovskaya N (2011) The scenario of a single freak wave appearance in deep water–dispersive focusing mechanism framework. Nat Hazard 11(1):127–134
25. Touboul J, Kharif C, Pelinovsky E, Giovanangeli JP (2008) On the interaction of wind and steep gravity wave groups using Miles' and Jeffreys' mechanisms. Nonlinear Process Geophys 15(6):1023–1110
26. Rapp RJ, Melville WK (1990) Laboratory measurements of deepwater breaking waves. Philos Trans R Soc Lond Ser A Math Phys Sci 331:735–800 (1622)
27. Baldock TE, Swan C (1994) Numerical calculations of large transient water waves. Appl Ocean Res 16(2):101–112
28. Perlin M, He J, Bernal LP (1996) An experimental study of plunging deepwater breakers. Phys Fluids 8(9):2365–2374
29. Chaplin JR (1996) On frequency focusing of unidirectional waves. Int J Offshore Polar Eng 6(2):131–137
30. Hughes SA (1993) Physical models and laboratory techniques in coastal engineering, vol 7. World Scientific
31. Goda Y (2010) Random seas and design of maritime structures, vol 33. World Scientific Publishing Company
32. Onorato M, Residori S, Bortolozzo U, Montina A, Arecchi FT (2013) Rogue waves and their generating mechanisms in different physical contexts. Phys Rep 528(2):47–89

Physical Model Study on the Soft Option of Coastal Protection Works by Vegetation Meadow—A Review

Surakshitha, Manu, and Subba Rao

Abstract As the frequency of occurrence of the coastal hazards increasing along with sea level rise the number of hard structures installed to mitigate the beach erosion, flooding needs to be increased or upgraded. Attention on strategically utilizing the ecosystem service provided by vegetation to tackle such hazard is increasing in the coastal engineering field as the negative impact on the environmental and ecological system is less in this approach compared to conventional approach. The resistance offered by the vegetation meadow on wave energy depends on the submergence ratio, density of the plant per area, the rigidity of vegetation, and also on hydrodynamic characteristics. Prediction of behavior and effect on the wave propagation is necessary to determine the degree of effectiveness of the vegetation field in coastal defense. The physical model study which involves laboratory testing of small-scale models is one of the tools to examine and verify the effectiveness of structure under the action of the wave. The present paper focuses on the review of physical model study, their key findings and highlighting the criteria based on which material is selected to model the various real plants.

Keywords Wave flume experiment · Vegetation model · Coastal vegetation · Living breakwater

1 Introduction

Pressure on coastal areas is increasing due to an increase in the number of coastal infrastructures and human settlements; as a result equilibrium of coastal process and the ability of the coast to withstand the natural disaster such as storm surge, flooding hurricane are declining thereby risking the life and valuable property. Breakwater, seawall, and groins are extensively used to protect such areas. These are called the as hard solution of coastal protection. These approaches focus more on dissipation and

Surakshitha (✉) · Manu · S. Rao
Department of Water Resources and Ocean Engineering, National Institute of Technology, Surathkal, Karnataka 575025, India
e-mail: Surakshithaks14@gmail.com

P. V. Timbadiya et al. (eds.), *Coastal, Harbour and Ocean Engineering*, Lecture Notes in Civil Engineering 321, https://doi.org/10.1007/978-981-19-9913-0_4

constraining the impact of such events on the affected area rather than maintaining the natural steady condition along the coastal belt. More often hard structures constructed in particular coast deployed to reduce erosion, cut off alongshore sediment supply to the nearby beach and cause erosion problem in that site. Soft solution of coastal protection concentrates on utilizing the protective service provided by coastal habitat.

There has to be an interaction of coastal process with landscape for sustaining the system equilibrium, starting from seabed elevation which provides bottom friction, facilitates breaking of a wave. The potential of coastal vegetation to trap the sediment preventing re-suspension along with wave decay makes it a significant feature [1]. Having a gentle slope when the wave is about to hit the shore still more reduces the intensity of the wave, ultimately minimizing the energy required for the onshore-offshore movement of sand, consequently maintaining the shoreline. The coast without such provisions experiences erosion which is slowly balanced by the continuous supply of sediment by rivers. Rivers not only provides sediment but also helps to maintain freshwater exchange for flourishing marshes and keep the shallow water level in the wetland as sea-level rises [2], those will provide storage for flood water as well as reduce the energy of storm surge forcing toward the community area [1, 3].

Because of sea-level rise, the existing coastal defense infrastructure needs to be improved in its dimensions and may require to be redone in the near future to counteract the constantly increasing sea level. This is not only expensive but also adversely affect a newly adopted ecological community [4]. The wetland having dense forest offers resistance to free-flowing wind thereby reduce the formation of the surface wave [3]. In recent years a considerable attention has been given to incorporating natural feature in traditional hard approaches to improve the depleting coastal biodiversity and further reduce the environmental impact. Extensive research is required to adopt such a new concept for coastal resilience.

Vegetation offers resistance to the free flow of energy that creates a damping effect on the incident wave, reduces turbulence, and creates a calm condition. Prior studies have shown that vegetated foreshore modifies coastal hydrodynamics. The wave damping capacity of the vegetated area can be easily determined once the drag coefficient of the vegetation is known [5]. Close to realistic results can be obtained in coastal hydrodynamic modeling if this effect is included, it can be done by representing them as friction factor, high viscous layer, or bottom drag coefficient [6].

2 Material Properties

Plant undergo reconfiguration that changes their shape and reduce the length so that the drag force acting on them reduces, meaning the resistance offered by the plant area on the flow decreases and associated dissipation is less. If the deflected length is not considered in the numerical analysis, the result shows more dissipation leading to overestimation [7]. The degree of reconfiguration depends on material properties such as modulus of elasticity and flexural rigidity. It is mandatory to know

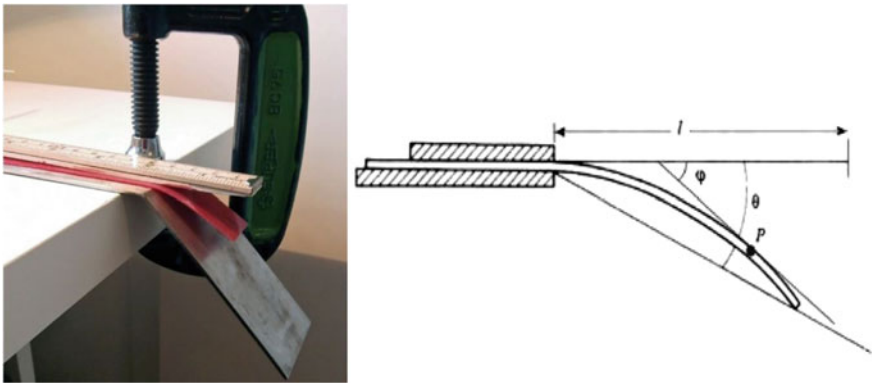

Fig. 1 Piers cantilever test

the biomechanical properties of vegetation to further evaluate the flow interaction for both physical and numerical study. Choosing the correct material to create the artificial vegetation of the real plant is a crucial process in order to get accurate wave transformation as that of the field.

Pier cantilever test is one of the methods used to determine the highly flexible vegetation such as seaweed. Here the sample is cut into a rectangle shape of a specific length (20 cm × 2.5 cm) and placed on the horizontal part of the apparatus as shown in Fig. 1, and then the specimen is slowly pushed toward the edge till it touches the inclined plane which is inclined to a known angle to the horizontal. Cantilever length and weight per unit area of the sample is noted and from Peirce's formula flexural rigidity "I" is calculated [8].

$$\mathrm{j} = \mathrm{wl}^3\left[\frac{\cos(\theta/2)}{8}\tan\theta\right]$$

where j is the flexural rigidity per unit width of the sample, θ is bending angle as shown in Fig. 1, l is the cantilever length and the weight per unit area of the sample is w.

Material properties can also be obtained by Instron materials-testing machine (Model 5544, Norwood, MA, USA) where the sample is held between the grip and tension is applied till it breaks [9].

3 Importance of Physical Study

The coastal region is commonly affected by wind, current, waves and frequently occurring storm, such extreme weather event makes the ocean a complex environment. The physical model study involves generation of this environment in a

controlled facility. Any innovative structure introduced for the shore protection needs thorough evaluation to determine the performance to accurately predict their consequence before the installation, this enables the designer to closely examine the failure mode, make necessary correction and optimize the parameter if required. Because the method involves less assumptions and direct measurement of response, the physical model study is one of the effective tools to examine and verify the effectiveness of structure under the action of wave in the ocean engineering field. It is achieved by laboratory testing of small-scale model.

To obtain a good agreement between up scaled response of model and response of prototype in real scenario, the following parameter should be scaled that is, dimension of the prototype, fluid property such as surface tension, viscosity, fluid density, and characteristic velocity, property of the structure (e.g., E = Young's modulus) and acceleration due to gravity and the atmospheric pressure [10, 11]. This will maintain the geometric similarity which preserves the shape, kinematic similarity maintains identical ratios of time, velocity, acceleration, and discharge between the prototype and the model thus ensures the similarity of particle motion between the prototype and the model. The hydrodynamic similarity ensures similar interaction between the structure and fluid for both prototype and the model [12]. There is several scaling law, the chosen law must govern the physical process. Since breakwaters are gravity-based structures, they are scaled by Froude's law. For the structures which are determined by elasticity, Cauchy number is considered additionally. Compliant towers, risers, and tendons are some of the example for Elastic structure.

4 Factor Affecting Wave Transformation

The optimum density of the vegetation per area, dimension of the vegetation field, stiffness, geometry, diameter or thickness of vegetation is some of the factors that determine the degree of wave damping. Bao et al. [13] analyzed mangrove forest structure to determine optimum forest width for the Vietnam coast for effective coastal resilience against the wave. 32 mangrove forests each of 4000 m^2 is selected on the southern and northern side of Vietnam. Data on wave height, mangrove forest structure in terms of mangrove height, forest closure, species, and density of shoots were collected along the coast, and then the wave attenuation was analyzed. An integrated equation was proposed which explains the relationship between wave decay to initial wave height and mangrove forest structure. They conclude that when the mangrove forest is dense and tall, the width of the forest required to obtain safe wave dissipation is less but when the height and density of the forest is less large mangrove forest width is required.

$$W_h = (0.9899 \times I_{wh} + 0.3526) \times e^{(0.048 - 0.0016 \times H - 0.00178 \times \ln(N) - 0.0077 \times \ln(CC) \times B_w)}$$

W_h is wave height behind the mangrove forest band in cm, I_{wh} is initial sea wave height in cm, H is the average mangrove height in m, N is the no. of tree per area, CC is the percentage of canopy closure, and B_w is the width of the forest in m.

Similarly, although the rigid model displays more dissipation than the flexible one, Paul et al. [14] found more dissipation for flexible vegetation when the density per unit area was increased.

Later mangrove replica with stiff wooden rods of 0.01 m diameter and 0.36 m length and are varied canopy densities of 62, 139, and 556 stems/m^2 were studied experimentally by Hu et al. [15]. The result of which showed the higher wave dissipation for dense stem configuration and lower submergence ratio. Another study used cross-linked polyolefin (XLPO) tubing to replicate the saltmarsh vegetation Spartina alterniflora, the modulus of elasticity of the material (172.4 MPa) was closer to that of the real plant measured by the author (Ev = 159.8 MPa) but same species displayed Ev = 1410 ± 710 MPa in another study, large difference because of the same vegetation was collected from two different locations. This shows that giving exact value of stiffness for a particular vegetation species is may not be justified, since roots, stem, joints, and leaves are made of different tissues, moreover, material property within a species also shows a different value depending on age, season [9], and exposure condition [16]. Further insight into the wave attenuation ability was determined by varying the stem density and submergence ratio. The higher order wave system dissipated more energy compared to the lower frequency wave system [17].

The ratio of water depth to vegetation height is called the submergence ratio; this is one of the important factors which affect the wave dissipation characteristics of vegetation. To understand the relationship between the two, the vegetation height needs to be varied according to the observed submergence ratio of the field condition and keeping the constant water depth. If the water depth is varied the other wave parameter such as wave height, wave period also varies, making it difficult to distinguish whether the submergence ratio affected the wave dissipation or the other hydrodynamics parameter.

Since coastal vegetation such as mangrove and salt marsh vegetation is always affected by waves and tides, some experiments introduced the effect of current in the flume study. With 2 different flexible materials (cable ties and poly ribbon) and a wide range of vegetation height (10–30 cm), leaf width(1.8–2.2 mm), and densities (500–8000 plant per m^2), the seagrass species Z. noltii model was studied in flume by Paul et al. [14]. However, in the real scenario, specific vegetation has particular flexibility and height. Therefore the experiment result was not only expected to represent the wave attenuation characteristics of Z. noltii but also of general sea vegetation. Here the experiment was conducted under pure wave conditions and other condition was a combination of wave-current conditions. Results revealed that the presence of current reduced the wave dissipation characteristics of the vegetation and as the submergence ratio increases the wave dissipation decreases. Among submergence ratio, underlying current, leaf index area (LAI), submergence ratio had the least effect on wave dissipation, and leaf index area (LAI) is found to be the dominant parameter.

Yin et al. [18] analyzed the performance of the mangrove forest on wave attenuation using polyvinyl chloride (PVC) cylinder (1:10 scale). Interestingly here elastic

property of the model (3.14–3.92 GPa) is different than that of the prototype (15Gpa) but the material is chosen because of its property to stay undamaged under the effect of the wave. Here Froude's scaling is only applied to the wave condition, not on the vegetation model. Down-looking Acoustic Doppler Velocimeter (ADV) was used to determine the current velocity. Eight capacitance-type wave gauges are used to determine the free surface elevations. After analyzing the damping data it is concluded that opposing current along with wave gives more wave damping. The wave dissipation in the case of the following current with the wave depends on the ratio of current velocity and wave velocity but opposing current always enhances the dissipation. Wave damping due to two species of real vegetation on wave parameter in prototype scale is evaluated experimentally in Cantabria Coastal and Ocean Basin (CCOB) large basin by Losada et al. [7]. The non-dimensional deflected length found to be less for combined effect of waves and currents.

In the study by John et al. [19], because of the difficulty in finding material of the young's modulus (E) same as 1:30-scaled-down young's modulus of seagrass E. acoroides, the material selection was not based on youngs modulus basis but moment of inertia was considered to fabricate the model. Also the thickness, length, and width of the leaf were scaled to create the model. Later, to investigate the effect of plant density per unit area on the wave field, the replica of Indian mangrove species called Avicennia officianalis was studied in the flume. The model was prepared from nylon rods based on the scaled-down young's modulus of the prototype and the result of the experiment found more dissipation for higher density vegetation model John et al. [20].

The seagrass (P. oceanica) was modeled (Fig. 2) by Folkard [21] using polyethylene sheeting, where geometrical scaling was not applied since the author ensured the same discharge rate and speed of flow during the experiment. Yipping et al. [22] tested artificial plants of phragmites australis on wave dissipation using an open wave flume of 30 × 0.5 m × 1 m. The density and flexural rigidity of the actual plant was the basis to select the material. Because of the difficulty to create the exact morphology of the real plant, this author suggested to adopt a simplified or idealized form of the vegetation shape.

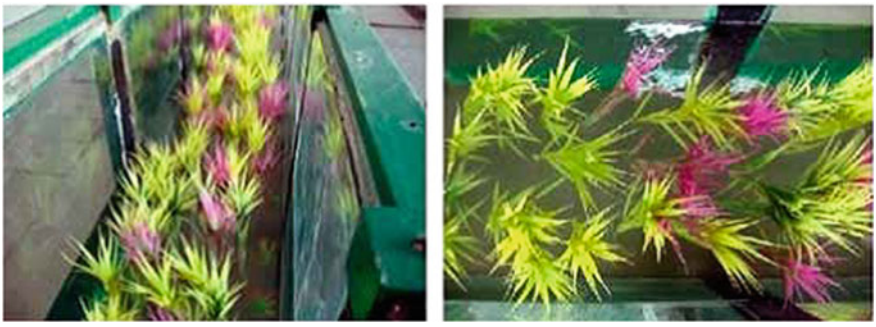

Fig. 2 Artificial phragmites australis plant in wave flume

Fig. 3 Plant model

Wave interaction of Phragmites australis (emerged vegetation) and Hydrilla verticalla (submerged vegetation) was studied in a flume with a vegetated replica by Li et al. [23]. The author made sure that the density, flexural rigidity, and morphologic resemblance of the model and prototype remains as close to similar as possible (Fig. 3).

Generally, a simple cylinder structure is used to evaluate the mangrove forest on wave dissipation characteristics where the complete structure of the Mangrove plant is ignored but because of the complexity to scale down each component. Only modulus of elasticity, diameter, and length of actual plant is considered to create a model [18]. This limitation is addressed in the study by He et al. [24], where the detailed model consisting of stem, root, and canopy of mangrove (Rhizophora) is evaluated in wave flume (40 × 0.5 m × 0.8 m). Roots from polyethylene, PVC stems of 1:10 scaled-down diameter, and the canopy model from high-density polyethylene was prepared as shown in Fig. 4. But only the diameter and length of the mangrove were scaled. Therefore, the upscaled result is not a true representative of the response of the mangrove (Rhizophora) forest in the actual field but it represents a range of bulk resistance conditions for wave propagation and the obtained experimental data can be useful for numerical model validation, where the effect of stem root and the canopy is considered to simulate the wave damping by coastal vegetation. The results showed maximum wave energy dissipation for the water level at the geometric

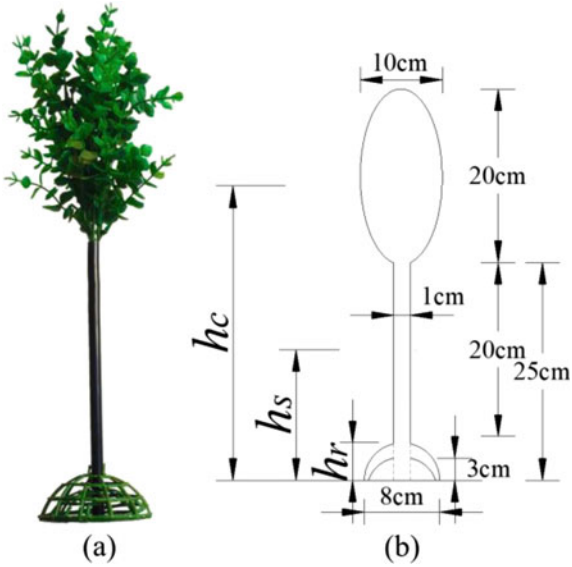

Fig. 4 Mangrove Rhizophora model

centroid of the canopy. In addition to that, an empirical formula was formulated to predict the wave transmission coefficient.

$$\mathrm{Kt} = -3.92 \times 10^{-9}\left(\frac{\mathrm{L}^2\mathrm{H}_0}{\mathrm{h}^3}\right)\left(\frac{\mathrm{h_s}}{\mathrm{h}}\right)^{0.18}\left[\left(\frac{\mathrm{h_r}}{\mathrm{h}}\right)^{-0.02}\right]^{\mathrm{l}}\left[\left(\frac{\mathrm{h_c}}{\mathrm{h}}\right)^{62.40}\right]^{\mathrm{j}} \times \left(\frac{\mathrm{B}}{\mathrm{L}}^{-96.37}\right)\psi^{4.528} + 0.777$$

Ψ is vegetation density, h_s/h, h_r/h, and h_c/h are the relative stem height, the relative root height and the relative canopy height, respectively. The term B/L is the relative width or horizontal extension of vegetation.

To analyze the effect of the vegetation biomass position with respect to depth on wave attenuation, Wu and Cox [25] conducted experiment with vegetation model of uniform biomass and a model of non-uniform biomass. Froude's scale 1:4 is adopted to fabricate salt marsh vegetation Schoenoplectus pungens using plastic strips or zip ties. To keep Reynolds number observed for the prototype in an actual condition similar to the model, the dimensions of the plant were not scaled. Since non-uniform vegetated biomasses have less area near the water surface compared to the uniform biomass model, they offer less wave resistance, and hence the dissipation recorded was less. The effect of flexibility of vegetation on wave damping is evaluated by Veelen et al. [26], where the rigid (bamboo dowel) and flexible vegetation (silicon sealant) model is examined under the wave field using flume experiment (Fig. 5a, b). There is no scale difference between the prototype and model but the author

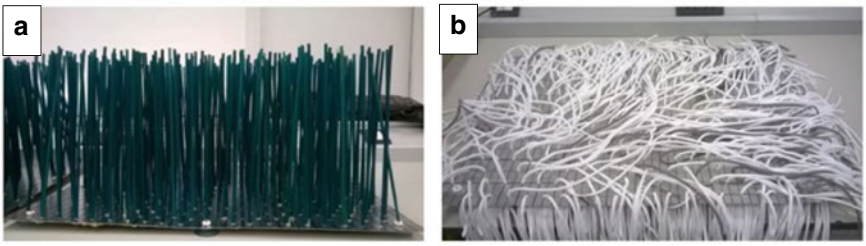

Fig. 5 **a** Artificial rigid vegetation. **b** Artificial flexible vegetation

made clear that wave vegetation interaction remains the same. The dimensions of the vegetation model (height, diameter, and density) are within the range of salt marsh vegetation present in South Wales and the wave condition selected is also similar to the observed condition of the field.

5 Summary

Coastal vegetation is an important feature because they affect flooding, inundation, and coastal erosion. They are represented as drag coefficients in the coastal hydrodynamic model. Since it cannot be directly measured in the field, experimental study provides an easy option. Moreover, research on the effect of vegetation characteristics on wave hydrodynamics is increasing to efficiently incorporate them in the coastal protection measure. This paper highlights research where artificial vegetation is studied. The studies started with a cylindrical mangrove model where diameter, length, and modulus of elasticity were the base to replicate the prototype. Now the delicate flexible vegetation such as salt marsh and seagrass is also being replicated and studied in the more recent research. Because of the difficulty in scaling the biomechanical property of the plant most of the studies adopt the scaling only to geometrical property and hydrodynamic property of testing condition. Therefore, the result will not be a true response expected to be in the field. More research and general guidelines are needed in the physical model study of the vegetation to get an accurate result.

References

1. Costanza R, Day JW, Mitsch WJ (2006) A new vision for New Orleans and the Mississippi delta. Appl Ecol Econ Ecol Eng 4(9):465–472
2. Temmerman S, Meire P, Bouma TJ, Herman PMJ, Ysebaert T, Vriend HJ De, Nargis C, Orleans N (2013) Ecosystem-based coastal defence in the face of global change. 1–5. https://doi.org/10.1038/nature12859

3. Jr JWD, Boesch DF, Clairain EJ, Kemp GP, Laska SB, Mitsch WJ, Orth K, Mashriqui H, Reed DJ, Shabman L, Simenstad CA, Streever BJ, Twilley RR, Watson CC, Wells JT, Whigham DF (2007) Restoration of the Mississippi Delta. Lessons from Hurricanes 315:1679–1684
4. Maris T, Temmerman S (2007) Tuning the tide: creating ecological conditions for tidal marsh development in a flood control area Tuning the tide: creating ecological conditions for tidal marsh development in a flood control area. https://doi.org/10.1007/s10750-007-0650-5
5. Chen H, Ni Y, Li Y, Liu F, Ou S, Su M, Peng Y, Hu Z, Uijttewaal W, Suzuki T (2018) Deriving vegetation drag coefficients in combined wave-current flows by calibration and direct measurement methods. Adv Water Resour 122:217–227. https://doi.org/10.1016/j.advwatres.2018.10.008
6. Augustin LN, Irish JL, Lynett P (2009) Laboratory and numerical studies of wave damping by emergent and near-emergent wetland vegetation. Coast Eng 56(3):332–340. https://doi.org/10.1016/j.coastaleng.2008.09.004
7. Losada IJ, Maza M, Lara JL (2016) A new formulation for vegetation-induced damping under combined waves and currents. Coast Eng 107:1–13. https://doi.org/10.1016/j.coastaleng.2015.09.011
8. Paul M, Henry PYT, Thomas RE (2014) Geometrical and mechanical properties of four species of northern European brown macroalgae. Coast Eng 84:73–80. https://doi.org/10.1016/j.coastaleng.2013.11.007
9. Burnett NP, Koehl MAR (2019) Mechanical properties of the wave-swept kelp Egregia menziesii change with season, growth rate and herbivore wounds. J Exp Biol 222(4). https://doi.org/10.1242/jeb.190595
10. Taylor P, Heller V (2011) Scale effects in physical hydraulic engineering models. https://doi.org/10.1080/00221686.2011.578914
11. Heller V, London IC (2012) Development of wave devices from initial conception to commercial demonstration. In: Comprehensive renewable energy, vol 8. Elsevier Ltd. https://doi.org/10.1016/B978-0-08-087872-0.00804-0
12. Chakrabarti SK (2005) Physical modelling of offshore structures. Elsevier Ltd., Handbook of offshore engineering. https://doi.org/10.1016/B978-0-08-044381-2.50020-5
13. Bao TQ (2011) Effect of mangrove forest structures on wave attenuation in coastal Vietnam. Oceanologia 53(3):807–818. https://doi.org/10.5697/oc.53-3.807
14. Paul M, Bouma TJ, Amos CL (2012) Wave attenuation by submerged vegetation: combining the effect of organism traits and tidal current. https://doi.org/10.3354/meps09489
15. Hu Z, Suzuki T, Zitman T, Uittewaal W, Stive M (2014) Laboratory study on wave dissipation by vegetation in combined current-wave flow Laboratory study on wave dissipation by vegetation in combined current-wave flow. https://doi.org/10.1016/j.coastaleng.2014.02.009
16. Armstrong SL (1988) Mechanical properties of the tissues of the brown alga Hedophyllum sessile (C. Ag.) Setchell: variability with habitat. https://doi.org/10.1016/0022-0981(88)90134-7
17. Anderson ME, Smith JM (2014) Wave attenuation by flexible, idealized salt marsh vegetation. Coast Eng 83:82–92. https://doi.org/10.1016/j.coastaleng.2013.10.004
18. Yin Z, Wang Y, Liu Y, Zou W (2020) Wave attenuation by rigid emergent vegetation under combined wave and current flows. https://doi.org/10.1016/j.oceaneng.2020.107632
19. John BM, Shirlal KG, Rao S, Rajasekaran C (2016) Effect of artificial seagrass on wave attenuation and wave run-up. https://doi.org/10.1177/1759313115623163
20. John BM, Shirlal KG, Rao S (2019) Laboratory investigations of wave attenuation by simulated vegetation of varying densities. https://doi.org/10.1080/09715010.2017.1398112
21. Folkard AM (2014) Hydrodynamics of model Posidonia oceanica patches in shallow water. 50(5):1592–1600
22. Yiping L, Anim DO, Wang Y, Tang C, Du W, Lixiao N, Yu Z, Acharya K, Chen L (2015) Laboratory simulations of wave attenuation by an emergent vegetation of artificial Phragmites australis: an experimental study of an open-channel wave flume. J Environ Eng Landsc Manage 23(4):251–266

23. Li Y, Anim DO, Wang Y, Tang C, Du W, Yu Z, Acharya K (2014) An open-channel flume study of flow characteristics through a combined layer of submerged and emerged flexible vegetation. https://doi.org/10.1002/eco.1384
24. He F, Chen J, Jiang C (2019) Surface wave attenuation by vegetation with the stem, root and canopy. https://doi.org/10.1016/j.coastaleng.2019.103509
25. Wu W, Cox DT (2015) Effects of vertical variation in vegetation density on wave attenuation. https://doi.org/10.1061/(ASCE)WW.1943-5460.0000326
26. Van VTJ, Fairchild TP, Reeve DE, Karunarathna H (2020) Experimental study on vegetation flexibility as control parameter for wave damping and velocity structure. https://doi.org/10.1016/j.coastaleng.2020.103648

Harbour Tranquillity and Prediction of Shoreline Evolution—A Case Study

Vaibhawi Roy, Santosh Kori, Jiweshwar Sinha, and Prabhat Chandra

Abstract Before finalizing the layout of breakwaters for a harbour, it is necessary to obtain an acceptable level of wave disturbance within the harbour basin. This is required to facilitate safe berthing of desired variety of ships in the harbour. Also, to address the problem of scarcity of land in highly populated coastal zones of India, it has been very important to mitigate the erosion at the shoreline. In view of this, it becomes necessary to predict the effect of coastal structures on shoreline and save usable land. In the present study, an attempt is made to check the effect of a proposed fishing harbour on the wave tranquillity inside the harbour and the probable effect on the shoreline due to littoral drift thereof. For this purpose, the site of Murdeshwar coast located by the side of a 500 m × 370 m normal headland at the central west coast of India is selected. The proposed fishing harbour consists of only one breakwater of length 820 m and width 120 m at the south side with an opening from westerly direction. Numerical modelling is done to arrive at erosion-accretion pattern on both sides of the proposed harbour over a period of 10 years. The wave tranquillity studies are conducted for assessment of wave tranquillity in the proposed harbour using MIKE 21 software. Littoral drift model used for the analysis of the shoreline changes determining the coastline position. According to the studies, the yearly net sediment transport is about 0.064 Mm^3 from south to north direction and the gross transport is about of 0.178 Mm^3. Numerical modelling revealed that the

V. Roy (✉) · S. Kori · J. Sinha · P. Chandra
Mathematical Modelling in Coastal Engineering, Central Water and Power Research Station, Pune 411024, India
e-mail: roy.v@cwprs.gov.in

S. Kori
e-mail: kori.sk@cwprs.gov.in

J. Sinha
e-mail: sinha.j@cwprs.gov.in

P. Chandra
e-mail: prabhat.chandra@gov.in

P. V. Timbadiya et al. (eds.), *Coastal, Harbour and Ocean Engineering*, Lecture Notes in Civil Engineering 321, https://doi.org/10.1007/978-981-19-9913-0_5

headland existing at the north of the harbour plays major role in tranquillity in the harbour basin as well as in establishing the shorelines at the site.

Keywords Wave transformation · Wave tranquillity · Coastal erosion · Littoral drift

1 Introduction

A major part of the world's population inhabit in the coastal zone. Also, water transport is one of the oldest means of transport all over the world. Harbours provide safe anchorage of ships to the shore. They also provide the undisturbed transfer of cargo and passengers between ships and the shore. In other words, coastal development can majorly contribute to the economical development of a country since trade volume directly depends on the smoothness of transfer of cargo between ships and shore. This is the basis of development of a harbour at seashore facing open sea. At the same time it is a fact that the man-made evolutions built in the form a coastal structure often change natural shoreline at many places and the ecological balance of nature gets disturbed in the long run. It leads to erosion and accretion in the vicinity of the structure along the shore. So, the aim of the researcher becomes to evolve a structure which makes minimum damage to the natural coastline and to predict the effect of the proposed structure over a period of time.

In the present paper studies are conducted to analyse the effect of a proposed fishing harbour at Murdeshwar in Karnataka on the wave tranquillity inside the proposed harbour and also the effect of the proposed harbour on the shoreline evolution over a period of years. It is situated at about 11 km north of Bhatkal. The proposed breakwater site is located by the side of a 550 m $\times$ 325 m headland at the central west coast of India. The proposed fishing harbour consists of only one breakwater of length 820 m and width 120 m at the south side with an opening from westerly direction.

Mathematical model studies of the proposed layout of the harbour were carried out from wave tranquillity and shoreline evolution viewpoint (Fig. 1).

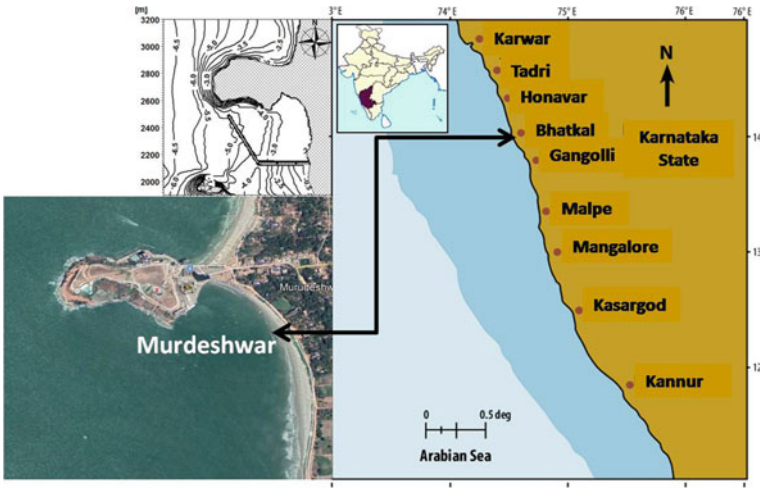

Fig. 1 Location map and the proposed layout

2 Site Conditions

Murdeshwar Fishery harbour is situated at 14°05′25″ N and Longitude 74°29′10″ E. Mean Highest High Water (MHHW) and Mean Lowest Low Water (MLLW) are 1.10 m and 0.1 m, respectively, with Mean Sea Level (MSL) as 0.7 m. The site is fully exposed to incident waves from the Arabian Sea with maximum waves upto 4.5 m height. In addition, presence of a rocky headland of about length 500 m and width 370 m normal to the coastline makes the site typical in nature.

3 Methodology

For carrying out simulation of wave tranquillity, littoral drift distribution and shoreline evolution studies, nearshore wave data such as significant wave height, mean wave direction, peak wave period is essential. Nearshore wave climate at the study site is obtained from the offshore wave data off Murdeshwar region reported by India Meteorological Department using MIKE21 Spectral Wave (SW) model [1]. For simulation of wave penetration and propagation in the harbour basin MIKE21 Boussinesq wave (BW) model [1] was used. LITPACK model was used for computation of quantum and direction of littoral drift and shoreline changes in subsequent years due to the proposed harbour.

4 Numerical Models Used in the Study

4.1 Spectral Wave Model

MIKE21 SW model is based on the wave action balance equation. In Cartesian co-ordinate system the wave action balance equation is given by,

$$\frac{\partial N}{\partial t} + \nabla \cdot \left(\overrightarrow{v} N\right) = \frac{S}{\sigma} \tag{1}$$

where

$N(\overrightarrow{x}, \sigma, \theta, t)$	is the action density
t	is the time
$\overrightarrow{x}(x, y)$	are the Rectangular co-ordinates
$\overrightarrow{v} = (c_x, c_y, c_{\sigma,} c_\theta)$	is the group velocity in the four-dimensional phase space $\overrightarrow{x}$ σ and θ
S	is the source term in energy equation
∇	is the four dimensional differential operator in $\overrightarrow{x}$ σ and θ space

4.2 Boussinesq Wave Model

MIKE21 BW model applied for harbour basin tranquillity simulation takes into account the impact of various hydrodynamic features such as wave diffraction, wave refraction, shoaling, bed resistance, partial reflection and transmission, frequency spreading and directional spreading. In this model time dependant depth averaged Boussinesq equations are solved. The corresponding governing equations are as under:

Continuity equation:

$$n\frac{\partial s}{\partial t} + \frac{\partial p}{\partial x} + \frac{\partial q}{\partial y} = 0 \tag{2}$$

Momentum equation in X direction:

$$n\frac{\partial p}{\partial t} + \frac{\partial}{\partial x}\left(\frac{p^2}{h}\right) + \frac{\partial}{\partial y}\left(\frac{pq}{h}\right) - \frac{\partial R_{xx}}{\partial x} + \frac{\partial R_{xy}}{\partial x} + F_x = 0$$

$$n^2 gh\frac{\partial s}{\partial x} + n^2 p\left(\alpha + \beta\sqrt{\frac{p}{h^2}^2 + \frac{q^2}{h^2}}\right) + \frac{gp\sqrt{p^2+q^2}}{h^2 C^2} + n\Psi_1 = 0 \tag{3}$$

Momentum equation in the Y direction:

$$n\frac{\partial p}{\partial t} + \frac{\partial}{\partial y}\left(\frac{p^2}{h}\right) + \frac{\partial}{\partial x}\left(\frac{pq}{h}\right) + \frac{\partial R_{yy}}{\partial y} + \frac{\partial R_{xy}}{\partial y} + F_x = 0$$

$$n^2 gh\frac{\partial s}{\partial y} + n^2 p\left(\alpha + \beta\sqrt{\frac{p^2}{h^2} + \frac{q^2}{h^2}}\right) + \frac{gp\sqrt{p^2+q^2}}{h^2 C^2} + n\Psi_2 = 0 \qquad (4)$$

The parameters used in the relationship include:

s water surface level above the base level (m)
p flux density along X-direction ($m^3/s/m$)
q flux density along Y--direction($m^3/s/m$)
h total water depth (m)
H average flow depth (m)
n porosity value
α resistance coefficient for laminar flow in porous media
β resistance coefficient in turbulent flow in porous media

4.3 LITDRIFT Model

LITDRIFT is a module of LITPACK software [2] used for simulating hydraulic and non-cohesive sediment transport in coastal area. The module simulates the longshore transport of the sediment. Incident predominant wave characteristics such as wave direction and magnitude, current and sediment properties play an important role in quantifying the longshore sediment transport. The sediment transport model is an intra-wave-period model which takes into account time-varying distribution of both suspended load and bed load within the wave period in combined wave and current motion including the effect of wave breaking, when relevant [2]. The model gives cross-shore distribution of longshore sediment transport for an arbitrary, non-uniform bathymetry and sediment profile [2]. The sediment transport from every single wave incidence occurring during the entire year contributes to the quantity of annual sediment.

The longshore current computation is based on the following equation expressing equilibrium between radiation stresses, flow resistance, wind shear stress and transfer of momentum.

$$-\frac{1}{\rho}\frac{\partial S_{xy}}{\partial x} + \frac{1}{\rho}\tau_W \sin\theta + gDI = \frac{V^2}{C^2} - \frac{\partial}{\partial x}\left[ED\frac{\partial V}{\partial x}\right] \qquad (5)$$

where r = density of sea water, D = water depth, V = mean velocity over the depth, C = resistance factor, S_{xy} = shear radiation stress, τ_w = Wind shear stress, I = longshore slope of the water surface, θ = angle between the wind direction and the coast normal, E = momentum exchange coefficient, g = acceleration due to gravity and x = distance in shore normal direction.

4.4 LITLINE Model

The module gives special variation of the coastline obtained as a result of changes in the longshore sediment transport. The model also simulates the impact of structures and sediment sources/sinks [2]. The prevailing wave climate in the form of time series is used as an input. The model is based on continuity equation for simulation of coastline evolution. It uses implicit Crank–Nicholson scheme [1].

The beach is assumed to be divided into a number of cells of equal dimensions. The model determines the quantities of sand entering and leaving a cell and the remaining sediment mass in each cell gives the net sediment (shoreline position at that cell). This cumulative and combined result gives the net shoreline position.

The continuity equation for sediment volumes is numerically solved

$$\frac{\partial y_c}{\partial t} = -\frac{1}{h_{act}} \frac{\partial Q}{\partial x} + \frac{Q_{sou}}{h_{act} \Delta x} \tag{6}$$

where y_c = shoreline position, t = time, h_{act} = height of active cross-shore profile, Q = longshore transport of sediment expressed in volume, x = longshore position, Δ_x = longshore discretization step and, Q_{sou} = source/sink term expressed in volume/Δ_x. Thus the term Q_{sou} can be used to include sand bypassing arrangement. This equation is solved numerically using implicit Crank–Nicholson scheme.

5 Model Simulations and Results

5.1 Wave Transformation from Offshore to Nearshore

Bathymetry of the model area (about 120 km × 100 km) is shown in Fig. 2. It was discretized using unstructured mesh. The SW model was run to obtain nearshore wave climate at −10 m depth contour for the entire period (Jan–Dec). It is evident that nearshore waves at −10 m depth are incident from 202° to 315° N direction. The predominant critical wave incident conditions lie in the quadrant 225° N to 292° N quadrant with maximum wave height of about 3.0 m. The corresponding offshore and nearshore wave rose diagram are shown in Fig. 3a, b, respectively.

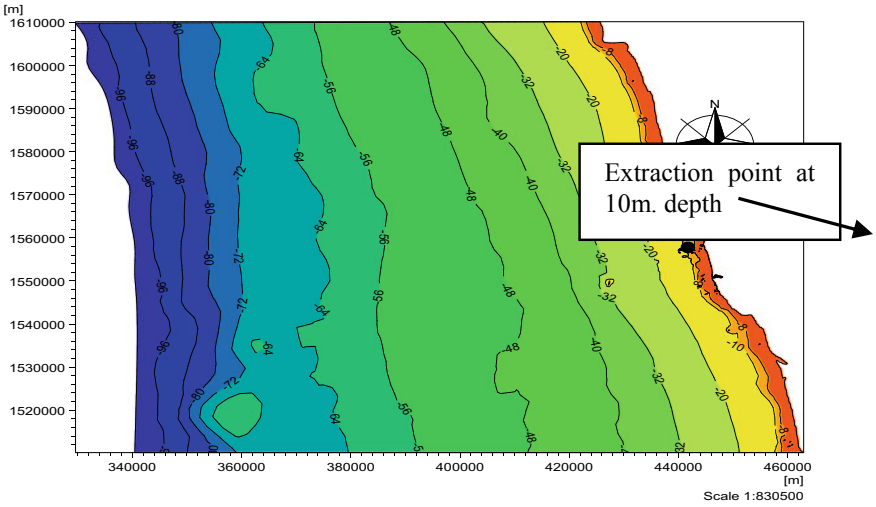

Fig. 2 Bathymetry plot for SW model with the near shore climate extraction point

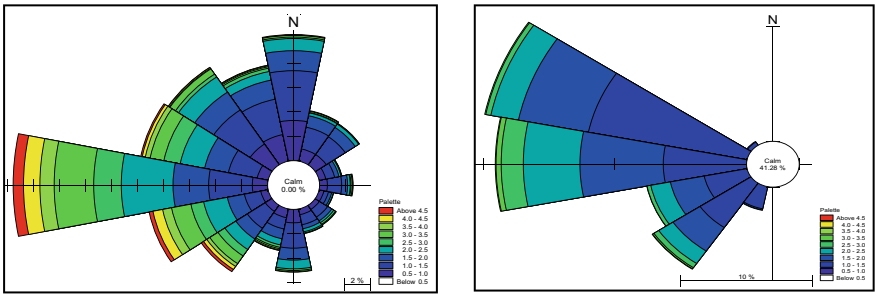

(a) Offshore wave rose diagram for Murdeshwar region

(b) Nearshore wave rose diagram at Murdeshwar site (-10 m water depth)

Fig. 3 **a** Offshore wave rose diagram for Murdeshwar region. **b** Nearshore wave rose diagram at Murdeshwar site (−10 m water depth)

5.2 BW Simulation

BW model was used to check tranquillity conditions inside the harbour using the nearshore wave climate. The model was set up for the maximum grid spacing in horizontal directions so that the minimum wave length was resolved. The time step was adjusted accordingly to get the Courant number less than 1. Grid with spacing 2.5 m × 2.5 m was used for the model simulations. A porosity layer was applied on the outer face of the breakwater to allow wave energy to pass out of the model area so as to avoid unrealistic reflection at the open boundaries. Layers of sponge

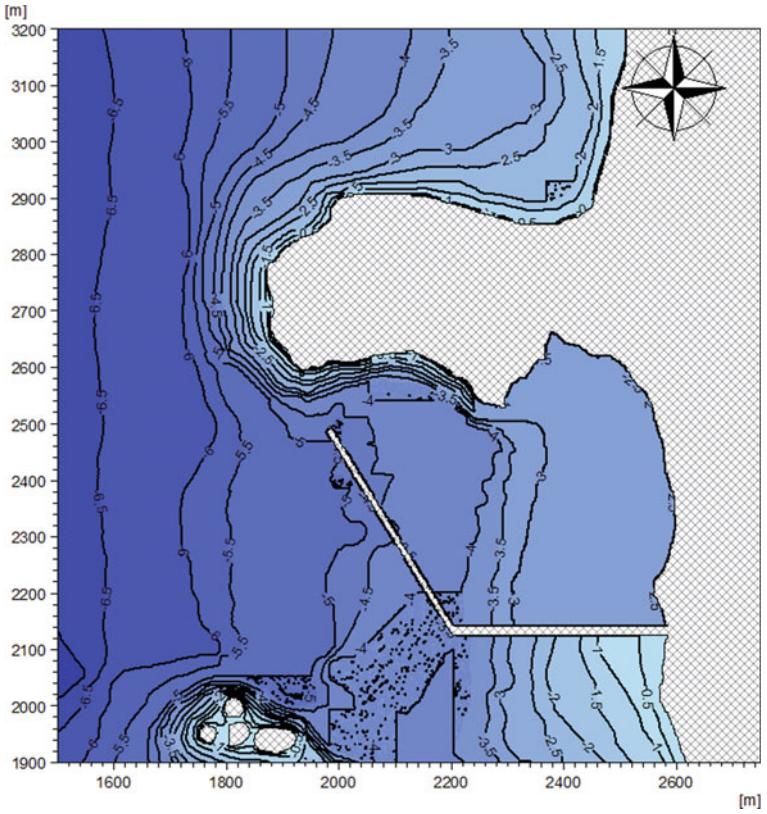

Fig. 4 Bathymetry plot for BW model

along closed boundaries were applied as absorbing medium. The model bathymetry incorporated with the proposed harbour layout is shown in Fig. 4.

The BW model was simulated for the predominant incident wave directions of SSW, SW, WSW, West, WNW and NW. The plots for the critical directions such as WSW, West and WNW are presented in Fig. 5a–c, respectively.

It is evident from the wave distribution plots that wave disturbance inside the harbour basin remains within the permissible limit of 0.30 m for all the predominant directions of incident waves throughout the year. The berthing operation may be carried out in the areas along the lee side of the breakwater and near the breakwater root where wave tranquillity holds good throughout the year.

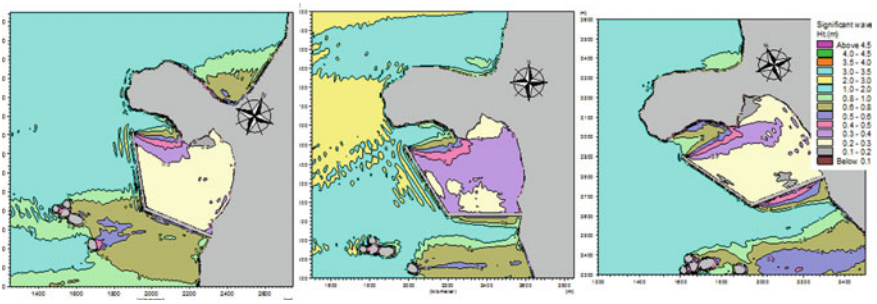

Fig. 5 Wave height distribution inside the harbour for waves incident from **a** WSW, **b** West, **c** WNW

5.3 Littoral Drift and Shoreline Evolution Modelling

The cross-shore beach profile used for littoral drift computation extended for 3.5 km in the sea to attain a depth of −10.0 m CD. Profile is discretized with uniform grid size of 5 m. The prevailing grain size at the study site was about 0.32 mm (d_{50}). The general orientation of coastline at the site was about 258° N. The model was calibrated and was simulated for nearshore wave climate for annual period. The annual net transport of about 0.064 × 10^6 m^3/year was obtained. Annual northward and southward drift distribution for the mentioned cross-shore profile is shown in Fig. 6.

According to model results, the annual net sediment transport was about 0.064 Mm^3 and the gross was 0.178 Mm^3. The annual transport rates are presented in Table 1. Here, the northward drift is indicated as positive and the southward drift is indicated as negative. From Fig. 6, it was seen that the peak sediment transport occurred at about 250 m from the shore and about 75% of the total transport occurred within a range of 400 m from the shore i.e. between +0 to –2.0 m depth contours.

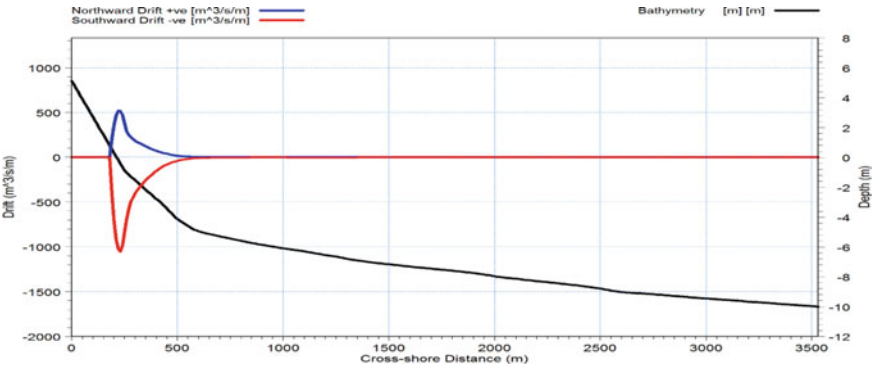

Fig. 6 Cross-shore distribution of littoral drift for annual period

Table 1 Littoral transport rate ($\times 10^6$ m^3)

Location	Northward	Southward	Net	Gross
Cross shore profile	0.057	0.121	-0.064	0.178

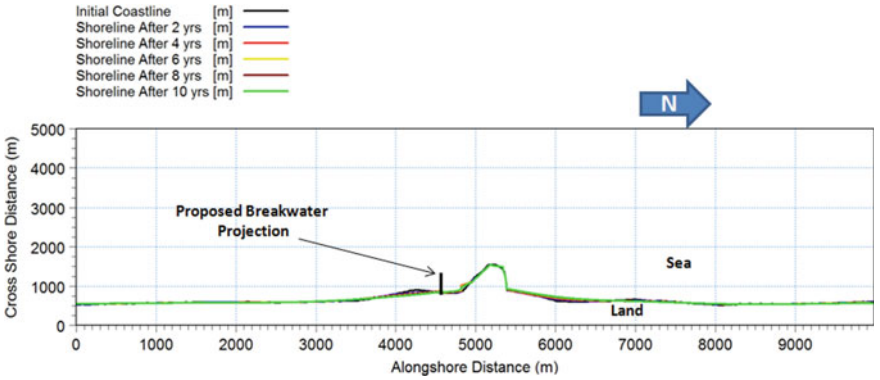

Fig. 7 Shoreline evolution after 2nd, 4th, 6th, 8th, 10th year

The coastline of 10.0 km length was considered for predicting the shoreline evolution. It was divided into 1000 cells (grid points) of 10 m length each. The stretch of the coastline was so chosen that the shoreline evolution on the northern side and the southern side of the proposed harbour could be modelled. The littoral drift rates computed earlier were used as an input to the shoreline evolution model. Projection of the proposed breakwater was one of the important inputs in the model since it directly obstructs the sediment movement and contributes majorly in the change in the shoreline over a period of years. It was seen that projection adopted was found to be appropriate for the optimized proposal (see Fig. 1) based on wave tranquillity studies. The deposition on northern side of the breakwater was seen as a result of southward net sediment transport.

Model was simulated for a period of 2, 4, 6, 8 and 10 years and accordingly, the shoreline change was predicted (Fig. 7). Maximum cross-shore advancement for each period was obtained as 52, 71, 86, 98 and 109 m, respectively, at northern side of the breakwater (see Fig. 7). At the same time, advancement of sea towards land was also observed of the order of 70, 88, 100, 110 and 117 m at south of the breakwater and the headland in 2,4,6,8 and 10 years, respectively.

6 Conclusions

The main findings of the wave tranquillity and the shoreline changes model studies for the proposed fisheries harbour at Murdeshwar are as below:

- The predominant wave directions are from 225° to 292° N and MIKE21BW model indicates that the proposed harbour layout is adequate to provide the desired wave tranquillity in the harbour basin against the wave attack from all the predominant directions throughout the year.
- At the site net sediment transport in a year is about of 0.064 Mm^3 and is towards south and gross transport is of the order of 0.178 Mm^3 [3]. As such, with the construction of proposed breakwater, there will not be significant changes in the existing shorelines on the north and south of breakwater
- The location of the proposed development gets a natural protection from the incident waves due to the existing rocky headland on its north. The sediment does not bypass the headland and the sediment movement is seen to be confined within the cell.
- Considering the simulation results, the layout is found suitable for the proposed fishing harbour at Murdeshwar as headland plays important role in achieving required wave tranquillity and stable shoreline.

References

1. MIKE21 (2014) User manual. Danish Hydraulic Institute (DHI), Denmark
2. LITPACK (2005) An integrated modelling system for littoral processes and coastal kinetics. Danish Hydraulic Institute
3. CWPRS Technical Report No. 5852 of September 2020, Mathematical model studies for wave tranquility and shoreline evolution for development of fisheries harbour at Murdeshwar, Karnataka'

Rejuvenation of Fishing Harbour Heavily Affected by Impact of High Waves and Sedimentation Using Numerical Methods

R. K. Chaudhari, S. K. Kori, and Prabhat Chandra

Abstract Design of fishing harbour is always site specific with required consideration of prevailing waves, tide and current conditions. In most of the cases when development is exposed to sea, the wave is the single parameter which affects the design considerations. Generally, the action of the waves is the principal cause of wave disturbance and movement of the sediment inside the harbour. The fishing harbour layout should be optimized enough to get the desired wave tranquillity inside the harbour with minimum siltation criteria. In the present paper, the case study of a already existing fishing harbour Marvanthe has been discussed which at present is facing high impact of waves and siltation inside the harbour basin and the studies undertaken may helped to over-come this problem. The location at Marvanthe is fully exposed to the incident waves from the Arabian sea with maximum significant waves of upto 4.0 m height. Numerical Model MIKE 21-SW, BW and LITPACK were used to evolve the optimum layout for the fishing harbour. Two alternative layouts; one having entrance in north direction and other layout having mouth opening in south direction, were assessed through numerical modelling. It is found that both layouts are providing enough tranquillity inside the harbour. However, the littoral drift studies shows that the net littoral drift is towards south so the mouth opening towards north may require periodically dredging at entrance. Hence, the layout having south side opening was recommended for the proposed Marvanthe fishing harbour. The details of the studies have been described in this paper.

Keywords Wave tranquillity · Numerical model · Shoaling · Refraction · Fishing harbour

1 Introduction

To cater the growing needs of the fishery industry, the development of fishing harbour with efficient and safe berthing facility is required. The coastal states where the fishing

R. K. Chaudhari (✉) · S. K. Kori · P. Chandra
Central Water and Power Research Station, Khadakwasla, Pune 411024, India
e-mail: chaudhari_rk@cwprs.gov.in

P. V. Timbadiya et al. (eds.), *Coastal, Harbour and Ocean Engineering*, Lecture Notes in Civil Engineering 321, https://doi.org/10.1007/978-981-19-9913-0_6

is the major food industry, need to develop fishing harbours at their coast to overcome needs of fishermen. But it is seen that due to lack of proper planning with consideration of the prevailing environmental conditions at the site, the implementation of fishing harbour carried in such condition leads to many problems. In the present case, a fishing harbour was constructed at Marvanthe in coastal region of Karnataka (Fig. 1). Maravanthe harbour consists of two breakwaters; north breakwater of 240 m length and south breakwater of 546 m length with mouth opening as 450 m constructed way back in the year 2014–15 (Figs. 2 and 3). The location at Maravanthe is fully exposed to the incident waves from the Arabian sea with maximum waves of upto 4.0 m height. The wave tranquillity conditions in the harbour with the present layout are not adequate for operation of the fishing vessels due to the exposure to the high waves particularly during the SW monsoon season. Also, inside the port basin, the beach erosion and accretion are taking place due to the attack of monsoon waves through the wide opening. To rejuvenate the fishing harbour, the mathematical modelling technique has been used, considering the prevailing environmental condition the modification in the layout of fishing harbour has been suggested to get required tranquillity with minimum siltation in the harbour. As per natural phenomena, waves attack coastal structure and infiltrate harbour entrance, generating disturbance inside the harbour areas. Hence, it is necessary to know beforehand the magnitude and direction of predominant propagating waves to design the optimal layout of harbours. MIKE 21-SW wave model was used to transfer offshore wave data of wave heights and wave propagation directions to the project site at (−) 8 m depth. Further, Boussinesq wave model (MIKE 21-BW) was used for prediction of the wave fields due to combined refraction and diffraction of directional random waves inside the harbour. These models were used to examine wave tranquillity in the proposed harbour and simultaneously the length and alignment of breakwater were optimized to get the desired wave tranquilly in the harbour. In this present case, the harbour opening is very large so the main target was to optimize the harbour breakwater length as well as suggest the proper alignment/layout so that the safe navigation of fishing boats at entrance should be feasible as well as wave disturbances inside the harbour should be minimum throughout the year. The alongshore sediment transport quantity and direction were also assessed through the numerical model LITPCK. In the present paper, the details of the mathematical model studies used to evolve suitable modification in the existing fishing harbour at Marvanthe, Karnataka, have been described.

2 Site Conditions

Marvanthe fishing harbour is situated at 50 km north of Udupi at the latitude of 13.7° N and the longitude of 74.6° E as shown in Fig. 1. The coastline consists of long, narrow sandy beaches and is oriented in NNW-SSE direction. The nearshore bathymetry is steep with straight and parallel depth contours. The tidal range at Marvanthe is about 1.2 m. Beaches at the site are having fine sand. The average

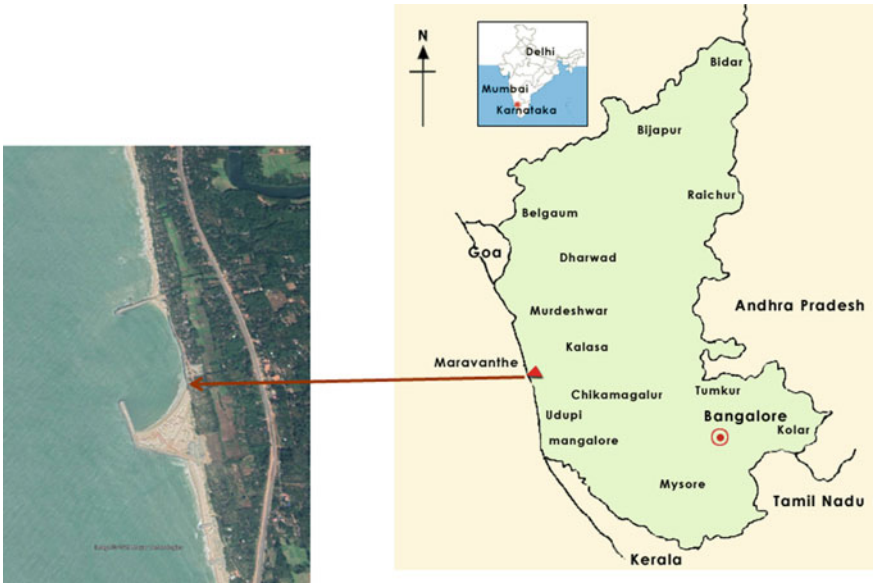

Fig. 1 Location map of Maravanthe site

value of D_{50} (mm) from various sand samples is about 0.25 mm and the same has been used for the model runs. Wave is a very important parameter which influences the littoral drifts that causes the erosion of coastlines. In absence of the measured wave data, the offshore wave data of 14 years from year 2001 to 2014 off Marvanthe fishing harbour as observed by India Meteorological (IMD) from ships plying in deep waters were analysed. This wave data information was considered at the offshore end of the model limits. The frequency distribution of wave heights for entire year for the above offshore wave data is presented in form of wave rose diagram shown in Fig. 4. It could be seen that the predominant wave directions in deep water are from 225° to 360° N with maximum wave heights of 4.5 m. These deep water wave data were transformed using the mathematical model MIKE 21-SW to get the nearshore wave climate near the Marvanthe.

3 Numerical Modelling Techniques

For rejuvenation of fishing harbour some modification in harbour layout carried out with use of mathematical models like MIKE 21-SW, MIKE 21-BW. These studies were mainly carried out in three following stages

1. Transformation of wave height and wave direction from deep water to (−) 8 m depth using spectral wave model MIKE 21-SW model.

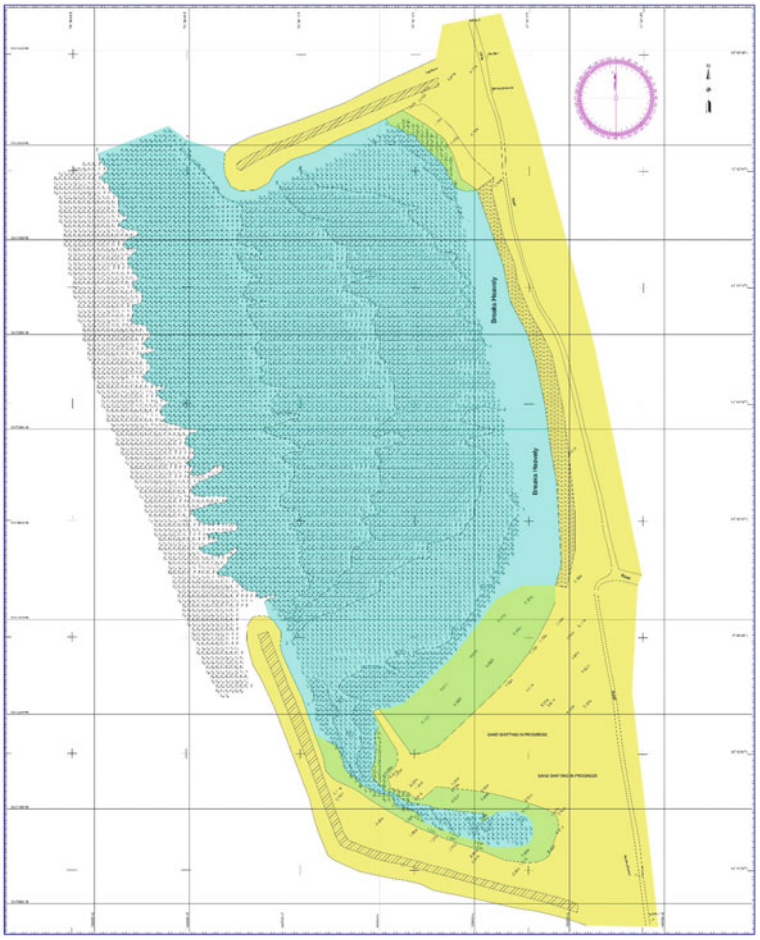

Fig. 2 Existing layout of the Marvanthe fishing harbour

2. Simulation of wave propagation in the harbour to obtain wave height distribution in the existing harbour as well as modified layouts using MIKE. 21-BW model.
3. Estimation of littoral drift movement.

3.1 Transformation of Wave Height and Wave Direction from Deep Water to (−) 8 m Depth

As waves propagate towards shore, a combination of shoaling, refraction, reflection, diffraction and breaking effects modify the waveform and the wave characteristics will be very different from those in deep water. To get the wave conditions from

Fig. 3 Marvanthe site photograph

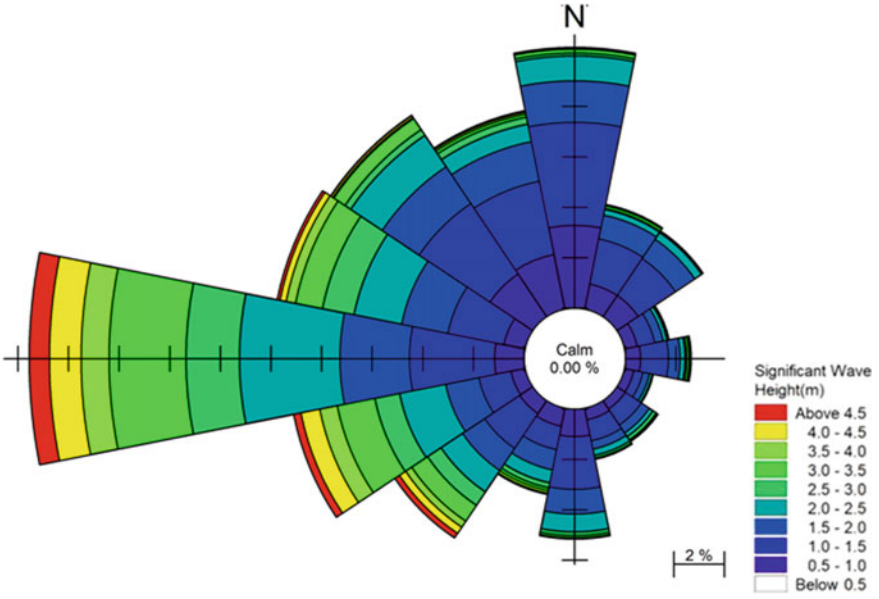

Fig. 4 Offshore wave rose diagram for entire year

offshore to nearshore at (−) 8 m depth, the numerical model MIKE21-SW was used. This is a state-of-the-art third generation spectral wind wave model based on unstructured mesh. The model simulates the growth, decay and transformation of wind generated waves and swells in offshore and coastal areas. It takes into account refraction and shoaling of waves, which are important in the transformation of waves from offshore to inshore. It also includes physical phenomena of wave growth by

action of wind, dissipation due to white-capping, dissipation due to bottom friction and dissipation due to depth induced wave breaking. In the absence of measured wave data of at least one year near the proposed site of development, the nearshore wave climate at Maravanthe was obtained by transforming the ship observed deep water wave data using MIKE21-SW model. Model area considered for MIKE 21-SW model is shown in Fig. 5. Bathymetry in the model region of about 60 km × 88 km area was discretized using unstructured mesh. The model was run to obtain nearshore wave climate at the inshore point in (−) 8 m depth contour. The wave directions and ratio of wave heights at (−) 8 m depth to deep water wave height, with different directions of wave incidence at the offshore boundary are obtained. After applying the ratio of deep water wave height and direction as shown in rose diagram (Fig. 4), the frequency distribution of waves in (−) 8 m depth were obtained shown in Table 1 and corresponding rose diagram (Fig. 6).

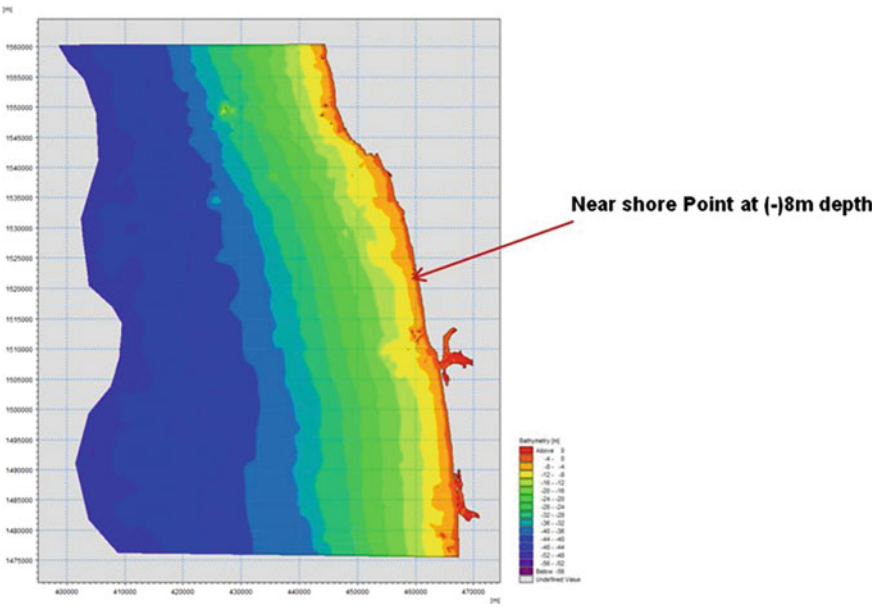

Fig. 5 Bathymetry for wave transformation from offshore to nearshore

Table 1 Input wave conditions for MIKE21-BW model

Wave direction (° N)	Peak wave period Tp (s)	Significant wave height (m)
225	10	2.5
247.5	10	3.5
270	10	3.5
292.5	10	2.5

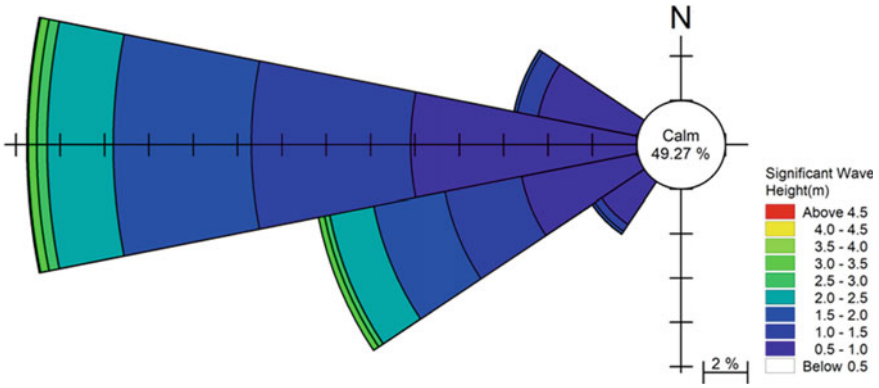

Fig. 6 Rose diagram at (−) 8 m depth (Year)

Based on the studies of wave transformation, following input significant wave conditions at (−) 8 m depth were considered for simulation of wave propagation in the proposed harbour using MIKE 21-BW model.

3.2 Model Simulation of Waves Inside the Harbour Basin for Different Layouts

The permissible wave disturbance at the berthing place depends on the ship size, mooring and berthing system. A permissible limit of 0.3 m for wave heights in the harbour is considered for of fishing harbour keeping in view the size of fishing boats. The modified layout was evolved considering the orientation of the entrance, littoral drift distribution and the wave tranquillity inside the harbour throughout the year. Due consideration was also given to ensure the safe navigation conditions of fishing vessels through the harbour entrance and an overlap was provided between two breakwaters to avoid broadside wave attack at the entrance. The numerical model MIKE21-BW was used for studying the wave disturbances in the harbour. This model is based on time dependant Boussinesq equations of conservation of mass and momentum obtained by integrating the three-dimensional flow equations without neglecting vertical acceleration. They operate in the time domain, so that irregular waves can be simulated. These equations include nonlinearity as well as frequency dispersion. The frequency dispersion is included in the flow equations by taking into account the effect of vertical acceleration or the curvature of stream lines on pressure distribution. The model simulates the processes of shoaling, refraction, diffraction from breakwater tips and bed friction. It also takes into account partial reflections from the boundaries, piers and breakwaters (DHI-2005) [1].

Wave propagation inside the harbour was simulated using MIKE21-BW model for input wave conditions as shown in Table 1. Simulations were carried out for the

tidal level at +1.5 m corresponding to MHWS. The wave propagation studies to assess the wave condition inside the harbour basin carried out for different layouts, viz. Existing layout, Alternative-1 and Alternative-2 layout, are detailed as below:

3.3 Existing Layout

The studies were conducted to examine wave propagation for the existing harbour layout at Maravanthe. This layout consisted of two breakwaters; 240 m long northern breakwater and 546 m long southern breakwater with 450 m wide harbour entrance as shown in Fig. 7. Total length of breakwater in existing condition is 786 m.

The MIKE 21-BW simulations were carried out for all the four predominant directions mentioned in Table 1. The simulations plots of most critical and having maximum occurrence percentage has been shown in Fig. 8a, b.

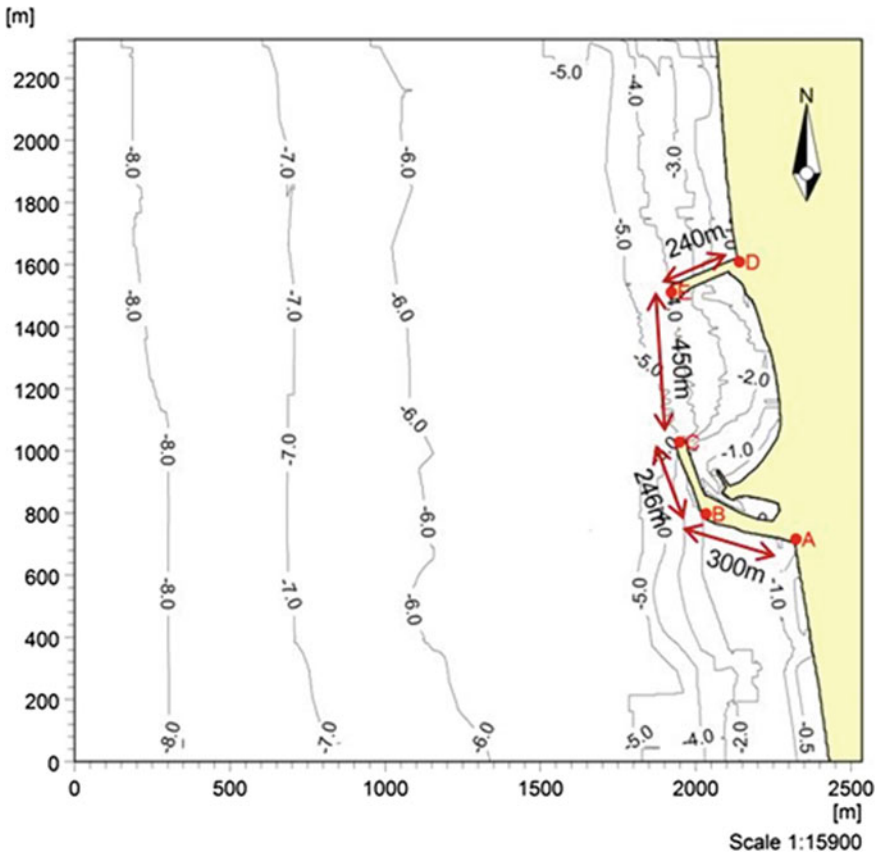

Fig. 7 Bathymetry and layout of existing harbour

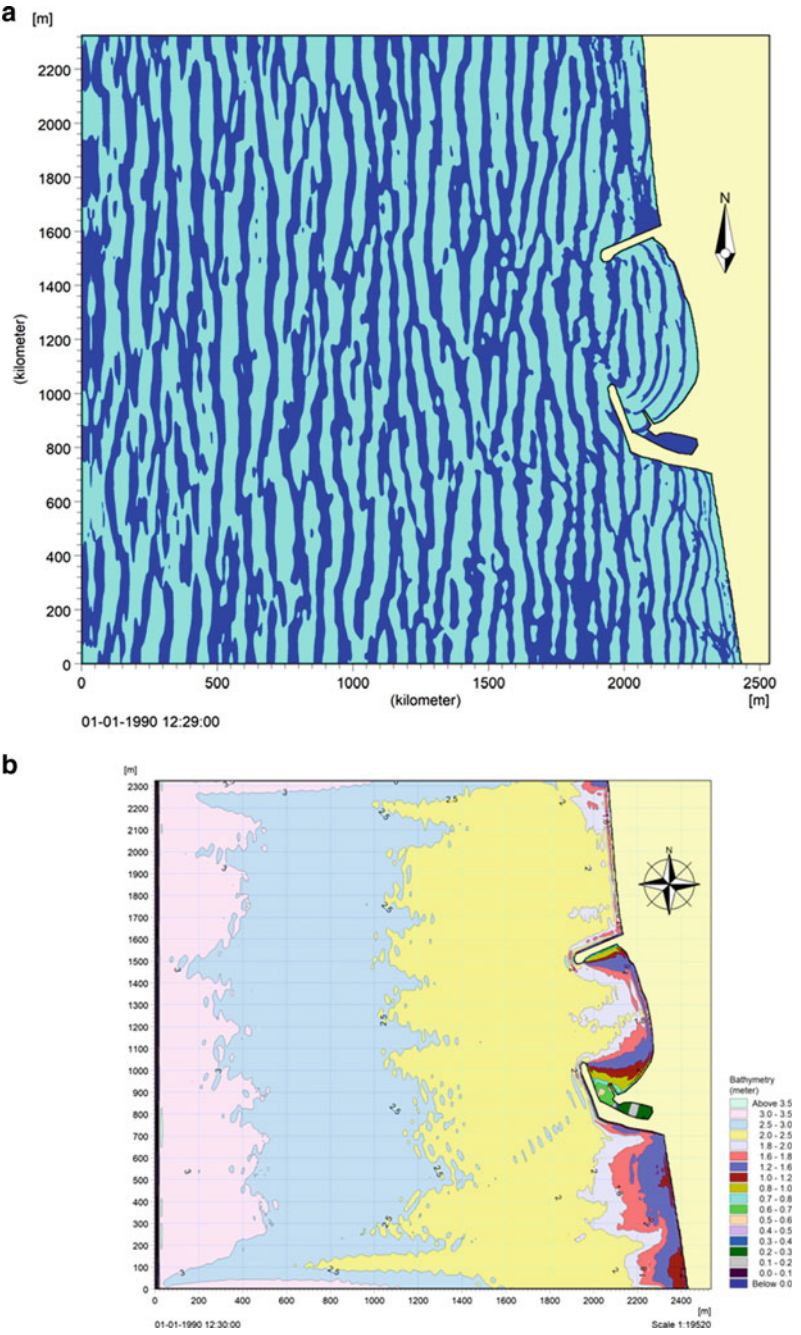

Fig. 8 **a** Wave propagation plot for waves incident from WEST (2700 N) direction. **b** Wave height distribution plot for waves incident from WEST (270° N) direction (Incident Wave Height: 3.5 m)

It is clearly seen from the wave distribution plots that the maximum significant wave heights of range of 1.8–2.0 m are seen inside the harbour basin which are much more than the permissible wave height of 0.30 m, also the fishing harbour entrance was exposed to the wave heights of order of 2.0 to 2.5 m. These wave conditions are not suitable for the safe operation of fishing harbour. A modified layout was evolved as alternative-1 details of model simulation given in next Para.

3.4 Alternative-I Layout

In order to provide required tranquillity inside the harbour and at the entrance of the fishing harbour a layout was suggested by CICEF the same has been taken as alternative–I. The studies were conducted to examine wave propagation in the proposed alternative–I harbour layout at Maravanthe. This layout consisted of two breakwaters; northern breakwater of 560 m more length than the existing Layout (total length of north breakwater is 800 m) while the southern breakwater having 65 m more length the existing layout (total length of south breakwater is 611 m) the harbour entrance is 105 m wide as shown in Fig. 9. Total length of the breakwater for this layout would be 1411 m. the entrance of the proposed harbour is situated in the south direction.

The MIKE 21-BW simulations were carried out for all the four predominant directions mentioned in Table 1. The simulations plots of most critical and having maximum occurrence percentage have been shown in Fig. 10a, b.

It was observed from above wave distribution plot from west and the plots from other predominant incident directions that the desired wave tranquillity in the harbour area would be achieved for all incident wave directions. Significant wave height is in range of 0.30 m for all four predominant directions inside the harbour basin would be obtained, suitable for berthing operations. It is also seen that the wave heights near the harbour entrance are higher in range of 1.2 m. During the SW monsoon season, there could be manoeuvring and navigation problems near the entrance facing south direction due to the presence of broad crested waves. Keeping in view such navigational difficulties, an alternative layout (alternative-II) was evolved at CWPRS having almost same breakwater length as the layout proposed by CICEF with harbour entrance on the north side.

3.5 Alternative-II Layout

An alternative layout was evolved at CWPRS with harbour opening on the north. This layout consisted of two breakwaters; northern breakwater consisted of 60 m more length than the existing layout (total length of north breakwater is 300 m) with breakwater tip at (−) 4.5 m while the southern breakwater having 550 m more length the existing layout (total length of south breakwater is 1105 m) with breakwater tip

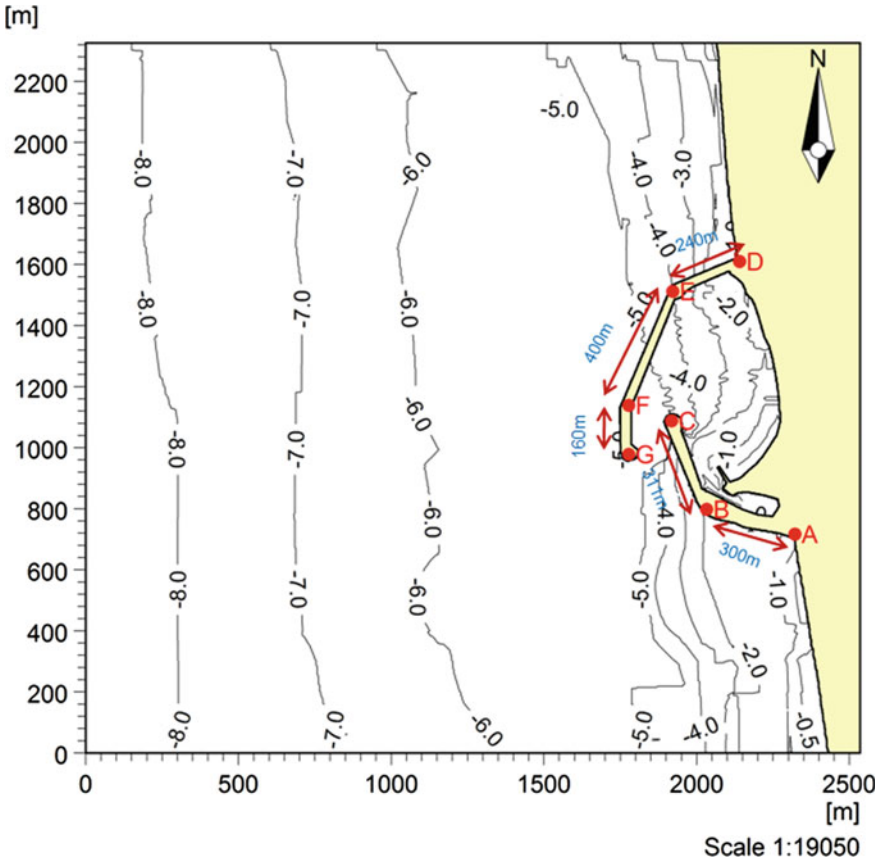

Fig. 9 Bathymetry and layout of modified harbour Alternative-I

at (−) 5.2 m and the harbour entrance is 110 m wide as shown in Fig. 11. Total length of breakwaters for this modified layout would be 1405 m.

The MIKE 21-BW simulations were carried out for all the four predominant directions mentioned in Table 1. The simulations plots of most critical and having maximum occurrence percentage has been shown in Fig. 12a, b.

It is seen from above simulation plot from west and with other prevailing incident directions that wave disturbances for the alternative layout-II will remain within the permissible limit of 0.30 m almost for all the predominant directions of incident waves. Only during the monsoon seasons, the waves would be more than the permissible limit for few days.

Consideration of the net littoral drift direction at the proposed site is essential in order to decide the suitable layout. In this regard, littoral drift studies were carried with the help of numerical model LITPACK.

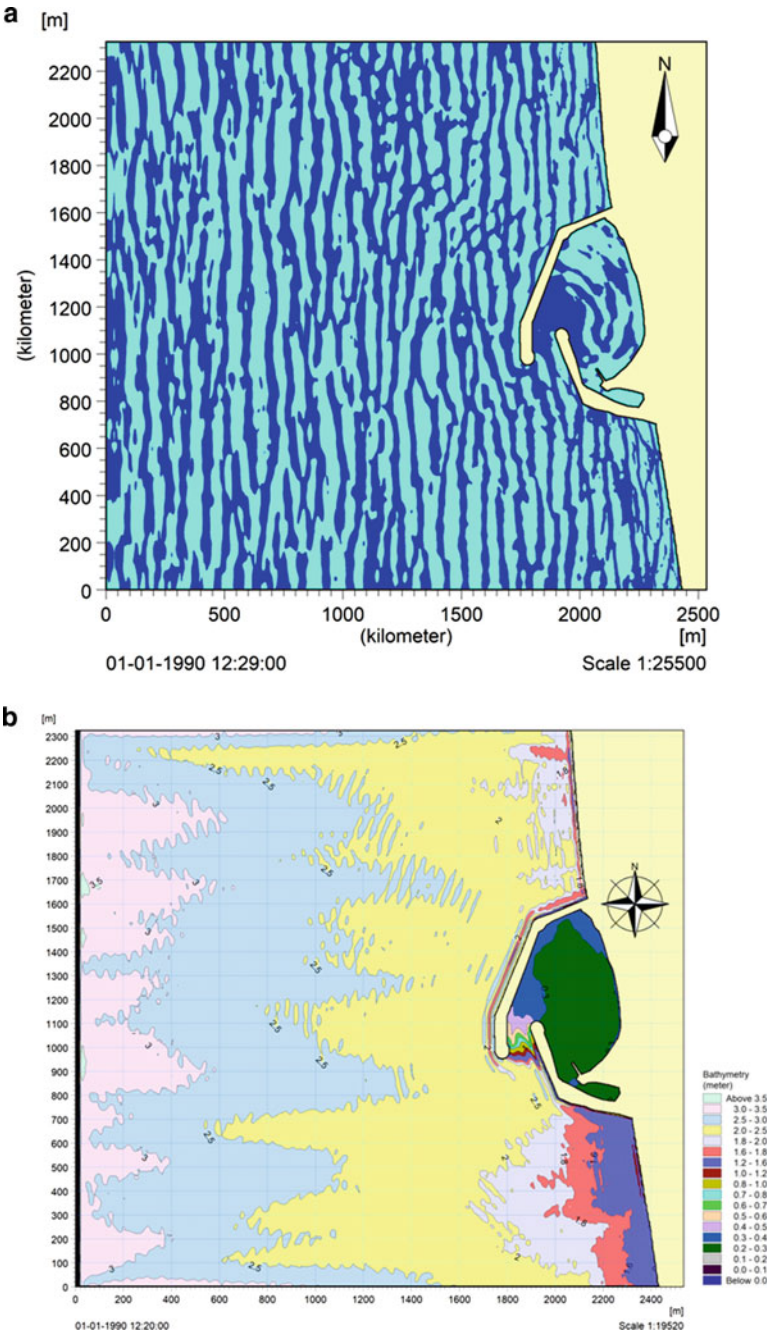

Fig. 10 **a** Wave propagation plot for waves incident from WEST (2700 N) direction, **b** Wave height distribution plot for waves incident from WEST (270° N) direction (Incident Wave Height: 3.5 m)

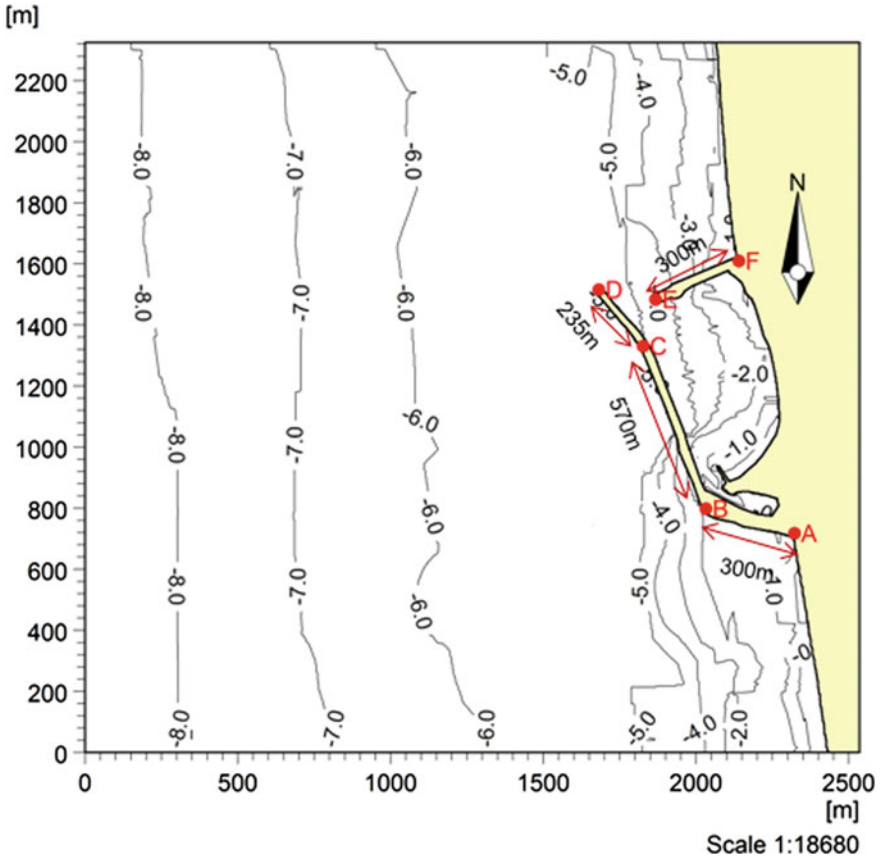

Fig. 11 Bathymetry and layout of modified harbour Alternative-II

3.6 Estimation of Littoral Drift Movement

The present studies were carried out using wave data mentioned above for years 2000 to 2014 in which wave heights ranged between 0.5 m and 4.5 m and wave directions between third quadrants. LITPACK model was used to estimate annual littoral drift rates and its distribution on the profile. Normal to the shoreline, i.e. 260° N, Fig. 13a shows the location of two cross shore profiles, one of northern side (Profile P1) (Fig. 13b) and other on the southern side (Profile P2) (Fig. 13c) of harbour, same were used for drift computation.

The both profiles cover a distance of 2.9 km extending up to about −10 m depth contour (with respect to chart datum) Fig.13b, c. The profiles were discretized with grid size of 5 m. Grain size distribution, fall velocity and roughness coefficients over the profile were required for computation of littoral drift. At the site, grain size is observed to be of the order of 0.25 mm. The Longshore sediment transport rates for

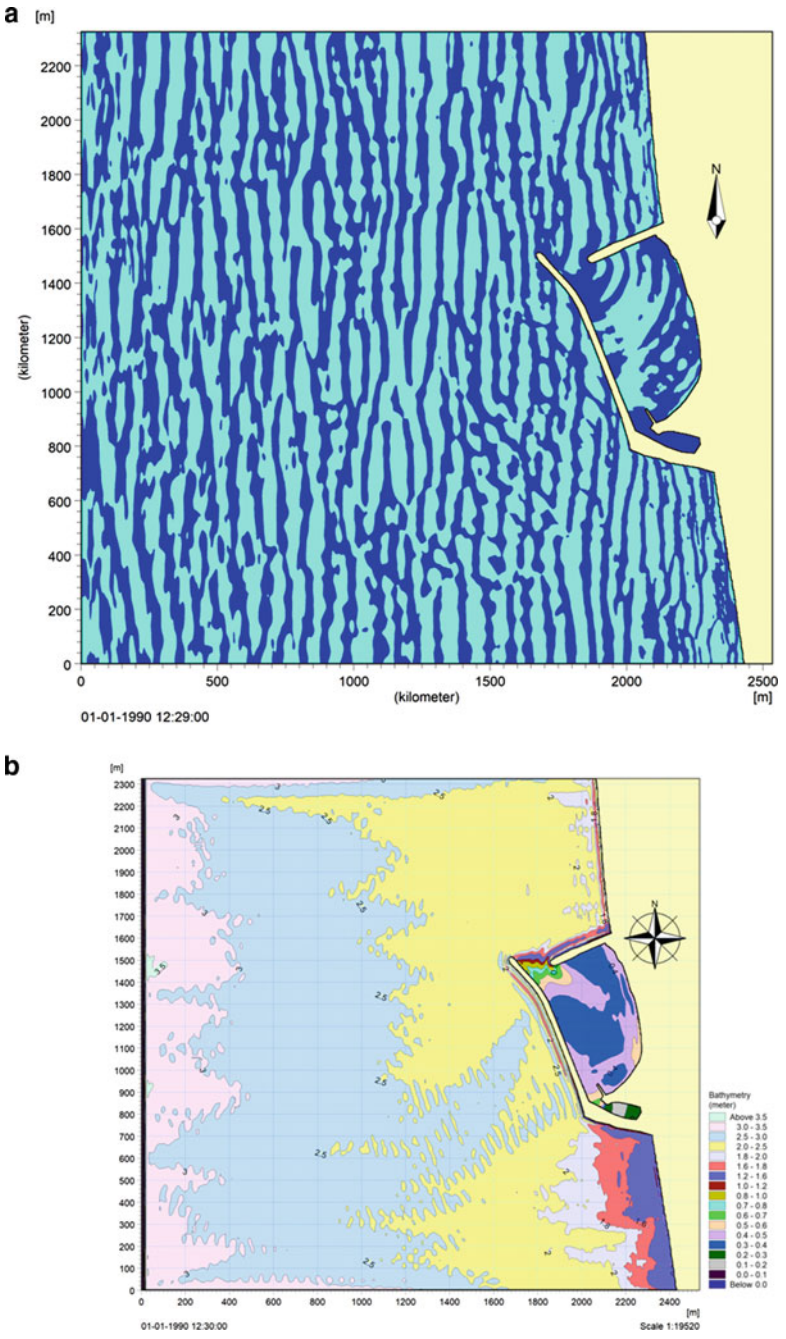

Fig. 12 **a** Wave propagation plot for waves incident from WEST (2700 N) direction, **b** Wave height distribution plot for waves incident from WEST (270° N) direction (Incident Wave Height: 3.5 m)

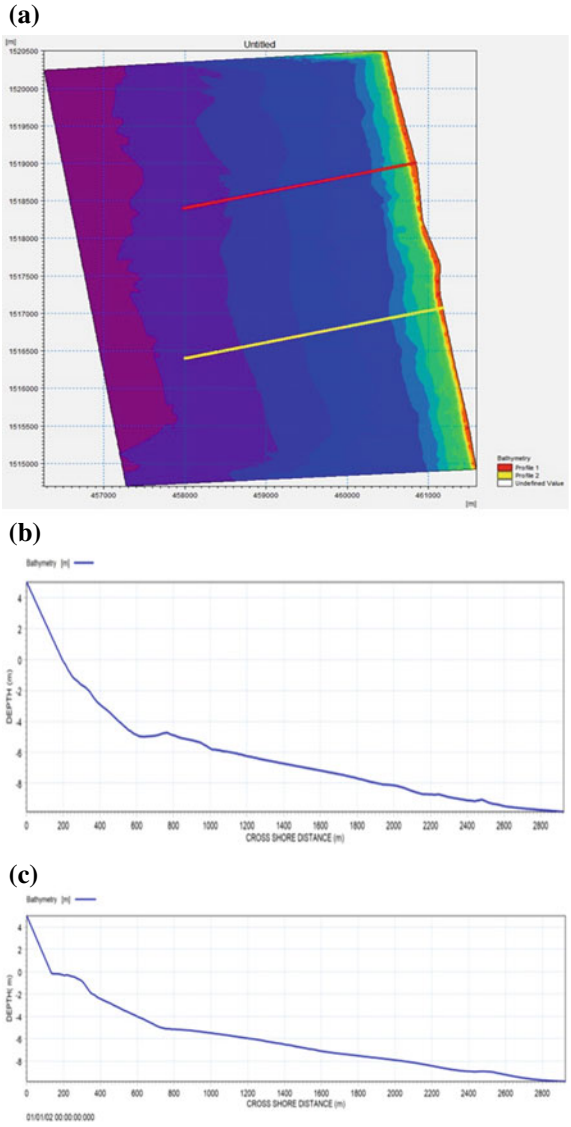

Fig. 13 **a** Location of cross shore profiles, **b** Cross shore profile P1, **c** Cross shore profile P2

the Maravanthe Coast were estimated by Sanil Kumar [2]. The annual net sediment transport estimated by Sanil Kumar was 0.025×10^6 m^3 in the northerly direction and the annual gross sediment transport was 0.029×10^6 m^3. In PhD thesis by Vijaya Kumar G T [3] annual net sediment transport at Maravanthe is estimated to be 0.35×10^6 m^3 towards southward the annual gross sediment transport was 1.12×10^6 m^3. By discussions with local people during field visit to Maravanthe, drift towards south was recognized. Seasonal changes in shoreline were observed from the past

Google earth images. Annual net sediment transport of 0.35×10^6 m^3 towards south was considered for the model calibration.

The model was calibrated using bed roughness to get the annual net transport of the order of 0.34×10^6 m^3/year. The model was run for annual nearshore wave climate described above. Annual northward and southward drift distribution across the cross shore two profile is shown in Fig. 14a, b and also in Table 2. The northward drift is plotted positive as while southward drift is plotted as negative.

Net transport in a year is of the order of 0.34 million cum and is towards south and gross transport is of the order of 1.48 million cum.

As net littoral movement at the site was towards south, it means the harbour mouth towards the north side may get some sedimentation problem at mouth and may require periodically dredging at entrance. Considering above the fishing harbour layout (alternative–I) having south side mouth will be more suitable for fishing harbour.

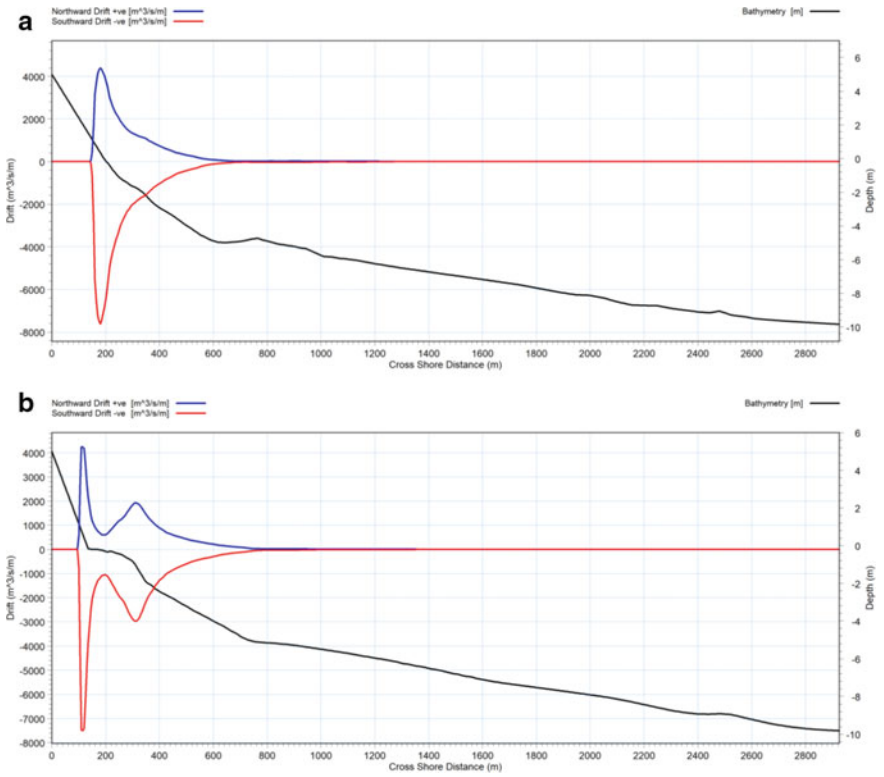

Fig. 14 **a** Cross shore distribution of northward and southward littoral drift during entire year for profile P1, **b** Cross shore distribution of northward and southward littoral drift during entire year for profile P2

Table 2 Littoral transport rate (m^3)

Location	Northward	Southward	Net *	Gross
Profile 1	583,600	928,400	−344,800	1,512,000
Profile 2	559,700	890,300	−330,600	1,450,000

Note * '−ve' Southward '+ve' Northward for the Net Drift

4 Conclusions

The main conclusions derived from above studies as follows:

- Wave propagation studies carried out for transformation of deep water wave conditions to (−) 8 m depth showed that the predominant directions of wave approach at the site of development are from 225° N, 247.5° N, 270° N and 292.5° N
- From the wave tranquillity studies carried out with alternative-I and alternative-II, it was found that both layouts were providing sufficient tranquillity inside the harbour basin but alternative-I having marginally better wave conditions than layout-II.
- LITDRIFT studies indicate that at the proposed site, sediment transport in a year is of the order of 0.34 million cum and is towards south and gross transport is of the order of 1.48 million cum.
- Considering these studies, the alternative-I layout was more suitable for the proposed rejuvenation of the Marvanthe fishing harbour.
- From above studies, it was found that numerical models may be used for rejuvenation of highly wave affected silted fishing harbour in very efficient and cost effective manner.

Acknowledgements Authors are grateful to Shri A.K. Agrawal, Director, Central Water and Power Research Station for his continuous encouragement and motivation during the course of studies and for granting permission to publish this paper.

References

1. Danish Hydraulic Institute (2005) MIKE 21 Boussinesq Wave and Spectral wave Module, User Guide and Reference Manual. Website. https://www.mikepoweredbydhi.com
2. Jena BK, Chandramohan P, Sanil Kumar V (1994) Surf zone dynamics along the south Karnataka coast between Bhatkal and Ullal, west coast of India. IJMS 23
3. Vijaya Kumar GT. A study of littoral processes and longshore sediment transport along the coast of Dakshina Kannada and Udupi Districts Karnataka, PhD thesis

A Numerical Approach for the Efficiency of Submerged Breakwater to Reduce Wave Impact on an Eroding Beach Adjacent to Estuary

Rahul Sawant, K. H. Barve, L. R. Ranganath, and J. D. Agrawal

Abstract Essar Bulk Terminals Limited (EBTL) operates a Port Terminal at Hazira, Gujarat on the west coast. EBTL has carried out reclamation of 350 Ha area for the proposed future development of the port. Reclamation was carried out by utilizing dredged material from deepening of the navigational channel and turning circle. However, in every monsoon, there is depletion in the area of the reclamation. The reclamation adjacent to the channel is eroded, and a hump is formed in the approach channel. Hump recurred even after dredging that area to the original depth and this hump causes difficulty in the navigation of the vessels along the approach channel. It is observed that there is considerable erosion on the corner of reclamation and the eroded sediments get deposited in the approach channel resulting in the formation of hump. The wave impact on the reclamation is the main reason which results in the erosion of reclaimed area. Three-phase wave modelling is used for modelling the wave conditions in the area of vicinity to understand and determine a method to arrest the formation of the hump. A regional model is developed with wind time series as the input. From the results, time series of wave parameters was obtained near the entrance of gulf of Khambhat. The output wave parameters were used for the local mathematical model encompassing the reclamation, and the wave climate at the reclamation is simulated. To reduce the wave impact on the reclamation corner, submerged breakwater consisting of length 300 m, 3.5 m height above the chart datum, located at 150 m to the west of the channel and 100 m away from the shoreline is considered. The results indicated that the proposed solution of submerged breakwater is effective in reducing the wave impact and thus erosion; which will prevent the formation of the hump and the results are discussed in the paper.

Keywords Numerical model · Wave tranquillity · Time series · Reclamation

R. Sawant (✉) · K. H. Barve · L. R. Ranganath · J. D. Agrawal
Central Water and Power Research Station, Khadakwasla, Pune 411024, India
e-mail: sawant.rahul@cwprs.gov.in

P. V. Timbadiya et al. (eds.), *Coastal, Harbour and Ocean Engineering*, Lecture Notes in Civil Engineering 321, https://doi.org/10.1007/978-981-19-9913-0_7

Fig. 1 Location map

1 Introduction

Essar Bulk Terminals Limited (EBTL) operates a Port Terminal at Hazira, Gujarat on the west coast. The port is located along the Tapi estuary as shown in Fig. 1. EBTL has carried out reclamation of 350 Ha area for the proposed future development of the port. Reclamation was carried out by utilizing dredged material from deepening of the navigational channel and turning circle. However, in every monsoon, there is depletion in the area of the reclamation. The reclamation adjacent to the channel is being eroded. There is a hump formation in the channel. Hump recurred after dredging that area to the original depth. The hump is causing problems in the navigation of the vessels.

2 Modelling Techniques

Mathematical model studies were carried out to evaluate suitable measures to minimize the recurrent problem of erosion at the corner of the reclamation and the formation of the hump in the channel. The eroded material is transported inside the channel by wave action and tidal forcing and gets deposited to form the hump. For wave transformation studies, module of MIKE21 software, i.e. MIKE21 SW, was used for

estimation of nearshore wave field in the harbour. Brief description of this model is given below.

2.1 MIKE21 SW Model

There is change in the wave direction and wave height when the coastal waves travel from deep to shallow zone. This happens due to the phenomenon of refraction and shoaling. This transformation of coastal waves from deep to shallow zone can be carried out using MIKE21 SW model. MIKE21 SW model is third generation spectral wind-wave model. The MIKE21 SW model simulates transformation due to refraction and shoaling, wave growth caused by wind action, decay due to white capping and bottom friction. The effects of wave-current interaction, nonlinear wave-wave interaction, time-varying water depth and diffraction are also included within the model [1]. The model is based on flexible mesh which allows for coarser resolution for offshore area and high-resolution mesh in the area of interest.

3 Methodology of the Study

The southern part of the reclamation has eroded due to the severe wave attack during the south-west monsoon. The reclamation near the channel is washed out, and the eroded material moves in to the channel and forms the hump. Mathematical model studies were carried out to explore the wave conditions in the vicinity of the reclaimed area and approach channel in EBTL, Hazira and to find a suitable solution to arrest the erosion at the reclaimed face and thereby reducing deposition in the channel. The studies were carried out in two stages [2]. First stage is the simulation of wave propagation in the area covering the reclamation and approach channel to compute wave height and direction at the specified locations near the mouth of channel considering existing bathymetry using MIKE21 SW model, and second stage is to arrive at the optimal solution for reduction in the wave attack on the reclamation by performing extensive wave model studies with various different layouts of protective structures.

4 Mathematical Model Studies for Wave Transformation

The wave parameters at the reclamation and the channel were obtained in three steps. Simulation of wave transformation over a large area using wind forcing is the first step. This is referred as regional model studies. The mesh prepared for this study is referred as Mesh 1 (regional model). The results are extracted at the entrance of the Gulf of Khambhat. This boundary is approximately at the −30 m depth contour. In the second step, the wave conditions obtained in the step 1 at the beginning of the

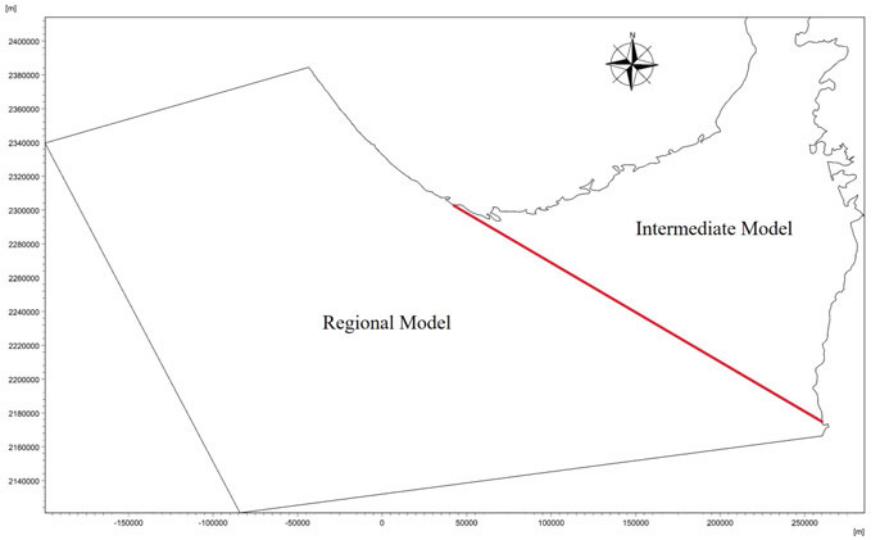

Fig. 2 Regional model and intermediate model

Gulf of Khambhat are used as input and wave climate is extracted at the location at the depth of −23 m near the reclamation. The mesh prepared for this study is referred as Mesh 2 (intermediate model). This step is necessary because swell waves start dominating the sea state at the entrance of Gulf of Khambhat. So, it is proper to give the waves as input for the further wave transformation studies. In the final third step, the result of the wave transformation from the step 2 simulation is used as input and the wave climate at the reclamation is obtained. A mesh with fine resolution, referred as Mesh 3 (local model), is created for the simulation. The three steps also help in resolving the bathymetry accurately while keeping the number of elements and nodes under control. The boundaries of the regional model, intermediate model and the local model are shown in Figs. 2 and 3.

4.1 Wave Transformation Studies for the Regional Model (Step 1)

Wind generates waves by interacting with the water surface. In particular in the deep sea, wind is the major force that generates waves. The offshore wind data reported by India Meteorological Department (IMD) in deep-water off Hazira from years 1984 to 2000 were analysed. Annual time series of wind parameters was prepared, and the time series was given as input to the wave transformation for the regional model. MIKE21 spectral wave model was used for the simulation of wave propagation from offshore to nearshore location. Bathymetry encompassing Lat 18°56′ N to Lat

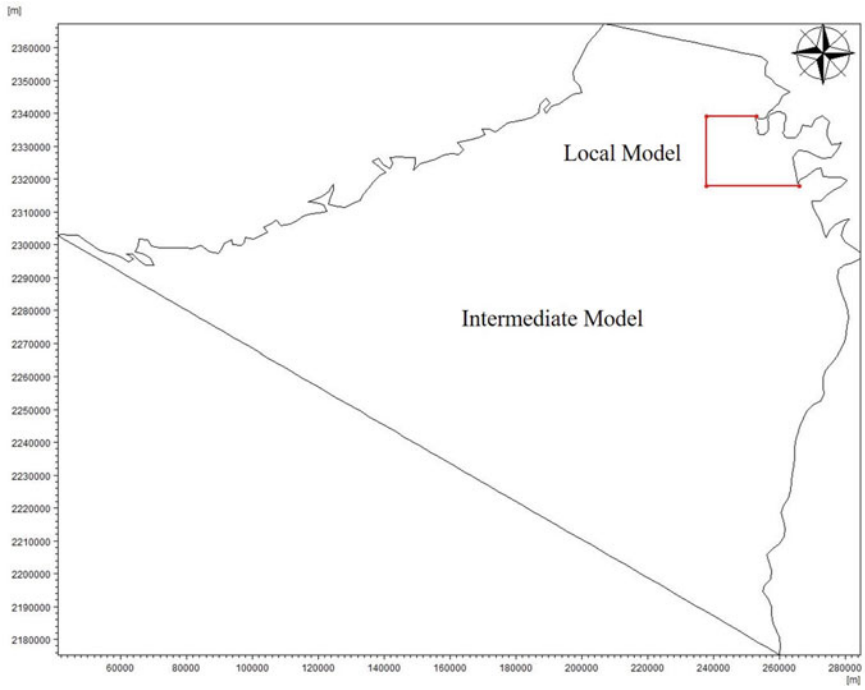

Fig. 3 Intermediate model and local model

21°54′ N and Long 68°10′ E to Long 73°6′ E, a region of 410 km by 260 km area with offshore depth of −2500 m is prepared on the flexible mesh using MIKE zero mesh generator tool. The mesh has 5269 nodes and 9616 elements as shown in Fig. 4. This is referred as Mesh 1. The bathymetry covers the region south of the Tapi estuary and encompassing it towards west. This model is referred as regional model henceforth. The wind time series of wind magnitude and wind direction was used as input is plotted in Fig. 5. This way we have simulated wind generated waves. Waves of varying magnitude, direction and period one after the other are generated due to the force of time dependent wind velocities. The model is simulated for a complete year. The typical wave vector plot over the complete region is shown in Fig. 6. Predominant wave directions at the entrance of the gulf are west, WSW, SW and south and maximum wave height up to 2.5 m was observed. The wave parameters obtained from the regional model studies, at the entrance of the Gulf of Khambhat, are used for further simulations.

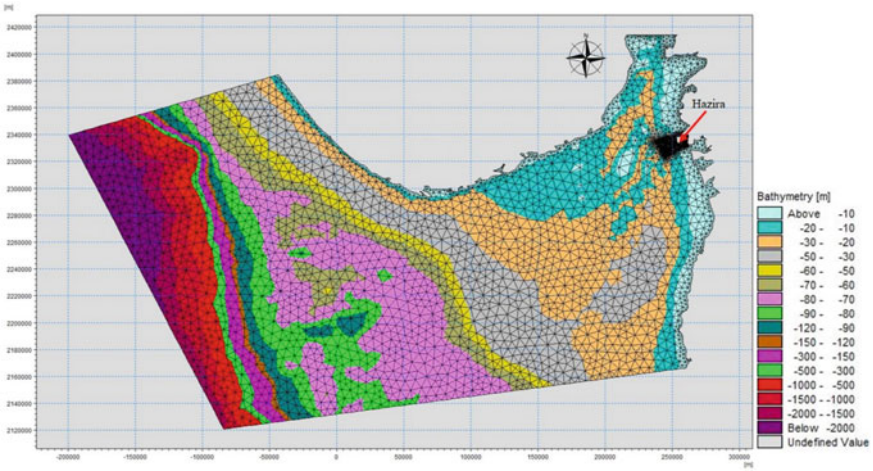

Fig. 4 Regional model bathymetry (Mesh 1)

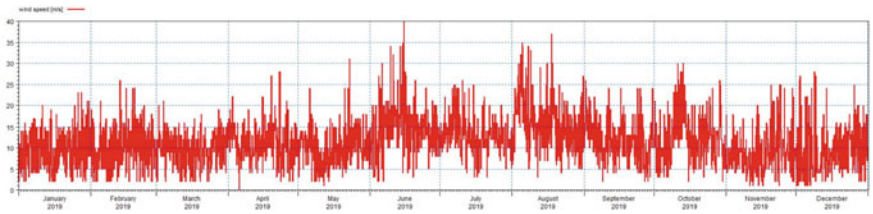

Fig. 5 Wind magnitude time series taken from IMD

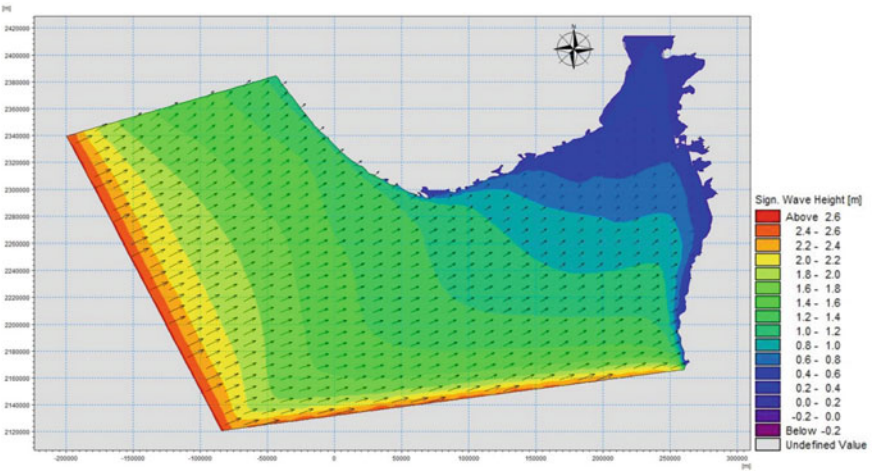

Fig. 6 Significant wave height vector plot of the regional model (SW monsoon)

4.2 Wave Transformation Studies for the Intermediate Model (Step 2)

A bathymetry and mesh as shown in Fig. 7 is prepared. It spans the area of 200 km by 160 km. The mesh consists of 1823 nodes and 3228 elements. The time series of wave parameters is extracted from the result of the regional model, at the south-west boundary of the Mesh 2, as shown in Fig. 8. The time series of wave parameters such as wave height, wave direction, wave period and constant wind speed of 15 m/s, from 220° N are the input parameters for the simulation of the intermediate model. Values of wind speed and direction are chosen from IMD data. The wind speed is considered on the higher side than the average wind speed. The wind direction is the predominant direction as observed by IMD. A typical wave vector plot obtained from the MIKE21 SW simulation for the intermediate model is shown in Fig. 7. The wave heights are between 0.8 m and as high as 2.5 m in the monsoon. The wave directions are from 210° to 250°. These results are used as the input for further studies.

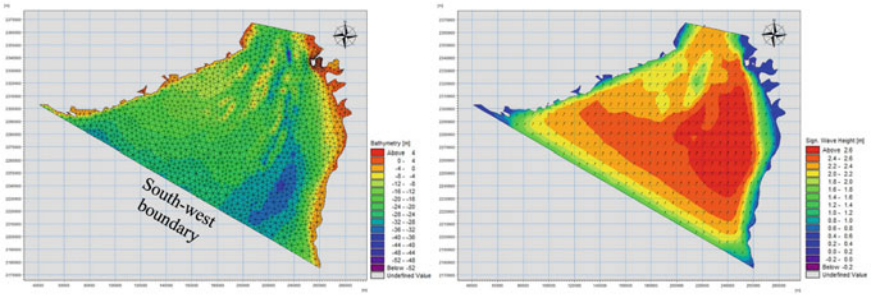

Fig. 7 Intermediate bathymetry with element mesh (Mesh 2) and significant wave height vector plot of the intermediate model (SW monsoon)

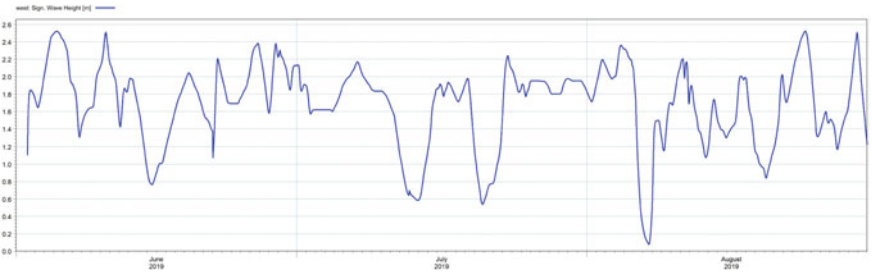

Fig. 8 Input significant wave time series for south-west boundary of intermediate model extracted from regional model (SW monsoon)

4.3 *Wave Transformation Studies for the Local Model (Step 3)*

This is third and final step in the transformation of waves to obtain wave climate at the reclamation and the channel corner. The studies are referred as the local model studies. A bathymetry and element mesh of 28 km by 21 km with 8132 nodes and 13,382 elements was considered for MIKE21 SW model simulation of step 3 as shown in Fig. 9. This is referred as Mesh 3. This has fine resolution. The wave parameters obtained from the intermediate model studies (step 2) are used for the further simulations in the local model. Time series of wave parameters, extracted from the results of intermediate model, along the boundary A and boundary B are shown in Figs. 10 and 11. The extracted time series of waves obtained from the intermediate model study is used as input for the simulation of the local model. In addition to this, local wind of 15 m/s in 220° direction is considered for the simulation. Along with it, water levels corresponding to tide near Hazira taken from CMAP were included in the simulation. Typical wave vector plot for south-west monsoon is shown in Fig. 12.

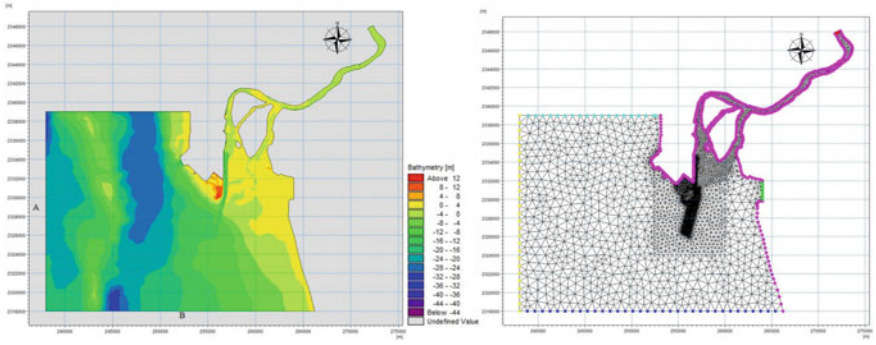

Fig. 9 Bathymetry and element mesh of local model for existing condition (Mesh 3)

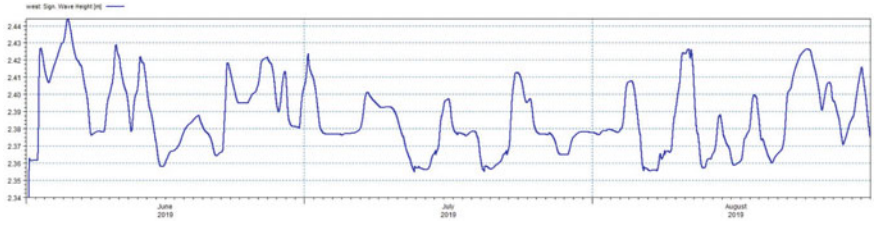

Fig. 10 Input significant wave time series for boundary A of the local model extracted from intermediate model

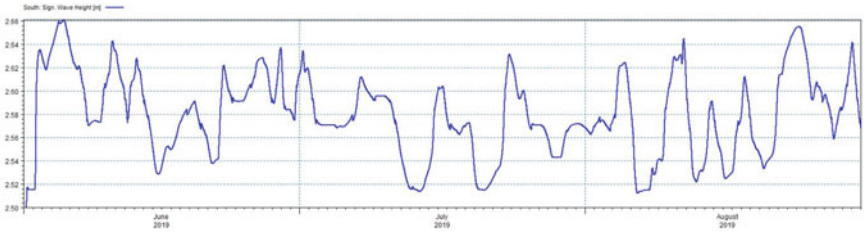

Fig. 11 Input significant wave time series for boundary B of the local model extracted from intermediate model

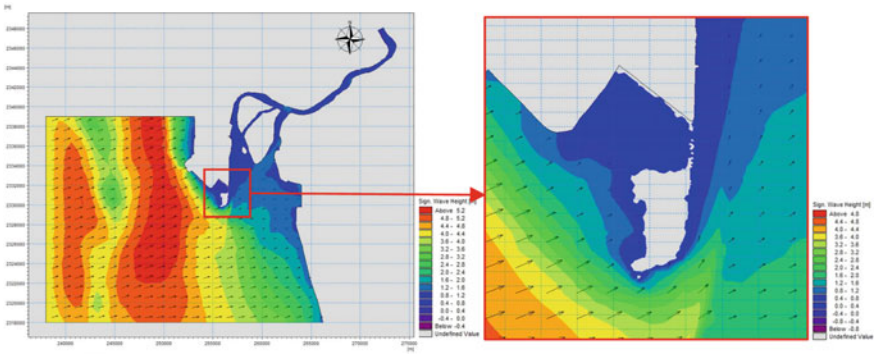

Fig. 12 Significant wave height vector plot of the local model (SW monsoon)

5 Wave Transformation for Proposed Condition

Primary objective of the study is to minimize the hump formation at the reclaimed area near the mouth of the channel so that the approach channel should be functional without any disturbance. Major objective of the study is to assess the reasons of the washing off of the reclaimed portion and how to mitigate it. The wave attack is responsible for drifting the sediment from the reclaimed area towards the channel and depositing at the corner every year. It is the main cause of the erosion of the beach. This eroded material moves towards the channel. It is not washed off completely. Thus, some material gets deposited and forms the hump. This may obstruct the movement of vessels in the channel. In the nature, three prominent forces are acting simultaneously namely wave force, tidal force and wind force. In this region, effect of wind is significant. All the three forces by preparing/extracting the wave and wind time series and water level time series corresponding to the tidal levels have been used. Wave transformation from the boundary of the local model to the area of interest was carried out. Wave impact on the region was assessed. Wave heights obtained from simulation with the existing bathymetry shows quite high wave impact in the area of interest. There are several methods to protect a shore. In the present scenario, it was anticipated to recover the beach/reclamation as much as possible.

These requirements can be achieved by constructing submerged breakwater. Thus, the innovative and environment friendly technique for the protection of the affected area, by a submerged breakwater was studied. To provide the protection for the reclamation and the SE corner, a protective structure in the form of submerged breakwater was envisaged. Many trials with different layouts of the submerged breakwater were performed. For different layouts with submerged breakwaters, wave climate was obtained. Multiple trials were taken to optimize the orientation, length and height of proposed submerged breakwater. Considering the reduction in the wave height and the direction of wave approach at the shoreline, submerged breakwater of 300 m length, 3.5 m height above the chart datum, located at 150 m from the channel and 100 m away from the shoreline resulted into satisfactory reduction in wave heights. This proposed submerged breakwater is incorporated into the existing bathymetry as shown in Fig. 13. Thus, comprehensive study was done. Study of wave, wind and tide simultaneously is a very complex phenomenon. It was carried out successfully. Model was simulated using MIKE21 SW for whole year and results, i.e. wave parameters (significant wave height, wave period and wave directions) are calculated. These runs were carried out for the monsoon season which is critical. Typical wave vector plot at 15 June, 4 pm in the south-west monsoon is shown in Fig. 14. The wave heights of magnitude 1–2 m are approaching the reclamation face for most of the year. Results showed that the maximum wave height is 2.5 m. Also, significant wave height vector plots of the local model with submerged breakwater during high water and during low water are shown in Fig. 15.

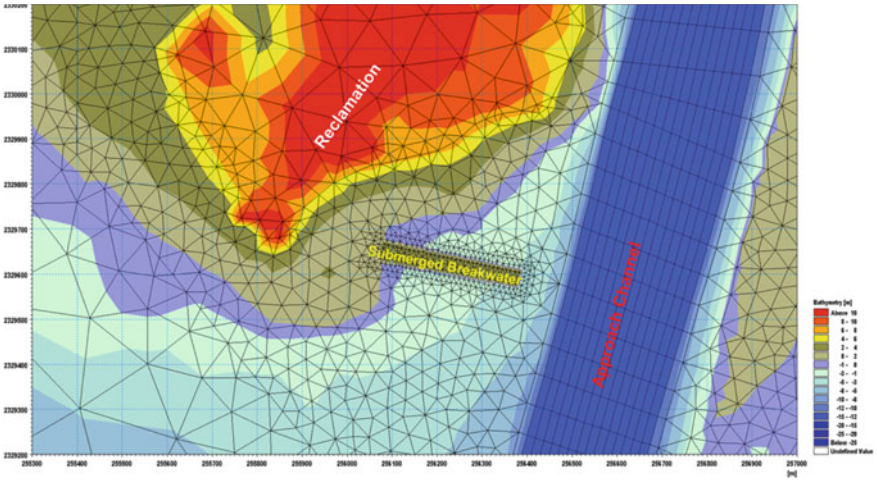

Fig. 13 Location of submerged breakwater

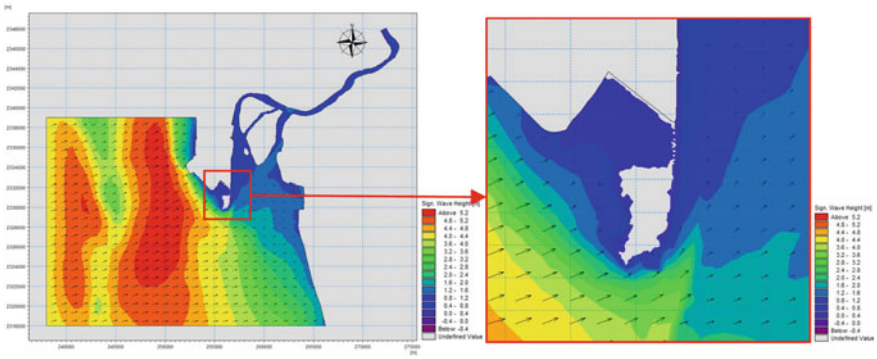

Fig. 14 Significant wave height vector plot of the local model with submerged breakwater (SW monsoon)

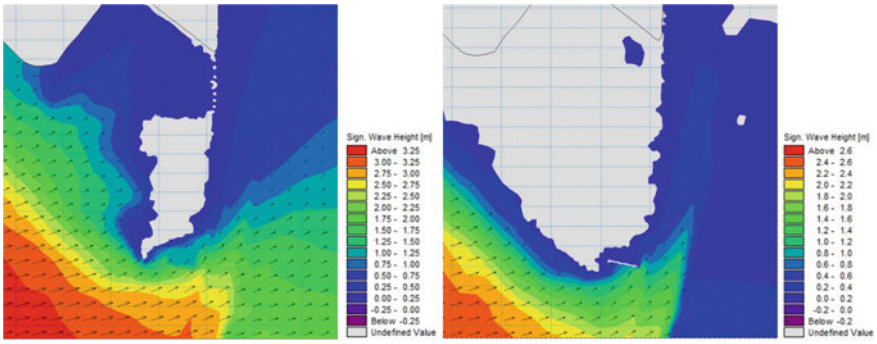

Fig. 15 Significant wave height vector plot of the local model with submerged breakwater during high water and low water

6 Discussion of Results

To estimate the reduction of wave height, wave parameter time series was extracted at three points as shown in Fig. 16. These three points are taken at the sea side, the lee side of submerged breakwater and one point away from the submerged breakwater shown as Point 1, 2 and 3, respectively. To get the clear idea of the reduction in the wave heights, the time series of wave height was extracted at the points, for existing bathymetry and with the proposed layout (Table 1). Comparison of wave heights with submerged breakwater and without submerged breakwater for existing and proposed condition is shown in Fig. 17.

At point 1, it is observed that at low tide, the wave height increases due to reflection. With the increasing submergence, there is a small increase in the wave heights as well. On an average, there is very little change in the wave heights at the point in front of the submerged breakwater. Immediately behind the submerged breakwater

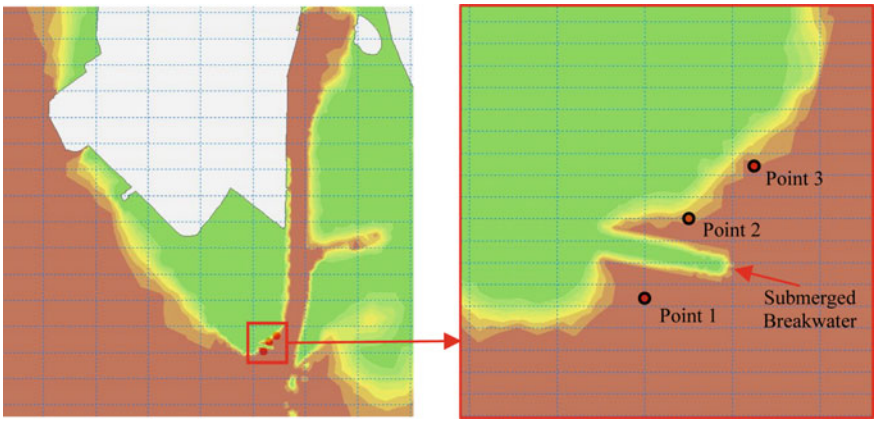

Fig. 16 Points at which wave data extracted

Table 1 Percentage reduction of wave heights (Avg) with the final layout at the locations in the lee of the breakwater

Points	Without submerged breakwater (H_1)	With submerged breakwater (H_2)	Percentage reduction in wave height
Point 2	1.26	0.40	69.00
Point 3	1.25	0.79	37.20

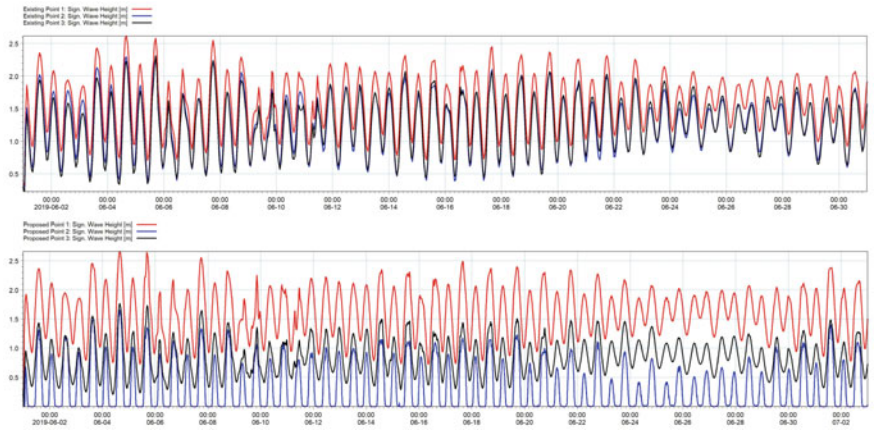

Fig. 17 Comparison of significant wave heights without submerged breakwater and with submerged breakwater

the reduction is very high. The waves from the sides of the breakwater and diffracted waves reach the shore behind the breakwater. This shows that the physics is simulated correctly. Thus, simulation with submerged breakwater was successful and the results are reasonable.

For every time step, percentage reduction is calculated as follows:

$$\text{Percentange reduction at time } t_i = P(t_i) = \left(\frac{H_1(t_i) - H_2(t_i)}{H_1(t_i)}\right) \times 100$$

$$\text{Average Percentage reduction} = \sum_{i=1}^{n} P(t_i)/n$$

where

$H_1\ (t_i)$ = significant wave height without submerged breakwater for given time 't'.

$H_2\ (t_i)$ = significant wave height with submerged breakwater for given time 't'.

n = total number of observations.

Thus, the effect for the complete SW monsoon period is represented. The wave energy is directly proportional to square of the wave height [3]. Thus, reduction in the wave height by 37%, results in the reduction of the wave attack by 55%. This reduction would arrest the erosion.

7 Conclusions

The following conclusions are derived from the foregoing study:

- In the navigational channel leading to Hazira EBTL terminal, a hump was formed which recurred even after it was dredged to the original depth. This shows that there is a continuous supply of sediment approaching that location. Erosion is due to the severe wave attack.
- Studies to assess the impact of the waves were carried by wave transformation studies on the regional model followed by extensive studies with the model in the area near the reclamation and the navigational channel (local model). The wind forces generate waves. In the regional model, wind time series of complete year was used as the input on the boundary of the model. The time series provides better representation of the sea state than giving discrete value of wind magnitude and the direction.
- Swell waves start dominating the sea state, from the entrance of Gulf of Khambhat. So, wave forcing should be given as input for the further wave transformation studies. Hence, a model extending from the entrance of Gulf of Khambhat to the −25 m near the reclamation was considered. Wave climate at the boundaries of the intermediate model were calculated from the results of the regional model.

Predominant wave directions at the entrance of the gulf are west, WSW, SW and south and maximum wave height up to 2.5 m was observed.

- The last stage of the wave transformation is to calculate wave climate at the reclamation. For this purpose, simulations with the local model were carried out. The wave time series at the boundaries of the local model were obtained from the intermediate model. Near the estuary, wind velocities and the changing water level at every time interval needs to be considered to simulate the wave heights and directions. From the IMD data, it was observed that maximum wind speed is 15 m/s. Wind forcing and the water levels at every time step were included as input. The simulation is as comprehensive as possible. The waves at the shore approach from 210° to 250° quadrant. The results show that wave heights up to 2.5 m attack the shoreline under study. Thus, it is necessary to reduce the impact of the waves.
- A submerged breakwater as a protection measure reduces the wave attack and also let waves pass to the shore for some time of the tidal cycle and eventually a beach behind the submerged breakwater is formed. Hence, submerged breakwater was envisaged as the protective measure. Various different layouts of submerged breakwater with different locations, orientation and lengths were studied. The wave time series comparisons at three locations on the seaside of the breakwater, just behind the breakwater and near the shore were compared to arrive at the optimal layout. It consists of submerged of length 300 m, 3.5 m height above the chart datum, located at 150 m to the west from the channel and 100 m away from the shoreline. The results indicated that submerged breakwater is effective in reducing the erosion and mitigating the formation of the hump.

Acknowledgements The authors wish to thank the Director, Central Water and Power Research Station (CW&PRS) for his consistent support, encouragement and kind consent for publishing this paper.

References

1. Holthuijsen L, Herman A, Booij N (2003) Phase-decoupled refraction-diffraction for spectral wave models. Coast Eng 49(4):291–305
2. CWPRS Technical Report No. 5845 (2020) Mathematical model studies for wave tranquillity and shoreline changes due to reclamation proposed by M/s EBTL at Hazira, Gujarat
3. Coastal Engineering Manual (2008) EM 1110-2-1100 (Part II)

Future Sea Level Rise at Indian Ports Using a Combined Numerical and Data-Driven Approach

P. S. Somaiya and M. C. Deo

Abstract The estimation of future sea level rise (SLR) under the changing climate at India's major ports is necessary considering India's large port infrastructure, spread across its ~7000 km of coastline. In this study, the future SLR for next 30 years is predicted using a combination of general circulation models (GCMs) and artificial neural networks (ANNs) to take advantage of both physics-based as well as data-driven approaches. For every port, monthly means of six climatic causal variables, namely sea surface temperature, precipitation, sea level pressure, surface salinity, wind speed, and surface height above geoid were used as input to the ANN to obtain the output of monthly mean sea levels. In the training, past sea levels recorded by tide gauges were used as output. The climatic input variables pertained to eleven different CMIP6 GCMs with SSP2-4.5 as the future climate scenario. Using the trained network and for every GCM, monthly sea levels were predicted for next 30 years, where the input was the future causal parameters. The rate of SLR was determined by fitting regression to the variation of the sea levels against time. This process was repeated for all GCMs. The median of all such GCM-yielded SLR, derived for each port, was compared with the same based on a software protocol called: SimCLIM which is based on the use of GCMs alone. It was found that such ANN-based SLR rate at major Indian ports was lower than the SimCLIM-based one, and it varied from 1.94 mm/year (Chennai) to 4.11 mm/year (Mumbai). The proposed approach is site-specific and hence more appropriate to use than the spatially averaged projections from SimCLIM or satellite data.

Keywords Sea level rise · General circulation models · SimCLIM · ANN · Tide gauge data

P. S. Somaiya · M. C. Deo (✉)
Department of Civil Engineering, Indian Institute of Technology Bombay, Mumbai 400 076, India
e-mail: mcdeo@civil.iitb.ac.in

P. V. Timbadiya et al. (eds.), *Coastal, Harbour and Ocean Engineering*, Lecture Notes in Civil Engineering 321, https://doi.org/10.1007/978-981-19-9913-0_8

1 Introduction

The coastal regions over the world are subjected to multiple hazards including sea level rise and associated land inundation. It has been recently recognized that the major cause of the present sea level rise (SLR) is the climate change induced by global warming [24]. The rise in earth's temperature, accelerated by human interference in the atmosphere, causes melting of ice cover on the land surface as a result of which the volume of water in oceans increases, and further, the surface water expands. Together with this is the resulting changes in water density and salinity, changes in water coming from land that contribute to the change in sea levels, both globally as well as regionally. The United Nations sponsored Inter-governmental Panel on Climate Change (IPCC) has pointed out an increasing trend of the global mean sea level [14]. The SLR is not uniform everywhere and depends on local factors including sea floor movements, land water changes, and regional water circulation. Its magnitude can vary even by 3 times or more compared to the globally averaged rise, and further, it could be negative as well [5]. Thus, it is always necessary to carry out location-specific studies on sea level changes.

The assessment of the impact of global climate change is commonly done through General Circulations Models (GCMs) developed by groups of world's climate scientists. A GCM essentially encapsulates the climate system behavior into differential equations representing conservation of mass, momentum, energy, and a few other laws related to air and water circulation and solves them using numerical methods with appropriate initial and boundary conditions. The GCMs yield their output at certain intervals in the form of various climatic parameters for past as well as future time periods. For this purpose, they are run on the basis of various climate change scenarios and societal responses [30]. The IPCC's most recent and sixth assessment report AR6 identifies five such cases called shared socioeconomic pathways (SSPs) that follow certain warming and response pathways to reach a particular situation at the end of the present century [25, 33].

The regional SLR is influenced by many met-ocean parameters in different proportions including temperature rise and resulting density and salinity change, sea level pressure, wind speed and direction, precipitation, and fresh water flow. The effect of (i) temperature-induced thermal expansion and ice melting was discussed by Bindoff et al. [3]; (ii) salinity, by Llovel and Lee [17]; (iii) sea level pressure, by Albrecht and Weisse [1]; (iv) wind speed and direction, by Gerkema and Duran-Matute [11], and (v) rainfall and fresh water inflow by Stammer et al. [29]. Apart from this, the impact of deformation or rebound of the earth's surface after removal of ice load of the ice age was studied by Mitrovica et al. [18]; that of land subsidence by Oppenheimer et al. [20] and that of El Nino Southern Oscillations (ENSO) by Fasullo et al. [10].

As regards the estimation of SLR rates for India, fairly large number of studies are available, starting with the early work of Emery and Aubrey [9] and including the recent ones of Black et al. [4] and Krishnan et al. [16]. Typically, while past tide gauge observations have shown a lower rate of SLR of 1.06–1.75 mm/year, the recent short-term satellite-based information has indicated an accelerated SLR

rate of 3.28 mm/year in Indian Ocean region. [6, 31, 32]. More relevant and recent studies related to the present work are due to Patil and Deo [22] who used data of tide gauges and CMIP5 GCMs for SLR projections for India and, Somaiya et al. [28] who inter-compared tide gauge, altimeter as well as CMIP5-based futuristic GCM data.

Although GCM-based evaluations are attractive due to their physics basis, they suffer from the problem of low-resolution and hence may need some local level tuning. Typically, the CESM2-WACCM GCM has a resolution of $0.94° \times 1.250$ for atmosphere and 0.470×1.120 for ocean. In order to obtain local level SLR, therefore, a combined approach of using the physics-based GCMs and a suitable data-driven technique reflecting location-specific met-ocean conditions can be attempted, as done successfully in the past in case of sea surface temperature and wave heights by Patil et al. [21] and Deshmukh et al. [8], respectively. For the data-driven technique, artificial neural networks (ANNs) can be advantageously employed in view of their abundant applications for this purpose [7].

Thus, in this study, we have evaluated SLR at 10 major ports of India located along the peninsular region as shown in Fig. 1 using monthly means of six causal parameters derived from the latest Climate Model Inter-comparison (CMIP) 6 GCMs. (Note that two other major ports, namely JNPT and Ennore are not considered separately since they are very close to Mumbai and Chennai, respectively, and further, the major port of Port Blair could not be included due to the very low data completeness (29%) or very high gaps in the tide gauge data). The input parameters include sea surface temperature and salinity, sea level pressure, wind speed and precipitation, and further, height above geoid to reflect dynamic changes in monthly sea levels. These are provided as input to an ANN to obtain its output in the form of monthly sea levels. The training of ANN was done using tide gauge data to reflect site-specific conditions. Such trained networks were run using projected or futuristic causal variables to get the monthly sea levels for a future period of 30 years. The results so obtained are compared with those of the commercial SimCLIM software that uses downscaled but relatively much low-resolution CMIP5 GCMs [26].

2 Materials and Methods

2.1 Artificial Neural Networks

As widely known, ANNs represent a network of computational elements called neurons or nodes that mimic the cognition process of human brain in that each neuron receives the input, sums it up, transforms the sum using certain transfer function, and passes on the result to the next layer of neurons. The neurons are configured into an architecture like feed forward in which the information flow is along one direction, i.e., from the input layer of neurons to the hidden layer/s and thereafter to the output layer, while in a recurrent network, backward or lateral flow is allowed.

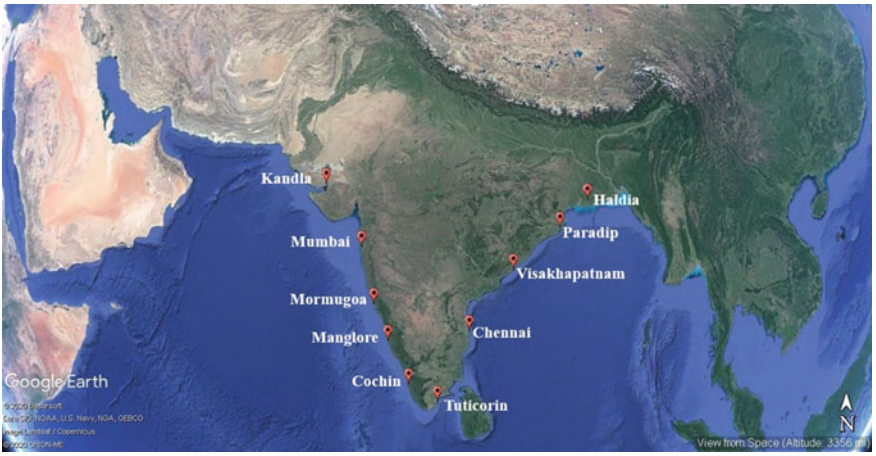

Fig. 1 Study locations along the Indian coast. (Image Landsat/Copernicus © 2020 ORION-ME)

In our work, we initially used both these configurations; however, later the recurrent one or specifically its variant called Long Short-Term Memory (LSTM) was found to impart better training as judged by the error statistic of coefficient of determination, R2, and hence, the same was employed for further analysis. In LSTM, long-term memory is created in a repeating unit or cell through short-term memories which are preserved through "gates" that decide on remembering or forgetting information and sending it further. More details can be seen in Hochreiter and Schmidhuber [13]. Before using any network, it is required to be trained using examples of input–output pairs for their processing with the help of a mathematical training algorithm [33]. The algorithm used was Adaptive Moments Estimation or ADAMS which is presented by Kingma and Lie Ba [15]. The free and open source machine learning library of Keras 2.3 that provides a Python interface for ANNs with TensorFlow 2.0 backend was used to carry out the training.

2.2 Data Used

The ANNs at each port location were trained using historical data of causal variables as input and corresponding tide gauge observations as output. The trained networks were thereafter used to predict the future SLR with the help of futuristic causal variables.

The tide gauge records belonged to the database of Permanent Service to Mean Sea Level (PSMSL) [22, 23]. They were in the form of monthly and annual mean sea levels. The lengths of the records were varying and further involved certain gaps of different lengths. As the basic gauge data at a given site are relative to a local chart datum, they are converted to a global reference datum of −7 m by PSMSL forming

the Revised Local Reference (RLR) data. The network input of causal variables pertained to the GCMs from latest global project: CMIP6 (https://esgf-node.llnl.gov/projects/cmip6/) [19]. Six input or causal parameters were identified. The first is the temperature, a major contributor to the SLR. The change in the precipitation patterns affects the rainfall distribution causing thereby increase or decrease in fresh water flows from rivers. It also changes salinity and the density of the sea water in turn affecting the volume of water and hence the SLR. The sea level pressure produces a reverse barometric effect on SLR. The wind drives and transports the warm ocean currents from one place to another. The dynamic variations in the sea level also forms an input to the ANN, and it can be extracted from the GCM data. The middle-of-the-road SSP2 4.5 scenario was used. The monthly means of such data from GCMs were available in NetCDF format as a 3D matrix for given latitude and longitude. There are many GCMs available under the CMIP6 project and this gives rise to varying results and uncertainty or bias in resulting estimates. One method to reduce such uncertainty is to use their ensemble median as done by Grose et al. [12] in their study involving downscaling of dynamic sea levels.

As mentioned earlier, for the purpose of comparison of our futuristic SLR, we have obtained the SLR from the commercial software protocol: SimCLIM (version 4.9.411) developed by CLIM-systems, New Zealand [34] and as previously done by Patil and Deo [21]. The underlying algorithm uses a certain pattern matching technique [35] and also an earlier CMIP5 project-based climate data for future projections. The SLR scenario generator tool was used to project the future SLR. The method of downscaling GCMs allows to use 28 CMIP5 GCMs and obtain ensemble averages avoiding thereby very high or low values. In such downscaling by the pattern matching technique the local MSL anomaly or the difference in values between future (2080–2100) and past (1986–2005) time slices is tagged with the corresponding global level difference. In this study, we have used the option of medium warming scenario: RCP-4.5 [26].

3 Results and Discussions

3.1 Historical SLR

As the recorded tide gauge levels get affected by local Vertical Land Movement (VLM) as well as Glacial Isostatic Adjustment (GIA), corresponding corrections were applied. The GIA corrections were obtained from Peltier GIA datasets [22]; (https://www.psmsl.org/train_and_info/geo_signals/gia/peltier/). The GIA correction is positive as it tends to underestimate the absolute SLR [32]. The VLM data belonged to the app "sea level rise for cities" in the SimCLIM software protocol that is based on GPS data from project: SONEL. The rising land has a positive VLM value and vice versa. These corrections are arithmetically added or subtracted from

the relative SLR rate to obtain the absolute SLR rate. (The details of underlying values were reported in Somaiya et al. [27].

For every port, the SLR rate was found out by fitting a linear regression to the plot of monthly tide gauge-based water levels, corrected as above, and corresponding time. It was found that the SLR rates for the east coast ports were 1.91 mm/year, 0.63 mm/year, 0.17 mm/year, −1.16 mm/year, and 0.1 mm/year at Haldia, Paradip, Vizag, Chennai, and Tuticorin, respectively, while the same was 0.86 mm/year, 1.71 mm/year, 1.10 mm/year, 0.07 mm/year and 0.88 mm/year, respectively, at Cochin, Mangalore, Mormugao, Mumbai, and Kandla, respectively of the west coast. The high rate at Haldia could be due to the high siltation from river deltas raising the water level rapidly while the negative trend at the Chennai port could be because of high VLM of 2.25 mm/year. The SLR rate so obtained in this work was found to be consistent at 95% confidence with corresponding trends of National Aeronautics and Atmospheric Administration (NOAA) bases on monthly PSMSL data (https://tidesandcurrents.noaa.gov/sltrends/sltrends_station.shtml?id=500-041).

3.2 Future SLR Using ANN

The Network and its Training

In this study, ANNs were used to find the dependency between the six causal variables and the mean sea level. The monthly mean values of these variables were used. Once the historical relationship was established by training the ANN, the same weights and bias were used along with future causal variables to get future monthly sea level as output. Thereafter, a linear regression line was fitted across such input and output to obtain the rate of future SLR. It is to be noted that since the ANN always has extra degrees of freedom in its configuration, it is presumed that this would enable it to adapt to the dependency between the input and output into the future as well, although the same was based on past structure.

Before training, all values were normalized in the range of 0 to 1 in order to remove the scaling bias. The input dataset was split into two parts: training and validation in proportion of 80:20. For this purpose, random sampling was done rather than sequential one which otherwise would have been desirable for a trend detection exercise. The training efficiency of the ANN was checked by the coefficient of variation, R2, of training and validation sets. For a well-trained network, the R2 values for both training and validation need to be close to each so that overfitting does not happen.

First the efficiency of feed forward type of ANN was tested for a typical site of Haldia port. The network had two hidden layers with 64 and 32 nodes in each, respectively. The R2 for the training set was 0.83 while the same for the validation set was 0.72. For the LSTM network the R2 for the training set was 0.83 while the same for the validation set was 0.84. Thus, the LSTM type of ANN was found to perform better than the feed forward one. This ANN configuration was therefore used

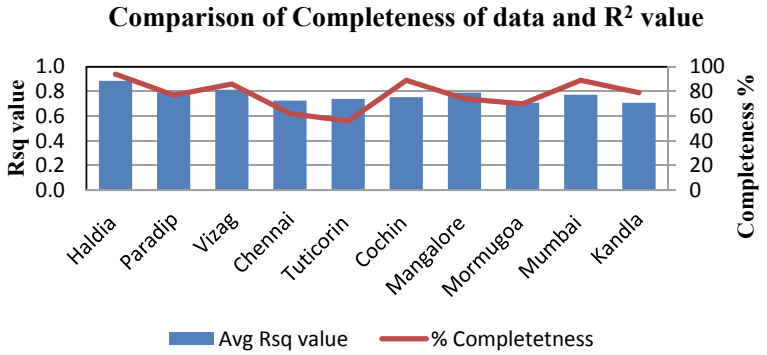

Fig. 2 Comparison between R2 score and completeness of data

further. In order to understand if there existed a relationship between the R2 values and the number of gaps in data, Fig. 2 was drawn which showed that lower number of missing information or higher completeness of data provides better training.

4 Projection of Future Sea Level

The trained network was used to predict the monthly sea levels over the next 30 years, that is, from the year 2020 to 2050 from the futuristic monthly averaged values of all causal variables. Thereafter, a linear regression was fitted to the outcome after making the VLM and GIA corrections to obtain the absolute rate of SLR at different port locations. Such correction was necessary since the output of sea levels was based on uncorrected tide gauge data.

The SLR rates for all locations derived using 11 different GCMs under the CMIP6 umbrella are shown in Fig. 3. This figure also shows the median ensemble of all these estimations. Different GCMs involve different sub-process modeling as well as computing schemes, and hence, very large variations in the outcome can be seen even for a given port. Further, a given GCM may perform well for some region but not for another one. Such bias can be removed by using typically their median ensemble [2, 16]. Therefore, in the present work, all GCMs were ranked as per their descending order of SLR values, and their median was derived and used further.

The resulting absolute SLR rates are shown in Fig. 4 (the blue colored ordinates), referred to later. As shown, these rates varied from 1.94 mm/year to 4.11 mm/year with maximum SLR rate at Mumbai port and minimum at Chennai port. The average SLR rate along the Indian coastline was thus 3.2 mm/year. It can be seen that the SLR rate at the west coast was more than the one at the east coast. It may be noted that SLRs from different locations will vary due to a variety of reasons such as local GIA and VLM corrections, shape of the basin, topography of the sea bed, changing flow of fresh water from the land. Larger bed sloes and water depths cause deeper

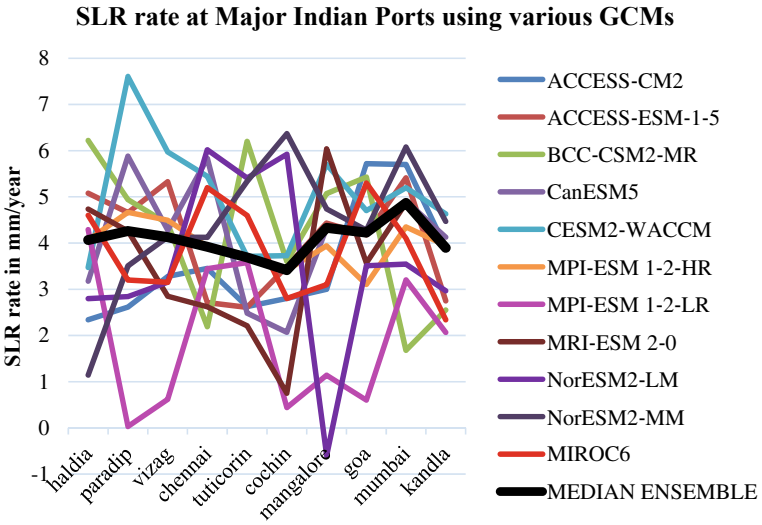

Fig. 3 Median ensemble of SLR rate from all GCMs

thermal mixing and hence smaller surface expansion. Also, local current circulation can result in either accumulation or diversion of water.

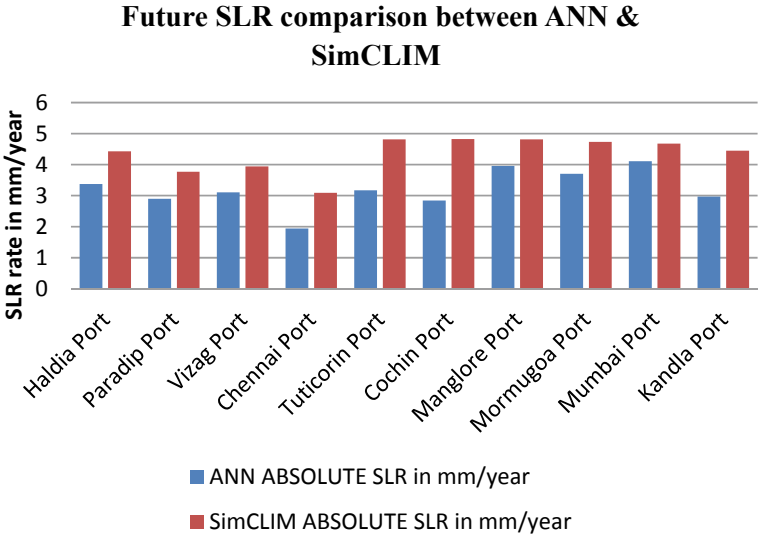

Fig. 4 SLR rate comparison between SimCLIM and ANN

5 Comparison with SimCLIM-Based Projections

In a previous study, Patil and Deo [21] had used the SLR scenario generator of the software: SimCLIM to obtain the future SLR up to the 2100. These rates were regional averages as dictated by the GCM resolutions. The base year was taken as 1995 for the evaluation of SLR. The SLR rate was obtained for the median ensemble (50th percentile) of all 28 GCMs under the earlier CMIP5 umbrella by fitting regression to the cumulative SLR data. The resulting rate of the relative SLR for the Indian port varied from 3.10 mm/year to 4.82 mm/year with a minimum at Chennai port and a maximum at Cochin and nearly same at Mangalore and Tuticorin.

In the present study, a combination of process-based and data-driven technique is used to obtain location-specific SLR. As against this, the fully GCM-based pattern scaling approach incorporated in the SimCLIM protocol tags changes in regional sea levels to the global ones. Figure 4 compares the results obtained from both these approaches. It shows that both results are consistent with each other, but the site-specific SLR is on the lower side.

The difference across the two methods under comparison could be attributed to the different approaches involved. The proposed method maps the causal variables with local tide gauge data and is more region specific, whereas the fully GCM-based method produces spatially averaged values. The tagging of location-specific SLR with in situ tide gauge data seems to produce lower values, and this is consistent with the observations in some of the past studies as well as in this one (as mentioned in section Historical SLR) that the tide gauge-based SLR rates are lower than the spatially averaged satellite or GCM-based evaluations [4, 21]. The type of input is also different for these two methods. The SimCLIM uses 28 GCMs of CMIP5 project, whereas for the ANN-based evaluation 11 CMIP6 GCMs were employed. Although both sets of evaluations use the moderate climate scenarios leading to 4.5 W/m2 radiative forcing at the end of the century, corresponding pathways, namely RCP-4.5 and SSP2-4.5 are not exactly same and can exhibit dissimilar regional pattern of the climate change [18].

From Fig. 4, it can be seen that, common to both methods, the SLR rate on the east coast would be generally lower than the west, which could be due to higher bed slopes as well as water depths within the eastern continental shelf leading to lower thermal expansion because of the deeper mixing in this region. The other reasons could be the effect of varying seasonality, tapping of salinity water coming from Bay of Bengal by the Lakshadweep islands [25, 31].

6 Conclusions

The following conclusions are drawn from the present study:

- The absolute SLR rate derived from monthly mean sea levels recorded by tide gauges was maximum at Haldia port (1.91 mm/year) and minimum at Chennai

port (−1.16 mm/year). The high rate at Haldia could be due to the high siltation from river deltas raising the water level rapidly while the negative trend at the Chennai port could be because of the high VLM.

- The absolute SLR rate projected for next 30 years and up to the year 2050 obtained from the pattern matching scheme of the software tool: SimCLIM, involving a median ensemble of 28 CMIP5 GCMs, varied from 3.10 mm/year (Chennai) to 4.82 mm/year (Cochin, Mangalore and Tuticorin).
- The training of ANN done to estimate the SLR from the causal variables coming from 11 CMIP6 GCMs was associated with high coefficient of variation: R2. It was seen that the network learned more accurately when data were continuous and with small number of missing values.
- The use of above-mentioned ANN to predict futuristic SLR rate up to the year 2050 indicated that such rate at major Indian ports would vary from 1.94 mm/year (Chennai) to 4.11 mm/year (Mumbai).
- The future projections of SLR from both ANN and SimCLIM approaches showed that the east coast would have lower rates than the west due to steeper bed slopes and water depths at the east which in turn would help in deeper thermal mixing. The lowest SLR rate at Chennai port might be arising out of a local current circulation pattern prohibiting water accumulation and because of very high VLM rate.
- The absolute SLR rate obtained from ANN is consistent with that of the SimCLIM, although lower in magnitude. The difference could be due to the use of tide gauge data for network training apart from the use of GCM-based data of two different CMIP projects and different methods of evaluations. However, the proposed ANN technique is site-specific and hence more applicable for the Indian major ports than the projections from SimCLIM as well as those from satellite data.

References

1. Albrecht F, Weisse R (2012) Pressure effects on past regional sea level trends and variability in the German Bight. Ocean Dyn 62(8):1169–1186
2. Arritt RW, Rummukainen M (2011) Challenges in regional-scale climate modeling. Bull Am Meteor Soc 92(3):365–368
3. Bindoff NL, Willebrand J, Artale V, Cazenave A, Gregory JM, Gulev S, ... Shum CK (2007) Observations: oceanic climate change and sea level. In: Solomon S, Qin D, Manning M, Chen Z, Marquis M, et al (eds) Climate change 2007: the physical science basis: contribution of working group I to the fourth assessment report of the intergovernmental panel on climate change. Cambridge University Press, Cambridge, pp 385–432
4. Black, KP, Baba M, Mathew J, Kurian NP, Urich P, Narayan B, Stanley DO (2017) Climate change adaptation guidelines for coastal protection and management in India. Global Environment Facility and Asian Development Bank, FCGANZDEC, New Zealand
5. Church JA, Clark PU, Cazenave A, Gregory JM, Jevrejeva S, Levermann A, Merrifield MA, Milne GA, Nerem RS (2013) Sea level change. In: Stocker TF, Qin D, Plattner GK, Tignor M, Allen SK, Boschung J, Nauels A, Xia Y, Bex V, Midgley PM (eds) Climate change (2013) The physical science basis. Contribution of working Group I to the fifth assessment report of the

intergovernmental panel on climate change, vol 1140. Cambridge University Press, Cambridge, UK
6. Church JA, White NJ, Konikow LF, Domingues CM, Cogley JG, Rignot E, ... Velicogna I (2011) Revisiting the Earth's sea-level and energy budgets from 1961 to 2008. Geophys Res Lett 38(18)
7. Deo MC (2010) Artificial neural networks in coastal and ocean engineering. Indian J Geo-Mar Sci 39(4): 589–596
8. Deshmukh A, Deo M, Bhaskaran P, Balakrishna Nair TM, Sandhya KG (2016) Neural network based data assimilation to improve numerical ocean wave forecast. IEEE J Oceanic Eng 41(4):944–953
9. Emery KO, Aubrey DG (1989) Tide gauges of India. J Coastal Res 489–501
10. Fasullo JT, Boening C, Landerer FW, Nerem RS (2013) Australia's unique influence on global sea level in 2010–2011. Geophys Res Lett 40(16):4368–4373
11. Gerkema T, Duran-Matute M (2017) Interannual variability of mean sea level and its sensitivity to wind climate in an inter-tidal basin. Earth Syst Dyn 8(4):1223–1235
12. Grose MR, Narsey S, Delage FP, Dowdy AJ, Bador M, Boschat G, ... Power S (2020) Insights from CMIP6 for Australia's future climate. Earth's Future 8(5):e2019EF001469
13. Hochreiter S, Schmidhuber J (1997) Long short term memory. Neural Comput 9(8):1735–1780
14. IPCC (2013) Climate change 2013: the physical science basis. In: Stocker TF, Qin D, Plattner G-K, Tignor M, Allen SK, Boschung J, Nauels A, Xia Y, Bex V, Midgley PM (eds) Contribution of working group I to the fifth assessment report of the intergovernmental panel on climate change. Cambridge University Press, Cambridge, United Kingdom and New York, NY, USA, 1535 pp. https://doi.org/10.1017/CBO9781107415324
15. Kingma DP, Ba J (2014) Adam: A method for stochastic optimization. arXiv preprint. arXiv: 1412.6980
16. Krishnan R, Sanjay J, Gnanaseelan C, Mujumdar M, Kulkarni A, Chakraborty S (2020) Assessment of climate change over the indian region: a report of the ministry of earth sciences (MoES). Government of India. https://doi.org/10.1007/978-981-15-4327-2
17. Llovel W, Lee T (2015) Importance and origin of halosteric contribution to sea level change in the southeast Indian Ocean during 2005–2013. Geophys Res Lett 42(4):1148–1157
18. Mitrovica JX, Gomez N, Morrow E, Hay C, Latychev K, Tamisiea ME (2011) On the robustness of predictions of sea level fingerprints. Geophys J Int 187(2):729–742
19. O'Neill BC, Tebaldi C, Vuuren DPV, Eyring V, Friedlingstein P, Hurtt G, ... Sanderson BM (2016) The scenario model intercomparison project (ScenarioMIP) for CMIP6. Geosci Model Dev 9(9):3461–3482
20. Oppenheimer M, Glacovic B, Hinkel J, Van De Wal R, Magnan A, Abd-Elgawad A, Cai R, Cifuentes-Jara M, Deconto R, Ghosh T, Hay J, Isla F, Marzeion B, Meyssignac M, Sebesvari Z (2019) Sea-level rise and Implications for low lying islands, coasts and communities. Special report on the ocean and cryosphere in a changing climate (SROCC)
21. Patil K, Deo MC, Ravichandran M (2016) Prediction of sea surface temperature by combining numerical and neural techniques. J Atmos Oceanic Technol 1715–1726
22. Patil RG, Deo MC (2020) Sea level rise and shoreline change under changing climate along the Indian coastline. J Waterw Port Coast Ocean Eng 146(5):04020002
23. PSMSL (2020) Permanent Service for Mean Sea Level (2020): "Tide gauge data". https://www.psmsl.org/data/obtaining/. Accessed 09 Feb 2020
24. Rahmstorf S (2010) A new view on sea level rise. Nat Clim Change 1(1004):44–45
25. Riahi K, Van Vuuren DP, Kriegler E, Edmonds J, O'neill BC, Fujimori S, ... Tavoni M (2017) The shared socioeconomic pathways and their energy, land use, and greenhouse gas emissions implications: an overview. Global Environ Change 42:153–168
26. Shankar and Shetye (2001) Emery KO, Aubrey DG (1989) Tide gauges of India. J Coastal Res 5(3):489–501
27. SimCLIM Systems (2003) User's manual. SimClim, New Zeeland. https://www.climsystems.com/slr-cities-app/technical/#data-andmethods

28. Somaiya P, Patil RG, Deo MC (2021) Historical and future sea level rise at major Indian ports. In: Hydro-2020 International conference, N I T Rourkela, March 26–28, vol 1, pp 602–612
29. Stammer D, Cazenave A, Ponte RM, Tamisiea ME (2013) Causes for contemporary regional sea level changes. Ann Rev Mar Sci 5:21–46
30. Taylor KE, Stouffer RJ, Meehl GA (2012) An overview of CMIP5 and the experiment design. Bull Am Meteor Soc 93(4):485–498
31. Unnikrishnan AS, Shankar D (2007) Are sea-level-rise trends along the coasts of the north Indian Ocean consistent with global estimates? Global Planet Change 57(3–4):301–307
32. Unnikrishnan AS, Kumar KR, Fernandes SE, Michael GS, Patwardhan SK (2006) Sea level changes along the Indian coast: Observations and projections. Curr Sci 362–368
33. Van Vuuren DP, Stehfest E, Gernaat DE, Doelman JC, Van den Berg M, Harmsen M, ... Tabeau A (2017) Energy, land-use and greenhouse gas emissions trajectories under a green growth paradigm. Global Environ Change 42:237–250
34. Wasserman PD (1993) Advanced methods in neural computing. Van Nostrand Reinhold, New York
35. Yin C, Li Y, Urich P (2013) SimCLIM 2013 data manual. CLIMsystems Ltd., Hamilton, New Zealand

Impact of Wave Dynamics on Shoreline Changes Due to Proposed Reclamation by Numerical Models in Tapi Estuary for M/S EBTL, Hazira

Komal S. Vighe, Rahul Sawant, and L. R. Ranganath

Abstract Tapi estuary near Surat city in Gujarat has vital importance due to its conducive hydrodynamic aspects. This led to development of large number of coastal infrastructures. The river bifurcates into two branches, viz. main Tapi river channel and Dumas creek. Several companies like Essar, L&T, RIL, NTPC, KRIBHCO, ONGC, MAGDALA AND GUJARAT AMBUJA CEMENT LTD have come up along the banks of Tapi channel. All ports have developed their captive jetties and successfully harnessed the power of ports to propel their economic growth. Port development in Tapi estuary requires intermittent dredging in channels and the estuary consists of many channels. Developing a deep channel would involve considerable capital dredging and necessitate maintenance dredging in future. Essar Bulk Terminals Limited (EBTL) has developed all weather Deep-Draft Terminal which is advantageously located on the western shore of Tapi Estuary that has come up with a very ambitious proposal of developing a common navigational channel for all ports by deepening the Tapi channel and Dumas creek. The proposal includes widening and deepening of the channel to 12 m depth, and the dredged material is intended to reclaim area between both the channel which comprises Kadia bet and Mora bet with the intention to develop a port city. To check the impact of proposed reclamation from wave perspective wave transformation, wave tranquility and changes in shoreline studies carried out and described in this paper. MIKE21-SW and BW models are used for wave studies and LITDRIFT and LITLINE modules of LITPACK that are used for shoreline evolution studies. The model studies indicated that the proposal is feasible from the wave tranquility and littoral drift aspects.

Keywords Mathematical model · Wave tranquility · Littoral drift · Wave disturbance

K. S. Vighe (✉) · R. Sawant · L. R. Ranganath
Central Water and Power Research Station, Khadakwasla, Pune 411024, India
e-mail: vighe.ks@cwprs.gov.in

P. V. Timbadiya et al. (eds.), *Coastal, Harbour and Ocean Engineering*, Lecture Notes in Civil Engineering 321, https://doi.org/10.1007/978-981-19-9913-0_9

1 Introduction

Essar Bulk Terminals Limited (EBTL), an-all weather, Deep-Draft Terminal is advantageously located on the western shore of Tapi Estuary along the western side of Hazira Peninsula in Gulf of Khambhat. In May 2014, MoEF gave EC (Environment Clearance) for extending the channel from 6.2 km to 17.6 km, deepening from 12 to 16 m and widening of channel to 300 m with two additional TC (Turning Circle), reclamation of 334 ha south of mangrove. Till date channel is dredged to 12 m below CD (chart datum). Two additional TCs have not been undertaken so far. With respect to reclamation of 350 ha, reclamation is still ongoing. Currently, the terminal is operating 5 Berths with a total Quay length of 1,450 m with operational draft ranging 12 m to14 m. The main navigation channel is 7 km long marked with beacons and buoys having a depth of 12 m below CD with width of 300 m and turning circle radius of 600 m (Fig. 1). EBTL has a proposal for the development of Port City in the Tapi estuary with reclamation of total 5114 ha area. In the original layout, the Dumas channel (800 m wide $\times$ -14 m deep) on East side of the proposed reclamation ended in the shallow depth, i.e., at -5 m depth contour, but it has to be extended up to -14 m depth contour which is about 15 km southward in the offshore. It is not advisable for navigation of vessels and sedimentation point of view due to occurrence of cross currents perpendicular to the channel and also the channel passing nearer to Purna River confluence. Hence, the original proposal in consultation with EBTL has been modified by restricting the channel depth to -12 m and extending up to -12 m depth contour in south-west direction into the offshore for hydrodynamic studies, and the same proposal has been considered for wave tranquility, and littoral drift studies are shown in Fig. 2.

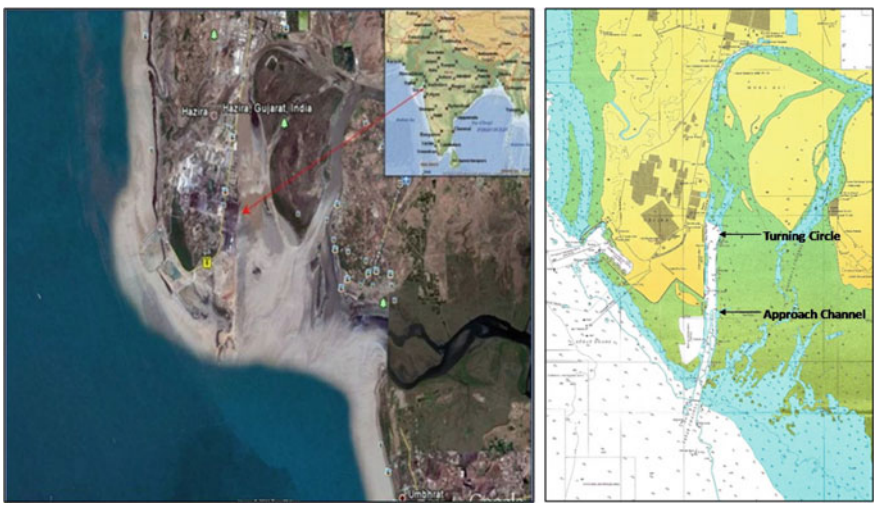

Fig. 1 Location plan of Essar port

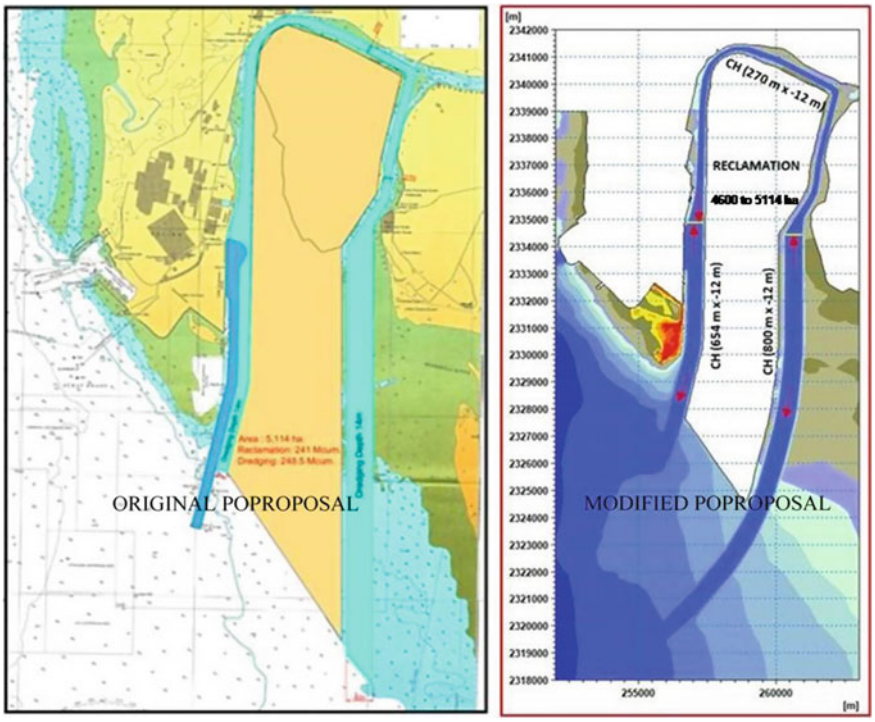

Fig. 2 Layout of the proposed reclamation (original and modified)

To check the impact of proposed reclamation from wave perspective wave transformation, wave tranquility and changes in shoreline studies carried out and described in this paper with different module of MIKE21 software.

2 Site Conditions

2.1 Wave Climate in Deep Sea

To study wave tranquility, nearshore wave data is essential. Instrumentally observed wave data at the site over a period of several years, if available, is best suited for this purpose. However, if such data are not available, the nearshore wave climate can be obtained by mathematically transforming offshore wave data to the nearshore location. For this purpose, the India Meteorological Department (IMD) reported wave data observed by ships plying in the offshore region between latitude 20–25° N and longitude 65–75° E from 1986 to 2000 for 15 years were analyzed. This wave data information was considered at the offshore end of the model limits. The frequency

Table 1 % Occurrence of wave height and direction off Hazira for entire year (Jan–Dec)

Wave ht (m)	0–0.5	0.5–1	1–1.5	1.5–2	2–2.5	2.5–3	3–3.5	3.5–4	4–4.5	Total
Direction (°N)										
22.5	0.00	1.33	0.58	0.58	0.42	0.00	0.00	0.00	0.08	3.00
45	0.00	0.42	1.17	0.83	0.25	0.25	0.08	0.17	0.33	3.50
67.5	0.00	0.33	0.58	0.92	0.33	0.17	0.17	0.17	0.00	2.67
90	0.00	0.25	0.92	0.92	0.50	0.58	0.42	0.00	0.00	3.59
112.5	0.00	0.17	0.25	0.25	0.17	0.00	0.00	0.00	0.00	0.83
135	0.00	0.33	0.25	0.00	0.08	0.00	0.00	0.00	0.00	0.67
157.5	0.00	0.08	0.25	0.42	0.08	0.00	0.00	0.00	0.08	0.92
180	0.00	0.67	1.00	1.17	0.75	0.42	0.42	0.25	0.25	4.92
202.5	0.00	0.33	0.83	0.92	1.42	1.75	0.67	0.58	0.50	7.01
225	0.00	0.75	1.92	2.92	3.17	3.67	2.09	1.00	2.42	17.93
247.5	0.00	0.75	2.00	2.50	2.50	2.25	3.67	1.42	2.42	17.51
270	0.00	1.25	4.09	3.17	2.17	0.75	1.50	0.42	1.83	15.18
292.5	0.00	0.83	2.42	1.33	0.67	0.33	0.25	0.00	0.75	6.59
315	0.00	0.92	1.67	1.17	0.67	0.17	0.08	0.00	0.33	5.00
337.5	0.00	0.83	1.33	0.50	0.67	0.17	0.08	0.00	0.00	3.59
360	0.00	1.67	1.67	0.92	1.00	0.58	0.75	0.08	0.42	7.09
Total	0.0	10.9	20.9	18.5	14.8	11.1	10.2	4.1	9.4	100.0

distribution of wave heights from different directions during the entire year for the above offshore wave data is given in Table 1. A corresponding wave rose diagram is shown in Fig. 3.

The input wave directions and wave height in deep water are obtained from Table 1 and mentioned in Table 2. These deep water wave data were transformed using the mathematical model MIKE21-SW to get near shore wave climate near the harbor entrance.

3 Modeling Techniques

The mathematical models, viz. MIKE21-SW (wave transformation and wave propagation for existing condition) and MIKE21-BW (wave tranquility for proposed condition) were utilized for wave tranquility studies, LITDRIFT module of LITPACK software for littoral drift distribution and LITLINE module used for assessment of shoreline changes. Brief descriptions of these models are given below.

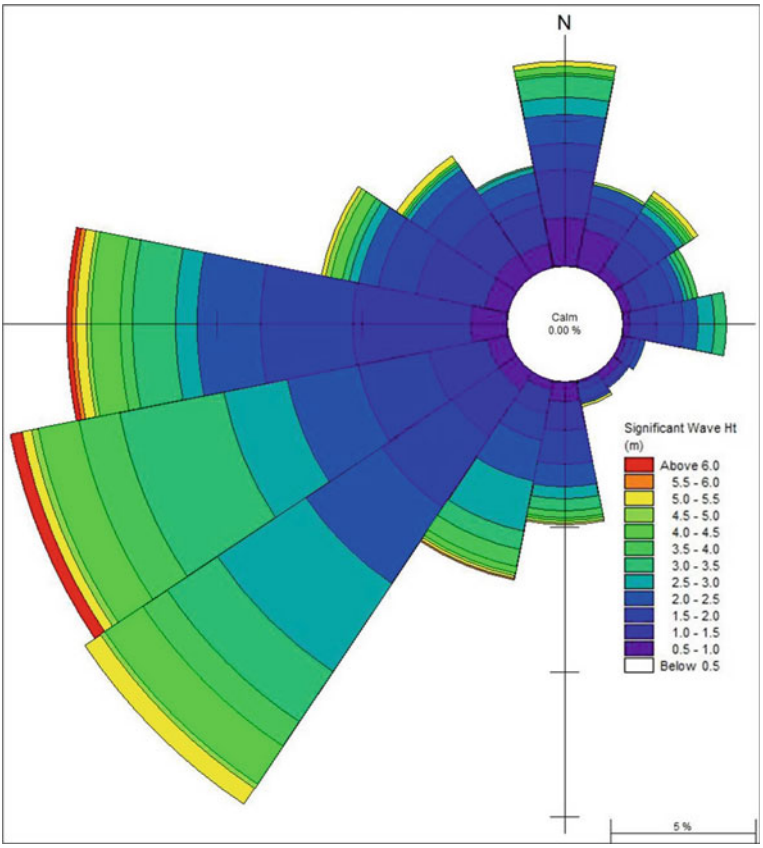

Fig. 3 Offshore rose diagram for entire year

Table 2 Input wave condition

Offshore direction (°N)	Wave height (m)	Offshore direction (°N)	Wave height (m)
22.5	2.5	202.5	4
45	4	225	4.5
67.5	3.5	247.5	4.5
90	3	270	4.5
112.5	2.5	292.5	4.5
135	2.5	315	4
157.5	2.5	337.5	3
180	4	360	4

3.1 MIKE21-SW Model

As waves travel from deep sea to shallow coastal waters, they undergo changes in direction and height due to the processes of refraction and shoaling. The computation of wave transformation from deep to shallow coastal waters was carried out using MIKE21-SW model. MIKE21-SW is a state-of-the-art third generation spectral wind wave model based on unstructured mesh. The model simulates the growth, decay and transformation of wind generated waves and swells in offshore and coastal areas. It takes into account refraction and shoaling of waves. It also includes physical phenomena of wave growth by action of wind, dissipation due to white-capping, dissipation due to bottom friction, and dissipation due to depth induced wave breaking. The effects of wave-current interaction, non-linear wave-wave interaction, time-varying water depth and diffraction are also included within the model. The model is based on flexible mesh which allows for coarse spatial resolution for offshore area and high-resolution mesh in shallow water and at the coastline [3].

3.2 MIKE21-BW Model

Mathematical model MIKE21-BW was used for studying the wave disturbance in the harbor area. The model is based on time dependent Boussinesq equations of conservation of mass and momentum obtained by integrating the three-dimensional flow equations without neglecting vertical acceleration. They operate in the time domain, so that irregular waves can be simulated. The frequency dispersion is included in the flow equations by taking into account the effect of vertical acceleration or the curvature of stream lines on pressure distribution. The model simulates the processes of shoaling, refraction, diffraction from breakwater tips and bed friction. It also takes into account partial reflections from the boundaries, piers and breakwaters [4].

3.3 LITPACK Model

LITPACK software is used for computation of littoral drift and simulation of shoreline changes due to construction of the breakwaters or any development on the shoreline, or due to any break in the sediment movement such as in the case of inlet. LITPACK is a professional engineering software package for the modeling of non-cohesive sediment transport in waves and currents, littoral drift, coastline evolution and profile development along quasi-uniform beach.

The LITDRIFT module simulates the cross-shore distribution of wave height, setup and longshore current for an arbitrary coastal profile. It provides a detailed deterministic description of the cross-shore distribution of the longshore sediment

transport for an arbitrary bathymetry for both regular and irregular sea states. The longshore and cross-shore momentum balance equation is solved to give the cross-shore distribution of longshore current and setup. Wave decay due to breaking is modeled, either by an empirical wave decay formula or by a model of Battjes and Janssen.

LITDRIFT calculates the net/gross littoral transport over a specific design period. Important factors, such as linking of the water level and the beach profile to the incident sea state, are included.

LITLINE simulates the coastal response to gradients in the longshore sediment transport capacity resulting from natural features and a wide variety of coastal structures. LITLINE predicts the coastline evolution by solving a continuity equation for the sediment in the littoral zone. The influence of structures, sources and sinks is included. With jetties and breakwaters, the influence of diffraction on the wave climate is also included [5].

4 Wave Transformation from Deep Water to Nearshore Region

In the absence of measured wave data near the proposed site of development, the nearshore wave climate at EBTL Hazira was obtained by transforming the ship observed deep water wave data using MIKE21-SW Model. Model area considered for MIKE21-SW model is shown in Fig. 4. Bathymetry in the model region of about 410 km by 260 km area was discretized using unstructured mesh. The model was run to obtain nearshore wave climate at the Inshore Point in (−) 20 m depth contour (Fig. 4). The wave directions and ratio of wave heights at (−) 20 m depth to deep water wave height, with different directions of wave incidence at the offshore boundary are given in Table 4. This transformation was applied to deep water wave data (Table 4) to obtain frequency distribution in (−) 20 m depth for entire year for the above offshore wave data which is given in Table 5. Corresponding wave rose diagrams are presented in Fig. 5. On the basis of wave transformation studies, it is clear that waves are incident from 180° N direction to 247.5° N at (−) 20 m depth. The following input wave conditions, given in Table 6, were considered for simulation of wave propagation in the proposed harbor using MIKE21-BW model and for existing condition using MIKE21-SW model at (−) 20 m depth.

5 Wave Tranquility Studies for the Existing and Proposed Condition

Wave propagation inside the harbor for existing condition was simulated using MIKE21-SW model for input wave conditions as given in Table 6. The bathymetry

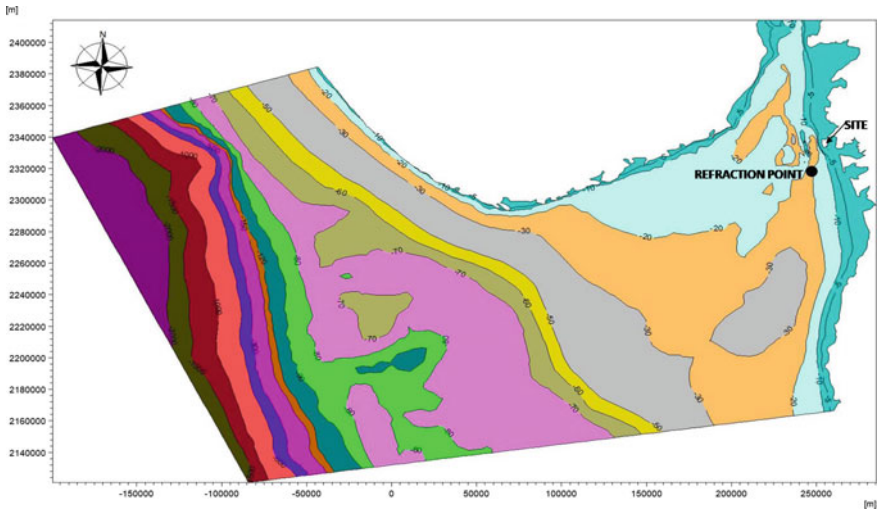

Fig. 4 Bathymetry for the wave transformation studies

Table 4 Wave transformation from deep to shallow coastal water

Sr. No	Offshore direction (Deg. N)	Inshore direction (Deg. N)	Wave height ratio (Hi/Ho)
1	90	181.465	0.0034
2	112.5	182.337	0.0177
3	135	184.626	0.0622
4	157.5	187.094	0.1832
5	180	191.105	0.4196
6	202.5	206.803	0.7099
7	225	224.817	0.5516
8	247.5	242.110	0.4240

Hi = Wave height at Inshore Point Ho = Offshore wave height

Table 5 % Occurrence of wave height and direction in Hazira for entire year (Jan–Dec)

Wave ht (m)	<0.5	<1	<1.5	<2	<2.5	<3.0	<3.5	<4.0	<4.5	Total
Direction (°N)									Calm	32.27
180	1.79	2.39	1.29	0.20	0.10	0.00	0.00	0.00	0.00	5.78
202.5	0.40	1.00	2.79	2.09	1.49	0.30	0.10	0.20	0.00	8.37
225	0.90	5.78	8.17	3.69	2.09	0.80	0.00	0.00	0.00	21.41
247.5	10.0	10.0	9.16	1.99	0.40	0.50	0.00	0.00	0.00	32.17
Total	13.1	19.2	21.41	7.97	4.08	1.59	0.10	0.20	0.00	100.0

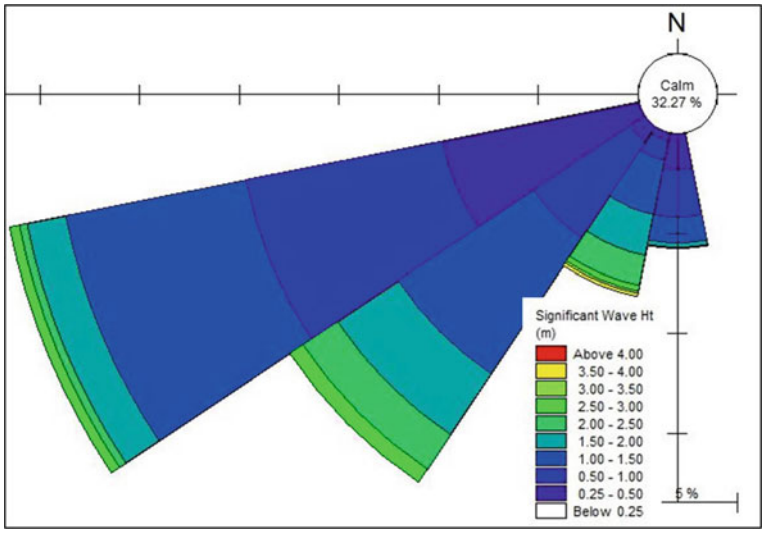

Fig. 5 Inshore rose diagram for entire year

Table 6 Design significant wave heights for wave tranquility studies

Wave direction (°N)	Significant wave height (m)
180	2.5
202.5	4
225	3
247.5	3

of area of 14 km × 24 km for MIKE21-SW model was prepared from C-MAP database and the nearshore bathymetry provided by authority as shown in Fig. 6. The plots for wave height distribution for the existing condition for predominant directions (SW and WSW) are shown in Fig. 7. The bathymetry for MIKE21-BW model for proposed condition was prepared from C-MAP database and the nearshore bathymetry provided by authority. Area of 15 km × 28 km was discretized with a grid of 5 m × 5 m as shown in Fig. 6. Simulation was carried out for tidal level + 4.5 m corresponding to MSL. The plots for wave height distribution and propagation for the proposed condition for predominant directions (SW and WSW) are shown in Fig. 8a, b.

It is seen that the waves are unable to reach the site hence the site of development will be tranquil considering the tranquility limit of 0.5 m. The wave tranquility studies to assess the wave tranquility at the site with proposed reclamation were carried out with the same predominant directions.

It is seen that the waves are unable to reach the site hence the site of development will be tranquil considering the tranquility limit of 0.5 m. The waves do not reach the site through the channel. The results indicate that, at the jetty location, the wave

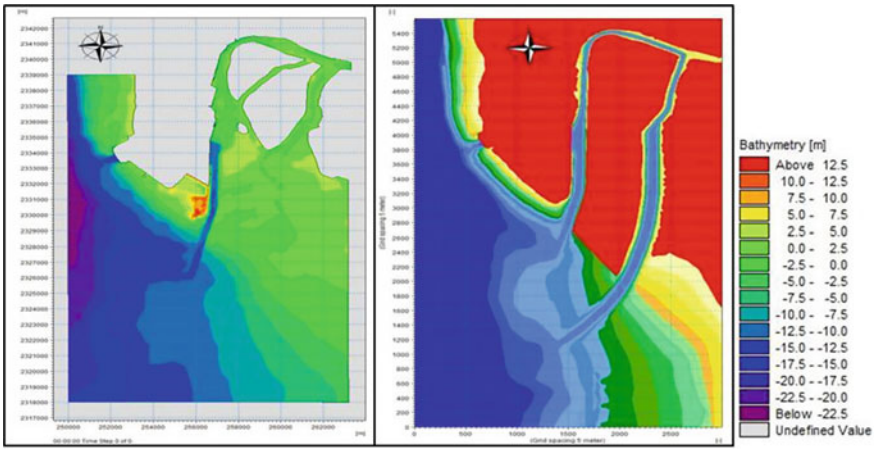

Fig. 6 Bathymetries for the wave tranquility studies for existing and proposed condition

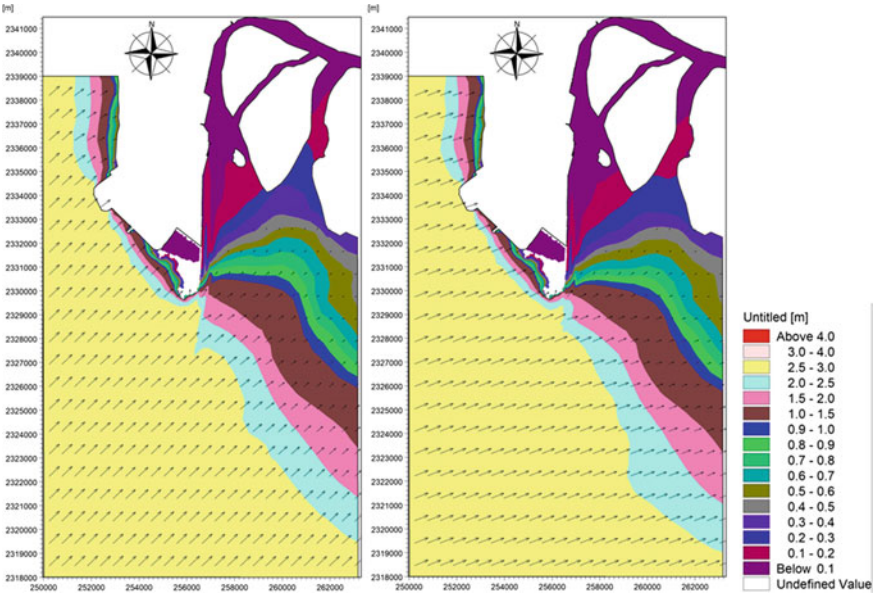

Fig. 7 Wave height and wave vector plot for wave's incident from SW and WSW direction with incident wave height 3.0 m for existing condition

heights are less than 0.5 m which is the permissible wave tranquility limit. The proposed development will be safe from the wave tranquility point of view throughout the year.

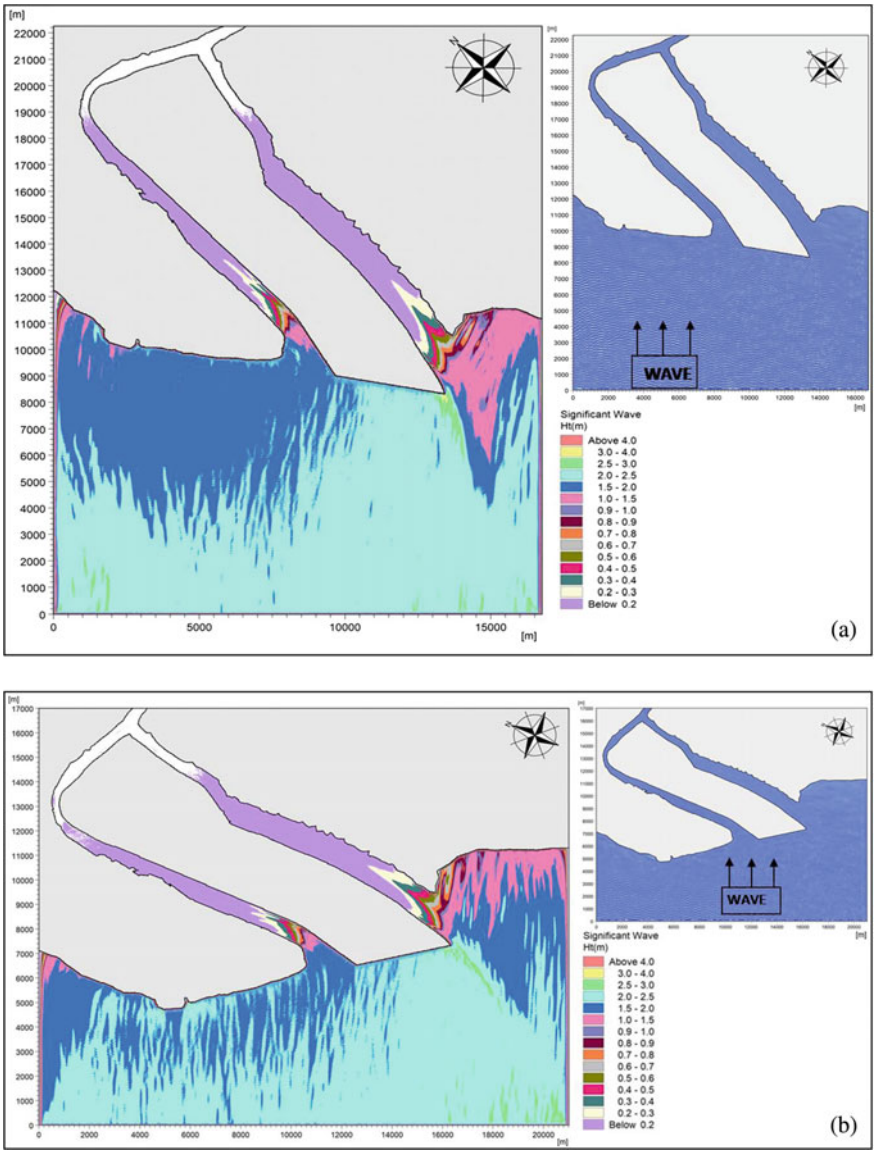

Fig. 8 **a** Wave height distribution and surface elevation plot for wave's incident from SW direction with incident wave height 3.0 m for proposed condition, **b** Wave height distribution and surface elevation plot for wave's incident from WSW direction with incident wave height 3.0 m for proposed condition

6 Littoral Drift Studies

It is understood from the earlier studies that the South Gujarat coast experiences a high sediment transport of the order of 1.52 Mm^3 [1]. Specifically, along the Valsad coast, the estimated southerly and northerly sediment transports are 0.594 and 0.98 Mm^3, respectively. It is seen that the drift is s northward direction. Valsad located near about 90 km from Hazira. The littoral drift study was conducted and a technical report No. 5845 was submitted in August 2020; the net drift 0.58 Mm^3 is reported [2]. The study of sediment movement along the shore is carried out by LITPACK model.

6.1 Estimation of Littoral Drift Rate

The littoral drift along the Hazira coast is estimated using LITDRIFT module of LITPACK software. The location of cross-shore profile is shown in Fig. 10. The profile is taken normal to the shoreline orientation. Littoral drift depends on the shoreline orientation and the near shore depth contours. Thus, the quantity of the drift changes with the orientation, and cross-shore bathymetry. The profile is normal to shoreline is at 225° N. The profile shown in Fig. 9 is prepared, and the littoral drift passing through this profile is calculated. The wave climates are prepared by extracting wave parameters at the (253,031 E, 2,330,975 N, −9.92 m depth). The profile shown in Fig. 9 covers a distance of 1650 m extending up to about −9.92 m depth contour (with respect to Chart Datum). The profile was discretized with grid size of 10 m. The ratio of wave height at the nearshore point (−9.92 m) to the incident wave height and inshore wave directions as given in Table 7 are obtained from the wave transformation studies explained in the paragraph 5.1. The annual wave climate table and the rose diagram are presented in the Table 8 and Fig. 10. When the wave heights are less than 0.2 5 m, the sea state is assumed to be calm, and the percentage of occurrence of waves less than 0.25 m constitutes calm percentage.

The model was simulated for period of one year to arrive at Northward and Southward drift. Littoral drift was computed and is shown in Fig. 11. The northward drift is plotted as positive while southward drift is plotted as negative. The northward, southward, net and gross transport rates are given in Table 9. Net drift is of the order of 0.147 million cum and is toward north, and gross transport is of the order of 0.874 million cum. The maximum transport occurs at −1.8 m depth contour. The surf zone is of the order of 450 m. The net drift may deposit in the channel at the East side of the reclamation. To minimize this problem, yearly maintenance dredging will be required.

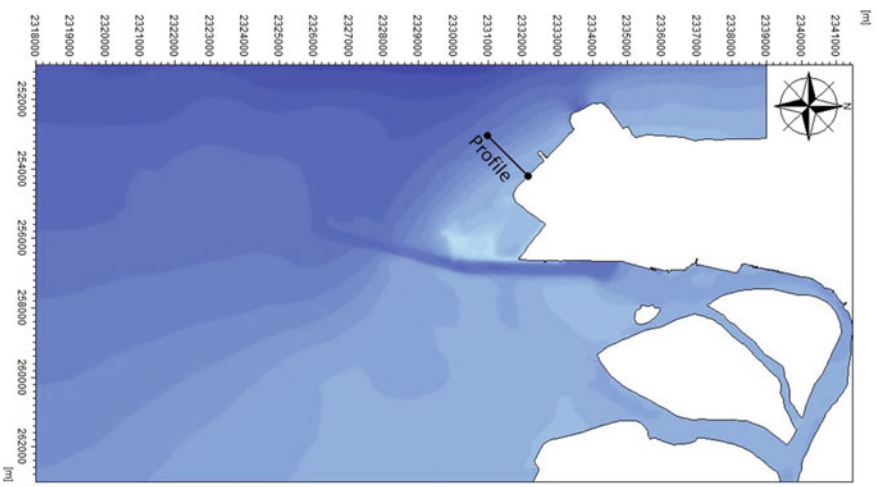

Fig. 9 Bathymetry near shoreline showing the profile

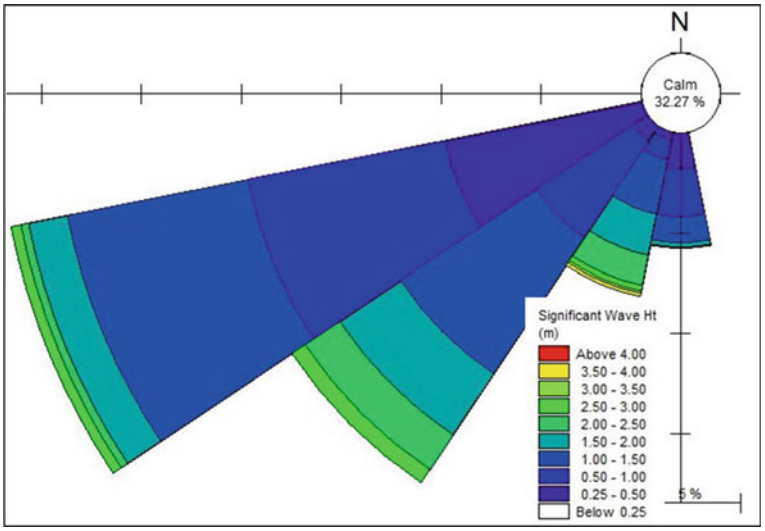

Fig. 10 Inshore wave rose diagram at profile

6.2 Shoreline Evolution

In order to assess the impact of the reclamation on the coastline, LITLINE module of LITPACK software was used for Hazira. The results are given below. The study of shoreline changes at Hazira due to the proposed reclamation shoreline of length 20 km was considered. Shoreline extended about 11 km toward north of the reclamation and

Table 7 Transformation from coastal water for south deep to shallow

Sr No	Offshore direction (Deg. N)	Inshore direction (Deg. N)	Wave height ratio (Hi/Ho)
1	112.5	187.426	0.0153
2	135	191.679	0.0533
3	157.5	195.041	0.1554
4	180	198.592	0.3552
5	202.5	209.236	0.6346
6	225	224.699	0.4702
7	247.5	241.551	0.3675
8	270	244.336	0.1549
9	292.5	244.745	0.0482
10	315	242.122	0.0124

Table 8 % Occurrence of wave height and direction in Hazira for entire year (Jan–Dec)

Wave ht (m)	<0.5	<1	<1.5	<2	<2.5	<3	<3.5	<4	<4.5	Total
Direction (°N)									Calm	32.03%
202.5	1.85	5.45	2.83	3.38	0.76	0.44	0.22	0.00	0.00	14.92
225	2.51	7.95	7.52	3.38	1.09	0.00	0.00	0.00	0.00	22.44
247.5	8.39	12.42	8.50	0.76	0.54	0.00	0.00	0.00	0.00	30.61
Total	12.75	25.82	18.85	7.52	2.40	0.44	0.22	0.00	0.00	100.00

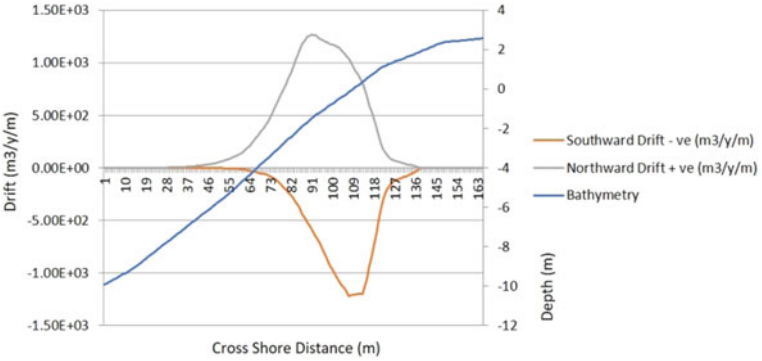

Fig. 11 Annual northern and southern littoral drift for entire year

Table 9 Littoral transport rates (million m^3/year) for South

Season	Northward	Southward	Net *
Annual	0.51	0.36	0.147

Note *For the net drift '+ve' Northward '−ve' Southward

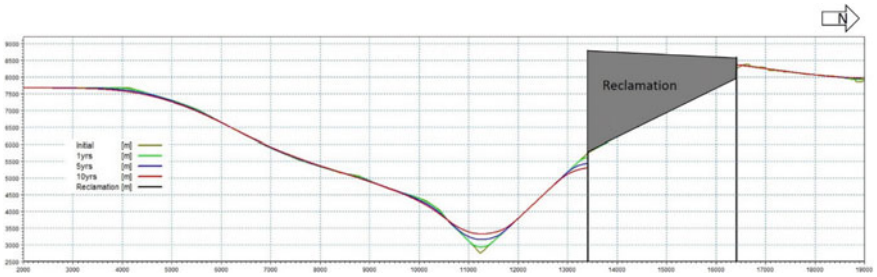

Fig. 12 Shoreline evolution for Hazira

about 9 km toward south of the reclamation. It was divided into 2000 grid points of grid size 10 m. Since LITPACK is a one-dimensional model, hence shore connected breakwaters are assumed as obstructions which are perpendicular to shoreline. The proposed reclamation was represented by two breakwaters with the blocking length of 3000 m and 1000 m with one offshore breakwater joining both the tips of the breakwater which extends clearly beyond surf zone. The model was run for 1, 5 and 10 years with the proposed reclamation as shown in Fig. 12.

7 Conclusions

- The predominant wave directions in deep water are 22.5° N to 360° N with maximum wave heights of 4.5 m were obtained by analyzing 15 years IMD data for Latitude 20–25° N and Longitude 65–75° E for the wave transformation study.
- Wave propagation studies were carried out for transformation of deep to (−) 20 m depth (Table 1D and Fig. 3D) showed that the predominant directions of wave approach at the site of development are South, SSW, SW and WSW with incident wave height 2.5 m, 4.0 m, 3.0 m and 3.0 m, respectively.
- Wave tranquility studies carried with existing and proposed layout of reclamation 4600 ha and Dumas channel with a width of 800 m and depth of 12 m below CD extending up to −12.0 m contour which is about 15 km long. The results show that the jetty and development area are tranquil with respect to wave disturbance considering the permissible limit of 0.5 m. Thus, the area of jetty will be tranquil throughout the year with proposed reclamation and channel.
- The cross-shore profile with the angle normal to the coast 2250N is considered for littoral drift study. The LITPACK model was run for annual period. Annual northward and southward, transport rates were computed for this profile.
- Net transport in a year is of the order of 0.147 million cum and is toward north, and gross transport is of the order of 0.847 million cum. The maximum transport occurs at −1.8 m depth contour. The surf zone is of the order of 450 m. The net drift may deposit in the channel East side of the reclamation. To minimize this problem, yearly maintenance dredging will required.

- For shoreline evolution, LITLINE model was run for 1, 5 and 10 years with the proposed reclamation. It is seen that the sediment will be deposited at north side of proposed reclamation and eroded at south side of proposed reclamation with increasing trend of deposition and erosion periodically.
- Considering all the three aspects of wave tranquility, littoral drift and shoreline evolution, it can be concluded that the reclamation for port city development is feasible with maintenance dredging and monitoring the changes in the shoreline periodically so that suitable remedial measures can be adopted.

Acknowledgements The authors are thankful to the Director, CWPRS, for his kind permission for publication of this paper.

References

1. Nayak BU and Chandramohan P (1992) A longshore sediment transport estimation for the Indian coast. Physical Processes in the Indian Sea. In: Proceedings of first convention of ISPSO
2. CWPRS Technical Report No 5845 (2020) Mathematical model studies for wave tranquility and shoreline changes due to reclamation proposed by M/S EBTL at Hazira, Gujarat
3. DHI, Denmark (2020) MIKE 21 SW model-user reference manuals
4. DHI, Denmark (2020) MIKE 21 BW model-user reference manuals
5. DHI, Denmark (2020) MIKE 21 LITPACK model-user reference manuals

River-Bay Model for Simulating the Compound Effect of River Flow and Storm Surges

B. Sridharan and Soumendra Nath Kuiry

Abstract Coastal flooding caused by riverine flow or storm surges, or the combined river flow and storm surges induced by tropical cyclones produce significant causalities and huge loss of properties in low-lying areas. The successive or co-occurrence of riverine flow and storm surges exacerbates the flood risk more than due to individual occurrences. The efforts to reduce the aftereffect of coastal flooding motivated many studies to simulate compound floods using the combinations of hydrodynamic and hydraulic models. These models are combined in loosely coupled or tightly coupled ways. Due to its faster computations, the existing studies often employed the loosely coupled model developed using the 2D storm surge model and 2D flood models or simple 1D–2D research codes. So far, the suitability of the loosely coupled approach to analyse the compound flood effects from river flow and storm surge has not been dealt with in detail. Further, the models developed based on the tightly coupled approach are very few, and their application has proven that these models suffer from model instability and computational burden. Therefore, an unstructured grid-based river-bay model is developed in this study for the stable and efficient simulation of coastal floods.

Keywords Coastal flooding · River flow · Storm surges · Loosely coupled model · Tightly coupled model

1 Introduction

Flooding is a natural disaster that has resulted in damage of U.S. $24 billion per year, with more than 220,000 fatalities worldwide [1, 2]. The flood risk is expected to worsen in the upcoming years due to sea-level rise [3], urban expansion of the coastal cities and climate change [4]. The flooding in the low-lying area occurs mainly from two sources such as storm surges and fluvial floods in the inland region. The simultaneous or successive occurrence of storm surges of tropical cyclones and

B. Sridharan · S. Nath Kuiry (✉)
Department of Civil Engineering, Indian Institute of Technology Madras, Chennai 600036, India
e-mail: snkuiry@civil.iitm.ac.in

P. V. Timbadiya et al. (eds.), *Coastal, Harbour and Ocean Engineering*, Lecture Notes in Civil Engineering 321, https://doi.org/10.1007/978-981-19-9913-0_10

fluvial flood flooding resulting from torrential rainfalls is called compound floods, and such events are termed compound events. Compound floods exacerbate the flood risk more than individual occurrences of river flow and storm surges. Therefore, it is mandatory to understand compound floods to develop a reliable flood prediction system.

The two primary approaches to simulating compound flooding are (i) decoupled or one-way coupling approach and (ii) tightly coupled or two-way coupling approach. The storm surge is first simulated on the ocean side by forcing the cyclonic wind and pressure data in the decoupled approach. The results from the storm surge model are then input into the inland flood model as boundary conditions. Finally, the inland model simulates the combined flood effects in the inland region. Extensive research works are available on the development of inland flood models (e.g. HEC-RAS: [5]; MIKE21: [6]; TELEMAC: [7]; LISFLOOD-FP: [8]; IITMFLO-2D: [9, 10]) and storm surge models (e.g. ADCIRC: [11]; FVCOM: [12]; SELFE: [13]; IITD 2D storm surge model: [14]). The research attempts to develop the combined river-bay model are very sparse [15–18]. The exiting combined river-bay simulation models suffer from instability problems and substantial computational costs. The shortcomings of existing studies are enlisted below.

- The suitability of the existing riverine flow models for urban areas is suspected of posing computational time and numerical stability problems. This is due to the requirement of high-resolution simulations to handle the detailed representation of topographical features. This aspect of inland modelling demands consideration.
- The existing storm surge models need too many iterations to generate a mesh that yields a stable solution and hence suffers from instability issues.
- The inland model chosen for combined flood simulation studies is mostly freely available 2D or 1D–2D numerical models and research codes. Little attention has been paid to hydraulic models used in the river-bay framework.
- The suitability of the two coupling approaches in simulating the compound flood has been not addressed.

Therefore, this research focuses on developing an unstructured grid-based two-dimensional river-bay model for stable and efficient simulation of surge and inundation. This work is organized as follows: first, the governing equations and the numerical schemes are described. Then, the developed model is validated for wind and surge height by simulating the historical cyclone, Thane. Then, developed IITMflo-S2D model is applied to simulate the compound flood. Finally, the summary and conclusions are discussed.

2 Governing Equations and Methods

The proposed storm surge model is developed by solving two-dimensional (2D) shallow water equations (SWEs). The governing 2D equations can be written as

$$\frac{\partial h}{\partial t} + \frac{\partial (q_x)}{\partial x} + \frac{\partial (q_y)}{\partial y} = 0 \tag{1}$$

$$\frac{\partial (q_x)}{\partial t} + \frac{\partial}{\partial x}\left(\frac{q_x^2}{h}\right) + \frac{\partial}{\partial y}\left(\frac{q_x q_y}{h}\right) = \mu\left(\frac{\partial^2 (hu)}{\partial x^2} + \frac{\partial^2 (hu)}{\partial y^2}\right) - gh\frac{\partial}{\partial x}\left(\frac{P_s}{\rho g}\right) + f(hv) + ghS_{0x} - \tau_{bx} + \tau_{sx} \tag{2}$$

$$\frac{\partial (q_y)}{\partial t} + \frac{\partial}{\partial x}\left(\frac{q_x q_y}{h}\right) + \frac{\partial}{\partial y}\left(\frac{q_y^2}{h}\right) = \mu\left(\frac{\partial^2 (hu)}{\partial x^2} + \frac{\partial^2 (hu)}{\partial y^2}\right) - gh\frac{\partial}{\partial y}\left(\frac{P_s}{\rho g}\right) - f(hu) + ghS_{0y} - \tau_{by} + \tau_{sy} \tag{3}$$

where h is water depth above the bed; q_x and q_y are unit discharges along x– and y–directions and g is acceleration due to gravity. μ is eddy viscosity coefficient; P_s denotes atmospheric pressure; ρ represents density of water; $f = 2\omega sin\phi$ is Coriolis parameter, wherein the angular frequency of earth rotation is ω and ϕ is the latitude, $S_{0x} = -\partial z/\partial x$ and $S_{0y} = -\partial z/\partial y$ are bed slopes; τ_{bx} and τ_{by} are bottom friction coefficients; τ_{sx} and τ_{sy} are the surface wind stresses, along x- and y-directions, respectively (Fig. 1).

These equations are solved numerically using the finite volume discretization scheme. For this purpose, the computational domain is divided into finite number of triangular cells. Then, the equations are integrated in space (over triangular cell) using Green-Gauss theorem and in time using Euler forward time marching scheme to obtain

$$\frac{h_i^{n+1} - h_i^n}{\Delta t} A_i + \sum_{j \in k_i} Q_{ij}^n = 0 \tag{4}$$

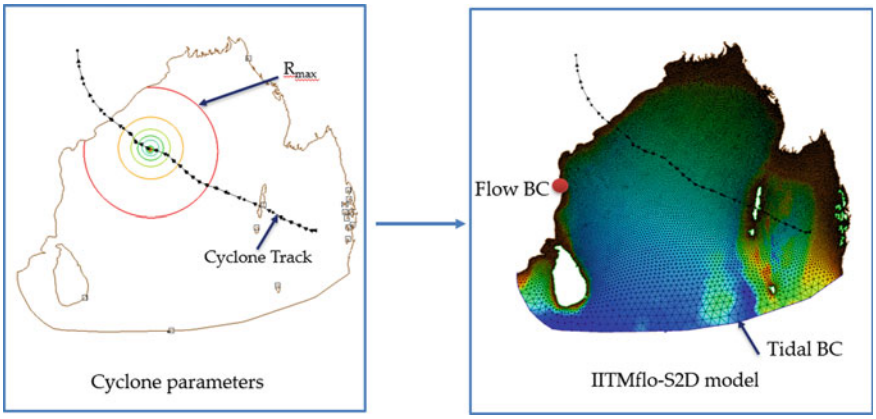

Fig. 1 Model set-up of the IITMflo-S2D model

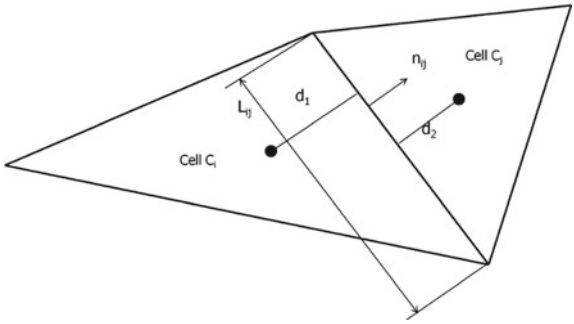

Fig. 2 Finite-volume discretization used in the present work

$$\frac{q_{x,i}^{n+1} - q_{x,i}^{n}}{\Delta t} A_i + \sum_{j \in k_i} F_{x,ij}^{n} = (T_{x,i}^{n+1} - g h_i^n S_{x,i}^{n}) A_i \tag{5}$$

$$\frac{q_{y,i}^{n+1} - q_{y,i}^{n}}{\Delta t} A_i + \sum_{j \in k_i} F_{y,ij}^{n} = (T_{y,i}^{n+1} - g h_i^n S_{y,i}^{n}) A_i \tag{6}$$

where Ki accounts for all interfaces of the considered cell C_i (as shown in Fig. 2) and A_i is the area of the cell Ci, Q_{ij} is the numerical approximation of the mass fluxes and $F_{x,ij}$, $F_{y,ij}$ are, respectively, x– and y–directions momentum fluxes, $S_{\mathrm{x,i}}$ and $S_{\mathrm{y,i}}$ are bed slope terms along x– and y–directions, $T_{x,i}$ and $T_{y,i}$ are source terms (i.e. bottom friction, Coriolis and wind stress and atmospheric pressure). A simple upwinding scheme is used to compute the fluxes, which aids in improving the stability of the model in the wetting–drying front. The bed slope term is discretized using the centred scheme.

The overall framework of the IITMflo-S2D model is shown in Fig. 3. The primary inputs required computational mesh, wind field, pressure field and tidal (downstream) boundary conditions. Software like SMS and the BlueKenue model can be used to discretize the computational domain into triangular cells. The elevations of the triangular cells are interpolated using the 30 arc second bathymetry data from the General Bathymetric Chart of the Oceans. The tidal boundary condition is imposed along the open sea using the LeProvost database. The cyclonic wind and pressure fields are generated with the help of the Holland wind model [19] generated within the IITMflo-S2D model using cyclone track data.

3 Results and Discussion

The performance of the proposed model IITMflo-S2D is first validated for wind velocity and then for storm surge height using the Thane cyclone. Finally, compound floods in the Adyar River are simulated using the proposed river-bay model IITMflo-S2D.

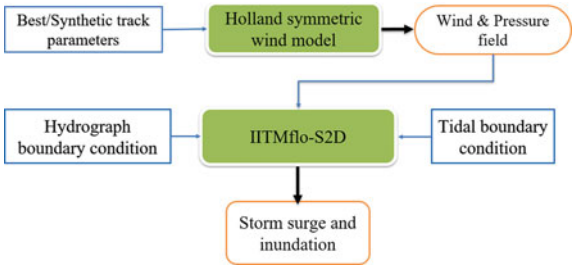

Fig. 3 Overall framework of the IIMflo-S2D model

3.1 Validation of IITMflo-S2D for Cyclonic Wind

The wind component of the IITMflo-S2D model is validated by simulating the cyclone, Thane. This cyclone started its journey on 25 October and continued to intensify. On 28 October, (IMD) India Meteorological Department reported it as a severe cyclonic storm. On 30 October, it made landfall between Cuddalore and Pondicherry along the Tamil Nadu coast. The maximum wind speed was 120 km/h, and the minimum central pressure was 956 MB. Figure 4 shows the historical track of Thane downloaded from the Joint typhoon warning centre.

Figure 5 shows the simulated wind fields at different instances during the Thane cyclone. These wind fields are reported here to compare the simulated maximum wind speed against the observed one. The observed maximum wind speed (reported by IMD) of the Thane cyclone is 38.55 m/s. Figure 5 shows that the simulated wind speed of 40.3 m/s closely matches the reported maximum wind speed. Further, to

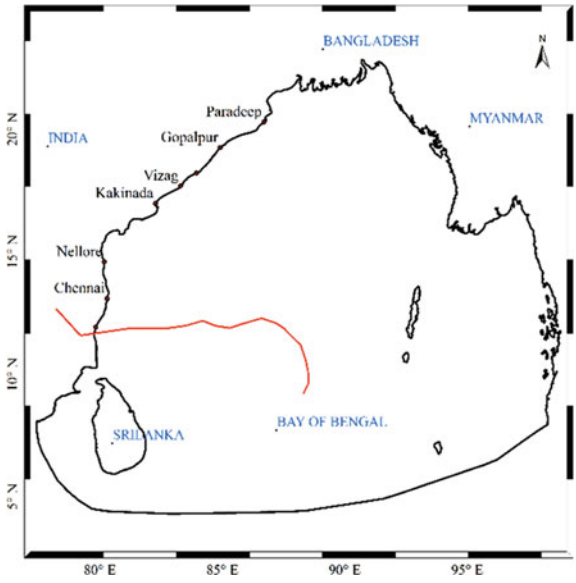

Fig. 4 Best track of Thane cyclone

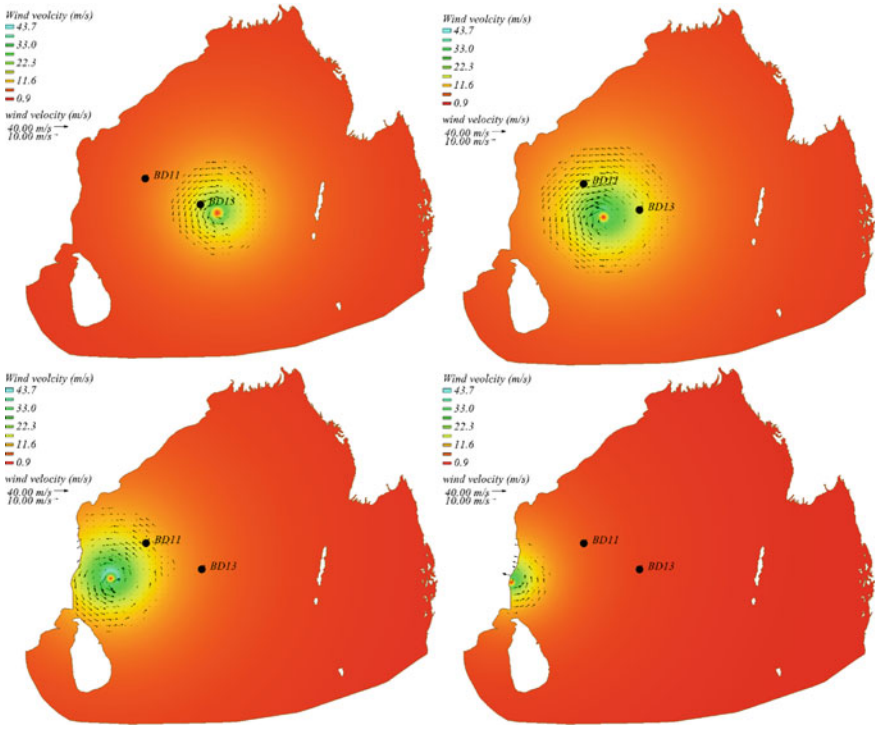

Fig. 5 Simulated wind field during Thane cyclone

quantify the accuracy, the time series of the wind data are compared at two buoys, BD11 and BD13. At station BD11, the simulated time series matches the observed wind data between 18 and 70 h, as seen in Fig. 6a. There is a small under-prediction at the beginning and towards the end because the parametric wind model tends to under-predict the wind speed when the radial distance (i.e. wind station location) is far away from the eye of the cyclone. At station BD13, the simulated wind time series agree well with the observed data (Fig. 6b). Overall, it is clear that the wind component of the IITMflo-S2D can reproduce the wind data, and it, therefore, can be used for storm surge simulations.

3.2 Validation of IITMflo-S2D for Storm Surge

The proposed IITMflo-S2D is now applied to simulate surge due to the Thane cyclone. Figure 7 shows the computational domain chosen for the simulation. The domain extends up to 1320 km along the coastal line and 1050 km in the offshore direction. It is discretized into 170,000 elements and 86,000 nodes (Fig. 7a) using a triangular mesh with a spatial resolution varying from 200 m along the mainland to 25 km

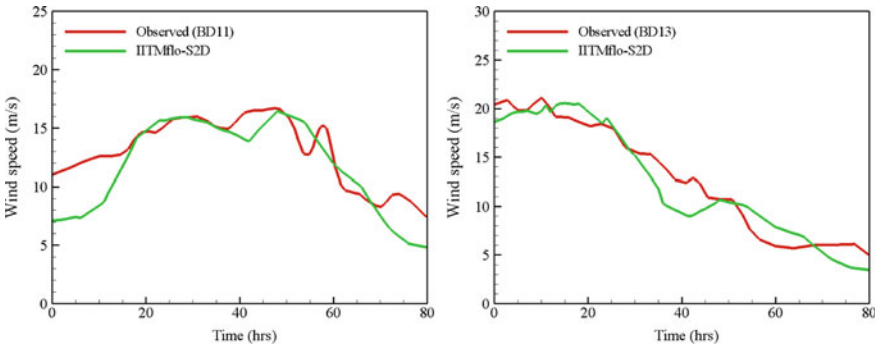

Fig. 6 Validation of wind model in IITMflo-S2D against BD11 and BD13 buoy records during Thane cyclone

along the open boundary [20]. Bathymetry data from GEBCO is used to interpolate the modal elevation of the discretized domain (Fig. 7b). Tidal boundary condition is imposed at the open boundary. The wetting–drying boundary is assigned towards the coast.

The simulated maximum surge height (Fig. 8) of 1.0 m by the IITMflo-S2D shows a good agreement with that reported by both IMD (1–1.4 m) and Baskaran et al. (2014) (1.15 m). The simulated water levels are compared at Ennore and Nagapattinam tide gauges maintained by INCOIS. The computed waters agree with the observed data with the root mean square error of 0.10 m and 0.13 m, respectively, at Ennore and Nagapattinam (Fig. 9). Also, the simulated water levels are in good agreement with Bhaskaran et al. [20]. Hence, it can be concluded that the IITMflo-S2D accurately predicts the general surge trend during cyclone Thane.

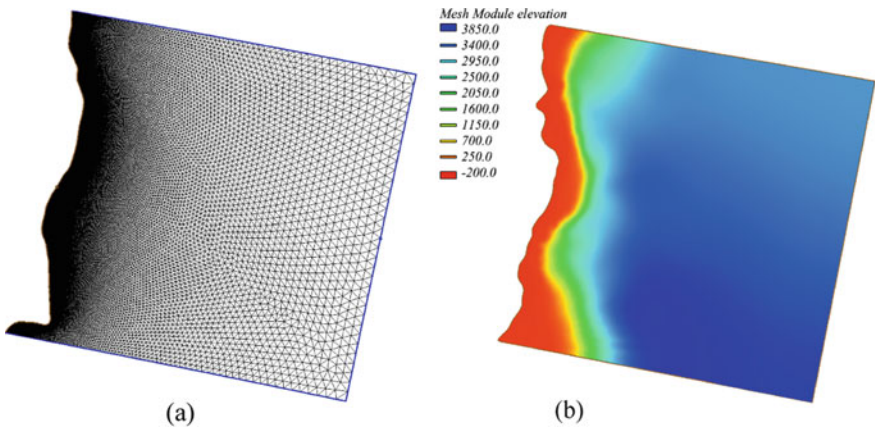

Fig. 7 **a** Unstructured triangular mesh used for Thane cyclone and **b** bathymetry of the study domain

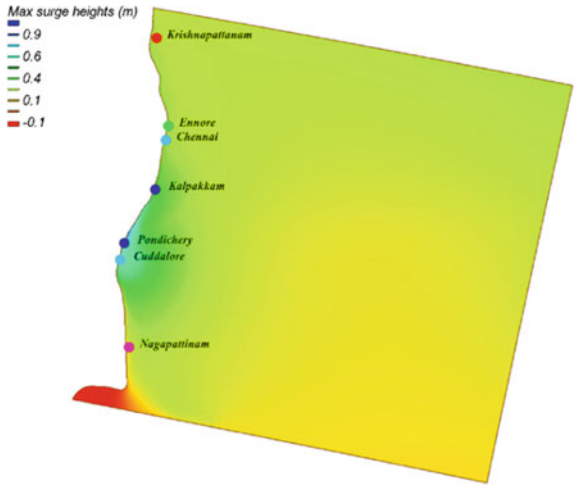

Fig. 8 Maximum surge heights obtained using IIMTflo-S2D model (in m)

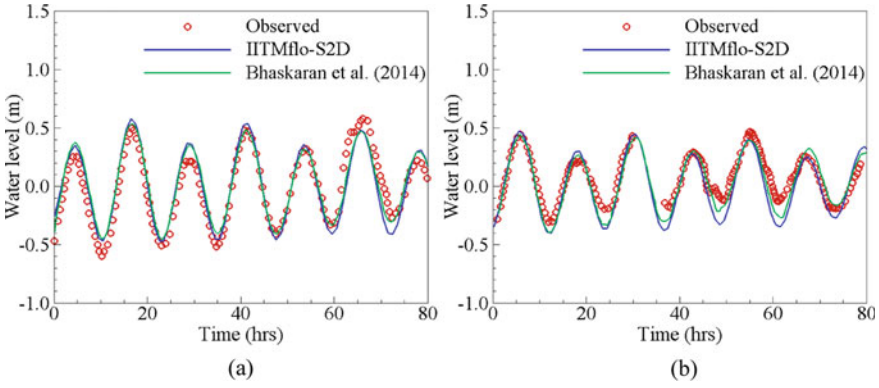

Fig. 9 Comparison of simulated and observed water level during Thane at **a** Ennore and **b** Nagapattinam

3.3 Application of the IITMflo-S2D Model

The developed model is applied to the Adyar River, which discharges into BoB in Chennai. The combined river-bay simulations are done using hypothetical events due to the absence of direct cyclone hits in the Adyar river bay. Among many possible scenarios of a cyclone hit, the worst-case scenario is selected for analysis. Hydrographs of different return periods (Fig. 10a) are imposed to specify the flow boundary condition. Synthetic tracks (Fig. 10b) are used to derive the surge boundary conditions (i.e. at the downstream of the inland model). The Adyar River experiences the maximum surge heights when the synthetic cyclone makes landfall 25 km away

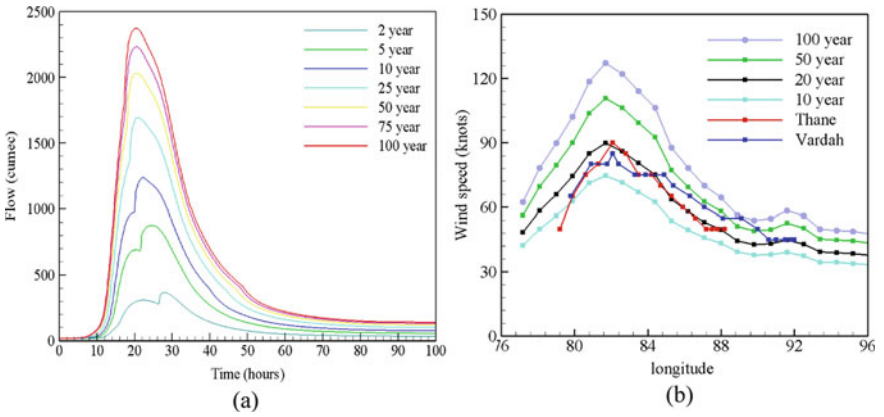

Fig. 10 **a** Upstream hydrograph and synthetic cyclone track used in the river-bay simulation

in the south direction. After identifying the worse-case landfall location, the river-bay interaction in the Adyar River is simulated using tightly coupled and decoupled river-bay models. The tightly coupled model uses the same computational domain (Fig. 11a) to simulate inland flood and storm surge. The decoupled model is an alternative to a tightly coupled model, wherein the compound flood mechanism is carried out by transferring the result of the surge model to the inland flood model (Fig. 11b) as a boundary condition.

In the case of decoupled model, the upstream boundary of the surge model is taken either at the coastline or a 10 m line along the coast as in previous studies on storm surge models. However, neither of these upstream boundaries can resolve the

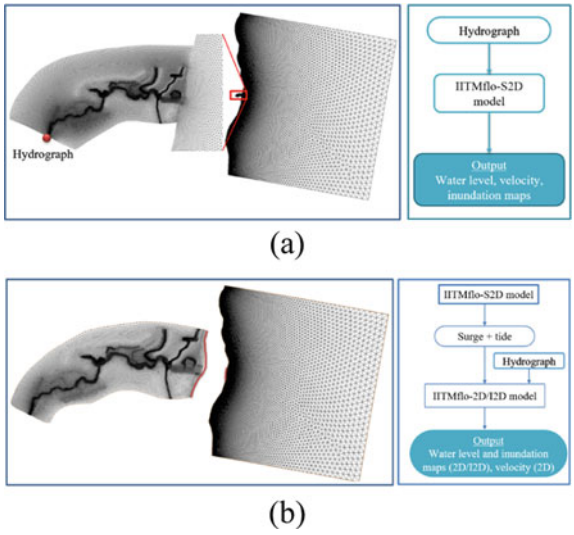

Fig. 11 **a** Tightly coupled and **b** traditional loosely coupled river-bay model

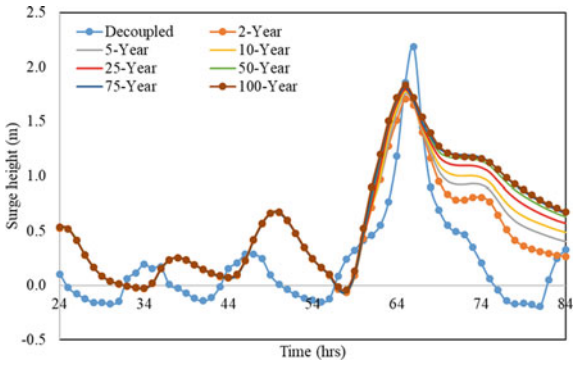

Fig. 12 Storm surge for decoupled model and tightly coupled model (shown as 2–100-year) for 100-year wind speed (~120 knots)

river mouth as the inland and storm surge model works independently. This leads to over-prediction of surge height as shown in Fig. 12, for they either create a virtual wall piling up the water in the seaside or ignore the surge propagation inside the river. Further, the over-predicted time series lead to subsequent over-prediction of the inundation extent as shown in Fig. 13.

There are no attempts done to address this over-prediction aspect in decoupled modelling approach. For this purpose, the computational domain is extended up to the region of the influence of the surge. Identifying this region of influence is a trial-and-error process in decoupled approach. It is a straightforward task in the tightly coupled river-bay model, as it considers the non-linear interaction of the surge and river flow. Therefore, the region of influence identified from the coupled model is used directly in the decoupled approach. It is found that inside the Adyar River, the surge influence is felt up to Jafferkhanpet. The inclusion of region of influence in the traditional decoupled approach helps to combat the over-estimation of surge characteristics. However, the computational time increases by 1.1 times when compared to the traditional one. Nevertheless, the results from the modified decoupled approach show slight under-prediction of inundation extent and surge time series. On the other hand, the tightly coupled approach can capture the non-linear interaction of the compound flooding more realistically with a slight increase (<5\%) in computational time compared to the modified decoupled approach. Hence, it is clear that the use of tightly coupled is necessary to capture the river-bay interaction that is closer to reality. The flooding due to a 50-year synthetic track for various return period hydrographs is shown in Fig. 14.

4 Conclusions

A novel coupled river-bay model is developed in this study using 2D SWES, and it is named as IITMflo-S2D model. The developed model is validated for wind storm surge height using the historical cyclone Thane. Then it is applied to simulate compound

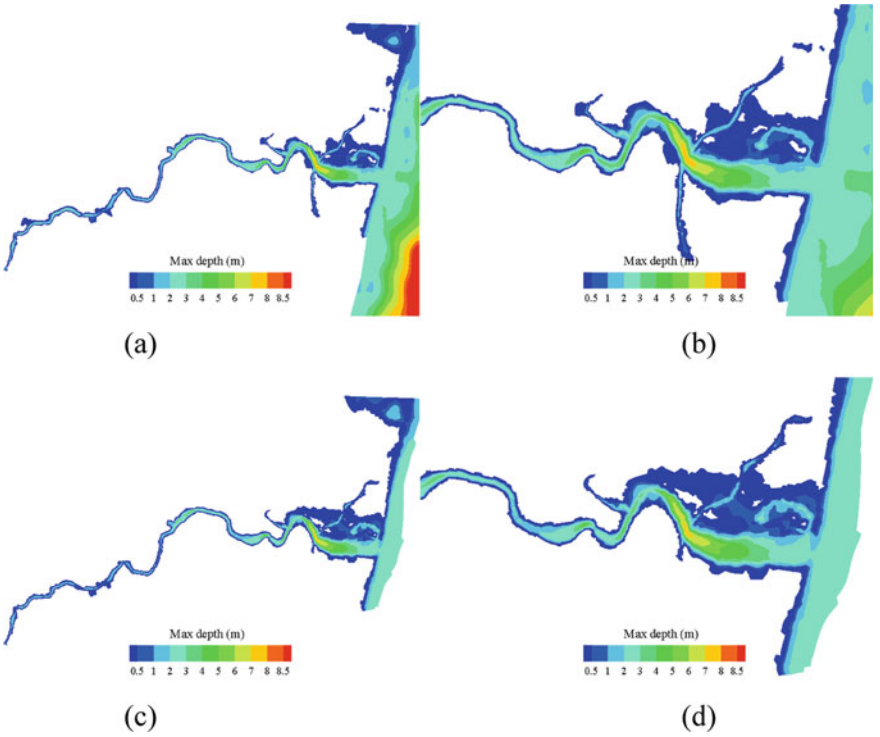

Fig. 13 Inundation map: **a** tightly coupled model, **b** closer view of **a**, **c** loosely coupled river-bay model and **d** closer view of **c** for 2-year hydrograph and 100-year wind combination

flood in the Adyar River. Since no actual events are available in the selected area, hypothetical events are generated using synthetic tracks. The tightly coupled and the traditional loosely coupled river-bay models are applied to simulate storm surge in the Adyar River basin along the BoB coast. Results show that the impact of surge increases with the increase in the wind speed in the downstream boundary. Further, the surge effect is modified depending on the magnitude of the hydrograph (i.e. higher the magnitude of the hydrograph, the lower will be the surge). These varying effects of different upstream boundary conditions make it clear that the existing decoupled models cannot capture the river-bay interaction's real nature. Hence, it is suggested to use a tightly coupled approach by accepting the small increase of computational effort. The validation and application of the developed models prove their robust nature and appropriateness to simulate river-bay interactions with reasonable accuracy at any area of interest.

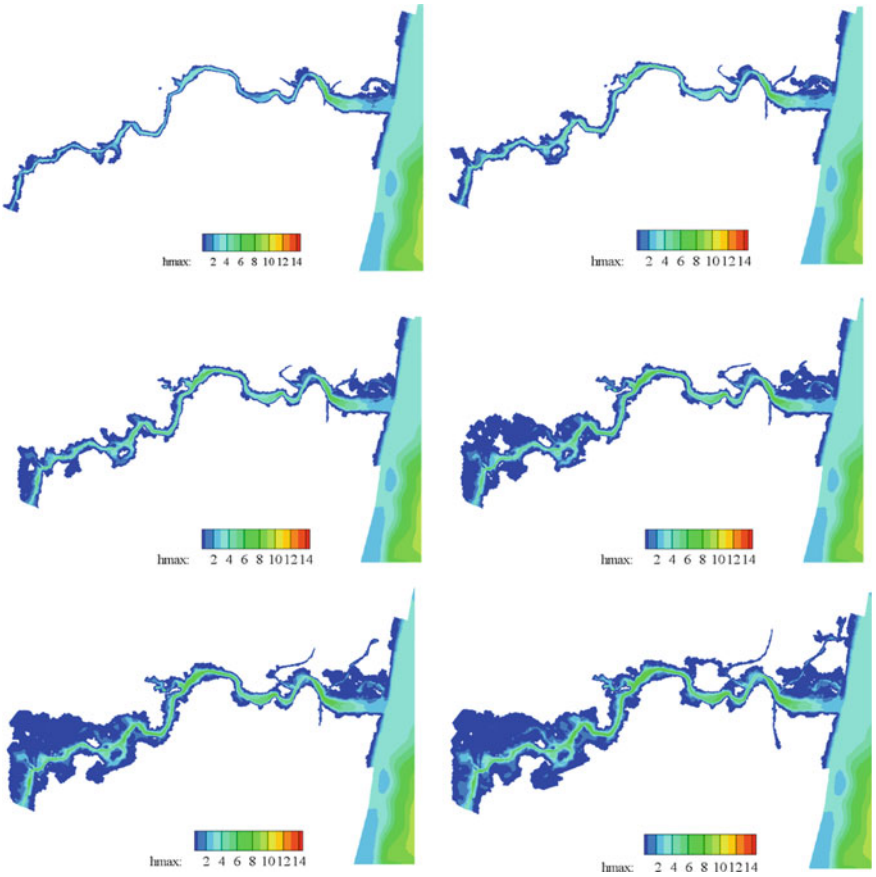

Fig. 14 Comparison of inundation map for 50-year return period wind sped with

Acknowledgements This research is funded by the Department of Science and Technology, India, under the SPLCIE climate change programme through the Grant No.DST/CCP/CoE/141/2018c.

References

1. Kundzewicz ZW, Kanae S, Seneviratne SI, Handmer J, Nicholls N, Peduzzi P et al (2014) Le risque d'inondation et les per- spectives de changement climatique mondial et régional. Hydrol Sci J 59:1–28. https://doi.org/10.1080/02626667.2013.857411
2. Winsemius HC, Aerts JCJH, Van Beek LPH, Bierkens MFP, Bouwman A, Jongman B et al (2016) Global drivers of future river flood risk. Nat Clim Change 6:381–385. https://doi.org/10.1038/nclimate2893
3. Nicholls RJ, Cazenave A (2010) Sea-level rise and its impact on coastal zones. Science 80(328):1517–1519. NOAA

4. Hallegatte S, Green C, Nicholls RJ, Corfee-Morlot J (2013) Future flood losses in major coastal cities. Nat Clim Change 3:802
5. Brunner GW (2016) HEC-RAS river analysis system, hydraulic reference manual (Version 5), US Army Corps of Engineers, Davis (2016). https://apps.dtic.mil/dtic/tr/fulltext/u2/a311952.pdf
6. Doan QT, Nguyen CD, Chen YC, Mishra PK (2015) Application of environmental sensitivity index (ESI) maps of shorelines to coastal oil spills: a case study of Cat Ba Island Vietnam. J Environ Earth Sci 74(4):3433–3451
7. Hervouet JM, Van Haren L (1996) Recent advances in numerical methods for fluid flows. Floodplain processes, 183–214
8. Bates PD, Horritt MS, Fewtrell TJ (2010) A simple inertial formulation of the shallow water equations for efficient two-dimensional flood inundation modelling. J Hydrol 387(1–2):33–45. https://doi.org/10.1016/j.jhydrol.2010.03.027
9. Sridharan B, Bates PD, Sen D, Kuiry SN (2021) Local-inertial shallow water model on unstructured triangular grids. Adv Water Resour 103930
10. Sridharan B, Gurivindapalli D, Kuiry SN, Mali VK, Nithila Devi N, Bates PD, Sen D (2020) Explicit expression of weighting factor for improved estimation of numerical flux in local inertial models. Water Resour Res 56(7):e2020WR027357
11. Luettich Jr, RA, Westerink JJ, Scheffner NW (1992) ADCIRC: an advanced three-dimensional circulation model for shelves, coasts, and estuaries. report 1. Theory and methodology of adcirc-2ddi and adcirc-3dl. Technical report, Coastal engineering research center Vicksburg, MS
12. Chen C, Liu H, Beardsley RC (2003) An unstructured grid, finite-volume, three-dimensional, primitive equations ocean model: application to coastal ocean and estuaries. J Atmos Oceanic Tech 20(1):159–186
13. Zhang Y, Baptista AM (2008) SELFE: a semi-implicit Eulerian-Lagrangian finite-element model for cross-scale ocean circulation. Ocean Model 21(3–4):71–96
14. Dube SK, Sinha PC, Roy GD (1985) The numerical simulation of storm surges along the Bangladesh coast. Dyn Atmos Oceans 9(2):121–133
15. Bunya S, Dietrich JC, Westerink JJ, Ebersole BA, Smith JM, Atkinson JH, ... Roberts HJ (2010) A high-resolution coupled riverine flow, tide, wind, wind wave, and storm surge model for southern Louisiana and Mississippi. Part I: model development and validation. Mon Weather Rev 138(2):345–377
16. Agnihotri N, Chittibabu P, Jain I, Sinha PC, Rao AD, Dube SK (2006) A bay–river coupled model for storm surge prediction along the Andhra coast of India. Nat Hazards 39(1):83–101
17. Gori A, Lin N, Smith J (2020) Assessing compound flooding from landfalling tropical cyclones on the North Carolina coast. Water Resour Res 56:e2019WR026788. https://doi.org/10.1029/2019WR026788
18. Pandey S, Rao AD, Haldar R (2021) Modeling of coastal inundation in response to a tropical cyclone using a coupled hydraulic HEC-RAS and ADCIRC model. J Geophys Res: Oceans, e2020JC016810
19. Holland G (1980) An analytic model of the wind and pressure profiles in hurricanes. Mon Weather Rev 108:1212–1218
20. Bhaskaran PK, Gayathri R, Murty PLN, Bonthu S, Sen D (2014) A numerical study of coastal inundation and its validation for Thane cyclone in the Bay of Bengal. Coast Eng 83:108–118. https://doi.org/10.1016/j.coastaleng.2013.10.005

Evolving Fishing Harbour Layout Using Mathematical Models

J. D. Agrawal, H. C. Patil, and Sagar Chanda

Abstract Fisheries sector is a powerful sector for employment generation as it stimulates growth for a number of subsidiary industries, most importantly it is the source of livelihood for a large population in India. A fishing harbour, intended to provide better landing and berthing facilities to fishing craft requires feasibility studies that consist of Hydrodynamics, sediment transport, Shore line changes and Wave tranquility studies. Wave propagation studies play a very important role in deciding the orientation and length of the breakwater in fishing harbour layout. The Mathematical model study is one of the tools to help in finalizing the most suitable harbour layout for inventive and cost-effective solution. The present paper describes a case study for the proposed development of a fishing harbour at Thrikkunnapuzha, Alappuzha district in Kerala state for finalization of layout from wave tranquility considerations using mathematical model techniques. Two-dimensional mathematical model MIKE-21 SW has been used for the wave climate transformation from offshore region to near-shore region. The model provides the Incident wave conditions in the near-shore region, which are likely to affect the harbour basin area. MIKE-21 BW model has been used for wave propagation in the near shore region and inside the fishing harbour basin. Based on the findings of MIKE-21 BW model simulations which are carried out for four different fishing harbour layouts for the incident wave direction from SSE, South, SSW, SW, WSW, West and WNW, the predicted safe berthing operation in terms of number of days in a year are found out. It is observed that there are appreciable differences in the layouts with concern of hydraulic aspects

J. D. Agrawal · H. C. Patil (✉) · S. Chanda
Ports & Harbours Division, Central Water & Power Research Station, Pune 411024, India
e-mail: patil.hansraj@rediffmail.com

J. D. Agrawal
e-mail: agrawal_jd@cwprs.gov.in

P. V. Timbadiya et al. (eds.), *Coastal, Harbour and Ocean Engineering*, Lecture Notes in Civil Engineering 321, https://doi.org/10.1007/978-981-19-9913-0_11

such as permissible wave height in the harbour basin. Based on the minimum non-operational days, easy manoeuvring of boats and other coastal phenomena like tidal hydrodynamics and littoral drift, etc., suitable layout is suggested. Thus it can be stated that for assessing the wave tranquility, mathematical model is the reliable technique for determining the fishing harbour layout.

Keywords Wave tranquility · Fishing harbour · Breakwater · Berth · MIKE 21 SW · MIKE-21 BW

1 Introduction

Proposed fishing harbour at Thrikkunnapuzha is situated at about 25.0 km south of Alappuzha district (Location: Latitude 09.25° and Longitude 76.40°) in Kerala state (Fig. 1) on the west coast of India. Wave tranquility studies are carried out to assess wave disturbance inside the fishing harbour proposed at Thrikkunnapuzha. This paper pertains to the wave tranquility studies [1].

Fig. 1 Location map of Thrikkunnapuzha, Alappuzha District, Kerala

If a port is to be developed most of the coastal phenomena such as tidal hydrodynamics, sedimentation, wave propagation which are important for designing the alignment and length of breakwater for fishing harbour, can be simulated using mathematical models. Wave tranquility at berthing area is one of the most important criteria in finalizing the fishing harbour layout.

The proposed harbour with different layouts are tested for the tranquility studies. MIKE-21 BW model is used to study the distribution of wave heights inside the harbour area with four layouts viz. Layout 1, Layout 2, Layout 3 and Layout 4. The model simulations are carried out for different fishing harbour layouts and the predicted improvement of wave tranquility in terms of percentage of tranquil area inside fishing area harbour.

2 Mathematical Modelling Techniques

Mathematical model studies are carried out in two stages. In stage-I, wave climate transformation from deep waters to near shore is done and in stage-II, wave tranquility inside the proposed fishing harbour area is simulated.

2.1 Wave Climate Transformation from Deep Sea to Near-Shore Region Using MIKE-21 SW Model

2.1.1 MIKE-21 SW Model Description

As waves travel from deep sea to shallow coastal waters, they undergo changes in direction and height due to the processes of refraction and shoaling. The simulation of wave transformation from deep sea to shallow waters is carried out using MIKE-21 SW (Spectral wave) model [3]. This model is a spectral wind wave model based on unstructured mesh, which takes into account all the important phenomena like wave growth by influence of wind, non-linear wave-wave interaction, dissipation due to white capping, bottom friction and depth-induced breaking. It can also model diffraction effects due to the presence of large structures like breakwaters, groins, etc. The effect of refraction and shoaling of waves due to depth variations and wave current interaction are also considered in the model. The output of the model are the regular wave parameters which include the significant wave height, mean wave period, mean wave direction, directional standard deviation and wave radiation stress. The model simulates the growth, decay and transformation of wind-generated waves and swell in offshore and coastal areas. The governing equation is the wave action balance equation. In horizontal Cartesian co-ordinates, the conservation equation for wave action is

$$\frac{\partial N}{\partial t} + \nabla.(\vec{\nu}\, N) = \frac{S}{\sigma}$$

where $N(\vec{x}, \sigma, \theta, t)$ is the action density, t is the time, $\vec{x} = (x, y)$ is the Cartesian co-ordinates, $\vec{\nu} = (C_x, C_y, C_\sigma, C_\theta)$ is the propagation velocity of a wave group in the four-dimensional phase space $\vec{x}$, σ and θ. S is the source term for the energy balance equation. ∇ is the four-dimensional differential operator in the $\vec{x}$, σ and θ space. The equation is solved using cell-centred finite volume method.

2.1.2 MIKE-21 SW Model Study

A bathymetry comprises of about 37 km (East–West) by 14 km (North–South) area has been prepared with the MIKE C-Map water Data and hydrographic survey data [2] carried out near the study area. The bathymetry extends beyond the depth of 45 m in the deep sea with a flexible triangular mesh (FM) is considered for *MIKE*-21 SW model study. The model is run with the Ship-observed wave data recorded by IMD as shown in Table 1. The wave rose plot for all the incident wave directions and heights at offshore is shown in Fig. 4 and NIOT Wave Atlas of the Indian Coast wave data [4] also provides wave rose plot for all the incident wave directions and heights at 25 m depth as shown in Fig. 4 (see Figs. 2 and 3).

MIKE-21 SW model output is a frequency distribution of wave heights from different directions at the depth of −8 m in inshore location. The corresponding wave rose plot at near-shore location is presented in Fig. 5.

From the analysis NIOT Wave Atlas [4] of the Indian Coast wave data and *MIKE*-21 SW model output such as percentage occurrence of wave heights, mean wave directions, input wave condition for *MIKE*-21 BW are determined. This wave data would be given as input (Table 2) to the MIKE-21 BW model for near-shore wave simulation.

Wave period of 10 s was considered for all incident wave direction.

2.2 Wave Tranquility Study Using MIKE-21 BW [3] Model

2.2.1 MIKE-21 BW Model Description [3]

The mathematical models for studying wave disturbances in the port/harbour area involve transformation of offshore wave climate to near-shore area and providing comprehensive wave action inside a harbour. The Boussinesq wave models are based on laws of conservation of energy and momentum concepts. The model simulates the processes of shoaling, refraction, diffraction from breakwater tips and bed friction. It also takes into account partial reflections from the boundaries, piers and breakwaters. This model is based on time-dependent Boussinesq equations for conservation of

Table 1 Percentage occurrence of wave heights and directions of Thrikkunnapuzha for entire year (IMD ship observed data)

Wave Ht. (m)	0.5	1.0	1.5	2.0	2.5	3.0	3.5	4.0	4.5	5.0	Total
Direction										Calm%	4.74
22.5	0.58	0.80	0.92	0.76	0.36	0.22	0.10	0.04	0.00	0.00	3.78
45.0	0.55	1.16	1.07	1.12	0.50	0.30	0.06	0.06	0.01	0.00	4.83
67.5	0.37	0.69	0.70	0.63	0.23	0.18	0.05	0.03	0.01	0.00	2.89
90	0.57	0.98	0.68	0.48	0.22	0.11	0.04	0.01	0.02	0.00	3.11
112.5	0.30	0.62	0.44	0.25	0.15	0.08	0.01	0.01	0.00	0.00	1.86
135.0	0.75	0.90	0.73	0.32	0.11	0.14	0.06	0.03	0.03	0.00	3.07
157.5	0.94	1.57	1.25	0.83	0.36	0.33	0.16	0.07	0.06	0.00	5.57
180	0.84	2.03	1.87	1.45	0.66	0.42	0.12	0.18	0.18	0.00	7.75
202.5	0.64	1.06	0.98	1.06	0.41	0.36	0.16	0.12	0.09	0.00	4.88
225.0	0.51	1.11	1.26	1.23	0.52	0.56	0.18	0.17	0.06	0.00	5.60
247.5	0.66	1.73	2.00	1.99	1.29	1.05	0.30	0.45	0.51	0.01	9.99
270.0	1.48	2.53	3.28	3.42	1.98	2.31	0.51	0.89	0.94	0.02	17.36
292.5	1.22	1.84	2.23	2.04	1.07	1.05	0.32	0.43	0.47	0.01	10.68
315.0	1.05	1.53	1.09	0.85	0.38	0.29	0.13	0.15	0.05	0.00	5.52
337.5	0.89	1.59	1.07	0.55	0.20	0.11	0.08	0.06	0.02	0.00	4.57
360.0	0.70	1.11	0.97	0.54	0.20	0.19	0.09	0.00	0.00	0.00	3.80
Total	*12.05*	*21.25*	*20.54*	*17.52*	*8.64*	*7.70*	*2.37*	*2.70*	*2.45*	*0.04*	*100.00*

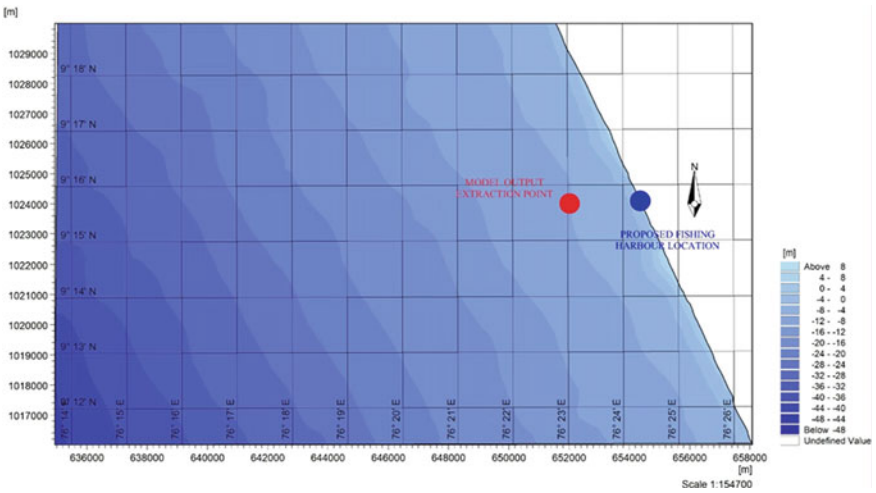

Fig. 2 Bathymetry for MIKE-21 SW wave transformation studies

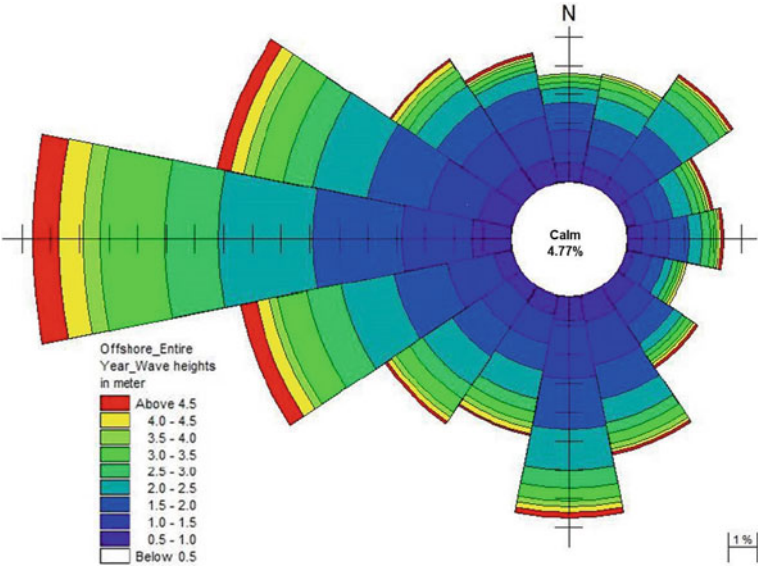

Fig. 3 Offshore wave rose diagram for entire year (IMD ship observed data)

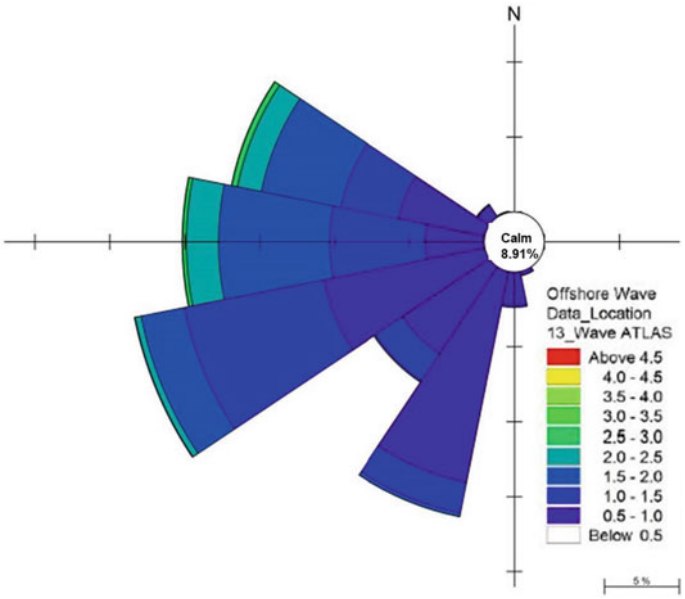

Fig. 4 Offshore wave rose diagram for entire year at 25 m water depth (NIOT wave atlas of the Indian coast, 2014)

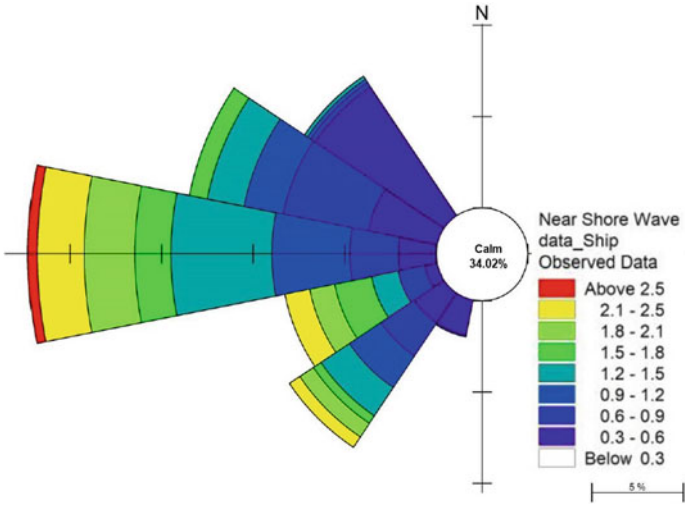

Fig. 5 Wave rose diagram at near-shore location (at 8 m depth)

Table 2 Input wave conditions for wave tranquility studies

Incident wave direction	Incident wave height (m)
WNW	1.5
West	2.0
WSW	2.0
SW	2.0
SSW	2.5
South	1.5

mass and momentum obtained by integrating the three-dimensional flow equations without neglecting vertical acceleration. They operate in the time domain, so that irregular waves can be simulated. These equations include non-linearity as well as frequency dispersion. The frequency dispersion is included in the flow equations by taking into account the effect of vertical acceleration or the curvature of streamlines on pressure distribution. This model is widely used to simulate wave propagation across the breakwater and to examine the wave height distribution inside the harbour. The governing equations are as follows:

Continuity Equation:

$$n\frac{\partial \varsigma}{\partial t} + \frac{\partial p}{\partial x} + \frac{\partial q}{\partial y} = 0$$

X Momentum Equation:

$$n\frac{\partial p}{\partial t} + \frac{\partial}{\partial x}\left(\frac{p^2}{h}\right) + \frac{\partial}{\partial y}\left(\frac{pq}{h}\right) + n^2 gh\frac{\partial \varsigma}{\partial x} + n^2 p\left(\alpha + \beta\sqrt{\frac{p^2+q^2}{h^2}}\right) - \frac{p^2}{nh}\frac{\partial n}{\partial x} - \frac{pq}{nh}\frac{\partial n}{\partial y} = n\frac{D^2}{3}\left(\frac{\partial^3 p}{\partial x^2 \partial t} + \frac{\partial^3 q}{\partial x \partial y \partial t}\right)$$

Y Momentum Equation:

$$n\frac{\partial q}{\partial t} + \frac{\partial}{\partial y}\left(\frac{q^2}{h}\right) + \frac{\partial}{\partial x}\left(\frac{pq}{h}\right) + n^2 gh\frac{\partial \varsigma}{\partial y} + n^2 q\left(\alpha + \beta\sqrt{\frac{p^2+q^2}{h^2}}\right) - \frac{q^2}{nh}\frac{\partial n}{\partial y} - \frac{pq}{nh}\frac{\partial n}{\partial x} = n\frac{D^2}{3}\left(\frac{\partial^3 q}{\partial y^2 \partial t} + \frac{\partial^3 p}{\partial x \partial y \partial t}\right)$$

where,

$\zeta(x, y, t)$ = water surface elevation above datum

$p(x, y, t)$ = flux density in x direction

$q(x, y, t)$ = flux density in y direction

$D(x, y)$ = still water depth, $h(x, y, t)$ = water depth

$n(x, y)$ = porosity, g = gravity

α = resistance coefficient for laminar flow in porous media

β = resistance coefficient for turbulent flow in porous media

x, y = space coordinates, t = time.

These above differential equations are solved using a time-centred implicit finite difference scheme with variables defined on a space-staggered rectangular grid. Output of Boussinesq Wave model is in the form of wave height distribution plot in the area of study. This plot gives the contours of the wave heights in the model area.

2.3 Description of Layouts and Model Output

2.3.1 Layout 1

The Layout 1 consists of north and south breakwaters as shown in Fig. 6. The north breakwater is of length about 970 m. The southern breakwater consists of shore-normal breakwater of length 270 m.

Most of the part of northern breakwater lies in 4.6–4.9 m depth. Depths inside the harbour have been considered as −3.0 m and below. The width of the entrance to the harbour is about 120 m and opens in SE direction. A typical Bathymetry which is used for this wave tranquility study is shown in Fig. 7.

The proposed Layout 1 is tested individually with all predominant wave directions which are likely to disturbance the tranquility, i.e. West, WSW, SW, SSW and South direction. Wave height distribution plot are the representative plots of wave propagation. Therefore, one sample plot of each has been given for South direction is shown in Fig. 8.

Wave tranquility study for this Layout 1 has indicated that the percentage of tranquil area inside the harbour decreases with the incident wave approaching from West direction to South direction. The highest wave height has been observed inside the harbour which is 1.448 m for significant wave height of the order of 1.5 m from South as is shown in Table 3.

Fig. 6 Proposed Layout 1

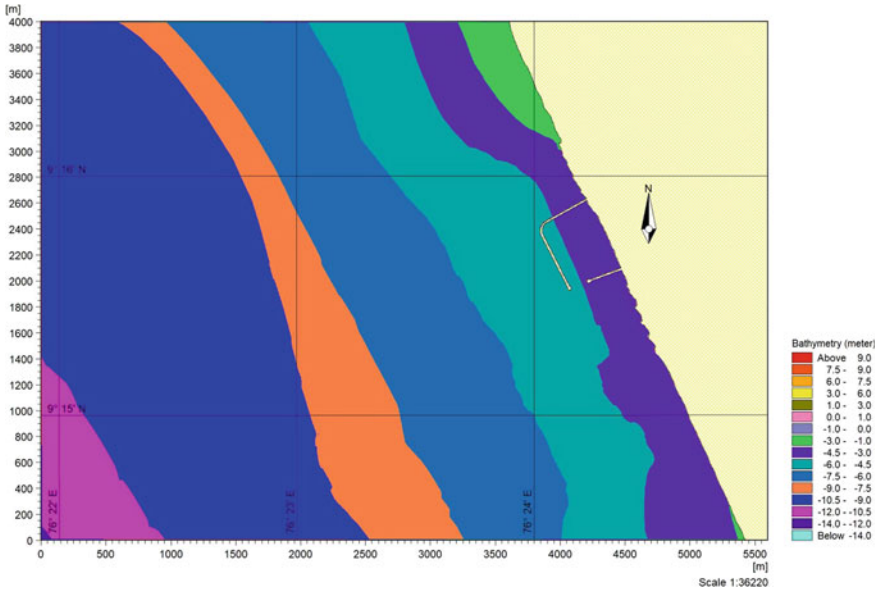

Fig. 7 Bathymetry for Layout 1 (Typical)

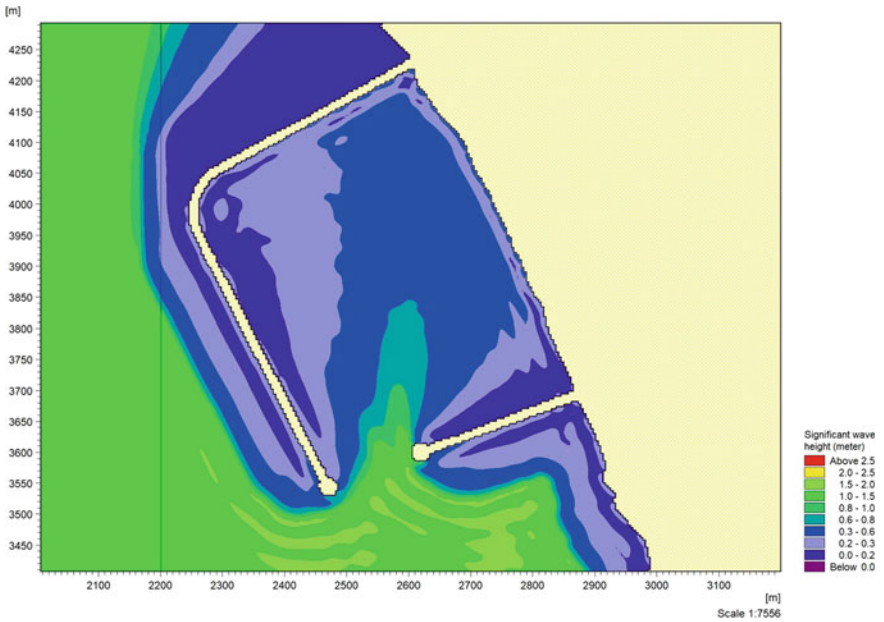

Fig. 8 Wave height plot for Layout 1 incident wave direction/height—south/1.5 m

Table 3 Wave height, average wave height and maximum wave heights of all the four layouts

Layout	Wave direction	Significant wave height (m)	Percentage of tranquil area inside harbour (%)	Average significant wave height inside harbour (m)	Maximum sig. wave height inside harbour (m)	Remarks
(1)	(2)	(3)	(4)	(5)	(6)	(7)
Layout 1	WNW	1.5	*	*	*	
	West	2.0	100	0.172	0.338	
	WSW	2.0	95.52	0.230	0.679	
	SW	2.0	71.58	0.292	1.144	
	SSW	2.5	37.10	0.386	1.721	
	South	1.5	44.60	0.369	1.448	
Layout 2	WNW	1.5	38.69	0.388	1.235	
	West	2.0	58.12	0.351	1.788	
	WSW	2.0	68.10	0.289	1.853	
	SW	2.0	95.27	0.183	0.979	
	SSW	2.5	*	*	*	
	South	1.5	*	*	*	
Layout 3	WNW	1.5	38.52	0.453	1.104	
	West	2.0	20.58	0.639	1.663	
	WSW	2.0	19.50	0.639	1.583	
	SW	2.0	31.03	0.567	1.496	
	SSW	2.5	35.82	0.583	2.007	
	South	1.5	78.89	0.224	1.058	
Layout 4	WNW	1.5	100	0.060	0.242	
	West	2.0	100	0.012	0.263	
	WSW	2.0	*	*	*	
	SW	2.0	*	*	*	
	SSW	2.5	*	*	*	
	South	1.5	*	*	*	

* No simulation is carried out as it is known that wave heights in the fishing harbour area will be well below the required limit

2.3.2 Layout 2

The Layout 2 as shown in Fig. 9 comprises of two breakwaters. The northern breakwater is shore normal and aligns straight for a length of about 360.0 m. The southern breakwater originates almost normal to the shoreline in SW direction and then bends towards NW totalling an approximate length of 960.0 m. Most of southern breakwater length extends up to 4.6–5.0 m depth. Depths inside the harbour have been

Fig. 9 Proposed Layout 2

considered as −3.0 m or below. The width of the entrance to the harbour is about 120 m and opens in NW direction.

The proposed Layout 2 is tested individually with all predominant wave directions which are likely to disturbance the tranquility, i.e. WNW, West, WSW and SW direction. Wave height distribution plot are the representative plots of wave propagation. Therefore, one sample plot of each has been given for West direction which is shown in Fig. 10.

Wave tranquility study for this Layout 2 has indicated that the percentage of tranquil area inside the harbour decreases with the incident wave approaching from SW direction to West direction. The highest wave height has been observed inside the harbour which is 1.853 m for significant wave height of the order of 2.0 m from WSW as shown in Table 3.

2.3.3 Layout 3

The Layout 3 as shown in Fig. 11 also comprises of two breakwaters. The northern breakwater is originated shore-normal and aligns towards SW direction for a length of about 540.0 m. Similarly, the southern breakwater originates almost normal to the shoreline and extends for a length of 590.0 m. Both the breakwaters converge at the entrance at depth of 5.0 m for a width of about 160.0 m.

The proposed Layout 3 is tested with all predominant wave directions which are likely to disturbance the tranquility, i.e. WNW, West, WSW, SW, SSW and South direction. Wave height distribution plot are the representative plots of wave

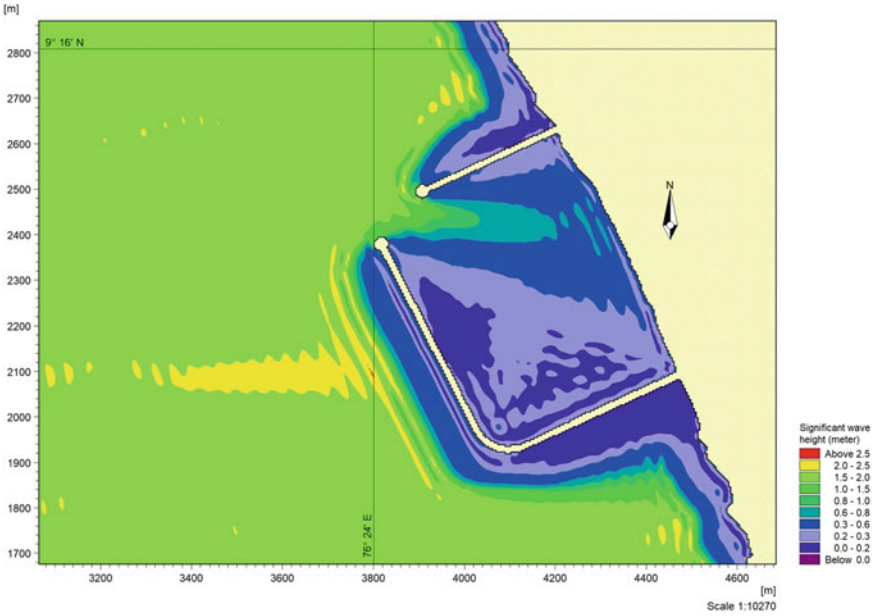

Fig. 10 Wave height (H_s) distribution plot for Layout 2 for incident wave direction/height—west/2.0 m

Fig. 11 Proposed Layout 3

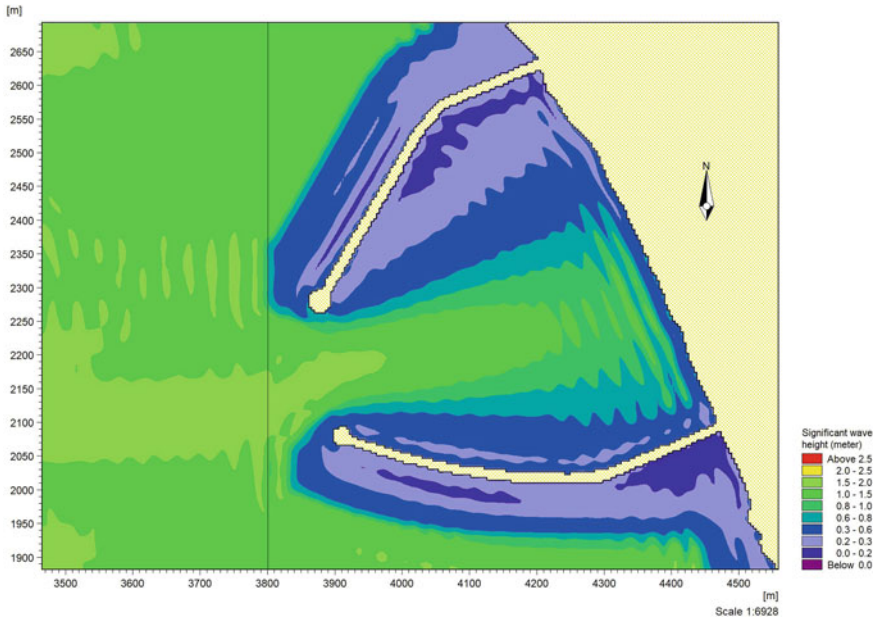

Fig. 12 Wave height (H_s) distribution plot for Layout 3 for incident wave direction/height—west/2.0 m

propagation. Therefore, one sample plot of each has been given for West direction which is shown in Fig. 12.

Wave tranquility study for Layout 3 has indicated that the percentage of tranquil area inside the harbour less than 100% for all directions. The highest wave height observed inside the harbour is 2.007 m for significant wave height of the order of 2.5 m from SSW is shown in Table 3.

2.3.4 Layout 4

This layout is also comprised of two breakwaters namely North and South Breakwater. The north breakwater is similar to earlier Layout 3 and having a length of about 490 m. South breakwater is also shore-normal but aligns along a curve and extends beyond the tip of north breakwater. The length of this breakwater is about 960 m. These breakwaters extend in depth of about 5.0 m.

Wave tranquility study for Layout 4 has indicated that the proposed harbour is tranquil for the all predominant incident wave directions. Wave height distribution plot and surface elevation plots are shown in Figs. 13 and 14 for WNW and West Direction respectively.

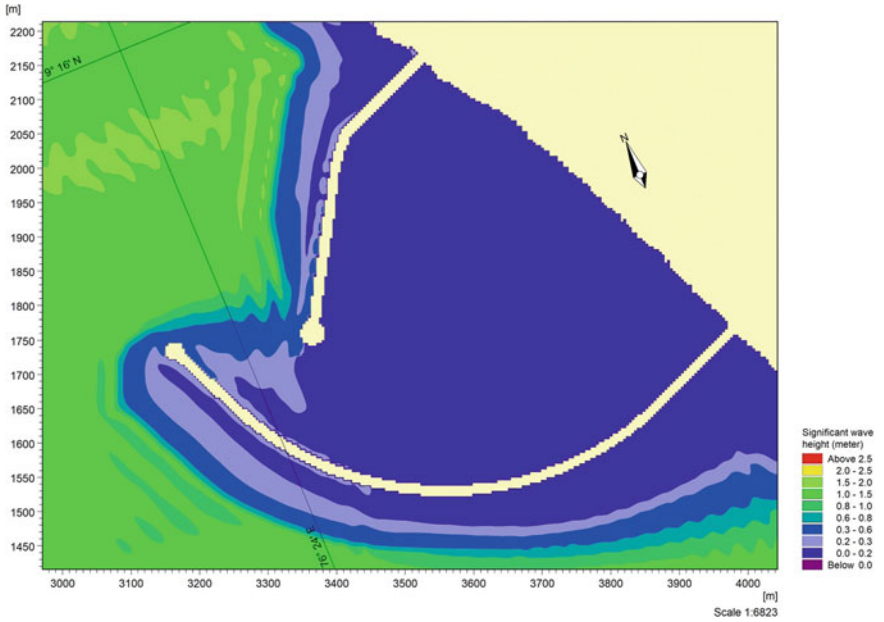

Fig. 13 Wave height (H_s) distribution plot for Layout 4 for incident wave direction/height—WNW/1.5 m

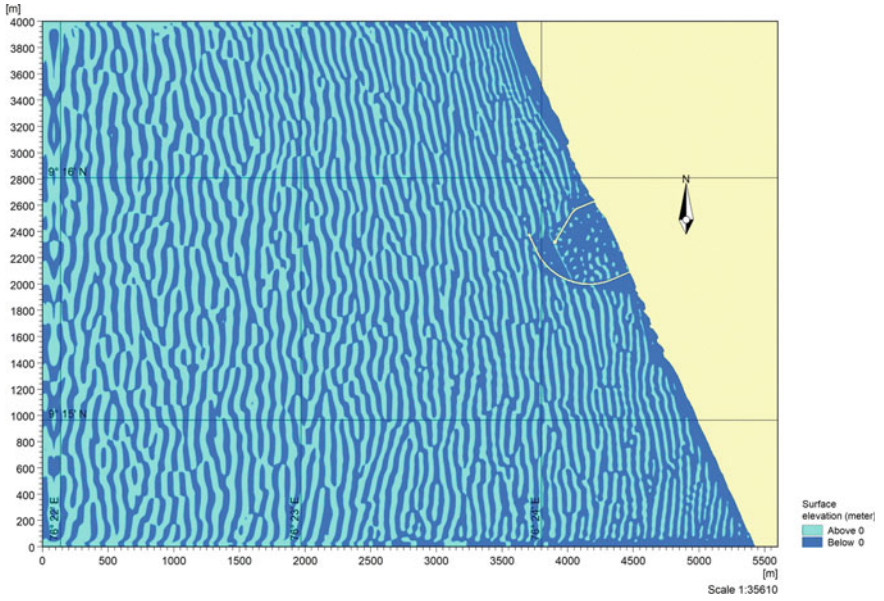

Fig. 14 Surface elevation plot for Layout 4 for incident wave direction/height—west/2.0 m

Gist of wave heights inside the harbour, average wave height in the area having wave heights exceeding the tranquility limit, i.e. 0.3 m, for all given four layouts is given in the Table 3.

3 Concluding Remarks

Wave tranquillity studies of all the three proposed layouts have indicated that waves inside the harbour area are exceeding the assumed tranquility limit of 0.3 m for few directions. This will make the fishing harbour non-operational for few days in a year. Additional Layout 4 is also examined so that fishing harbour remains operational throughout the year except for the stormy weather is shown in Table 3. Layout 4 may pose slight navigational inconvenience for the boats while entering and leaving the harbour. This can also be reduced if the boats reach the harbour through NW direction.

Acknowledgements The authors are thankful to Shri A. K. Agrawal, Director, Central Water and Power Research Station, Pune for his continuous encouragement and kind permission to publish the paper.

Review 1

Submission: 451

Title: Evolving Fishing Harbour layout using Mathematical Models

Authors: J. D. Agrawal, H. C. Patil and Sagar Chanda

Overall evaluation

Score: 1 (weak accept)

Text:

The paper deals with optimizing the port layout for a location on the Kerala Coast. The authors have considered state-of-the-art numerical model (MIKE—SW & BW) and the method adopted is acceptable.

Comment 1: Two different database for wave climate (Ship observed and NIOT wave atlas) was mentioned and the more recent database of NIOT wave atlas was not considered. The reason for this may be indicated.

Reply: When the study was taken up during 2018, NIOT Wave ATLAS of 2014 was only available and the same was used as an additional database for determining predominant wave direction, heights and other wave parameters.

Comment 2: Joint distribution of wave height and wave period is missing.

The important parameter of Wave Period is missing in the entire manuscript. Wave period plays a major role in assessing the harbor tranquility. This needs to be addressed.

Reply: Each of these Layouts were evaluated for achieving the desired wave tranquility by every possible wave direction, heights and their period. Wave period is adopted as 10 s for each case. The measured wave data in the vicinity of the proposed site location supplied by the project authority shows that the predominant wave period is in the range of 8–10 s. Accordingly, wave period of 10 s was considered for study.

Comment 3: While there are many ways of port layout, few options with one opening is considered. The reason for not considered two openings to allow sediment movement in and out of the port may be included.

Reply: The different layouts were provided by the project authority for evaluating the wave tranquility inside the harbour. The modification of the layouts like entrance of harbour is subjected to the projects authority. As far as the sediment problems are concerned, effort has been made to place the harbour entrance at the deeper water (approximately 5 m depth) where the concentration of suspended sediments are not significant. This shall avoid siltation in the harbour.

Review 2

Submission: 451

Title: Evolving Fishing Harbour layout using Mathematical Models

Authors: J. D. Agrawal, H. C. Patil and Sagar Chanda

Overall evaluation

Score: 2 (accept)

Text:

Authors have presented a case study in which they have examined a few alternative breakwater alignments to ensure clam water conditions inside a harbour off the Kerala coast. For this purpose they have used the MIKE-21 modelling software. The manuscript can provide guidance to all those who wish to know practical applications of the related DHI models.

Comment 1: Reference citations as well as their listing needs to be as per the required format.

Reply: Incorporated in the revised manuscript.

References

1. CWPRS Technical Report No. 5671 (Feb 2019) Mathematical model study for Wave Tranquility for proposed fish landing facility at Thrikkunnapuzha, Kerala
2. Harbour Engineering Investigation Subdivision (South Zone), Thangassery, Kollam, Kerala, Investigation Studies of Thrikkunnapuzha Fishing Harbour, December 2015.
3. MIKE 21 Reference manuals (2014) Danish Hydraulic Institute, Denmark
4. Wave Atlas of the Indian Coast, 2014 published by National Institute of Ocean Technology, Chennai

Wave Propagation Through the Long Navigational Channel Using Mathematical Modelling

S. S. Hulawale, S. N. Wankhade, K. P. Patil, S. S. Agrawal, H. C. Patil, and J. D. Agrawal

Abstract West coast of India has got a flatter continental slope as compared to East Coast, resulting into the long navigational channel on the West Coast Ports, such as New Mangalore Port and Cochin Port. Wave refraction takes place in the long navigational channel, as they travel, resulting in very good wave attenuation at the entrance to the Port. An attempt has been made to study this phenomenon. Wave propagation from deep water to the shallow coastal regions has different processes as compared to wave propagation from shallow region to inside the port or coastal area. In order to accommodate these processes two mathematical model MIKE 21 SW and MIKE 21 BW have been used. Wave transformation from deep water to mouth of navigational channel has been done using MIKE 21 SW model. Results of same indicate that WNW, West, 259°N (along the navigational channel), and WSW wave directions are predominant at the entrance to the channel. All these wave conditions are used for wave propagation along the navigational channel. Analysis of these data has indicated that wave propagation along the channel has maximum attenuation as compared to wave with some angle with channel alignment. It is also seen due to refraction of wave energy from the side slope of navigational channel, wave energy concentration is seen on side slopes. It can be concluded that long navigational channel is good from the wave tranquillity aspects.

Keywords Navigational channel · Wave transformation · Wave propagation · MIKE 21 BW · MIKE 21 SW

S. S. Hulawale (✉) · S. N. Wankhade · K. P. Patil · S. S. Agrawal
Department of Civil Engineering, Sinhgad College of Engineering, Pune 411041, India
e-mail: sakshihulawale2831@gmail.com

H. C. Patil
Central Water and Power Research Station Khadakwasla, Pune, Maharashtra 411024, India

J. D. Agrawal
Department of Civil Engineering, Dr. D. Y. Patil Institute of Technology, Pimpri, Pune 411018, India
e-mail: jagottam.agrawal@dypvp.edu.in

P. V. Timbadiya et al. (eds.), *Coastal, Harbour and Ocean Engineering*, Lecture Notes in Civil Engineering 321, https://doi.org/10.1007/978-981-19-9913-0_12

1 Introduction

The last decade has witnessed an enormous growth along Indian coastal region, such as development of commercial ports, development of infrastructure facilities in existing ports. There have been significant innovations in coastal technologies that have led to the development of the maritime industry. Seaborne trade has also emerged as the most affordable mode of bulk transport. This ultimately led to increase in the vessel size of modern bulk carriers. Thus, with the purpose of providing access to these vessels inside the harbours, long and wider navigational approach channels have to be dredged outside the sheltered area of the harbour. The requirement of long navigational approach channel is relevant to the harbours on west coast of India. The west coast of India is well known to be having flatter sea bed slope of 1:300–1:500, thus result in the very long navigational channel of about 5–10 km [1]. The presence of a long navigational channel alters the wave field approaching a harbour as it significantly modifies the amount of wave energy penetrating into a harbour [2]. Analysis of wave transformation along such channel is essential for economic and efficient design of port layout [3]. The important parameters at play are reflection, refraction of waves over the side slopes of the channel, diffraction of wave energy due to steep bathymetric variations along the side slope of the channel and bottom friction [4]. The relative importance of these phenomena is investigated using mathematical model studies for New Mangalore Port which is situated on West Coast of India. The objective of this paper is to demonstrate the significance of 'Wave Attenuation Associated with Long Navigational Channel' in engineering design of ports and harbours with mathematical model studies.

2 Mathematical Model Description

2.1 MIKE 21 SW (Spectral Wave) Model

Waves undergo changes in direction and height as they travel from deep sea to shallow coastal waters due to the processes of refraction and shoaling. The MIKE 21 SW model has been used for simulation of wave transformation from deep to shallow coastal waters. MIKE 21 is a spectral wind wave model based on unstructured mesh and takes into account all the important phenomena like wave growth by influence of wind, bottom friction and depth-induced breaking, nonlinear wave-wave interaction, and dissipation due to white capping. It also models diffraction effects due to the presence breakwaters, groins, etc. The effect of wave-current interaction and refraction and shoaling of waves due to depth variations have also been considered in the model. The model outputs are the regular wave parameters which include the significant wave height, mean wave direction, mean wave period, wave radiation stress, and directional standard deviation. The model simulates the transformation of wind-generated waves and swell, their growth, and decay in offshore and coastal

areas. The wave-action balance equation is the governing equation. The conservation equation for wave action in horizontal cartesian co-ordinates is

$$\frac{\partial N}{\partial t} + \nabla.(\vec{\nu}\, N) = \frac{S}{\sigma}$$

where $N(\vec{x}, \sigma, \theta, t)$ is the action density, $\vec{v} = (C_x, C_y, C_\sigma, C_\theta)$ is the propagation velocity of a wave group in the four dimensional phase space, $\vec{x} = (x, y)$ is the cartesian co-ordinates $\vec{x}$, σ and θ. S is the source term for the energy balance equation, ∇ is the four-dimensional differential operator in the $\vec{x}$, σ and θ space, and t is the time. The equation has been solved using cell-centred finite volume method [5].

The mathematical model MIKE 21 SW (Spectral Wave) has been used for wave climate transformation from deep water to the mouth of the navigational channel. Results of the same indicate that WNW, West, 259°N (along the navigational channel), and WSW wave directions are predominant at the entrance of the navigational channel. The results were verified with the help of the Technical Report of Mathematical Model Studies which was carried out on New Mangalore Port at CW&PRS, in 2010 [6]. These wave conditions are used for wave propagation studies along the navigational channel.

2.2 MIKE 21 BW (Boussinesq Wave) Model

MIKE 21 BW (Boussinesq Wave Model) has been used to investigate the wave propagation over long approach channel. The mathematical model is based on time-dependent Boussinesq equations of conservation of mass and conservation of momentum obtained without neglecting vertical acceleration by integrating the three-dimensional flow equations. Irregular waves can be simulated as it operates in the time domain. These equations include frequency dispersion as well as nonlinearity. The model simulates the processes of refraction, shoaling, diffraction due to irregular bathymetric variations and structures and bed friction. It also takes into account partial reflections from boundaries, breakwaters, and piers. This has been done by including porosity terms in governing equations. The governing equations are

Continuity Equation

$$n\frac{\partial \xi}{\partial t} + \frac{\partial P}{\partial x} + \frac{\partial Q}{\partial y} = 0$$

X Momentum Equation

$$n\frac{\partial P}{\partial t}+\frac{\partial}{\partial x}\left(\frac{P^2}{h}\right)+\frac{\partial}{\partial y}\left(\frac{PQ}{h}\right)+\frac{\partial R_{xx}}{\partial x}+\frac{\partial R_{xy}}{\partial x}+$$

$$n^2gh\frac{\partial \xi}{\partial x}+n^2P\left[\alpha+\beta\frac{\sqrt{P^2+Q^2}}{h}\right]+\frac{gP\sqrt{P^2+Q^2}}{h^2C^2}+n\psi_1=0$$

Y Momentum Equation

$$n\frac{\partial Q}{\partial t}+\frac{\partial}{\partial x}\left(\frac{Q^2}{h}\right)+\frac{\partial}{\partial y}\left(\frac{PQ}{h}\right)+\frac{\partial R_{xx}}{\partial x}+\frac{\partial R_{xy}}{\partial x}+$$

$$n^2gh\frac{\partial \xi}{\partial y}+n^2Q\left[\alpha+\beta\frac{\sqrt{P^2+Q^2}}{h}\right]+\frac{gQ\sqrt{P^2+Q^2}}{h^2C^2}+n\psi_2=0$$

where

$\xi(x, y, t)$ = water surface elevation above datum

$P(x, y, t)$ = flux density in x direction

$Q(x, y, t)$ = flux density in y direction

$d(x, y)$ = still water depth

$h(x, y, t)$ = water depth

$n(x, y)$ = porosity

g = gravity

α = resistance coefficient for laminar flow in porous media

β = resistance coefficient for turbulent flow in porous media

x, y = space coordinates

t = time.

The above equations are solved using a time-centred implicit finite difference scheme and variables defined on a space-staggered rectangular grid. Output of this wave model is in the form of wave height distribution plot in the area of study. This plot gives the contours of the wave heights in the model area [7].

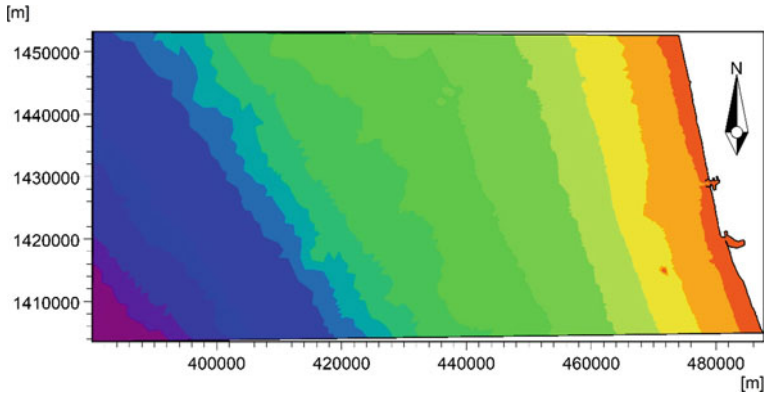

Fig. 1 Bathymetry for MIKE21 SW model

3 Model Studies

3.1 Wave Transformation Studies for Nearshore Wave Conditions Using MIKE 21 SW Model

The domain with 55 km length in the offshore direction and 50 km length along the coastline with an unstructured mesh was considered for studies using MIKE 21 SW (Spectral Wave) model which extends beyond 1000 m depth in deep sea as shown in Fig. 1. The model was run for the offshore wave climate data given in Table 1 (the offshore wave data is reported by IMD) for all the incident wave directions and heights.

Results of same indicate that WNW, West, 259°N (along the navigational channel), WSW wave directions and 1.5, 3.5, 3.5, 3.5 m wave heights, respectively, are predominant at the entrance of navigational channel. These wave conditions have been used for wave propagation studies using MIKE 21 BW model along the navigational channel.

3.2 Wave Propagation Studies Using MIKE21 BW Model

The domain is 8 km long and 10 km wide with grid spacing of 4 m. The typical 7.5 km long navigational channel of width 250 m, 1:20 side slope, and depth 15.4 m is shown in Fig. 2. Numerical model studies have been carried out with this idealized bathymetry. MIKE 21 BW model using unidirectional irregular waves with JONSWAP spectrum with high frequency cut-off and directional = ±30° was applied for simulation.

Table 1 Percentage occurrence of wave height and direction off New Mangalore entire period (Jan–Dec)

Wave height (m)/wave direction (0°)	0–0.5	0.5–1	1–1.5	1.5–2	2–2.5	2.5–3	3–3.5	3.5–4	4–4.5	Total
22.5	1.03	1.03	1.48	0.30	0.0	0.00	0.00	0.00	0.00	3.84
45	0.52	0.59	0.37	0.15	0.07	0.00	0.00	0.00	0.00	1.70
135	0.07	0.07	0.00	0.00	0.00	0.00	0.00	0.00	0.00	0.15
157.5	0.30	0.00	0.00	0.07	0.0	0.07	0.00	0.00	0.00	0.44
180	0.74	0.59	0.22	0.30	0.00	0.07	0.00	0.07	0.00	1.99
202.5	0.07	0.44	0.15	0.66	0.30	0.44	0.30	0.07	0.00	2.44
225	0.96	1.33	1.11	2.29	1.18	1.48	0.52	1.03	0.22	10.11
247.5	0.15	1.33	0.81	2.80	1.48	3.10	2.14	1.48	0.30	13.58
270	1.62	3.62	3.10	2.80	2.95	3.17	1.62	1.40	0.30	20.59
292.5	0.74	3.03	3.54	0.96	0.59	0.37	0.37	0.30	0.07	9.96
315	2.51	3.47	3.17	0.89	0.22	0.07	0.15	0.07	0.00	10.55
337.5	1.70	2.88	1.70	0.89	0.37	0.07	0.00	0.00	0.00	7.60
360	3.10	5.83	4.13	2.21	0.59	0.59	0.22	0.22	0.15	17.05
Total	13.51	24.21	19.78	14.32	7.75	9.45	5.31	4.65	1.03	100.00

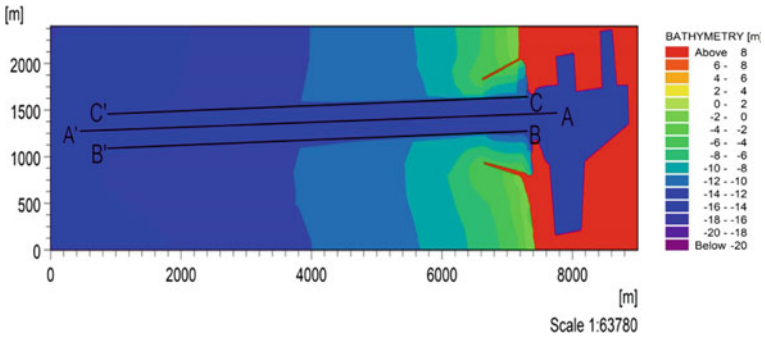

Fig. 2 Bathymetry for MIKE21-BW model

Following wave conditions were used for the wave propagation studies over the navigational channel by varying various parameter, viz incident wave heights and direction. The side slope of channel, i.e. 1:20 and wave period, i.e. 8 s was kept constant for all condition.

Condition 1. The incident wave height 1.5 m, wave direction WNW

Condition 2. The incident wave height 3.5 m, wave direction West

Condition 3. The incident wave height 3.5 m, wave direction 259°N (along the navigational channel)

Condition 4. The incident wave height 3.5 m, wave direction WSW.

4 Results and Discussions

4.1 Condition 1

The result revealed that wave heights observed at the end point of the channel (at 7500 m from the entrance of navigational channel), for the centre of the channel (Section 'AA'), north side of navigational channel (Section 'CC'), and south side navigational channel (Section 'BB') are 0.42, 0.33, and 0.37 m, respectively, as shown in Fig. 3 and Table 2. The results revealed that considerable wave attenuation occurred along navigational channel, i.e. up to 65.43%, as shown in Table 2 and Fig. 3.

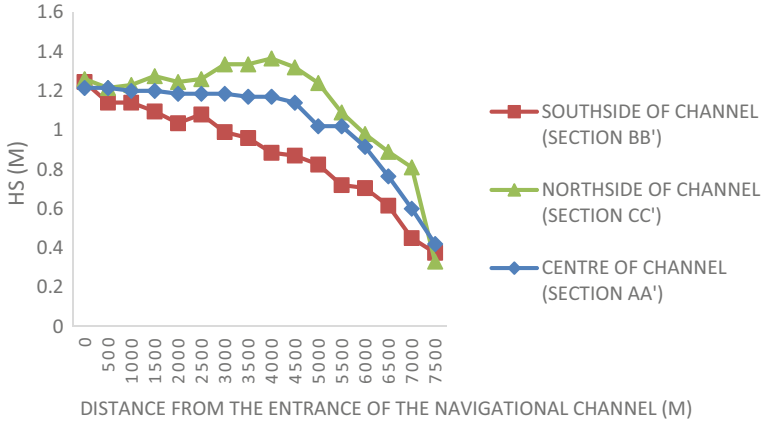

Fig. 3 Wave height plot along navigational channel for incident wave direction WNW and wave height 1.5 m

4.2 Condition 2

The result revealed that wave heights observed at the end point of the channel (at 7500 m from the entrance of navigational channel), for the centre of the channel (Section 'AA'), north side of navigational channel (Section 'CC'), and south side navigational channel (Section 'BB') are 0.94, 0.42, and 0.73 m, respectively, as shown in Fig. 4 and Table 2. The results indicated that considerable wave attenuation occurred along navigational channel, i.e. up to 71.58%, as shown in Table 2 and Fig. 4. Typical wave heights distribution plot for Condition 2 as shown in Fig. 5.

4.3 Condition 3

The result revealed that wave heights observed at the end point of the channel (at 7500 m from the entrance of navigational channel), for the centre of the channel (Section 'AA'), north side of navigational channel (Section 'CC'), and south side navigational channel (Section 'BB') are 0.49, 0.42, and 0.52 m, respectively, as shown in Fig. 6 and Table 2. The results have indicated that maximum wave attenuation occurred along navigational channel, i.e. up to 83.33%, as shown in Table 2 and Fig. 6.

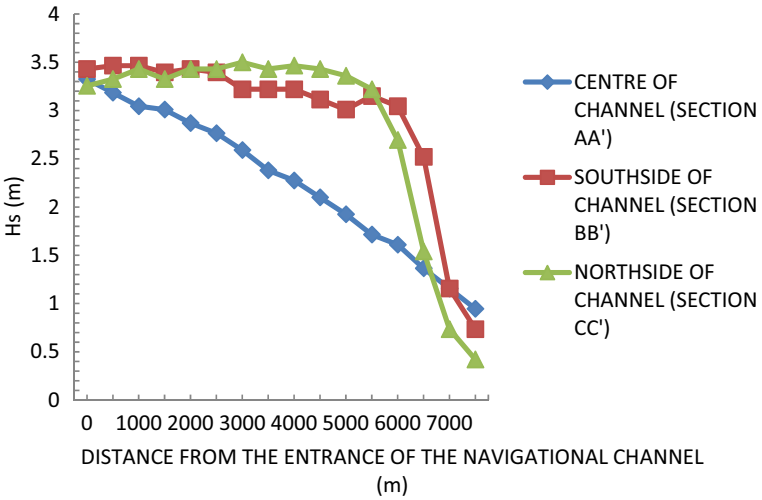

Fig. 4 Wave height plot along navigational channel for incident wave direction WEST and wave height 3.5 m

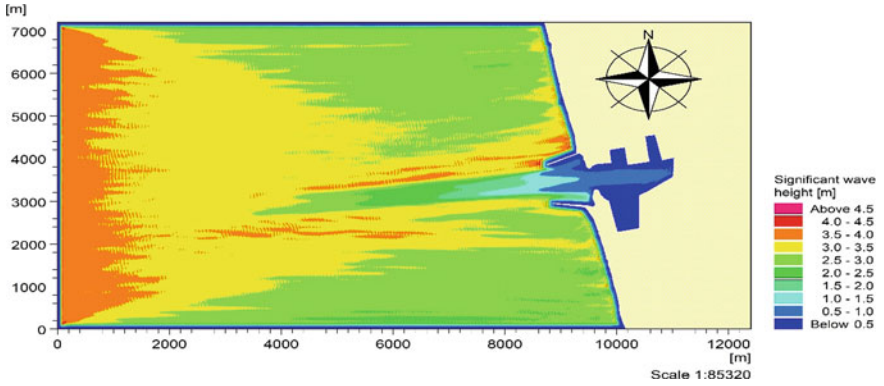

Fig. 5 Typical significant wave height distribution plot for incident wave direction West/wave height 3.5 m

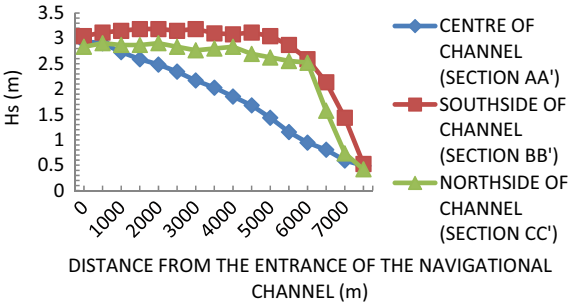

Fig. 6 Wave height plot along navigational channel for incident wave direction 259°N and wave height 3.5 m

4.4 Condition 4

The result revealed that wave heights observed at the end point of the channel (i.e. 7500 m from the entrance of navigational channel), for the centre of the channel (Section 'AA'), north side of navigational channel (Section 'CC'), and south side navigational channel (Section 'BB') are 1.05, 0.84, and 1.47 m, respectively, as shown in Fig. 7 and Table 2. The results have indicated that considerable wave attenuation occurred along navigational channel, i.e. up to 66.67%, as shown in Table 2 and Fig. 7.

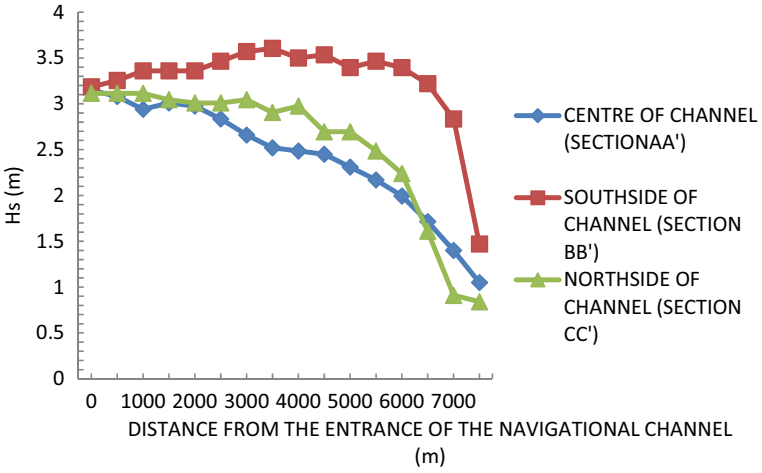

Fig. 7 Wave height plot along navigational channel for incident wave direction WSW and wave height 3.5 m

Table 2 Wave heights and percentage wave attenuation at different locations along the Navigational channel and sides of navigational channel

Wave direction/wave height (m)	Wave height (m) at section 'AA' (Center along channel)		Percentage wave attenuation at section 'AA' (Center along channel)	Wave height (m) at section 'CC' (North side of channel)		Wave height (m) at section 'BB' (South side of channel)	
	Entrance of channel	End point of channel/7500 m		Entrance of channel	End point of channel/7500 m	Entrance of channel	End point of channel/7500 m
WNW/1.5 m	1.21	0.42	65.43%	1.26	0.33	1.24	0.37
WEST/3.5 m	3.32	0.94	71.58%	3.25	0.42	3.43	0.73
*259°N/3.5 m	2.94	0.49	83.33%	2.83	0.42	3.04	0.52
WSW/3.5 m	3.15	1.05	66.67%	3.11	0.84	3.18	1.47

(*Along Navigational channel)

5 Analysis of Result

Analysis of results of these four conditions indicates that when the waves are incident along the channel maximum attenuations at the end point of the channel are seen due to refraction of waves on the sides of the channel and wave energy concentration is seen in the sides. However, when the wave is incident with an angle to the navigational channel, either South or North, it is seen that wave attenuates in the side slopes from where waves are trying to enter the channel. In case of wave incident from WNW direction, attenuation on the other side of the channel was maximum over larger than the attenuation along the centre of the channel. This is due to difficulties of wave crossing the slopes of the channel from shallow water to deep water and due to refraction, they bend towards shallower portion.

6 Comparison Between Physical Model Studies and Mathematical Model Studies Results

The results of mathematical model studies conducted were compared with physical model studies that were carried out in CWPRS in the year 2019 [8]. The physical model studies had wave attenuation of 74% for the West Direction, whereas mathematical model studies showed wave attenuation of 71.58% as shown in Table 3 and Fig. 8. The wave attenuation along the navigational channel appeared to be almost 96% comparable.

Table 3 Comparison between physical model studies results and mathematical model. Studies results for incident wave direction West and wave height 3.5 m

Location for result extraction	Physical model	Mathematical model
At entrance of channel (wave height)	2.5 m	2.37 m
At end point of channel (wave height) (entrance of harbor)	0.65 m	0.67 m
Wave attenuation	74%	71.58%

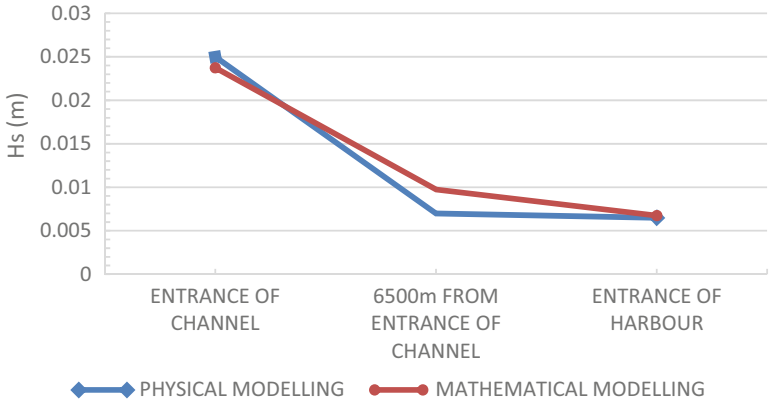

Fig. 8 Comparison of result between Physical and Mathematical model studies for wave heights along navigational channel for incident wave direction West/wave height 3.5 m

7 Conclusions

The following conclusions are derived from the foregoing study:

- Wave propagation along the long and wide navigation channels has been studied using a mathematical model based on MIKE 21 BW model (Boussinesq wave equation).
- Approach channels are very effective wave attenuators causing wave attenuation of more than 80% by natural process of refraction.
- On the West Coast of India, the waves from the west direction are dominant, the orientation of approach channel approximately towards West would be effective in reducing the length of breakwater.
- The studies indicated that there is significant influence on the incident wave field, which leads to wave attenuation and amplification. Both these effects, in turn, critically influence inputs to design and planning of port infrastructure as well as assessment of harbour agitation and downtime.
- Mathematical model was able to reproduce the simulation results comparable to physical model results.

Acknowledgements The authors are thankful to Shri A.K. Agrawal, Director, CW&PRS (Ministry of Jal Shakti, Government of India), for the permission to conduct the research work in the institute. The authors are also thankful to Dr. S.S. Shastri, HOD Sinhgad College of Engineering and Shri D.K. Rajmane, Assistant Professor Sinhgad College of Engineering for their guidance and valuable suggestions. The authors are thankful to Shri Sagar Chanda, R.A of CW&PRS (Ministry of Jal Shakti, Government of India), for constant guidance.

References

1. Pardeshi AB, Patil HC (2010) Wave attenuation in artificially dredged channels for ports. In: ICHE 2010 Chennai, India
2. Zwamborn JA, Grieve G (1974) Wave attenuation and concentration associated with harbour approach channel. In: Coastal engineering proceedings, January 1974, pp 2068–2085
3. Pardeshi AB, Agrawal JD, Kudale MD (2014) Sensitivity analysis of wave propagation through the long approach channel a port. In: INCHOI, June 2014
4. Kanetkar CN, Joshi VB, Agrawal JD (1994) Wave propagation in a navigational channel to harbour. In: INCHOE 1994 CSIR-NIO Goa, India
5. MIKE21 Spectral Wave Modelling User Guide, Denmark
6. Technical Report No. 4780 September 2010, CWPRS (2010) Mathematical model studies for wave propagation for proposed defending of existing channel and development of outer harbour for LNG terminal at new Mangalore port, Karnataka
7. Abott M, Sorenson (2001) Scientific Documentation of MIKE21 BW DHI
8. Technical Report No. 5706 May 2019, CWPRS (2019) Physical model studies for wave tranquility for the proposed development of coast guard jetty at new Mangalore port, Karnataka

Observation of Flow Pattern at Dahej in Gulf of Khambhat

J. A. Shimpi, S. G. Manjunatha, L. R. Ranganath, K. B. Bobade, and Vivek Saxena

Abstract The Gulf of Khambhat (GoK), formerly known as the Gulf of Cambay situated between Saurashtra peninsula and main land of Gujarat. The peculiarity of GoK is due to its funnel shape geometry which has width of 80 km at the mouth and funnel down to 25 km over a longitudinal reach of 140 km. This inherent important geometric characteristic of GoK results to form the quarter wavelength resonance of the tides. Tides which are semi-diurnal type with a large diurnal inequality, get amplified significantly from South to North due to its geometrical shape and varying bottom friction coefficients (Nayak and Shetye (May 2003) Tides in the Gulf of Khambhat, west coast of India estuarine. Coast Shelf Sci 57(1–2):249–254 [2]). In the North Arabian Sea, the maximum tidal range is found in GoK with an average tidal range of 10 m near to Bhavnagar which is situated at West coast of GoK and around 25 km away from Dahej, which is situated at East Coast of GoK. However, during the data collection at Dahej, the minimum tidal range observed was 3.8 m on 25th February 2018 at 11:45 h., while maximum tidal range was 9.77 m on 4th March 2018 at 12:45 h. Large tidal range is responsible for maximum tidal currents and morphological changes in the GoK. The coastal parameters, viz., tide, tidal currents, suspended concentration, type, and particle size of the bed material are essential and required to be collected for specific site to provide as input parameter to mathematical model studies. This paper describes about coastal data collection at Dahej, in GoK. Highly sophisticated self-recording type Acoustic Doppler Current Profiler (ADCP) were used for current measurement and self-recording type M/s. Vale-port make Wave cum tide gauge was used for water level measurement. To analyse suspended sediment concentration, water samples were collected at different locations at different stages of tide during spring and neap tidal condition. Bed samples were also collected at different locations to analyse the type of bed material. The field data collected would be used for calibration and validation of the model to address the siltation problems near the berthing area in the port of Dahej.

J. A. Shimpi (✉) · S. G. Manjunatha · L. R. Ranganath · K. B. Bobade · V. Saxena
Central Water and Power Research Station, Khadakwasla, Pune 411024, India
e-mail: shimpi899@gmail.com

S. G. Manjunatha
e-mail: manjunatha.sg@cwprs.gov.in

P. V. Timbadiya et al. (eds.), *Coastal, Harbour and Ocean Engineering*, Lecture Notes in Civil Engineering 321, https://doi.org/10.1007/978-981-19-9913-0_13

Keywords Gulf of Khambhat · Current Profiler · Tide gauge · Suspended sediment concentration

1 Introduction

The coastal zone, where the land, sea, and air meet, is one of the most complex areas for civil engineering design. This coastal zone which includes coastline, estuaries and creeks is subjected to various environmental factors. Most of the coastal processes occur over relatively long time spans, having large spatial extents, as well as influenced by meteorological conditions.

Field studies play vital role to study any hydraulic phenomena in prototype. Waves, tides, currents and winds, suspended sediment concentration, bed sample, temperature, bathymetry, topography, beach profiles, etc., are the important parameters which need to be considered for any developments in coastal environment. The effect of these environmental parameters varies over space and time. The knowledge of these parameters is essential in planning and design of harbour works, shore protection works, maintenance of waterways, alignment of jetty, groynes, breakwater, reclamations and its effects on surrounding flow patterns, computation of siltation, capital and maintenance dredging, scheduling of maintenance dredging, shore line changes, to address the problems to accretion and erosion, disposal of dredged spoil, beach nourishments, locating intake and outfall structures, etc. All these works require a systematic collection of data on above-mentioned parameters. Due to dynamic behaviour of the most of coastal processes, understanding of these processes is quite complex without field data collections as well as laboratory model studies. The systematic collection of field data provides baseline information to address various coastal problems.

The field data collection frequency and its methods govern the quality and accuracy of the field data. The duration of data collection depends on the purpose behind collection of data and the risk involved in extrapolation of the data. It is obvious that more the data better the predictions, thus leading to more sound and reliable solutions. However, it should be collected for a period of not less than a year so that all the seasons are well covered. Before carrying out any field survey, proper knowledge about site, nearby topography and morphology, and type of water body, i.e. river, estuary, ocean, etc., is essential. The environmental data which needs to be collected, instruments/equipment required with its capabilities and analysis of data is described in following paragraphs.

2 Study Area

The study area is located in gulf of Khambhat (GoK) (Fig. 1). The location of South and North jetties of M/s PLL is shown in Fig. 2. Locations of field data collected at the vicinity of the jetties are shown in Fig. 3. The gulf is known for high tidal ranges. Due to the large tidal range, strong currents are observed in the Gulf. Large inter-tidal zone exists due to high tidal amplitude. The major rivers viz. Narmada, Tapti, Mahi and Sabarmati form estuaries, and their inflow carries heavy load of suspended sediments in the Gulf. The river Narmada enters the Gulf just south of the southern jetty of M/s. PL. The tidal information of the Luhara (21°' 39' N, 72°' 33' E) is given below (Source: Admiralty Chart No. 2082; Dahej harbour & Approach to Dahej) (see Table 1).

2.1 Data Collection and Analysis

Field data collection was carried out at site during 22nd February 2018 to 8th March 2018 to cover neap and spring tide. Following oceanic parameters were collected during the field data collection.

(i) Tide
(ii) Currents at two locations.
(iii) Water samples at different stages of tide for computation of suspended sedimentation concentration.

Fig. 1 Location map of Dahej in GoK

Fig. 2 Location of South and North Jetties of M/s PLL

Fig. 3 Locations of field data collected

Table 1 Tidal water levels in Gulf of Khambat near Dahej

Tidal levels	Levels in Meter
Mean high water spring (MHWS)	8.80
Mean high water neap (MHWN)	7.0
Mean sea level (MSL)	5.10
Mean low water neap (MLWN)	3.20
Mean low water spring (MLWS)	1.40

(iv) Bed samples at two locations to find the type of bed material

(i) Tides: Tides observed in this region are mixed semi-diurnal type with a large diurnal inequality. A self-recording wave cum tide gauge manufactured by M/s. Valeport, UK, was installed during the data collection at the Northern jetty of M/s. PL. The instrument recorded the data at an interval of every 15 min. The data was retrieved after returning from the site. The tide data recorded by the instrument is presented by time series plot of water level variation observed during the period of data collection at site (Fig. 4). It is observed from the analysis of tidal data that, the predicted tidal values of high water and low water at Dahej match well with the observed values at site. The differences in values are marginal. During the data collection, the minimum tidal range observed was 3.8 m on 25th February 2018 at 1:45 h, while maximum tidal range was 9.77 m on 4th March 2018, at 12:45 h.

(ii) **Tidal Currents**: The tidal currents were measured using Acoustic Doppler Current Profiler (ADCP) manufactured by M/s RDI, USA. It measures the

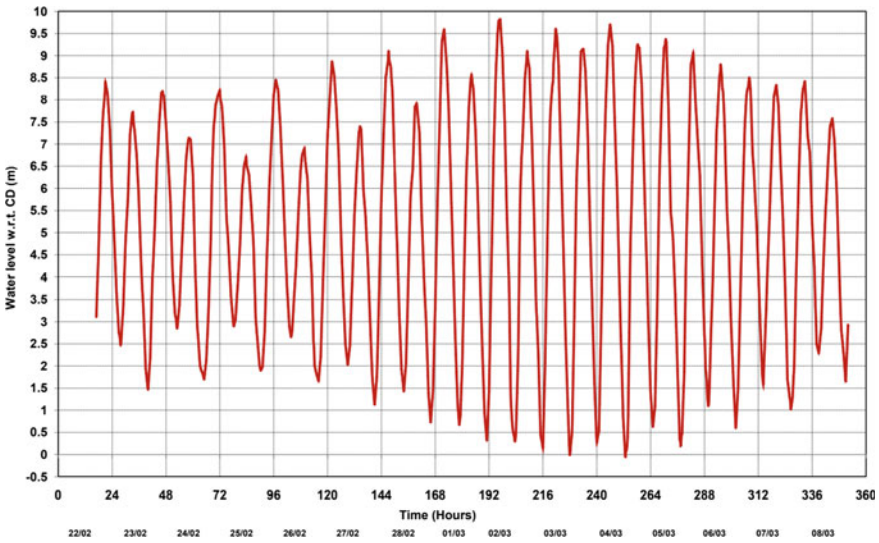

Fig. 4 Tidal variation at Dahej

current magnitude and direction over a depth at specific interval of depth. The data recorded on the instrument was retrieved and then converted into engineering units. The tidal currents were measured at every 15 min interval continuously round the clock at two locations: one was at south of the southern jetty, and another one was at North of the Northern jetty.

3 Tidal Currents at Location C1

ADCP deployed at the location C1 (21° 39.8' N, 72° 30.6' E) to measure magnitude and direction of tidal currents. The currents were measured from 1 m below the free water surface. The analysis of the data has been carried out for three different depths, viz., 1.5, 6.5, and 11.5 m from the water surface. For every day, Figs. 5 and 6 shows the specimen graphs for tidal currents observed at location C1 & C2 on 23 February 2018 at 1.5 m below free water surface. Based on the data observed, it is noted that in general, tidal currents at the site were strong. The maximum current observed at location C1 was 2.30 m/sec. The maximum, minimum and average values of magnitude of currents during neap tide at 1.5 m depth were 1.98, 0.03 and 1.02 m/s, respectively, whereas during spring tide these values were 2.30, 0.02 and 1.37 m/s, respectively. The maximum, minimum and average values of magnitude of currents during neap tide at 6.5 m depth were 1.72, 0.01 and 0.92 m/s, respectively, while during spring tide these values were 2.20, 0.02 and 1.22 m/s, respectively. At 11.5 m depth, the maximum, minimum and average values of magnitude of currents during neap tide were 1.64, 0.02 and 0.82 m/s, respectively, whereas during spring tide these values were 1.80, 0.01 and 1.01 m/s, respectively The maximum ebb and flood currents observed at site were 2.2 and 2.3 m/s, respectively. The current direction during flood phase of the tide varied between 3° and 360°N. Similarly, the variation in flow direction during ebb phase was between 133° and 186°N (see Figs. 7 and 8).

3.1 Tidal Currents at Location C2

The tidal currents at location C2 (21°42.6' N, 72° 30.2' E), which was on North side of the Northern jetty of PLL were measured simultaneously with location C1. The magnitude and direction of the currents observed at different depths viz. 1.5, 6.5 and 11.5 m from the water surface. Based on the data observed, it is noted that in general tidal currents at the site are very strong. The maximum tidal current observed at location C2 was 2.25 m/sec. The maximum, minimum and average values of magnitude of currents during neap tide at 1.5 m depth were 1.93, 0.01 and 1.09 m/s, respectively, whereas during spring tide the values were 2.25, 0.02 and 1.33 m/s, respectively. At 6.5 m depth, the maximum, minimum and average values of magnitude of currents during neap tide were 1.77, 0.02 and 0.98 m/s, respectively, while during spring tide these values were 2.15, 0.02 and 1.22 m/s, respectively. The

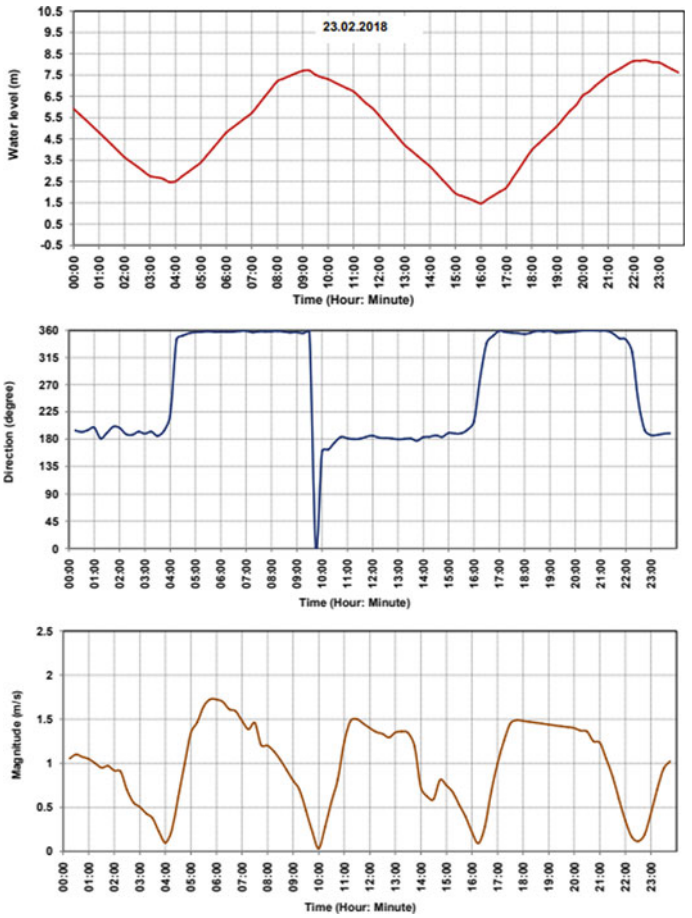

Fig. 5 Tide and tidal currents at location C1

maximum, minimum and average values of magnitude of currents during neap tide at 11.5 m depth were 1.62, 0.01 and 0.87 m/s, respectively, and during spring tide, these values were 2.05, 0.01 and 1.11 m/s, respectively. The maximum ebb and flood currents observed at site were 2.20 and 2.25 m/s, respectively, at 1.5 m below water surface. The current direction during flood phase of the tide varied between 6° and 359°N. Similarly, the variation in flow direction during ebb phase was between 172° and 179°N.

(iii) **Suspended sediment concentration**: During the field data collection, water samples of 2 L were collected from near mid depth at both the locations of current observations, i.e. at locations C1 and C2. The samples were collected during neap and spring tide at different tidal stages viz. low water slack, mid of flood, high water slack and mid of ebb. The water samples collected at site were

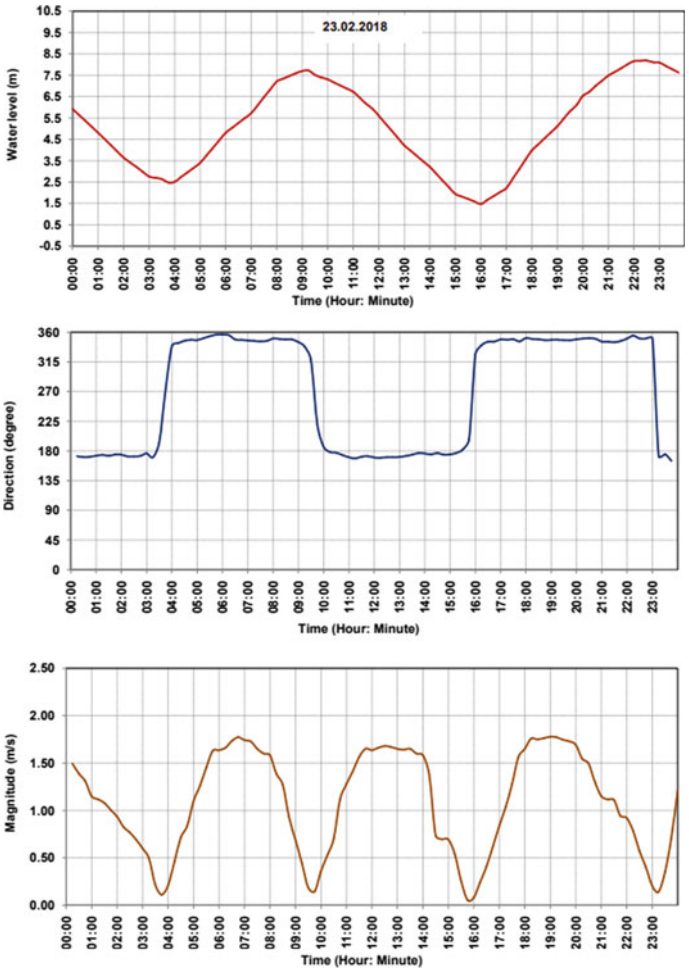

Fig. 6 Tide and tidal currents at location C2

analysed to determine the suspended sediment concentration. Due to strong flood and ebb currents, the water remains always turbid with high suspended sediment concentration. The suspended sediment concentrations measured was varied between 950 and 2849 mg/lit. The sediment concentration was relatively low during flood phase and high-water slack period. During the low water slack and mid of ebb, the suspended sediment concentration was found to be relatively higher.

(iv) Bed sample analysis: The bed samples were collected at both the locations of current observations, i.e. at locations C1 and C2 using grab sampler as shown in Fig. 9. The mechanical analyses of samples were carried out. The results are presented in the form of gradation curves are shown in Fig. 10. The bed

Fig. 7 ADCP deployed at location C1

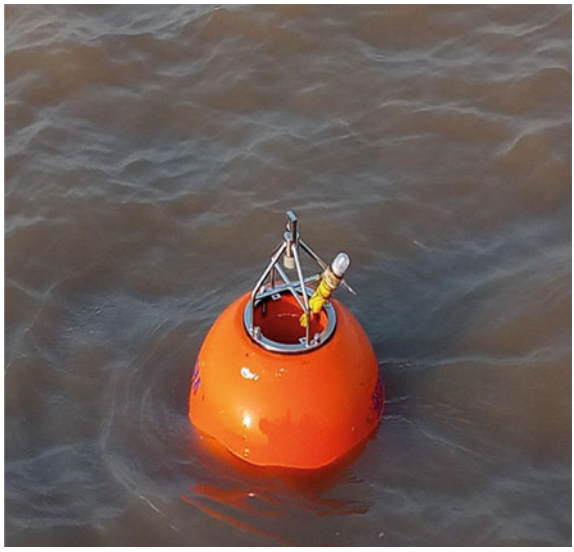

Fig. 8 ADCP deployed at location C2

materials at location C1 and C2 have D50 values of 0.429 and 0.245 mm, respectively. The type of bed material was fine sand.

4 Conclusions

It was observed from the field data collection and analysis that tides observed at Dahej are mixed semi-diurnal type with a large diurnal inequality in nature. The flow field

Fig. 9 The particle size distribution curve (for location C1)

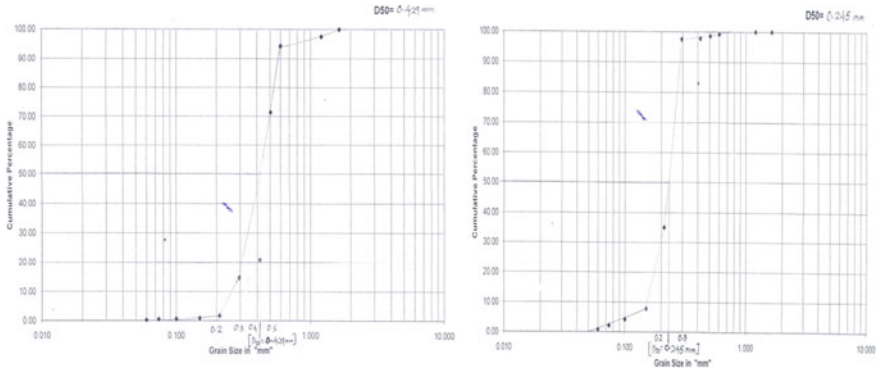

Fig. 10 The particle size distribution curve (for location C2)

in the gulf of Khambhat is complex and dynamic in nature. The Maximum tidal range observed during the spring tide was 9.77 m, while during the neap tide was 3.80 m. Large tidal range is due to its inherent geometrical funnel shape which leads to quarter wavelength resonance of the tides. The high tidal ranges cause strong tidal currents in the range of 2.2–2.3 m/sec during ebb and flood tidal condition. The suspended sediment concentrations measured was varied between 950 and 2849 mg/lit. Bed sample analysis indicated that the bed materials at locations C1 and C2 have D_{50} values of 0.429 and 0.245 mm respectively. The type of bed material was fine sand [1]. The collected data is useful for potential professionals and others working for this region. The data collected was used for the hydraulic model studies to resolve the siltation and other hydrodynamic problems of that particular area.

Acknowledgements The authors are thankful to Shri. A. K. Agrawal, Director, CWPRS for his kind permission to publish this paper. Authors are also thankful to the M/s PLL for the necessary arrangements at site during field data collection.

References

1. CWPRS Technical Report No 5657 Year 2018 (2018) Field data collection and analysis for Mathematical Model studies for M/s Petronet LNG Limited at Dahej, Gujarat
2. Nayak and Shetye (May 2003) Tides in the Gulf of Khambhat, west coast of India estuarine. Coast Shelf Sci 57(1–2):249–254

Mitigation of Sedimentation in Approach Channel and Harbour at Passenger Jetty, Mandwa, Maharashtra

V. B. Sharma, V. P. Konde, and Prabhat Chandra

Abstract Mandwa port is situated on the West coast of India which connects Mumbai to Alibag by establishing inland water transport to reduce travel time and traffic on the road. The port comprises a breakwater of length 360 m and a navigational channel of length 1.8 km, 150 m wide dredged initially to (−) 4.0 m below Chart Datum (CD). The clear depths in the channel are required be maintained at about 2.5–3.0 m below chart datum throughout the year. At present, the port is facing severe problem of sedimentation in the navigational channel. The sedimentation in the approach channel and in the harbour areas occurs mainly due to the deposit of the sea-borne suspended sediments in the dredged areas. There is no significant contribution in the overall sedimentation due to the littoral or river discharges. The annual sedimentation in the approach channel is about 2.0 m, and this would not facilitate availability of clear depth of more than 2.5 m throughout the year in the channel and in harbour area. In order to mitigate this problem of sedimentation two proposed scenarios were studied, namely, proposed condition-I with additional dredging in the channel and harbour areas and other proposed condition-II with modification in the channel alignment (orientation) to align it along the currents to reduce sedimentation in the channel. The MIKE-HD/MT model was utilised for the studies which was calibrated with the collected field data. In second proposal, length of channel slightly reduces by about 100 m. In first proposal, both initial cost and maintenance cost would increase marginally, while in second proposal, initial cost of dredging will be very high as new approach channel needs to be dredged but its maintenance cost will be much less. The detailed findings of this study would be discussed in the paper.

Keywords Tide · Current · Sedimentation · Maintenance dredging · Approach channel

V. B. Sharma (✉) · V. P. Konde · P. Chandra
Central Water and Power Research Station, Khadakawasla, Pune 411024, India
e-mail: vipin_bihari@yahoo.com

P. V. Timbadiya et al. (eds.), *Coastal, Harbour and Ocean Engineering*, Lecture Notes in Civil Engineering 321, https://doi.org/10.1007/978-981-19-9913-0_14

1 Introduction

Mandwa port is situated on the west coast of India which connects Mumbai to Alibag in by establishing inland water transport to reduce travel time and traffic on the road. In line with the Government's increasing thrust on waterborne transportation, MMB in April 2018, completed construction of state of the art Ro-Ro jetty, breakwater, and allied facilities at Mandwa (Fig. 1). Roll on and Roll off (Ro-Ro) services between Mumbai and Mandwa have also been launched in March 2020. The port comprises a breakwater of length 360 m and a navigational channel of length 1.8 km, 150 m wide dredged initially to about (−) 4.0 m below Chart Datum (CD). It was indicated by the project authorities that the port is to be used for Ro-Ro vessels of about 20 m beam for two way operation in the channel. The clear depths in the channel are required to be maintained at about 2.5–3.0 m below chart datum throughout the year. At present, the port is facing severe problem of sedimentation in the navigational channel. The sedimentation in the channel can be attributed to mainly high sediment concentration levels in the region and the strong currents normal to channel. A capital dredging of about 4,26,000 cubic metre was carried out to achieve initial dredged depths of about −3.5 to 4.0 m below CD in the navigational channel. During the monsoon period, sedimentation in the navigational channel is of the order of 0.2 Million cum as observed from the bathymetric charts of the year 2018 which accounts for about 80% of total annual sedimentation. The sedimentation in the approach channel and in the harbour areas occurs majorly due to the deposit of the sea-borne suspended sediments in the dredged areas. There is no significant contribution in the overall sedimentation due to the littoral or river discharges.

The present paper model studies carried out using MIKE-21 HD/MT for assessing the hydrodynamics and sedimentation patterns in the approach channel and harbour areas at Mandwa jetty have been presented, and suitable recommendations to mitigate sedimentation problems have to been suggested.

2 Data Analysis

The prototype data is used to calibrate the model. This calibrated model is used to predict the impact of proposed or existing maritime structures on hydrodynamics and sedimentation. The Bathymetry was taken from C-map data available in MIKE-21 software. The bathymetry indicates that existing Mandwa jetty is in shallow water at about (−) 2.5 m depth contour. As the average tidal range is of the order of 5 m, and large area is subjected to flooding and drying. The bathymetry in the vicinity of shown in Fig. 2.

The tides at Mandwa are semi-diurnal in nature. It can be observed from figure that the maximum tidal range during spring tide is about 5 m, while during neap tide it is about 1 m. This observed tide was used for simulation and calibration of the model.

Fig. 1 Location plan

Observed currents were available at two locations (Fig. 3) C1 and C2 as shown in Figs. 4 and 5 which were used to calibrate the model. The maximum currents recorded in harbour area are of the order of 0.8 m/s while at C2 location, the maximum currents are of the order of 1.4 m/s.

The observed suspended sediment concentration suspended solids varies from 100 to 1000 mg/l during non-monsoon and monsoon period, respectively.

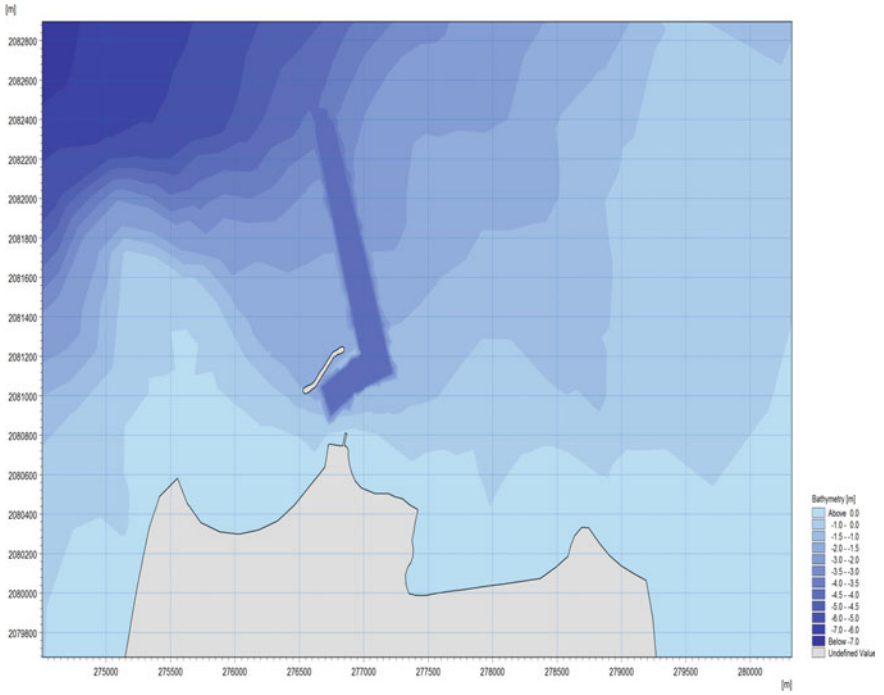

Fig. 2 2D view of bathymetry

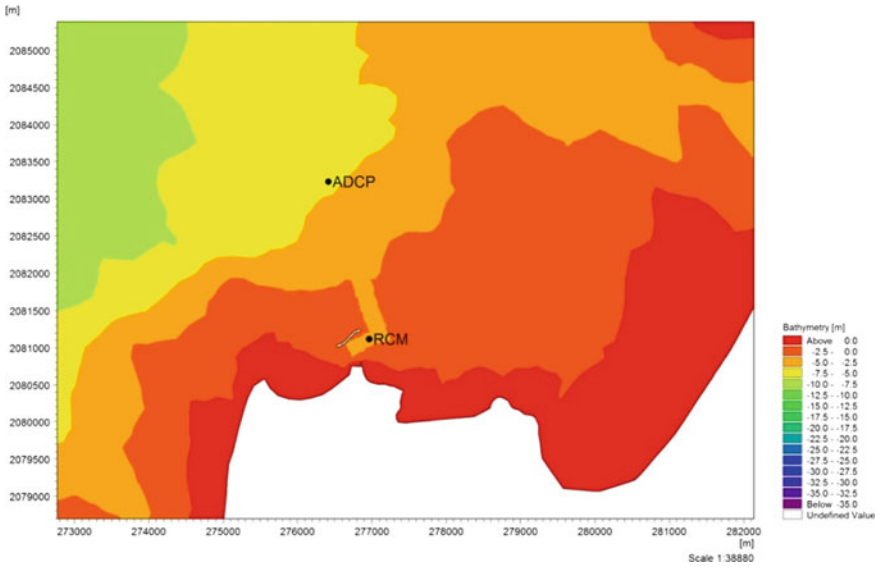

Fig. 3 Observed current data locations

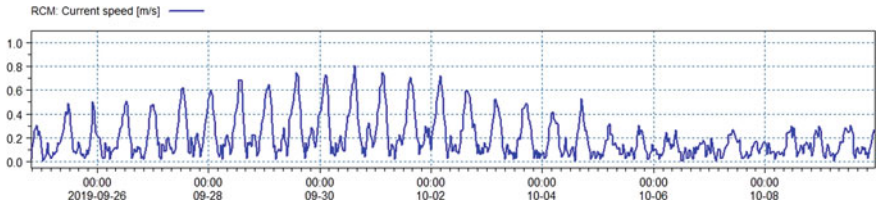

Fig. 4 Observed current in harbour A C1

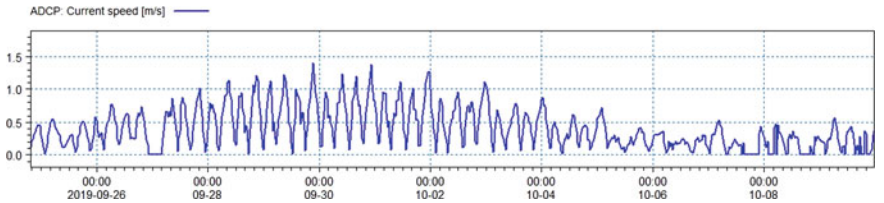

Fig. 5 Observed current in channel area C2

3 Modelling Approach

Coastal hydrodynamics refers to the part of the coastal process which deals with tide, wave, its transformation and dissipation. Radiation stresses also play an important role in coastal process. These are the depth integrated and wave averaged excess momentum fluxes due to waves as defined by Longuet-Higgins and Stewart (1964). Radiation stresses are responsible for set-up, set-down, and longshore current in the nearshore zone. This approach is used in MIKE-21 SW model to simulate radiation stresses. In MIKE-21 HD model, turbulence modelling is included in the momentum equations in the terms containing laminar stresses and Reynolds stresses. It can be either used as a constant in the horizontal stress terms or by using the Smagorinsky's formulation (1963) to express sub-grid scale transports by using an effective eddy viscosity related to characteristic length scale (Lily 1989).

In order to simulate dynamics of cohesive sediment, it is necessary to initially compute the hydrodynamics of water body in terms of velocity and water level fluctuations. Thus, MIKE-21 HD model has been used for simulating hydrodynamics, while MIKE-21 SW (short wave) model has been used to simulate wave-induced radiation stress which is input to MIKE-21 HD Model. MIKE-21 HD model is based on the numerical solution of the two-dimensional incompressible Reynolds averaged Navier–Stokes equations invoking the assumptions of Boussinesq and of hydrostatic pressure. The spatial discretization of the primitive equations is performed using a cell-centred finite volume method.

Further, for simulating sediment transport, Mud Transport Model (MIKE-21 MT) which is based on advection–dispersion equation was used which describes erosion and deposition of mud or sand/mud mixtures under the action of currents and waves.

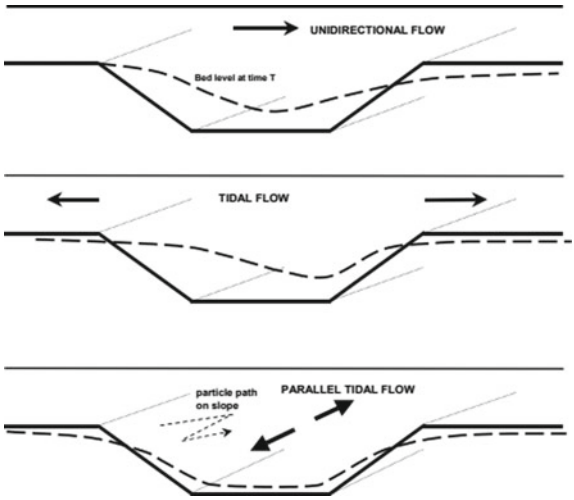

Fig. 6 Sedimentation in channel for different flow conditions and different channel orientation

The two-dimensional depth-averaged sediment transport model (MIKE-21 MT/AD) takes into account conservation of mass of sediment, depth-averaged velocities, longitudinal dispersion coefficient, lateral diffusivity, settling velocity, critical deposition stress, and critical erosion stress for the given sediment. Flocculation of mud particles is described as function of suspended sediment concentration as given by Burnt 1986. The numerical values of these parameters were modified within their ranges such that the prevailing sedimentation in the existing approach channel is achieved.

Sedimentation in approach channel is influenced by the orientation of approach channel with respect to direction of flow. Sedimentation in channel is maximum when flow is perpendicular to approach channel, and it is minimum when flow is parallel to channel orientation. Figure 6 shows sedimentation pattern in approach channel.

Channel orientation perpendicular to the flow causes reduction of velocities in the deeper zone of the channel. This is significant in the near-bed layer where adverse pressure gradients cause a strong reduction of the flow and flow separation and reversal will occur Van Rijn [1], 2012 as shown in Fig. 7. Sedimentation depends the ratio of existing depth and dredged depth ratios [2]. According to Gole and Tarapure [2] sediment-carrying capacity is proportional to the square of the velocity, the rate of infilling was derived to be $h_d{}^2 - h_a{}^2/h_d{}^2$

h_d = depth of initially dredged channel, and h_a = ambient depth upstream

Galvin in 1992 improved the Gole and Tarapure formula considering suspension and bypassing of sediment as shown in Fig. 8

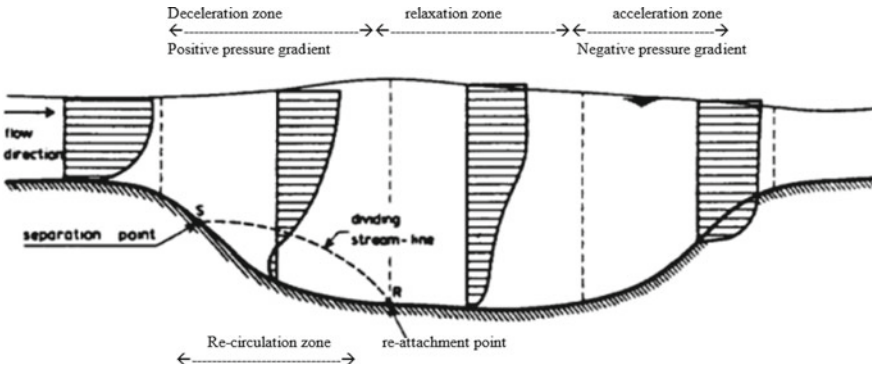

Fig. 7 Channel perpendicular to flow direction, flow velocity profiles in channel

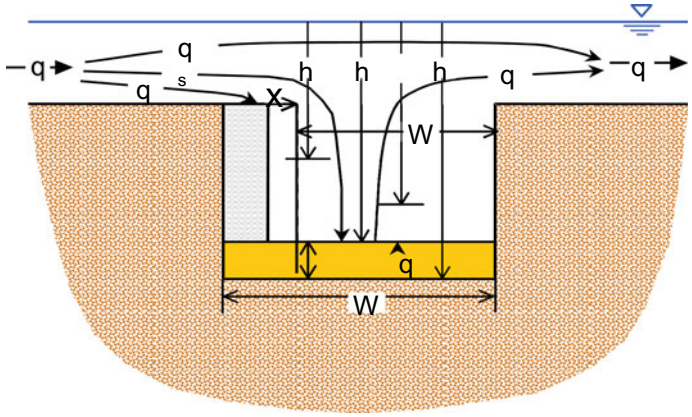

Fig. 8 Gavin method approach

4 Model Calibration

The computational model considered for tidal flow simulation covered an area of 50 km × 60 km. The model area covers entire Mumbai creek up to (−) 28 m depth contour. Model simulations were carried out for existing condition. This comprises a breakwater of length 360 m and a navigational channel of length 1935 m oriented at 340ºN dredged to −4 m. Mesh and bathymetry files were generated using MIKE-21 tools. In the vicinity of Mandwa Port, fine mesh was generated, while in remaining model area, coarse mesh was generated to reduce the simulation time.

The model area consists of three open boundaries at sea side. Predicted tidal levels obtained from C-map were supplied at north and south boundaries with appropriate level differences. As the flow is almost parallel to the contours along western

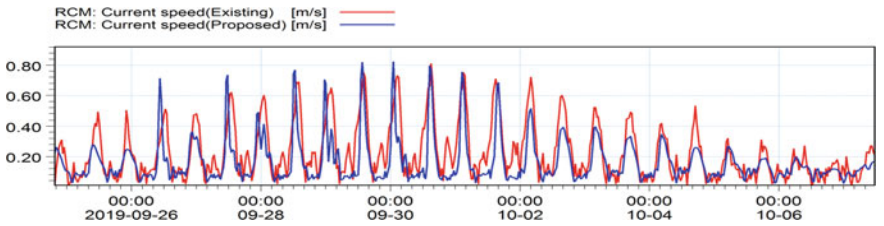

Fig. 9 Calibration of currents at location C1

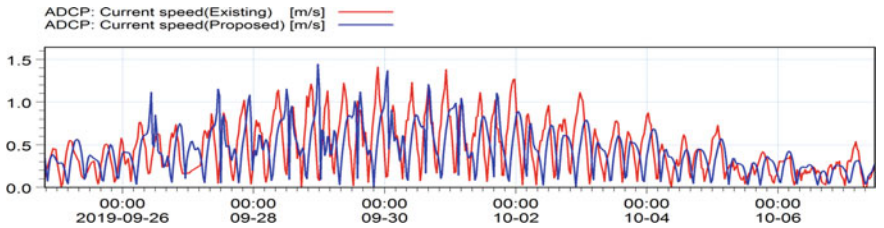

Fig. 10 Calibration of currents at location C2

boundary, no cross-flow condition was provided at this boundary. The model parameters like bottom roughness coefficient, surface elevation, etc., were adjusted to get the required prototype conditions in the model. The simulations were repeated by changing model parameters until the computed values matched with the field observed data. The changes in flow fields were computed at every time step of 30 s, and results are recorded at every 30 min time interval. The computed values of currents were compared with the field observed data. The calibration of currents at two locations is shown in Figs. 9 and 10. It can be observed that the currents match well with the prototype data.

Typical flow behaviours during peak flood and peak ebb are shown in Figs. 11 and 12. The length of vector shows the magnitude of current, and arrowhead of vector indicates the direction of flow. It can be observed that flow is almost perpendicular to channel. This is the worst scenario from the considerations of sedimentation.

5 Sedimentation Studies

The output of hydrodynamics was used in MIKE 21 MT model to evaluate sedimentation in the channel. The hydrographic surveys during different seasons were provided by the MMB and these were analysed to assess the sedimentation in the channel and harbour areas and the same were used to calibrate the sediment model. It can be observed that maximum sedimentation in the channel is in it's mid portion and harbour area. Mike-21 MT model was simulated for 15 days to cover both spring and

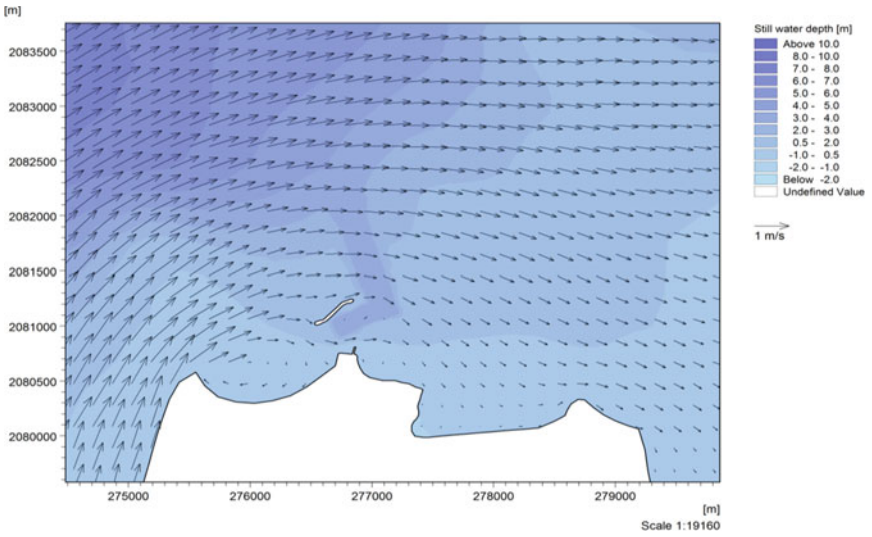

Fig. 11 Flow pattern in model area during peak flood

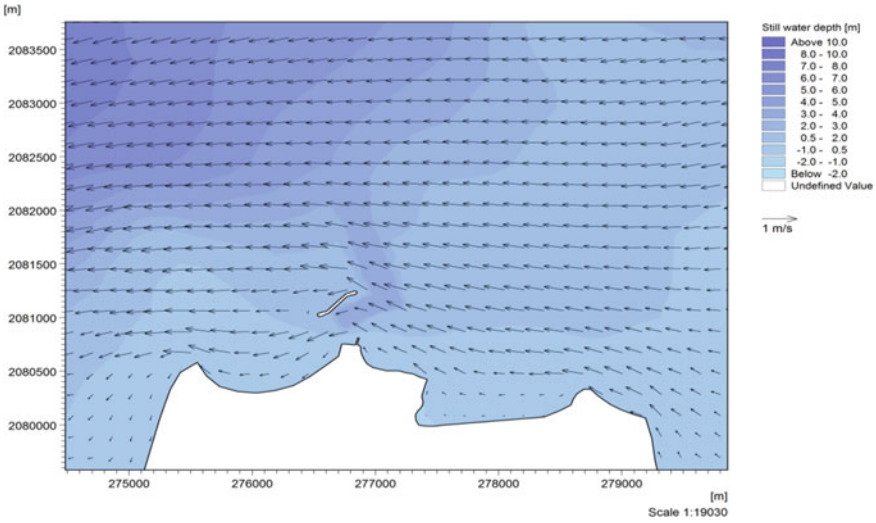

Fig. 12 Flow pattern in model area during peak Ebb

neap tide. Typical plot of sedimentation in the channel after 15 days of simulation is shown in Fig. 13. Model calibration for sedimentation in navigational channel is shown in Fig. 14.

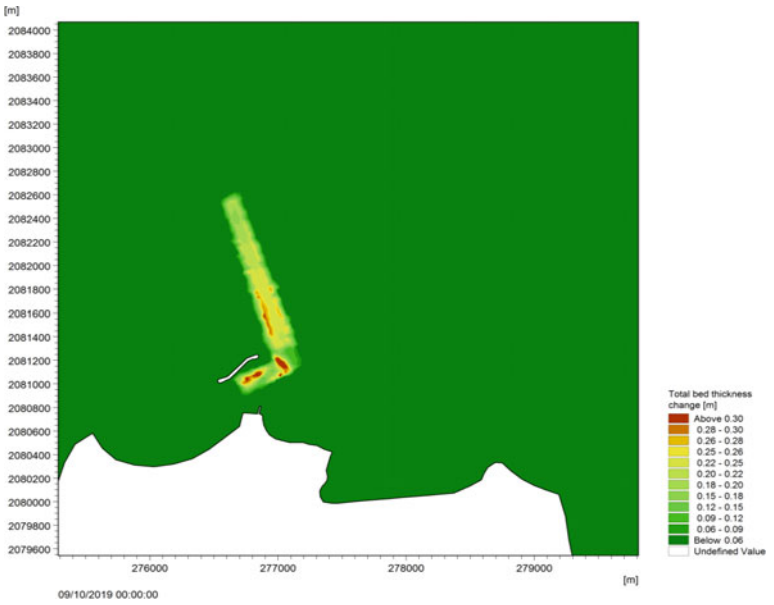

Fig. 13 Sedimentation in existing condition after 15 days during monsoon

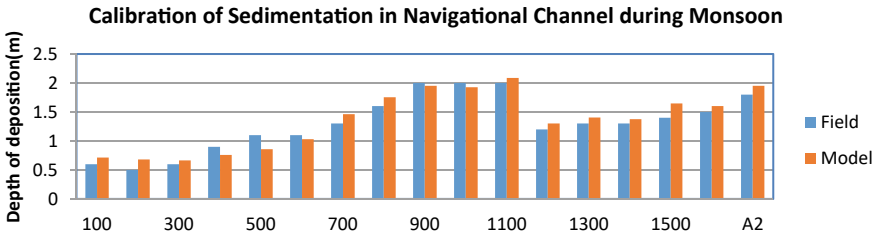

Fig. 14 Calibration of sedimentation in navigational channel during monsoon

5.1 Proposed Alternative Scenarios

Sedimentation in a channel depends upon various parameters like currents, waves, suspended sediment concentration, bed material characteristics, and angle between flow and axis of channel. Sedimentation is maximum when flow is perpendicular to channel and its minimum when flow is parallel to channel. In the present scenario, parameters like currents, waves, suspended sediment concentration, and bed material characteristics cannot be changed as these are site dependent. Thus, the only variable which can be varied is angle between current direction and channel axis. Additionally, as per the study of the sediment patterns, the dredged depth can be increased in high deposition zones to provide additional cushion for ship to enable maintaining a depth of about 2.5–3.0 m throughout the year. It may be noted that

as the depth of dredging increases, the rate of deposition also increases resulting in more requirement of maintenance dredging. As per the existing condition, it is difficult to maintain the required depth of 2.5–3.0 m in the existing channel due to the sedimentation. Considering all these factors, following two alternative scenarios/ proposed conditions were conceptualized, studied, and evaluated.

1. Proposed Condition 1–Additional dredging in high deposition zones of existing channel
2. Proposed Condition 2–Modifying the navigation channel alignment along the flow.

5.1.1 Proposed Condition 1 with Additional Dredging

It is evident from Fig. 14 that the rate of sedimentation is more after 800 m chainage upto the harbour area. This zone is termed as Zone-I while up to 800 m chain age from sea end, it is termed as Zone-II. Under this proposed condition 1, the zone-I is proposed to be dredged to −5 m depth below CD, while Zone-II to −4 m depth contour as shown in Fig. 15. Hydrodynamic model was simulated for this condition without changing the hydraulic parameters used in calibrated of model (existing condition).

Mud transport model was simulated for proposed condition 1 with variable depth of dredging without changing the parameters for which model was calibrated in existing condition. Typical plot of sedimentation in the channel after 15 days of simulation is shown in Fig. 16.

It can be observed from the figure that the annual sedimentation in the Zone-I (dredged depth of −5 m) increases by about 25% while in Zone-II, it remains almost same.

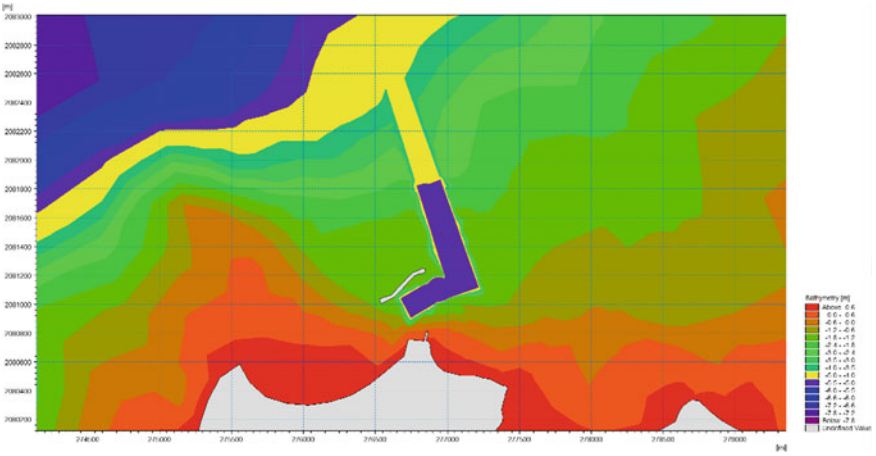

Fig. 15 2D View of Bathymetry in vicinity of port area (proposed condition-1)

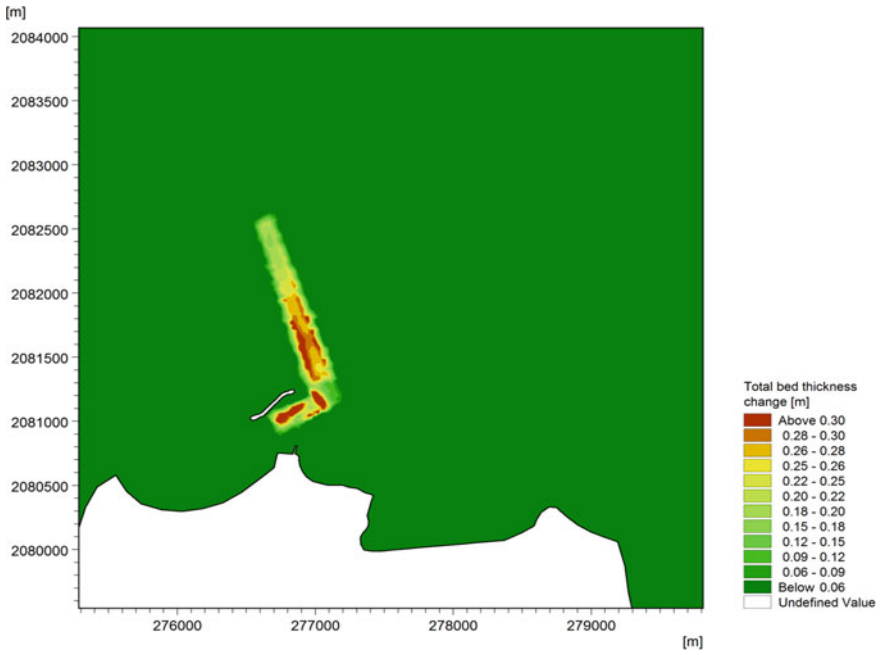

Fig. 16 Sedimentation in proposed condition-1 after 15 days during monsoon

Average depth of annual sedimentation in this scenario at an interval of 100 m is compared with the existing sedimentation in the channel and is shown in Fig. 17. The annual sedimentation in zone-I is of the order of 2.5 m which was about 2.0 m in existing condition.

A clear depth of more than 2.5 m below CD is assured in the channel and harbour areas throughout the year for proposed condition 1.

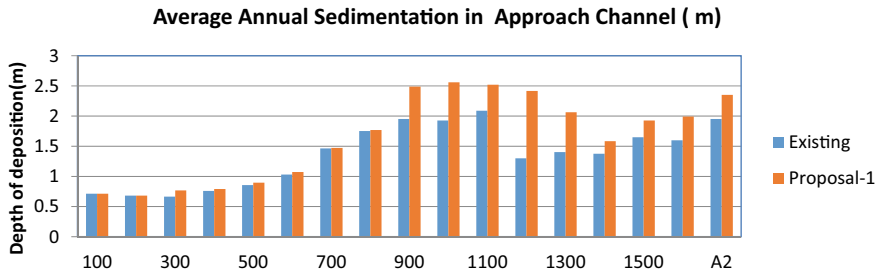

Fig. 17 Comparison of annual deposition in existing and proposed condition 1

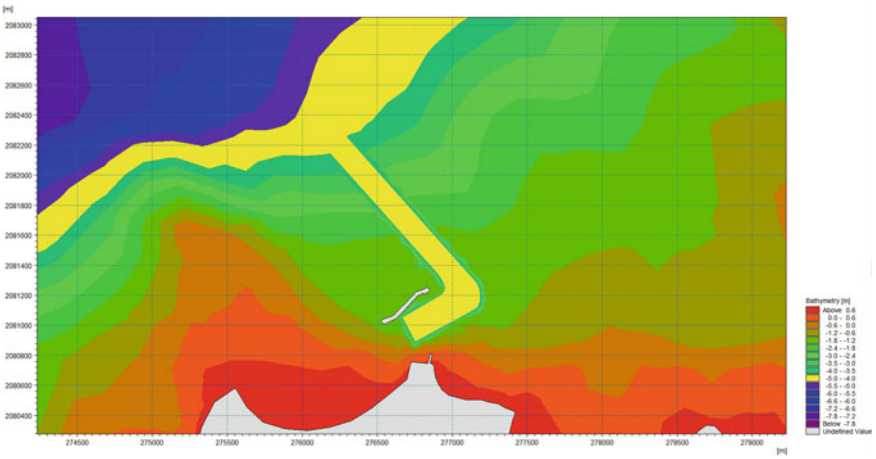

Fig. 18 2D bathymetry for proposed-II condition (channel orientation 320ºN)

5.1.2 Proposed Condition 2: Modification in Alignment of Channel

The bearing of existing channel is 340ºN. The current direction is oblique to the axis of channel. More sediment is trapped when it moves oblique or near normal to the channel. In order to align the channel along the flow, channel orientation has been changed to 320ºN from 340ºN and dredged initially to −4 m below CD. In this proposed condition2, the length of channel is also reduced marginally by about 100 m. This proposal was studied to reduce the maintenance dredging requirement further. This proposal was incorporated in the bathymetry as shown in Fig. 18, and hydrodynamic and sedimentation studies were carried out.

Mud transport model was simulated for proposed condition-2 without changing the parameters for which model was calibrated in existing condition. Typical plot of sedimentation in the channel after 15 days of simulation is shown in Fig. 19.

It can be observed from the figure that sedimentation deposition in the channel reduced significantly. Average depth of annual sedimentation in this scenario (Proposed-2) at an interval of 100 m is compared with the existing sedimentation and proposed condition-1 and shown in Fig. 20. It can be observed that maximum annual sedimentation in the channel is about 1.2 m as compared to 2 m in existing condition. There is an overall reduction in the depth of deposition. On an average 40–50% reduction in sedimentation is observed in the sedimentation patterns compared to prevailing sedimentation in the channel.

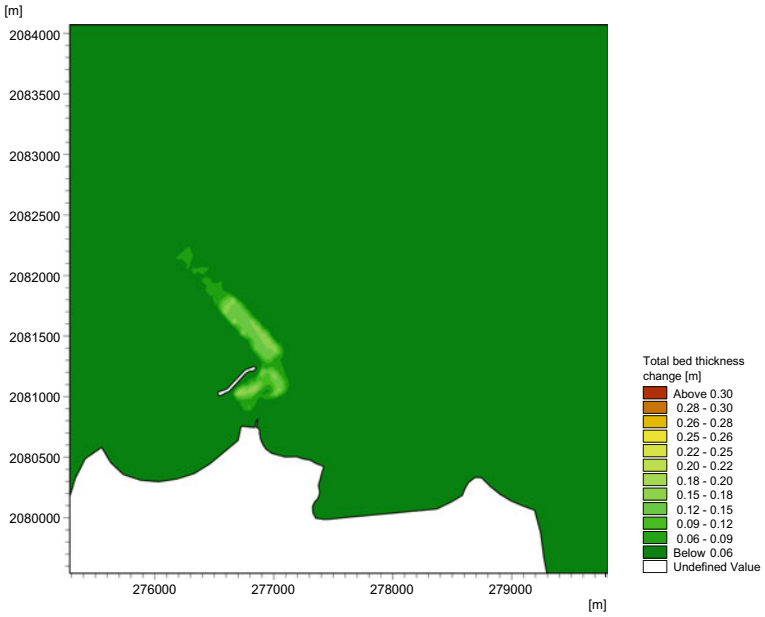

Fig. 19 Sedimentation in proposed condition-2 after 15 days during monsoon

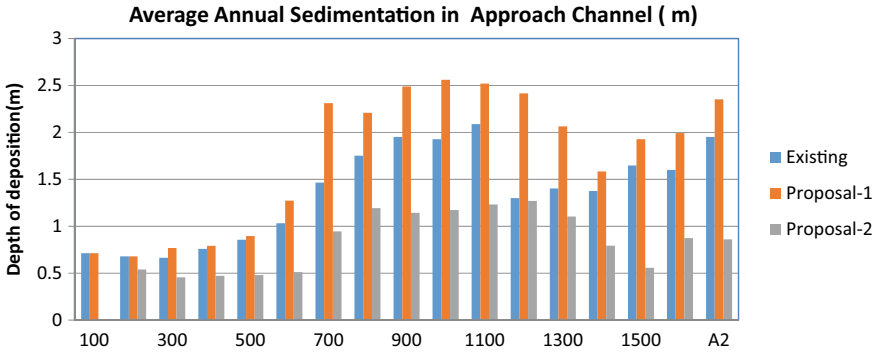

Fig. 20 Comparison of annual deposition in existing and proposed-1 and 2 conditions

6 Conclusions

On the basis of preliminary mathematical model studies for assessment of hydrodynamics and sedimentation in the channel and harbour areas of Mandwa jetty, the main findings are as below:

- The maximum currents in the harbour area are about 0.8 m/s, whereas these are 1.4 m/s in the open channel area. The sediment concentration values range from 100 to 1000 ppm in the region.
- Under the existing condition, the annual sedimentation in the approach channel dredged to (−) 4 m below CD is about 2.0 m and this would not facilitate availability of clear depth of more than 2.5 m throughout the year in the channel and in harbour area. The sedimentation is comparatively less in Zone 2 (up to 800 m from the sea end of the channel), but it is quite more in Zone 1 (beyond 800 m up to harbour).
- Two proposed scenarios were studied; (i) proposed condition-1 with additional dredging in the channel and harbour areas Zone 1 to −5.0 m and Zone 2 to −4.0 m (Fig. 13) for the existing alignment of the channel, (ii) proposed condition-2 with Modification in the channel alignment to bearing 320ºN (Fig. 19) more along the current with dredging at (−) 4.0 m below CD.
- For proposed condition-1, the annual sedimentation in the channel and harbour areas in Zone 1 would be increased to about 2.5 m, but with the additional cushion dredging provided, a clear depth of more than 2.5 m below CD would be available throughout the year in the channel and harbour areas.
- For Proposed Condition 2 with modification in the channel alignment (Fig. 19), the sedimentation would be reduced by 30–40% in comparison to the existing scenario, and the annual sedimentation would be about 1.2–1.4 m. The channel length would also be reduced marginally by about 100 m. The navigation and manoeuvring aspects need to be seen by the project authorities for the modified alignment of channel.

Acknowledgements The authors are thankful to Shri A. K. Agrawal, Director, CWPRS for his kind permission to publish this paper.

References

1. Van Rijn LC (2006) Principles of sedimentation and erosion engineering in rivers, estuaries and coastal seas
2. Gole CV, Tarapore ZS (1971) Prediction of siltation in harbour basins and channels. In: Proceeding of the 14th congress of IAHR, Société Hydrotechnique de France, Paris, France, D5-1-D-5-8

Beach Profile Changes Along an Open Coast and Near an Estuary

S. Vasanthakumar, S. A. Sannasiraj, K. Murali, and V. Sundar

Abstract The beach profile changes form the primary aspect of the field study in understanding coastal processes as they vary concerning different coasts, site conditions, and wave characteristics. In this study, beach profile changes on an open coast and near an estuary are quantified through field investigations conducted over a couple of years. The changes in the beach profiles are compared temporally and spatially. The data was collected on the first spring of every month using Real-Time Kinematic Global Positioning System (RTK-GPS) from May 2017 to April 2019. The accuracy of data collected using RTK-GPS is 8–15 mm. The study areas are considered an open coast in Devaneri, Tamil Nadu, and near an estuary with its mouth being trained by a pair of training walls in Karaikal, Puducherry, India. Both the sites are located along the Southeast coast of India and are 300 km apart. The open coast has remained constant with minor changes in the profiles, and the one near an estuary coast undergoes significant changes seasonally and spatially. It is observed that the presence of coastal structures dictates the terms in the erosion/accretion process on the coast.

Keywords Beach profile · Open coast · Estuary · RTK-GPS

S. Vasanthakumar (✉) · S. A. Sannasiraj · K. Murali · V. Sundar
Department of Ocean Engineering, Indian Institute of Technology Madras, Chennai, Tamil Nadu, India
e-mail: vasanth.kumar1122@gmail.com

K. Murali
e-mail: murali@itm.ac.in

V. Sundar
e-mail: vsundar@iitm.ac.in

P. V. Timbadiya et al. (eds.), *Coastal, Harbour and Ocean Engineering*, Lecture Notes in Civil Engineering 321, https://doi.org/10.1007/978-981-19-9913-0_15

1 Introduction

The beach profile changes are one of the most studied features in understanding the morphology of a coast prior to considering any development. Hence, it is essential to regularly monitor the spatial and temporal evolution of the beach profiles. Though several models have been developed to estimate their changes, the field data helps in cross-referencing and benchmarking the models. An open coast is primarily dominated by the action of waves and other natural factors. The erosion and/or accretion processes along the coast might not follow a particular trend or the drift pattern for certain stretches of the coast, whereas in a few other stretches, the beach may remain stable with just minor changes. Morphologically, estuarine coasts have been categorized into five profile shapes created by dominating non-storm factors, including local wave generation, beach orientation, beach width and slope, and sediment grain size [9]. The presence of hard protection structures dictates the erosion/accretion pattern along a coast [4, 5]. Beach profiles with nearshore bathymetry are an estimate of erosion/accretion patterns, more importantly in artificial beach nourishment in the vicinity of coastal structures [1]. The changes in the beaches are seasonal, while severe storms or other extreme coastal hazards impact the coast. Usually, the sediments from beaches are removed and deposited as an offshore bar. Once the storm recedes, the offshore bar is driven back to its original location by the waves. Continuous monitoring of beach profiles provides great hindsight into its changes, sometimes being rapid. The rate of erosion/accretion, due to the normal and extreme weather events and the shoreline response to engineering structures can be estimated through regular field surveys, which also serve as ground truth for validation of numerical models. With more intense and finer spatial and temporal scales, the coast's localized impacts can be easily quantified. Any line perpendicular to the beach and intersecting the sea is called a beach profile. The present study explores the site-specific impact of longshore drift on beach morphodynamics. The long-term net littoral drift is toward the north on the east coast of India [7]. In this study, beach profile changes on an open coast and near an estuary are quantified through field investigations over a couple of years. Understanding the behavior of the estuarine coast in a coastal environment is a very important aspect of the coastal process.

2 Materials and Methods

2.1 Beach Profiling Techniques

The beach profile can be obtained with different types of equipment varying from simply graduated rods and chains [3] to standard stadia rods and levels to a more accurate auto-tracking geodimeter with a reflecting prism [2]. A typical shore-normal beach survey provides a one-line cross profile of beach that represents the relative

elevation of the beach from a standard reference. This profile includes the position of key beach features, such as shoreline, berm, dunes, sand bar, and vegetation cover. A typical reference point for each profile is sited over a permanent structure to re-establish the profile origin for successive surveys. For accuracy, the survey is accomplished on the same line each time because any slight deviation from the prior established orientation could yield results that can lead to misinterpretation. Another difficulty inherent with profiling is the necessity to adopt linearity between successive data points along the profile line. It is therefore vital that all crest and berm features, which are present across the profile, are surveyed so that a true representation of the beach-profile surface can be recorded. An awareness of these limitations ensures that the measurements are taken in the field to eliminate or reduce factors liable to cause potential errors in surveying and the interpretation of resulting data [10]. Comparing successive beach profiles produces a two-dimensional cross-sectional area, representing the amount of beach erosion and accretion between the surveys. A three-dimensional volumetric change in the beach is computed by integrating adjacent cross-profile areas and comparing them with prior surveys. [8]. Three potentially significant errors are associated with these approaches in estimating beach erosion or deposition. The first is that all the measurements are relative to a standard benchmark. If this reference disappears or is lost, it is challenging to compare it with the previous profile or make it more accurate with subsequent surveys. The second potential error occurs if subsequent surveys do not follow the same orientation as the previous survey. The third possible error involves the three-dimensional interpolation from two-dimensional data. Interpolated results are subject to significant errors if the two-dimensional comparisons neglect subtle changes in the beach surface or if the adjacent profiles are widely spaced. Practical limitations associated with conventional beach monitoring are:

- The long time required to conduct extensive surveys,
- The common loss of "permanent" reference where the beach is either rapidly eroding or subjected to substantial wave penetration during storms, and
- The errors associated with estimating volumetric changes from inadequate data.

2.2 Beach Profiling Using RTK-GPS

There are several survey techniques available for obtaining the beach profiles. Of all those techniques, data collection by the Real-time Kinematic-Global positioning system (RTK-GPS) provides the best data of the highest quality and is quick. It is a satellite navigation technique used to enhance the precision of position data derived from satellite-based positioning systems (Global Navigation Satellite Systems, GNSS) using base station. The base station is a ground-based fixed reference point near the survey area. The major setups in the instrument are reference ellipsoid (WGS 1984), Local geoid (EGM2008), Projection (UTM-44), and exact position of receiver antenna. Since all the profiles' starting point is preloaded in the

instrument, rapid erosion need not be worried. The spatial and temporal analysis of data provides the volumetric changes per unit shoreline.

2.3 Study Area

The study areas are considered as an open coast in Devaneri, Tamil Nadu, and near an estuary with its mouth being trained by a pair of training walls in Karaikal, Puducherry, India. Both the sites are located along the Southeast coast of India and are 300 km apart.

2.3.1 Devaneri (Open Coast)

The study area is an open coast along with the coastal fishing village in Devaneri. This coast is located about 50 km south of the metropolitan city Chennai along the Southeast coast of India. The project site (12° 38 ′55″ N to 12° 39 ′15″ N and 80° 12 ′14″ E to 80° 12 ′35″ E) is bordered by the Bay of Bengal on its east. This fishing village is just about 4 km close to the major tourist attraction, viz., Mahabalipuram, a UNESCO World Heritage Site of 7th- and 8th-century monuments, one which is the shore temple, the details of which are as shown in Fig. 1.

2.3.2 Karaikal (Near Estuary

Karaikal is a coastal town with a minor port occupying an area of 160sq.km which was formerly part of French India (Fig. 2). The site falls within the Latitude between 10° 54′ 25″ N to 10° 55′ 08″ N and Longitude 79° 51’ E to 79° 51′ 23″ E. The coastal stretch of the Karaikal is dominated by sandy beaches and tidal flats. The vast alluvial plains occur in the eastern part of the Karaikal region. Arasalar River, a tributary of the river Cauvery, empties itself into the Bay of Bengal at Karaikal. To prevent the sand bar formation near the mouth of the estuary and to train the discharge of the river, a pair of training walls have been constructed on either side of its mouth. These training walls provide a safe passage for fishing vessels to the fishing harbor, located inside the Arasalar River. The beach to the north of the training walls is an open beach where the coastal community often relaxes. Further north, the coast is protected by a dense vegetation cover, beach to the north of training walls consists of dunes and dunes protected by creepers. The beach to the south of training walls is a less popular one comparatively and has less footfall. This side of the beach is protected by dense vegetation and withstood the winds of Gaja cyclone [4].

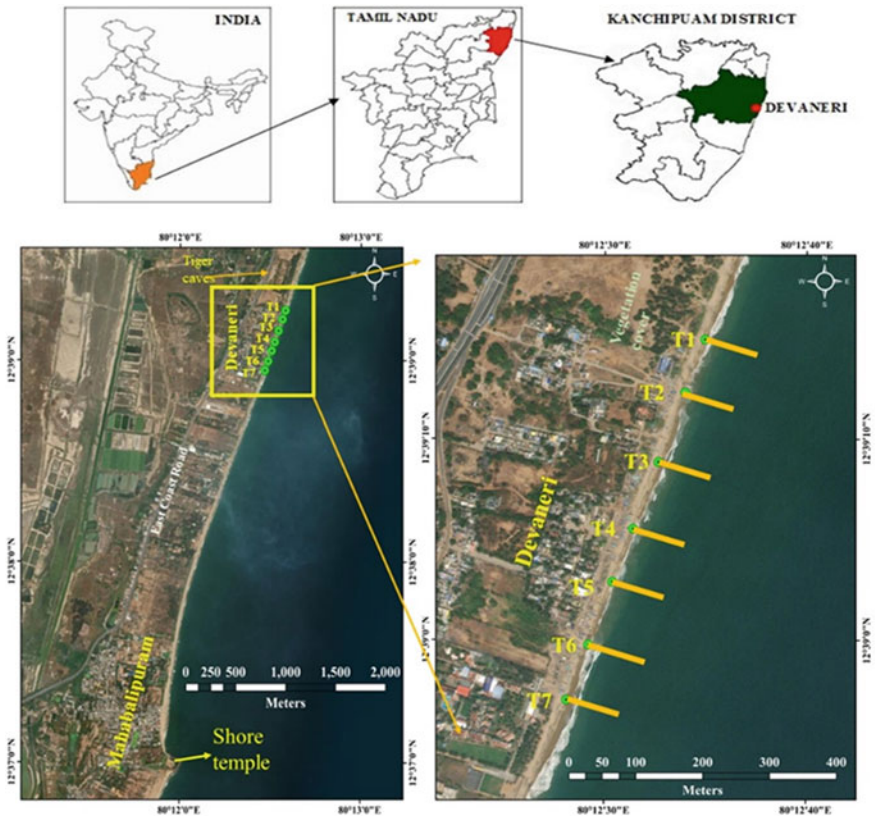

Fig. 1 Devaneri study area and location of Transects (T1-T7)

2.4 Field Survey

The collection of beach profiles dates a log back to the modern method reported in 1960. Setting the location of profiles along the coast plays a major role in assessing the beach morphology changes for that particular coastal stretch. In an open and plain coast, profiles can be spaced uniformly. Beach profiles can be placed with a maximum spacing of 150 m for better three-dimensional interpolation from two-dimensional data [11]. A total of seven exchanges were considered in this Devaneri region. Each transmission is 50–70 m cross length from the village (Fig. 1). The profiles monitored are directly related to the hamlet. The coastal length of the study area is 600 m with 390 m as the hamlet center, 390 m to the north of the hamlet center point is transect 1, and 210 m to the south of the hamlet center point is transect 7. Transects 1 and 7, T1 and T7, as indicated in Fig. 1, are positioned around 100 m beyond the village's boundary. At the same time, the other five transects are placed inside the village boundary. Each transect is 100 m apart from the subsequent ones. A pseudo-baseline

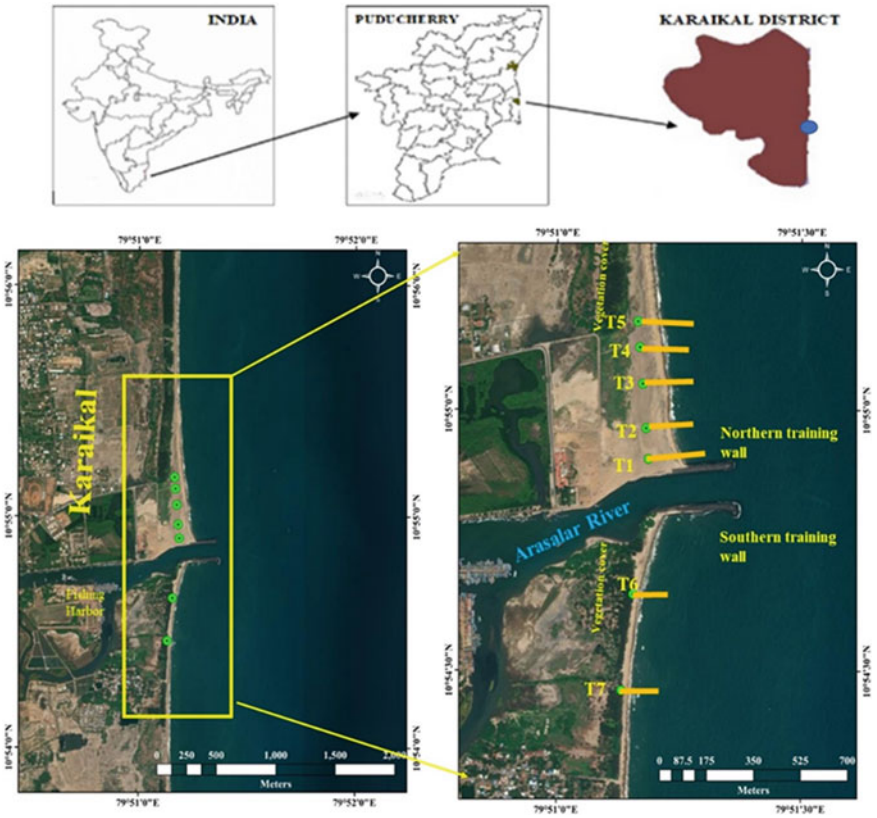

Fig. 2 Karaikal study area and location of Transects (T1–T7)

is established for spatial and temporal analysis. A coast with engineering structures, dunes, and vegetation cover needs proper attention while planning the profiles. The impact of the shore-connected structures on the coastline varies from 1:1 to 1:10 of the perpendicular distance of the structure [6]. This structure causes erosion on its down-drift side and accretion on the up-drift side. Along the east coast of India, drift varies bi-directionally with the season, and predominant drift toward the north [7], so the coast on both sides of the training walls needs to be monitored on temporal and spatial scales. Five transects on the north and two on the south of the Arasalar river mouth were established for continuous monitoring, as shown in Fig. 2. The beach profiles to the north of training walls were spaced 80–120 m depending on the site conditions. The first two transects are placed on the part of the plain beach; third and fourth transects are placed between dunes. To the north, the first transect (T1) is located about 30 m from the northern training wall. The T2 and T3 transects are located 120 m and 280 m from T1, respectively. Transect T4 is located 130 m north of transect T3. The last Transect T5 is located in front of the vegetation cover and dunes; Transect T5 is 80 m north of Transect T4. The presence of dunes along

the south coast is less, and it is a flat beach. Just two transects above 300 m apart were monitored. Transect T6 is placed over a dune, while Transect T7 is placed on a plain turf. The pseudo-baseline is considered for performing spatial and temporal analysis for both north and south of training walls separately. The coastal length of the study area is above 600 m on either side of the training walls in Karaikal. The data was collected on the first spring of every month from May 2017 to April 2019.

3 Results and Discussions

The variations in the beach profiles are superposed for the selected months of all three seasons, i.e., Non-monsoon (April), SW-monsoon (August), and NE-monsoon (November) from the year 2017 to 2019.

3.1 Devaneri (Open Coast)

The dynamic portion for beach profiles, i.e., the area after the baseline, is taken for comparison. The typical transects T1, T3, and T7 are projected in Figs. 3, 4 and 5. The seasonal variations of all transects are computed, and seasonal volumetric changes from the beach profile variation over a unit shoreline of the stretch are projected in Fig. 6. It is observed that throughout the year, no significant accretion/erosion pattern is witnessed when the change in the quantity over each of the months is considered is found less. The stretch of the coast considered herein experiences the South-west monsoon from June to September, the North-East monsoon from October to December, while January to May is a non-monsoon season. Although accretion along with the profile during the south-west monsoon season is noticed, the dynamic of impact is found to be relatively less. It is found that during the northeast and post-monsoon season, the profiles tend to erode, and accretion processes commence during the south-west monsoon season. The foreshore slopes of all transects mostly look similar, and no major changes in the beach width are observed. The spatial changes between all transects are similar because it is an open coast with no coastal structures in the vicinity.

3.2 Karaikal (Near Estuary)

Since the Karaikal study area is located adjacent to the training walls, the direction of the monsoon plays a vital role in determining accretion/erosion processes. During monsoon season, the beach to the north of the training walls undergoes erosion, while the coast to the south undergoes accretion. Once the post-monsoon started, the processes witnessed a reversal. The beach to the north of the training walls

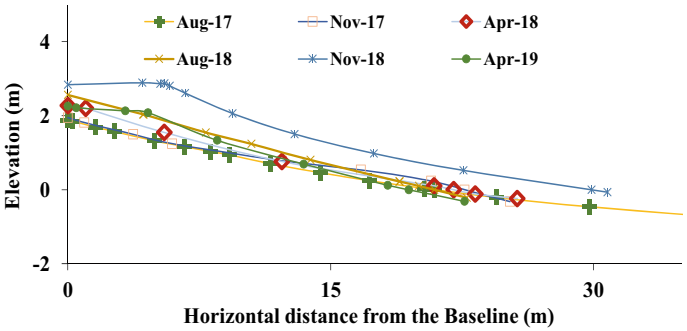

Fig. 3 T1-Beach profiles from Aug-2017 to April-2019 (Devaneri)

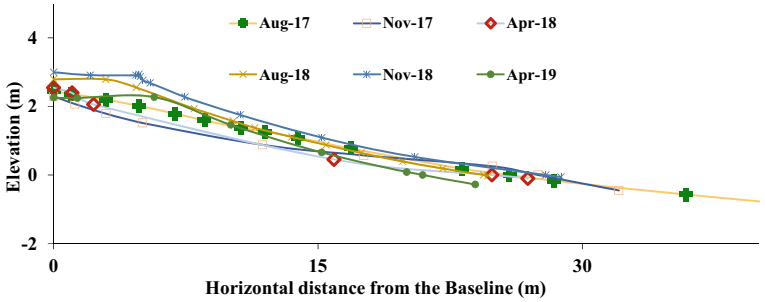

Fig. 4 T3-Beach profiles from Aug-2017 to April-2019 (Devaneri)

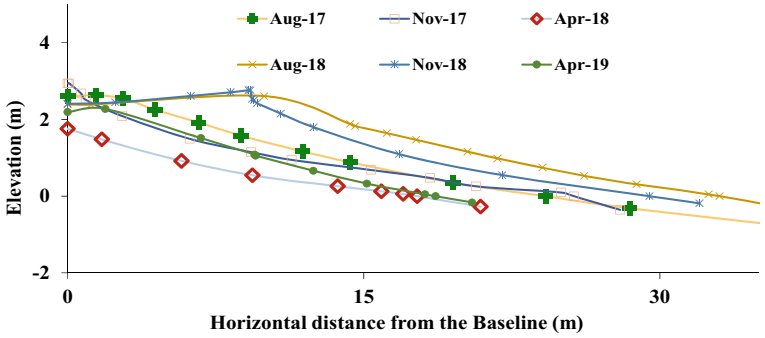

Fig. 5 T7-Beach profiles from Aug-2017 to April-2019 (Devaneri)

undergoes accretion, while the beach to the south undergoes erosion. The changes during the northeast monsoon are vigorous, and maximum changes occur during this season. Typical temporal changes in the coast during August 2017–April 2019 are compared in results, superposed in Figs. 7, 8, 9, 10 and 11. The seasonal volumetric changes per unit shoreline for all profiles are shown in Fig. 12. Transects 1–4, close

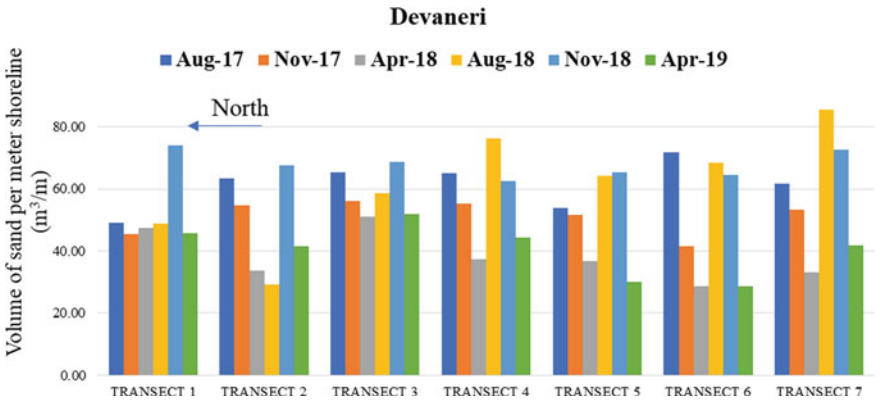

Fig. 6 Seasonal volume changes from 2017 to 2019 (Open coast)

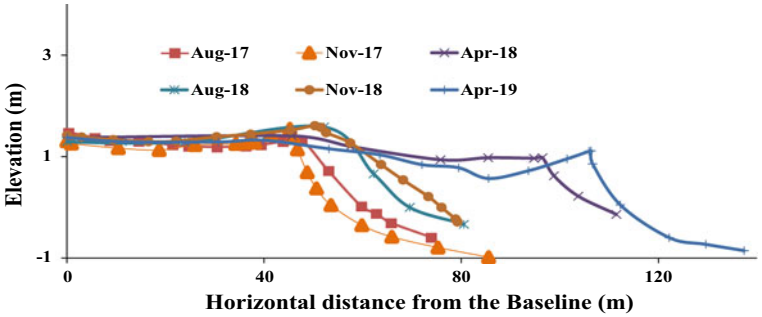

Fig. 7 T1-Beach profiles from Aug-2017 to April-2019 (Karaikal-North)

to the northern training wall, are found witnessing rigorous erosional activity during monsoon compared to T5, which is located a little away from the training wall. Furthermore, this transect is situated on the sand dune and near vegetation. The beach profiles T1–T3 on the northern side of the training walls and the T6 and T7 profiles on the southern side of the training walls undergo enormous beach width and slope dynamics. The Northeast monsoon always dominates the East coast of Tamil Nadu, so the south side beach of training walls witnesses more accretion while the north side witnesses erosion during monsoon.

4 Conclusions

The beach profile changes in the open coast and the near estuary have been discussed above. The advantage of using RTK-GPS for beach profile surveys over conventional methods has been discussed. It is observed that the open coast beaches and the coast

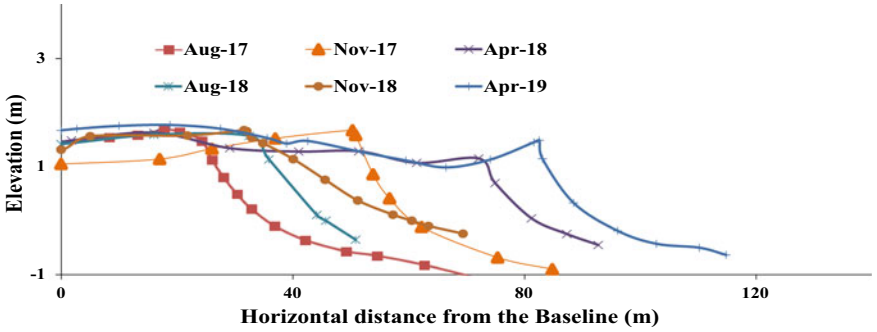

Fig. 8 T2-Beach profiles from Aug-2017 to April-2019 (Karaikal-North)

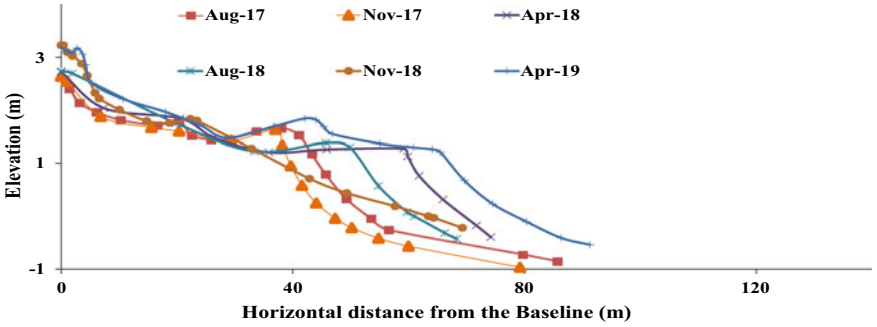

Fig. 9 T5-Beach profiles from Aug-2017 to April-2019 (Karaikal-North)

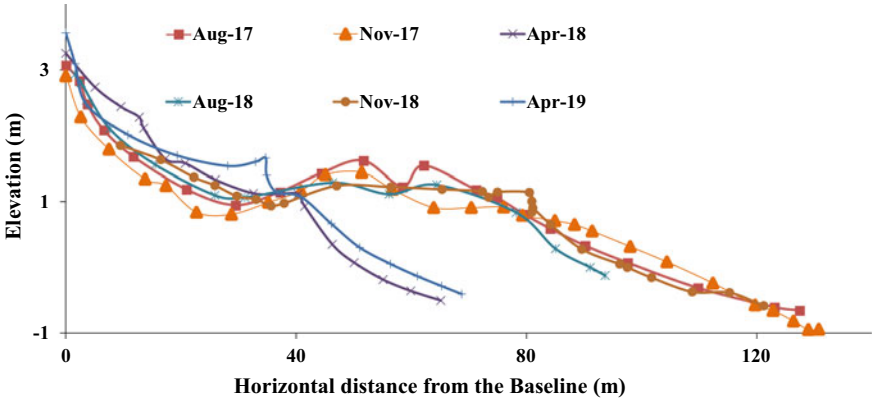

Fig. 10 T6- Beach profiles from Aug-2017 to April-2019 (Karaikal-South)

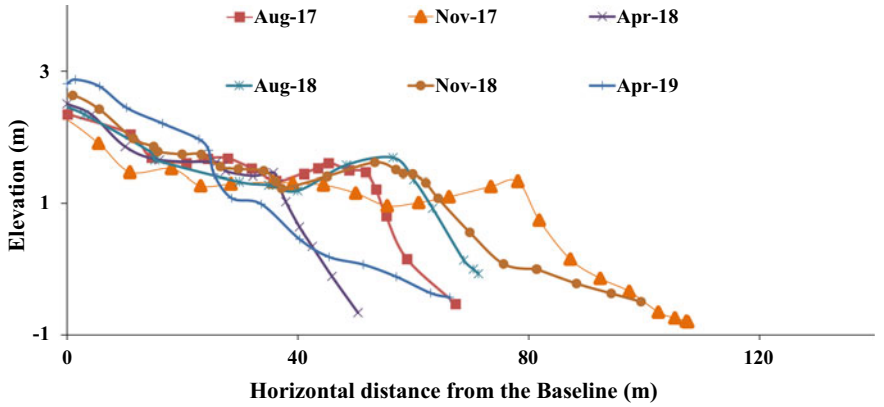

Fig. 11 T7-Beach profiles from Aug-2017 to April-2019 (Karaikal-South)

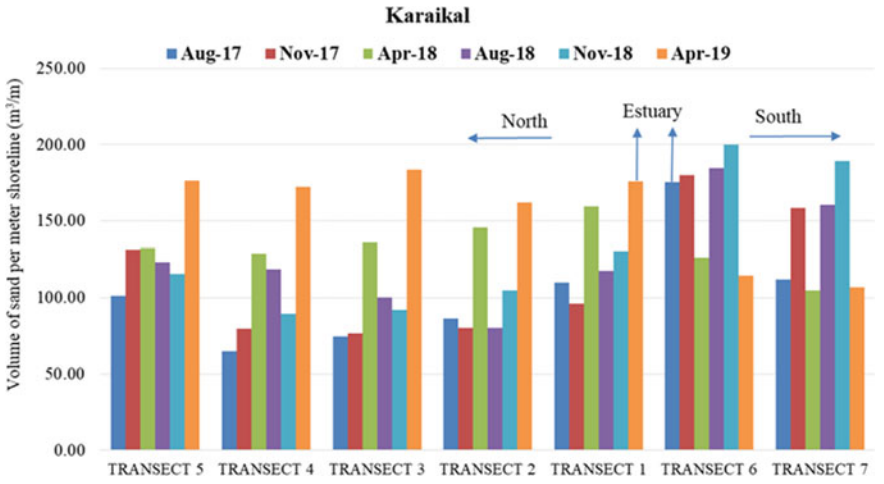

Fig. 12 Seasonal volume changes from 2017 to 2019 (Near estuary)

remains constant through time, with minor profile changes. No major accretion/ erosion is witnessed on the open coast. The presence of hard protection structures in the near estuary coast dictates the erosion/ accretion pattern. Though the beach regains on a yearly scale, the seasonal changes are very dominant in this region.

Acknowledgements The study was supported by the central water Commission (CWC), Ministry of Jal Shakti, Dept. of Water Resources, RD & GR, Government of India. A part of the research study is sponsored by the Department of Science and Technology (DST) under the "SPLICE-Climate Change" Program with the reference number DST/CCP/CoE/141/2018(C).

References

1. Ananth PN, Sundar V (1990) Sediment budget for Paradip port, India. Ocean Shorel Manag 13(1):69–81
2. Birkemeier WA, Bichner EW, McConathy MA, Eiser C (1991) Nearshore profile response caused by Hurricane Hugo. J Coast Res 81(8):113–127
3. Emery KO (2016) A simple method of measuring beach profiles. Limnol Oceanogr 6(1):90–93
4. Jeyagopal S, Vasanthakumar S, Dhananjayan M, Sundar V, Sannasiraj SA, Murali K (2020) Very severe cyclonic storm impacts to shoreline and beach profiles along the Karaikal coast of India. ISH J Hydraul Eng 28(1):439–448
5. Kannan R, Anand KV, Sundar V, Sannasiraj S, Rangarao V (2014) Shoreline changes along the Northern coast of Chennai port, from field measurements. ISH J Hydraul Eng 20(1):24–31
6. Kudale M (2010) Impact of Port development on the coastline and the need for protection. Indian J Geo-Mar Sci 39:597–604
7. Kunte PD, Alagarsamy R, Andursthouse AS (2013) Sediment fluxes and the littoral drift along northeast Andhra Pradesh Coast, India: estimation by remote sensing. Environ Monit Assess 185(6):5177–5192
8. Morton RA, Leach MP, Paine JG, Cardoza MA (1993) Monitoring beach changes using GPS surveying techniques. J Coast Res 9(3):702–720
9. Nordstrom K, Jackson N (2013) Removing shore protection structures to facilitate migration of landforms and habitats on the bayside of a barrier spit. Geomorphology 199:179–191
10. Thomas T, Phillips MR, Morgan A, Lock G (2018) Morphostat: a simple beach profile monitoring tool for coastal zone management. Ocean Coast Manag 153:17–32
11. Timothy WK, Christopher JA (1994) Beach profile spacing practical guidance for monitoring nourishment projects. Coast Eng, 2100–2114

Estimation of Nearshore Sediment Transport Along the North Konkan Coast—A Numerical Approach

H. Lavanya, Jyoti P. Kerkar, and Jayakumar Seelam

Abstract One of the critical segments of the Indian coastline currently being studied for its intricate hydro and sediment dynamics is the Konkan coast, which makes up the bulk of the Western Ghats. The study region focuses on the numerical modelling of the Goa, South Maharashtra, and Karwar coastal stretches. This work includes calculating sediment transport rates in the north Konkan coast's nearshore sections and the 2D coupled numerical modelling of hydrodynamics and sediment transport. Waves, tides, currents, and winds were taken into consideration. One month of post-monsoon simulations from mid-December 2018 to mid-January 2019 was performed using the model. It was discovered that the model findings were in excellent agreement with the data. Sediment circulation was found to be mainly in a north and cross-shore direction. The sediment transfer was evaluated between several depth contours, including 0–2, 0–5, 0–10, 0–20, and 0–30 m of water. Over 386 kms, the average sediment transport rate for the area between 0 and 2 metrres of water was roughly 4.75 Mm^3/year. According to the model's findings, there is significant sediment movement between 10 and 20 m of water (133 Mm^3/year). During the simulated period of post-monsoon 2018, it was discovered that the total sediment

H. Lavanya (✉) · J. P. Kerkar · J. Seelam
Ocean Engineering Division, CSIR-National Institute of Oceanography, Dona Paula, Goa 403004, India
e-mail: laavhemanath.1512@gmail.com

J. P. Kerkar
e-mail: jyoti2317@gmail.com; jkerkar@nio.org

J. Seelam
e-mail: jay@nio.org

J. P. Kerkar
Research Scholar, Bharathidasan University, Tiruchirappalli, India

P. V. Timbadiya et al. (eds.), *Coastal, Harbour and Ocean Engineering*, Lecture Notes in Civil Engineering 321, https://doi.org/10.1007/978-981-19-9913-0_16

transfer throughout the coastline length between 0 and 30 m of water was about 144.5 Mm^3/year.

Keywords Sediment transport · Hydrodynamics · MIKE21 · Gross transport · Circulation

1 Introduction

Sediment transport rates are primarily responsible for the coastline changes that directly impact the coastal habitats and infrastructure. There is little information on estimates of the sediment transport at the nearshore for the entire Indian coastal region. The sediment transport involves complex interactions between waves, current, and sediment. So far, the estimation has been carried out based on equations derived from controlled laboratory conditions and riverine studies. Indian coastal conditions cannot derive accurate estimates from existing empirical equations as various seasonal factors control it. Since there have not been any sediment transport models in the vast region from Ratnagiri in Maharashtra to Karwar in Karnataka, it is proposed to generate a knowledge base on sediment transport through numerical modelling. The hydrodynamic and sediment transport model results and measured information will be used to understand the sediment transport rates for the region considered in this study. A sediment transport model for the nearshore region (30 m water depth) of a comparatively large domain considered would place this study ahead of the sediment transport studies reported so far.

2 Materials and Methods

Many numerical, physical, and mathematical models have been suggested to understand the hydrodynamics of a coastal area; the state of art modelling software MIKE21 by DHI is one amongst the commercially proposed numerical modelling systems. The present study is carried out in the MIKE21 modelling suite, and the model is well calibrated with the measured hydrodynamic parameters [1].

2.1 Model Description

In this work, the flow (HD), sediment transport (ST), and wave computations are dynamically coupled using the MIKE21 coupled flexible mesh flow model (FM) (SW). This approach fully accounts for variations in bed level when calculating flow and waves. The core computational element of the overall MIKE21 Flow Model FM modelling system is the Hydrodynamic Module. The MIKE21 Flow Model is a

modelling framework that uses a flexible mesh method to provide the hydrodynamic foundation for the Mud Transport (MT) Module and Sand Transport (ST) Module, as well as input for changes in water level for the spectral wave (SW) model. The depth-integrated incompressible Reynolds averaged Navier–Stokes equations, which are the foundation of the modelling system, are solved numerically for shallow water in two dimensions. Equations for continuity, momentum, temperature, salinity and density make up the model. Both spherical and Cartesian coordinates can be applied to the horizontal domain. By subdividing the continuum into non-overlapping pieces or cells, the cell-centred finite volume approach discretizes the fundamental equations' spatial domain.

The important rivers, including Bankot, Tirakol, Chapora, Zuari, Mandovi, Sal, and Kali, were included in the hydrodynamic model, which was constructed from the Bankot River in south Maharashtra to Karwar in north Karnataka. From mid-December 2018 to mid-January 2019, the model uses tide, wave, currents, and wind as inputs. The variations in flow patterns were examined by contrasting the tidal heights and flow velocities at various points within the domain. Depth-averaged flow velocities were taken at various alongshore sites to confirm the alongshore and cross-shore variance of the current velocity calculated using the 2DH technique.

2.2 Study Area

2.2.1 North Konkan Coast

India has an approximately 7517 km long coastline [2]. The study region extends from Ratnagiri headland in South Maharashtra to the Karwar headland in the North Karnataka, comprising the entire coastline of the state of Goa between them (Fig. 1). Along the central west coast of India, Goa is a narrow coastal strip that lies between the latitude 14°48′ N and 15°48′ N and longitude 75°40′ E and 74°20′ E. It is located on the feet of Western Ghats and combines submerged and emergent coasts, as evident from the geological map of Goa. The coast between river Tirakol and Mandovi is emergent and between Mandovi and Zuari is submergent coast. The entire coastline covers a total stretch of 386 km approx. From the Ganapatipule beach in Maharashtra to the Rabindranath Tagore (RTK) Beach in Karwar beach forms the crux area for estimating sediment transport.

Waves of monsoon winds mainly influence the stretch of the coastline and associated littoral drift, the adjoining Arabian Sea, is influenced by different conditions during the year, viz., Southwest monsoon SW (June to September), Northeast monsoon NE (December to February), and a transition period between these two seasons. The study area extends up to 114 km in the north to 95 m water depth and 80 km in the south to 80 m, covering a vast coastal stretch of 386 km. Along this stretch, the key areas of interest include Ratnagiri, Marmagao, and Canacona.

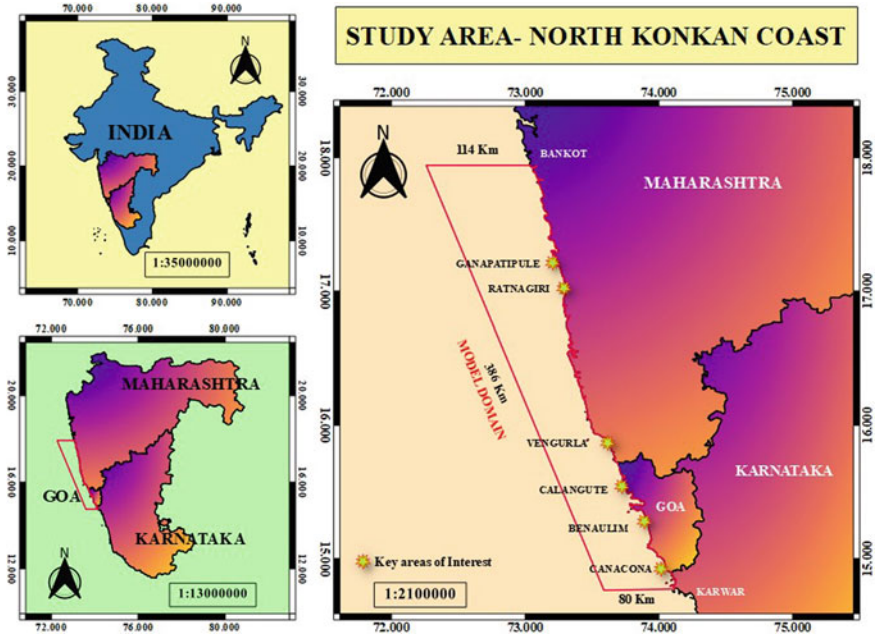

Fig. 1 Study area–North Konkan coast

2.2.2 Data Collection

The input parameters considered for the model were obtained from various sources. The model domain considered for the study, along with the mesh and bathymetry, is shown (Fig. 2). The bathymetry contours for the study area were obtained from the National Hydrographic Organisation (NHO) charts by the Govt. of India. A bathymetry survey was carried out along the selected domain locations, which was interpolated along with the NHO bathymetry to obtain the overall bathymetry of the model domain considered. The water level recorders (Tides), recurring current metres (Currents), and wave tide gauges (Waves) were deployed at selected locations along the study area during Dec 2018 and Jan 2019 for one month to obtain the in-situ data for the locations, which in turn were used to calibrate the model.

2.3 Selection of Input Parameter

A nested grid is used in the current numerical model. The model consists of triangular nested mesh set up with sizes varying between 100 and 150 m at the surf zone and from 1 to 2.5 km in the offshore region. The inputs selected for the model were water levels, waves, winds, currents, and sediment size distribution. The water level

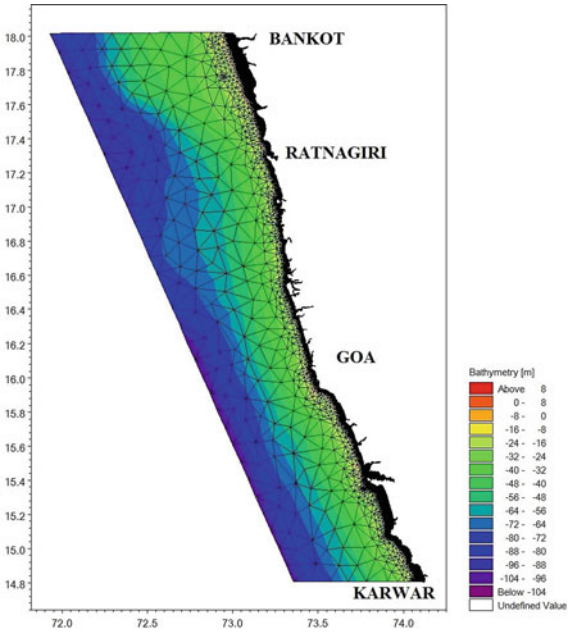

Fig. 2 Study area and model domain showing bathymetry contours and the mesh

inputs for the model were extracted from the MIKE21 toolbox, which has the inbuilt global tide model for the generation of water levels at specific locations. The mean sea-level values (1.3 m for Mormugao) added to the extracted water levels served as the tidal inputs at the open boundaries. The wave forcing for the model was provided as radiation stresses along the open boundaries. The radiation stresses were extracted from a well-calibrated spectral wave model (Fig. 3) output established for the Indian Ocean [3].

The CSIR-National Institute of Oceanography Automated Weather Station data was sourced to obtain the wind speed and direction as wind input to the model (Fig. 4). The AWS winds were chosen instead of ECMWF and NCEP wind databases due to their acceptable temporal resolution of 10 min. Moreover, the model outputs with AWS winds provided better results than the ECMWF and NCEP-sourced winds. The wind speed and wind direction were provided as time series input to the model.

The sediment grain size distribution based on water depths was input to the sediment transport model, and the sediment transport tables were generated using the MIKE21 toolbox. The sediment size distribution was between fine and medium sand on the nearshore, as reported in the previous studies [4]. The sediment grain sizes varied between 0 and 15 m water depths. The D50 sediment size distribution 0.2 mm for 0–2 m water depth, 0.01 mm for 2–7 m water depth, and 0.075 mm for 7–15 m water depths, was adopted. A uniform sediment distribution of silty sand (0.075 mm) was assumed beyond 15 m water depth, which is the minuscule proper size in the sediment transport (ST) module.

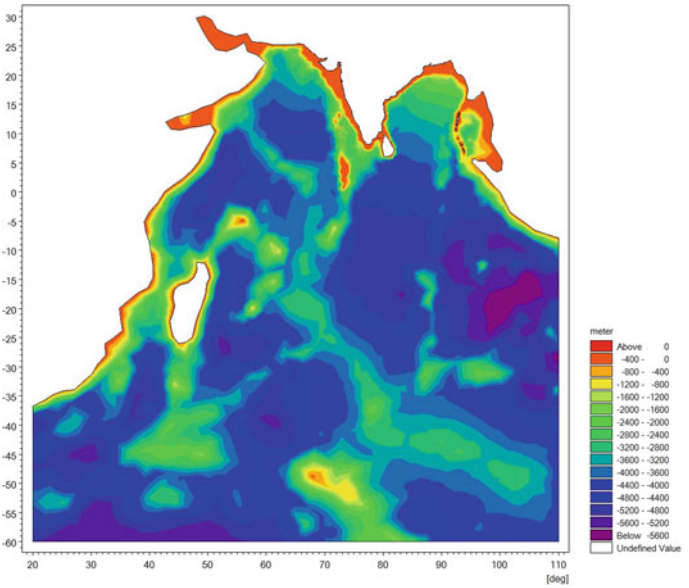

Fig. 3 Domain considered for the large-scale calibrated Spectral wave model

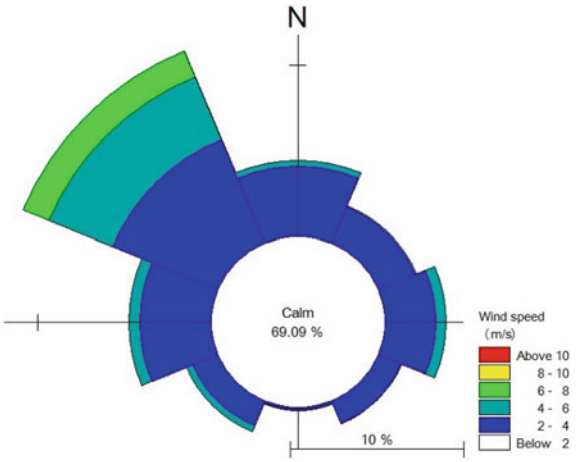

Fig. 4 Automated weather station winds during December 2018–January 2019

The HYbrid Co-ordinate Ocean Model (HYCOM)-derived U and V Velocities were obtained from https://www.hycom.org/ [5], a consortium for assimilative data modelling and provided as inputs along the north and south boundaries of the model. The north boundary was provided with pure current forcing, while the south boundary with a Flather condition including both extracted water levels and HYCOM currents

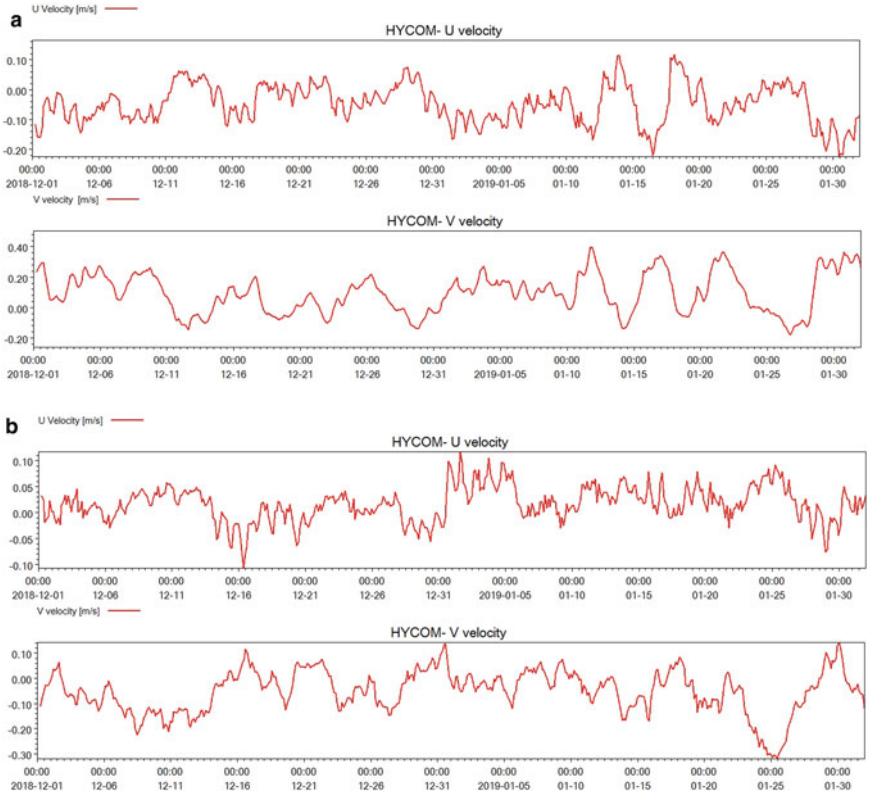

Fig. 5 HYCOM extracted U and V velocity inputs along the (**a**) south (**b**) north boundary

(Fig. 5). Apart from the major parameters mentioned, the rivers in the domain were provided with minimum discharge values ranging from 0.001 m^3/s to 10 m^3/s. The manning's roughness coefficient of 32 was adopted as a constant throughout the domain.

3 Results and Discussion

The model simulations were carried out for a month from mid-December 2018 to mid-January 2019 with a minimum time step between 0.1 s and 100 s, keeping the CFL limit up to 0.8. Few selected locations known as the key locations were picked along the coast to observe the sediment dynamics, current circulation, and sediment transport estimation. Four sections contain six places, viz., Ganapatipule, Ratnagiri, Vengurla, Calangute, Benaulim, and Karwar (Fig. 6) were considered for the study.

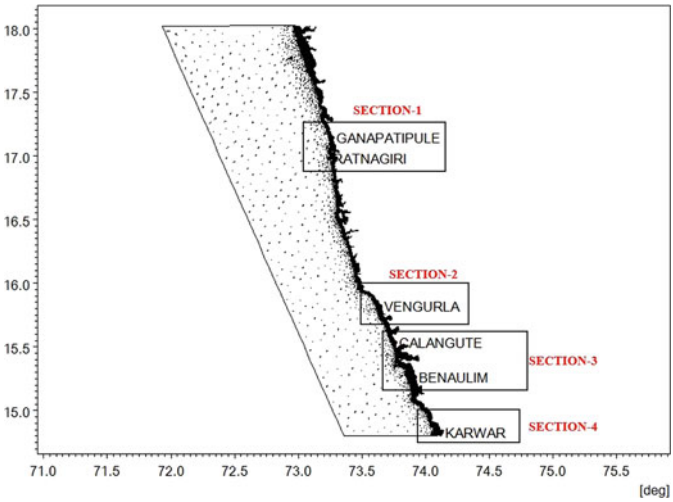

Fig. 6 Key areas considered for the estimation of sediment transport rates

3.1 Hydrodynamics

The current speed and direction were compared at two locations along the domain. Recurring current meter measurements off Ratnagiri and Canacona at 15 m water depths were compared with the nearshore modelled currents extracted at the same depth. The current speed and direction variations between the measured and modelled outputs at Ratnagiri are illustrated (Fig. 7). The measured and modelled currents match with an average velocity of 0.182 m/s, a maximum velocity of 0.24 m/s [6], and a minimum of 0.01 m/s with the predominant flow in the North-Northeast direction. In a few locations, the velocity peaks did not pick up as expected, attributing to other factors influencing the hydrodynamics of the region apart from the input parameters considered.

Canacona near Karwar bay is a critical location with complex hydrodynamics in place. A fair comparison was observed between this location's measured and modelled current velocities. An exact match was observed at particular duration sets

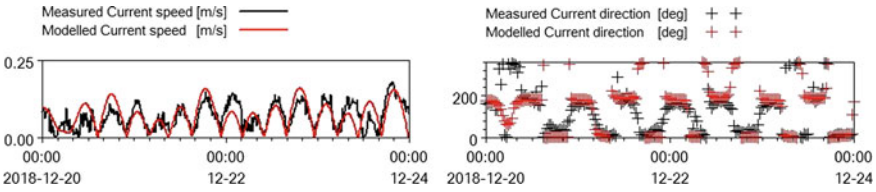

Fig. 7 Comparison of measured and modelled currents at Ratnagiri

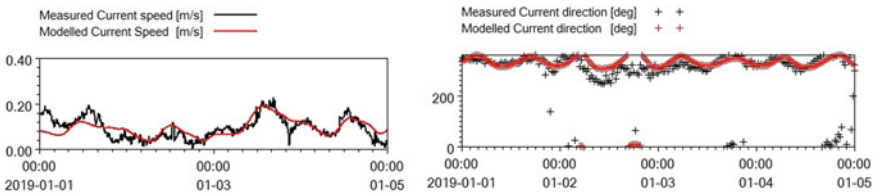

Fig. 8 Comparison of measured and modelled currents at Canacona

26-Dec 2018 to 3-Dec 2018, 3-Jan 2019 to 5-Jan 2019 (Fig. 8), and 15-Jan 2019 to 20-Jan 2019. The dissimilarities in the intermediate locations were due to the presence of small islands around the measured location, whose hydrodynamic complexities are yet to be studied in detail. The average current velocities observed at Canacona are 0.153 m/s, the maximum being 0.3 m/s and the minimum around 0.015 m/s, with the average predominant current direction along the north-northwest direction.

The correlation for modelled and measured current velocities at Ratnagiri and Canacona showed a positive correlation above 80%, denoting a significantly good numerical model calibration (Fig. 9). The model calibration is justified by the 96.8% correlation achieved at Ratnagiri and 84.6% at Canacona, respectively. Water levels along the model domain were compared at Canacona, Ratnagiri, and Marmagao. The water levels extracted from WX-Tide [7] at the three locations were compared with the modelled water levels, which were a proper match (Fig. 10). The water levels at Ratnagiri varied between a maximum of 1.9 m and a minimum of 0.5 m, whereas at Canacona, the levels were between −0.3 m and 1.2 m. Marmagao water levels ranged between −0.1 and 1.5 m, respectively. The spring and neap tides influence the water levels and hydrodynamics of the location to a considerable extent.

The west coast of India experiences high wave activity during the southwest monsoon season and remains calm for the rest of the year [2], which is proved by the modelled waves in this study. Nearshore waves were extracted from the model at six different locations, viz., Ganapatipule, Ratnagiri, Vengurla, Calangute, Benaulim,

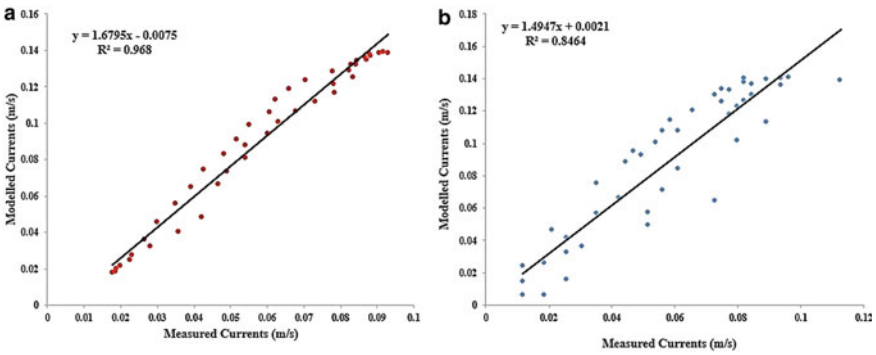

Fig. 9 Correlation plots for measured and modelled currents at **a** Ratnagiri and **b** Canacona

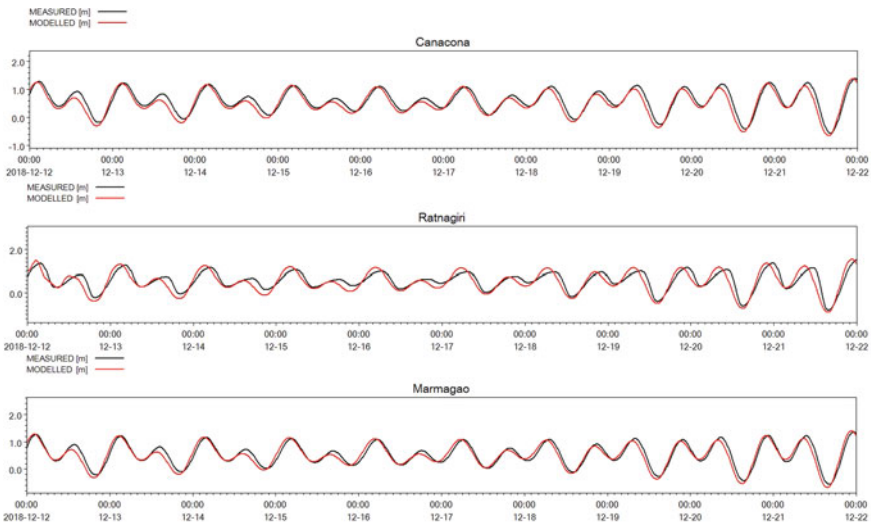

Fig. 10 Comparison of measured and modelled water levels at Canacona, Ratnagiri, and Marmagao

and Karwar to observe the variations in significant wave height (Hs) and wave direction. A gradual drop in the significant wave heights from north to south along the coast is shown (Fig. 11). The rose plots indicate that the Hs values vary between 0.5 m and 1 m along Ganapatipule, Ratnagiri, and Vengurla and drop to 0.2 m and 0.4 m at Calangute and Benaulim. Karwar witnesses Hs between 0.8 m and 1 m. The waves overall seem to be directed in the North-Northwest direction.

3.2 Circulation in the Key Areas

The U and V velocity vectors along the four sections were averaged monthly to obtain the mean vectors. The averaged current vectors were directed towards the north during the simulation period (Fig. 12). Hence the current circulation, in that case, is predominantly north. The formation of localized eddies was witnessed at the Vengurla (Fig. 12b). Localized eddies play a vital role in sediment transport in that particular region. Localized eddies were also noticed around the small islands near Karwar. Figure 12a indicates the presence of currents of magnitude 0.14 m/s at Ratnagiri directed towards the shore. Few eddies were also observed in the same area, possibly indicating a high volume of sediment movement of 0.012 Mm^3/year cross-shore (Fig. 13a). Current speeds at Vengurla creek were around 0.18 m/s showing evidence for 0.220 Mm^3/year sediment load directed cross-shore (Fig. 13b). Current speeds seem to reduce from 0.18 m/s to 0.05 m/s moving from south to north alongshore. The current circulation pattern changes gradually from North West to North moving from south to north alongshore with the drop in current speeds. Formation of eddies

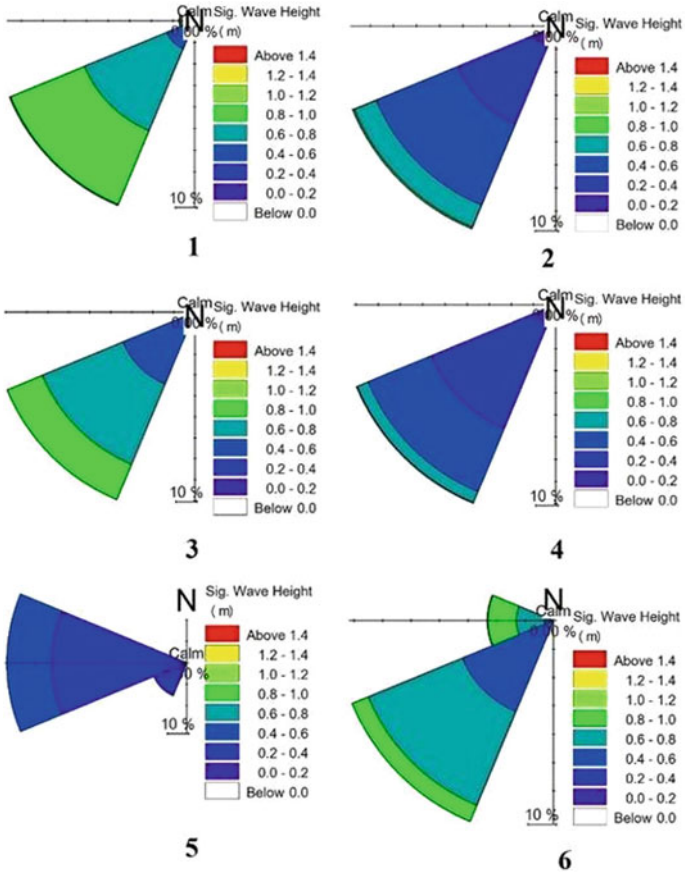

Fig. 11 Wave rose plots of modelled significant wave heights at 1. Ganapatipule 2. Ratnagiri 3. Vengurla 4. Calangute 5. Benaulim and 6. Karwar

along Mandovi and Zuari estuaries (Fig. 12c), with high current speeds of 0.14 m/s, is witnessed. The north-westerly currents from the south seem to form localized eddies along Mandovi Zuari estuaries and Vengurla, which gradually change direction to the north when moving further alongshore. In locations with high speeds, sediment transport volumes were also high.

3.3 Sediment Flow Pattern

The sediment flow pattern along the four sections was analysed, corresponding to their current circulation. The locations in Vengurla where eddies were observed seem to have vast volumes of sediment transport of order 0.220 Mm^3/year. A pattern was

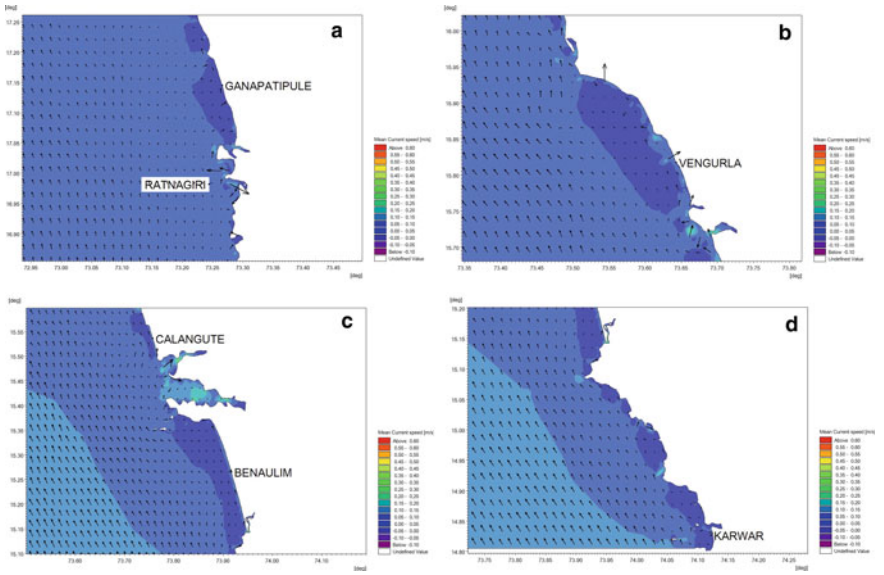

Fig. 12 One month averaged Current speeds along the four sections

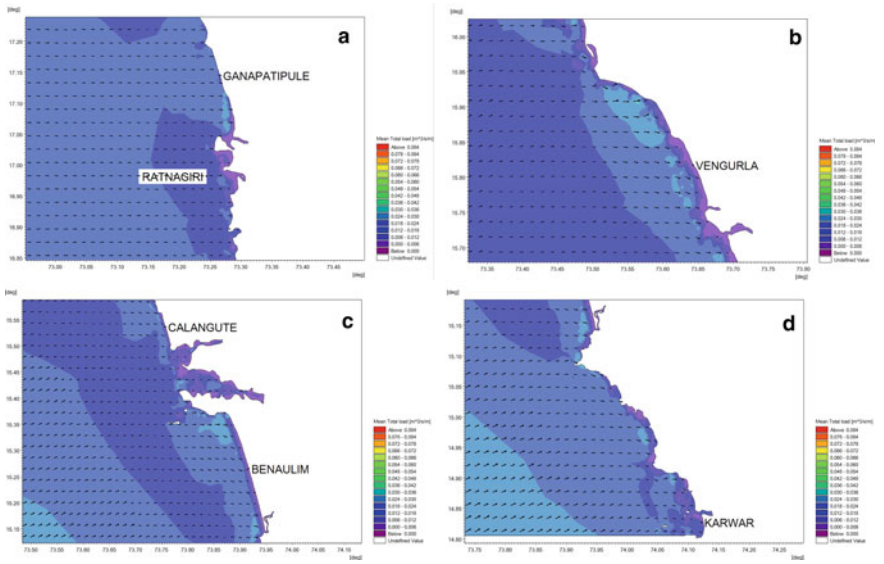

Fig. 13 One month averaged total sediment load vector plots along the four sections

observed in the sediment circulation in the sections considered. The southern stretch of Goa and Karwar witnesses sediment movement towards the northwest and north, while Ratnagiri is directed cross-shore towards the coast. Sediment transport reversal is observed in the Vengurla section, where the sediment transport is partly north and partly south due to local eddies (Fig. 13b). At South Goa, typically at Velsao, the movement in a very high order of 0.012 Mm^3/year is observed. Similar to Vengurla, there is a change in sediment flow pattern observed at Benaulim. The locations above Benaulim experience northerly movement, while those below observe it southerly. The sediment circulation is bi-directional during the winter, partly north and partly south (Fig. 13) along the west coast [8, 9]. The circulation directions in the surf zone are such that the flow is part towards the south and north [10, 11, 12, 13, and 14], while most of the flow is directed on-shore. It is directed uniformly towards the north in the nearshore regions.

The grain size distribution for the study was between 0.2 mm and 0.075 mm, due to which the patches signifying massive sediment transport are observed offshore. The preliminary study was focused only on silty sand type up to 30 m water depth, while clay proportions (Mud transport) were not considered in the study. The presence of high-magnitude offshore currents was also attributed to the same reason. Overall, the mean sediment transport observed at the locations varied between 0.007 Mm^3/year and 0.220 Mm^3/year.

3.4 Estimation of Sediment Transport

The sediment transport along the domain was estimated by two strategies, viz., (i) Linear estimation of mean sediment load based on cross-sections taken across the key locations (Ganapatipule, Ratnagiri, Vengurla, Calangute, Benaulim, and Karwar) and understanding of the sediment transport at different depths till 30 m, (ii) Collective estimation of mean sediment load for the entire stretch between diferent depth levels till 30 m. The former will provide the localized sediment transport between different depths, while the latter focuses on quantifying the overall sediment transport at various depths. Linear cross-sections were drawn across the key locations, and the sediment loads were extracted to 30 m water depth. The extracted points along the line were not uniformly placed since the model is designed with a nested triangular mesh of varying resolution. The depths under consideration were 0–2 m, 0–5 m, 0–10 m, 0–20 m, and 0–30 m, respectively (Table 1). The cross-section estimates of sediment transport indicate a considerable sediment movement between 10 and 20 m water depths. A comparatively high rate of 0.645 Mm^3/year was observed at Vengurla between 0 and 5 m water depth, which can be attributed to the presence of localized eddies in that area. Between 0 and 5 m water depth at Karwar, it is 1.680 Mm^3/year due to the presence of high magnitude currents around the small islands in that area. Vengurla also witnesses a surf zone sediment transport of 0.220

Table 1 Sediment transport estimates for the key sections based on cross sections

Location	Sediment transport observed between different water depths along the cross section at key locations (Mm^3/year)				
	0–2 m	0–5 m	0–10 m	0–20 m	0–30 m
Ganapatipule	0.007	0.289	2.132	6.817	8.162
Ratnagiri	0.012	0.347	0.805	3.695	5.735
Vengurla	0.220	0.645	3.723	7.574	8.447
Calangute	0.005	0.281	1.252	5.642	6.984
Benaulim	0.017	0.429	4.540	8.193	8.934
Karwar	0.032	1.680	4.634	7.927	10.000

Table 2 Gross sediment transport estimates for the domain at varying water depths

Sediment transport was observed between different depths during Dec 2018–Jan 2019 (Mm^3/year)				
0–2 m	0–5 m	0–10 m	0–20 m	0–30 m
4.751	9.094	9.968	142.820	144.500

Mm^3/year between 0 and 2 m water depth. Overall, Karwar experiences a higher rate of nearshore sediment transport of 10 Mm^3/year, while at Ratnagiri it is significantly less of order 5.735 Mm^3/year.

The gross sediment transport estimates in Table 2 agree with the sediment movement along the nearshore water depths observed in the cross-section estimation method. The sediment transport between 0–10 m and 0–20 m water depth contours was estimated to be 133 Mm^3/year for a 386 km long coastal stretch, which is more than the longshore sediment transport of 9.968 Mm^3/yr observed between 0–2 m to 0–10 m. The reason for this could be the presence of increased current speeds in the nearshore area. Other factors contributing can be rainfall, river discharges, and anthropogenic activities at every location along the coast, which is quite difficult to be incorporated into a numerical model for a vast stretch; region-specific models, in that case, would serve the purpose better. The total sediment transport along the coastal stretch considered between 0 and 30 m water depths during mid-December 2018 and mid-January 2019 was estimated to be about 144.5 Mm^3/year, the majority of which is contributed between 10 and 20 m water depths.

4 Conclusions

A comprehensive numerical model simulation comprising hydrodynamics, sediment transport, and spectral waves for the north Konkan coastal stretch of 386 km was established. It is well calibrated at the different locations of Ratnagiri, Marmagao,

and Canacona with the measured tides and currents. The current and sediment circulation patterns were observed at four selected key sections, revealing that the current direction during Dec 2018 and Jan 2019 was predominantly north-northwest. For sediments, it was cross-shore and towards the north. In magnitude and direction, sediment circulation in the northern half was completely different from the south. The impact of localized eddies in the sediment transport was noticed in parts of Vengurla, Mandovi-Zuari estuaries and Benaulim.

The total sediment transport estimated in the north Konkan coast during the simulation period of mid-December 2018 and mid-January 2019 up to 30 m water depth was 144.5 Mm^3/year. Sediment transport between 10 and 20 m depths was more than that between 0 and 10 m, which must be further studied to improve the model input conditions. Considering clayey sediments and silty sand in the proposed coupled model (Mud transport) will better understand the nearshore morphodynamics. The current study must be expanded to other seasons of the year to understand the hydrodynamics effectively, delineate the sediment cells, and estimate sediment budgets, which will be the scope for future work in this arena.

Acknowledgements The authors acknowledge the financial support from the National Centre for Coastal Research (NCCR) Chennai, under the Ministry of Earth Sciences, the Government of India, to carry out the present work. The authors are also thankful to the Director, CSIR-National Institute of Oceanography, Goa, for providing all necessary resources to carry out the research. We acknowledge the scientific, technical, project staff and students who were of great support during data collection and other field operations.

References

1. DHI, MIKE21, Flow model hydrodynamic module: scientific documentation, 2012
2. Kumar VS, Pathak KC, Pednekar PNSN, Raju NSN, Gowthaman R (2006) Coastal processes along the Indian coastline. Curr Sci 530–536
3. Kerkar JP, Seelam JK, Jena BK (2020) Wave height trends off central west coast of India. J Coastal Res 89(SI) 97–104
4. Kumar VS, Anand NM, Chandramohan P, Naik GN (2003) Longshore sediment transport rate—measurement and estimation, central west coast of India. Coast Eng 48(2):95–109
5. Chassignet EP, Hurlburt HE, Smedstad OM, Halliwell GR, Hogan PJ, Wallcraft AJ, Bleck R (2007) The HYCOM (hybrid coordinate ocean model) data assimilative system. J Mar Syst 65(1–4):60–83
6. Chandramohan P, Kumar VS, Nayak BU, Pathak KC (1993) Variation of longshore current and sediment transport along the south Maharashtra coast, west coast of India. Indian J Marine Sci 22:115–118
7. WXTide: www.wxtide32.com
8. Shanas PR, Kumar VS (2014) Coastal processes and longshore sediment transport along Kundapura coast, central west coast of India. Geomorphology 214:436–451
9. Murty CS, Veerayya M (1985) Longshore currents and associated sediment transport in the nearshore areas of Kerala and Goa, west coast of India. Mahasagar 18(2):163–177
10. Kunte PD (1994) Sediment transport along the Goa-north Karnataka coast, western India. Mar Geol 118(3–4):207–216

11. Kunte PD, Wagle BG, & Sugimori Y (2002) A review and re-assessment of sediment transport along the Goa coast, India. J Coastal Res 612–621
12. Chandramohan P, Nayak BU (1989) Distribution of longshore sediment transport along the Indian coast based on empirical model. In Proceedings of Third International Conference on Dock and Harbour Engineering, KREC Surathkal, India; 6–9 December 1989. vol. 2, 1989, 501–508
13. Chandramohan P, Nayak BU (1991) Longshore sediment transport along the Indian coast. Indian J Marine Sci 20:110–114
14. Chandramohan P, Nayak BU (1992) Longshore sediment transport model for the Indian west coast. J Coastal Res 775–787

Coastal Data Collection at North Maharashtra and South Gujarat: A Case Study on Planning, Challenges and Strategies

S. N. Jha, H. B. Jagadeesh, and Prabhat Chandra

Abstract Field observed data on coastal processes is one of the essential requirements for evolving long-term plans and coastal protection measures. In view of this, for collection of such data, a scheme of Coastal Management Information System (CMIS) is being implemented by the Government of India under the on-going Scheme 'Development of Water Resource Information System (DWRIS)' of Ministry of Jal Shakti, Department of Water Resources, River Development & Ganga Rejuvenation (MoWR, RD & GR). CWPRS is the implementing agency for coastal data collection at North Maharashtra and South Gujarat. Two sites were identified for CMIS, viz. Satpati in North Maharashtra, Nani Danti-Moti Danti in South Gujarat by CWPRS with the help of respective state governments. These sites were identified considering the vulnerability of coastal erosion and severity of its impact on local population and need for coastal data collection for providing a comprehensive coastal protection plan for these areas. The total duration of the project is about three years wherein various coastal data such as coastal bathymetry, wave, tide, tidal currents, shoreline changes and cross-shore profile, suspended and bed sediments, river /creek discharges, winds, rainfall, temperature, humidity, etc., is being collected during different period of all the seasons and processed so as to be used at front-end and linked to Centralised Data Centre (CDC). The data collection program comprises of procurement of standard equipments following the government procedure, its installation at sites, and collecting data in standard format. The present paper discusses about the practical problems, while implementing this program at sites, challenges faced during the pandemic and its impact on CMIS program, and strategies adopted to overcome these challenges. General data trends observed at these sites will also be presented.

Keywords CMIS · Data collection · Coastal erosion · Tide · Sediment

S. N. Jha (✉) · H. B. Jagadeesh · P. Chandra
Central Water and Power Research Station, Khadakwasla, Pune 411024, India
e-mail: jha.sn@cwprs.gov.in

P. V. Timbadiya et al. (eds.), *Coastal, Harbour and Ocean Engineering*, Lecture Notes in Civil Engineering 321, https://doi.org/10.1007/978-981-19-9913-0_17

1 Introduction

Field observed data on coastal processes is one of the essential requirements for evolving long-term plans and coastal protection measures. In view of this, a scheme of Coastal Management Information System (CMIS) is being implemented by the Government of India under the on-going Scheme 'Development of Water Resource Information System (DWRIS)' of Ministry of Jal Shakti, Department of Water Resources, River Development & Ganga Rejuvenation (MoWR, RD & GR) for collection of such field data. CWPRS is the implementing agency for coastal data collection at North Maharashtra and South Gujarat.

The main objectives of the implementation of the Coastal Management Information System (CMIS) at two sites one each in the North Maharashtra and South Gujarat is detailed as under:

- Identification of suitable sites preferably at vulnerable reaches, procurement and installation of state-of-the art equipment, recording and reporting of data to the shore station/site office/Data Processing Centre, processing of the raw data, validation, and transmission to the Centralized Data Centre.
- Determination of causes of erosion/sediment transportation/sediment budget etc. for the selected sites based on the above data collection and documentation for the same.
- Development of suitable SOP/Manual/Guideline for coastal data collection and training/workshop for dissemination of the knowledge gained during the project including the design of coastal protection works, SOP, data collection methods, etc., for the benefit of limited audiences of maritime states/UTs, and central Government organization concerned with coastal protection.

The total duration of the project is three years with total estimated amount of Rs. 6.95 crores. The Tripartite MoU was signed with CWC and the states of Gujarat and Maharashtra in January 2019 at CWC Office Gandhinagar. The first instalment of 30% of total estimated amount was released in June 2019, while the Project Monitoring Committee (PMC) was constituted vide CWC letter dated 19.07.2019.

The Maharashtra Maritime Board officers suggested two alternatives sites viz. Kegaon and Satpati in the Northern Maharashtra for CMIS project. The team comprising the officers from Central Water Commission (CWC), Central Water and Power Research Station (CWPRS) and Maharashtra Maritime Board (MMB) visited these sites. Similarly, The Gujarat State Irrigation officers suggested three sites viz. Nanidanti Motidanti, Udvada and Kosamba in Sothern Gujarat for CMIS project. The team comprising the officers from Central Water Commission (CWC), Central Water and Power Research Station (CWPRS) and Gujarat State Irrigation visited these sites in August, 2019.

The site selection was done keeping in view the following.

i. States/UTs priority for protecting the vulnerable reach,
ii. Vulnerability of site from the erosion point of view.
iii. Providing adequate coverage of data collection for whole sediment cell,

iv. Avoiding duplication of effort with any other agency engaged in such activity
v. Type of activities and density of the dwelling units along the coast and probable benefits for future projects.

After the joint site inspection, discussions with MMB officials, Govt. of Maharashtra, Irrigation Department, Govt. of Gujarat and CWC and approval of project monitoring committee (PMC), following sites were identified as the site for CMIS:

1. Satpati in North Maharashtra
2. NaniDanti- Moti Danti in South Gujarat.

Satpati is located at 19° 43′ 39.6″ N and 72° 42′ 19.2″ E nearly 80 km North of Mumbai. At this location, Banganga creek is connected through sea during high water. Many small and large boats are normally anchored in the creek. A zone of about 800 m was exposed in front and on the south side of the creek during the low tide. The spring tidal range is about 5.3 m. Creek was mostly devoid of any water during low tide except at isolated fragments. Boats could come inside the creek only during high tide. It appeared that while the creek inlet was facing the problem of sedimentation, the southern side of the creek was facing the problem of severe erosion (Figs. 1 and 2).

Apparently, due to the erosion on the beach, the crest level of the sea wall also appeared to go down allowing waves to overtop it. The erosion appeared more prominent at Shirgaon which is 1 km on the southern side from the creek mouth. A big fishing community of about 30–40 thousand people lived there which is getting affected by this erosion. There was an imminent threat to their life and property due

Fig. 1 Erosion at Satpati Site

Fig. 2 Erosion at Nani Danti Moti Danti Site

to the prevalent erosion. The effect of erosion was visible for a length of about 1.0–1.5 km from the southern side. Water current velocity towards creek was very high during flooding. It was observed from the admiralty charts that—5 m depth contour was about 3.6 km away from shore, while—10 m depth contour was about 4.8 km away from shore. The site Nanidanti−Motidanti is located at the estuary mouth of Ambika river at about 25 km from Valsad. The waves of about 1.5 m height were seen approaching the shore. The tidal range is about 5.5 m in this region. It was observed that a beach of about 1.5 km in a stretch was eroding near the mouth. The temporary protection works in a reach of about 1.0 km by dumping stones randomly were put but these were not effective. It was assessed by talking to the local people that the crest level of the temporary protection works sank by more than 2.0 m in a period of last two or three years due to the erosion. A lot of population of the fishermen resided there and the nearby structures appeared to be in danger due to the erosion in the area. It was observed that the foundation of a temple near the shore was also exposed due to the erosion in the monsoon season. It was informed that some erosion was noticed even in the upstream reaches of Ambika river. Some reach of the beach on the south side was well protected by using the proper sea wall.

1.1 Procurement of Equipments

- Identification of equipment requirement considering the usability of equipment on other sites on rotational basis.
- Finalization of specifications for equipment to be procured.
- Procurement and installation of state-of-the-art equipment.

The following instruments were procured by CWPRS after being duly approved by Project Monitoring Committee (PMC).

Table 1 Instrument Procured for CMIS project and its objective

S. No	Equipment	Purpose	Quantity approved
1	Directional Wave Rider Buoy(DWRB)	To measure wave characteristics	2
2	Acoustic Doppler Current Profiler (ADCP)	Provides the velocity profile across the water column	2
3	River ADCP	For Data related to Riverine processes such as Discharge	1
4	Pressure-Based Tide gauge	To measure tidal amplitudes in shallow waters	2
5	LISST	To determine mean suspended sediment concentration; particle size distribution etc	1

(continued)

(continued)

S. No	Equipment	Purpose	Quantity approved
6	Echo sounder (dual) with data logger & RTK GPS dual frequency (GNSS RTK)	To measure bathymetry (water Depth) and Shoreline changes with position accuracy	2
7	Automatic weather station (AWS)	To measure weather parameters; temperature, wind, rainfall, humidity	2
8 (a)	Theodolite	For Land Survey	1
8 (b)	Hand held GPS	getting Geo-positions during land survey	2
9	Computer, On site Data Acquisition/ Retrieval System and Printer, UPS	For Field Data Collection and Data Processing at the office, Power Backup for Computer Systems	9
10	Sieve Shaker	For grain size distribution /mechanical analysis or gradation of soil and bed-material samples	1
11	CTD meter	For determination of Electrical conductivity, Temperature and Depth of a water sample at the time of collection	1
12	Grab and Water Sampler	Used to collect bed samples and water samples from any desired depth	2 each

Items were procured as per the standard CPWD manual procedures. CWPRS has an internal committee that oversees all the procurement process. Each stage of procurement is supervised which includes.

(a) Approval of specification.
(b) Notice inviting tender.
(c) Technical bid opening.
(d) Financial bid opening and.
(e) Award of supply order to L1.

2 Field Studies

2.1 Establishment of Benchmark

The setting of benchmark is one of the most significant activity as all the level of beach profile, bathymetry and coastline are based on it. The benchmark for the data collection program were obtained from the state Government agencies at the start of

CMIS programme. Correspondences were also made with Survey of India for cross verification and establishment of permanent benchmark at the sites.

2.2 Testing and Installation at Sites

All the supplied equipments were thoroughly tested at CWPRS and both the sites. The first phase of testing was done in the month of September 2020, while second phase of testing was done in January 2021 before installation.

The testing of bathymetric survey system was carried out at both sites during 15–20 Sep-2020, while the work of pre monsoon bathymetry survey was successfully completed during 24 January to 02 February 2021 at these two sites while the post monsoon bathymetry survey was successfully completed during September 2021.

Installation, testing and commissioning of Automatic Weather Stations (AWS) were successfully completed during January 2021. Data of weather parameters like wind speed, rainfall, humidity are being collected using AWS which are transmitted directly to CWPRS. Testing and installation of Pressure Tide Gauge (PTG) for tide measurement and Marine ADCP for sea current measurement was carried out during January 2021 at both sites. It included procurement of mooring material, safety equipment, etc., and preparation of mooring lines for deploying the equipment at a water level of −8 m were carried out.

River ADCP and CTD were procured in September 2021, and the site data for river current, conductivity and temperature were collected for September 2021. Similarly, LISST has been procured and tested recently and will be used for collection and analysis suspended sediment data.

Four beach surveys and sediment sampling at both the sites (Nani Danti–Moti Danti, Gujarat and Satpati, Maharashtra) have been carried out so far. The first beach survey was carried out in the month of December 2019, while the second beach survey was carried out during September 2020. The third beach survey was carried during January, 2021, while fourth beach survey was carried out during September 2021. These surveys were carried out using digital theodolite and GPS procured under CMIS project. Beach sediment data was analysed using sieve shakers procured under CMIS project.

3 Results

Beach profile data collected so far advancement of shoreline in non-monsoon months at both the sites, while severe erosion is observed during south west monsoon months. Average humidity of 74% and wind speed of 1.12 m/s was found at Satpati, while humidity of 78% and wind speed of 4.49 m/s was found at Nani Dani Moti Danti. The average temperature at both sites was about 25.5 °C (Figs. 3 and 4).

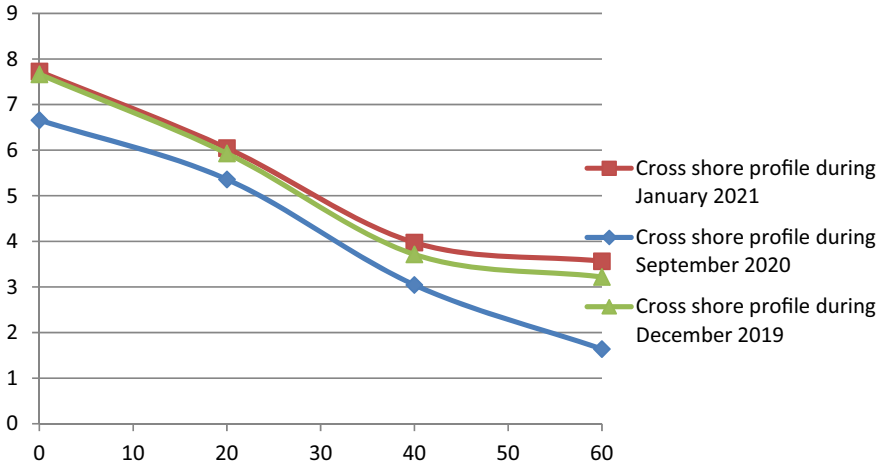

Fig. 3 Typical profile change at satpati site observed during study

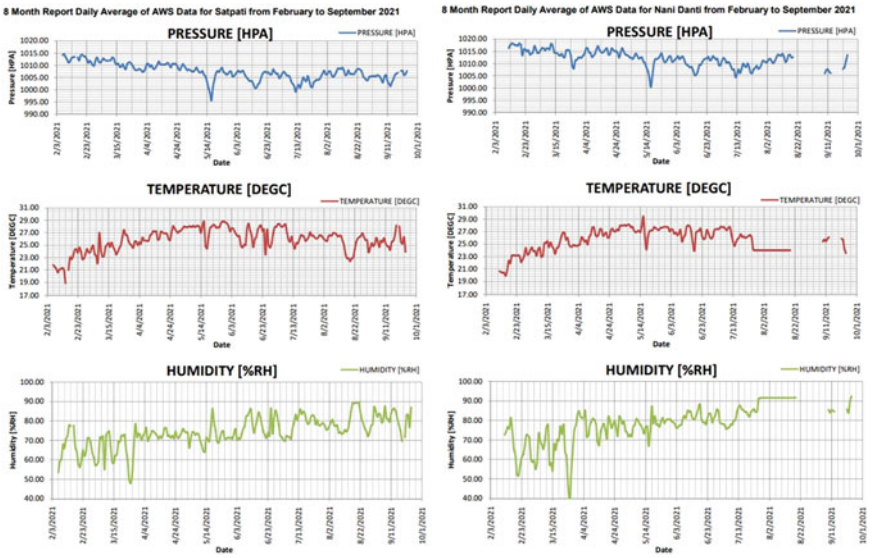

Fig. 4 Data collected from AWS

4 Major Challenges

4.1 Pandemic of COVID-19

CMIS project was awarded to CWPRS in July 2019, while the specification of equipments were approved in PMC meeting held in September 2019. The procurement process was set into motion immediately after. While some items were procured by March 2020, many equipments could not be procured due to sudden lockdown. Even those items for which supply order was issued got delayed as suppliers expressed their inability to deliver and most of the time CWPRS had no option but to extend deadline. The timeline for whole project got derailed. An extension of four months was provided by PMC meeting, held online, in the month of August, 2020. Most of the items for which budget was available were procured by then. In January 2021, these equipments were installed at both the sites following standard COVID protocols. As the project started gathering pace 2nd wave of COVID-19 struck in April 2021. The effect was especially severe in Maharashtra and especially in Pune. As per one estimate during the study period (March 2020 till May 2021), of the 465,192 COVID-19 cases in Pune city, a total of 162,182 (35 per cent) were reported in the first wave while 27,517 (6 per cent) cases were registered during the maintenance period. The second wave reported 275,493 (59 per cent) cases. The second wave lasted till June 2021. Now, every attempt is being made to expedite the project.

4.2 Availability of Fund

The first financial release was made in July 2019. As per MoU at least 50% of the allotted fund must be utilized before fresh funds could be demanded. Thus the allotted money was not sufficient to buy all instrument at once and had to be carried out stages. As procurement process of first stage itself got delayed due to pandemic, the 50% expense requirement was met only by October 2020. Demand for second release was made in November 2020, but the second financial release was finally received in July 2021. The process to purchase DWRB and LISST was done out only after the release of second installment.

4.3 Loss of Equipments

Tide gauge and Marine ADCP were installed at both the sites in January 2021. Sinker weight of 400 kg were put during mooring to avoid any drift of the installed equipments. No insurance company acceded to request of CWPRS for insurance of these equipments during their deployment period in sea. CWPRS decided to hire security personnel for these equipments at both the sites and job work was awarded

to the agency. The contract included ensuring safety and security of the deployed land and water instruments and also to provide video or photograph on daily basis with geotagging and live calls. Awareness campaign was done to ensure safety and security of instruments. Villagers were briefed about the research activity by officers of CWPRS and respective State Government. State Government also issued written communication to fishermen for ensuring safety of equipments.

The JTWC issued a Tropical Cyclone Formation Alert on May 13. Movement in sea was totally stopped by coast guards, and the security firm expressed its helplessness in the situation. On May 17, Tauktae reached its peak intensity as an extremely severe cyclonic storm, with maximum 3-min sustained winds of 185 km/h. As per the reports, Mumbai recorded a whopping 300 mm highest amount of rainfall recorded in May since records began in the nineteenth century. Squally winds reaching more than 100 km/h (62 mph) were recorded. The maximum wind speed recorded was 108 km/h (67 mph), the highest recorded wind gust in last 70 years. The movement in sea was restored only after Monsoon period was over, and it was found that both ADCP and CTD were not present at the sites. The situation was unprecedented and despite taking all safety Measure the instruments got dislocated from its place of installation and could not have been recovered so far. Still efforts are being made to make search for the equipments using divers and side scan sonar surveys.

4.4 Coordination Aspects

CMIS recognizes the importance of role of state Government agencies for successful completion of the project. This is further highlighted by the fact that state Government are part of the tripartite MoU at the beginning of project. Some the key areas in which support of state government is envisaged essential during the course of project are (a) equipment monitoring ensuring availability of suitable boat with skilled boat drivers, staff and labour (b) restricting fishing activities near deployed instruments (d) minor timely repairs like battery monitoring, cleaning of AWS etc.

For continuous long period data collection, the support services and coordination amongst various agencies like harbour department, maritime board, village panchayat, Police department Coast guards, etc., is very essential. Further, for successful completion of project, community plays a very important role. Thus, it is essential to involve all the stakeholders at every stage of planning and execution of the project. Moreover, it is equally important to disseminate and engage with local community about the benefits of the project.

5 Conclusion and Recommendations

1. The procurement of all instruments except DWRB is complete in all respects. Bathymetric survey for pre and post monsoon season has been carried out. AWS

was installed at both sites and data is being received continuously. Beach surveys were carried out at both sites in December 2019, September 2020, January 2021 and September 2021.
2. The testing and installation of two units of each instruments Pressure Tide Gauge (Two units), Marine ADCP (Two units) were carried out in January 2021 taking all safety measures, but these instruments are missing at both sites since May 2021 after cyclonic storm Tauktae hit Indian Coast.
3. Due to Covid lockdown conditions, all procurement actions and subsequent data collection have been delayed.
4. Lots of initial preparation is required to procure the equipments following all Government norms as per GFR. As the activity is quite time consuming and instruments are very costly, extreme caution on price and specifications needs to be taken while procuring them.
5. Timely release of funds is very crucial to avoid delays and expenditure envisaged on instruments should be released in totality at the beginning of project.
6. Support services and co-operation from the local bodies play a very crucial role in the data collection program like CMIS.
7. Non availability of insurance for the equipments deployed at sea is a major constraint, particularly under rough sea condition like cyclones, extreme monsoon condition, etc.

Acknowledgements The authors acknowledge with thanks the financial support received from Central Water Commission (CWC) for CMIS project. The authors are also thankful to Shri R. S. Kankara Director, CWPRS for his support at each stage of CMIS project and his kind consent to publish this paper.

Effect of Super Cyclone AMPHAN on Structure: A Case Study

P. Haldar, S. Karmakar, and S. Roy

Abstract Over the past few years, India has faced different super cyclonic storm (SuCS) rises from the Bay of Bengal (BOB) source. "AMPHAN" is another powerful reported tropical cyclone (TC) after the Odisha SuCS of 1999. It made landfall with incredible atrocity along the coast of Odisha and West Bengal (WB) states of India and the Hatiya islands of Bangladesh (BD) on the same day. It caused massive devastation and damage along the coastal regions, specifically Sundarbans. It causes inevitable disturbance to the people dependent on the fragile landscape for life and biodiversity, which entailed a careful study to evaluate the resilience of structure and emergency maintenance response. The current paper analyzes the effect of wind on the structure after tracking down the cyclone path based on India Meteorological Department (IMD) records. Further, the study of the impact on structure and bridge during the post-AMPHAN period compared to the pre-AMPHAN situation. This paper also presents a comprehensive disaster mitigation report illustrating the damages with photographs, which helps to understand the catastrophic intensity caused by the cyclone.

Keywords Cable-supported bridge · Disaster mitigation · Super cyclone · Wind-induced vibrations

P. Haldar (✉) · S. Karmakar
Department of Civil Engineering, National Institute of Technology Durgapur, Durgapur 713209, India
e-mail: ph.19ce1103@phd.nitdgp.ac.in

S. Karmakar
e-mail: somnath.karmakar@ce.nitdgp.ac.in

S. Roy
Department of Civil Engineering, Narula Institute of Technology, Kolkata, West Bengal 700109, India

P. V. Timbadiya et al. (eds.), *Coastal, Harbour and Ocean Engineering*, Lecture Notes in Civil Engineering 321, https://doi.org/10.1007/978-981-19-9913-0_18

1 Introduction

Cyclones are considered the most destructive natural disaster amongst floods, earthquakes, landslides, and pestilences, compared to their duration, severity, and areas of destruction. Again, cyclone in the atmosphere is an intense vortex, specified by the rotation of high wind about a centre of low atmospheric pressure in clockwise and anti-clockwise directions in the southern and northern Hemispheres, respectively. The pressure increases outwards, and the movement of the centre is onward. The wind strength and the cyclone intensity depend upon the rate at which it extends outwards and the pressure in the centre.

The most significant results of this disaster may be enormous damage to communication systems, transports, properties (buildings and other structures), marine facilities, crops, and human and animal loss. Besides, millions of trees can be uprooted in a matter of hours, which may be the reason for extensive damage to the ecosystem [1–4]. Hence, the cyclone epidemic mitigation is essential. Unlike earthquakes, cyclones' average life period is around five days from their formation time and landfall on the coast. In contrast, earthquakes occur suddenly and for a few seconds [5]. It has been estimated that the number of deaths related to cyclone in the past two centuries is nearly 1.9 million, 27% in India and 42% in BD [6]. SuCS "AMPHAN" (uttered as UM-PUN means sky) has named by Thailand in 2004. The name is adopted by the World Meteorological Organization, the grouping of countries. The panel includes Thailand, Sri Lanka, Oman, the Maldives, Pakistan, Myanmar, BD, and India, naming cyclones for this region [7].

AMPHAN formed over Northwest BOB, crossed WB–BD coasts as a very severe cyclonic storm (VSCS). It stroked this region with a very high wind speed of 155–165 Kmph, causing colossal property damage and life loss. This SuCS is also gusting to 185 Kmph across Sundarbans, as per the IMD 2020 press release [8]. Figure 1 shows the cyclone's observed track, and details of cyclone classification as per the IMD scale are presented in Table 1. This cyclone termed SuCS by following the IMD scale [7, 9] is considered the second-worst storm in this decade (after Phailin, 2013) in India.

Storm-water surges, very high-intensity winds, saline water invasion, tidal inundation, and flash floods are also associated with this cyclone "AMPHAN." The principal ambition of this vulnerability assessment is to explore the role of its damage and effect on structure, especially bridge-type. This study has considered the previous damage by the other cyclones, which are originated from BOB and the Arabian Sea and affect India. All the data are collected from Vogue media, government reports, NGO reports, etc. Besides, due to the pandemic situation of COVID-19, the researcher cannot meet the victimized area. Therefore, following IMD; Regional Meteorological Centre Kolkata; WB Disaster Management & Civil Defence Department; National Disaster Management Authority [10]; The Orissa Disaster Mitigation Authority [11]; The Orissa Disaster Mitigation Programme (ODMP); Orissa State Branch (OSB); and The Indian Red Cross Society (IRCS), this case study has completed.

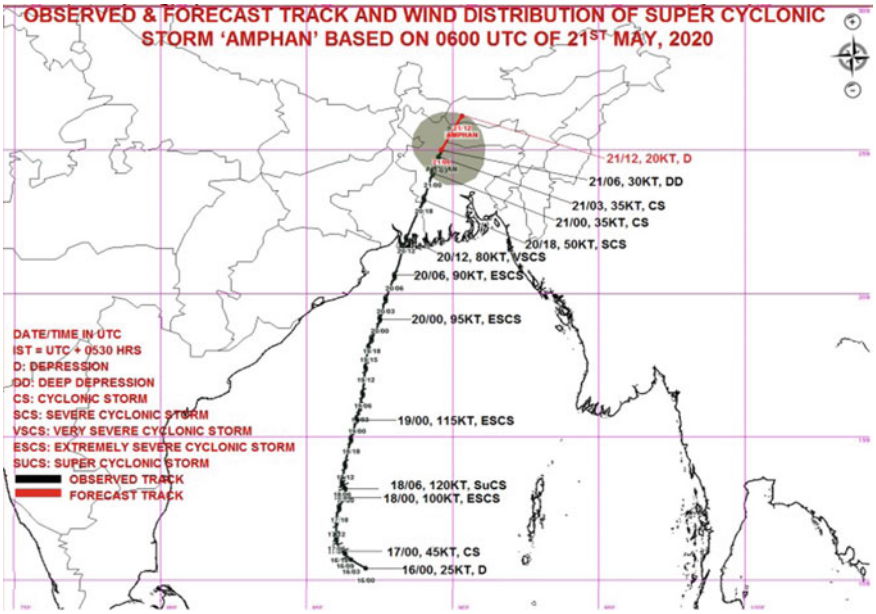

Fig. 1 Route of SuCS AMPHAN as per IMD

Table 1 Details of the classification of cyclone as per the IMD scale

Intensity (Kmph)	Expected devastation
DD (50–61)	Minor damage to unsecured and loose structures
CS (62–88)	Spoil to thatched huts, communication and power lines, tree branches
SCS (89–117)	The uprooting of large avenue trees. Extensive damage to thatched roofs
VSCS (118–166)	Minor disruption of road traffic and rail
ESCS (167- 221)	Some wear to old buildings and power lines disruption in large scale
SuCS (222 or more)	Extensive structural damage to industrial and residential buildings. Large-scale trouble of road traffic and rail due to extensive damage to bridges

2 Cyclone–Typhoon–Hurricane: The Difference

Scientists have identified the cyclone by various names in different regions of the world, according to its native land. The weather phenomenon that evolves over the North-western Pacific and Philippines is named "typhoon." In the Eastern Pacific Ocean or the Atlantic and the West Indian islands in the Caribbean Sea, the same powerful storms are named "hurricane," which is the name of the Caribbean god of evil [12, 13]. These are also known as "Willy-willies" in Western-north Australia, "Tornados" in the Southern USA and Guinea lands of West Africa, and "cyclone"

in the Indian and South Pacific Ocean [10]. Further, it is termed "severe tropical cyclones" when it is in South-eastern Indian, and the South-western Pacific Ocean originated Cyclones. Again, "severe cyclonic storm" when it appears in the Northern Indian Ocean. They are just "TC" in the South-western Indian Ocean. The most specific criteria for the announcement of any storm as a hurricane, typhoon, or cyclone are its wind speed, which must reach at least 119 kmph. Hurricane and typhoon can be upgraded to an "intense hurricane" and "super typhoon" if their wind speed hits 179 kmph and 241 kmph, respectively. Whilst the "SuCS" term comes for 222 kmph [13].

3 Two Significant Cyclones During the Last Decades in India

TC hits India almost every year, and this TC's disaster potential is becoming high after the landfall due to storms, tidal waves, and strong wind. The worst affected terrain is the Indian sub-continent as its coastline is 7516 km, and 40% of India's total population lives within 100 km of coastline. Also, 13 coastal states/U.Ts surrounding 84 districts are affected by the cyclone, and 370 million people are exposed to this disaster in India as per NDMA 2019 publication [14]. The states overwhelmed by cyclone have listed in Table 2.

Again, Table 3 shows the list of most destructive cyclones with in the last two decades, amongst which Phailin (2013) and Fani (2019) are the most terrible.

3.1 Phailin Cyclone (2013)

The VSCS "Phailin" has battered at the coast of Odisha on 12th October 2013, near Gopalpur in the Ganjam district. It was created as a tropical depression in Thailand bay from a remnant cyclonic circulation on 4th October [15]. Therefore, the name of this SuCS has been given as "Phailin," which is the Thai language that means "sapphire" [16]. On 10th October, it boosted speedily and became a cyclone

Table 2 List of states vulnerable to cyclone

States/U.T.s vulnerable to cyclone			Other state affected by cyclone		
Eastern Coast		Western Coast	Easter Coast	Western Coast	
Andhra Pradesh (AP)	Odisha	Gujarat	Andaman Nicobar (A & N) Island	Goa	Maharashtra
Tamil Nadu (TN)	WB			Daman & Diu	Lakshadweep
Pondicherry				Kerala	Karnataka

Table 3 Previous cyclone details in India [12, 18–20]

Sl. No	Name	Year	Origin	Affected area	Max. speed kmph	Named by	Impact
1	Bhola	1970	CBOB	BD	240	-	$86.4 million
2	Sidr	2007	CBOB	Patuakhali, Dhaka, Sundarbans	248	Oman	$1.7 billion
3	Fanoos	2005	BOB	TN	110	Pakistan	$21.4million
4	Nisha	2008	BOB	Sri Lanka (SL.), TN, Puducherry	85	BD	–
6	Jal	2010	BOB	SL., India, Borneo, Brunei, Malaysia	–	India	–
7	Thane	2011	BOB	TN, Puducherry, AP	145	Myanmar	–
8	Nilam	2012	BOB	A.P., TN, SL	101	Pakistan	–
9	Phailin	2013	East Central BOB	Odisha, AP	215/260	Thailand	$4.26 billion
10	Hudhud	2014	Andaman Sea	A&N, AP., Odisha, Nepal	175/185	Oman	$3.58 billion
11	Nilofar	2014	Arabian Sea	Coastal Gujrat, Pakistan	125	Pakistan	-
13	Vardha	2016	Southeast BOB	A&N Islands, Thailand, Sumatra, Malaysia, SL	130, 155	Pakistan	$3.37 billion
14	Ockhi	2017	Southwest BOB	Kerala, TN, Gujarat	155, 185	BD	$920 million
15	Gaja	2018	Thailand	TN	165	Sri Lanka	$2.5 trillion
16	Titli	2018	BOB	Odisha, AP	165	Pakistan	–
17	Fani	2019	Indian Ocean	Odisha	205	BD	$2352 million
19	AMPHAN	2020	BOB	Odisha, WB, BD	185	Thailand	$13.2billion
20	Nisarga	2020	Arabian Sea	Maharashtra	110	BD	–

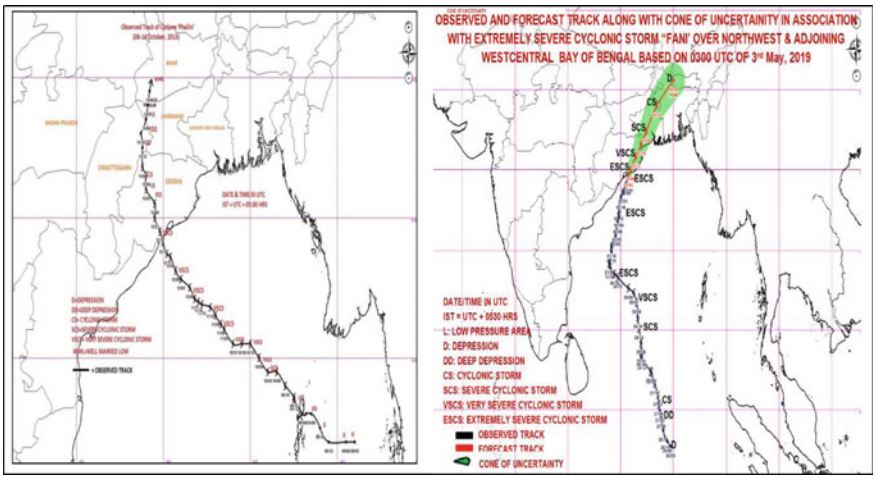

Fig. 2 Observed track of Phailin during 8th–14th October 2013 and Fani on 2nd May 2019

equivalent to a category one hurricane as per Saffir–Simpson Scale. It exploded into a SuCS and made landfall on 12th October with a wind speed of 220 kmph. The second most robust cyclone hits the state after the 1999 super cyclone [15–17]. The rapid damage and needs assessment (RDNA) team has estimated about INR 89,020 million loss and damages due to this cyclone. Figure 2 shows the observed track of Phailin and Fani as per IMD.

3.2 Fani Cyclone (2019)

Cyclone Fani made landfall at Satapada, near Puri, on 3rd May 2019 at about 8:30 a.m. with a max wind speed of 175–180 kmph gusting to 205 kmph. It is the other most robust cyclone in the last 20 years [19]. The origin of Fani was formed on 26th April 2019 in the Indian Ocean. On 30th April, it turned into a VSCS Fani over Southeast and adjoining the southwest BOB. Further, it intensified to extremely severe cyclonic storm (ESCS) on 1st May, equivalent to category-4 hurricane as per Saffir–Simpson Hurricane Scale [21]. It moves towards Tamil Nadu, but surprisingly, it changes its direction and moves towards Odisha's coastal area. Fani caused enormous damage till 4th May early morning [19, 21].

4 The Disaster: Cyclone "AMPHAN"

4.1 Formation of AMPHAN and Wind Analysis

According to IMD Report, a clear-cut low-pressure area has formed on the 15th morning, over the southeast BOB persists. Depression is concentrated in the early morning of 16th May on this pressure area over the same region. This weak system boosted up into a deep depression (DD) in the afternoon over the same place. Further, in the same evening, it forms into a cyclonic storm over the south BOB's central parts, being classified as "AMPHAN." It also intensified into a SuCS after characterizing all stages in the afternoon of 18th May 2020 over west-central BOB. This SuCS has crossed WB–Bangladesh's coast, at 17:30 h on 20th May, as a VSCS. Its speed was 155–165 kmph. As described above, it gusting to 185 kmph across Sundarbans near latitude 21.9°N and longitude 88.4°E. This storm is about 70 km, nearly to the south of Kolkata, 35 km northeast of Sagar Island, 95 km east-northeast of Digha (WB), and 185 km south-southwest of Khepupara (Bangladesh). It has caused widespread damage in WB as this place was the epicentre of the cyclone's landfall. Kakdwip and Namkhana in South 24 Parganas and Minakha and Hingalganj in North 24 Parganas are the worst affected by the cyclone, which made landfall near Sagar Island. Detailed stages of the cyclone have illustrated in Fig. 3. It weakened slightly before the landfall, though high cyclonic winds were noticed around the cyclone's eye. It lay over WB as a VSCS, gradually moving northeastwards from late evening to 20th May.

Figure 4 shows the wind direction and speed by the wind rose diagram with the help of the IMD Report. Figure 5 shows the best track positions and other SuCS parameters, "AMPHAN" from MERRA2 [22].

4.2 Impact of AMPHAN on Structures

The damages details for the "AMPHAN" are discussed in this segment considering the WB Government declaration. Almost 8.13 lakh people were evacuated at that time, and six crore people were affected directly or indirectly, along with 87 deaths. The road communication became completely immobilized as 4,710 km of rural roads and 317 km of PWD roads were damaged, including 300 small culverts or bridges. Figure 6 shows a scene of the impact of AMPHAN in a different area. The cyclone had destroyed the unstructured building and heavy damage to many institutional/school buildings, factory buildings, industrial structures, and destroyed Kolkata Airport. The total loss evaluated caused by the cyclone was about 13.2 billion USD, out of which for 10 lakh (1 million) dwelling damage [23]. The excessive uplift wind forces are effectively resisted by the RC roof system's heavy dead weight. Thus, maximum devastation happened to AC sheets, thatch, tiles roof cladding house. Many thatched dams were damaged over Kalindi, Ichhamati, Rai Mangal, and Sahebkhali rivers on

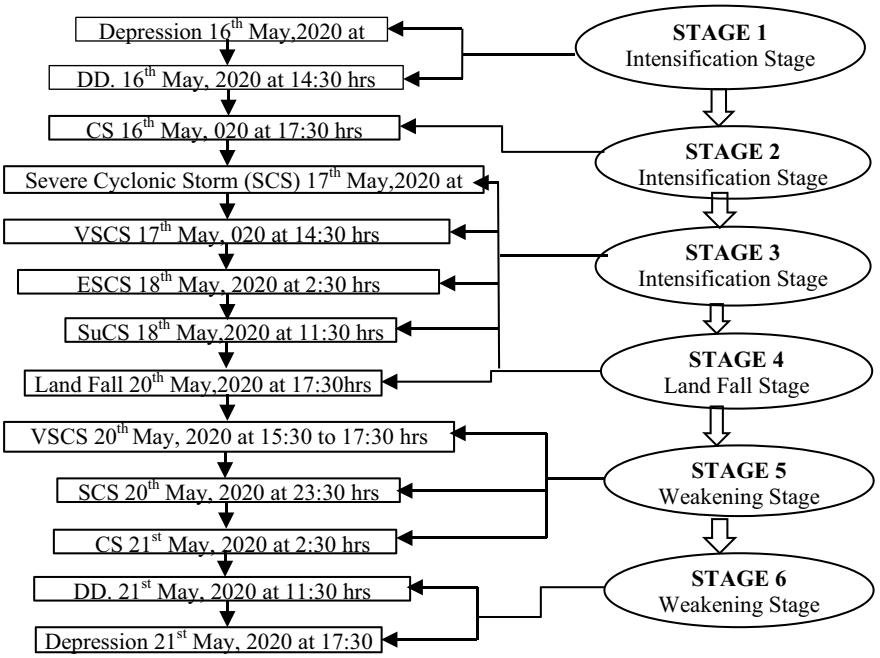

Fig. 3 Stage wise AMPHAN details

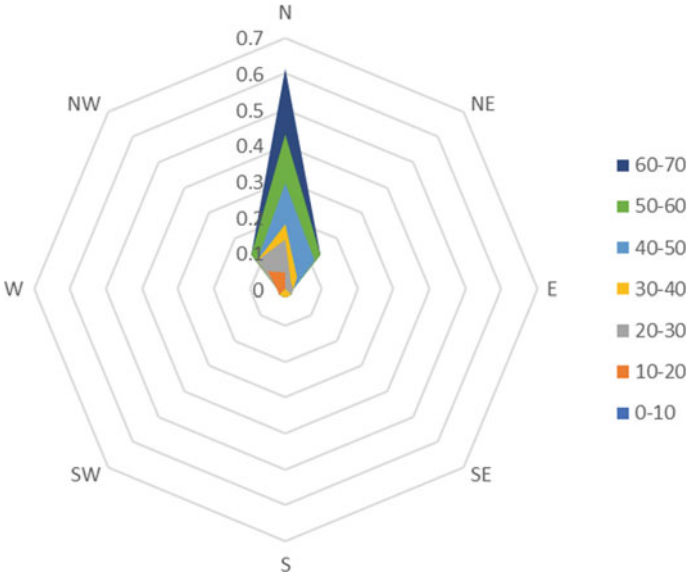

Fig. 4 Wind rose diagram (wind in m/s)

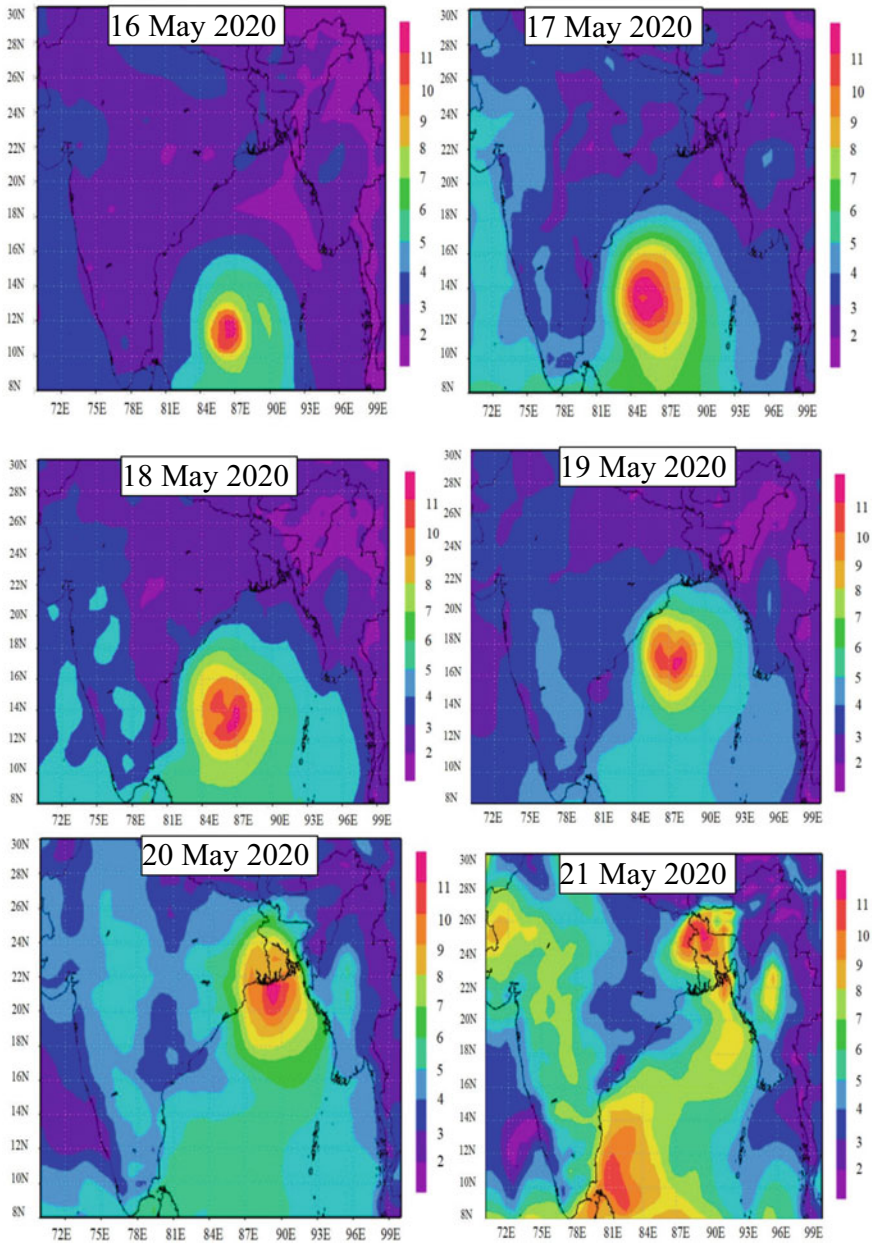

Fig. 5 Best track positions and other parameters of SuCS, "AMPHAN" from MERRA2

the coastal belt close to the Sundarbans due to high tidal waves prompting the local administration to repair them immediately.

4.3 Effect of AMPHAN on Bridges

Cyclones, besides causing massive damages to the unstructured buildings and different semi-engineered structures, the engineered structures may be affected by it. These reasons caused severe engineering concerns and need further research to enhance the analysis of cyclones' behaviour against wind forces. Several bridges are in the path of the "AMPHAN," amongst which some are cable-supported suspension bridges.

In the present day, genuinely speaking, predicting wind effect on bridges with the global climate change and enlarging span length is undoubtedly tricky. The significant factor for bridge design with a long span is wind-induced vibrations (WIV). The four major classifications of WIV based on wind mechanisms are Flutter, galloping, vortex-induced vibration (VIV), and buffeting. The other are rain and wind-induced vibration (RWIV), wake induced vibration, coupling of VIV and galloping, coupling of buffeting, and Flutter. Figure 7 shows the position of bridges in a map along the AMPHAN affected area. With 822.96 m length, Vidyasagar Setu is a cable-stayed suspension bridge in the route of "AMPHAN." This bridge may be a subject of concern as the cable-stayed bridge deck is prone to Flutter, the pylon may be affected by galloping, vortex-induced vibration (VIV). At IISC Bangaluru, a section model concept-based circuit wind tunnel has been conducted for the wind analysis of this bridge. It revealed that the cross section of the deck does not undergo any significant bending, torsion, galloping, and Flutter oscillations up to a wind speed of 250 KMPH [24]. As per the press release by IMD, AMPHAN was a SuCS with a wind speed of 200–210 kmph, which enhanced the requirement for monitoring this bridge because this bridge was constructed 18 years before and situated about 360 km south of Paradip. Another example is 73 years old Howrah Bridge, a truss bridge. Compared to a girder stiffened bridge, the truss-stiffened section bridge is more favourable as it blocks less wind. But generally, the truss-stiffened bridge is less stiff against torsion. Therefore, torsional moment due to wind is a concern on the Howrah bridge.

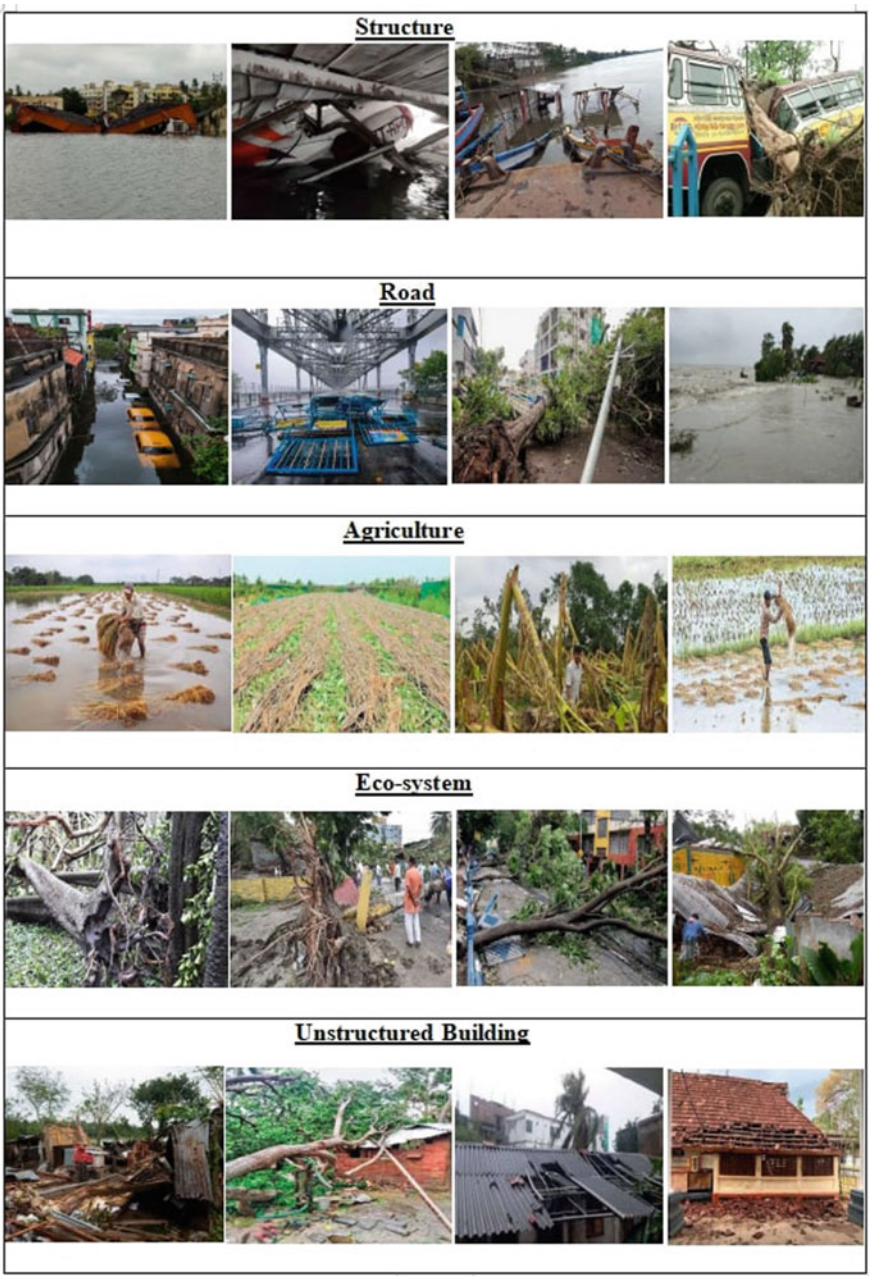

Fig. 6 Impact of "AMPHAN" in a different area

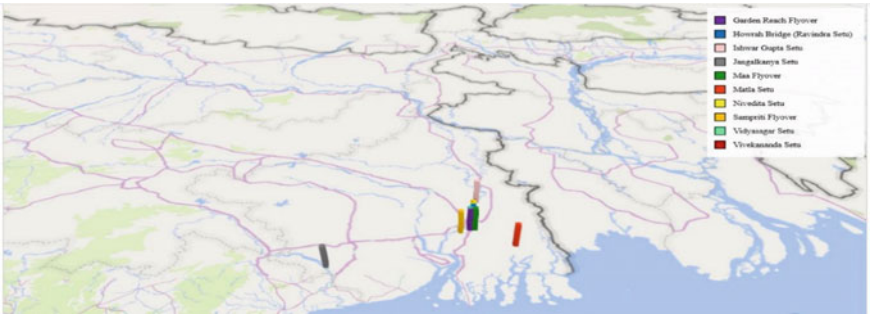

Fig. 7 Position of bridges in a map along the AMPHAN affected area

5 Conclusions

The states like WB and Odisha have a long history of disasters, especially floods and cyclones that affect thousands of people every year. "AMPHAN" is one of the destructive cyclones in the last years. It caused excessive damage to infrastructure along with loss of life. According to the survey by the government, it was noticed that several structural damages occur depending on engineering attention in varying degrees. This attention is applied to the structure during the construction and design stages. The authors have discussed the probable causes of the observed failures and their impact on other fields. Further, India has inadequate documentation on wind evolution and its resisting structure. Therefore, simple and practical measures have been suggested to mitigate the damage caused by cyclone, along with the importance of construction aspects and structural detailing. Moreover, the author focusses on the effect cyclone on bridges situated on cyclone path. The listed bridge should monitor and maintain with great concern that could mitigate the vulnerabilities of the region during the post-AMPHAN periods. This would further ensure fruitful results with minimal damage during similar natural disasters in the future.

Acknowledgements Data from MERRA2 are acknowledged, thankfully.

References

1. Mehta KC (1984) Wind-induced damage observations and their implications to design practice. Eng Struct 6(4):242–247
2. Walker GR (1985) Cyclonic storms and related design criteri. Asia Paci"c Symposium on Wind Engineering, University of Roorkee, Roorkee, India, December 1985, pp XVI–XXVI
3. Venkateswarlu B (1987) Extreme wind hazards in Asia. In: Proceedings of the US-Asia Conference on Engineering for Mitigating Natural Hazards Damage, Bangkok, December 1987, pp. A1–1–14
4. Sarker AK (2017) Cyclone hazards in the Arabian sea–A numerical modeling case study of Cyclone Nilofar. Water Environ J 31:284–295

5. Shanmugasundaram J, Arunachalam S, Gomathinayagam S, Lakshmanan N, Harikrishna P (2000) Cyclone damage to buildings and structures a case study. J Wind Eng Ind Aerodyn 84:369–380
6. Nicholls RJN, Mimura N, Topping JC (1995) Climate change in South and South-east Asia: some implications for Coastal Areas. J Global Environ Eng 1:137–154
7. WMO/ESCAP Panel (2015) on Tropical Cyclones (8th June 2015) A Report: Tropical Cyclone Operational Plan for the Bay of Bengal and the Arabian Sea 2015 (PDF) (Report No. TCP-21). World Meteorological Organization. pp. 11–12. Retrieved 29 March 2015.
8. IMD (2020) Press Release of India Meteorological Department on 20th May 2020.
9. IMD 2009 Best track data of tropical cyclonic disturbances over the north Indian Ocean(PDF) (Report). India Meteorological Department. 14th July 2009. Retrieved 31 October 2015. http://www.rsmcnewdelhi.imd.gov.in/images/pdf/archive/best-track/bestrack.pdf
10. NDMA, An explanation about Cyclone by NDMA, https://ndma.gov.in/Natural-Hazards/Cyclone
11. OSDMA (2019) Cyclone Fani 2019 Odisha DLNA (Damage, Loss, and needs assessment) Report, May 2019, Odisha Government, https://www.osdma.org/publication/cyclone-fani-2019-dlna-report/
12. Nair AG, Annadurai R (2018) A study on various tropical Cyclone hits in India – Through GIS approach. Int J Pure Appl Math 119(14):589–595
13. Than K (2019) Cyclone, hurricane, typhoon: What's the difference? *An article on National Geographic*, 12th June 2019, https://www.nationalgeographic.com/news/2019/6/130923-typhoon-hurricane-cyclone-primer-natural-disaster/
14. NDMA (2019) Study Report on Gaja Cyclone 2018, A publication of National Disaster Management Authority, September 2019
15. Parida BR, Beherab SN, Oinam B, Patel NR, Sahooe RN (2018) Investigating the effects of episodic Super-cyclone 1999 and Phailin 2013 on hydro-meteorological parameters and agriculture: An application of remote sensing. Remote Sens Appl: Soc Environ 10:128–137
16. Murty PLN, Sandhya KG, Bhaskaran PK, Jose F, Gayathri R, Balakrishnan TM et al (2014) A coupled hydrodynamic modelling system for PHAILIN cyclone in the Bay of Bengal. Coast Eng 93:71–81
17. IMD (2013) Very Severe Cyclonic Storm, Phailin over the Bay of Bengal (08–14 October 2013). Cyclone Warning Division, India Meteorological Department, New Delhi. http://www.rsmcnewdelhi.imd.gov.in/images/pdf/publications/preliminary-report/phailin.pdf
18. Frank NL, Husain SA (1971) The deadliest tropical Cyclone in history? Bulletin American Meteorological Society 52(6):438–445
19. Basa EA (2019) Management of an extremely severe cyclonic storm–FANI–A case study from India. World Engineering Convection, Australia, 2019, 20–22 November, Melbourn Convention, Exhibition Center
20. Sharma SK, Misra SK, Singha JB (2020) The role of GIS-enabled mobile applications in disaster management: A case analysis of cyclone Gaja in India. Int J Inf Manage 51:102030
21. Mohanty CR, Mb J, Radhakrishnan RV, Mohanty PC, Panda R (2020) Tropical cyclone Fani perspective from the trauma and emergency department of an affected tertiary hospital. Chin J Traumatol 23(4):243–248
22. Mishra AK, Vanganuru N (2020) Monitoring a tropical super cyclone Amphan over Bay of Bengal and nearby region in May 2020. Remote Sens Appl: Soc Environ 20:100408
23. Beer T. (2020) 500,000 Families May Be Homeless Due To Devastation From Cyclone Amphan. Retrieved from https://www.forbes.com/sites/tommybeer/2020/05/22/500000-families-may-be-homeless-due-to-devastation-from-cyclone-amphan/#284210522cdd
24. West Bengal PWD, Highway bridges in west Bengal – vol III with major highway projects. A report by West Bengal PWD.

Effect of Cyclone Yaas on Digha Sea Beach and Adjoining Coastal Areas in West Bengal

Mayuraksha Bardhan

Abstract A very severe Cyclone Yaas hit the Digha Coast and adjoining coastal areas in West Bengal on 26.5.2021. Process of landfall commenced from 8.30 A.M and it continued for about four hours to complete the whole process. Maximum Storm Surge Level recorded at Digha was about 7.20 m. Maximum wind velocity observed at Digha was about 150 km/h with direction s-s-e. Many places in Howrah, North 24 Parganas, South 24 Parganas and East Midnapore districts got marooned on 26.5.2021 after sea water and river water gushed into villages following damage to river embankments due to high storm surge soon after Cyclone Yaas made a landfall near Dharma Port in Odisha on 26.5.2021. About 156 km of river embankments in these districts were either damaged or breached. Embankments along rivers Hooghly, Rupnarayan and Haldi were damaged at several places causing the disaster. A number of villages and settlements in the riverine areas of these districts were inundated. Affected areas include Digha, Tajpur, Mandermoni, Haldia of East Midnapore district. Breaches in river embankments left thousands of villages and settlements inundated in areas like Kakdip, Sagar, Ghoramara island, Patharpratima, Bakkhali, Sandeshkhali, Mousuni island, Fraserganj and Hingalganj in South 24 Parganas. In East Midnapore, nearly 12 blocks were marooned due to surge in sea water and river water levels. Water overtops Guard Wall at Digha and New Digha on 26.5.2021 morning with embankment breach and destruction of Guard Wall at several places. Entire Sea Embankment from Sankarpur to Tajpur was badly affected due to cyclone. In Mandermoni, several hotels and shops were destroyed. This paper reports damage caused due to Cyclone Yaas in West Bengal. Preventive measures to be taken in case of future storms to minimize damage and loss of life have been discussed.
also.

Keywords Torm surge · Wind velocity · Embankment breach · Sea embankment

M. Bardhan (✉)
River Research Institute, P.O.-Mohanpur, District- Nadia, West Bengal 741246, India
e-mail: mayur.bardhan@gmail.com

P. V. Timbadiya et al. (eds.), *Coastal, Harbour and Ocean Engineering*, Lecture Notes in Civil Engineering 321, https://doi.org/10.1007/978-981-19-9913-0_19

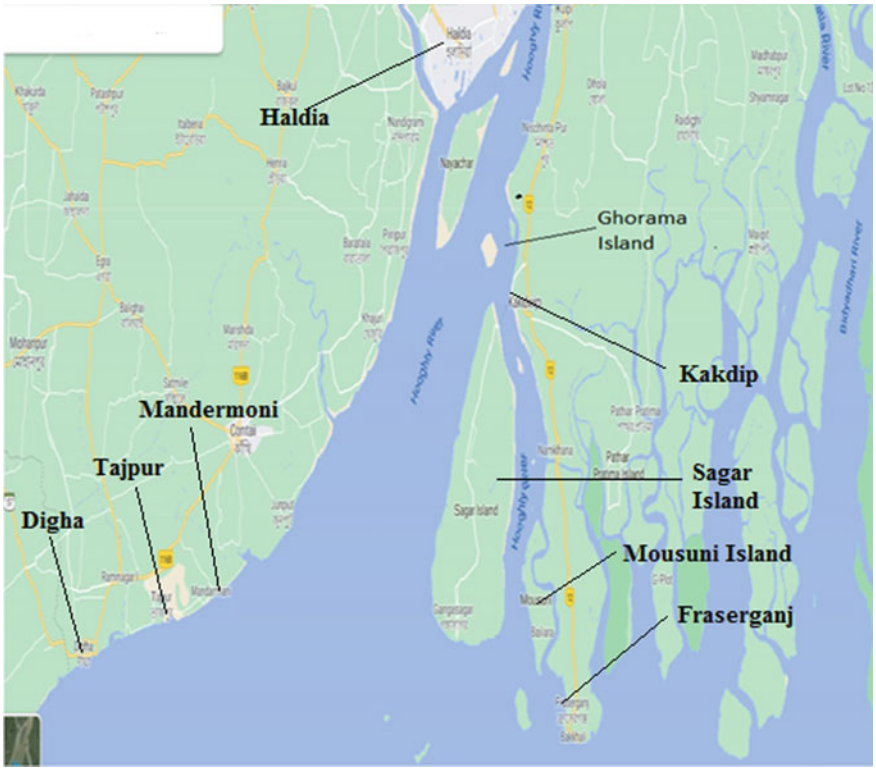

Fig. 1 Areas affected due to Cyclone Yaas

1 Introduction

A very severe Cyclone "Yaas" hit the Digha Coast and adjoining coastal areas in West Bengal on 26.5.2021. Affected areas include Digha, Tajpur, Mandermoni, Haldia of East Midnapore district and areas like Kakdip, Sagar, Ghoramara island, Patharpratima, Bakkhali, Sandeshkhali, Mousuni island, Fraserganj and Hingalganj in South 24 Parganas. The affected areas are shown in Fig. 1. Table 1 depicts damages due to Cyclone Yaas in the district of East Medinipur in West Bengal [1]. This paper reports damage caused due to Cyclone Yaas in West Bengal with special emphasis on Digha Sea Coast.

2 Review of Literature

"Examination of the storm data of the past 45 years or so indicates that the most likely periods for storms are the months of advancing and retreating south-west monsoon,

Table 1 Damages due to Cyclone Yaas in East Midnapore district of West Bengal

Sl. No	Items	Quantity
1	Villages affected	1200 Nos
2	Population affected	9 Lacs
3	Cattle lost	236 nos
4	Agricultural land	50,000 Ha
5	Houses damaged	50,000 nos
6	Fruit, flowers and vegetables	8000 Ha
7	Roads	150 km
8	Embankment	72 km
9	Trees	25,000
10	Electrical wires	15,000 km
11	People shifted in relief camps	4.5 Lacs

Source http://www.anandabazar.com.

i.e. May and October. The statistical analysis indicates that for Sagar, extrapolating the 100-year range the Sagar water level is 11.95 ft. (3.643 m) above the mean sea level to which at least another 3.50 ft. (1.067 m) may be added to arrive at the storm level at Digha for the shallowness of the coast. In other words, the height of storm levels may be taken as 15.45 ft. (4.710 m) above the mean sea level for Digha and due allowance may be made for the free board."—"Stability of the beach at Digha" conducted by Hydraulic Study Department, KPC, Calcutta, June-1966, TR No-32 [2].

3 Analysis of Hydro-Meteorological Data Observed During Cylone "Yaas"

The storm surge height due to cyclone Yaas is presented in Table 2.

Table 2 Storm Surge at Digha and Sagar on 26.5.2021

Location	Predicted maximum tide level		Maximum measured storm surge level in metre (GTS)		Storm surge in metre
	In chart Datum in metre	In metre (GTS)	In chart Datum in metre	In metre (GTS)	
Sagar Island	5.71	2.89	8	5.18	2.29
Digha	6.78	3.96		7.20	3.24

Source Kolkata Port Trust

Table 3 Observed wind speed on 26 May 2021

Time	Speed in km/h	Direction	Remark
8.0AM	100.00	S-S-E	Instrument was Anemometer [S-S-E South-South-East]
9.00AM	120.00	S-S-E	
10.00AM	135.00	S-S-E	
11.00AM	150.00	S-S-E	
11.30AM	125.00	S-S-E	
12.30PM	100.00	S-S-E	
1.00PM	69.00	S-S-E	

Source River Research Institute, W.B.

3.1 Wind Speed and Direction

From different reports of the River Research Institute [3], it has been observed that dominated wind direction at Digha for the months of May to October is south-west. It was observed that the wind direction during Cyclone YAAS was south-south-east and maximum wind speed 150 km/h as presented in Table 3.

The storm surge height (SSH) 7.2 m (GTS value) was recorded on 26th May 2021 by the Digha Meteorological Observation Site Office of River Research Institute under I&W Directorate, Govt. of West Bengal.

4 Effect of Cyclone Yaas in the State of West Bengal

4.1 Effect of Cyclone Yaas on Digha Sea Beach

Figure 2 depicts coast line around Digha from River Mouth Subarnarekha to Rasulpur. The entire coast line around Digha is divided in different stretches.

4.2 Shankarpur Bus Stand to Jaldah/Tajpur (Length 3.8 km)

The tagging end of block protection near Shankarpur Bus stand was fully damaged for a length of around 80.0 m (Fig. 3). Guard wall, retaining wall after walkway at country side, was completely damaged. Concrete block at sea face displaced, damaged and boulder soling beneath was exposed, stone boulders were scattered all round. The guard wall stood almost intact where there was infinite back filling near bus stand. Figure 4 depicts damaged Guard Wall at Jaldah.

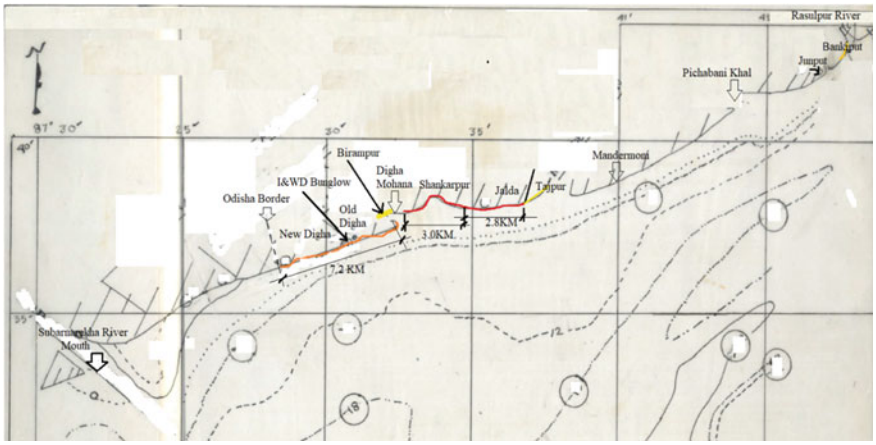

Fig. 2 Schematic view of coast line around Digha from River Mouth Subarnarekha to Rasulpur

Fig. 3 Damaged sea wall in country side at Shankarpur bus stand as observed on 28.5.2021

Fig. 4 Guard wall damaged and black top road behind damaged, washed out at Jaldah as observed on 28.5.2021

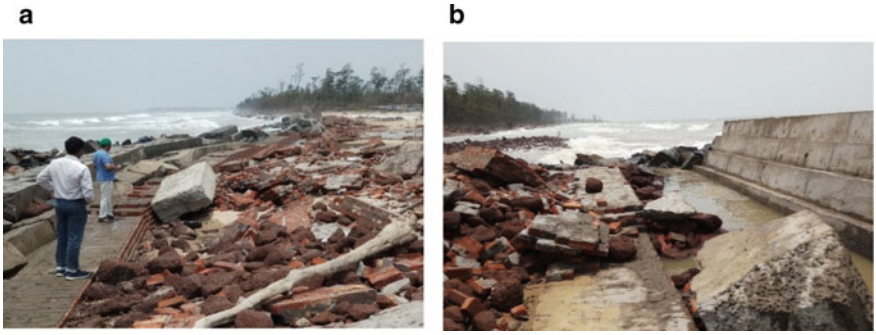

Fig. 5 **a** and **b**: Damaged guard wall and masonry retaining wall at Nayak Ghat, Shankarpur (Harbour) as observed on 28.5.2021

4.3 Shankarpur Bus Stand to Digha Mohana (Length 3.0 km)

Length 3.0 km, out of which concrete guard wall and masonry retaining wall both were constructed for a length of 1.0 km which was completely damaged (Fig. 5a & b).

4.4 Digha Mohana to Hotel Sea Hawk (Length 2.33 km)

The block protection from hotel Sea Hawk to Digha Mohana, length of about 1.73 k.m, was intact (Fig. 6a) except damages to boulder protection near Sea Hawk (Fig. 6b), approximate length of 0.60 km and one drainage sluice at this point got damaged. Here too the surge was above the guard wall top and it overflowed towards the country side but there was almost no damage to the concrete blocks as well as the black top road behind the masonry retaining wall at country side.

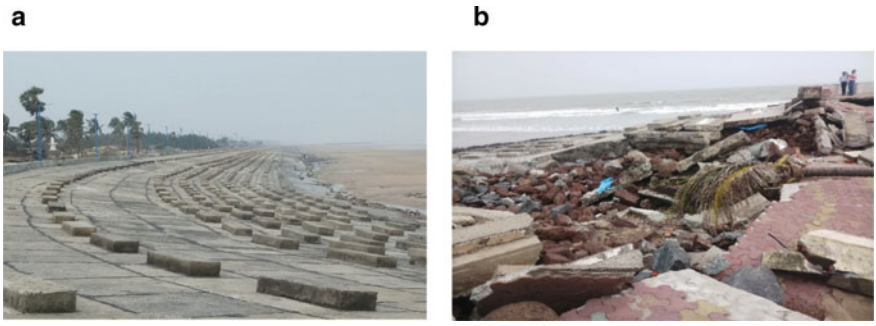

Fig. 6 **a** Intact block protection, Sea Hawk to Digha Mohana and **b** Damaged protection just near Sea Hawk as observed on 28.5.2021

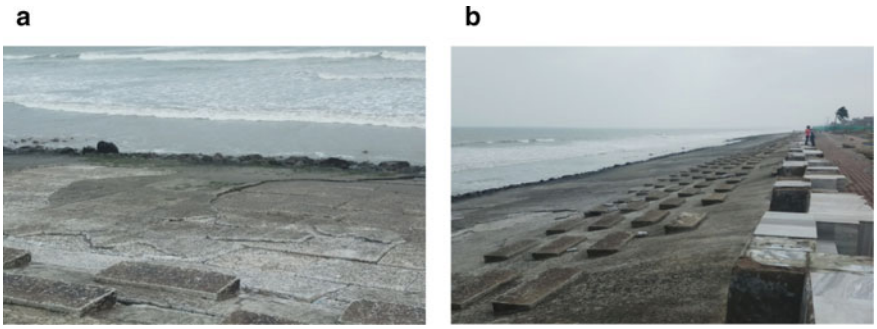

Fig. 7 **a** Area near Hotel Sea Hawk and **b** Eastern side of Jatranullah Inlet as observed on 28.5.2021

4.5 Sea Hawk to Eastern Side of Jatranullah Inlet (Length—3.37 km)

At this stretch (Figure 7a and b), the block protection was almost intact with minimum wear and tear.

4.6 New Digha (from Eastern Side of Jatranala Inlet to Udaypur, Bengal Orissa Border, Length—1.50 km)

Figure 8a and b depict stone boulders accumulated from sea face slope in Jatranala Inlet.

Fig. 8 **a** Stone boulders from sea face slope, got accumulated near and **b** Guard wall overtopped to C/S as observed on 28.5.2021

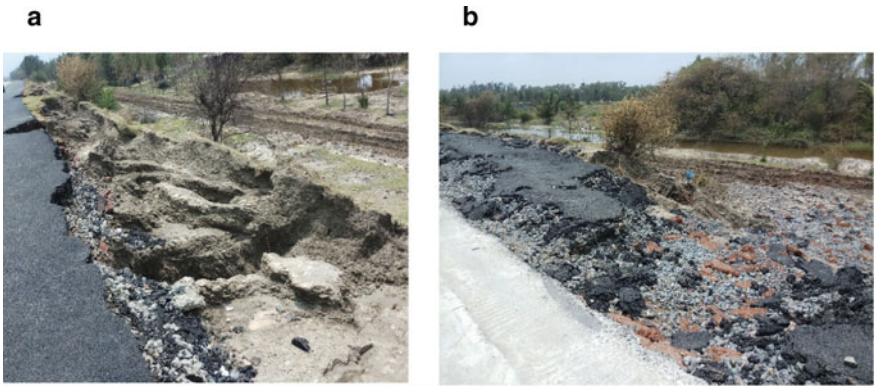

Fig. 9 **a** Overtopped surge made huge rain cut at country side and **b** subsequent damage to the black top road at Birampur as observed on 29.5.2021

4.7 Birampore, Digha

Average black road top level here was 6.25 m G.T.S. The surge overtopped too at this stretch, damaged the black top, formed rain cuts at country side and damaged the existing block lining as well as the nose of proposed view point (Fig. 9a and b).

The sloped block lining here was very steep, in the tune of 1(H):1(V) which was not at all permitted at sea face. It was gathered that the sea dyke too got lowered during construction of black top road over it, which was a self-destructive measure.

4.8 Bankiput

The protection at sea face was almost intact with minor damage to the boulder pitching over slope. The surge too here overtopped the guard wall and made huge rain cut like depression at country side (Fig. 10 a and b).

4.9 Probable Causes of Failure

Out of all the coast line protection, the worst hit was the stretch between Shankarpur Bus Stand to Tajpur. The wind velocity and HHTL were similar in all the stretches but somewhere the effect was minimum and somewhere it was maximum. Maximum top level of guard wall was 6.25 metre (G.T.S), somewhere lower than this too. The RL of total column of water including surge was 7.20 metre (G.T.S), causing spill over the guard wall towards country side. Where there was infinite backfill at country side behind the masonry retaining wall, the spilled water thrust causes minimum damages

Fig. 10 **a** and **b** Damaged Sea Wall at Bankiput, near Junput as observed on 29.5.2021

as the horizontal backfill pressure resisted the masonry retaining wall from getting tilted but where there was no infinite fill, the masonry retaining wall, PCC guard wall did not get any horizontal support, either got tilted or damaged.

The above Fig. 11 shows the force diagram, while a wave hits the sloped embankment. The forces are named below.

Pu = Uplift pressure over lining block at the moment of fall of the wave over slope
Hw = Horizontal thrust of wave over slope
Pp = Passive earth pressure
W = Self weight of masonry retaining wall
R = Resultant force over masonry wall.

$Now,\ resul\tan t\ ,\ R = \sqrt{\left(H_w - P_p\right)^2 + W^2}$ .....(Bera 2021)... [4]

The wall is safe against overturning till the resultant, R, is within the base of the wall. Where there is no infinite soil wedge, Pp = 0 and the wall is likely to fail in overturning.

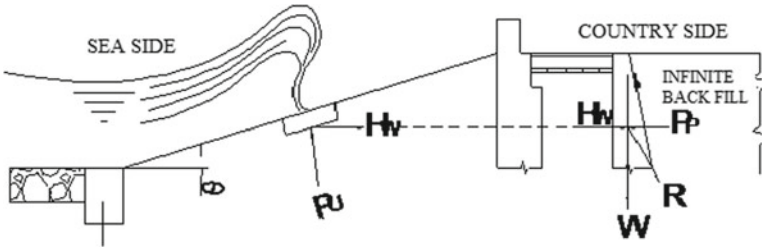

Fig. 11 Schematic diagram of forces acting on masonry retaining wall

Fig. 12 Inundation of flood water in Ghorama Island of South 24 Parganas district due to embankment breach of Muriganga river as observed on 26.5.2021

Fig. 13 Flood in Uttarmamudpur of Hingalganj of South 24 Parganas district due to embankment breach of Icchamati river as observed on 26.5.2021

4.10 Effect of Cyclone Yaas in South 24 Parganas District

Figure 12 depicts inundation of flood water in Ghorama Island of South 24 Parganas district due to embankment breach of Muriganga river. Figure 13 depicts flood in Uttarmamudpur of Hingalganj of South 24 Parganas district due to embankment breach of Icchamati river. Figure 14 depicts embankment breach in G-Plot area of South 24 Parganas.

5 Discussion

As per Daskaviraj and Sarkar [5], any embankment/sea dyke protection is designed considering the optimum natural effect which is neither maximum nor the minimum. Considering the worst effect to design such kind of protection, it will be uneconomical as such type of natural calamity is not usual though we have faced two such natural

Fig. 14 Embankment breach in G-Plot area of South 24 Parganas as observed on 26.5.2021

calamities in two consecutive years. Kumar [6] reported that Cyclone "AMPHAN," in the year of 2020, was much stronger but the landfall completed two and half hours before the time of peak high tide but the cyclone "YAAS" used the blood moon tide to hit the worst.

6 Conclusions

The following conclusions are drawn from the above study:

- In view of the lowering of beach due to the hard protection adopted so far in Digha sea beach, there is increasing impact on the slope protection works due to the momentum of increased height of water column. As such, beach nourishment is necessary to reduce such impacts and also for use of the beach by the tourists for longer time in any day.
- Removal of sand dunes from country side and lowering of sea dyke top Level have caused the surge to overtop to the country side to a large extent.
- Mangroves need to be planted and maintained in coastal areas because they are the first and a very important line of defence against storm and surging water.
- Shelters for storm affected people need to be built and maintained properly specially in coastal areas. The affected people must be explained well the need to move to safe shelters.

References

1. Anandabazar Patrika dated 27.5.2021 http://www.anandabazar.com
2. "Stability of the beach at Digha" (1966) Hydraulic Study Department, KPC, Calcutta, June 1966, TR No. 32
3. Monthly Report (2021) of Digha Observation Station of River Research Institute, West Bengal, May 2021
4. Bera AK (2021) Technical Report on the effect of Cyclone "Yaas" submitted to the Irrigation & Waterways Department, Government of West Bengal, India, 2021
5. Daskaviraj SK, Sarkar SK (1985) "Hydraulic aspects of Sea Wall design for the east coast of India with reference to Digha", paper no. 9, 52nd R & D Session of C.B.I & P, India, 1985
6. Shubham K, Preet L, Amit K (2021) Influence of Super Cyclone "Amphan" in the Indian Subcontinent amid COVID-19 Pandemic. Remote. Sens. Earth Syst. Sci. 4:96–103

Suitable Coastal Protection Measures for a Vulnerable Coastal Site Using Numerical Techniques

Prabhat Chandra, R. K. Chaudhari, and S. K. Kori

Abstract Due to human intervention and nature's fury, coastal morphology is continuously changing. Some time, longshore transport equilibrium is disturbed due to manmade coastal structure or due to natural wave attack. In such conditions, heavy erosion or accretion takes place at the coastal site. Coastal erosion is loss of land area due to action of waves, currents, winds and gradual increase in the sea level due to global warming. Coastal erosion is a severe problem needing immediate attention to this in an effective manner with a scientific base for evolving suitable design of coastal protective structure. In present paper, some coastal protection measures were evolved for the vulnerable site Sasihithlu, Dakshina Kannada District Karnataka along the west coast of India. Some shops and other buildings have been totally demolished by the severe shore erosion at the present site. Near the site, there is a combined river mouth for two rivers named as Sambhavi river and Nandani river. The mouth is located in the open coast and subjected to high waves of up to 4 m associated with the significant littoral drift. As a result, the severe erosion has been taking place at the south of the river mouth near Sasihithlu. In order to stabilize the shoreline near Sasihithlu, suitable coastal protection measures were suggested by using numerical model LITPACK. For shore protection at Sasihithlu, the performance of two types of protective measures, i.e. groyne field and offshore breakwaters, was assessed through model studies. From model studies, it was found that with six groyne in series, maximum 10 m of accretion would take place between the groyne fields after 10 years. While with offshore breakwaters, maximum 4 m of accretion would occur between the shore and offshore breakwaters in 10 years. The suggested coastal protection works are expected to stabilize the eroding coast line at Sasihithlu.

Keywords Numerical model · Groyne · Offshore breakwater · Erosion · Accretion

P. Chandra (✉) · R. K. Chaudhari · S. K. Kori
Central Water and Power Research Station, Khadakwasla, Pune 411024, India
e-mail: pchandra_2003@yahoo.co.in

P. V. Timbadiya et al. (eds.), *Coastal, Harbour and Ocean Engineering*, Lecture Notes in Civil Engineering 321, https://doi.org/10.1007/978-981-19-9913-0_20

1 Introduction

Coastal erosion is a severe problem for maritime developing countries like India. Coastline is acting as dynamic interface between the land and sea. This is under continuous attack by sea waves which is the dominant factor for movement of sediment along coastline causing erosion or accretion. It is observed that coastline at different places in India faces serious erosion. It is also noticed that the magnitude and nature of erosion change from place to place. However, in some places, temporary erosion takes place during the monsoon season and again built up of beach is restored during non-monsoon season. Whereas, in some places, permanent erosion takes place and serious damages may occur to manmade monuments building roads, etc. To mitigate this type of erosion, coastline is required to be protected as per the priority. Coastline near Sasihithlu, Mangalore, Karnataka (Fig. 1) faces serious erosion and some shops near the coastline have been totally demolished due to this (Photos 1 and 2). The site is heavily affected by the erosion due to continuous shifting of river mouth towards south. It is also seen from the recent Google images that a significant amount of erosion has taken place since previous years (Fig. 2). For such a vulnerable site, attention should be paid to design suitable measures to combat coastal erosion which should be economical without sacrificing the safety and functional requirement. In order to protect this vulnerable coast site from severe erosion, only hard measures such as groynes, seawall and offshore breakwater can be used. To evolve the suitable costal protection measures, the effect of these possible protections on the shore line can be assessed through numerical model. In the present study, the effect of putting a series of groynes and offshore breakwaters to save the coastline and for maintenance of beach has been assessed through the numerical model LITPACK. In the present paper, the details of the mathematical model studies using numerical model for evolving suitable coastal protection measures at Sasihithlu, Mangalore, have been described.

2 Site Conditions

The Sasihithlu site is situated at about 30 km north of Mangalore in Udupi District at the latitude of 13.070250 degree and the longitude of 74.776920 degree as shown in Fig. 1. The Sasihithlu beach is located at just at south of the combined river mouth for two rivers named as Sambhavi and Nandani rivers. The coastline at the site consists of long, sandy beaches and is oriented in NNW-SSE direction. The nearshore bathymetry is steep with straight and parallel depth contours. The tidal range at Sasihithlu is about 1.65 m. Beaches at the site are having fine sand. The average value of D50 (mm) from various sand samples is about 0.368 mm and the same has been used for the model runs. Wave is a very important parameter which influences the littoral drifts that causes the erosion of coastlines. In absence of measured wave data, the offshore wave data of 14 years from year 2001 to 2014 off

Fig. 1 Location map of Sasihithlu site

Photo 1 Image showing the demolished shop

Photo 2 Image showing the present river mouth

Fig. 2 Google Image showing the distortion in shoreline from 2004 to 2019

Sasihithlu site as observed by India Meteorological (IMD) from ships plying in deep waters were-analysed. This wave data information was considered at the offshore end of the model limits. The frequency distribution of wave heights for entire year for the above offshore wave data is presented in form of wave rose diagram as shown in Fig. 3. It could be seen that the predominant wave directions in deep water are from 220° to 360° N with the maximum wave heights of 4.5 m. These deep water wave data were transformed using the mathematical model MIKE 21-SW to get the nearshore wave climate near the Sasihithlu.

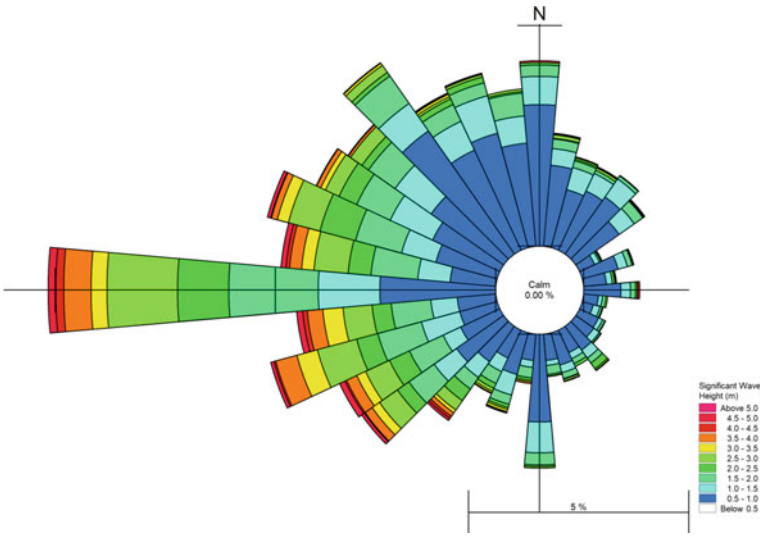

Fig. 3 Offshore wave rose diagram for entire year

3 Numerical Modelling Techniques

For evolving suitable coastal protection measures at vulnerable coastal site Sasihithlu, Mangalore, mathematical models like MIKE 21-SW, LITPACK have been used. These studies were mainly carried out in two following stages:

1. Transformation of wave height and wave direction from deep water to (−)10 m depth using MIKE 21-SW model.
2. Estimation of Littoral drift distribution and simulation of shore line changes using LITPACK model.

3.1 Transformation of Wave Height and Wave Direction from Deep Water to (−) 10 m Depth

As waves propagate towards shore, a combination of shoaling, refraction, reflection, diffraction and breaking effects modify the waveform and the wave characteristics will be very different from those in deep water. To get the wave conditions from offshore to nearshore at (−) 10 m depth, the numerical model MIKE21-SW was used. This is a state-of-the-art third generation spectral wind wave model based on unstructured mesh. The model simulates the growth, decay and transformation of wind generated waves and swells in offshore and coastal areas. It takes into account refraction and shoaling of waves, which are important in the transformation of waves from offshore to inshore. It also includes physical phenomena of wave growth by

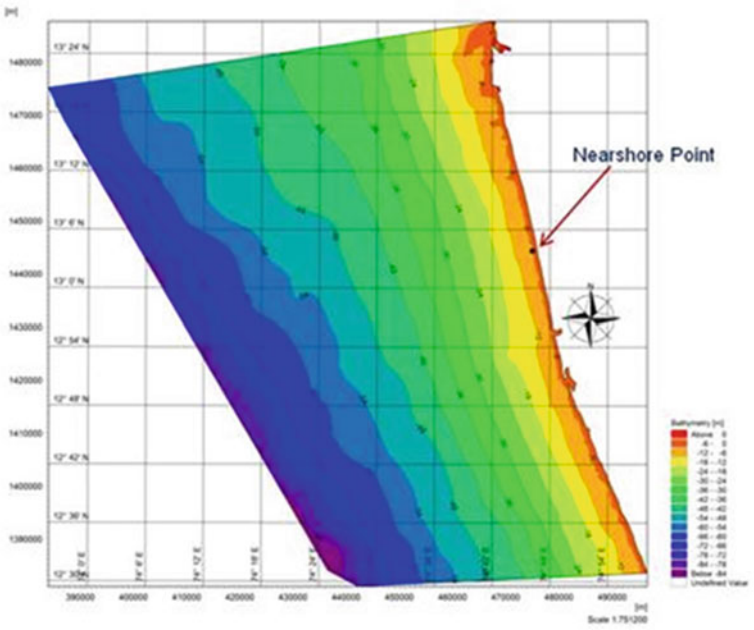

Fig. 4 Bathymetry for wave transformation from offshore to nearshore

action of wind, dissipation due to white-capping, dissipation due to bottom friction and dissipation due to depth induced wave breaking. In the absence of measured wave data of at least one year near the proposed site of development, the nearshore wave climate at Sasihithlu was obtained by transforming the ship observed deep water wave data using MIKE21-SW Model. Model area considered for MIKE 21-SW model is shown in Fig. 4. Bathymetry in the model region of about 76 km × 93 km area was discretized using unstructured mesh. The model was run to obtain nearshore wave climate at the Inshore Point in (−) 10 m depth contour. The wave directions and ratio of wave heights at (−) 10 m depth to deep water wave height, with different directions of wave incidence at the offshore boundary are obtained. After applying the ratio of deep water wave height and direction as shown in rose diagram (Fig. 3), the frequency distribution of waves in (−) 10 m depth was obtained as shown in Table 1 and corresponding rose diagram (Fig. 5).

3.2 Estimation of Littoral Drift Distribution and Simulation of Shore Line Changes

Mathematical model studies for estimation of littoral drift distribution and simulation of shoreline changes were carried out using LITPACK model. LITPACK software

Table 1 Percentage occurrence of wave height and direction at Sasihithlu in (−)10 m depth for entire period (Jan-Dec)

WAVE HEIGHT (m)	0–0.5	0.5–1	1–1.5	1.5–2	2–2.5	2.5–3	3–3.5	3.5–4	4–4.5	Total
DIRECTION(degN)										
210	5.34	1.98	0.15	0.00	0.00	0.00	0.00	0.00	0.00	7.47
220	0.88	1.84	0.73	0.10	0.15	0.02	0.00	0.00	0.00	3.72
230	0.66	1.81	1.30	0.64	0.47	0.15	0.10	0.02	0.02	5.17
240	0.81	1.98	3.18	1.00	1.59	0.83	0.07	0.24	0.02	9.75
250	0.37	0.71	2.35	0.61	1.13	1.20	0.05	0.10	0.00	6.51
260	0.34	0.73	1.84	0.54	0.81	1.00	0.12	0.12	0.05	5.56
270	1.10	3.38	6.39	2.06	3.26	1.54	0.42	0.24	0.02	18.42
280	1.05	4.07	3.33	1.98	1.37	0.32	0.12	0.00	0.00	12.25
290	2.50	6.27	2.18	0.71	0.10	0.02	0.00	0.00	0.00	11.78
300	14.99	3.85	0.39	0.12	0.02	0.00	0.00	0.00	0.00	19.37
Total	28.04	26.62	21.85	7.76	8.89	5.09	0.88	0.73	0.12	100.00

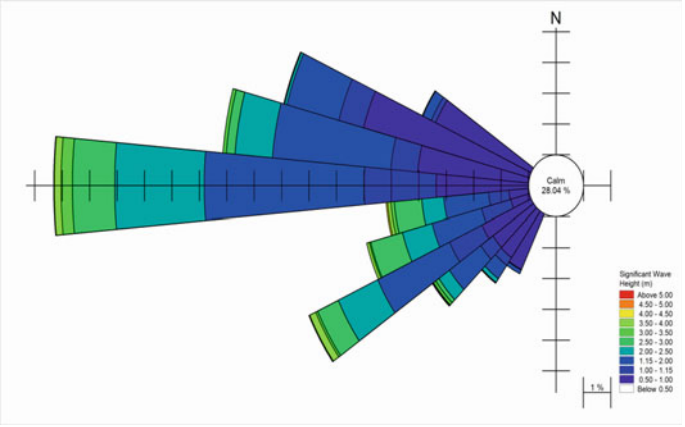

Fig. 5 Rose diagram at (−)10 m depth (Year)

was used for computation of littoral drift and simulation of shoreline changes due to construction of the breakwaters. LITPACK is a professional engineering software package for the modelling of non-cohesive sediment transport in waves and currents, littoral drift, coastline evolution and profile development along quasi-uniform beach (DHI 2014)[1]. The two modules of LITPACK, i.e. LITDRIFT and LITLINE are used in the present study.

LITDRIFT module simulates the cross-shore distribution of wave height, setup and longshore current for an arbitrary coastal profile. It provides a detailed deterministic description of the cross-shore distribution of the longshore sediment transport for

an arbitrary bathymetry for both regular and irregular sea states. The longshore and cross-shore momentum balance equation is solved to give the cross-shore distribution of longshore current and setup. Wave decay due to breaking is modelled, either by an empirical wave decay formula or by a model of Battjes and Janssen. LITDRIFT calculates the net/gross littoral transport over a specific design period. Important factors, such as linking of the water level and the beach profile to the incident sea state, are included. Wave climate is described in time series file in LITDRIFT. Each set of items in wave climate describe the characteristics of one wave incident and duration of wave incident is in percentage fraction of year. Thus, the total annual drift Qannual is sum of contributions from all wave incidents.

$$Qannual = \sum_{i=1}^{NSETS} Qs(i).Duration(i) \tag{1}$$

where

NSETS is the total number of wave incidents.

Qs Sediment quantity.

The annual drift Qannual is obtained when the total duration in the wave climate is one year.

LITLINE simulates the coastal response to gradients in the longshore sediment transport capacity resulting from natural features and a wide variety of coastal structures. LITLINE predicts the coastline evolution by solving a continuity equation for the sediment in the littoral zone. The influence of structures, sources and sinks is included. With jetties and breakwaters, the influence of diffraction on the wave climate is also included. The main equation in LITLINE is the continuity equation for sediment volumes expressed as

$$\frac{\partial \mathrm{yc(x)}}{\partial t} = -\frac{1}{hact(x)} \frac{\partial Q}{\partial x} + \frac{Q_{sou}(x)}{h_{act}(x)\Delta x} \tag{2}$$

where

Yc(x) is distance from baseline to coastline t is time.

$h_{act}(x)$is height of active cross-shore profile.

$Q(x)$ is longshore transport of sediment expressed in volume.

x is the longshore position.

$Q_{sou}(x)$ source/sink term expressed in volume/Δx.

Δx is longshore discretization step.

3.3 Estimation of Littoral Drift Rate

LITPACK model was used to estimate annual littoral drift rates and its distribution on the profile. Normal to the shoreline, i.e. 257° N. Figure 6 shows the cross-shore profile near the Sasihithlu and the same was used for drift computation.

The profile covers a distance of 3.2 km extending up to about −10 m depth contour (with respect to chart datum) as shown in Fig. 6. The profiles were discretized with grid size of 5 m. Grain size distribution, fall velocity and roughness coefficient over the profile were required for computation of littoral drift. At the site, mean grain size is observed to be of the order of 0.368 mm. In the studies of longshore sediment transport rates for the Indian Coast made by Chandramohan and Nayak in 1991[2], it is estimated that the northerly drift along the Mangalore coast is 3.62×10^5 m3/year and the southerly drift is 10.69×10^5 m3/year. Study by Jayappa K S (1996) [3] reported net transport of 0.043 million cum towards South. In an estimate by Sanil Kumar (2006) [4], annual net transport of 0.036 million cum towards South at Ullal was reported. Additionally, as seen from various Google Earth images that the net drift is towards South and shorelines in the neighbourhood of New Mangalore Port Trust (NMPT) does not show any long-term trend of erosion or accretion. The model was calibrated using bed roughness to get the annual net transport of the order 0.047 × 106 m3/year. The model was run for annual nearshore wave climate given in Table 1. Annual northward and southward drift distribution across the cross-shore profile is shown in Fig. 7 and in Table 2. The northward drift is plotted positive as while southward drift is plotted as negative.

Net transport in a year is of the order of 0.047million cum and is towards south and gross transport is of the order of 0.23 million cum.

According to cross-shore distribution plot (Fig. 7), the maximum transport occurs at about 40 m from the shoreline (i.e. High Water Line) at 0.29 m depth contour. The sediment transport occurs between 1.2 m and (−) 5.8 m depth contours.

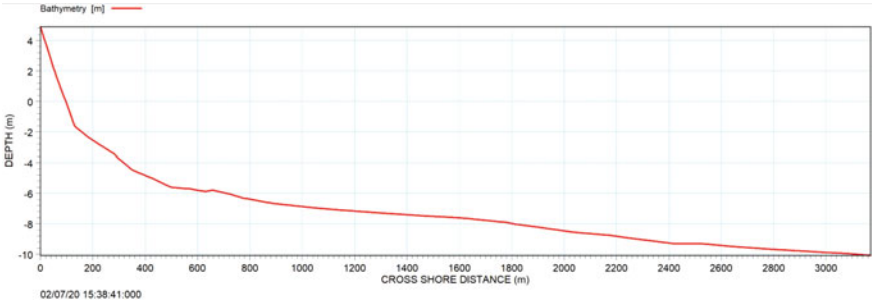

Fig. 6 Cross-shore profile

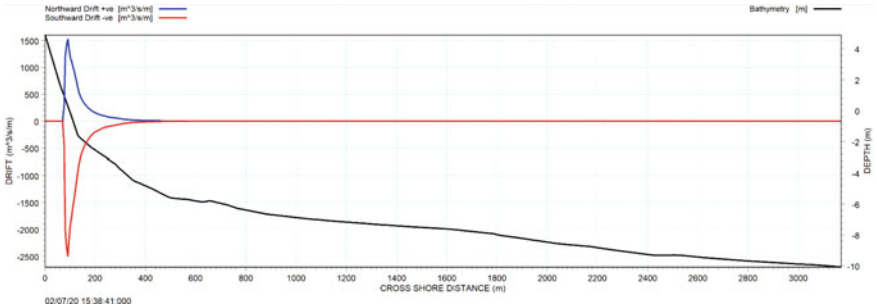

Fig. 7 Cross-shore distribution of northward and southward littoral drift during entire year

Table 2 Littoral transport rate (m^3)

Northward	Southward	Net *	Gross
93,100	140,700	−47,600	233,800

Note * '−ve' Southward ' + ve' Northward for the Net Drift

3.4 Shoreline Evolution

In order to stabilize the river mouth, the river training wall had been proposed and to assess the impact of the shore connected breakwaters on the coastline, LITLINE module of LITPACK software was used. It may be noted that LITPACK is a 1D model, in which the shore connected breakwaters are assumed as obstructions which are perpendicular to shoreline. Therefore, projections of the breakwaters were considered in the simulation. The model was run for 1, 2, 4, 6, 8 and 10 years with proposed North and South breakwaters as shown in Fig. 8. The length of the shoreline considered for the studies is 6 km, extending about 3 km towards north of the breakwater and about 3 km towards south of the breakwater. It is divided into 1200 grid points of grid size 5 m. Two shore connected breakwaters of lengths 395 m (Southern) and 360 m (Northern) were included perpendicular to the shoreline; the length of the breakwaters are measured from the MHHW line, and the separation distance between two breakwater is considered as 120 m.

The LITLINE model was run for 1, 2, 4, 6, 8 and 10 years with the proposed breakwaters. It is estimated from the model that shoreline would advance by 41 m, 50 m, 62 m, 74 m, 85 m and 91 m on the North of Northern breakwater in 1, 2, 4, 6, 8 and 10 years, respectively. The shoreline erosion on south of southern breakwater was observed from the model results. It is estimated that shoreline would erode by 6 m, 11 m, 16 m, 19 m, 23 m and 26 m on the south of southern breakwater in 1, 2, 4, 6, 8 and 10 years respectively. In order to protect a reach of about 1.2 km near the Sasihithlu site, two options of protective measures have been assessed through the model studies; Groyne field and offshore breakwaters.

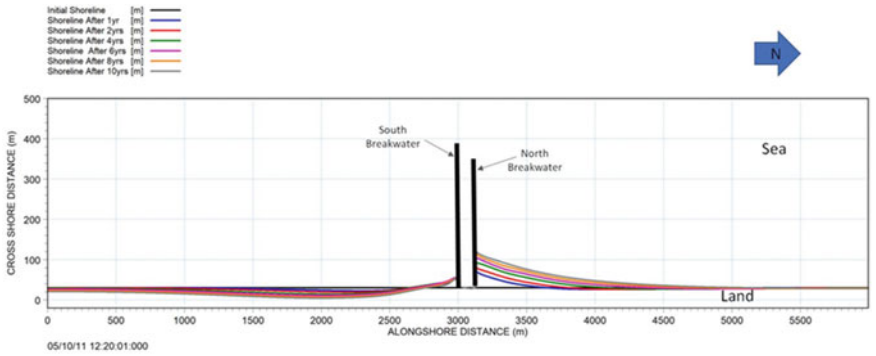

Fig. 8 Shoreline changes plot with proposed North and South breakwater

3.5 Option-1

For shore protection of Sasihithlu site, six groynes in series with of 60 m length with 200 m spacing between them were considered for reducing erosion. The effect of the groynes has been assessed through the model studies as shown in Fig. 9 below:

The model was run for 1, 2, 4, 6, 8 and 10 years with the proposed groyne field. It was noticed from the model outcome that maximum 10 m of accretion will be between the groyne fields after 10 years. More erosion on the south of groyne field was also observed.

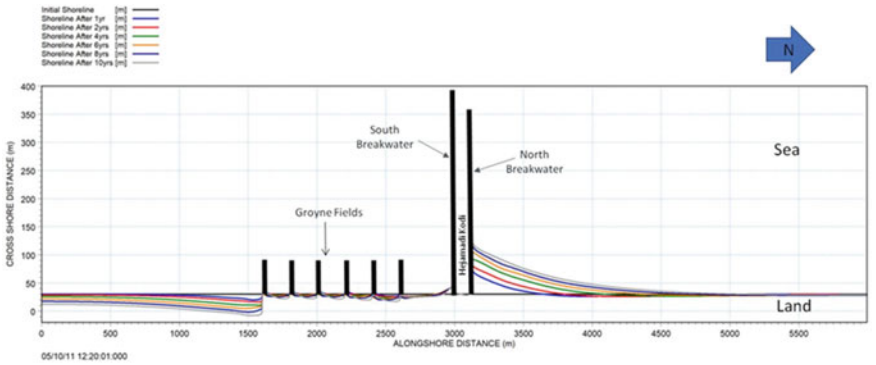

Fig. 9 Effect on shoreline changes with the six groynes in series

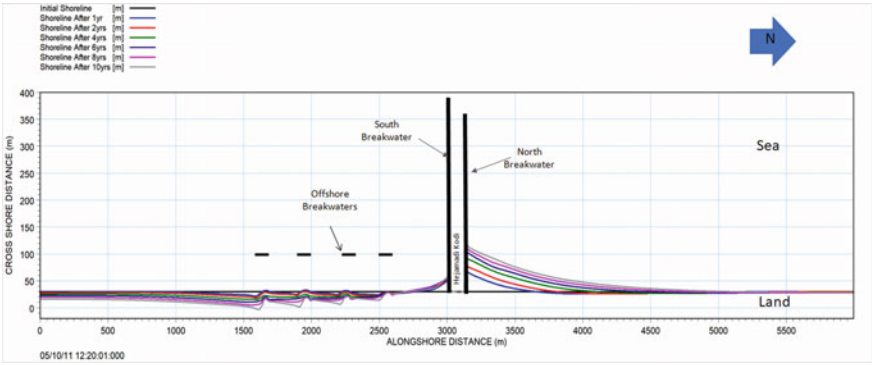

Fig. 10 Shore line evolution with four offshore breakwaters

3.6 Option-2

As a shore protection measure, other option of four offshore breakwaters of length 100 m each with 200 m spacing between them at a distance of 100 m (−2 m depth contour) from the shore was also considered for reducing erosion. The model output is shown in Fig. 10 below.

The model was run for 1, 2, 4, 6, 8 and 10 years with the proposed offshore breakwaters. It was seen that maximum 4 m of accretion would be between the shore and offshore breakwaters in 10 years.

4 Conclusions

The main findings of the mathematical model studies for shoreline changes to evolve the suitable coastal protection work near Sasihithlu are as below:

- Wave transformation studies indicate that the predominant wave directions at the nearshore (−) 10 m depth are from 210° to 300° N.
- LITDRIFT studies indicate that at the proposed site, the net annual sediment transport is of the order of 0.047 million cum and is towards south and gross annual drift is of the order of 0.23 million cum. The extreme indices during the historical period at annual scale.
- Shoreline changes studies indicate that as a result of construction of proposed breakwaters (training wall), there would be accretion at north of the north breakwater up to 41 m, 50 m, 62 m, 74 m, 85 m and 91 m in 1, 2, 4, 6, 8 and 10 years, respectively, and shoreline would advance up to depth of (−) 2 m contour after 10 year. Erosion of shoreline would be observed at south of south breakwater by 6 m, 11 m, 16 m, 19 m, 23 m and 26 m in 1, 2, 4, 6, 8 and 10 years, respectively.

- With the option of groyne fields (6 nos. of 60 m length each at 200 m spacing) for coastal protection, it was found that maximum 10 m of accretion would be between the groyne fields after 10 years.
- With the option of offshore breakwaters (4 nos. of 100 m length each with 200 m spacing) for coastal protection, it was found from the studies that maximum 4 m of accretion would be between the shore and offshore breakwaters in 10 years.
- Numerical models are efficient to assess the impact of coastal protection. It is cost effective and less time consuming. Assessed protection layout can be applied to protect the vulnerable coast site.

Acknowledgements Authors are grateful to Shri A.K. Agrawal, Director, Central Water and Power Research Station for his continuous encouragement and motivation during the course of studies and for granting permission to publish this paper.

References

1. Danish Hydraulic Institute (2014) LITPACK, LITDRIFT (Longshore Currents and Littoral drift) , LITLINE (Coastline Evolution) Module, User Guide and Reference Manual Website: https://www.mikepoweredbydhi.com
2. Chandramohan P, Nayak BU (1991) Longshore sediment transport along the indian coast. Indian J Mar Sci 20:110–114
3. Jayappa KS (1996) Longshore sediment transport along the mangalore coast west coast of India. Indian J Mar Sci 25: 157–159
4. Sanil Kumar V, Pathak KC, Pednekar P, Raju NSN, Gowthaman R (2006) Coastal processes along the Indian coastline. Curr Sci 91(4)

Morphological Response of Sandy Beaches to Tauktae Cyclone in Goa, West Coast of India

S. Rajendiran, Jaya Kumar Seelam, Raghavendra Talawar, H. Lavanya, S. Malavika, Ritesh K. Vanjari, Mandar Naik, Vinayak Yerudkar, and Abdul V. Sayyed

Abstract Extremely severe cyclonic storm Tauktae traversed along the west coast of India during 14–19 May 2021 and reached its peak on 17 May 2021. The cyclone passed along the Goa coast on 16 May 2021, wherein the eye of the cyclone was about 100 km from the coastline. The effect of this cyclone was felt severely along the coastal stretches due to increased wave and wind effects over the beaches. The influence of the Tauktae cyclone on beach morphology has been studied in this paper. A total coastal stretch of about 27 km long in South Goa and 7 km in North Goa is considered. Beach profiles at 9 locations were measured before and after the cyclone, and volumes on the foreshore were compared. The cyclone waves and wind impact on the beaches resulted in erosion at most locations. The retreat of the berm was between 5 and 16 m, while the foreshore erosion volumes ranged between 25.82 and 132.5 m^3/m. Profiles measured between 8 and 27 June, i.e. within one month of the cyclone passage, showed varying rates of accretion/erosion. Further measurements of monthly profiles are carried out. The cyclone impact on the beach profiles in terms of changes in morphology features and beach volumes is presented in this paper.

Keywords Cyclone Tauktae · Beach profile · Accretion · Erosion · Beach recovery

S. Rajendiran (✉) · J. K. Seelam · R. Talawar · H. Lavanya · S. Malavika · R. K. Vanjari · M. Naik · V. Yerudkar · A. V. Sayyed
Ocean Engineering Division, CSIR-National Institute of Oceanography, Dona Paula, Goa, India
e-mail: rajendiransundar22@gmail.com

J. K. Seelam
e-mail: jay@nio.org

A. V. Sayyed
e-mail: asayyed@nio.org

P. V. Timbadiya et al. (eds.), *Coastal, Harbour and Ocean Engineering*, Lecture Notes in Civil Engineering 321, https://doi.org/10.1007/978-981-19-9913-0_21

1 Introduction

The tropical Indian Ocean, which plays a predominant role in the socio-economic activities happening over the country, is prominent for the formation of tropical cyclones during the pre- and post-periods of the Southwest monsoon season. Tropical cyclone Tauktae was one such kind, which developed over the Arabian Sea in the pre-monsoon period of the year 2021 in May. Apart from the devastations all over the west coast, Tauktae has taken several lives and been illustrated as the deadliest cyclone over the decade.

Beaches are the part of a coastal zone where maximum spatial and temporal variation occurs. So there is a need for efficient management of beaches for effective coastal management. Beach environments are always dynamic due to continuous and vigorous natural hazards happening season by season, which bring out changes in the action of waves, currents and winds.

More recently, Priestas and Fagherazzi [7] studied dune recovery on Barrier Island in Florida after Hurricane Dennis (2005). They concluded that the overwash due to the cyclone destroyed the berm region of the beaches. This depends on the dune morphology other than wave climate and current due to the cyclone. The beach morphodynamic studies are carried out to assess the state of the coast, which further results in taking action for shore protection for the benefit of the coastal community. A continuous study was carried out along the Goa coast by periodically measuring the beach profiles to understand the beach morphology changes due to cyclone impact.

As mentioned above, the parameters on which the dynamic behaviour of the beach depends are waves, currents, and wind. These basic parameters show significant changes during cyclones and other natural hazards. This work mainly comprises the response of the cross-shore profiles of the Goa coastal region. This study aims to analyse dune recovery processes along Goa beaches after the Tauktae cyclone on 16 May 2021 and to quantify morpho-sedimentary changes along the Goa coast using pre- and post-cyclone beach morphological surveys. We had considered a total of 9 locations along the Goa stretch where the survey had been carried out. Of the 9 locations, mainly 4 locations are presented in this paper, which have more socio-economic importance when compared to other locations. The effect of the cyclone along the coast can be assessed by analysing the profiles before and after the cyclone at these four locations (Fig. 1).

2 Materials and Methods

The standard fly levelling method adopted during this survey is the beach survey procedure. The procedure involves fixing the benchmarks (Permanent structures, electric posts, etc.) along the survey locations. The levelling is performed using the surveyor's level and 5 m levelling staff with the least count of 0.005 m. The profiles are measured from the benchmark, a point on the beach that remains stable to the sea.

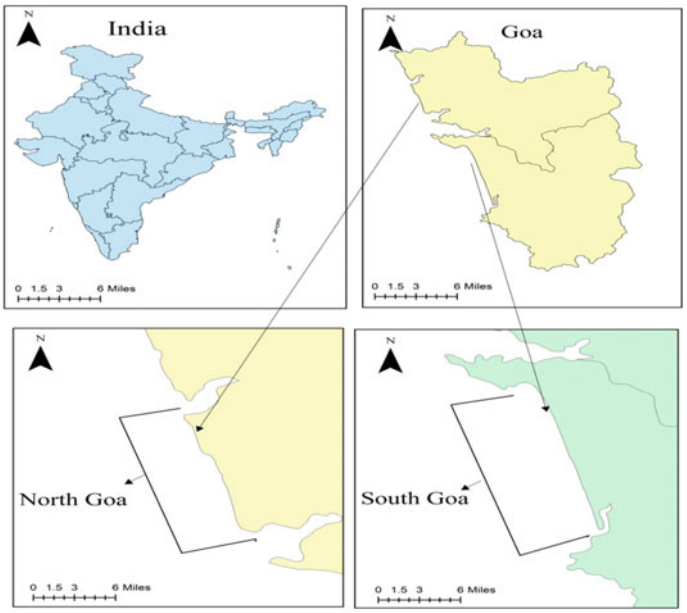

Fig. 1 Study area considered for the work

The profiles are taken monthly at the selected locations from the fixed benchmark to the low water line.

2.1 Study Area and Data

Periodical observation of beach profiles has been carried out for the past two decades by CSIR-NIO for a better understanding of the dynamic behaviour of the beaches, especially during catastrophic activities like cyclones, storm surges, etc. In this study, we have considered the beach profiles taken from March to September 2020 and 2021. The profiles for the post- and pre-cyclones are considered for the year 2021, and the same is followed for 2020 to cross-compare the profiles. Beach profile for April 2020 could not carry out due to the outbreak of COVID-19 followed by lockdown all over the country.

As mentioned above, the study area chosen for this work is along India's Goa coast-Central West coast. Initially, along the coast, 4 locations are chosen from North Goa which is of 8 km stretch, and 5 locations are chosen from South Goa which is 27 km. Out of the 9 stations along the coast, 4 stations are presented here, as they have a large amount of human interference. The collected beach profiles are initially with respect to benchmark and are further processed with respect to mean sea level.

Then the volume for all the profiles is calculated along the cross-shore direction, starting from the benchmark to the WL or MSL (considered 0 m elevation).

3 Results and Discussions

Beach profiles collected are processed periodically to estimate the change in the volume of sand per metre width along the cross-shore. And particularly after the cyclone hit on 16 May 2021, the profiles were taken very frequently till the end of June-2021 to understand the beach recovery process. Then, the volume change is represented graphically for the 4 locations along the Goa coast. Similarly, the same exercise was done previously for 2020, and the volume change is represented graphically.

3.1 South Goa Profiles and Their Respective Volumes

SG-1 is the location chosen at the northernmost part of the South Goa beaches. In this location, there is a fall of 2.1 m berm height after the cyclone hit, which is visible from the profiles April-2021 and May-2021 mentioned above. Similarly, if we consider the same month profiles for the year 2020, there is a gradual retreat of the berm towards land during the initiation of the monsoon. When considering March-2020 and June-2020 profiles, 1 m fall of berm height is noted (Figs. 2 and 3).

When we analyse the volume plots, it is clearly visible that there is a sudden fall to 100 m^3 during the year 2021 and a gradual decrease during 2020.

Similarly, when SG-2 is considered, there is less retreat of the berm towards the land by 5 m after the cyclone hit. Also, there is not much beach erosion that took place both due to the cyclone and monsoon. This can be clearly inferred from the volume plots mentioned for the SG-2 location for the year 2021. When we consider 2020 profiles, comparatively, there is an increased foreshore dune erosion because of the commencement of the monsoon. And the beach started rebuilding itself during the retreat of the monsoon. This rebuilding process can be seen from the beach profile plot (Sep-20 profile) and the volume plot of SG-2.

3.2 North Goa Profiles and Their Respective Volumes

Considering the NG-1 profile, during the month of April-2021, the berm of around 2.2 m high washed away due to the cyclone. As a result, the beach width increased due to the accumulation of sand near the shoreline. This is visible from the May-2021 profile of NG-1. When we compare this with 2020 profiles, there is a 1 m berm height

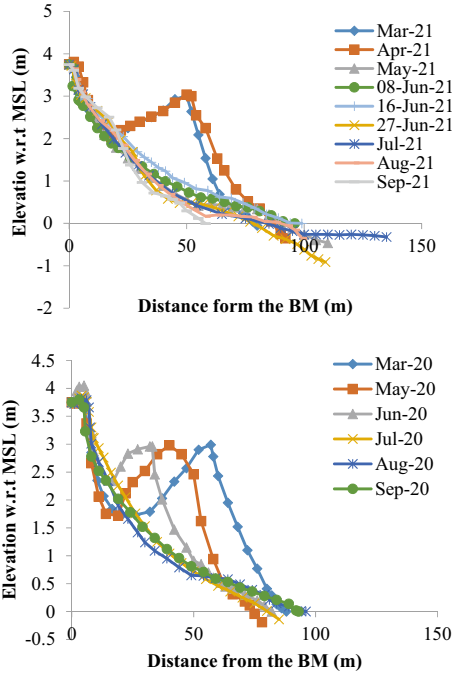

Fig. 2 Beach profiles for SG-1 for the years 2021 and 2020

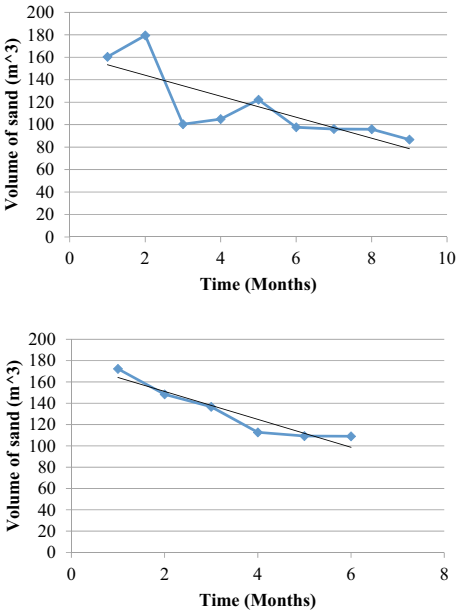

Fig. 3 Respective volumes of the profile SG-1 for the years 2021 and 2020

fall from May-2020 to June-2020. This profile doesn't have much volume variation during the cyclone hit and initiation of the monsoon (Figs. 4 and 5).

When we consider NG-2, there is a 16 m retreat of berm towards the land from the month of Apr-2021 to May-2021. After that, the beach recovered gradually, inferred

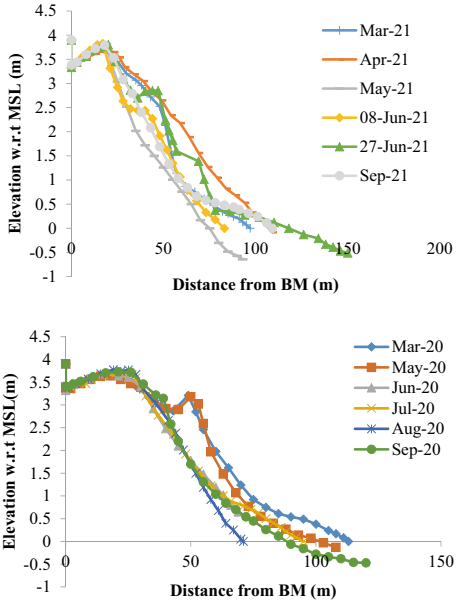

Fig. 4 Beach profiles for SG-2 for the years 2021 and 2020

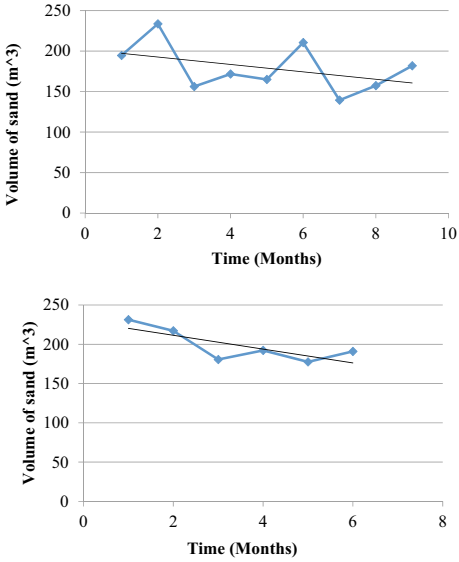

Fig. 5 Respective volumes of the profile SG-2 for the years 2021 and 2020

from the profiles above for the year 2021. Also, there is an increase in the volume around 180 m^3 towards Sep-2021. When we consider 2020 profiles, there is not much berm disturbance, and the profile volume is more or less similar (Figs. 6, 7, 8 and 9).

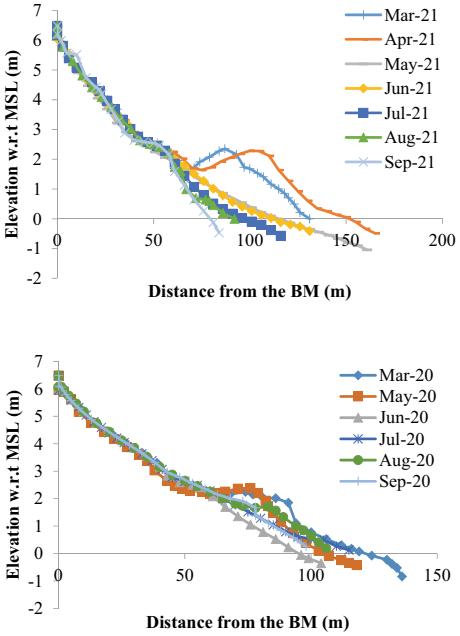

Fig. 6 Beach profiles for NG-1 for the years 2021 and 2020

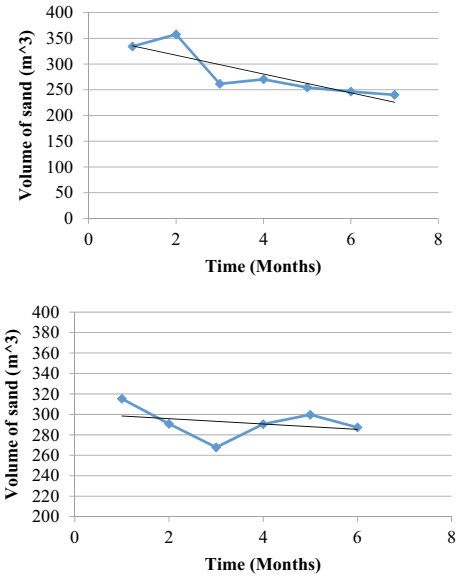

Fig. 7 Respective volumes of the profile NG-1 for the years 2021 and 2020

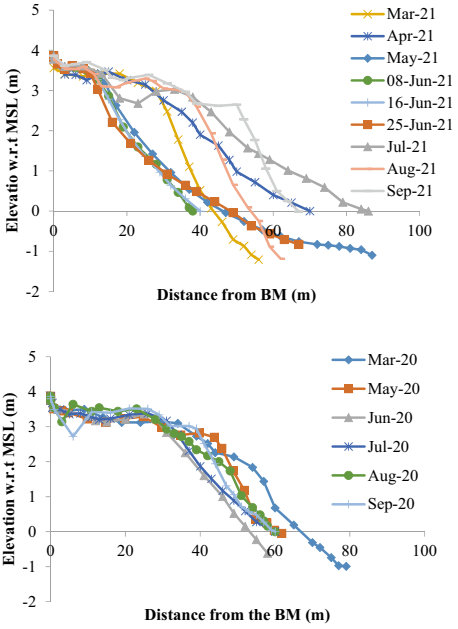

Fig. 8 Beach profiles for NG-2 for the years 2021 and 2020

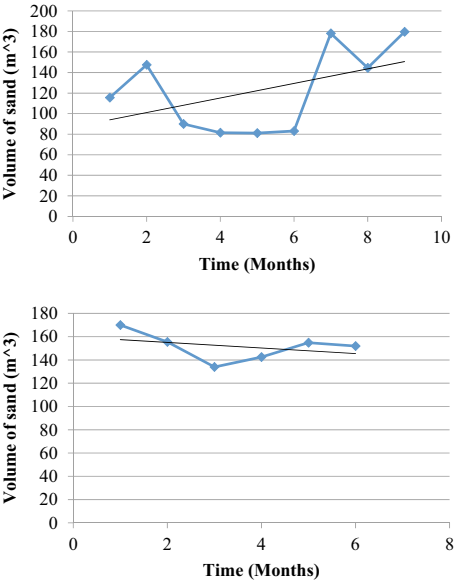

Fig. 9 Respective volumes of the profile NG-2 for the years 2021 and 2020

3.3 Significant Wave Height Reanalysis Data

The significant wave height during the time the survey was carried out is analysed. This significant wave height is obtained from ECMWF reanalysis data. There is a steady increase in the height towards the initiation of the monsoon, which attains its maximum during July or August 2020, a normal phenomenon happening over the Goa coast. But during the year 2021, the wave height reached its maximum of 8 m during May, which clearly infers the impact of the Tauktae cyclone along the Goa coast.

As the wave height increases, a more dynamic situation occurs in the surf zone due to the high wave breaking activity. Eventually, sand from the beach area is disturbed and transferred either offshore or alongshore, depending on the wave direction (Figs. 10 and 11).

The sudden peak in wave height during May-2021 at both the study locations (North and South Goa) resulted in obtaining the minimum volume of sand (i.e. minimum beach area) calculated from the beach profiles during that particular time. So it is evident that the wave height during the cyclone plays a major role in littoral transport, which can be seen from the beach profiles or volume of the profiles.

Unlike in 2020, there is a gradual increase in the wave height when approaching the Southwest monsoon, which is a normal phenomenon along the West coast of India. As a result, a gradual decrease in the sand volume and beach width is measured

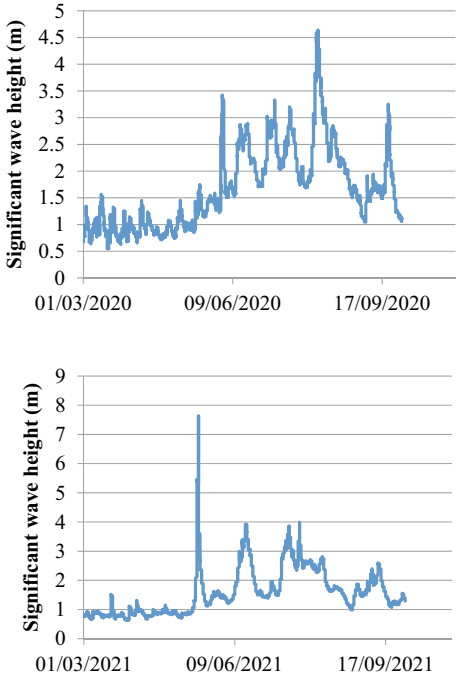

Fig. 10 Significant wave height reanalysis data-South Goa in the years 2020 and 2021

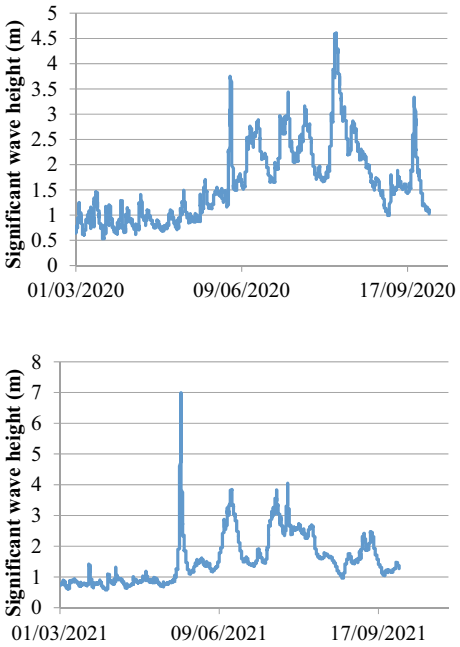

Fig. 11 Significant wave height reanalysis data-North Goa in the years 2020 and 2021

during the year 2020 from March to August. During September, there is a slight increase in the beach volume at a few coastal locations, which reveals that the beach is accreting.

4 Conclusions

In this paper, studies are carried out to analyse the beach dynamics pre and post-effects of the Tauktae cyclone. Beach profiles from March-September 2020 and March-September 2021 are analysed, and analysis showed significant changes in their volumes.

- March-September 2020 showed a gradual decrease in volume at the onset of the southwest monsoon; however, it shows a sudden decrease in the volume of sand due to the cyclone.
- From the analysis of beach profiles, it is evident that the berm of Goa beaches eroded in May-2021 (i.e. after the cyclone hit). And eventually, there is a sudden fall in the volume of sand. But for the same months of 2020 profiles, there is a gradual decrease in the volume of sand. This gradual decrease is due to the initiation of the southwest monsoon.
- From the day of the cyclone hit, there are three profiles within the month of June-2021 showing no significant trend.

- At stations NG-1 and NG-2, the sand from the berm settled near the surfzone, increasing the beach width to a greater extent. At the onset of the monsoon, sand at the surfzone is carried further offshore away, thus reducing the length of the beach.
- At stations SG-2 and NG-2, the beach started rebuilding at the end of the monsoon.

References

1. Aravind P, Amrutha MM, Kumar VS (2021) Ocean wave dynamics in the coastal area of the central west coast of India and its variability. Ocean Eng 227:108880
2. Dora GU, SanilKumar V, Philip CS, Johnson G (2014) Observation on foreshore morphodynamics of microtidal sandy beaches
3. Ganesan P, Gaonkar SS (2006) Seasonal beach profiling along Malvan and Kotharwadi coast, southern Maharashtra, central west coast of India. National Institute of Oceanography, Goa
4. Kumar KV, Aboobacker VM, Saheed PP, Vethamony P (2012) Coastal circulation along the central west coast of India during cyclone Phyan: measurements and numerical simulations. Nat Hazards 64(1):259–271
5. Moulton MA, Hesp PA, da Silva GM, Keane R, Fernandez GB (2021) Surfzone-beach-dune interactions along a variable low wave energy dissipative beach. Mar Geol 435:106438
6. Murty CS, Veerayya M, Varadachari VVR (1982) Morphological changes of the beaches of Goa
7. Priestas AM, Fagherazzi S (2010) Morphological barrier island changes and recovery of dunes after Hurricane Dennis, St. George Island. Florida. Geomorphology 114:614–626
8. Suanez S, Cariolet JM, Cancouët R, Ardhuin F, Delacourt C (2012) Dune recovery after storm erosion on a high-energy beach: Vougeot Beach, Brittany (France). Geomorphology 139:16–33
9. Tsoar H (1994) Bagnold, RA 1941: The physics of blown sand and desert dunes. London: Methuen. Prog Phys Geogr 18(1):91–96

Impacts of Coastal Structures in Typical Bays on Different Shorelines

B. Gopikrishna and J. D. Agrawal

Abstract Coastal structures are built to provide permanent solutions to safeguard the harbouring operations. The structures such as breakwaters and seawalls are important infrastructures that are commonly built near coasts and have strong influences in bringing changes to the shorelines. The combined effect of these structures was studied in the present paper with two typical sites located in different bays situated in Andaman and Nicobar Islands and west coast of the country. Both the sites were studied for the shoreline dynamics by imposing seawalls and breakwaters as hard structures. MUS harbour was located within a crenulated shape of the bay in Nicobar Islands and was provided with permanent harbour facilities. The shoreline and part of the breakwater have been damaged under tsunami waves of 2004. A seawall was proposed inside the bay to protect the shore. The impact of the seawall in the neighbouring locations was studied to arrive at the optimal length of seawall in the presence of the shore parallel breakwater. The other harbour is located at Navabag, west coast of India that is situated between the two headlands with a small inlet at the north headland where tidal flow with sediment causes hindrance to the navigational boats. In this case study, the impact of the shore perpendicular breakwater for channelising the flow in the presence of the seawall was studied. A 1-D model in flexible mesh was set up for both the sites for the known site conditions. Based on the simulations of shorelines for different periods, the optimum length of seawalls of 450 m at MUS harbour and 500 m length of breakwater at Vengurla site were arrived. The effect of breakwater of length 500 m at Vengurla site is 1 m and 2.5 m of deposition of sediment in a span of 10 and 30 years, respectively.

Keywords Breakwater · Seawall · Bay · Erosion · Shoreline change

B. Gopikrishna (✉) · J. D. Agrawal
Central Water & Power Research Station, Khadakwasla, Pune 411 024, India
e-mail: bgk9@yahoo.com

J. D. Agrawal
e-mail: agrawal_jd@cwprs.gov.in

P. V. Timbadiya et al. (eds.), *Coastal, Harbour and Ocean Engineering*, Lecture Notes in Civil Engineering 321, https://doi.org/10.1007/978-981-19-9913-0_22

1 Introduction

The coastal structures like breakwaters are constructed to protect the harbour in acquiring the appropriate tranquil conditions on the lee side and at the same time obstructing the movement of sediment on the wind side to prevent the approach channels from being silted up. The seawalls are basically built to prevent the erosion along the coast. However, these structures alter the hydrodynamic conditions when interact with the predominant waves [1]. In some coasts, it may happen to propose both the structures to acquire tranquil conditions on the one side of the coast and protect the coast from erosion on the other side. This kind of situation is required in bay locations along the coast wherein the energy of the monsoon waves is absorbed by the shore parallel breakwaters and by obstructing the movement of longshore sediment by shore perpendicular breakwaters. In both cases, the interaction of the seawall with the waves will impart changes in morphology in different ways. Such a combination is very rare as of now in the Indian coasts. The present study deals with proposed seawall in one location with existing shore parallel breakwater and proposed shore perpendicular breakwater with the existing seawall at other location. The study of impact of combined structures of seawall and breakwaters in bays at different locations at neighbouring coasts is described. This paper also aims at explaining how the negative impact of seawall is diminished due to the existence of the breakwater at both the sites without comparing the outcomes of both the models.

MUS is a principal village in the Car Nicobar Island and is positioned geographically at 9°14′28” N and 92°46′32” E. Initially, the harbour was protected by a breakwater of length 490 m (Fig. 1) and a jetty of 90 m length on lee side of breakwater was constructed for facilitating berthing of ships. Now, it is proposed to construct a seawall or shore protection to the shoreline of MUS for a length of 800 m (A-B-C of Fig. 1) to prevent the erosion likely to happen inside the harbour basin. However, the present study deals with deciding the optimum length of seawall that serves the same purpose as that of proposed 800 m.

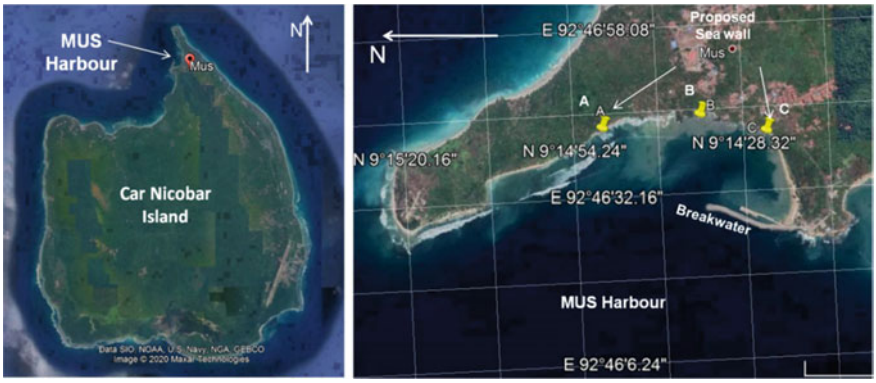

Fig. 1 Car Nicobar Island and location of MUS harbour along with proposed location of seawall

Fig. 2 Location of Vengurla and its bay between two headlands

The other site in the west coast, i.e. Navabag, is located in Vengurla Tehsil at geographical coordinates 15° 51′23.92" N, $73^0$37′15.19" E in Sindhudurg district of Maharashtra state, India. The location is situated 12 km North of Redi port located in the same district of Maharashtra and just above the North of Goa state (Fig. 2). Vengurla is one of the typical pocket beaches located between two headlands of 500 m and 300 m lengths in the west coast of India. The Commissioner of Fisheries, Government of Maharashtra, Mumbai, proposed to provide the infrastructure along with post-harvesting facilities to the fishermen. As a part of this development inside the bay, a breakwater of length 500 m was proposed.

The earlier studies [5] in combination with the seawall and breakwater indicated that the wave forcing could be reduced over the seawall by placing a submerged breakwater. As a result, the run up over the seawall was reduced by 20–60% and reflection coefficients up to 70%. Similar study with the help of laboratory wave flume [7] with low crested offshore breakwater as a rehabilitation structure and damaged vertical seawall. The results of the model studies indicated reduction of wave forces on seawall.

2 Materials and Methods

2.1 Study Area

2.1.1 MUS

The shoreline simulation in 1D requires to have a longshore profile and a few cross-shore profiles at various locations. The longshore profiles were delineated from the

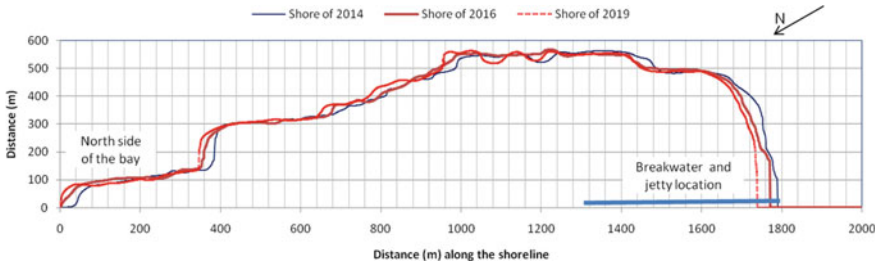

Fig. 3 Delineated shorelines of different years from satellite imageries

USGS earth explorer Landsat imageries for the available years of 2014, 2016 and 2019. Since the resolution for the imageries considered is same in the same area, the difference would not depict any kind of irrelevant changes. The baseline of 2 km was considered oriented to 180° N. The delineated longshore profile of approximate length of 2 km with a crenulated shape was computed from baseline orthogonally with a grid interval of 1 m. The grid interval of 1 m is so chosen to reproduce the curvatures along the shoreline and to minimise the likely refractive errors arise during computation. The annual gross littoral drift in the area outside the bay is towards North and is estimated to be 0.4 million m^3 and inside the bay 0.3 million m^3. The little difference in net- and gross-accumulated drift is an indication of unidirectional drift over the area throughout the year. The details of the computation of littoral drift at this location are disseminated through a separate paper of this conference.

The comparison of the delineated imageries of different years indicates certain amounts of deposition and erosion patterns inside the bay. The erosion is observed near the tip of the MUS Island and all along the shoreline from 360 m distance to the end of the seawall-proposed location, i.e. at +1400 m chainage (Fig. 3). The pattern is, however coincidental, with google earth imageries of the same years. The accretion is noticed from +1400 m chainage on shoreline up to the breakwater position at the end of shoreline considered. The rate of erosion and the rate of accretion all along the shoreline vary from 0.5 m to 10 m per year at different locations as estimated by end point rate in a span of 5 years. It is also noticed that the rate is not the same year over year in a span of 5 years.

2.1.2 Vengurla

The Vengurla beach is one of the pocketed beaches located in the west coast of India. The bay location is situated between headlands with a narrow opening of about 100 m at the corner of the north headland. The tidal flow passes through the narrow opening along with sediment while flooding and reverses while during ebbing. In this way, the narrow opening acts as sink while flooding and source while being in ebbing phase of the tide. The Google imageries of different years from 2014 to 2020 (Fig. 4) have been marked for sediment deposition patterns in front of entrance and have

been supplied to CWPRS. The indicated markings in red colour in each imagery signify the deposition inside as well as outside of the entrance to the harbour. Since the phase of the tide is not known, there is every possibility that the bars may get exposed during low tide. The entrance is more likely to deposit sediments during the ebb phase of the tide as the case of the imagery post-monsoon of the year from 2014 to 2018.

Such deposition of the sediments is disappeared in the imagery of the year 2020. However, the bar inside the harbour is seen till the year 2018. The imageries of the different years indicated that the seawall had been constructed between the years

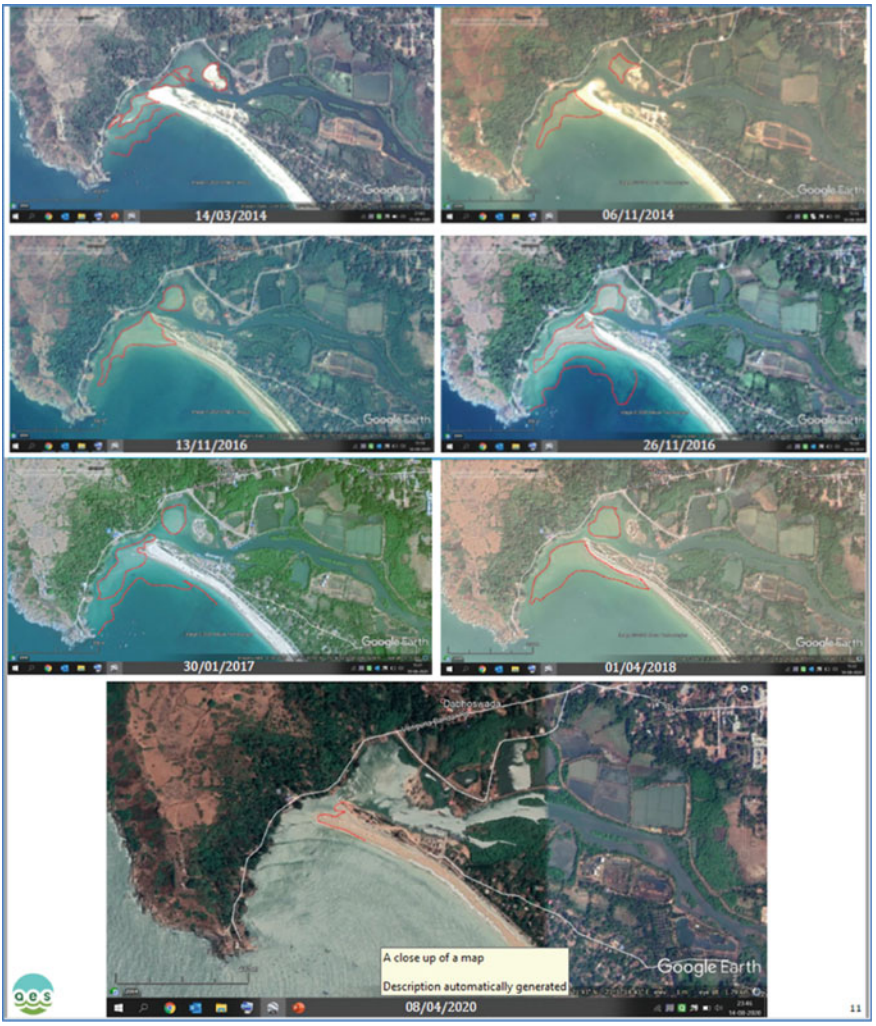

Fig. 4 Google imageries of Vengurla site for different years in existing condition

2010 and 2013. Post-seawall effect has been analysed by comparing the cross profiles of the year 2020 (Fig. 4) extracted from CMAP with that of the year 2015 based on the observed profiles [8]. The cross-shore profile as extracted from the location of the seawall across shore for the year 2020 indicated that the contour of 8 m depth at 1 km from shoreline takes a flat slope to 10 m contour of 3.5 km from shoreline. The nearshore contours of 0 m at around 800 m shoreline falls steep to 8 m contour within a distance of around 250 m. Such a steep profile with the observed data of 2015 indicated to rise from 500 m from the shoreline. Since after the construction of seawall, it is observed that from the year 2015 to 2020 indicated a shift of contour depths of up to 8 m by 250 m towards sea.

The past studies of Navabag indicated that the sand dunes are present throughout the backshore of the site and there exists a seawall of about 0.8 km length along the southern sector and a paved path about 0.4 km in the northern part. As per the studies done by Kunte and Wagle [6] using remote sensing products, it is mentioned that the sediment transport direction observed to be bi-directional and seasonal dependent along the Maharashtra coast, and the resultant sediment transport is southward. The longshore current direction is variable at Vengurla with an annual net southward drift of 0.05 million m^3 as estimated by field measurements whereas along Ratnagiri coast the littoral drift direction is predominantly southwards and is estimated to be 0.12 million m^3. Negligible annual net sediment transport was observed in the vicinity of Vengurla based on Shore Protection Manual equation. The same method when applied along the west of India overestimated the drift. The annual net transport direction varies along the west coast showing southerly at Ratnagiri, Tadri and Mangalore and northerly along Vengurla, Goa and Coondapur Kunte [6]. The recent studies of the year 2020 [4] at Vengurla site confirmed the same, i.e. towards North with 0.019 to 0.037 Mm^3 of net annual longshore sediment transport rate (LSTR). This change in direction in net LSTR is due to slight change in direction of breaking wave angle.

2.1.3 Data and Its Analysis

For any site-specific modelling work in 1D, the data required are mainly beach profiles, longshore profiles, tides, waves, wind, currents, sediment data and sediment-laden river discharges along with the satellite imageries of the study region. Here, for both the study regions ship observed annual averaged wave data for 30 years obtained from IMD was used. The predominant direction of waves approach during monsoon is from WSW, SW and SSW directions offshore with magnitudes up to 4.5 m. However, the frequency of these highest waves is very minimal in a year and 75% of waves of height 2 m or less prevails at MUS site. The scene at Vengurla site was that during monsoon the waves approach from W and SW directions with up to 4.5 m in height. The other monsoon climate in west coast is subject to waves of 3 m in height between NNW and NE directions, while in non-monsoon the predominant direction is from NW of varying heights of waves up to 3 m.

The sediment data collected at site were analysed for D_{50} at CWPRS. The D_{50} size at jetty location is 0.24 mm and 0.21 mm at the beginning of proposed seawall. The size at location far end of the seawall is 0.53 mm. The sediment size D_{50} at Vengurla has been observed to be between 0.06 and 0.5 mm from literature. A constant value of 0.2 mm has been used for the study. The three cross-shore profiles considered were up to 20 m contour depths at MUS site: one in the North (Profile 1) and others in the centre of bay (Profile 2) and South (Profile 3) sides. These cross-shore profiles were interpolated offshore to onshore with a grid interval of 1 m. It is observed from North profile to South profile that the distance of the 20 m contour from the 5 m contour is increased from 375 to 1200 m. The distance between these contours at centre of bay is at 840 m. Thus, it indicated the deeper contours gradually taken the shape of the bay. Owing to the shape of the bay at Vengurla, only two cross-shore profiles were considered up to 10 m offshore depths in a distance of 3.5 km from shoreline: one in North and other in South.

The shoreline along the bay between the headlands is an important input to the model for shoreline morphology calculations. The longshore profiles were delineated from the USGS earth explorer Landsat imageries for different years. These profiles were used for calibrating the shoreline model in existing condition and further used by incorporating the proposed structures. Since the site at Vengurla had been studied by various researchers in the recent past and hence the known littoral drift was calibrated. This involved the use of roughness and fall velocities of sediments determined during the calibration of the littoral drift model.

3 Methodology

3.1 MUS

The baseline of 2 km was considered oriented to 180° N. The delineated longshore profile of approximate length 2 km with a crenulated shape was computed from baseline orthogonally with a grid interval of 1 m. The grid interval of 1 m is so chosen to reproduce the curvatures along the shoreline and to minimise the likely refractive errors arising during computation. The other required model inputs like dune position, dune height, distance of deep water contour position and angle of deep water contour to baseline were appropriately given in the model. The active depth and roughness considered in the model were adjusted to tune the model with the delineated longshore profile for other years and finally arrived at 5 m. The model was calibrated against known shoreline configurations using the ship observed data of the past 30 years. During calibration, it is assumed that the annual wave climate would have occurred repeatedly for 5 years. The simulated shorelines after 2 years and 5 years with an initial shoreline of 2014 were compared with the delineated shorelines of 2016 and

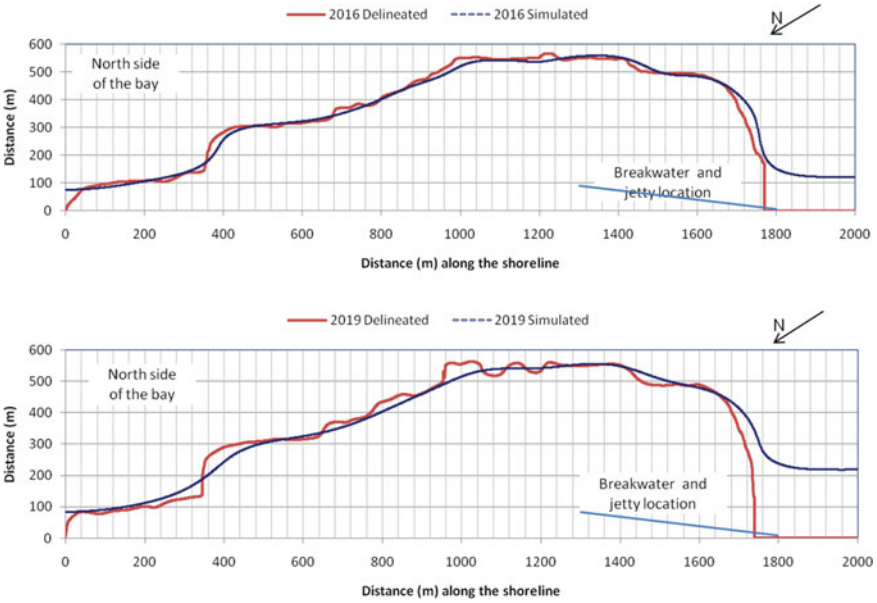

Fig. 5 Comparison of shorelines for different years

2019 incorporating the breakwater. The delineated and simulated longshore profiles for different years are shown in Fig. 5. The comparison shows good agreement excepting at positions steep or abrupt curvatures.

3.2 Vengurla

Littoral drift was computed at two cross sections whose depth contours were extracted from the latest data of CMAP belong to the year 2020 to understand the site condition. This involved the use of roughness and fall velocities of sediments determined during the calibration of the shoreline model. The bed roughness and depth of closure played a crucial role in calibrating the model. The primary input to model is the annual wave climate as observed by ships. This was obtained from the averaged conditions of wave climate of 33 years. It is presumed that the wave climate and cross-shore depths do exist for the future periods as well. From the results of the littoral drift, it is observed that the northerly and southerly drifts are more or less similar in magnitude and are insignificant. However, the net drift is taking place from South to North. Such a small magnitude in drift is contemplated due to the frequencies of the predominant wave directions of different magnitudes prevail from the West and SW. The annual net drift towards North based on North profile was estimated to be of the order of 90 m^3/m. Similarly, based on the South profile, the annual net drift towards North

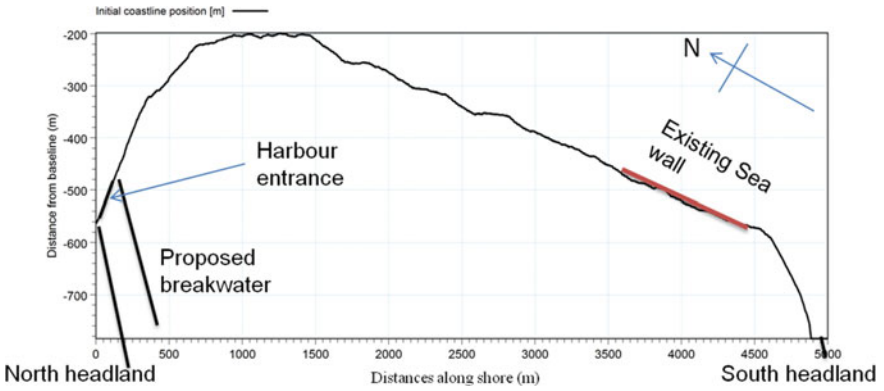

Fig. 6 Longshore profile of Vengurla Bay with different structures

is estimated to be 190 m^3/m. The estimated transport of drift northwards by South profile is 560m^3/m which is more than North profile in the same direction. However, the southward movement of the same was 390m^3/m and 150 m^3/m by South and North profiles, respectively. The annual gross and net longshore sediment drift at Vengurla are 0.25 to 0.22 million m^3 and 0.04 million m^3 towards North, respectively.

Having calibrated the model for littoral drift, the following experiments were done using shoreline model to study the effect of structures. The existing and proposed structures are shown in the delineated shoreline of the year 2009 in the diagram (Fig. 6).

1. Existing condition without seawall.
2. Existing condition and seawall of length 800 m.
3. Proposed condition with breakwater of length 500 m.
4. All the above conditions with a source and sink in the model.

4 Results and Discussions

The composite structure interaction was studied with the help of modelling through a software developed by Mike21. Depending on the existing condition with a particular structure, i.e. in the case MUS breakwater, the influence of breakwater lies not only on creating the tranquil conditions on the lee side but also reduces the reflectivity of waves from the seawall structure owing to the reduced wave conditions. The placement of the seawall was economically done as a shore protective structure whose actual impact is minimal in reflecting the waves due to the presence of the shore parallel breakwater. The other site at Vengurla described the existing condition with the seawall in the bay as a shore protective structure. The influence of this seawall was seen at site in frontal erosion or shifting of deep water contours. However, the breakwater which when interrupts the longshore drift may help in nourishing the

deficit zone depending on the seasonal predominant directions of waves. The details of the composite structure interaction are explained separately in the subsequent lines.

4.1 MUS

It is required to simulate the shorelines for the future changes under the impact of the proposed seawall or revetment of length 800 m along the shore. Accordingly, the revetment structure of length 800 m demarcated with A, B and C (Fig. 7) has been incorporated in the model. Experiments were conducted for future shoreline positions in a span of 5 years for 20 years with the initial shoreline of 2014. For the purpose, the annual averaged wave climate is assumed to be repeated for the next 20 years. The calibration parameters active depth and roughness have been used for further simulations. Experiments were done by incorporating the breakwater as simulated for calibration procedure. Since the shore inside the bay is having crenulated shape, the revetment structure for 800 m is split in small segments to keep its distance from shore to as minimum as possible. It is found from the figure that the impact of revetment is accretion at point C and minimum erosion beyond Point A. On average, it could be at the rate of 10 m accretion in a span of 20 years as obtained from the past wave climate and 5 m erosion beyond A at the rate of less than 5 m in a span of 20 years.

The shoreline behaviour for future years under the same wave conditions was simulated without incorporating the seawall in order to justify the need of the seawall or any shore protection work. It is noticed from the imageries that accretion has taken place from the breakwater root to the start of proposed seawall. Such an accretion is simulated for future periods for about a length of 500 m northwards, i.e. up to the position of chainage +910 m from +1410 m (Fig. 7). The rate of this accretion is simulated to be around 10 m in 20 years. The minimal erosion and no change situation were indicated by the model for rest of the portion. In order to optimise the length of the seawall, a series of experiments were conducted by reducing the length gradually from point C (from 800 to 225 m). The results of series of experiments indicated the similar pattern as that of no-seawall experiment (Fig. 7) i.e. South of seawall shows accretion and erosion at North of seawall.

The crenulated shape of bay was studied for shoreline changes with the existing breakwater of length 490 m. In usual case, the seawall or revetment along the coastline causes accretion on up-drift side and erosion on the down-drift side. In this case, the flow is restricted from one side by constructing a breakwater parallel to the coastline, and the accretion is simulated at far end of the revetment (Point C) due to reduction in littoral currents driven by the reduction in the momentum generated radiation stresses. However, for any structure of a kind of seawall or revetment, flanking or end wall effect which leads to erosion on down-drift side for some distance is inevitable. The other effect upon constructing the seawall is frontal effect or toe erosion. The contours in front of seawall will be deepened and shift towards the sea. This scenario

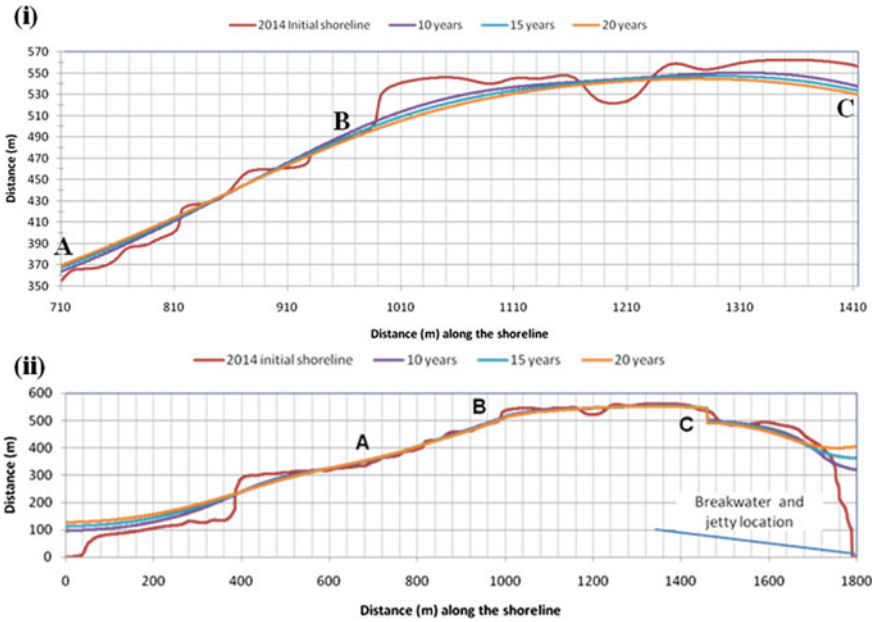

Fig. 7 Simulation of shorelines for different years (i) without seawall and (ii) with seawall

Fig. 8 Vengurla site showing the location of proposed breakwater at North Headland

will be required for any port or harbour locations provided that the appropriate toe protection is made.

In order to ascertain the impact of construction of seawall at adjacent coasts and ascertain the need of the wall, the calibrated model in existing condition was extended for 20 years, i.e. till the year 2034 under the influence of the same wave conditions without incorporating the seawall. The accretion at the rate of 10 m in

20 years was simulated near the far end of proposed location (point C) of seawall even without the seawall. This indicated that the impact of seawall neither increases nor decreases the accretion rate at South of the shoreline considered. The reason is due to the predominant direction of waves approach in the presence of shore parallel breakwater. The erosion rate at the near end of seawall (point A) decreases due to the construction of seawall to the extent of almost half as compared to the erosion with the existing condition, i.e. without seawall. However, from the far end of seawall for a distance of 500 m (approx. chainage from 1410 to 910), accretion is simulated for the same period of 20 years in the absence of seawall. This indicates that the accretion that has taken place so far behind chainage 1410 would be extended along the coast if there was no such proposal of seawall. Hence, along this stretch of 500 m length, the seawall purpose is not ascertained. However, the point A beyond for a length of 150 m remains under erosion at the rate of 0 to 5 m in a span of 20 m for all the scenarios. Finally, the length of seawall recommended is 800 – 500 + 150 = 450 m.

4.2 Vengurla

Initially, the need of the seawall was justified by simulating the erosion at the southern end of the shoreline for a distance of about 800 m within the bay. The rest of the location is in the zone of accretion. In the next scenario, the seawall was incorporated and effect of it was seen by simulating the shorelines with the same initial shoreline. The effect of seawall in shifting of the 8 m contour for a distance of 250 m in a span of 5 years was seen from the results of the simulation. This has been verified with the measured cross-shore profiles as given in the paper Noujas et al., 2018 at the same location in front of the seawall. This could be because the predominant direction of longshore transport is towards North, and much of the transport is taking place between 500 and 1000 m from the shore. The simulations for further 30 years with seawall along with the incorporation of source-sink scenario show that the accretion that was taken before the construction of seawall continued even after the incorporation of seawall till its starting point. This scenario is validated with the pattern of depositions with the google imageries (Fig. 4). These magnitudes of accretion and erosions are compared with experiments of proposed shore perpendicular breakwater.

It is found from the results of the simulation that the impact of breakwater is seen for a length of up to 2 km from North headland along the shoreline in a period of 30 years as simulated from the past wave data (Fig. 9). The change is estimated to be up to 1 m per decade and up to 2.5 m in a span of 30 years over and above the present rate of deposition. The reason is that breakwater is very close to the headland to help in channelising the flow and prevents the entry of sediment into the harbour while the drift is moving from South to North. It is obvious that the orientation of breakwater at the proposed location does hinder the movement of sediment and

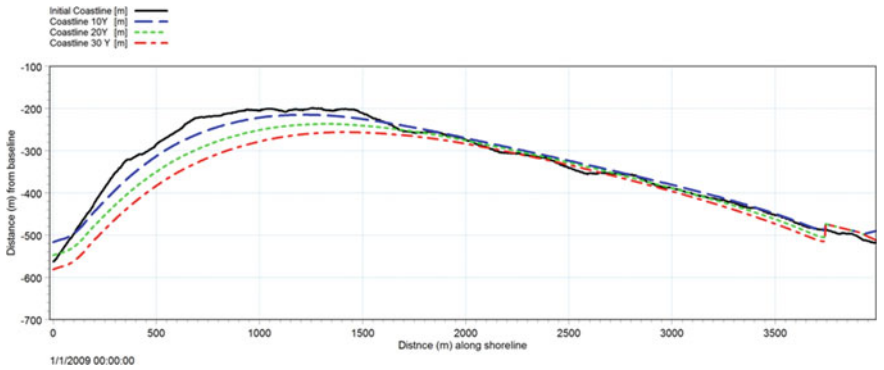

Fig. 9 Simulation of shorelines for various years with breakwater and seawall

cause to deposit on the seaside. This change in quantity would have entered into the harbour if the breakwater was not there. The erosion and accretion patterns have shown insignificant changes even after the incorporation of breakwater, i.e. up to 1 m in a span of 10 years and up to 2.5 m in a span of 30 years with the length of the breakwater equivalent to the length of the headland nearby. Its impact is justifiable to hinder the movement during North drift and to channelise the flow during both phases of tide.

5 Conclusions

The composite structure interaction of waves was studied with the help of numerical modelin 1-Dat MUS harbour in Car Nicobar Island and Vengurla sites. The absence of either one of these structures at both the sites will have left the site with more undesirable results like increase in reflectivity and erosional patterns. The need of the seawall as a shore protecting structure was ascertained at both the sites. The length of seawall was optimised to 450 m due to the presence of shore parallel breakwater at MUS harbour. The impact of the breakwater in changing the erosional and accretional patterns is minimal at Vengurla site up to 1 m accretion in a span of 10 years and up to 2.5 m in a span of 30 years over and above the present rate of deposition due to the North drift and channelising the flow on the lee side.

Acknowledgements The authors are thankful to Shri. A.K Agrawal, Director, CWPRS for his encouragement and support during the period of study and kind permission for publication of this paper.

References

1. Balaji R, Sathish K, AnkitaMisra (2017) Understanding the effects of seawall construction using a combination of analytical modelling and remote sensing techniques: Case study of Fansa. Gujarat, India. Int J Ocean Climate Syst 8(3):153–160
2. CWPRS Technical Report: 5891, Jan, 2021
3. CWPRS Technical Report: 5933, July, 2021
4. Jesbin George V, Kumar S, Gowthaman R, Singh J (2020) Nearshore waves and Littoral drift along a micro-tidal-wave dominated coast having comparable Wind-sea and swell energy. J Marine Sci Eng 8(55):2020
5. Koraim AS, Heikal EM, Abo ZaidA A (2014) Hydrodynamic characteristics of porous seawall protected by submerged breakwater. Appl Ocean Res 46:1–14
6. Kunte, Wagle (2001) Littoral transport studies along west coast of India – a review. Ind J Marine Sci 30:57–64
7. MuniReddy MG, Neelamani S (2005) Hydrodynamic studies on vertical seawall defenced by low-crested breakwater. Ocean Eng 32(5–6):747–764
8. Noujas V, Kankara RS, Rasheed K (2018) Estimation of longshore sediment transport rate for a typical pocket beach along West Coast of India. Mar Geodesy 41(2):201–216

Feasibility of the Proposed ROPAX Jetty Through Evaluation of Hydrodynamics by Mathematical Model Study

N. S. Jagatap, A. K. Singh, and L. R. Ranganath

Abstract The growth in international trade has made the developing countries to concentrate more on the development of their infrastructure, like roads, airports, seaports, which play an important role within the development of the economy. The government is committed to the sustainable development of Indian shipping industry, and the increase within the maritime economic happenings has encouraged a rapid development within the port sector. Hazira is a suburb and a transshipment port within the Surat City within the Gujarat state of India. It is located at the west most end of Surat. Hazira is one amongst most significant the ports of India and therefore the most important element of Surat Metropolitan Region. The town is the industrial hub of India and is found on the bank of the Tapti River, eight kilometres away from the Arabian sea. Deendayal Port Trust, Gujarat features a proposal to determine ROPAX Jetty in Hazira, Gujarat as a part of the ambitious project from PMO India. A two-dimensional mathematical model MIKE21 HD was used to study the hydrodynamics within the vicinity of the proposed ROPAX jetty area. The impact on the hydrodynamics within the vicinity of the proposed ROPAX jetty was studied with the assistance of mathematical model. The current measured at two locations varied from 0.3 m/s to 1.1 m/s in existing condition and reduces marginally in the order of 0.1 m/s at C1 location and 0.05 m/s at C2 location after proposed ROPAX jetty. The results from the hydrodynamics studies suggest that there aren't any significant changes within the flow pattern and no cross flow observed during the simulation. It absolutely was suggested that the project is executed and further maintained with maintenance dredging within the channel for smooth functioning of the project. This project will help immensely for saving time travelled by road and also reduce the gap between Hazira, Gujarat to Gogha, Gujarat from around 384 km to merely meagre 80 km.

Keywords Hydrodynamics · Jetty · Ropax · Circulation

N. S. Jagatap (✉) · A. K. Singh · L. R. Ranganath
Central Water and Power Research Station, Pune 411024, India
e-mail: naval.jagtap@cwprs.gov.in

P. V. Timbadiya et al. (eds.), *Coastal, Harbour and Ocean Engineering*, Lecture Notes in Civil Engineering 321, https://doi.org/10.1007/978-981-19-9913-0_23

1 Introduction

The economic development of any country is very much reliable on the improvement of their infrastructure, like roads, airports, seaports, etc., which is why the developing countries are persistently working in improving their infrastructure which also plays a pivotal role in growth of international trade. The rise in the maritime economic happenings has encouraged a rapid development in the port sector. The shipping industry is also valuable in terms of its capacity to move large shipments along with the ability to provide for its storage.

The government is committed to the sustainable development of Indian shipping industry the prominence in maritime economic undertakings has further led to the development of many ports related activities. It is widely acknowledged that time is a precious aspect of life. "Time is money", is a famous phrase in English that glorifies the importance of time. In today's fast paced world, it becomes necessary to cut time of logistics between different regions of economic important.

RoPax is a term generally used to exemplify ships having roll-on and roll-off facility for the carrying commercial and private vehicles along with the facility to accommodate large numbers of commuters independently, for shorter cruises. The word "RoPax" simply means "passenger RoRo vessel [2]. The RoPax and RoRo ships are expected to flourish even more in the forthcoming years. Particularly in India, the massive prospective for this flourishing usage of RoPax and RoRo ships is mostly to reduce the traffic on roads. "Highway at Sea" is the only "highway" in the world which has no traffic jams. With the growing emphasis over the use of RoPax for various purposes, both on domestic and international routes, it will draw new necessities with new features and improvements. Therefore, feasibility of such projects and their impact on the hydrodynamics in the vicinity of these projects is the prime need of the hour.

Hazira is a transshipment port in the Surat City in the Gujarat state of India. It is situated at the west end of Surat. Hazira is one of the major ports of India and the most significant part of Surat Metropolitan Area. Surat is also well-known as the industrial hub of India and is located on the bank of the Tapti River, 8 km away from the Arabian Sea. Deendayal Port Trust, Gujarat has a proposal to establish ROPAX Jetty in Hazira, Gujarat as part of the ambitious project from PMO India [1]. The ferry transport from Ghogha and Hazira port is about 60 km and facilitates easier access.

2 Methodology

A two-dimensional mathematical model was setup incorporating the features of the project site. MIKE21 HD model was used to simulate tidal flow pattern in the region by using the data related to bathymetry and other hydraulic factors like tide, current, waves, etc. The velocity field in the existing condition was simulated for various

tidal conditions. The model has been calibrated for hydrodynamics aspects for the existing condition using field observed data. The hydrodynamic model studies consist of simulation of flow pattern for the existing conditions as well as with the proposed ROPAX jetty. These model studies help in evaluating the probable variations in the hydrodynamic conditions and realization of tidal circulations, if any, due to the proposed jetty.

3 Data

3.1 Bathymetry Data

The bathymetric data for the offshore region has been obtained from the C-MAP, and admiralty charts were used for preparation of bathymetry for computational model.

3.2 Tide Data

Site observed tidal data was available for the month of May 2013. The same data has been used to provide appropriate boundary conditions with proper phase lag. The data analysis specified that the site observed tidal range was 7.05 m during spring tide and about 3.1 m during neap tide. The site observed tide was considered for the model studies. The tides in the area are very high due to which the estuary is highly dynamic in nature and also well-flushed. The boundary tide used for model simulation is shown in Fig. 2.

3.3 Current Data

Figure 3 shows the observed currents at CM1 and CM2 locations. Observed current data at two sites, i.e. CM1 and CM2 which showed that the currents near CM1 and CM2 were in the order of 0.3 m/s–1.1 m/s. The plot for observed current is shown in Fig. 4.

4 Hydrodynamic Model

Hydrodynamic studies include simulation of the flow field for the existing condition. At first, the flow simulations were carried out with the existing conditions. The model was then simulated with the proposed ROPAX jetty. Further, the simulations were

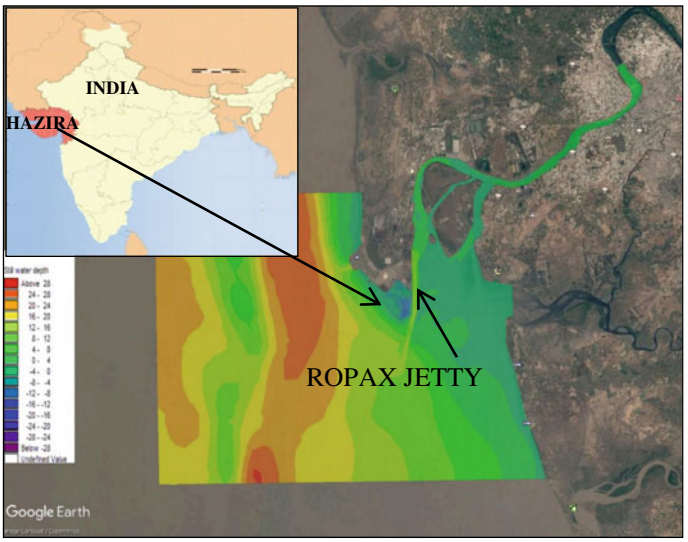

Fig. 1 Location map

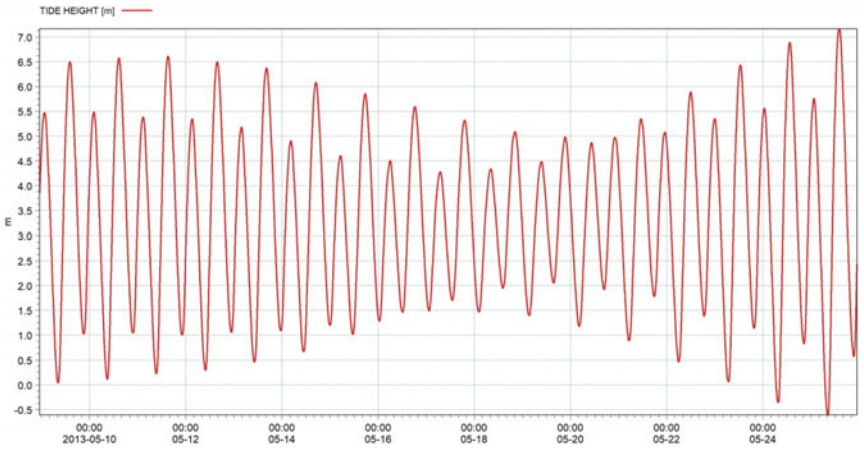

Fig. 2 Boundary tide

carried out to assess variations in the hydrodynamic condition and formation of tidal circulations if any, after studying the proposed jetty and changes in hydrodynamics. These simulations were carried out to find out the probable changes in current pattern as well as magnitude in the vicinity of the proposed ROPAX jetty at Hazira, Gujarat.

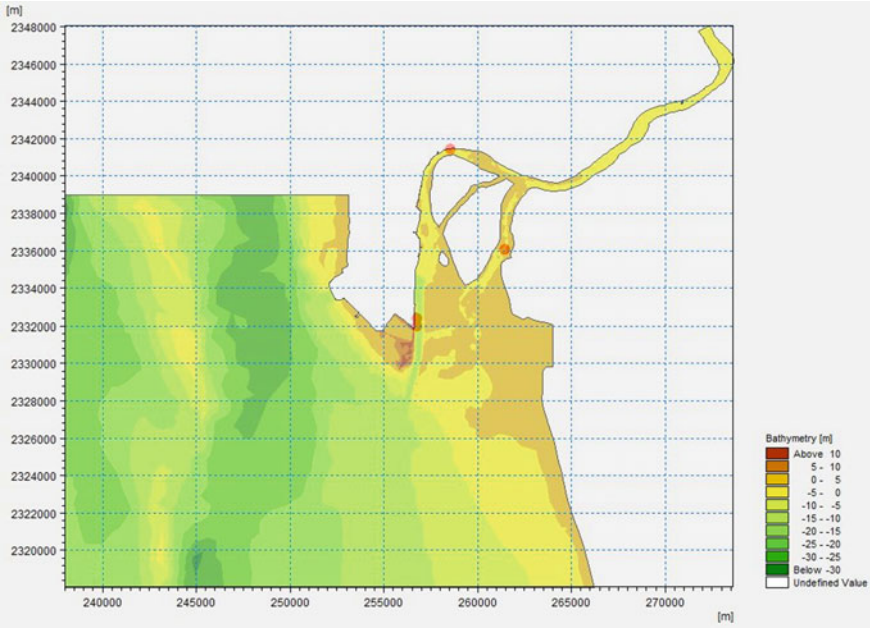

Fig. 3 Observed current speed and direction

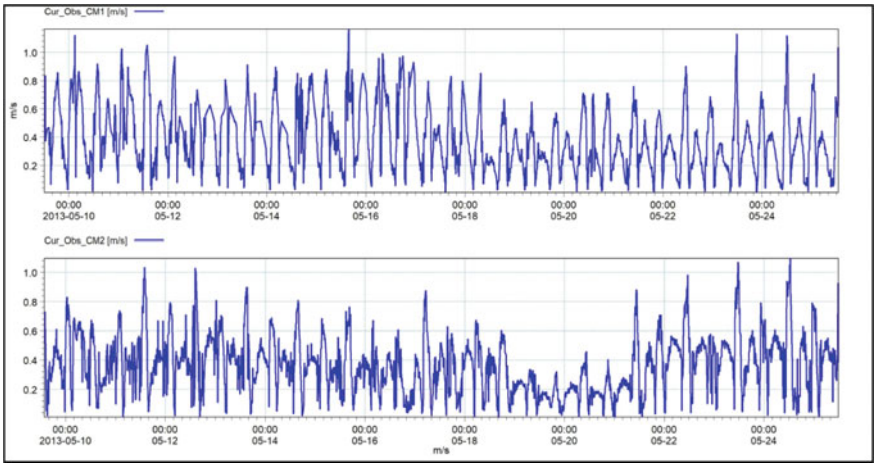

Fig. 4 Observed current at CM1 and CM2

4.1 Two-Dimensional Hydrodynamic Model

It is necessary to know dynamics of the water body in terms of velocity and water level fluctuations before undertaking any major developments in coastal areas. The suitable governing equations for understanding water flow variations in coastal areas are Shallow water equations based on 3D Governing Equations in Cartesian co-ordinates. The model study is based on the situation of the three-dimensional incompressible Reynold's averaged Navier–Stokes equations, subjected to the assumptions of Boussineq and hydrostatic pressure [3].

The continuity equation is given as.

$$\frac{\partial u}{\partial x} + \frac{\partial v}{\partial y} + \frac{\partial w}{\partial z} = S \tag{1}$$

The two horizontal momentum equations are given for the x- and y-components, respectively.

$$\begin{aligned} &\frac{\partial u}{\partial t} + \frac{\partial u^2}{\partial x} + \frac{\partial vu}{\partial y} + \frac{\partial wu}{\partial z} = fv - g\frac{\partial \eta}{\partial x} - \frac{1}{\rho_0}\frac{\partial p_a}{\partial x} \\ &-\frac{g}{\rho_0}\int_z^n \frac{\partial p}{\partial x}dz \frac{1}{\rho_0 h}\left[\frac{\partial s_{xx}}{\partial x} + \frac{\partial s_{xy}}{\partial y}\right] + F_u + \frac{\partial}{\partial z}[v_t \frac{\partial u}{\partial z}] + u_s s \end{aligned} \tag{2}$$

$$\begin{aligned} &\frac{\partial v}{\partial t} + \frac{\partial v^2}{\partial y} + \frac{\partial uv}{\partial x} + \frac{\partial wv}{\partial z} = -fu - g\frac{\partial \eta}{\partial y} - \frac{1}{\rho_0}\frac{\partial p_a}{\partial y} \\ &-\frac{g}{\rho_0}\int_z^n \frac{\partial p}{\partial y}dz - \frac{1}{\rho_0 h}\left[\frac{\partial s_{yx}}{\partial x} + \frac{\partial s_{yy}}{\partial y}\right] + Fv + \frac{\partial}{\partial z}[v_t \frac{\partial v}{\partial z}] + v_s s \end{aligned} \tag{3}$$

where

t = time, x, y and z = Cartesian co-ordinates, η = surface elevation,

d = still water depth, $h = \eta + d$ total water depth.

u, v and w = velocity components in the x, y and z direction., $f = 2\Omega \sin \Phi$

The horizontal stress terms are described using a gradient-stress relation, which is given as

$$F_u = \frac{\partial}{\partial x}\left(2A\frac{\partial U}{\partial X}\right) + \frac{\partial}{\partial y}\left[A\left(\frac{\partial u}{\partial y} + \frac{\partial v}{\partial x}\right)\right] \tag{4}$$

$$F_v = \frac{\partial}{\partial x}\left[A\left(\frac{\partial u}{\partial y} + \frac{\partial v}{\partial x}\right)\right] + \frac{\partial}{\partial y}\left(2A\frac{\partial v}{\partial y}\right) \tag{5}$$

where "A" is the horizontal eddy viscosity.

The surface and bottom boundary condition for u, v and w are.

At $z = \eta$:

$$\frac{\partial n}{\partial t} + u\frac{\partial \eta}{\partial x} + v\frac{\partial \eta}{\partial y} - w = 0, \left[\frac{\partial u}{\partial z}, \frac{\partial v}{\partial z}\right] = \frac{1}{\rho_0 v_t}\left(\tau_{sx}, \tau_{sy}\right) \tag{6}$$

At $z = -d$:

$$u\frac{\partial d}{\partial x} + v\frac{\partial d}{\partial y} + w = 0, \left[\frac{\partial u}{\partial z}, \frac{\partial v}{\partial z}\right] = \frac{1}{\rho_{0v_t}}\left(\tau_{bx}, \tau_{by}\right) \tag{7}$$

where $\left(\tau_{sx}, \tau_{sy}\right)$ and $\left(\tau_{bx}, \tau_{by}\right)$ are the x- and y-components of the surface wind and bottom stresses.

The total water depth h can be obtained from the kinematic boundary condition at the surface, once the velocity field is known from the momentum and continuity equations. However, a more robust equation is obtained by vertical integration of the local continuity equation

$$\frac{\partial h}{\partial t} + \frac{\partial h\overline{u}}{\partial x} + \frac{\partial h\overline{v}}{\partial y} = hS + \hat{P} - \hat{E} \tag{8}$$

where $\widehat{P}$ and $\widehat{E}$ are precipitation and evaporation rates, respectively, $\overline{u}$ and $\overline{v}$ are the depth-averaged velocities.

5 Computational Model for Hydrodynamic Studies

The model domain considered for tidal flow comprises total area of 35 km × 30 km. The computational model covers the entire Tapi Estuary and adjoining open sea. The complete model domain has been discretized into computational coarse and fine mesh near proposed jetty expansion. The bathymetry for the existing conditions was taken from C-MAP (DHI) and was used for the study.

5.1 Simulation of Flow Field with Existing Condition

At first, the studies were conducted with the existing conditions in the Tapi estuary. The model domain indicated that there are four open boundaries where flow conditions needed to be defined. At the start, the flow simulations were carried out by using site observed spring tide with a tidal range of 7.05 m, as the current observations are also available for the same time at CM1 location. The tidal boundary was defined at the northern and southern boundaries with suitable phase lag. It was observed that the flow is nearly parallel to the contours along the western boundary, no cross-flow boundary was considered. The model was calibrated for Tapi estuary by fine tuning

the model and simulations were carried out. The time history of velocities and water levels at different locations (CM1 to CM2) was observed. The typical velocity vector plots during different phases of the spring tide are shown in the Fig. 5a, b. The magnitude of velocity is indicated by the length of the vector to the scale and the direction of flow is represented by the arrowheads.

It was noticed that flow direction is nearly parallel to the Western buoyed channel and to the Dumas channel and no significant cross flow is observed within the straight stretches of the channel. The comparison of currents with the field observed and model result is shown in Fig. 6. The model results match well with the site observed data and hence there is a good agreement specifying that the model is proved.

5.2 Simulation of Flow Field with Proposed ROPAX Jetty

The model set up used for simulating existing condition was used to simulate hydrodynamics for the proposed condition with addition of the proposed ROPAX jetty. A 250 m ROPAX jetty with approach is proposed. The proposed jetty is a piled structure and the piers for the proposed jetty have been incorporated in the model. The model was simulated to observe changes in flow conditions if any due to this new development. A 2D view of the computational model is shown in Fig. 7.

The typical velocity vector plots during different phases of the spring tide are shown in the Fig. 8a, b.

It was observed that there is no cross circulation and slight change in current velocity near the jetty area at C1 and C2 Locations as shown in Fig. 9a. The current at C1 location reduced by around 0.1 m/s and at C2 location by 0.05 m/s in the proposed condition. It is inferred that with the new developments, there is not much change in the current pattern either in magnitude or direction. The current variation is shown in Fig. 9b.

6 Conclusions

A two-dimensional mathematical model MIKE21 HD was used to study the hydrodynamics in the vicinity of the proposed ROPAX jetty area.

The impact on the hydrodynamics in the vicinity of the proposed ROPAX jetty was studied with the help of mathematical model.

The hydrodynamic studies showed no significant changes in the flow pattern and there was no cross flow observed during the simulation.

The current at CM1 and CM2 location varies from 0.3 m/s to 1.1 m/s in existing condition. It was also observed from the model studies that the current at C1 and C2 location reduces marginally by 0.1 m/s and 0.05 m/s, respectively, after the proposed ROPAX jetty.

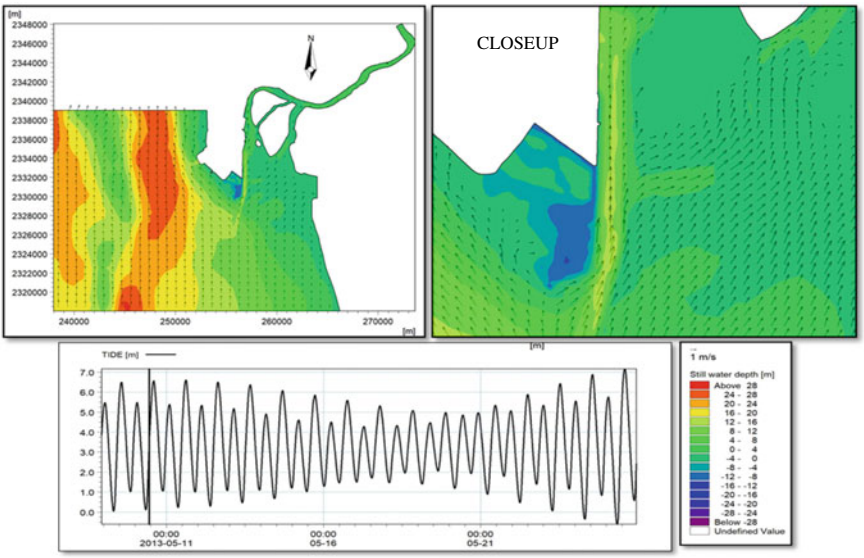

(a) Typical flow field during peak flood (existing condition).

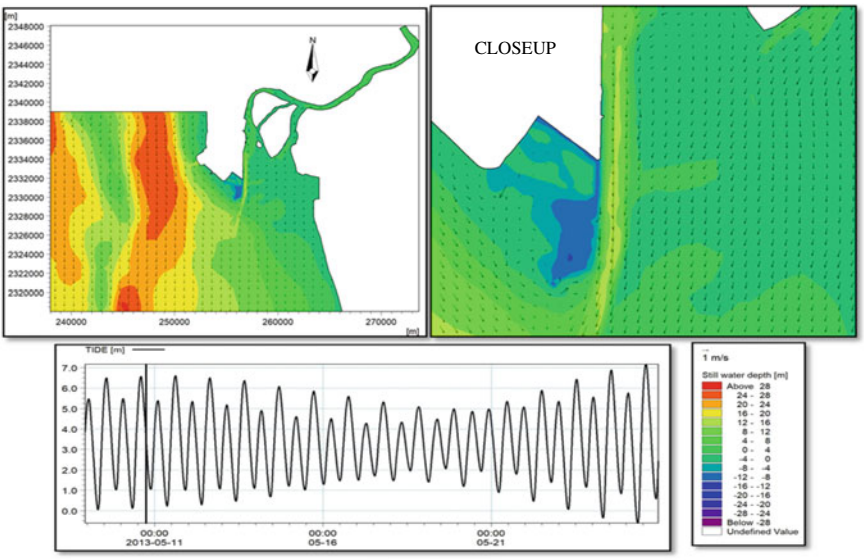

(b) Typical flow field during peak ebb (existing condition).

Fig. 5 **a** Typical flow field during peak flood (existing condition) **b** Typical flow field during peak ebb (existing condition)

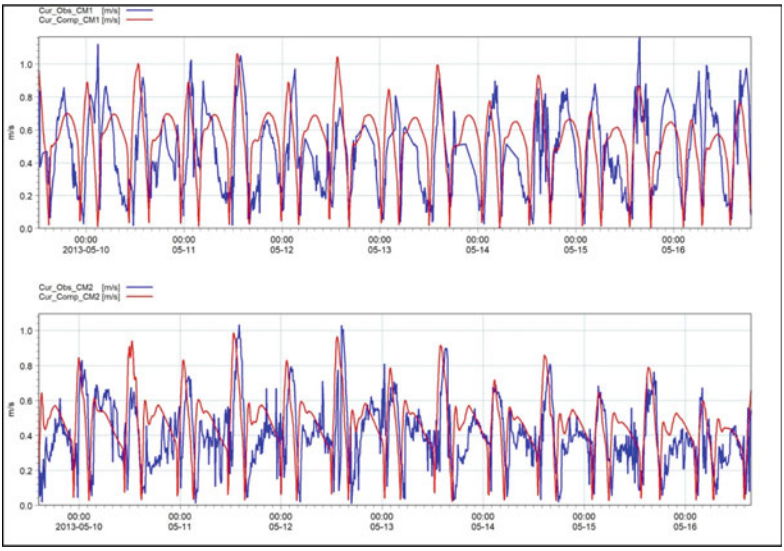

Fig. 6 Comparison of currents (observed Vs computed)

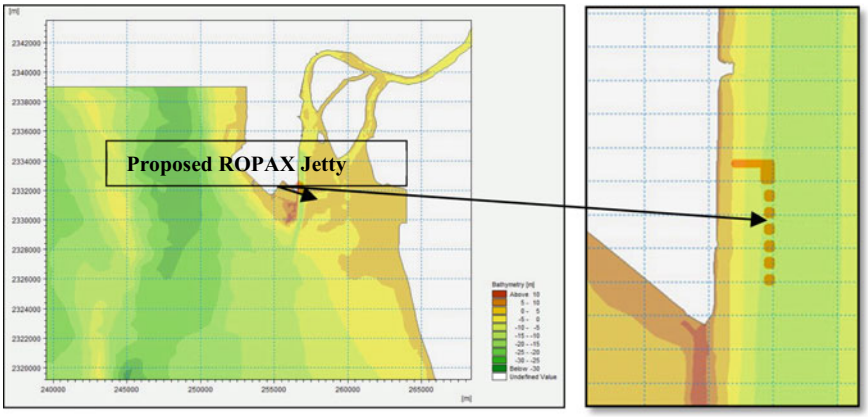

Fig. 7 2D view of computational model (proposed)

It is inferred that with the new developments, there is not much change in the current pattern either in magnitude or direction. Hence, the proposal of ROPAX jetty is feasible from flow conditions point of view as there is no adverse flow conditions for the movement of the vessels provided the desired depth is maintained with annual maintenance dredging.

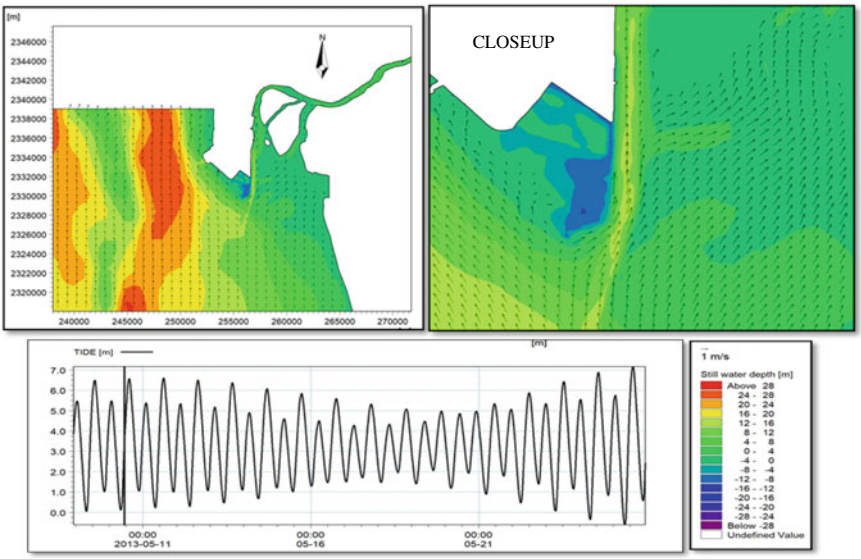

(a) Typical flow field during different peak flood (proposed condition).

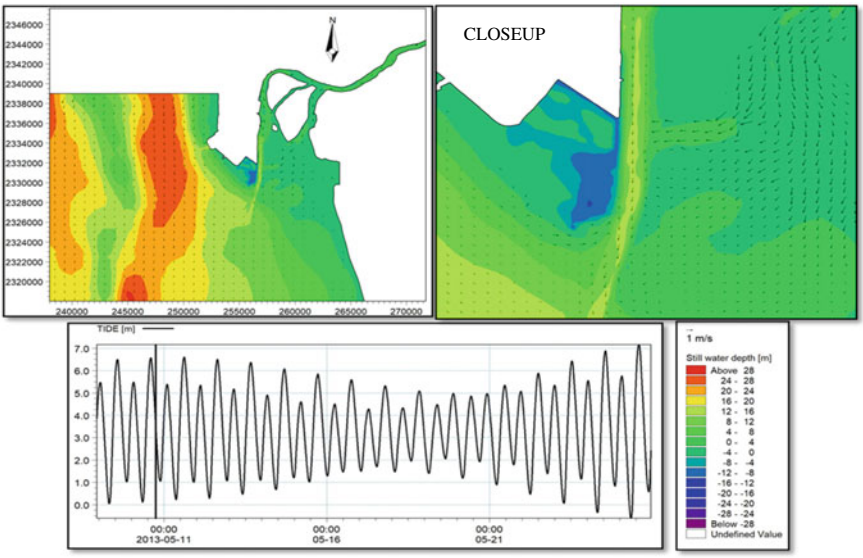

(b) Typical flow field during different peak ebb (proposed condition).

Fig. 8 **a** Typical flow field during different peak flood (proposed condition). **b** Typical flow field during different peak ebb (proposed condition)

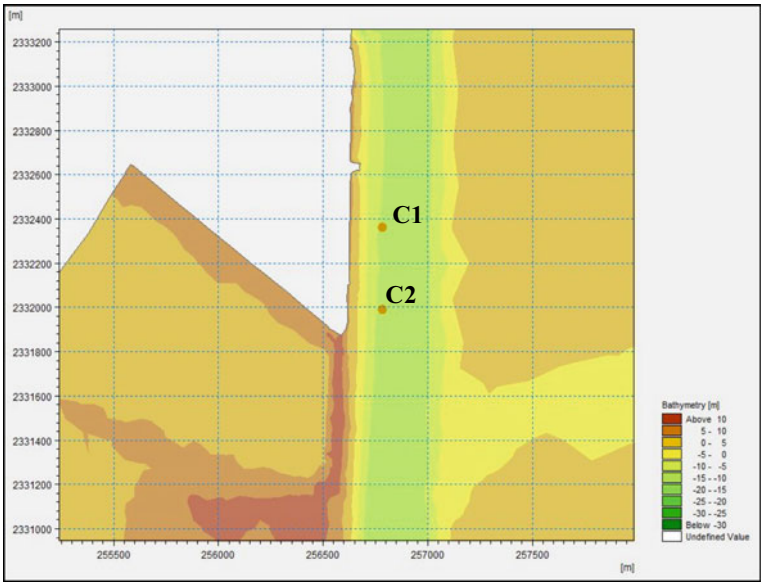

(a) Current measurement location at C1 and C2.

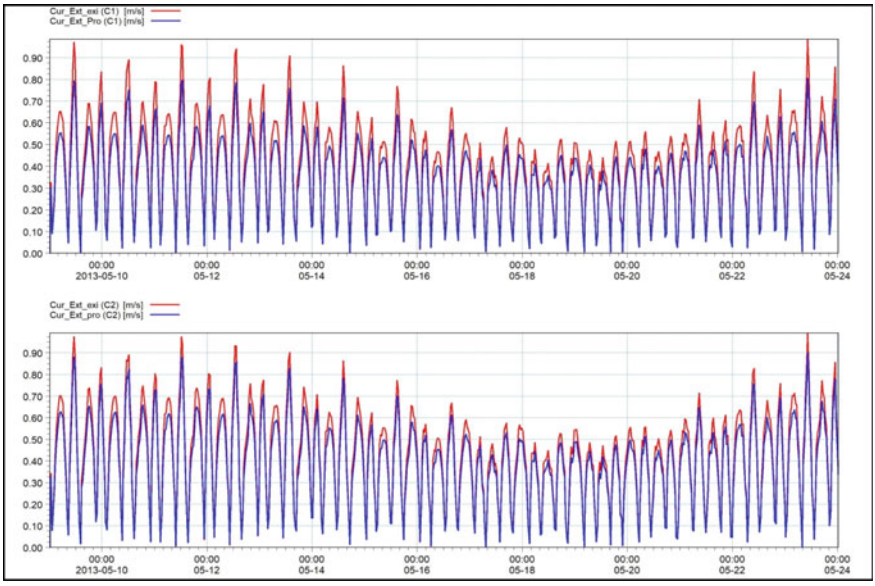

(b) Current comparison at C1 and C2 location (existing vs. proposed).

Fig. 9 **a** Current measurement location at C1 and C2. **b** Current comparison at C1 and C2 location (existing vs. proposed).

Acknowledgements The authors wish to acknowledge the Director, CWPRS for his consistent support, encouragement and kind consent for publishing this paper.

References

1. Technical report no 5905 (2021) mathematical model studies for evolution of hydrodynamics for the proposed ROPAX jetty at Hazira, Gujarat
2. https://www.norshipsale.com/functionality-and-uses-of-roro-and-ropax-vessels
3. MIKE manual 2020

Estimation of Sedimentation for a Harbour Located in a Bay by Different Methods

Om Nath Singh, B. Gopikrishna, J. D. Agarwal, and H. P. Singh

Abstract The coastlines of islands are always under threat by various environmental agencies. Coastal changes do happen by a wide range of oceanic processes. Comprehensive understanding of the coastal processes regulated by coastal hydrodynamics and the consequent movement of sediments is vital to the formulation of coastal zones management strategies. It is imperative to protect the dynamic environment against those processes cost effectively with minimal or no impact on neighbouring coasts. Some of the bay environments are protective from the seas naturally. However, coastal structures like breakwaters that were built for creating tranquil conditions provide hindrance to the movement of sediment passing alongshore. This study pertains to the study of estimation of this sedimentation by different methods for a harbour located in Car Nicobar Islands, viz. (1) Empirical methods, (2) Numerical modelling in 1D, and (3) Numerical modelling in 2D. The harbour is subjected to the seasonal variation in sedimentation, and in SW monsoon, the estimation with 2D model studies is 2200 m^3/m with little or no sedimentation in the harbour in other seasons and annual net variable littoral drift towards north direction varies inside the crenulated shape of the bay from 2300 m^3/m to 4600 m^3/m with a cumulative annual net drift of 0.26 to 0.32 Mm^3as simulated through 1D model. The longshore sediment drift as estimated by empirical methods varies from 0.28 to 0.31 Mm^3 for a typical slope of sea bed and breaking wave height. The estimated littoral drifts with 1D model are in agreement with the sand transport 2D simulations and empirical estimations.

Keywords Hydrodynamics · Sediment · Sediment transport · Littoral drift · Bay

O. N. Singh (✉) · O. N. Singh (✉) · H. P. Singh
Department of Water Engineering and Management, Central University of Jharkhand, Ranchi, India
e-mail: iwemomsingh@gmail.com

B. Gopikrishna · J. D. Agarwal
MMCE Division, Central Water and Power Research Station, 411024 Pune, India
e-mail: gopikrishna.b@cwprs.gov.in

J. D. Agarwal
e-mail: agrawal_jd@cwprs.gov.in

P. V. Timbadiya et al. (eds.), *Coastal, Harbour and Ocean Engineering*, Lecture Notes in Civil Engineering 321, https://doi.org/10.1007/978-981-19-9913-0_24

1 Introduction

The coastal zone has become one of the most important activity zones in the world as it is thickly populated and has several industries and other establishments. Coastal zone development operations must be planned and organized within the context of well-defined Coastal Zone Management Plans. For the formulation of coastal zone management plans, a thorough understanding of coastal processes regulated by coastal hydrodynamics and the associated sediment movement is required. Winds, waves, tides, and currents are the forces that drive coastal hydrodynamics.

Sediment movement is a vector containing both longshore and cross-shore components at a site in the nearshore zone. Longshore transport is predominantly caused by wave-induced longshore currents, whereas cross-shore transport is mostly caused by wave orbital motion and coastal currents. Longshore sediment movement has been researched for over five decades. Certain elements of this transportation component, such as the impacts of grain size diameter, barred terrain, and longshore transport cross-shore dispersion, are still subject to substantial ambiguity. The focus on cross-shore sediment movement is new, having begun around a decade ago, therefore, the uncertainty in forecast capabilities (including the impacts of all factors) may be much higher. In certain instances, it might also be due to the absence of sufficient wave data or a poor knowledge of transport mechanisms that restrict the accuracy of predictions for the two components [1].

Alongshore sediment movement on beaches is caused by a combination of wave-induced current in the surf zone and turbulence caused by wave breaking. Longshore currents are significantly responsible for sediment transfer along the coast. Sand is carried in suspension as well as along the bed (suspended and bed loads, respectively). Where wave breaking is most active, i.e. at the breaker line for diving breakers but more equally scattered over the surf zone for spilling breakers, the suspended load is rather large [1]. The direction of longshore sediment transport determined by incoming waves direction, which in turn determined the direction of longshore current [2].

One of the most important variables influencing coastal geomorphology is littoral drift, also known as longshore sediment transport (LST) (CERC 1984). The coastal zone greatly influenced by troubling the natural conditions resulting in abrasion all along the coastline and sediment deposited along the shoreline behind the breakwater. The port officials spend millions of dollars each year on sand pumping operations and dredging to feed the down drift beaches. As a result, for successful coastal design and management, understanding of sediment transportation rates inside and near any harbour is vital. For effective and economic preservation in the coastal area, the differences between net and gross transport rates and the orientations for coastal drift are chiefly useful.

Many researchers in the past have applied the empirical theories that have been well calibrated for various sites [3] estimated sediment transport rates at Visakhapatnam coast using energy flux method. [4] applied well-known formulae CERC, Kamphuis, etc., to Kundapura coast, Central west coast of India. Reference

[5] applied CERC, Kamphuis and VanRijin for the coast located along Puducherry. Wherein among all, the methods used it was made clear that CERC and Kamphuis have greater estimates for low breaking wave heights than VanRijin and Kamphuis predicts longshore sediment transport for sites whose average wave heights are of the order of 1 m. Further increase in wave heights yields higher rates. Another important derivation by VanRijn (www.leovanrijn-sediment.com) by field and laboratory methods for sand, gravel, and shingle sized materials reveals that the longshore transport is proportional to wave height raise to power 3.1 and grain size to the power −0.6 and to the beach slope to the power 0.4. The longshore transport is significantly affected by the profile shape. In the present study, the crenulated shape of bay was chosen with different cross-shore profiles and estimate of longshore transport was done with both empirical as well as deterministic based methods.

2 Study Area and Data Source

A typical shore in the Car Nicobar Island was chosen which is located in Nicobar district of Andaman Nicobar groups of islands (Fig. 1). It is located geographically at 9 ° 14′27" N and 92 ° 46′53" E North of Car Nicobar Island. The mean sea level (MSL) of Car Nicobar Islands is at 1.0 m. The tide whose gauge located at eastern shore of the island shows that the tidal range is 1.8 m with highest high water during spring is at 1.95 m while lowest low water at 0.1 m. Similarly, the highest and lowest water levels during neap tide are 1.25 m and 0.75 m, respectively. Initially, the harbour was protected by a breakwater of length 490 m and a jetty of 90 m length on lee side of breakwater. The inter islands vessels started utilizing the facility from Jan, 2003. Earlier studies of CWPRS at the same location indicated with different layouts by extending and realigning the breakwater to achieve the required tranquil conditions (CWPRS technical report No 3855, 2002 and 4391 of 2006).

The tidal currents differ from place to place based on the tide's character, sea depth, and coast configuration. The sailing directions (Enroute) India and Bay of Bengal prepared and published by National geospatial Intelligence agency, Virginia of the year 2013 was referred for the data on currents and flow directions. It is mentioned that the tidal currents off Sawai Bay whose latitude 9°14' N and longitude 92°45' E and located South of MUS harbour in Car Nicobar Island set NE on the flood tide. The flow direction during NE monsoon is from South to North with the currents set ESE direction as observed at Kimois (9°07' N, 92°46' E). However, the location Kimois is existing at southern side of Car Nicobar Island which is beyond the study domain considered. Inside the harbour, the tidal currents were expected up to 0.2 m/s (CWPRS Technical report No 4391, 2006). Based on CWPRS Technical report No. 5891 (2020), the net annual littoral drift computed from mapping the imageries of different years is 0.3 Mm^3 (Million m^3) in the direction of North.

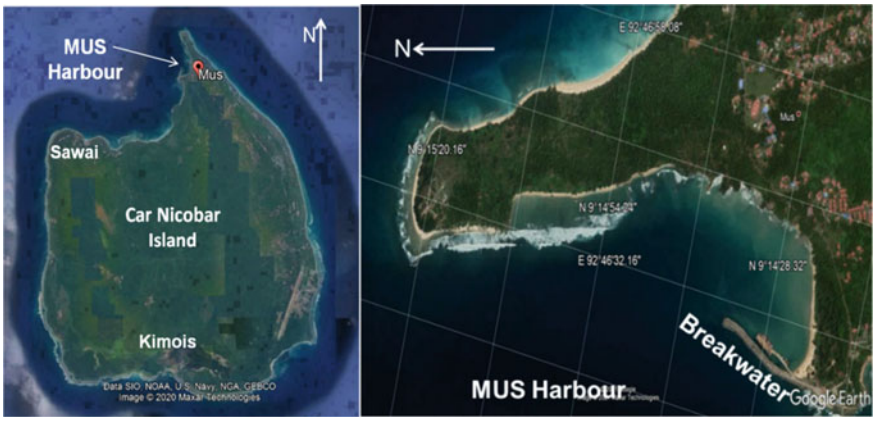

Fig. 1 Location of MUS harbour in Car Nicobar Island (Courtesy: Google Earth)

2.1 Data Used

The domain of the study area covering the large portion of the sea was chosen from C-MAP, 2020 developed by DHI, Denmark in order to reproduce the existing condition of the site in the model. The contour depths inside the harbour (Fig. 2) indicate that the depths are of the order of 10 m near the existing breakwater. The contours around the harbour took the crenulated shape of the bay nearshore from below 1.5 m to more than 25 m deep offshore parallel contours. The tide data were extracted by using a tool in Mike21 (Global Tide model) which predicts water levels at different location with respect to time by using harmonic coefficients of different locations. The sediment data with regard to bed samples were collected from the site at different locations, viz. Jetty and proposed sea wall at different chainages and sent to CWPRS by the project authority. The collected sediment was reanalyzed for different D_{50} sizes of the sediment at different locations and used for the present study. The D_{50} sizes at different locations inside the harbour are 0.24 mm, 0.21 mm, and 0.53 mm.

The ship data sailed in the offshore region between 8° N and 14° N and 90°–94° E reported by India Meteorological department (IMD) during the period of 1970 to 2000 were considered. The predominant directions during monsoon the waves approach from WSW, SW, SSW directions offshore with magnitudes up to 4.5 m. However, the frequency of these highest waves is very minimal in a year. The annual average offshore wave data as obtained from the measurements of the ship indicated that the frequency of about 10% of the period in a year the site is approached with waves of 3 m or more and 75% of the period with waves of 2 m or less. The frequency of waves in the range of 2 m to 3 m is less than 10% period in the year. Similar analysis for the SW monsoon indicated that the frequency of about 20%, 63%, and 14% of the periods in a year the waves approach the site with 3 m and above, 2 m and less, and between 2 and 3 m, respectively.

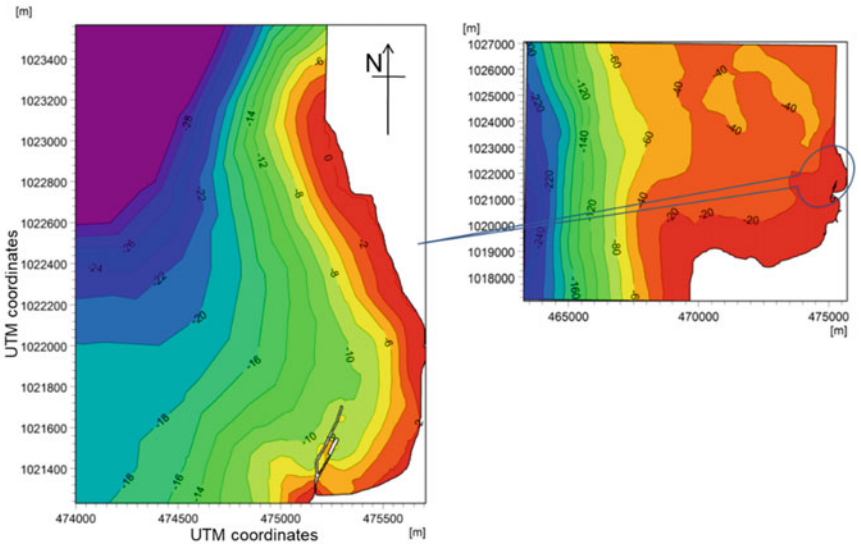

Fig. 2 Bathymetry of the area inside harbour extracted from C-Map, 2020

3 Methodology

3.1 Empirical Methods

In a true sense, computation of littoral drift is neither feasible in the field nor by any physical modelling techniques. However, traditionally some straight forward techniques involving short-term tracer experiments and longer-term trap experiments help in measuring longshore transport. The empirical formulations depend mostly on field measurements and remain site-specific. Empirical formulae correlate the transportation rate of longshore sediments with breaking point wave parameters. The wave parameter at the breaking point is the major source of input data for these empirical equations. Out of the most widely used empirical methods CERC (1984), Kamphuis (1991) formulae have been chosen based on data availability to estimate longshore sediment transport.

3.1.1 CERC (1984)

In CERC formula, the transport rate expressed as a function of wave height and wave incident direction at the breaker point [6]. LSTR was estimated by using empirical equation which relates longshore sediment transport rate to the longshore energy flux within the breaker zone. As per the CERC (1984) formula, the longshore sediment transport rate is given by

$$Q = \frac{K A \rho g H_b^2 T sin(2\alpha_b)}{64\pi}$$

where

A: $\frac{1}{(\rho_s - \rho)g(1-p)}$, Q: LSTR (m^3/yr.), H_b: Wave Height at breaker point,

K: Dimensionless empirical proportionality (0.39), g: Acceleration due to gravity, ρ_s: Sediment density, ρ: Sea water density, p: Porosity factor,

α_b : Angle between breaking wave and shoreline.

3.1.2 Kamphuis Formula (2002)

Based on laboratory tests and available field data, Kamphuis (1991) created an empirical formula that incorporates the beach slope, wave time, and sediment particle size. With further laboratory data and analysis, Kamphuis (2002) formula was shown to be relevant to both field and experimental data, and it is provided by

$$Q = \frac{2.27 H_b^2 T_p^{1.5} m_b^{0.75} d_{50}^{-0.25} sin(\alpha_b)}{(\rho_s - \rho)g(1-p)}$$

where
T_p: Wave Period (s), d_{50} : Sediment median grain size (mm), m_b: Slope of bottom in the surf zone.

The CERC formula has the advantage of being simple, allowing for the integration of contributions from waves received from different directions and the production of an analytical solution for LSTR estimation, but it ignores sediment size and longshore current it does not give more relevant values. As a consequence, Kamphuis can help with a better understanding of LSTR [4].

3.2 2D Numerical Modelling

3.2.1 Mike 21 HD (FM)

MIKE21 (FM) software, 2020 of DHI, Denmark has been used to set up hydrodynamics model in two dimension. The flexible mesh of MIKE21 is an unstructured mesh uses a cell centred finite volume solution technique based on linear triangular elements. A suitable mesh is essential for obtaining reliable results from the HD model. Setting up the mesh includes selection of the appropriate area to be modelled, adequate resolution of the bathymetry. The resolution in the geographical space must be selected with respect to stability considerations. The primary input to the model is the bathymetry of the area. Keeping in view the study region, i.e. harbour in the bay,

the domain of about 13 × 10 km was chosen to avoid boundary effects in around the harbour. The study area was discretized into number of elements and nodes utilizing flexibility inherited in the unstructured meshes. The existing condition of the harbour is shown in (Fig. 2). It is observed that the deep-water contours are aligned along the shore for some distance and later become parallel to the deep-water contours of the sea. The bathymetry of the study area was prepared using the land and water points extracted from C-Map database of DHI group.

The most critical aspect of any modelling methodology is to replicate field phenomena, which necessitates calibrating and validating the model against established observations. Calibration parameters include chezy's coefficient and eddy viscosity, which are adjusted to refine the model. The east coast circulation pattern suggests that the flow from West to East occurs during the SW monsoon, i.e. June to September. The Sawai Bay is subjected to NE currents. The HD model was simulated for existing condition for a typical period of two weeks (28-07-2020 to 12-08-2020) which includes spring tide, neap tide, and average tides. Similarly, HD model was simulated for NE monsoon covering the period from 7-11-2020 to 18-11-2020 covering all phases of tide. For the simulation during this period, the boundaries are adjusted such that the flow take place from South to North by adjusting slope of the water boundary.

3.2.2 Mike 21 ST (FM)

Mike 21 (sediment transport) ST module calculates the resulting transport of non-cohesive materials based on the flow conditions alone or combination of flow conditions with wave conditions in two dimensions while considering the morphological evolution in the model. The Sand Transport Module of Mike 21 is applied to the study of engineering problems such as sediment transport studies for non-cohesive materials or sand/ mud mixtures in estuaries and coastal areas. The solution to the sediments transport is achieved by solving the Advection Dispersion equation upon integrating over time explicitly. Because of the stability constraint imposed by adopting an explicit scheme, the time step interval must be chosen so that the Courant-Friedrich-Levy (CFL) number is less than one. In the calculation, a variable time step interval is employed, and it is set so that the CFL number in all computing nodes is less than a critical CFL number. This model can well be applied to the regions of transport of sediments in and around estuaries or inlets where sediment grading coefficient is less than 1.6 and mean grain diameter is greater than 0.15 mm. The flow chart representing the computation of sediment in terms of erosion and accretion is shown in Fig. 3.

Having calibrated the HD model for water levels and velocities, ST model has been set up considering hydrodynamic conditions. The coupled HD and ST model is simulated for existing condition for both the monsoon seasons for the same period as that of HD simulation periods covering spring, neap, and average tides. Before beginning the simulation for the sediment transport, the model requires generating the sediment tables that can accommodate the values of different sizes of sediment

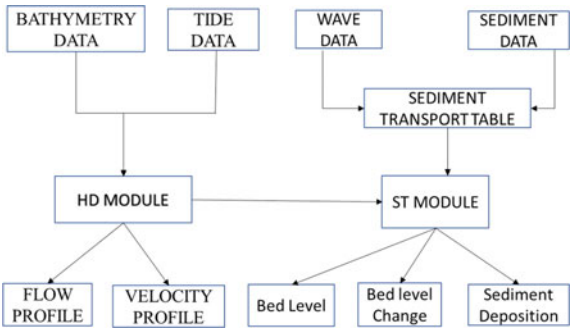

Fig. 3 Flow chart representing the coupled HD and ST simulation (MIKE DHI manual, 2021)

and different wave characteristics within the limits as per site conditions. The range of variations of every parameter relevant for sediment transport has been specified while generating the table. The waves and current theory for the sediment model has been used for simulations. The mean grain size diameter of 250 microns has been assumed to simulate the model. A major assumption in calculating deposition and erosion of sediment is that the spatial distribution of the bed-material D_{50} remains constant in time. The validity of this assumption is particularly at a specific site and the time scale under consideration.

The analysis of different years of imageries was considered to identify the pattern of deposition and erosion inside the harbour all along the shoreline. The bed-level change was simulated in the model for two weeks covering spring and neap tides. This pattern of changes in morphology well agrees with that of the analysis of imageries.

3.2.3 1D Numerical Modelling

DHI Water and Environment has created LITDRIFT module in LITPACK software package. Various beach and coastal evaluations are available, and the software package is integrated into a module of sediment transfer, i.e. sediment transport module (STP). LITDRIFT is a programme that simulates littoral drift and sediment movement along shorelines. The littoral drift for each wave condition, as well as the overall sediment budget for the year, is the model's outputs.

When waves come close to the shore, they shoal and finally break. This results in the release of energy, which is utilized for sediment re-suspension and the induction of a shore-parallel current. It is feasible to calculate the littoral drift precisely using wave data and the parameters of the coastline profile.

Three main forms of input are used in the simulations.

- The annual and seasonal wave climate file of arriving waves. This file comprised of frequency distribution of wave heights and directions.
- The profile description. This involved bathymetry, grain size diameter, bed roughness, properties of sediment about each cross-shore profile.

- Input file. The wave climactic file and description of the profile are described in this file, along with the solution approach.

The module simulates the shoreline distribution for each coastal profile of wave height, configuration and longshore current. It gives a complete deterministic description of the cross-shore distribution of along shore sediment drift under regular and irregular circumstances at sea for any bathymetry.

Since the bay is having crenulated shape and movement of the drift is not constant along the curved path of the shoreline, littoral drift was computed at three cross sections to understand the site condition. The three cross-shore profiles considered were up to 20 m contour depths. One in the North (Profile 1), other in the Centre of bay (Profile 2), and South (Profile 3) sides (Fig. 4). These cross-shore profiles were interpolated offshore to onshore with grid interval of 5 m. It is observed from North profile to South profile the distance of the 20 m contour from the 5 m contour is increased from 375 to 1100 m. The distance between these contours at the centre of bay is at 700 m. Thus, this indicates the deeper contours gradually taken the shape of the bay.

The primary input to the model is the annual wave climate. This was obtained from averaged ship observed wave climate of 30 years. From the data of the waves, it is observed from the annual data that the predominant direction of waves takes place from South to North. As a part of calibration process, the roughness value was so adjusted to meet the drift of the site condition as estimated in CWPRS technical report No 5891 (2021). A sensitivity analysis on roughness indicated that the transportation of drift decreases with the increase of roughness. The same has been obtained with all the cross-shore profiles considered in the study.

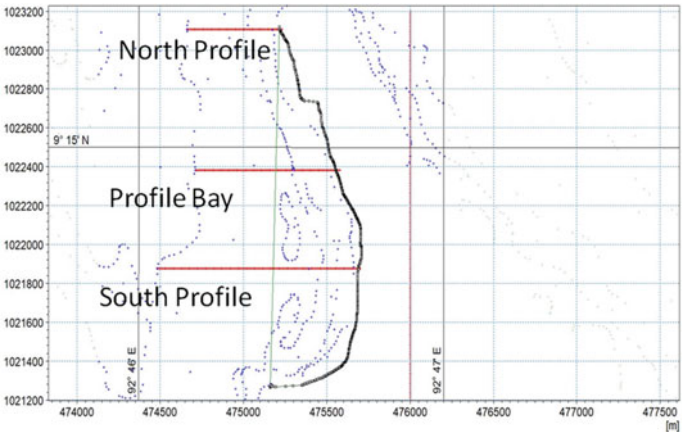

Fig. 4 Cross-shore profiles considered along the shoreline inside the bay

4 Results and Discussions

4.1 Empirical Based Estimation of Littoral Drift

The longshore drift was estimated by two methods, i.e. CERC (SPM 1984) and Kamphuis (Gowthaman et al. 2015) methods. The sensitivity analysis with different breaking wave heights and sea bed slopes was done to arrive at the longshore drift at the site. An attempt has been made to compute the drift by substituting the values of the following different variables.

K = 0.39, g = 9.81 m/s^2, p = porosity = 0.4, ρ = 1024 kg/m^3 ρ_s = 2650 kg/m^3, T = 8 s, $\alpha_b = 1^0$, $m_b = 0.2$

The longshore drift by CERC formula was estimated to be 0.287 Mm^3 and 0.138 Mm^{3}with different angles of wave approach to the shoreline and heights up to 4 m (Fig. 6). From the figure, it is noted that variation of drift magnitude is highly sensitive to the angle of wave approach. In comparison to the CERC method, Kamphuis considered T_b(10 s) and m_b (slope at bottom in surf zone) as additionally influencing variables. By substituting all the variables in the above equation, the influence of bed slope was studied here and the maximum slope obtained is used for different values of breaking wave heights (Fig. 5). The variation of littoral drift with different breaking wave heights is given in Table 1. The estimation of the drifts at the site by empirical formulae is well comparable with breaking wave height of 4 m with sea bed slope at surf zone of 0.2.

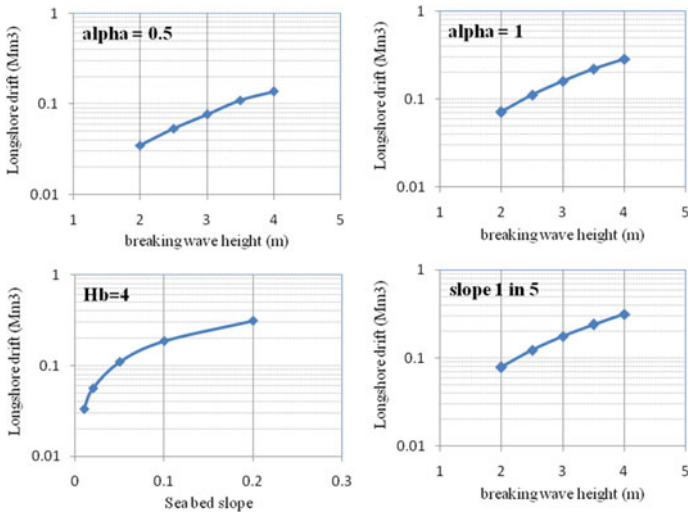

Fig. 5 Variation of longshore drift by different influencing variables

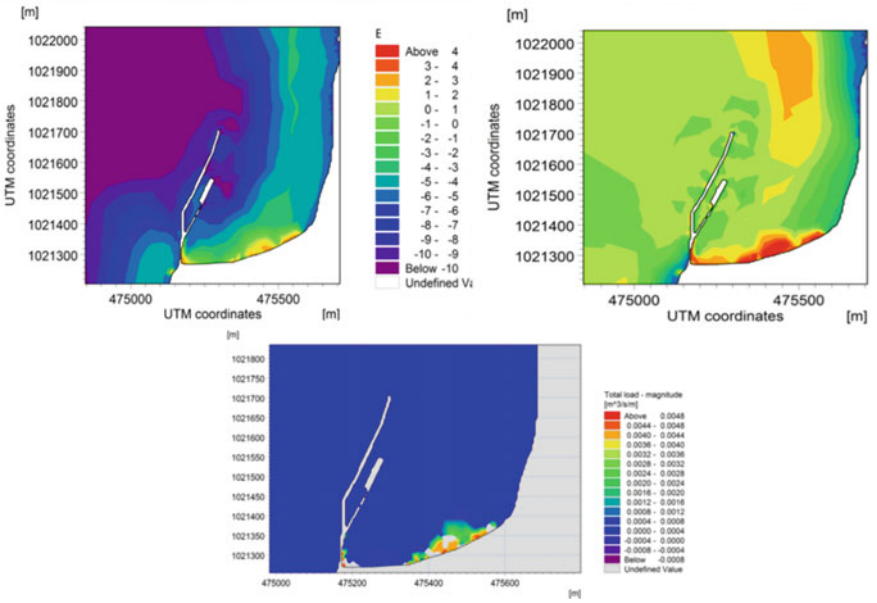

Fig. 6 Bed level, bed-level change, sediment deposition for 3 m significant wave height in SW monsoon

Table 1 Variation of littoral drift with different wave heights ($m_b = 0.2$)

Breaking wave with a bed slope of 1 in 5	2	2.5	3	3.5	4
Littoral drift per year (Mm^3)	0.0785	0.123	0.176	0.24	0.314

4.2 Deterministic-Based Estimations of Littoral Drift

4.2.1 2D Model

The results of the coupled model of hydrodynamics indicated that the deep sea velocities are of the order of 0.6 to 0.8 m/s in both the monsoon seasons and 0.1 to 0.2 m/s inside the harbour. The sediment transport model with hydrodynamics quantitatively reveals that certain amount of deposition at the coast adjacent to breakwater on the lee side. The deposited sediment in the SW monsoon period of four months has been ascertained to be 2220 m^3/m which leads to change in bed level between 3.0 m and 5.0 m. The rate of bed level varies from 0.6 m/day to 1.0 m/day behind the breakwater and beyond breakwater along the shoreline varies from −0.2 m to −0.8 m. The net change in bed level (Fig. 6) simulated to be significant by the end of the simulation since the 3 m significant waves were imposed constantly from SW direction throughout the simulation whose root mean square (RMS) wave height is of the order of 2 m.

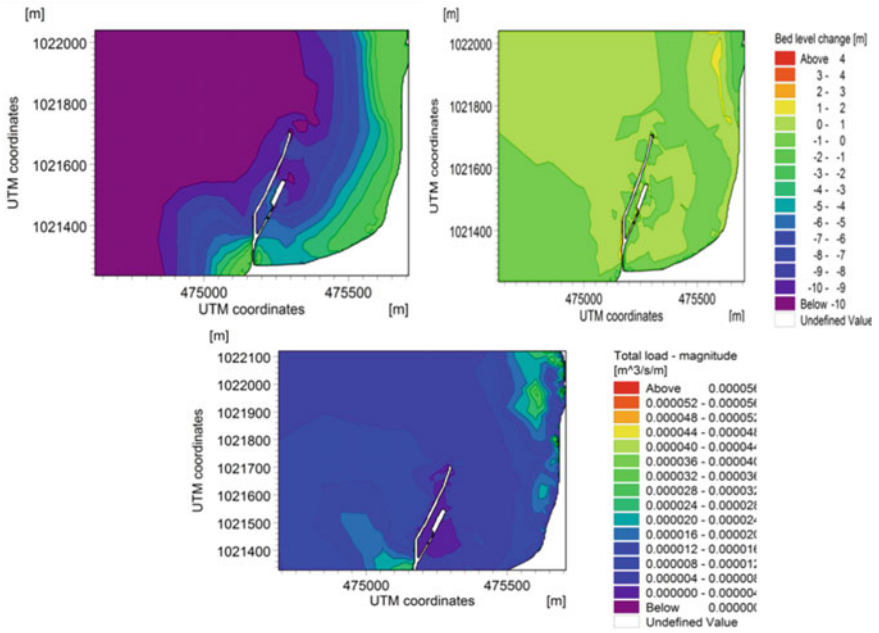

Fig. 7 Bed level, bed-level change, sediment deposition for 1 m significant wave height in SW monsoon

The existing condition with breakwater and jetty shows that the sediment deposited along the shoreline behind the breakwater and erosion all along the shoreline in the bay. The similar results with 1.5 m significant (RMS of 1 m) wave height imposed in the model from SW direction and NE directions are shown in (Fig. 7) and (Fig. 8). The flow direction in NE monsoon from south leads to flow from North to South inside the harbour due to crenulated shape of bay that causes marginal deposition along the shoreline. The sediment depositions with these magnitudes of waves inside the harbour is negligible as compared to that with 3 m significant waves. Since the known observations on sediment deposition are not available, these magnitudes of deposited sediment are to be correlated with that of 1D model results.

4.2.2 1D Model

Littoral drift was computed at three cross sections to understand the site condition (Fig. 4). This involved the use of roughness and fall velocities of sediments determined during the calibration of the shoreline model. The bed roughness and depth of closure played a crucial role in calibrating the shoreline model. The area is subject to longshore littoral drift towards North at an estimated 0.3 Mm^3. This value so arrived was based on the validation of the shoreline model by using a set of shorelines delineated from geo-referenced Landsat imageries (Technical report No 5891, Nov 2020).

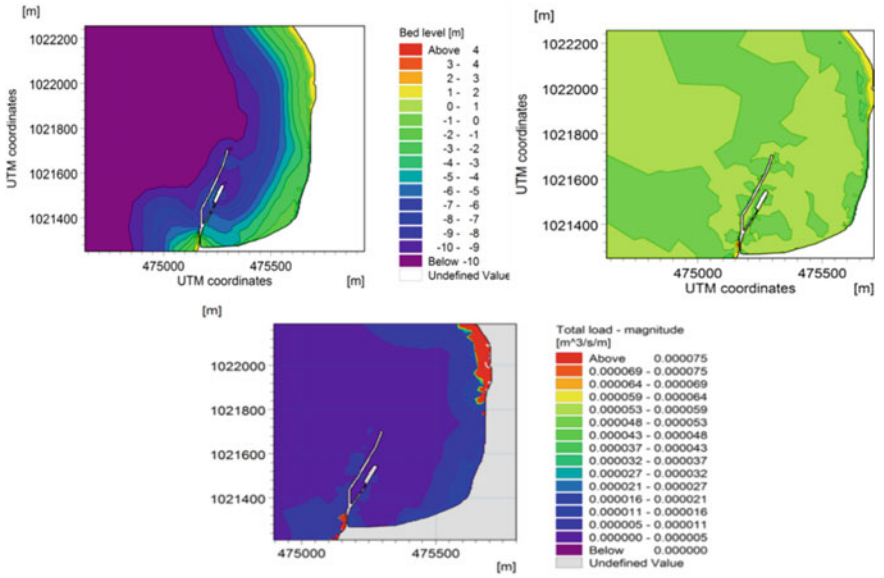

Fig. 8 Bed level, bed-level change, sediment deposition for 1 m significant wave height in NE monsoon

Here in this study, the littoral drift model was calibrated to obtain the drift prevails in the area by modifying the roughness in a set of experiments.

The net drift towards North based on profile south was estimated to be of the order of 5900 m^3/m/year and their accumulated drift estimated as 0.32 Mm^3. The roughness obtained was used for estimating drift with Profile Bay. The annual drift towards North estimated to be 0.26 Mm^3 indicating some amount of deposition to the extent of 0.06 Mm^3. The net drift of the order of 4600 m^3/m/year towards North was estimated in SW monsoon. Had there not been any breakwater constructed, the littoral drift of 0.32 Mm^3 per year would have transported into the harbour. Further away from the bay towards North profile, i.e. 0.29 Mm^3 with annual net drift of 5580 m^3/m/year was estimated by the model.

The seasonal littoral drift based on the seasonal past wave climate was also estimated. It is found from the computation of littoral drift in all the seasons the net drift is in the predominant direction of waves in the study area i.e. towards north with little or no transport towards south. The littoral drift computations for all the seasons and annual for all the profiles considered in the model were tabulated (Table 2). From the table, it can be inferred from the SW monsoon and annual observations the littoral drift contribution in SW monsoon alone contributes to 80% of the annual contribution.

The littoral drift is estimated by keeping constant grain size diameter. While calibrating the model for littoral drift, an attempt has been made to estimate the same with variable grain size diameter from offshore to onshore. The results indicated at no deviation in the estimation because of steeper slopes of the sea bed prevail in

Table 2 Annual and seasonal drifts for different profiles along the shoreline

Season	Net drift (m^3/m)	Accumulated net drift (Mm^3)
Annual (North)	5580	0.29
June-Sept (SW)	3220	0.23
Oct–Jan (NE)	420	0.027
Feb–May (Non-Monsoon)	429	0.028
Annual (Profile Bay)	4505	0.26
June–Sept (SW)	2366	0.21
Oct–Jan (NE)	360	0.035
Feb–May (Non-Monsoon)	366	0.035
Annual (profile South)	5900	0.32
June-Sept (SW)	4620	0.31
Oct–Jan (NE)	500	0.022
Feb–May (Non-Monsoon)	505	0.022

the area. This confirms that our assumption regarding grain size diameter assumed constant was correct. The hydraulic bed roughness value varies from 0.002 to 0.01 for an annual wave climate and SW monsoon seasons as well for all profiles considered.

5 Conclusions

The longshore sediment transport has been estimated by different methods, viz. empirical methods, 1D as well as 2D numerical models. The empirical methods like CERC (1984) and Kamphuis (2002) were applied. The annual longshore sediment transport was estimated to be 0.28 and 0.31 Mm^3, respectively, with the two methods. The 2D coupled model simulated the hydrodynamic flow conditions for different seasons and further the pattern of deposition and erosion under a set of wave conditions in different seasons. The model simulates the pattern of sediments under the impetus of 3 m significant waves constantly from SW direction and leaves inside the harbour at an average rate of 2200 m^3/m by the end of SW monsoon. Similarly, study with 2 m waves from the same direction leaves negligible sediment in the same location. This emphasizes the mobility of the sediment for 3 m or higher is significant for sediment deposition. The annual net littoral drift in the area outside the bay from the results of 1D model is towards North and is estimated to be 0.32 Mm^3 and inside the bay 0.26 Mm^3. Out of the SW monsoon and annual estimations, the littoral drift contribution in SW monsoon alone is 80% of the annual contribution. The variable net littoral drift with wave climate derived for SW monsoon contributes to about 2300 m^3/m to 4600 m^3/m as estimated for different profiles through 1D model. Both the numerical models estimated insignificant quantities in other seasons. The estimated littoral drifts with 1D model are in agreement with the sand transport 2D simulations and empirical estimations.

Acknowledgements The author(s) is thankful to Shri. A.K Agrawal Director, CWPRS for his kind permission for carrying out the studies at CWPRS and publication of this paper.

References

1. CWPRS Technical report No 5891 of Jan, 2021
2. Sorensen RM (2006) Basic coastal engineering. Springer Science+Business Media
3. Shetty A, Jayappa KS (2020) Seasonal variation in longshore sediment transport rate and its impact on sediment budget along the wave-dominated Karnataka coast, India. J Earth Syst Sci 129(1). https://doi.org/10.1007/s12040-020-01504-y.
4. Sarmat KGS, Reddy BSR (1988) Longshore Sediment Transport near Visakhapatnam Port, India
5. Shanas PR, Sanil Kumar V (2014) Coastal processes and longshore sediment transport along Kundapura coast, central west coast of India. Geomorphology, 214:436–451. https://doi.org/10.1016/j.geomorph.2014.02.027.
6. Rajab PM, Thiruvenkatasamy K (2017) Estimation of longshore sediment transport along Puducherry coast, Eastcoast of India; based on empirical methods and surf zone model
7. George J, Sanil Kumar V, Gowthaman R, Singh R (2020) Author Version of 2020

Extension of Breakwaters and Restoration of River Mouth Atkasargod Fishery Harbour, Kerala

Shivani Sahu, Jiweshwar Sinha, B. L. Meena, and Prabhat Chandra

Abstract Coastal areas play a vital role in the socio-economic development of a country because seaborne trade remains the cheapest method for importing and exporting large quantities of merchandise all around the world. Kasargod Fishing Harbour (12° 28′ 32.71" N and 74° 59′ 36.14" E) in Kerala state is situated at the confluence of the Northern creek and the downstream of the river Chandragiri. With the help of mathematical model studies from the considerations of wave tranquillity and littoral drift, a 700-m long curved breakwater as extension of northern breakwater was evolved to provide protection and tranquil conditions at the inlet, which would help in manoeuvring of the trawlers/boats of the fisherman through the entrance of inlet channel. A depth-averaged numerical model using MIKE 21 FM software has been developed to study tidal circulation in the creek inlet and nearshore region and to assess the changes likely to occur in hydrodynamics and siltation pattern in navigational channel and harbour region due to the proposed expansion. The model studies indicated that the maximum current magnitude of the order of 0.5 m/s and 0.75 m/s occurred in the inlet channel during non-monsoon and monsoon season, respectively. During high flow in the monsoon season, only ebb currents would persist in the inlet channel and during ebbs, irrespective of seasons a circulation always persists on the south side of the southern breakwater. Also, it is indicated that as compared to other nearby regions, sediment deposition in the inlet channel is quite less. However, a maintenance dredging of in the inlet channel would be required periodically for smooth functioning of the channel and manoeuvring of fishery boats.

Keywords Fishing harbour · Tide · Wave induced currents · Creek inlet and navigational channel

S. Sahu (✉) · J. Sinha · B. L. Meena · P. Chandra
Central Water and Power Research Station, Khadakawasla, Pune 411024, India
e-mail: sahushivani.cwprs@outlook.com

P. V. Timbadiya et al. (eds.), *Coastal, Harbour and Ocean Engineering*, Lecture Notes in Civil Engineering 321, https://doi.org/10.1007/978-981-19-9913-0_25

1 Introduction

Coastal zones are continually changing because of dynamic interaction between the ocean and land. Tides, waves, winds and currents are responsible for depositing sediment on a continuous basis along the Kerala coast. Deposition of sediment results in the formation of characteristic coastal landforms such as beaches, barrier and sand bars along the coast. The process of sediment transport and deposition can change the topography of the bed level of coastal area. The bypassing of littoral drift is a major cause of sedimentation in the harbours which are within surf zone.

Kasargod Fishing Harbour situated at the confluence of the northern creek and the downstream of the river Chandragiri in the West Coast of India in Kerala state. This fishing harbour is exposed to the waves and tides from the Arabian Sea. In the past years, sand bar movements were very versatile in nature along the coast, due to the littoral drift prevailing at the entrance of inlet gut as shown in Fig. 1a. Further, post construction of the breakwaters and the closure of the natural channel, net deposition of sediment occurred near both the breakwaters in recent years in Fig. 1b. Post construction of breakwaters causes the navigational problems for fishing crafts due to prevailing high wave and current actions in the entrance of the channel. It is likely that apart from littoral drift, the tide induced sediment transport may also have contributed deposition of sediment near the inlet channel causing inconvenience to the fishermen. In order to ease the difficulties of fishermen against the wave and the littoral actions near the entrance of channel, it is proposed to evolve a suitable layout of breakwater structure by extending the existing north breakwater and to restrain the fall of littoral sediment into the channel as well. As far as southward drift is concerned, northern breakwater is partially blocking the drift and remaining part enters into the harbour. From the considerations of wave tranquillity and littoral drift, an optimized breakwater layout with extension of 700 m.

In the present paper, the detailed mathematical model studies using MIKE 21 HD and MT (MIKE 21 Scientific background) have been carried out to assess the impact on tidal hydrodynamics and tide induced sediment transport due to the optimized breakwater layout.

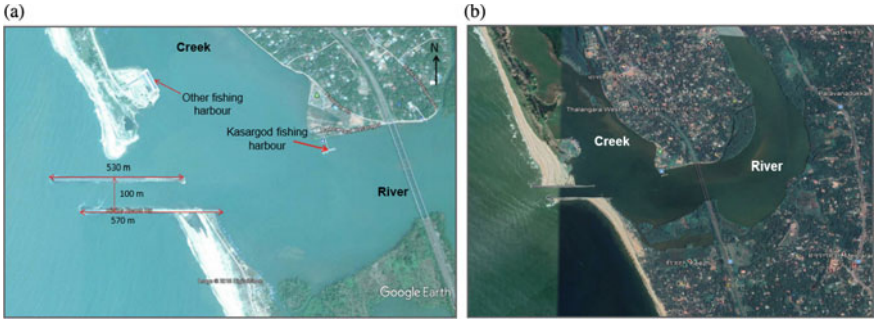

Fig. 1 **a** Fishing harbours and Intake channel. **b** Wave and current actions and net deposition after construction of breakwaters

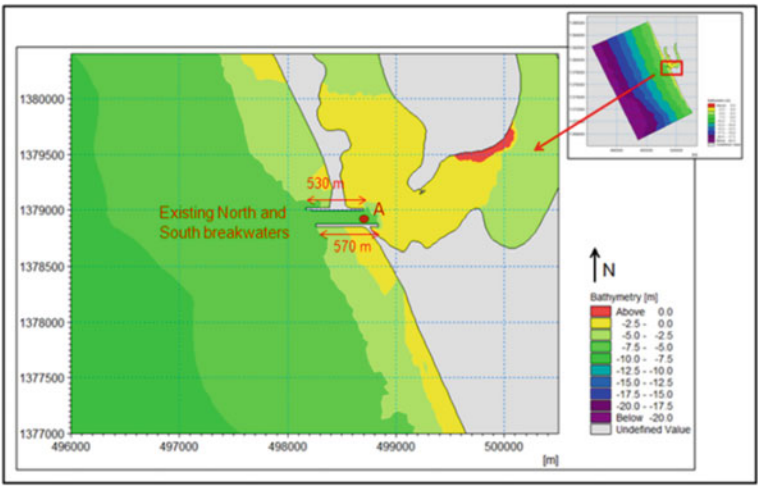

Fig. 2 Existing model bathymetry

2 Data Analysis

The basic inputs for hydrodynamic and sedimentation studies are mainly bathymetry, tidal data, wave data, current data, sediment characteristics, suspended sediment concentration, etc. Bathymetry of the area under the existing conditions is digitized from the hydrographic chart and from MIKE 21 C-map data as shown in Fig. 2, which includes land region in the east and offshore region up to −21.0-m depth contour in the west. In the east side, Kasargod fishery harbour exists at the right bank of River Chandragiri, where depth contours are available in the range of −2.0 to −3.0 m.

Tides in the region are semidiurnal with pronounced diurnal inequality having considerable difference in the tidal ranges and the elevation of low waters and high waters in the successive tidal cycles. The spring tidal range is about 1.6 m, while neap tidal range is 0.2 m as depicted in Fig. 3.

Water level, tidal current and current direction were observed at location A (Fig. 2) in the inlet channel for a period of seven days during the non-monsoon period as shown in Fig. 4a–c. The observed data was used for calibration in the model.

3 Mathematical Model

In order to simulate dynamics of cohesive sediment, it is necessary to initially compute the hydrodynamics of water body in terms of velocity and water level fluctuations. MIKE 21HD model has been used for simulating hydrodynamics, while MIKE 21 spectral wave (SW) model has been used to simulate wave induced stress which is input to MIKE 21 HD model. MIKE 21HD model is based on the numerical

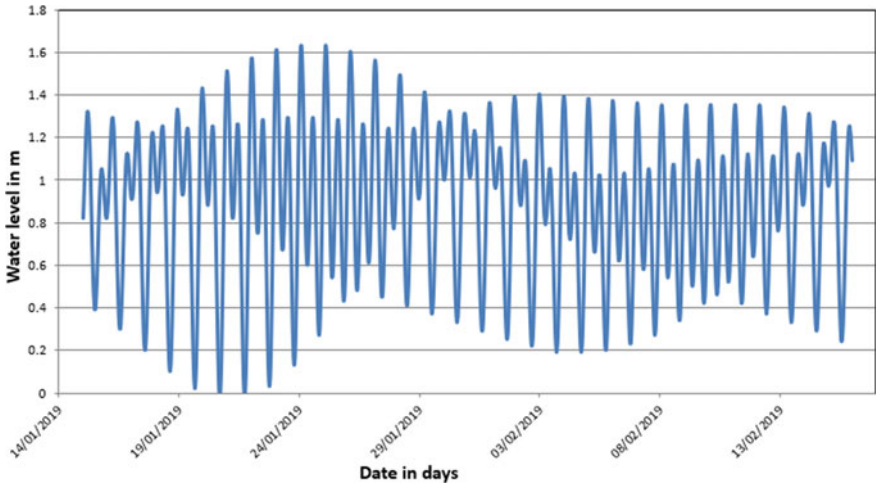

Fig. 3 Tidal level at Kasargod used as boundary

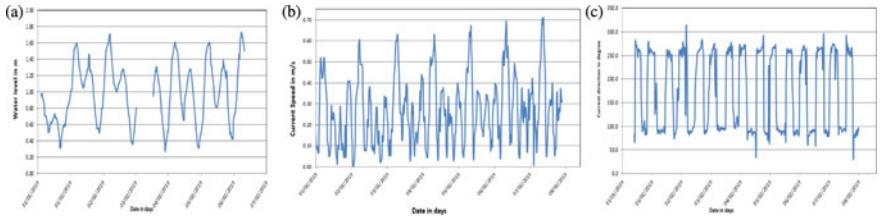

Fig. 4 **a–c** Observed water level, current speed and current direction at Location A

solution of the two-dimensional incompressible Reynolds averaged Navier–Stokes equations invoking the assumptions of Boussinesq and of hydrostatic pressure. The spatial discretization of the primitive equations is performed using a cell-centred finite volume method.

Further for simulating sediment transport, Mud Transport Model (MIKE 21MT), which is based on advection–dispersion equation, was used which describes erosion and deposition of mud or sand/mud mixtures under the action of currents and waves. The two-dimensional depth-averaged sediment transport model (MIKE 21MT) takes into account conservation of mass of sediment, depth-averaged velocities, longitudinal dispersion coefficient, lateral diffusivity, settling velocity, critical deposition stress and critical erosion stress for the given sediment. The numerical values of these parameters were modified within their range such that the prevailing sedimentation pattern in the vicinity of existing harbour area is achieved.

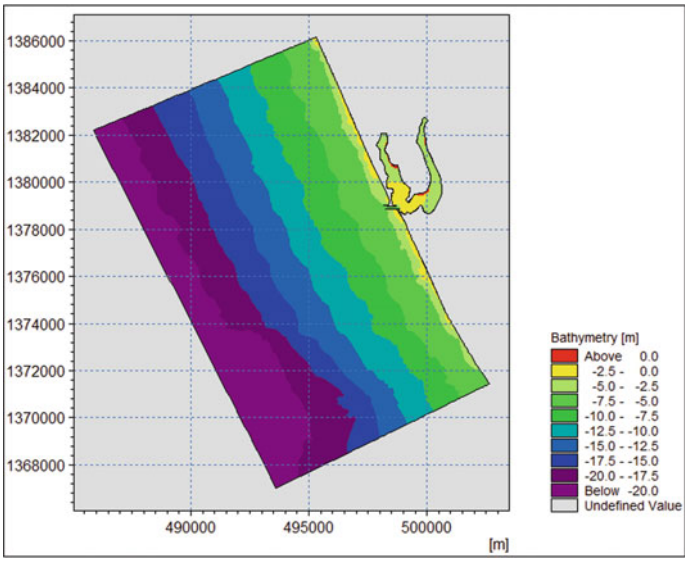

Fig. 5 Bathymetry for simulation in existing conditions

4 Model Simulation and Calibration in Existing Condition

Objective of mesh generation is to divide the whole model in to a number of individual triangular flexible cells to perform the fast and accurate computation. Digitized data from hydrographic charts provides bathymetric information and extracted data from MIKE C-Map about the study site was used for mesh generation. Land boundaries were incorporated with the generated flexible mesh, and bathymetry was prepared through the interpolation of the data incorporate with the generated mesh.

The two-dimensional hydrodynamic model of the Kasargod fishery harbour have been calibrated against water level, current speed and direction at locations 'A' (Fig. 2) comparing the model results with field measurement to make the model performance to a satisfactory level. A calibration of water level, current speed and direction between observed and simulation at −7.0-m depth contours is given in Fig. 6a–c.

The model simulation for hydrodynamic and siltation was carried. The tidal data was imposed as boundary condition and at the other end of the channel near the existing port; river discharge was imposed as a boundary condition. Instantaneous flow fields under existing condition in non-monsoon season are presented in Fig. 7a, b.

Hydrodynamic model under existing condition was run for monsoon period. For monsoon period, time series of a hypothetical discharge in the form of discharge hydrograph from the river were adopted as boundary conditions at the upstream end of the creek and the river. During monsoon period, maximum current magnitude of

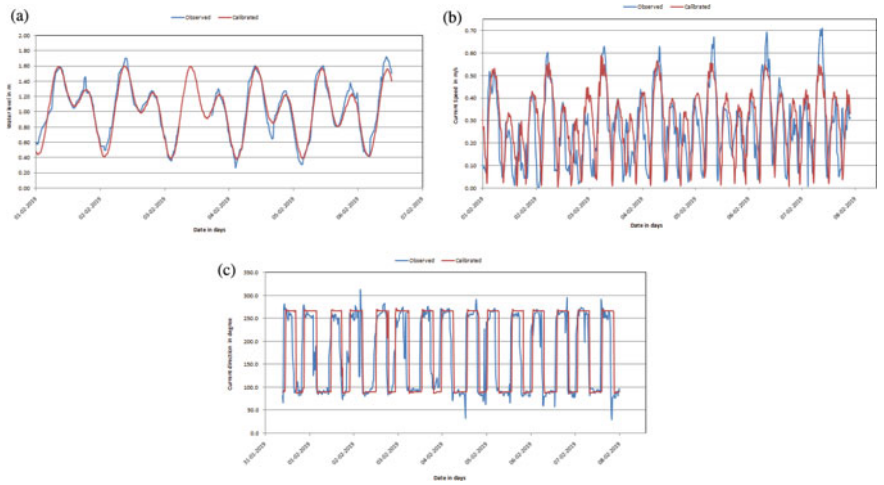

Fig. 6 **a** Comparison of water level. **b** Comparison of tidal currents. **c** Comparison of current direction

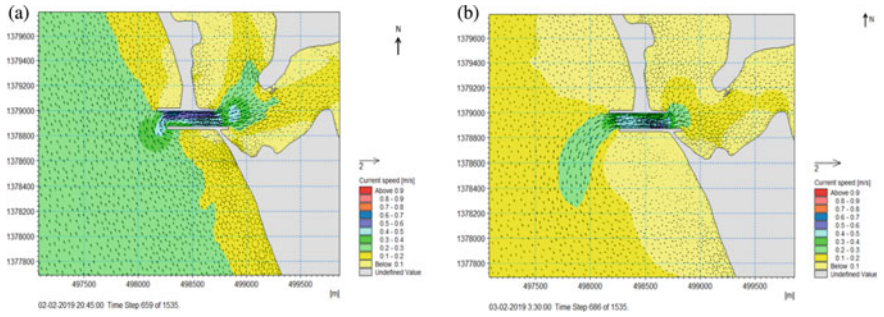

Fig. 7 **a**, **b** Instantaneous flow field during flooding and ebbing under existing condition

the order of 0.75 m/s was noticed in the inlet channel as depicted in Fig. 8, where length of vector represents the magnitude of flow and arrowhead shows the direction of flow.

Sediment transport model was run for non-monsoon season and monsoon season for a period of 15 days continuously under the prevailing site condition. The time series of a hypothetical sediment concentration discharge from the river and the creek was imposed as boundary conditions in the creek upstream and the river for monsoon season. The result in terms of change in total bed thickness at the end of simulation period is shown in Fig. 9a, b. Non-monsoon and monsoon both the seasons lesser sediment deposition occurred in the inlet channel as compared to its upstream and downstream regions.

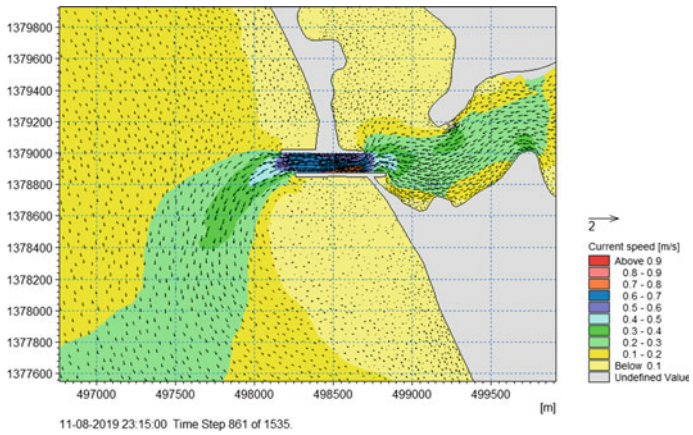

Fig. 8 Maximum current speed under existing condition during monsoon

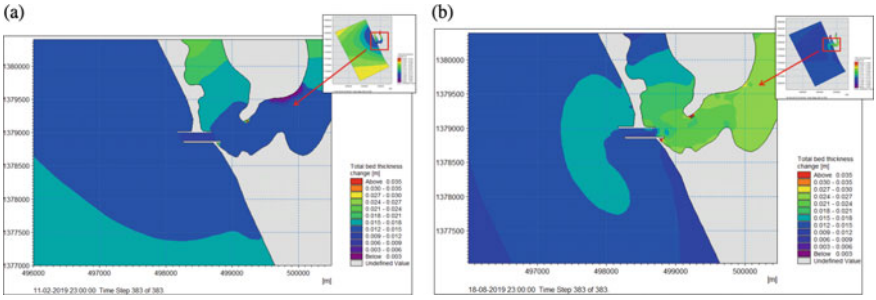

Fig. 9 **a** Simulated siltation pattern in non-monsoon. **b** Simulated siltation pattern in monsoon

5 Model Simulation for Modified Layout

The optimized layout of the breakwater extension based on wave tranquillity and littoral transport studies was simulated under proposed condition, wherein northern breakwater is proposed to be extended by 700 m in curved shape. The model was setup for the proposed condition with bathymetry as depicted in Fig. 10.

In order to visualize the probable changes occurring in hydrodynamics and siltation pattern, the hydrodynamic and sediment transport model was run for non-monsoon and monsoon periods. Instantaneous flow fields during both flooding and ebb tides for non-monsoon period are plotted as shown in Fig. 11a, b. It could be observed that magnitude of maximum current at creek inlet was almost similar to observed currents during non-monsoon period under existing condition.

During monsoon period maximum current magnitude are plotted as shown in Fig. 12. From the figure, it could be observed that magnitude of maximum current at creek inlet in proposed condition was almost similar to that observed during monsoon

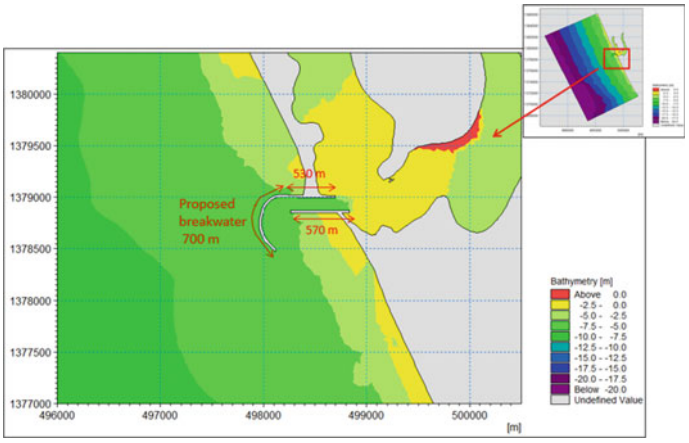

Fig.10 Model bathymetry used in simulations under proposed condition

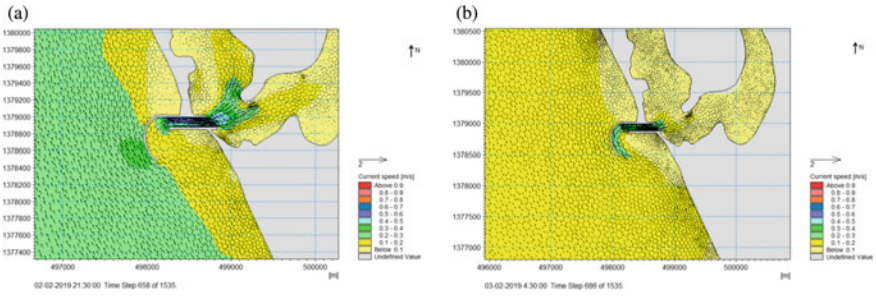

Fig. 11 **a**, **b** Instantaneous flow field during flooding and ebbing under existing condition

period for the existing condition. It is also seen that during ebb tides, circulations occurred on the south side of the southern breakwater.

The simulated sedimentation pattern in the model area at the end of the seasons was depicted in Fig. 13a, b which shows that sediment deposition of the order of 0.012 m is traced at the upstream of the inlet channel in non-monsoon, and in monsoon sediment, deposition occurred in the region is similar to that of the existing condition.

6 Model Results and Discussions

In order to visualize the flow behaviour and accretion of sediment in existing and proposed scenarios, two locations (Locations C1 and C2) are selected in model area as shown in Fig. 14.

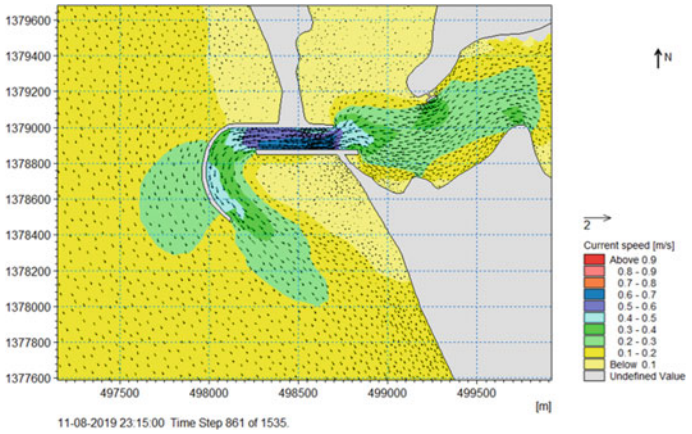

Fig. 12 Maximum current speed under proposed condition in monsoon season

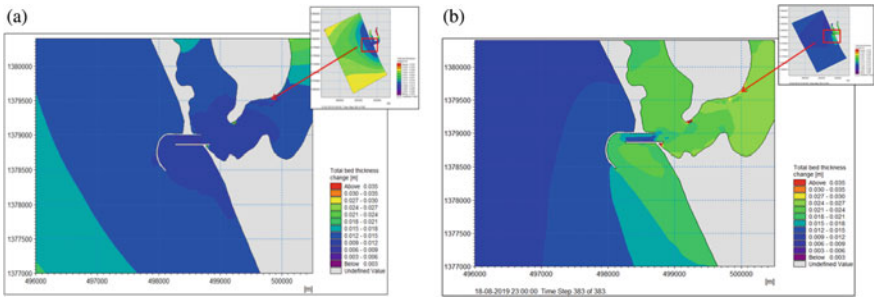

Fig. 13 **a** Simulated siltation pattern in non-monsoon. **b** Simulated siltation pattern in monsoon

Time series plot of flow speed at these locations under existing as well as under proposed scenarios (monsoon and non-monsoon). The variation of current speed at locations C1 is almost same both in the existing and the proposed conditions and at location C2 decreases by about 50% during flooding in the proposed condition as compared to the existing condition due to the curved shape of the breakwater extension as depicted in Fig. 15a, b.

From the simulation results of sediment transport model, lesser sediment deposition occurs in the inlet channel as compared to its upstream and downstream regions. Sediment deposition is traced in the lee side of both the breakwaters. Rate of siltation during non-monsoon period at locations C2 in the inlet channel between the existing and the proposed conditions is shown in Fig. 16a, b. It could be observed that siltation at locations was less in proposed condition during non-monsoon as compared to the existing condition and vice versa in monsoon.

However, it is observed in the region in front of the curved portion of the proposed extension of the northern breakwater sediment deposition of the order of 6300 cum

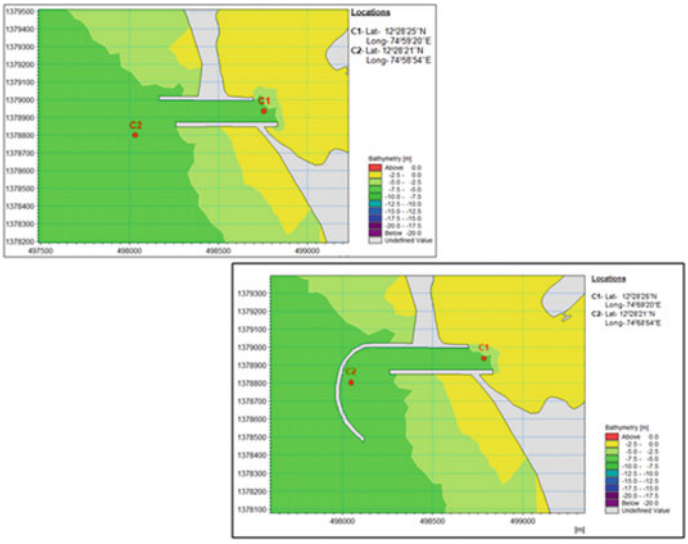

Fig. 14 Locations selected for comparison of variation in current speed

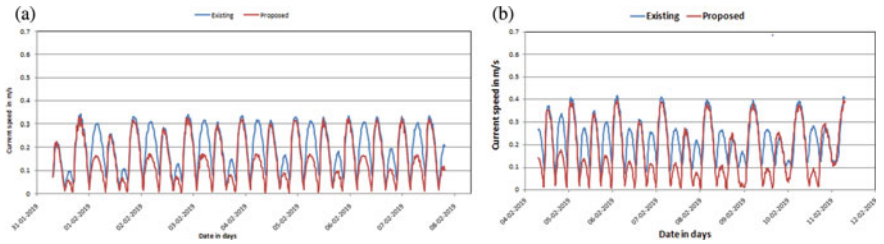

Fig. 15 **a** Current speed at location C2 in non-monsoon. **b** Current speed at location C2 in monsoon

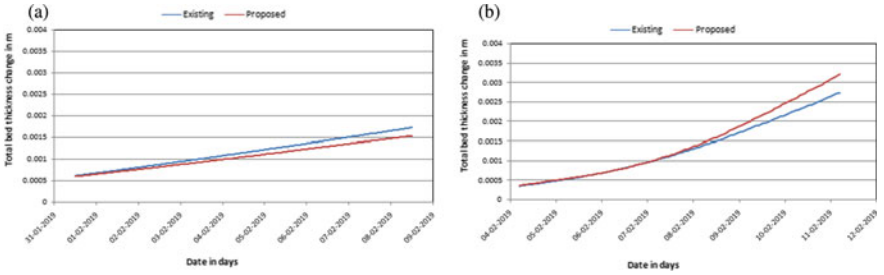

Fig. 16 **a** Rate of siltation at C2 in non-monsoon. **b** Rate of siltation at C2 in monsoon

and 16,500 cum occur during non-monsoon and monsoon seasons, respectively. However, for manoeuvring of fisheries, boats near the channel maintenance dredging of the order of 30,000 cum per annum would be required.

7 Conclusions

In this paper, the probable changes in the flow fields and siltation patterns in the inlet channel of harbour basin of the study area at Kasargod due to the proposed scenario are investigated through 2D mathematical model studies using MIKE 21 software. The following conclusions can be drawn from the model studies:

- Hydrodynamic and suspended sediment transport simulations for restoration of inlet channel can be undertaken using 2D numerical software.
- The mathematical model studies with MIKE 21HD model indicated that maximum current magnitude of the order of 0.5 m/s and 0.75 m/s occurred in the inlet channel during non-monsoon and monsoon seasons, respectively. During high flow in the monsoon season, only ebb currents persist in the channel.
- MIKE 21MT model indicated that as compared to surrounding nearby regions, sediment deposition in the inlet channel is less. The annual average depth of siltation is estimated as 10.0 cm in the area. However, a maintenance dredging of about 30,000 cum per annum in the inlet channel would be required for smooth functioning of the channel for manoeuvring of fishery boats for the optimized/ modified layout with 700 m curved extension of north breakwater. It is suggested to conduct maintenance dredging in the nearby region of inlet channel in every three to four years.
- In respect of the flow conditions and its pattern obtained in the hydrodynamic simulations, the modified proposed layout of the breakwaters for the Kasargod fisheries harbour is found to be suitable.

Acknowledgements The authors are thankful to A. K. Agrawal, Director, Central Water and Power Research Station, Pune for his kind permission to publish this paper.

Reference

1. MIKE 21 Scientific background - Flow Model FM, DHI, Denmark

Issues and Challenges of Mangrove Sustainability in Vietnam Considering Driver-Pressure-Impact-States-Response (DPSIR) Model

Nguyen Thi Ngoc Bich, Mitthan Lal Kansal, and Hai-Hoa Nguyen

Abstract The benefits of mangroves to the environment, people, and ecosystems are enormous. Mangroves play an essential role in processing, absorbing, and treating Carbon Dioxide, some greenhouse gases, and act as a giant reservoir to store these. Vietnam, with a 3260 km long coastline, has four major regions, i.e., the Northwest coast, the Northern Delta, Central coast, and the coast of Southern Vietnam. The coastal Mangroves in Vietnam play the role of barrier to protect it from saline intrusion, coastal erosion, and destructive climate change. However, there are many challenges to their sustainability. Recently, the Vietnam mangrove has changed in quantity and quality. The mangrove area in 1943 was over 400 000 ha which has reduced to 164 701 ha in 2017 (a decrease of 60%). There are many reasons for such declines, such as war, sea-level rise, anthropogenic activities, climate change. Human activities such as traditional logging, non-timber, traditional fishing and aquaculture, exploitation of mangrove produce, and interaction between agriculture with mangrove have affected its sustainability. Economic and tourism dynamics have caused pressure on the mangrove ecosystem. This study highlights the issues and challenges of mangrove development, management, and rehabilitation in Vietnam based on the theory of sustainability with the Driver-Pressure-State-Impact-Response (DPSIR) model. This model is reviewed from the socio-ecological point of view—a tool for assessing the interaction among the environment, ecology, and society. The study provides a comprehensive overview of the risks and hazards from the environment and human activities' point of view. Further, the study focuses on socio-ecological pressure, challenges of mangrove conservation and response of mangroves in Vietnam.

N. Thi Ngoc Bich (✉) · M. L. Kansal
Department of Water Resources Development and Management, Indian Institute of Technology Roorkee, Roorkee 247667, India
e-mail: bichnguyen@wr.iitr.ac.in

M. L. Kansal
e-mail: mlk@wr.iitr.ac.in

H.-H. Nguyen
Forest Resources and Environmental Management Faculty, Vietnam National University of Forestry, Hanoi 10000, Vietnam

P. V. Timbadiya et al. (eds.), *Coastal, Harbour and Ocean Engineering*, Lecture Notes in Civil Engineering 321, https://doi.org/10.1007/978-981-19-9913-0_26

Keywords Vietnam mangroves · Sustainability · Issues and challenges · DPSIR model

1 Introduction

Mangroves are unique ecosystems close to tropical and subtropical areas that grow in wetlands. These get evolved strong and succeeded in sheltered (muddy), high-salinity, wet, and warm environments, wherein only a few species of plants and animals can adapt. Mangroves are essential and unique ecosystems that provide a range of ecosystem services; safeguard the coastlines, reduce the damages caused by storms, waves, and floods; reduce erosion on the beach and coastline; and work for carbon absorption. Mangroves help alleviate the adverse impacts of climate change and help people and nature acclimate [1–6]. Mangroves provide direct and indirect benefits to the people, contribute to the rich biodiversity and significant ecological values, and connect people with the ocean. Thus, mangroves have enormous economic and societal values. They also provide a vast source of raw materials for humans and other living beings. Further, mangroves and associated land coastal areas can confiscate about 22.8 million tons of carbon/year. However, mangroves have covered only 0.1% of the earth's mainland surface, accounting for 11% of all terrestrial carbon inflowing the ocean [2, 7, 8]. More than 60% of the population living around the coastline depends on products and services from the sea [9]. Besides these, mangroves reduce the impacts of natural disasters from the ocean. The worldwide distribution of mangroves is shown in Fig. 1.

According to FAO [2], the mangrove area in Africa was 3,160,000 ha, Asia 5,858,000 ha, North and Central America 2,263,000 ha, Oceania 1,972,000 ha, South America 1,978,000 ha. The total area varies widely in time and space. In 2000, 137,760 sq. km belonged to tropical and subtropical regions, including 118 countries and territories worldwide [8]. Global Mangroves Alliance (GMA) [10] estimated the mangrove area of 135 882 sq. km in 2017. The mangrove area is distributed

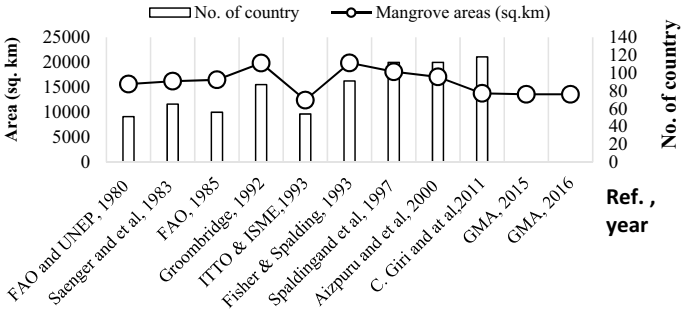

Fig. 1 Estimated mangrove area worldwide

in North and Central America and the Caribbean with about 20,962 sq. km (15.4%), Asia 52,352 sq. km (38.5%) [10]. Fifteen countries contain 75% of all mangroves, and only 6.9% are in protection areas [8]. It may be noticed that the total area under mangroves has decreased substantially from 1993 to 2011. The loss and change of mangrove areas are becoming more and more serious as almost 2% of mangrove area is getting lost per year globally [1, 2]. In some developing countries, the rate is up to 8% per year [11]. Since 1980, an average of 20–35% of mangroves, rainforests, or coral reefs have disappeared [2, 11, 12]. Spalding [5] reported losses of over 20% in all regions except Australia from 1980 to 2005.

Vietnam, with 3 260 km long coastline, has four zones of mangrove forests: the Northeast: Ngoc Cape—Do Son Cape with an area of 39,400 ha; the Northern Delta: Do Son Cape—Lach River with 7000 ha; the central coast: Lach River—Vung Tau Cape with an area of 14,300 ha as mangrove forests; the coast of southern Vietnam: Vung Tau Cape—Ha Tien province over 191 800 ha where is the largest and best biodiversity mangrove ecosystem in Vietnam [13, 14]. The topographic structure substantially influences the survival and formation of mangroves. The planned mangrove forest in Vietnam is 323,712 ha. The Mekong Delta contains more than 60%, distributing about 20% in the Southeast, and the remaining 20% on the northern coast and Red River Delta (MARD, 2014, 2018, Government of Vietnam, 2014).

2 Driver-Pressure-State-Impact-Response (DPSIR) Based Sustainability Framework

The concept of sustainability is important and developed for each sector in stages. All perspectives are based on the foundation of ecosystem sustainability. OCED developed this view of sustainability with the framework based on Pressures (P), States (S), and Responses (R) from 1994. The PSR indicators suggest estimating the human activities pressuring environmental states and providing politically aware responses to stretch a "desirable state." This model provides more rigorous and specific entanglement analysis making it easier to frame a policy for managing people, ecosystems, and the environment. In fact, the fluctuations of climate change and anthropogenic and socio-economic activities are increasingly affecting the ecosystem. Therefore, assessing pressure and response is no longer a comprehensive response to ecosystem sustainability [15–18]. Hence, the premise for developing many later assessment frameworks, such as the European Environment Agency, has added to this perspective with specificity and added many additional sub-indices to drivers-pressures-states-impacts-response indicator DPSIR (Fig. 2).

Following this framework, the social and economic development activities "Pressure" the environment and, consequently, the "State" of the environment, such as providing adequate conditions for health, resource availability, and biodiversity changes. Finally, the consequence of "Impacts" on human health and materials may result in a societal "Response" that feeds back on the "Driving forces" [18].

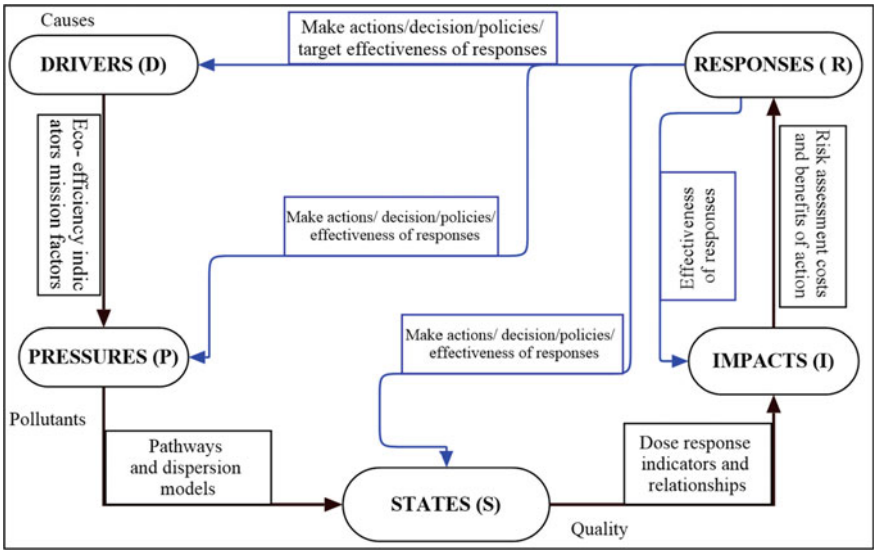

Fig. 2 The framework of DPSIR [15, 18, 19]

Peter Kristensen [15] suggests the DPSIR framework has a chain of causal links starting with "drivers"/"pressures" (economic sectors, human activities, emissions, waste, etc.) that results in "states"/"impacts" (physical, chemical, and biological) on institutional, human health and functions, eventually leading to political "responses" (prioritization, target setting, indicators). The explanation of causes results in a series of highly complicated motivations and results in sub-tasks. In contrast, assessing the relationship between the environment, ecology, mangroves, and natural and social factors in terms of sustainability results in the interactions between resource problems, human activities, and the governance system. The governance system influences resource use by defining rules [20]. The above model shows the relationship between cause and effect in social problems. However, the development of these evaluations is compatible with the selection of indicators for assessing environmental, social, and ecosystem causal interactions [15, 19]. When anthropogenic activities pressure the ecosystem, the sustainable development model will have to be seen from a more serious and relational point of view. The relationship social-ecological-system (SES) is formed when humans interact with the environment [21, 22]. It can also be seen that many studies apply the DPSIR model in predicting environmental degradation and making it easier for policymakers and decision-makers. In terms of ecology, many researchers and organizations have also used this model to assess the environment. Sirak Robele Gari [18] used the DPSIR model to analyze water issues in Colombia. Pressure and responsiveness in management and coastal areas are also recognized for mangroves in Vietnam [23–25].

3 Issues and Challenges of Mangroves Following the DPSIR Model

Based on the DPSIR sustainability assessment framework, this study highlights the impacts of anthropogenic activities, the quality and management of mangroves, and the pressure of human activities on mangroves. This study outlines the current conditions, problems, and challenges in mangroves' conservation and sustainable development in terms of Pressures-States-Response as shown in Fig. 3.

Human actions affect directly or indirectly through socio-economic activities mangroves ecosystems and change them. These are considered based on the DPSIR model. The above model identifies the main problems in creating pressure on mangroves: war, deforestation, overexploitation of resources, conversion of land use purposes, and an increasing population who have life dependent on the mangrove forest. Global climate change and extreme weather conditions also lead mangroves under much pressure. Challenges must be addressed to protect, conserve, and develop mangroves in terms of recognizing human activities, socio-economic development, and ecology to ensure the sustainability of mangroves.

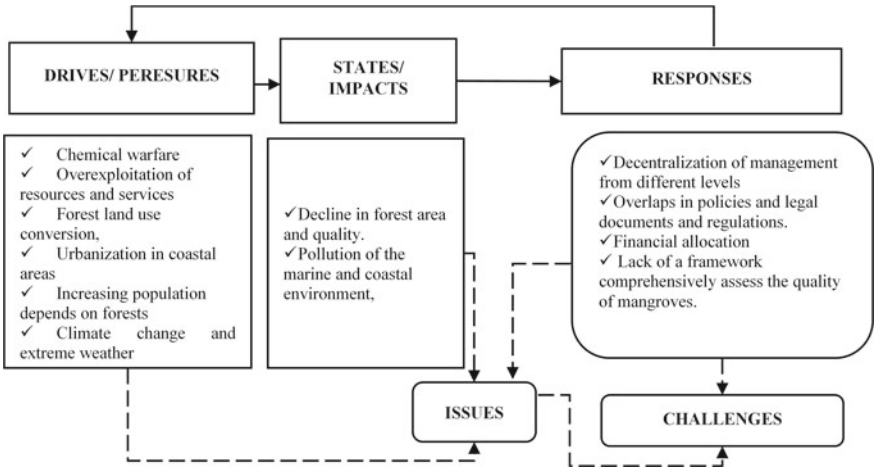

Fig. 3 Issues and challenges of mangroves in Vietnam following DPSIR model

4 Issues in the Pressure and Status of Mangroves in Vietnam

4.1 Impact of Human Activities on Mangroves

Changing the purpose of using mangrove forest land for aquaculture, infrastructure construction, tourism, and service development has taken place seriously. Not only Vietnam but also countries in the region showed that in the period 1975–2005, the area of mangroves in Asia converted to agricultural land was about 50% in Thailand, Malaysia (43%), and Myanmar (98%). The destruction of mangroves in Indonesia is due to aquaculture activities, in Asia lost 12% of its mangrove areas in the period 1975 to 2005. The aquaculture and agriculture expansion (by more than 90%), urbanization, and other factors like infrastructure have caused deforestation significantly [26]. Mangrove area has decreased rapidly due to the development of shrimp farms in the buffer zones, and even in the core zone, the encroachment and overexploitation of coastal resources continue (Katooba Workshop XVII, Nam Dinh, Vietnam, 2010). Nguyen Huu Dong and Tran Thi Tu [27] researched the mangrove in Ha Tinh, showing that there was 1392.79 ha of mangrove forest lost from 2000 to 2012. Change in land use purposes is also the cause of the fragmentation of mangroves. Fragmentation remains a legitimate threat; about 35.4% of mangroves in Ngoc Hien are part of inland forests [28]. Bijeesh Kozhticodan Veettil [29] estimated that a current sea-level rise of 1 m would erase 45.2% of the remaining mangrove area, 60.9% of the rice cultivation areas, and 65% of the aquaculture ponds, and agricultural activities, 46% of the province will disappear [IPCC, 2016; 30]. Following the General Statistics Office (GSO) (2020), fishery growth was 9.7%/year, and shrimp, fish, and aquaculture farming areas increased from 40,800 ha in 2015 to 46,900 ha in 2019 [29, 30].

The pressure from coastal people to exploit and use the benefits of mangroves is increasing. Hence, the process of harvesting mangroves will be stronger and more frequent. Consequently, this is deforestation, change in structure, pollution, and mangrove degradation. Nearly a third of the coastline is urban or residential. The coastal provinces are home to 46.6 million people in 28 coastal provinces (with 125 districts and 25 island districts) with a population density of 354 people/km^2 [31]. According to statistics [32], tourism contributes 70% of revenue to coastal cities. In the period 2015–2019, the number of tourists was over 10,000 turns/year in Ho Chi Minh City and over 7000 turns/year in Ha Long. Despite good economic development, this will also pressure coastal biodiversity management, protection, and development. Mangroves are not an exception to that risk shrimp farming also increased shrimp farming accounts for 30 to 70% of mangrove loss globally [33, 34]. Pham Tien Dat [35] researched in Bang La, mangrove plantations have attended by the upper and wealthy families are more frequently than the middle, and the low-income families did as well as they were more dependent on mangrove forests. In Ca Mau, Vietnam, having an average of 116,1 ha/year, the only remaining area of 775.83 ha of mangroves, 50% to shrimp farm expansion during 1973–2008 [36].

Particularly, the exploitation and export of wood and wood products in Vietnam are increasing. The export value of wood production increased by 7 billion USD (3.5 million m^3 of products) in 2019, proactive 75% of raw materials were timber for processing, production, domestic consumption, and export. Among these materials are raw materials from mangroves [37].

4.2 Impact of Natural Disasters, Extreme Weather, and Climate Change

In recent years, the Ranked of Vietnam was in the 10 countries most strongly affected by climate change. The IPPC (2007) climate change coastal scenario suggests that 30%, 40%, and 100% of mangroves could be lost within the next 100 years if the current loss rate keeps going the situation [38]. Under the climate change scenario, the sea level will increase by 30 cm by 2050 and 70 cm by 2100. Urban area flood risk is expected to increase to 7%, affecting over 4.5 million people in the coastal area [39]. Undoubtedly, it is also difficult for Vietnam to avoid this scenario. The drought in 2016 caused extremely saltwater intrusion, especially in the Mekong Delta, damaging more than 1.4 million ha of agricultural land nationwide and 22% of the cultivated rice area (12% of rice production and 8% of national agricultural GDP). Directly affecting the livelihoods of about 3 million farmers, 316,000 workers lost their jobs due to river floods and coastal floods. The total number of tropical cyclones from 1951 to 2010 equal 209 [35, 40] and in the period 1949–2018 had 453 storms and tropical depressions [39, 40]. Kevin and Whelan [41] studied how the impact of groundwater levels can directly affect soil elevation in the Shark River mangroves, comparing the difference between accretion and elevation that may be related to groundwater changes in or immediately after the storm. Mangroves are very sensitive to changes in the duration and frequency of inundation and salinity beyond species-specific physiological tolerance thresholds. A recent review of the literature on this matter, facing storms, floods, and frequent flooding causes plants to pass away at the seaward mangrove margins or changes in species composition, ultimately leading to reduced yields. Furthermore, storms also affect mangrove diversity, such as plants and crabs [29]. Mangroves significantly reduce the height and attenuation of waves affecting the coast [42]. Bryan [43], research in Cu Lao Dung, Vietnam, mangroves play a role in tidal dispersion, reducing water depth, and balancing tidal currents and flood flows. Furthermore, the coast also enhances sedimentation and helps to expand the area of mangroves [46–78].

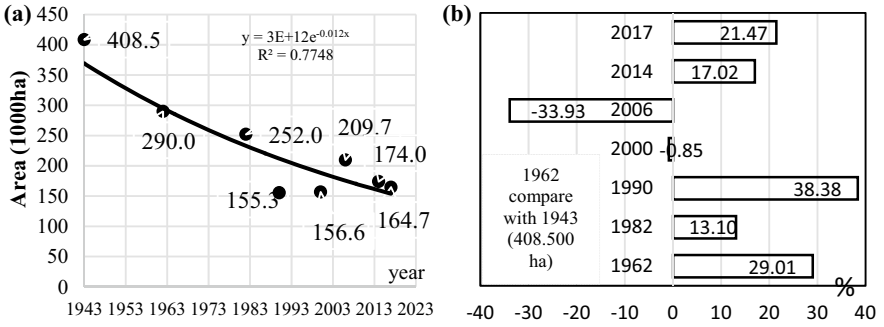

Fig. 4 **a** Variation of Vietnam's mangrove area [2, 13, 14, 38, 47, 48]. **b** Percentage of forest area reduction compared to the previous period

4.3 Changes in the Quality and Quantity of the Mangrove Areas

The mangroves area in Vietnam has declined significantly, from 408,500 ha in 1943 to 155 290 ha in 2000 [47]. By 2017, after 74 years, the forest area had only recovered to 164,701 ha [38, 48] (Fig. 4a, b). The main cause of deforestation in the 1940–1957 period was chemical warfare [49]. In the post-war period, many policies of economic development and land use conversion by the government or arbitrarily exploited and spontaneously converted use of mangrove land decreased the rate of mangrove forests significantly. On the other hand, the conversion of forest land to rice, shrimp farming, and other aquatic products has increased sharply [23, 49–51].

The decline of the forests is due to conversion to agriculture, aquaculture, tourism, urban development, and overexploitation [4, 8]. On the other hand, the expansion of aquaculture has also caused massive mangrove loss in Ca Mau. Following this data shows that after many years from 1943 to 2021, nearly 80 years, the area of forest recovered, including planting, has only reached about 33% compared to 1943 [13, 52–54].

Therefore, the loss of Mangroves will be a complex problem for ecological and environmental researchers and government to protect and develop mangroves despite great support from NGOs and public and private budgets. Only in the period, 2000–2012 Vietnam had about 0.25% of the forest area lost. Other countries in the region also have a significant reduction in area. The highest are Myanmar, Malaysia, and Indonesia [54] (Fig. 5 and Table 1).

4.4 Pollution in Coastal Areas

Vietnam has 114 estuaries, not only dividing mangrove forests into small areas but also creating an opportunity each year to discharge waste entering the ocean about

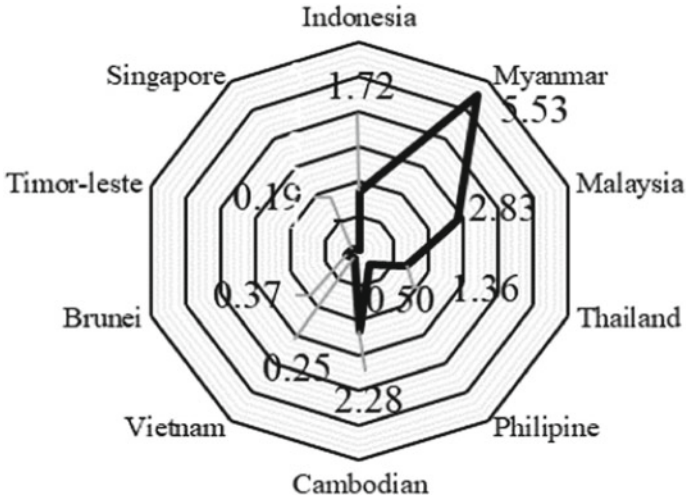

Fig. 5 Percentage of Mangrove areas loss between 2000 and 2012 in Southeast Asian countries

Table 1 Mangrove area lost in Southeast Asian countries 2000–2012 [54]

Countries	Mangroves deforestation, (ha)	Mangrove habitat area lost, (ha)
Indonesia	60,906	48,025
Myanmar	27,957	2,770
Malaysia	18,836	15,809
Thailand	3,504	3,344
Philippine	1,423	1,396
Cambodian	1,218	1,086
Vietnam	531	528
Brunei	48	41
Timor-Leste	2	2
Singapore	-	0
Southeast Asia	114,424	97,901

14.03 MT/year (about 38,500 tons/day, into plastic waste (0.28–0.73 MT, equal 6% of the world)) into the ocean, ranked 4th in the world. This is the source of the garbage drifting into the ocean. Industrial activities also contribute significantly to damaging marine ecosystems, including mangroves, millions of tons of heavy metals are discharged into rivers and into the. From 1995 to June 2002, there were 90 oil spill accidents, with 92,420 tons of oil spilt into coastal areas and the East Sea. The increasing exploitation of marine resources through 340 oil wells, 272 operational seaports, and various petroleum by-products (of the order of 550 tons/year) has polluted the seawater, affecting the mangrove system. Besides, the average annual

amount of waste generated is about 5,600 tons, and over 15,000 tons of oil and grease are floating, but only 67–70% of hazardous solid waste was treated [30, 32, 39]. Suspended solids (TSS) and ammonium content increased sharply when coastal agricultural and aquaculture activities increased, such as TSS, D.D.T., Ammonium, and Phosphate. The Cuu Long Delta is subject to significant fluctuations in salinity intrusion, with the highest concentration of 6.5 g/l and an average of 2–4 g/l, and the infiltration process is unstable [48]. Adding more affection impacts the development ability of mangroves because of the forest's sensitivity to excessive pressure from the aquatic environment. Tinh Hong Pham et al. (2020) [55] also showed that carbon sequestration in the mangrove restoration restores mangroves, thereby contributing to ameliorating climate change in Northern Vietnam. Overexploitation or destruction of mangroves will result in loss of organic carbon and carbon stocks in the soil under the mangroves [56].

5 Challenges in Mangrove Management and Development

Mangrove protection, conservation and management are challenging as there is no effective supervision. The mangrove management system is relatively cumbersome (Fig. 6), making it difficult to control, deal with protection and restoration, and the new planting. It lacks satisfactory supervisory devices for protecting mangrove ecosystems and sustainable development [57]. The regulatory framework for mangrove protection includes many legal and sub-law documents that are not highly synchronized and easily cause conflicts when putting into practice, such as Decision No. 178/2001/QD-TTg; Decree No. 117/2010/ND-CP, Law No: 18/2012/QH13-Vietnam's law of the sea, No: 55/2014/QH13- Law on environmental protection, Decision No. 120/2015/QD-TTg, Decree No. 119/2016/ND-CP, 2016; No. 16/2017/QH14. In addition, in Decree No. 151/2007/ND-CP of October 2007, the civil law also contains some articles on using marine resources. Further, in each stage of development, the government also add sub-law documents and develops policies for each program to address the inadequacies and dynamics of climate change, resources issues, and environmental pollution. The Government of Vietnam encouraged farmers to transform coastal land from rice fields and mangroves into shrimp aquaculture [51].

Furthermore, legal basis for managing and protecting particular mangroves is still not specific. There is no comprehensive quantitative assessment method for mangroves. The challenge for scientists, local leaders, and policymakers is to identify conservation limits and key impacts on deteriorating mangrove quality and the risk of mangrove. From the perspective of sustainable development, mangrove conservation is one of the most critical issues that should be part of national policies, actions, and outlines at the national level [59, 60].

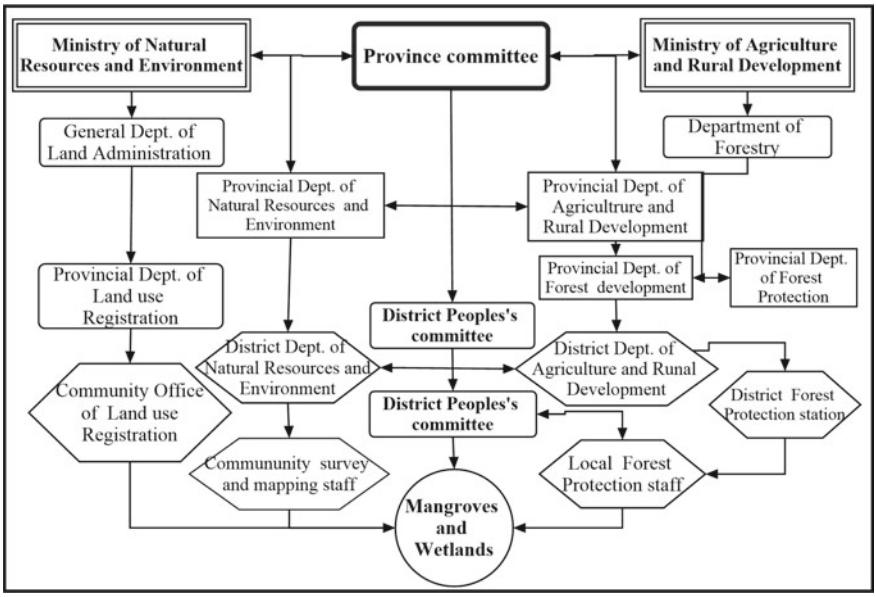

Fig. 6 System for management, control, and conservation of mangroves in Vietnam [58]

Linking management and development to economic development, ecological conservation, education, and climate change presents challenges. Many environmental issues, such as ecosystem conservation and maintenance, face the most significant financial challenge. It is not easy to allocate funds to various projects. Policies in bridging education and economy-related with mangroves are still fragmented, not meeting the level of vulnerability and urgent and long-term requirements. Capital investment for scientific research on mangroves is still very limited [37]. It has been observed that the budget containing both government and local bodies accounts for only 21.5% of the total budget. From 2006 to 2010, mobilization from NGOs, individuals, and households was more than 30%, and from 2011 to 2016, it increased to 48% of the forestry's budget for conservation and protection (Vietnam Government, 2018). This shows that the resources for the mangrove component are insignificant compared to the ecological and environmental role it plays.

Moreover, the quality of mangroves is realized mainly from the investment sources of NGOs (CIFOR, SEACAR, IEKA, and ODA funds). For instance, program 886, for four years (from 2016 onwards), outlaid an investment capital of 59,600 billion VND. (out of which government capital is 14,575 billion VND, and for other agencies, it is 45,025 billion VND). Thus, investment in resources for mangroves' development, restoration, and protection is low and highly dependent on NGOs and other development agencies (ODA).

6 Conclusion

Mangroves act as a shield against natural disasters but are sensitive ecosystems. The conservation and restoration of these are difficult and complex activity. Further, mangroves in Vietnam have suffered a lot due to chemical warfare, which has dramatically reduced the forest area and is difficult to restore or replant on the damaged land. Many forest restoration plans continue to be implemented. Economic, social activities, services, and conversion of forest land into agricultural land are still burning issues in mangrove conservation. Furthermore, Vietnam, as well as other countries in the world, are facing the issue of global warming and climate change. The challenge for mangrove sustainability in Vietnam is to agree on a common legal framework for the entire management system from central to provincial levels. The financial allocation itself needs to be more specific and reasonable. The role of individuals in the protection and reforestation of mangroves needs to be highlighted. Reducing the complexity of the regulatory framework for mangrove conservation and management will make controlling, developing, and protecting mangroves easier.

References

1. Duke NC, Meynecke J, Dittmann S, Ellison A, Anger KU, Berger U, Cannicci S, Diele K, Ewel K, Field C, Koedam N, Lee S, Marchand C, Nordhaus J, Dahdouh-Guebas F (2007) A world without mangroves? Science 317(5834):41–42
2. FAO (2007) The world's mangroves 1980–2005, A thematics study prepared in the framework of the Global Forest Resources Assessment ISBN 978-92-5-105856-5 153, 77
3. Barbier EB, Koch EW, Silliman BR, Hacker SD, Wolanski E, Primavera J, Reed DJ (2008) Coastal ecosystem-based management with nonlinear ecological functions and values. Science 319:321–323
4. Alongi DM (2008) Mangrove Forests: Resilience, protection from tsunamis, and responses to global climate change. Estuar Coast Shelf Sci 76:1–13
5. Spalding M, Kainuma M, Collins L (2010) World atlas of mangroves. ITTO, ISME, FAO, UNEP-WCMC, UNESCO-MAB and UNU-INWEH. Earth scan Publishers Ltd. London
6. Duke Norman C, Klaus S (2015) Mangroves: unusual forests at the seas edge. Tropical Forestry Handbook. Springer, Berlin, pp 1–24
7. Jennerjahn TC, Ittekkot V (2002) Relevance of mangroves for the production and deposition of organic matter along tropical continental margins. Naturwissenschaften 89:23–30
8. Giri C, Ochieng E, Tieszen LL, Zhu Z, Singh A, Loveland T, Masek J, Duke NC (2011) Status and distribution of mangrove forests of the world using earth observation satellite data. Global Ecol Biogeogr 20:154–159
9. Saito Y, Alino PM (2008) Region conditions. In: Mimura N (ed) Asia-pacific coasts and their management: states of environment. Springer, Netherlands, pp 255–331
10. Globale mangroves alliance (2021) The state of the Worlds Mangroves 2021. Report
11. Polidoro BA, Carpenter KE, Collins L, Duke NC, Ellison AM, Ellison JC, Farnsworth EJ, Fernando ES, Kathiresan K, Koedam NE, Livingstone SR, Miyagi T, Moore GE, Nam VN, Ong JE, Primavera JH, Salmo SG, Sanciangco JC, Sukardjo S, Wang Y, Yong JWH (2010) The loss of species: mangrove extinction risk and geographic areas of global concern. PLoS ONE 5:1–10
12. Valiela I, Bowen JL, York JK (2001) Mangrove Forests: one of the world's threatened major tropical environments. Bioscience 51:807–815

13. Hong PN, San HT (1993) Mangroves of Vietnam. IUCN. The world conservation Union, Bangkok, Thailand, vol 173, pp 3–11. ISBN 2-8317-0166-x
14. Hong PN (1996) Restoration of mangrove ecosystems in Vietnam: a case study of Can Gio District, Ho Chi Minh City. In: Field C (ed) Restoration of mangrove ecosystems. The international tropical timber organization and the international society for mangrove ecosystems, Okinawa, Japan, pp 76–79
15. Levrel H, Kerbiriou C, Couvet D, Weber J (2009) O.E.C.D. pressure–state–response indicators for managing biodiversity: a realistic perspective for a French biosphere reserve. Biodivers Conserv June 18(7):1719–1732
16. Kristensen P (2004) The DPSIR framework. National environmental research institute, Denmark. UNEP Headquarters, Nairobi, Kenya, pp 1–10
17. Ávila-Flores G, Juárez-Mancilla J, Hinojosa-Arango G, Cruz-Chávez P, López-Vivas JM, Arizpe-Covarrubias O (2020) A practical index to estimate mangrove conservation status: the forests from La Paz Bay, Mexico as a case study. Sustainability 12(858):1–16
18. Gari SR, Guerrero CEO, Bryann A-U, Icely JD, Newton A (2018) DPSIR-analysis of water uses and related water quality issues in the Colombian Alto and medio Dagua Community Council. Water Sci 32:318–337
19. EEA (1999) Environmental indicators: typology and overview. Technical report No 25, pp 1–19. ISSN 00231207
20. Stanners D, Bosch P, Dom A, Gabrielsen P, Gee D, Martin J, Weber JL (2007) Frameworks for environmental assessment and indicators at the EEA. Sustain Indic 127–144. ISBN 1597261319
21. Ostrom E (2009) A general framework for analyzing sustainability of social-ecological systems. Science 325(5939):419–422
22. Anderies JM, Janssen MA, Ostrom E (2004) A framework to analyze the robustness of social-ecological systems from an institutional perspective. Ecol Soc 9(1):18
23. Torell M, Salamanca AM (2003) Wetlands management in Vietnam's Mekong delta: an overview of the pressures and responses. Wetlands management in Vietnam: issues and perspectives. SIDA, WorldFish Cent Contrib Jutaprint Penang Malaysia 1692:1–19
24. Nguyen H-H, McAlpine C, Pullar D, Leisz SJ, Galina G (2015) Drivers of coastal shoreline change: case study of Hon Dat Coast, Kien Giang Vietnam. Environ Manag 55:1093–1108
25. Nguyen H-H, Nghia NH, Nguyen HTT, Le AT, Tran LTN, Duong LVK, Bohm S, Furniss MJ (2019) Classification methods for mapping mangrove extents and drivers of change in Thanh Hoa Province, Vietnam during 2005–2018. For Soc 4(1):225–242
26. Giri C, Zhu Z, Tieszen LL, Singh A, Gillette S, Kelmelis JA (2008) Mangrove forest distributions and dynamics (1975–2005) of the tsunami-affected region of Asia. J Biogeogr (J Biogeogr) 35:519–528
27. Nguyen HD, Tran TT (2019) Assessment of status management and spatial planning proposal for planting mangroves in Ha Tinh province. In: 3rd science and technology conference: effective management of natural resources and environment towards green growth, pp 450–463. ISBN: 978-604-73-4719-3
28. Hauser LT, Vu GN, Nguyen BA, Dade E, Nguyen HM, Nguyen TT, Le TQ, Vu LH, Tong AT, Pham HV (2017) Uncovering the spatio-temporal dynamics of land cover change and fragmentation of mangroves in the Ca Mau peninsula, Vietnam using multi-temporal SPOT satellite imagery 2004–2013. Appl Geogr 86:197–207
29. Veettil BK, Quang NX, Trang NTT (2019) Changes in mangrove vegetation, aquaculture and paddy cultivation in the Mekong Delta: a study from Ben Tre Province, southern Vietnam. Estuar Coast Shelf Sci 226:106273
30. MARD (2019) Overview of present management and effectiveness of policies on mangrove protection and development in Vietnam: future policy orientations and information gap. MARD, Hanoi, Vietnam
31. GOS (2020) Statues of population, labor and employment 2020, General statistics office of Vietnam, Vietnam Government. https://www.gso.gov.vn/px-web-2/?pxid=V0201&theme=D%C3%A2n%20s%E1%BB%91%20v%C3%A0%20lao%20%C4%91%E1%BB%99ng. Accessed Oct 2021

32. Vietnam National Administration of Tourism (2021) http://thongke.tourism.vn/index.php/statistic/cat/15. Accessed Oct 2021
33. GOS (2020) Economic structure and services report 2020, General statistics office of Vietnam, Vietnam Government. Accessed Oct 2021
34. MONRE (2021) National Environmental Status Report 2016–2020. Ministry of natural resources and environment of Vietnam, Dan Tri Publisher. ISBN: 978-604-331-818-0
35. Barbier EB, Cox M (2004) An economic analysis of shrimp farm expansion and mangrove conversion in Thailand. Land Econ 80(3):389–407
36. Dat PT, Yoshiro K (2012) Comparing mangrove forest management in Hai Phong City, Vietnam towards sustainable aquaculture. In: The 3rd International Conference on Sustainable Future for Human Security SUSTAIN; Procedia Environ Sci 17:109–118
37. Lam-Dao N, Pham-Bach V, Nguyen-Thanh M, Pham-Thi MT, Hoang-Thi P (2011) Change detection of land-use and riverbank in Mekong delta, Vietnam, using time-series remote sensed data. J Resour Ecol 2:370–374
38. CIFOR, Thuy PT, Van Dien N (2021) A decade of mangrove conservation achievements and challenges in Vietnam. CIFOR, no. 337
39. Duke NC, Schmitt K (2015) Mangroves: unusual forests at the seas edge. In: Tropical forestry handbook, p 1
40. MARD (2019) Planning for development economic in a period of climate changes MARD, Hanoi, Vietnam
41. MONRE (2021) No. 4944/BTNMT-TCBHĐVN announcing the State of the National Sea and Island Environment Status Report for the 2016–2020 period. Ministry of natural resources and environment, report Publication House, Hanoi, Vietnam
42. Hong Tinh P, Thi Hong Hanh N, Van Thanh V, Tuan MS, Van Quang P, Sharma S, MacKenzie RA (2020) A Comparison of soil carbon stocks of intact and restored mangrove forests in Northern Vietnam. Forests 660–670
43. Whelan KRT, Smith III TJ, Anderson GH, Ouellette ML (2009) Hurricane Wilma"s impact on overall soil elevation and zones within the soil profile in a mangrove forest. Wetlands 29(1):16–23
44. Bao TQ (2011) E**ff**ect of mangrove forest structures on wave attenuation in coastal Vietnam. Oceanologia 53:807–818
45. Bryan KR, Nardin W, Mullarney JC, Fagherazzi S (2017) The role of cross-shore tidal dynamics in controlling intertidal sediment exchange in mangroves in Cù Lao Dung, Vietnam. Cont Shelf Res 147:128–143
46. Yamamoto L (2014) Environmental displacement in Vietnam. Coastal disasters and climate change in Vietnam, 1st edn. Elsevier, pp 379–393
47. Bryan KR, Nardin W, Fagherazzi S (2017) The role of cross-shore tidal dynamics in controlling intertidal sediment exchange in mangroves in Cù Lao Dung, Vietnam. Cont Shelf Res 147:128–143
48. Fricke AT, Nittrouer CA, Ogston AS, Vo-Luong HP (2017) Asymmetric progradation of a coastal mangrove forest controlled by combined fluvial and marine influence, Cù Lao Dung, Vietnam. Cont Shelf Res 147:78–90
49. Sam DD, Binh NN, Que ND, Phuong VT (2005) Overview of mangrove forest in Vietnam. Agriculture Publication House, Hanoi, Vietnam
50. FIPI (2019) Report on forecasting water sources and saline intrusion in the dry season in 2018–2019 and proposing solutions to combat drought in the Mekong Delta, MARD 2019
51. Hue LTV, Scott S (2008) Coastal livelihood transitions: socio-economic consequences of changing mangroves forests management and land allocation in a commune of Central Vietnam. Geogr Res 46:62–73
52. Ha TTT, van Dijk H, Bush SR (2012) Mangrove conservation or shrimp farmer**'**s livelihood? The devolution of forest management and benefit sharing in the Mekong Delta, Vietnam. Ocean Coast Manag 69:185–193
53. Nguyen H-H, McAlpine C, Pullar D, Johansen K, Duke NC (2013) The relationship of spatial temporal changes in fringe mangrove extent and adjacent land-use: Case study of Kien Giang coast, Vietnam. Ocean Coast Manag 76:12–22

54. Binh TNKD, Vromant N, Hung NT, Hen L, Boon EK (2005) Land cover changes between 1968 and 2003 in CaiNuoc, Ca Mau Peninsula, Vietnam. Environ Dev Sustain 7:519–536
55. Hue L (2008) Economic reforms and mangrove forests in Central Vietnam. Soc Nat Resour 21:106–119
56. Richards DR, Friess DA (2012) Rates and drivers of mangrove deforestation in Southeast Asia 2000–2012 113(2):344–349
57. Pham TT (2003) Managing and classifying wetlands in the Mekong River Delta, Wetlands management in Vietnam: issues and perspectives, pp 31–43
58. Arias-Ortiz A, Masque´ P, Glass L, Benson L, Kennedy H, Duarte CM, Garcia-Orellana J, Benitez-Nelson CR, Humphries MS, Ratefinjanahary I, Ravelonjatovo J, Lovelock CE (2021) Losses of soil organic carbon with deforestation in mangroves of Madagascar. Ecosystems, Springer Nature 24:1–19
59. Tuan VQ, Kuenzer C (2012) Can Gio mangrove biosphere reserve evaluation – current status, dynamics, and ecosystem services. IUCN report, Hanoi, P 101
60. Hawkins S, Phuc XT, Phuong PX, Thuy PT, Tu ND, Cuong CV, Brown S, Dart P, Robertson S, Vu N, McNally R (2010) Roots in the water: legal frameworks for mangrove PES in Vietnam Katoomba Group's legal initiative country study series. Forest Trends, Washington, DC, p 55
61. Schmitt K, Duke NC (2015) Mangrove management, assessment and monitoring. Tropical forestry handbook. Springer, Berlin

Numerical Wave Modelling for the Development of Fishing Harbour—Case Study

Amol S. Borkar and Prabhat Chandra

Abstract Nearshore wave climate is an important factor for development of any port or harbour. Wave propagation inside the harbour should always be within the allowable safe limit for berthing of ships/boats. The wave propagation inside the harbour is minimised by providing proper sheltering through breakwater. The projection of breakwater should ensure minimum silt entry in the harbour, thereby reducing the dredging inside the harbour. Numerical modelling for present study is conducted for development of fishing harbour at Shiroor, Karnataka, on the west coast of India. Modelling is carried to derive the nearshore wave climate using Numerical spectral wave model (MIKE-21 SW). Wave propagation inside the fishing harbour was analysed using Numerical Boussinesq wave model (MIKE-21 BW) and the shoreline prediction by using LITPACK model. Near the point of interest at −7.5 m depth, the wave transformation studies indicated that predominant wave directions were from 225° N to 290° N directions, i.e. the site is exposed to predominant waves from South-West (SW) to WestSouthWest (WSW) directions and waves of significant height of about 3.0 m waves reach the proposed site. Wave climate inside the fishing harbour was assessed for the layout proposed by the project authority consisting of Northern breakwater of length of 205 m and Southern breakwater of length 315 m with 80 m wide opening from the westerly direction. The tip of the breakwater is proposed at (−) 3.3 m. The Numerical model studies carried out by using MIKE-21 BW model for this proposed layout indicated that the significant wave heights in the harbour basin would be are generally in the range of 0.25 m–0.10 m and the layout was adequate to provide desired tranquillity less than 0.3 m in the harbour basin for all the directions. Numerical model studies for shore line have shown that the net drift is towards the North direction and accretion would take place on the Southern side of South breakwater and erosion on the Northern side of North breakwater. Thus, the mathematical modelling studies to evolve fishing harbour layout satisfy tranquillity

A. S. Borkar (✉)
Scientist C CWPRS, Pune 411024, India
e-mail: newamol_borkar@rediffmail.com

P. Chandra
Scientist E CWPRS, Pune 411024, India

P. V. Timbadiya et al. (eds.), *Coastal, Harbour and Ocean Engineering*, Lecture Notes in Civil Engineering 321, https://doi.org/10.1007/978-981-19-9913-0_27

criteria and also ensure minimum siltation in the harbour basin. With the construction of proposed breakwater, there will not be significant changes in the existing shorelines on the North and South of breakwater.

Keywords Fishing harbour · Wave transformation · Wave tranquillity · Numerical modelling · Shoreline

1 Introduction

The longshore sediment movement and Nearshore wave climate at the coast are very important in understanding the environmental impact on the coast. Wave approaches at an oblique incident and results sediment movement due to the longshore currents. The present studies were carried to assess the impact of sediment transport and to ensure minimum silt entering inside the harbour, located at Shiroor, Karnataka, on the west coast of India, for the development of fishing harbour. Modelling is carried to derive the nearshore wave climate using Numerical spectral wave model and littoral drift and shoreline evolution by using LITPACK model. The location at Shiroor is fully exposed to incident waves from the Arabian Sea with maximum waves of 3.5 m height and predominant waves from SW to NWN reach the coast. The site is having rocky outcrops and headland towards the Northern stretch from the proposed development. The tidal range at the site is about 1.1 m. Sediment movement is visible in a stretch of about 7.5 km from South portion to the existing North breakwater. Wave climate inside the fishing harbour was assessed for the layout proposed by the project authority consisting of Northern breakwater of length of 205 m and Southern breakwater of length 315 m with 80 m wide opening from the westerly direction. The tip of the breakwater is proposed at (−) 3.3 m. The basin is required to be dredged to (−) 3.0 m for parking of the vessels and berthing operations.

2 Methodology

The offshore wave data reported by India Meteorological Department as observed from ships playing in deep waters of Shiroor Karnataka were transformed using DHI [2] MIKE-21 Spectral Wave (SW) model to get the nearshore wave climate at the fishing harbour. Estimation of littoral drift distribution and simulation of shoreline changes were carried out using LITPACK model.

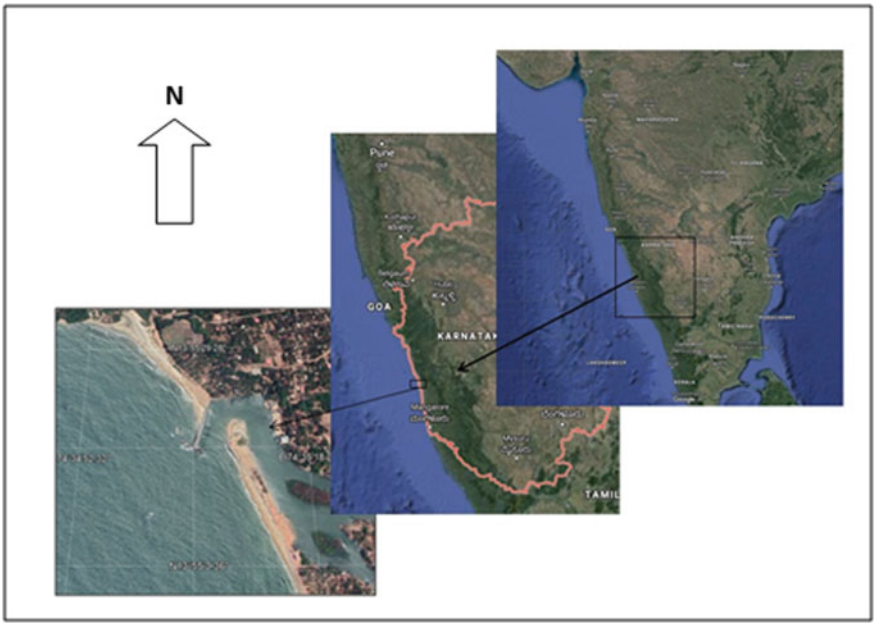

Fig. 1 Location of Shiroor fishing harbour

3 Study Area and Site Conditions

The study area is located (Lat 130 55′ 15″ N and Long 740 35′ 07″ E) at Shiroor, Karnataka, on the west coast of India (Fig. 1). The nearshore bathymetry at the site is having mild slope, and the coastline orientation is 260^0 N. The site is having rocky outcrops and headland towards the Northern stretch from the proposed development. The tidal range at the site is 1.1 m. The sediment concentration was analysed, and graded sediment having size d50 from 0.06 to 0.38 mm is considered in the present studies.

4 Wave Transformations from Deep Water to Nearshore Region

The nearshore wave climate at Shiroor was obtained by transforming the ship observed deep water wave data using spectral wave model. The total area covered in the model studies was about 40 km in the offshore and 90 km along the seashore. The offshore wave climate (Fig. 2a) during the entire year indicates that the predominant wave directions in deep water are from SSW to NNW with the maximum wave heights of the order of 3.5 m. These deep water wave data were transformed by

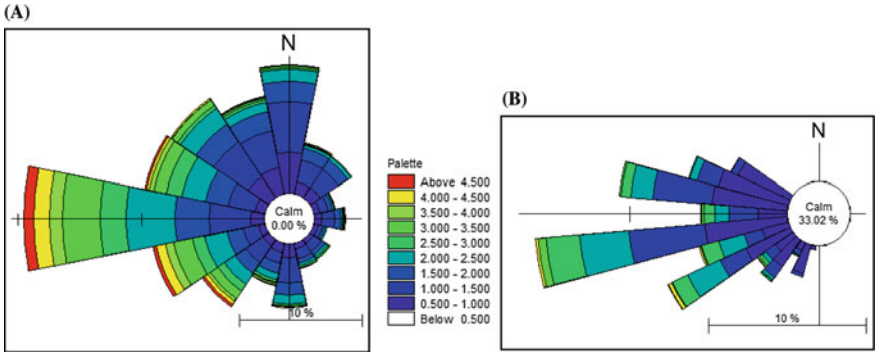

Fig. 2 **a** Offshore wave rose. **b** Offshore wave rose

MIKE-21 SW model to get the nearshore wave climate. The change in wave height from offshore to near shore at 7.5 m depth is presented in Fig. 2b.

From wave transformation studies, waves are incident from SSW° N direction to WNW° N. It is observed that in the nearshore region, the waves having the maximum wave height of the order of 3.5 m approach predominantly in the quadrant 200^0 N to 290^0 N (SSW to WSW direction) quadrant directions.

5 Littoral Drift Assessments

5.1 Earlier Studies for Estimation of Littoral Drift

The longshore sediment transport rates for Alivekodi which is very near the site about 2 km were estimated by Dinesh et al. [1]. The annual net sediment transport estimated was 0.302184×106 m^3 in Northerly direction. According to his work, annual net sediment transport at Alivekodi is of the order of 0.302184×106 m towards North.

5.2 Estimation of Littoral Drift

The littoral drift estimation was carried out using LITPACK model. The cross-shore profile is shown in Fig. 3. The profile is taken normal to the shoreline orientation. The profile is normal to shoreline which is at 260^0 N.

The model was simulated for a period of one year and depending on the wave direction with respect to shoreline. Littoral drift was computed and is shown in Fig. 4. The Northward drift is plotted as positive, whilst Southward drift is plotted as negative.

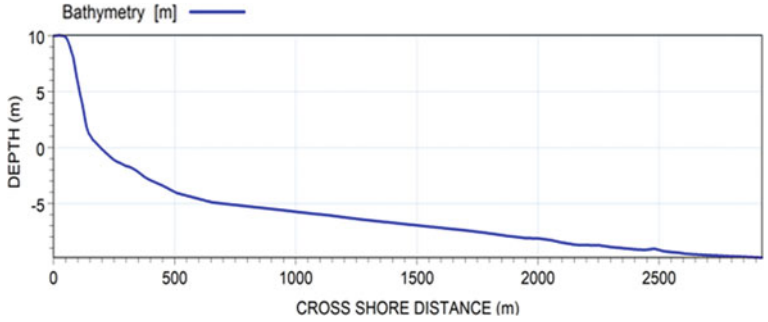

Fig. 3 Cross-shore profiles for drift

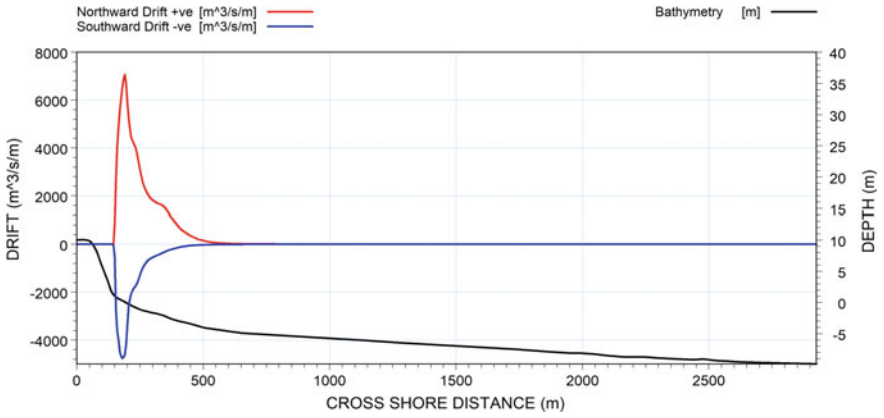

Fig. 4 Annual Northern and Southern littoral drifts for entire year

Studies for estimation of littoral drift indicated that Northward drift is of the order of 0.786 million cum and Southward drift is of the order of 0.377 million cum. Net transport is of the order of 0.409 million cum, and Gross transport is of the order of 1.16 million cum. The maximum transport occurs at about 60 m from the shoreline (i.e. High Water Line). The sediment transport occurs between 1.25 m and −4.75 m depth contours as shown in figure above.

6 Estimation of Coastline Evolution

In order to assess the impact of the breakwaters on the coastline, LITLINE module of LITPACK software was used. The length of the shoreline considered for the studies is extending about 1.5 km towards North of the breakwater and about 1 km towards

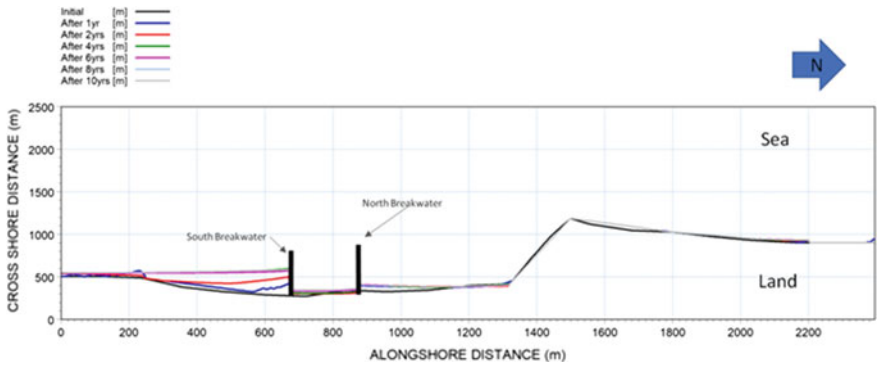

Fig. 5 Shoreline changes likely to occur after 1, 2, 4, 6, 8 and 10 years

South of the breakwater. It is divided into 480 grid points of grid size 5 m. The model was run for after 1, 2, 4, 6, 8 and 10 years which are considered for model studies.

The shoreline changes simulated for the proposed layout (Fig. 5) indicated that due to the construction of the breakwaters, shoreline changes likely to occur after 1, 2, 4, 6, 8 and 10 years with the proposed layout of breakwater length as recommended. It is estimated that shoreline will advance towards sea by 144, 225, 260, 293, 309 and 309 m at South of the South breakwater and 64, 67, 72, 71, 66 and 66 at North of the North breakwater in 1, 2, 4, 6, 8 and 10 years, respectively. With the construction of proposed breakwater, no significant changes in the shore line on the North and South sides of breakwater are expected.

7 Wave Tranquillity Studies

Wave propagation inside the harbour was simulated for the harbour layout at Shiroor, Karnataka, to achieve adequate wave tranquillity conditions inside the harbour throughout the year by using MIKE-21 BW. The model is based on time-dependent Boussinesq equations of conservation of mass and momentum obtained by integrating the three-dimensional flow equations without neglecting vertical acceleration. The model simulates the processes of shoaling, refraction, diffraction from breakwater tips and bed friction. It also takes into account partial reflections from the boundaries, piers and breakwaters.

7.1 Input Wave Conditions for the BW Model

Following (Table 1) are the input wave conditions obtained from wave transformation studies which were used for the BW model.

Table 1 Input wave conditions for wave tranquillity studies

Wave direction (N)	Peak wave period Tp (sec)	Significant wave height (m)
202.5	8	2.5
225	8	3.0
247.5	8	3.0
270	8	3.0
292.5	8	2.5

The studies were conducted to examine wave propagation for the proposed harbour layout at Shiroor. This layout consisted of the proposed breakwaters of length of 205 m and Southern breakwater of length 315 m with 80 m wide opening wide westerly opening harbour entrance as shown in Fig. 6.

Model area of 2.5 km by 2.0 km was discretised with a grid size of 3 m by 3 m. Wave height distribution in the port basin for layout for waves coming from SW and SSW directions was carried out for peak wave period of 10 s. The model studies the wave heights in the port basin which were generally in the range of 0.1–0.3 m for

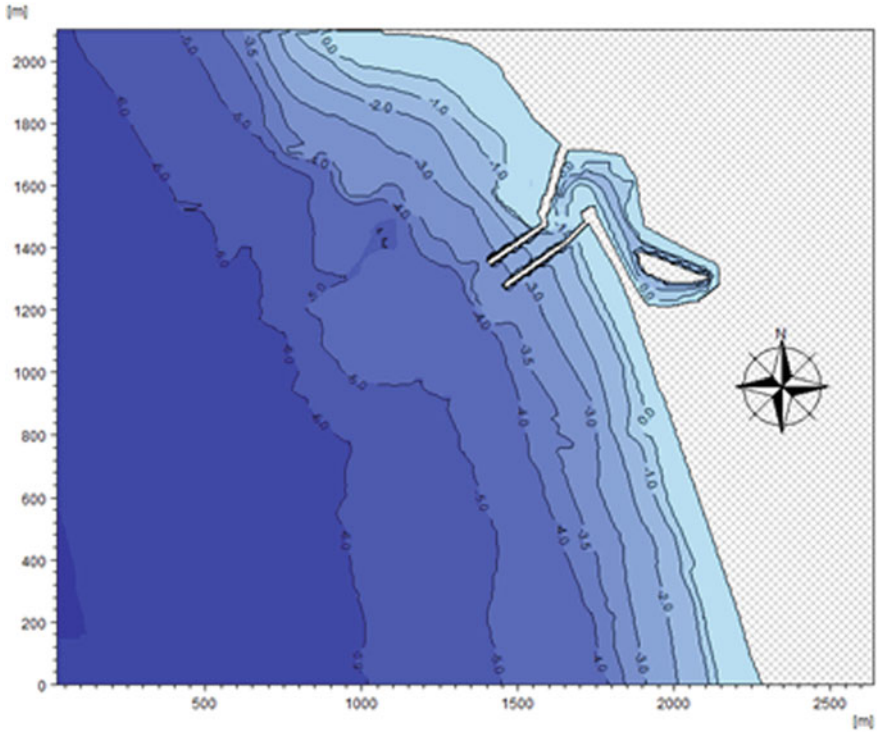

Fig. 6 Bathymetry for MIKE-21 BW model

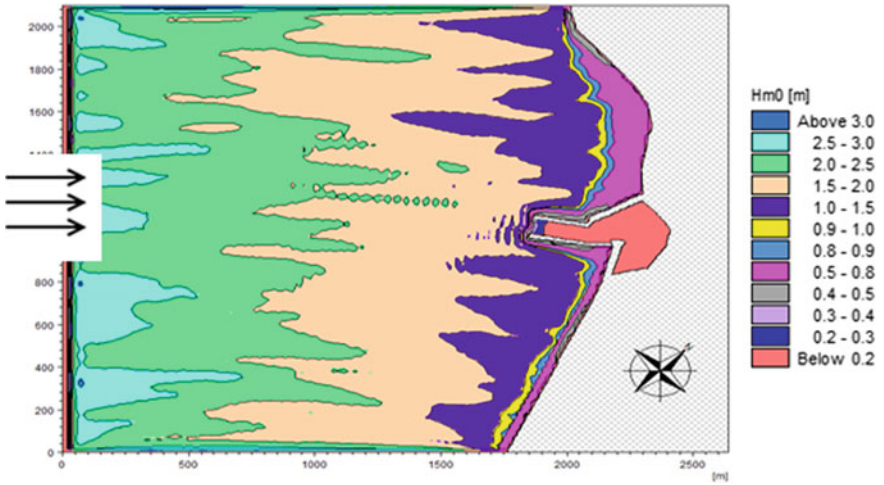

Fig. 7 Wave height distribution for waves incident from SW direction (Hs = 3.0 m)

harbour layout. The results of wave height distribution for a typical incident SW^{o} N (225^{0} N) direction are shown in Fig. 7.

From the model studies of wave tranquillity, the wave distribution plots show that wave disturbances for the layout remain within permissible limit of 0.30 m in the basin area for the predominant directions SW^{o} N (225^{0} N).

8 Conclusions

The following conclusions are derived from the present study:

(i) The proposed fishing harbour at Shiroor will have predominant incident wave directions in deep water which are from SSW to West directions at (−) 7.5 m depth.

(ii) At the proposed location, Northward drift is of the order of 0.786 million cum and Southward drift is of the order of 0.377 million cum. Net transport is of the order of 0.409 million cum, and Gross transport is of the order of 1.16 million cum.

(iii) With proposed Northern breakwater of length of 205 m and Southern breakwater of length 315 m with 80 m wide westerly opening indicate that the maximum wave heights inside the harbour basin would be less than 0.3 m in the designated berthing areas, which is well within the permissible limit.

(iv) With the construction of proposed breakwater, no significant changes in the shoreline on the North and South sides of breakwater are expected.

Acknowledgements The authors are grateful to Shri A.K. Agrawal, Director, Central Water and Power Research Station Pune, for his continuous encouragement and motivation during the course of studies and for granting permission to publish this paper.

References

1. Dinesh D, Jaya KS, Subba R (2016) Wave induced sediment transport in the vicinity of tidal inlets along Karnataka Coast. IIRSET J 5
2. D.H.I MIKE-21 Spectral wave model tool used for wave transformation, MIKE-21 Boussinesq Wave model tool used for wave trainquility studies, MIKE-21 LITPACK model tool used for Littoral drift and shoreline evolution studies

Role of Physical Wave Models in Optimization of Breakwater for Development of Harbours on Open Coast

Sudheer S. Chavan, M. D. Sawant, and Prabhat Chandra

Abstract Breakwaters are sound massive structures devised for providing tranquil conditions to facilitate loading and unloading operations at the berths, wharfs and jetties in harbour areas. The cost of breakwater construction governs about 70–80% of total capital cost of the coastal engineering project. Considerable economics can be achieved by using small-scale physical models which help in avoiding disastrous mistakes in prototype design. The present study emphasizes on the role of physical wave models for establishing wave tranquility conditions for the development of a jetty and passenger cruise terminal at Bhagwati Bunder in Ratnagiri district, Maharashtra, India. The part construction of west or commercial breakwater up to a length of 457 m was over in 1973. Maharashtra Maritime Board has proposed development of cruise terminal and jetty to cater to passenger ships with length of 245 m and draught of 7.9 m. The permissible wave limit for berthing operations at passenger jetty has been considered as 0.50 m. The physical wave model studies at geometric similar scale of 1/120 were conducted at CWPRS which consists of a three-dimensional model tray shallow wave basin equipped with the Random Sea Wave Generation facilities with SCADA control. The physical wave model studies were conducted for 100 m as well as 200 m extension of the existing breakwater for the three predominant wave directions, viz. WSW (Hs = 4.0 m, Tp = 12 s), West (Hs = 4.0 m, Tp = 12 s) and North West (Hs = 1.8 m, Tp = 6 s). The studies indicated that about 70–80 days will be lost for operation at the passenger berth during the monsoon season under existing condition. With 100 m extension of existing breakwater, the downtime will be about 10 days at the passenger berth during the monsoon season. The 200 m extension will provide just adequate wave tranquility throughout the year at the passenger berth for ship size of 245 m length with wave permissible limit as 0.50 m. The physical model studies were very useful in visualizing the complex interaction of wave patterns inside the harbour which helped in evolving the wave tranquility conditions at different berths, jetties, wharfs, etc.

S. S. Chavan (✉)
Scientist 'C', Central Water & Power Research Station, Khadakwasla, Pune 411 024, India
e-mail: sudheertask@rediffmail.com

M. D. Sawant · P. Chandra
Central Water & Power Research Station, Khadakwasla, Pune 411 024, India

P. V. Timbadiya et al. (eds.), *Coastal, Harbour and Ocean Engineering*, Lecture Notes in Civil Engineering 321, https://doi.org/10.1007/978-981-19-9913-0_28

Keywords Wave tranquility · Harbour · Breakwater · Berths · Wharf · Jetty

1 Introduction

A number of minor/intermediate ports and fishing harbours are coming up on open sea coast and estuarine region. The wave tranquility aspects are very important for berthing operations in ports and fishing harbours (Shore Protection Manual, 1984). The breakwater length and alignment are required to be optimized for providing safe-sheltered harbour areas. Breakwaters are sound massive structures which have been devised for providing tranquil conditions to facilitate loading and unloading operations at the berths, wharfs and jetties in harbour areas. The cost of breakwater construction governs about 70–80% of total capital cost of the coastal engineering project. Considerable economics can be achieved by using small-scale physical models which help in avoiding disastrous mistakes in prototype design. The Bhagwati Bunder is situated in Mirya Bay, in Ratnagiri district of Maharashtra state (Fig. 1) at Longitude 73°16′16″ E and Latitude 16°59′51″ N. The part construction of west or commercial breakwater up to a length 457 m was over in 1973. Maharashtra Maritime Board (MMB) has proposed development of cruise terminal and jetty at Bhagwati Bunder to cater to passenger ships with length of 245 m and draught of 7.9 m. The development area is exposed to incident waves during non-monsoon and monsoon seasons and diffracted waves from the existing breakwater reach the harbour. The layout of Bhagwati Bunder harbour basin with bathymetry is shown in Fig. 2.

Due to limitation of the space between proposed jetty and the existing clinker jetty, no turning circle was proposed by the Project Authorities and rather the ship movement from the entry and exit from the breakwater tip was proposed to be controlled by

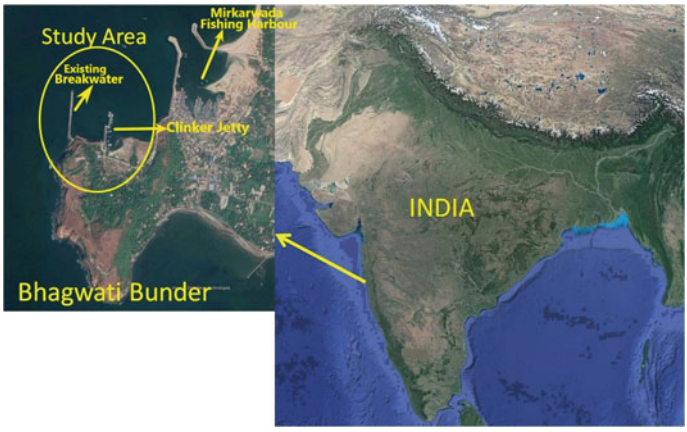

Fig. 1 Location plan

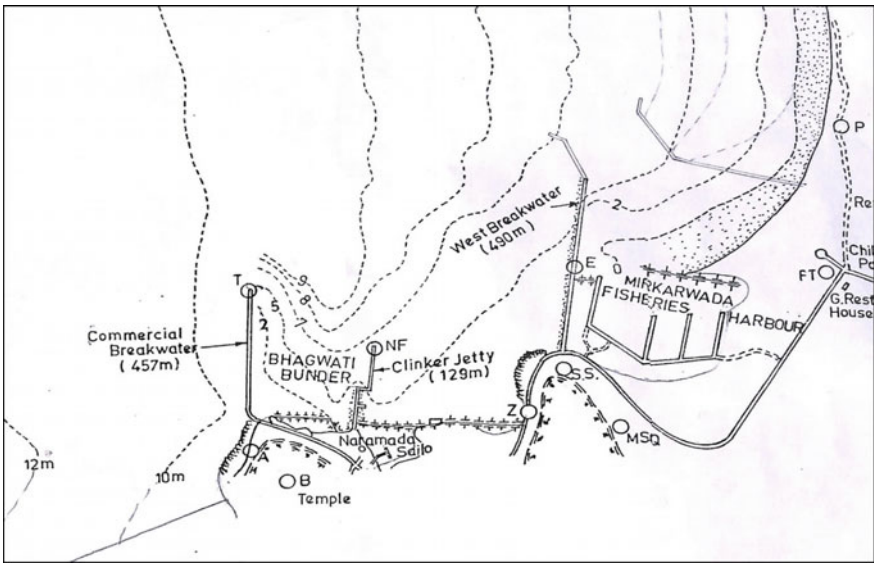

Fig. 2 Existing layout

tugs. Considering the beam and draught of the vessel, 150 m wide channel dredged to (−) 9.5 m below chart datum (CD) was suggested. In the initial proposal, an extension of 100 m of the existing breakwater as shown in Fig. 3 was suggested by the Project Authorities for obtaining the adequate tranquility at proposed passenger jetty for round-the-year operation. In order to suggest the suitability of proposed extension and to decide the optimum extension of the existing breakwater for providing wave tranquility from incident waves from different directions, the physical model studies were referred to CWPRS. The physical wave model studies at geometric similar scale of 1/120 were conducted at CWPRS in MPWB Hangar which consists of a three-dimensional model tray shallow wave basin equipped with the Random Sea Wave Generation (RSWG) facilities with SCADA control. The depth contours up to −16 m depth in vicinity of Bhagwati Bunder and Mirkarwada Port in Mirya bay is shown in Fig. 4. The site photograph of existing west or commercial breakwater 457 m long at Bhagwati Bunder is shown in Fig. 5. The photograph of existing clinker jetty (Narmada jetty) at Bhagwati Bunder is shown in Fig. 6. Presently, the crest level of the breakwater is at about +6.5 m and the armour and lee sides of the breakwater are partly damaged.

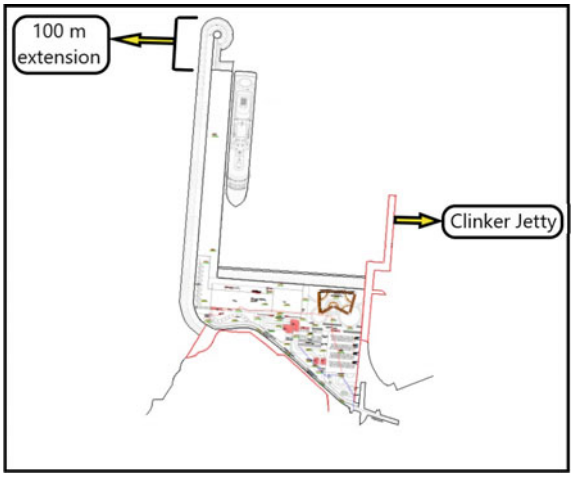

Fig. 3 Proposed 100 m extension of existing West breakwater

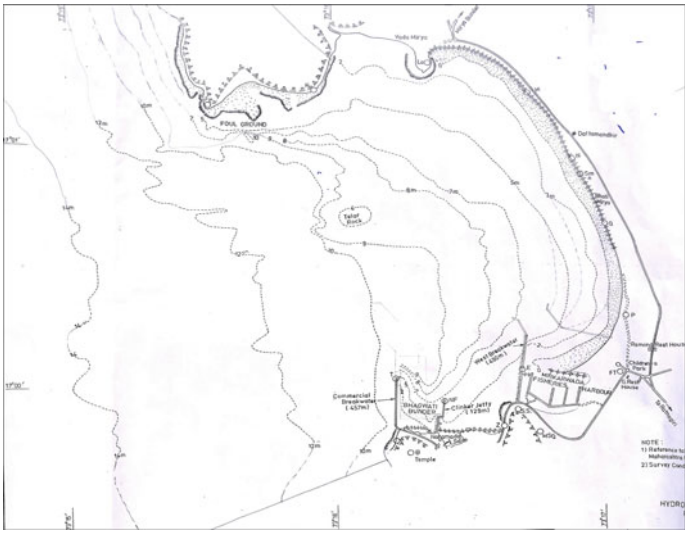

Fig. 4 Depth contours at Bhagwati Bunder and Mirkarwada Port in Mirya bay

2 Data Analysis

Analysis of data is the most important part of model studies as the results are dependent upon the accuracy of data. The basic inputs for wave model studies are bathymetry data, wave and tidal data.

Fig. 5 Layout of existing Breakwater 457 m long at Bhagwati Bunder

Fig. 6 Layout of existing Clinker Jetty at Bhagwati Bunder

2.1 Wave Data

The offshore wave data reported by India Meteorological Department (IMD) as observed from ships playing in deep water off Ratnagiri from 1986 to 2000 were analysed. The wave climate near Ratnagiri was obtained by transforming the ship-observed deepwater wave data, using MIKE-21 SW model. The model was run to obtain near-shore wave climate at the inshore point in −10 m depth contour. The wave data was also obtained from India Meteorological Department (IMD) at −15.5 m contour for annual period (January to December). The wave data have been analysed by CWPRS and it was found that waves incident from WSW (West of South West) to NW (North West) quadrant are more predominant in South-West monsoon season. An inshore rose diagram at −10 m depth is shown in Fig. 7. The significant wave heights (Hs) from WSW and West directions are 4 m each and will hardly exceed 3 days in a year. The significant wave height (Hs) from North West direction is 1.8 m and will not exceed at all in a year.

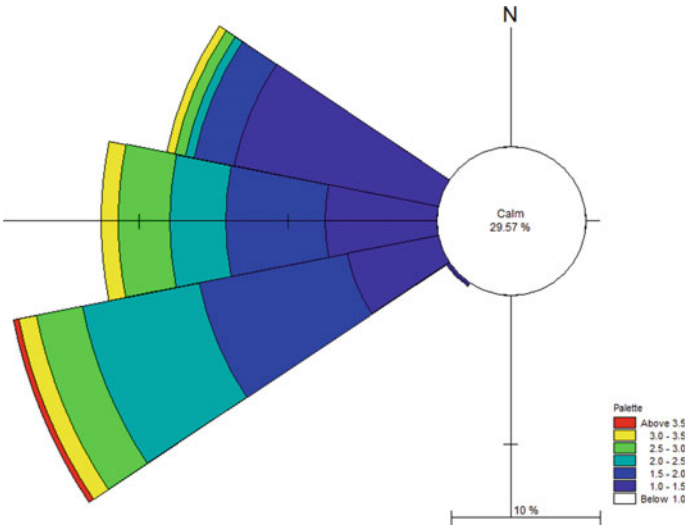

Fig. 7 Inshore rose diagrams at Ratnagiri for Entire Year at −10 m depth

Considering the existing breakwater layout, the following predominant incident significant wave conditions were adopted. The significant wave period for incident waves from the WSW and West directions is considered as 12 s and the 6 s for incident waves from the NW direction for the Physical wave model studies.

2.2 Bathymetry Data

The bathymetry of the study area was made available by the project authorities. The bathymetry was reproduced in the model to the scale as a rigid bed using hydrographic survey chart of January 2000 prepared by the Marine surveyor. It can be seen from bathymetry chart of the fishing harbour basin (Fig. 4) that the contours are more likely parallel to the coastline and the tip of existing west breakwater is at −5.0 m depth contour. At the entrance of the harbour, a deep channel can be observed adjacent to west breakwater tip.

2.3 Tide Data

The observed tide data by IMD at Bhagwati Bunder, Ratnagiri is plotted and typical tide is shown in Fig. 8. The high water level adopted during the model studies was considered as 3.15 m.

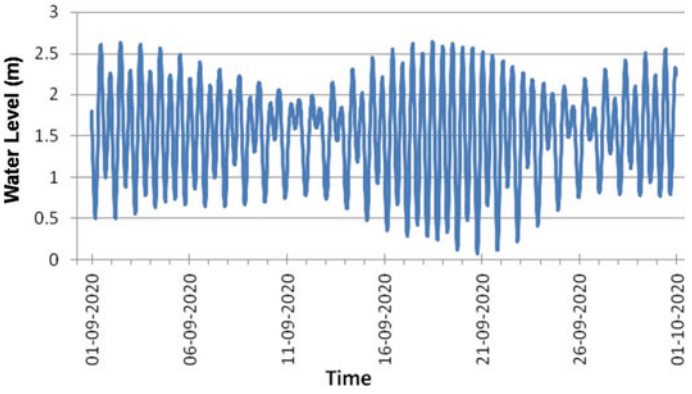

Fig. 8 Observed tide at Bhagwati bunder

3 Physical Wave Model Studies

3.1 Physical Wave Model

The physical wave model studies were conducted for fishing harbour at Bhagwati Bunder at geometric similar (G.S.) scale of 1:120 based on Froudian similarity (Huges Steven A., 1993) with Random Sea Wave Generation (RSWG) system with SCADA control and multichannel data acquisition system. Model tray is housed in the Multi-Purpose Wave Basin (MPWB) hangar of size 75 m × 60 m at CWPRS and the wave generators and data acquisition system control cabin are as shown in Figs. 9, 10 and 11. Two wave paddle units of 21 m each have been used for generating incident waves from West and North West directions in the model which corresponds to about 2.5 km long water face (wave front) in proto. One wave paddle unit of 14.1 m has been used for generating incident waves from WSW direction in the model which corresponds to about 1.7 km long water face (wave front) in proto. Power to wave paddles is supplied by the hydraulic power pack unit by creating required hydraulic pressures as per the input wave generation signal. Hydro Servo Actuator system is used for random sea wave generation. This RSWG system has the facilities for generation of waves in a frequency range of 0.3–3.0 Hz in model, significant waves of up to 10.0 cm and water depths of up to 25.0 cm in model. The matching of the wave spectrum for the three incident wave directions WSW, West, North–west and are shown in Fig. 12.

Fig. 9 MPWBH

Fig. 10 Wave generators

Fig. 11 RSWG, DAS, SCADA

3.2 Proposal Studied in the Physical Wave Model

The initial layout of approach channel for proposed development of cruise terminal and jetty is shown in Fig. 13. Earlier, in the initial layout, the approach channel

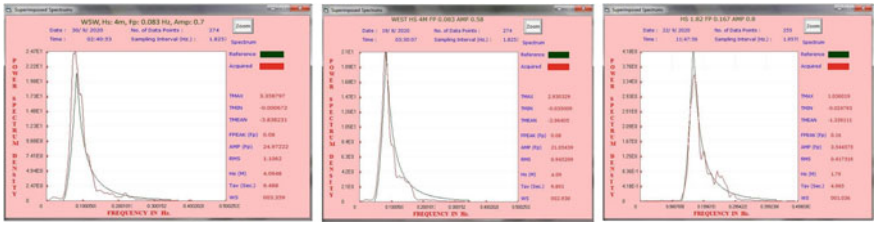

Fig. 12 Matching of wave spectrum in the model for WSW, West and NW directions

and harbour basin was proposed to be dredged to (−) 12 m. Subsequently, as per the draught considerations of the passenger ship, the dredging of the basin was suggested to be done at depth of (−) 9.5 m. Due to revision in dredged depth to (−) 9.50 m in revised layout, the length of approach channel would be reduced by 700 m approximately as compared to the initial layout. The revised layout of approach channel for proposed development of cruise terminal and jetty is shown in Fig. 14.

The crest level of the existing west or commercial breakwater was kept at (+) 7.0 m (C.D) and the crest level of proposed jetty along lee side of existing breakwater and the reclamation level were considered at (+) 5.5 m above CD. The experiments were conducted at high water level (HAT) which is (+) 3.15 m above C.D. The approach channel is 150 m wide and harbour basin was dredged to (−) 9.5 m (C.D.). The approach channel was extended beyond the tip of west breakwater towards sea side (North–west approx.) to a length of about 165 m. The existing clinker 129 m long jetty is located about 315 m from lee side of existing breakwater which is almost parallel to the existing breakwater alignment. The length of berthing face of proposed

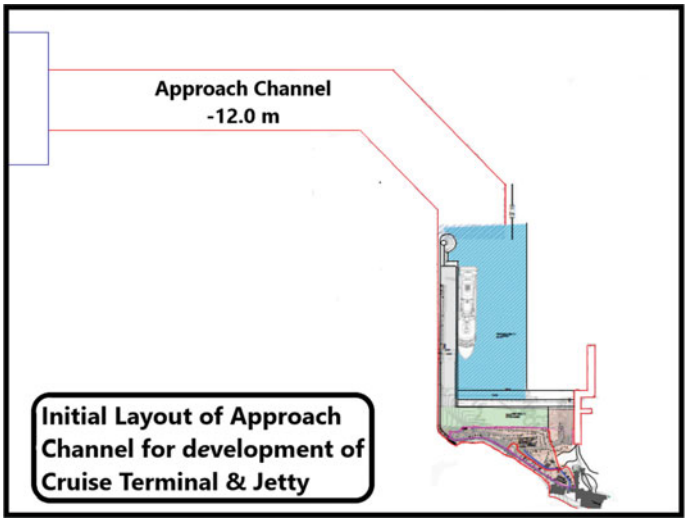

Fig. 13 Initial layout

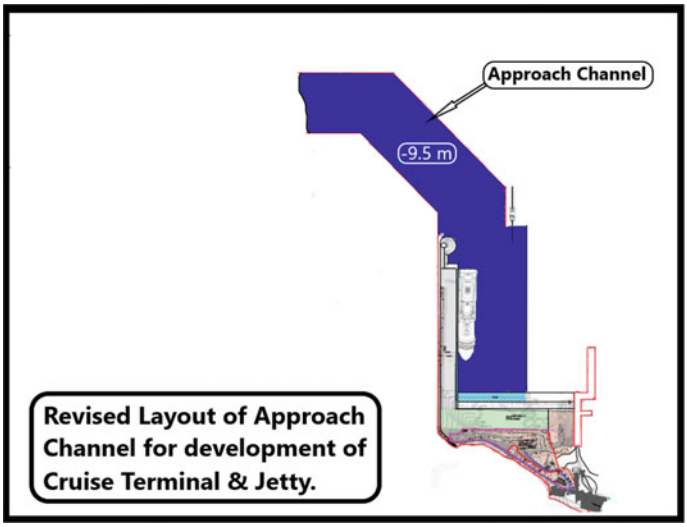

Fig. 14 Revised layout

cruise terminal shall be 283 m in order to accommodate ship/vessel having maximum length of about 245 m and beam width of 32 m. The proposed reclamation area behind the berthing face of cruise terminal shall be about 13,700 sq m approximately.

The predominant incident wave conditions from the West (Hs 4.0 m, Tp 12 s), WSW (Hs 4.0 m, Tp 12 s) and North West (Hs 1.8 m, Tp 6 s) directions were considered for the model studies as per Table 1. The physical model in 3D shallow wave basin of size 52 m × 57 m with bathymetry contours up to −16.5 depth and wave generators at Multi-Purpose Wave Basin Hangar is shown in Fig. 15.

Initially, the model studies were conducted with the proposed 100 m extension of existing breakwater and subsequently optimum extension length was evolved in order to obtain the desired wave tranquility limit of 0.50 m to achieve safe berthing operations at proposed passenger cruise terminal inside the harbour basin round the year. Many alternatives of existing breakwater extension as well as different angle of extension beyond the tip of existing breakwater were tried. Finally, 200 m extension of existing breakwater in line provided adequate wave tranquility conditions at

Table 1 Input wave conditions for wave tranquility studies

Incident wave direction	Significant wave height Hs(m)	Significant wave peak period, Tp (sec)
WSW	4	12
West	4	12
NW	1.8	6

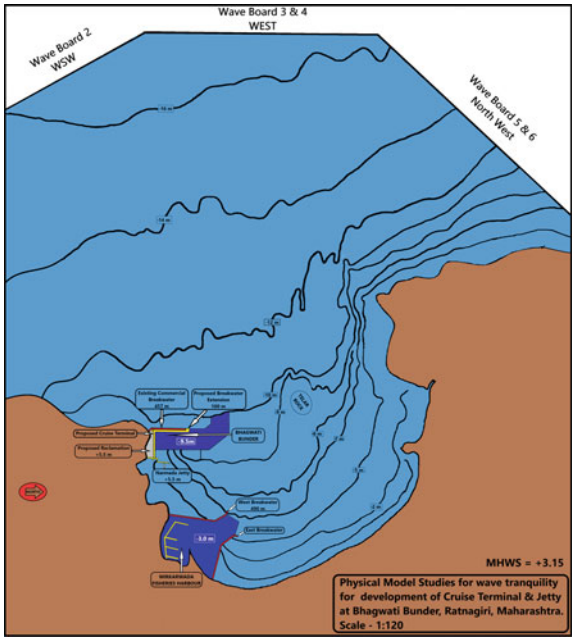

Fig. 15 The physical wave model (Scale G.S. 1/120) in 3D shallow wave basin of size 52 m × 57 m with bathymetry contours and wave generators

passenger cruise terminal for safe operations throughout the year. Therefore, physical wave model studies have been reported here with 100 m and 200 m extension for all three predominant wave directions, viz. WSW, West and North–west (Fig. 16).

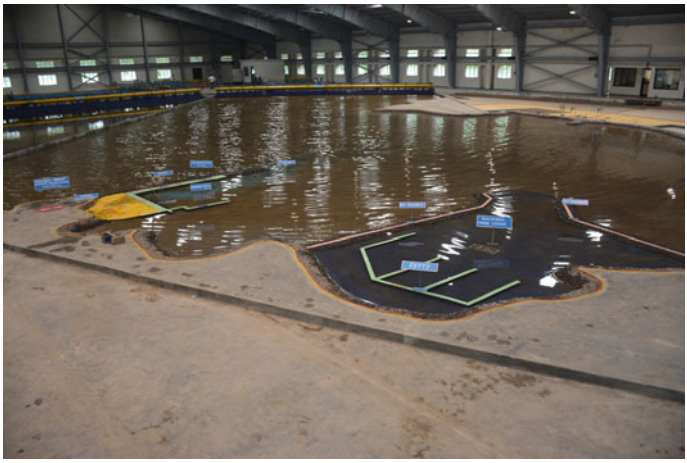

Fig. 16 View of wave model of Bhagwati Bunder (Scale G.S. 1/120) in-housed in 3D shallow wave basin at Multi-purpose Wave Basin Hangar with three wave directions

3.3 Wave Tranquility for Incident Waves from WSW Direction

The physical wave model studies were conducted for incident waves from WSW direction (Hs = 4.0 m, Fp = 0.08 Hz) corresponding to Southwest monsoon season. It was observed that mainly diffracted waves were approaching from West (Main or commercial) breakwater and entering the basin with slight wave attenuation in the existing condition, i.e. without any extension of breakwater. The wave disturbance at the tip of the main breakwater exposed to dominant waves in monsoon was observed to be 3.3 m. The wave disturbances were observed to be very high as 1.3 to 1.4 m on the leeside of the breakwater in the existing condition.

With 100 m extension of west breakwater, the wave disturbance at the tip of the existing breakwater was reduced to 1.10 m. The maximum wave disturbance of about 0.70 m was observed at the berthing face of passenger cruise terminal. The wave disturbance at the proposed reclamation face was about 0.70–0.80 m. The wave tranquility conditions are shown in Fig. 17. The wave disturbance at the middle of the clinker jetty was observed to be 0.70 m and at the tip of the clinker jetty, it was observed as 1.0 m.

The maximum wave disturbance of about 0.60 m was observed at the berthing face of passenger cruise terminal. The wave disturbance at the proposed reclamation face was about 0.50–0.60 m. The wave disturbance at the middle of the clinker jetty was observed to be 0.60 m and at the tip of the clinker jetty, it was observed as 0.9 m.

3.4 Wave Tranquility for Incident Waves from West Direction

The physical wave model studies were conducted for incident waves from West direction (Hs = 4.0 m, Fp = 0.08 Hz) corresponding to southwest monsoon season. It was observed that mainly diffracted waves were approaching from West (Main or commercial) breakwater and entering the basin with slight wave attenuation in the existing condition, i.e. without any extension of breakwater. The wave disturbance at the tip of the main breakwater exposed to dominant waves in monsoon was observed to be 3.3 m. The wave disturbances were observed to be very high as 1.3–1.4 m in the existing condition.

With 100 m extension of west breakwater, the wave disturbance at the tip of the existing breakwater was reduced to 1.10 m. The maximum wave disturbance about 0.75 m was observed at the berthing face of passenger cruise terminal. The wave disturbance at the proposed reclamation face was about 0.60–0.70 m. The wave disturbance at the middle of the clinker jetty was observed to be 0.85 m and at the tip of the clinker jetty, it was observed as 0.95 m.

With 200 m extension of west breakwater, the wave disturbance at the tip of the existing breakwater was reduced to 0.8 m. The maximum wave disturbance of about 0.55 m was observed at the berthing face of passenger cruise terminal. The

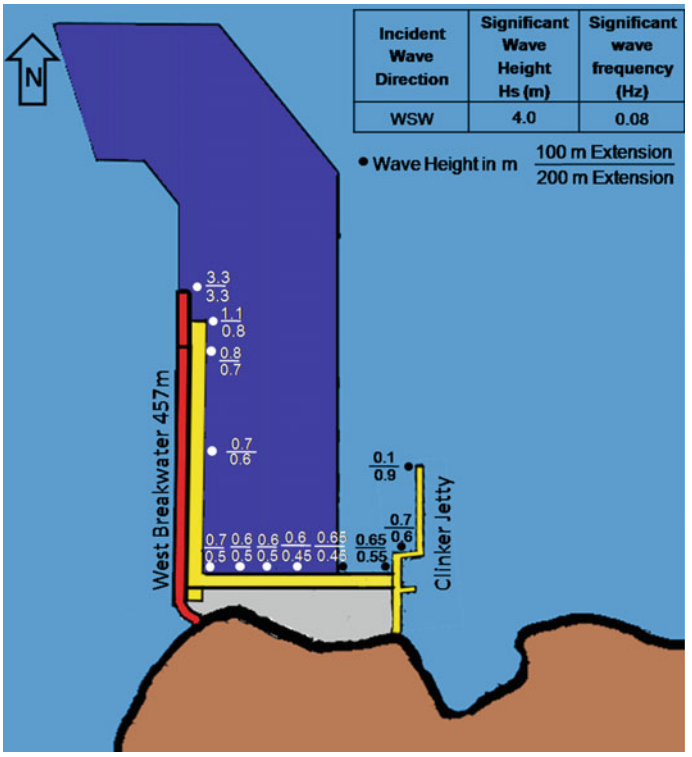

Fig. 17 Wave tranquility conditions for 100 m and 200 m extension

wave disturbance at the proposed reclamation face was about 0.50–0.60 m. The wave disturbance at the middle of the clinker jetty was observed to be 0.85 m and at the tip of the clinker jetty, it was observed as 0.95 m.

3.5 Wave Tranquility for Incident Waves from North West

The model studies were conducted for incident waves from North West direction (Hs = 1.8 m, Fp = 0.167 Hz). It was observed that direct as well as diffracted waves in non-monsoon are approaching the West (Main) breakwater and entering the harbour basin with very slight wave attenuation. The wave disturbances were observed to be 0.50–0.60 m on the lee side of the existing west breakwater in existing condition.

With 100 m extension of west breakwater, the wave disturbance at the tip of the extended breakwater was observed to be 1.20 m and the wave disturbance at the tip of the existing breakwater was reduced to 0.40 m. The wave disturbance on lee side of the existing breakwater around middle was reduced to about 0.35 m. The maximum wave disturbance of about 0.35 m was observed at the western end of berthing face

of passenger cruise terminal. The wave disturbance at the middle of the clinker jetty was observed to be 0.30 m and at the tip of the clinker jetty, it was observed as 0.35 m. The wave disturbance at the proposed reclamation face was about 0.30–0.40 m.

With 200 m extension of west breakwater, the wave disturbance at the tip of the extended breakwater was observed to be 1.20 m and the wave disturbance at the tip of the existing breakwater was reduced to 0.35 m. The wave disturbance on lee side of the existing breakwater around middle was also observed as 0.35 m. The maximum wave disturbance of about 0.30 m was observed at the entire berthing face of passenger cruise terminal. The wave disturbance at the middle of the clinker jetty was observed to be 0.30 m and at the tip of the clinker jetty, it was observed as 0.35 m. The results of wave tranquility conditions are shown in Figs. 18 and 19.

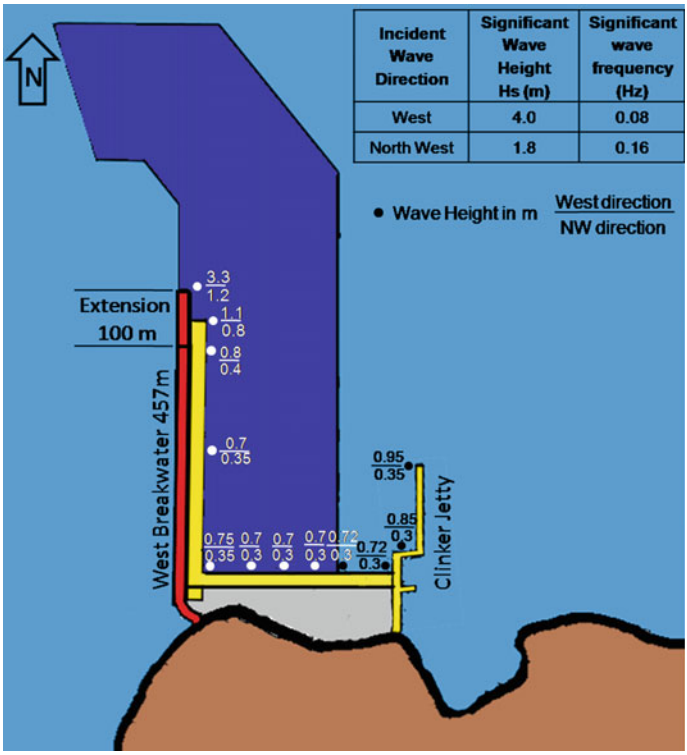

Fig. 18 Wave Tranquility Conditions for 100 m extension of west breakwater for incident waves from West (Hs 4.0 m, Tp 12 s) and North West (Hs 1.8 m, Tp 6 s) directions

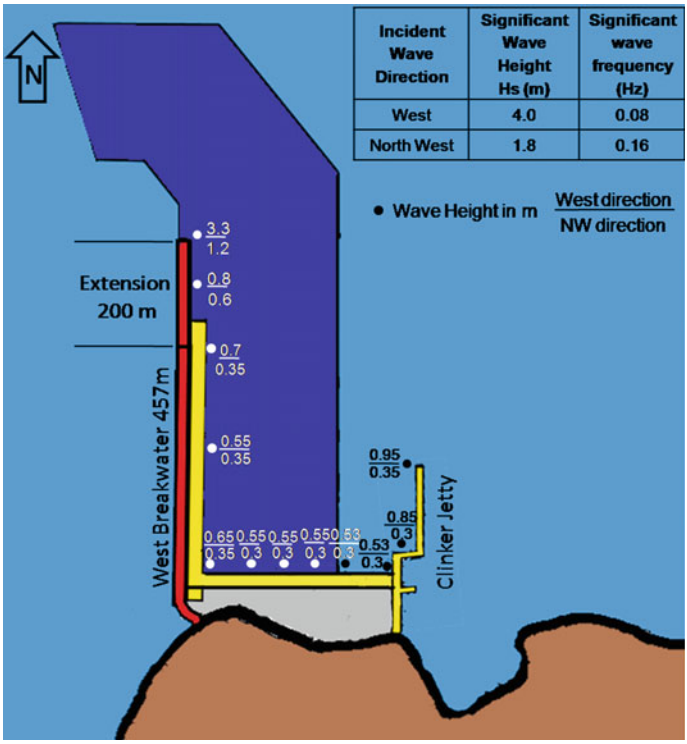

Fig. 19 Wave Tranquility Conditions for 200 m extension of west breakwater for incident waves from West (Hs 4.0 m, Tp 12 s) and North West (Hs 1.8 m, Tp 6 s) directions

4 Results and Discussions

The physical wave model studies were conducted with for 100 m as well as 200 m extension of the existing breakwater for the three predominant wave directions, viz. WSW (Hs = 4.0 m, Tp = 12 s), West (Hs = 4.0 m, Tp = 12 s) and North West (Hs = 1.8 m, Tp = 6 s). The monsoon waves from the West and West-south-west directions during the southwest monsoon season (June–September) are the most critical from the tranquility considerations. Considering the permissible wave limit of 0.50 m for operations at the passenger berth, about 70–80 days will be lost for operation at the passenger berth during the monsoon season under existing condition. The tranquility conditions during the non-monsoon season (October–May) are far better as compared to the monsoon season and provide tranquil conditions at the proposed passenger berth in the existing condition. The incident waves in monsoon mainly from WSW and West quadrant reach the harbour basin after getting diffracted from the tip of existing west or commercial breakwater. The maximum wave disturbance at the entrance of the Bhagwati Bunder was observed to be 3.30 m in monsoon which is quite high. This high wave disturbance at the entrance of the harbour can be attributed

to severe wave conditions prevailing in monsoon. Moreover, the harbour entrance is located at around (−) 10 m depth contour in open sea. The wave energy travelling from deep sea cannot be attenuated much due to lack of shoals or bars or island in its path. In the absence of any turning circle, suitable tug boats will be required for manoeuvring operations of the passenger ships during the entry and exit operations. The suitable depths will be available at the breakwater tip only. With 100 m extension of existing breakwater, the downtime will be about 10 days at the passenger berth during the monsoon season. The 200 m extension will provide just adequate wave tranquility throughout the year at the passenger berth for ship size of 245 m length with wave permissible limit as 0.50 m. In case, smaller ships or fishing crafts are planned in future, this 200 m extension may not provide round the year tranquility at passenger berth. The wave tranquility conditions at the passenger berth and along the proposed reclamation face are almost same, hence the reclamation face may also be utilized for berthing operations in future for other vessels. The breakwater crest has been taken at +7.0 m level as a non-overtopping section for operational conditions for the model studies. The correct crest level will be decided on the basis of wave flume studies only. The wave disturbances obtained in the physical wave model for above three incident wave conditions have been tabulated in Table 2.

5 Conclusions

1. The analysis of the wave data and the configuration of Bhagwati Bunder established that the most critical and predominant incident waves to be considered for the physical model studies are from the directions WSW (Hs = 4.0 m, Tp = 12 s), West (Hs = 4.0 m, Tp = 12 s) and North West (Hs = 1.8 m, Tp = 6 s).
2. The physical wave model studies were conducted using 3-D model with geometric similar scale of 1/120 using random sea wave generation system with multiple data acquisition system at CWPRS using all the three predominant directions WSW, West and North West for existing condition, 100 m extension as well as 200 m extension of the existing west breakwater.
3. The physical wave model studies indicated that under the existing condition, the wave disturbance inside the harbour basin was observed to be 0.4–0.45 m for waves incident from Northwest direction (Non-monsoon season) wave tranquility would be achieved. The maximum wave disturbance was observed to be 1.4–1.5 m inside the harbour basin for incident waves from WSW and West during the monsoon season which is far more than the permissible limit of 0.50 m. Therefore, it was contemplated to extend the existing west breakwater by 100 m and 200 m in the same line to achieve desired wave tranquility limit of 0.50 m throughout the year for safe berthing operations at the proposed passenger cruise terminal and inside the harbour basin.
4. The physical wave model studies indicated that the maximum wave disturbance at berthing face of proposed cruise terminal would be about 0.72–0.75 m with 100 m extension of existing breakwater (Figs. 11 and 12) in monsoon which

Table 2 Physical wave model results for incident waves WSW & West (Hs = 4.0 m, Tp = 12 s) and NW (Hs = 1.8 m, Tp = 6 s)

Sl. No	Location	Incident waves from WSW (Hs = 4.0 m, Tp = 12 s)		Incident waves from West (Hs = 4 m, Tp = 12 s)		Incident waves from NW (Hs = 1.8 m, Tp = 6 s)	
West breakwater extension		100 m	200 m	100 m	200 m	100 m	200 m
1	Tip of extended West Breakwater	3.3	3.3	3.30	3.30	1.20	1.20
2	Middle of extension	1.1	0.80	1.10	0.80	0.80	0.60
3	Tip of existing West Breakwater	0.80	0.70	0.80	0.70	0.40	0.35
4	Middle on the Lee side of existing West Breakwater	0.70	0.60	0.70	0.55	0.35	0.35
5	Western face of passenger cruise terminal	0.70	0.50	0.75	0.65	0.35	0.35
6	Near the western face of passenger cruise terminal	0.60	0.50	0.70	0.55	0.30	0.30
7	Middle of the passenger cruise terminal	0.60	0.50	0.70	0.55	0.30	0.30
8	Near middle of the passenger cruise terminal cruise terminal	0.60	0.45	0.70	0.55	0.30	0.30
9	Near the eastern face of passenger cruise terminal	0.65	0.45	0.72	0.53	0.30	0.30
10	Eastern face of passenger cruise terminal	0.65	0.55	0.72	0.53	0.30	0.30
11	Middle of clinker jetty	0.7	0.60	0.85	0.85	0.30	0.30
12	Tip of clinker jetty	1.0	0.90	0.95	0.95	0.35	0.35

would cause downtime about 10 days in monsoon. It was also envisaged that the wave tranquility of 0.50 m would be just achieved throughout the year for berthing operation at the proposed passenger cruise terminal with 200 m extension of existing west breakwater (Figs. 11 and 13).

5. It was observed from the model studies that under existing condition with breakwater length of 457 m, the downtime at proposed passenger jetty would be about 70–80 days during the monsoon season and it would be tranquil throughout during the non-monsoon season. With 100 m extension of breakwater, the downtime would be about 10 days during the monsoon season only. With 200 m extension of breakwater, the downtime would be almost nil throughout the year.
6. The physical wave model studies also indicated that the alignment of the proposed approach channel may be required to be shifted suitably towards north due to extension of the existing west breakwater. There is scope to study ship navigation aspects due to extension of the existing breakwater and shifting of the proposed channel.
7. The physical wave model is a very useful tool for realistic simulation of complicated wave patterns in the bay and near berths/jetties. Layout and configuration

of breakwater/s can be suitably decided by geometrically similar rigid bed wave modelling technique to optimize the capital cost of massive coastal structure like breakwater.

Acknowledgements The authors would like to acknowledge the Director, CWPRS, Ministry of Jal Shakti, Department of Water Resources, River Development & Ganga Rejuvenation, Government of India (GoI) for his guidance and constant encouragement during the course of study. The authors express their deep gratitude for according permission to publish this paper.

References

1. Shore Protection Manual (1984) Volume I, coastal engineering research center, department of the army, US Army Corps of Engineers, Washington DC 20314
2. Hughes SA (1993) Physical models and laboratory techniques in coastal engineering, coastal engineering research center, waterways experiments station, USA

Assessment of Vulnerability for Eastern India Coastal Region Using Geospatial Techniques

M. Ashiq Ahmed, Nilanjan Saha, and S. A. Sannasiraj

Abstract The increase in population and coastal infrastructure demands a rigorous assessment of coastal vulnerability for extreme events. The predictions by Intergovernmental Panel for Climate Change (IPCC) indicate that climate change will severely impact coastal regions, river systems, urban infrastructures and increase the frequency of inundation along coastal areas. This study emphasizes the need to use extreme events and socioeconomic data to evaluate the vulnerability of a given coast. This paper presents the vulnerability assessment of the Chennai coastal region using eight variables: coastal elevation, coastal slope, rate of shoreline change, tidal range, sea level rise, storm surge, Adyar flood and land use and land cover. A Coastal Vulnerability Index (CVI) is calculated by integrating the physical and social–economic variables. The Coastal Vulnerability Index for shoreline erosion ranges from 15 to 21 with a mean value of 18 and a standard deviation of 1.6, while the Coastal Vulnerability Index for inundation ranges from 4.1 to 12.7 with a mean value of 7.3 and a standard deviation of 1.4. The vulnerability maps show the exposed regions around river Adyar that are highly vulnerable to coastal erosion and floods, especially due to extreme events. The assessment indicated the variation in the vulnerability of inundation around the Chennai Port regions and the low vulnerability of the shoreline erosion in this region. The vulnerability assessment suggests that planning and adaptation of the coastal ecology for the future needs are to be performed with extreme caution.

Keywords Coastal Vulnerability Index · Coastal processes · Socioeconomic parameters · Extreme events · Climate change

M. A. Ahmed (✉) · N. Saha · S. A. Sannasiraj
Department of Ocean Engineering, Indian Institute of Technology Madras, Chennai 600036, India
e-mail: mashiqahmed@gmail.com

N. Saha
e-mail: nilanjan@smail.iitm.ac.in

P. V. Timbadiya et al. (eds.), *Coastal, Harbour and Ocean Engineering*, Lecture Notes in Civil Engineering 321, https://doi.org/10.1007/978-981-19-9913-0_29

1 Introduction

Coastal cities continue to be exposed to the effects of climate change, especially sea level rise and extreme events [2, 3, 17]. Accelerated development and anthropogenic activities of the coastal regions to meet the demands of the population have instigated burden on the coastal ecosystem and induced climate change hazards. Extreme events such as cyclones have always been part of the earth's system, but the frequency and intensity have increased as the world warms, and 90 percent of disasters are now classified as climate change-related, costing the global economy 520 billion dollars per year and pushing 26 million people into poverty [15]. The effects of climate change are visible in the form of rising sea levels and temperature, melting of arctic ice sheets, burning forests and more intense cyclones. It is requisite that vulnerability of coastal regions is assessed in the further planning and development of coastal infrastructure to address climate change hazards such as sea level rise and extreme events. The Coastal Vulnerability Index system is the most prevalent and widely adopted method for this purpose. The eastern coast of Indian state Tamil Nadu similar to numerous coastal regions in the world has a rich coastal ecosystem and biodiversity. Significant percentage of the population lives and thrives in the coast, and the coastal regions are a hub to several industries and infrastructures which provide resources and livelihood to the coastal population but due to increased anthropogenic activities, the effects of climate change have increased the intensity and frequency of extreme events like storms such as Hudhud-2014, Vardah-2016, Ochki-2017, Fani-2019, Amphan-2020, Tauktae-2021 and Yaas-2021. Hence, it is vital to assess the vulnerability to enable policymakers, decision-makers, stakeholders and port authorities to change the strategies for the better safety of the coast. This paper focuses on the vulnerability due to climate change, particularly sea level rise with extreme events and attempts to study the vulnerability of erosion, inundation and recommend suitable strategies exemplified as a case study along eastern India's—Tamil Nadu—coastal regions.

2 Materials and Methods

2.1 Coastal Vulnerability Index

There are various methods to assess the coastal vulnerability such as index-based methods, indicator-based approach, GIS-based decision support systems, methods based on dynamic computer models [11]. The index-based methods are perhaps the most common because it is simple, hasty and reliable [8]. The most popular is Coastal Vulnerability Index (CVI) which was first developed by Gornitz and Kanciruk [5] to assess the US East Coast to climate change, particularly sea level rise considering the risks to inundation and coastal erosion hazards. This study presents an attempt to estimate the Coastal Vulnerability Index using historical and simulated extreme events along with socioeconomic variables. The ocean and geomorphological variables,

identified as significantly contributing to vulnerability, are coastal slope, elevation, shoreline change rate, mean tidal range, sea level rise; in addition, extreme events-based hazards like storm surge and socioeconomic parameters like land use and land cover (LULC) are studied in this paper. This CVI presented in this paper is a combination of Physical Vulnerability Index (PVI) and Socioeconomic Vulnerability Index (SVI) which is often either averaged equally or given specific weights [1, 10, 13]. The CVI for this study has been separated into vulnerability due to shoreline erosion and vulnerability due to storm surge and inundation. The vulnerability of the shoreline erosion is calculated from the physical parameters such as coastal elevation, slope, rate of shoreline change, tidal range, sea level rise, storm surge.

The vulnerability due to inundation is calculated from physical parameters such as coastal elevation, slope, storm surge, 2015 Adyar Flood and socioeconomic parameters like land use and land cover. The CVI is computed as a combination of the Physical Vulnerability Index with a weight of 70% and Socioeconomic Vulnerability Index with a weight of 30% to capture the effect of climate change on the coast [10]. Based on the evaluated CVI, regions from very low (class 1) to very high (class 5) vulnerability were identified [4, 7, 9, 10, 14]. The formula to calculate the PVI, SVI and CVI are

$$\text{PVI or SVI} = \sum_{i=1}^{n} W_i V_i, \tag{1}$$

$$CVI = SUM\,(PVI, SVI), \tag{2}$$

where n = Total number of variables, W_i = Weight, V_i = Vulnerability score.

2.2 Study Area and Data Sources

The study area is along the eastern coast of India in state Tamil Nadu along the Bay of Bengal, which stretches from the Chennai Port (13.081384° N, 80.292045°E) to the Adyar River (13.013432° N, 80.272965° E) as shown in Fig. 1. The study region also covers the river Cooum mouth which is just south of the Chennai Port. The various data sources and their period used for the assessment of vulnerability like digital elevation, slope, rate of shoreline change, sea level rise, tidal range, storm surge, simulated Adyar flood and sentinel 2A images for land use and land cover mapping for the region are shown in Table 1.

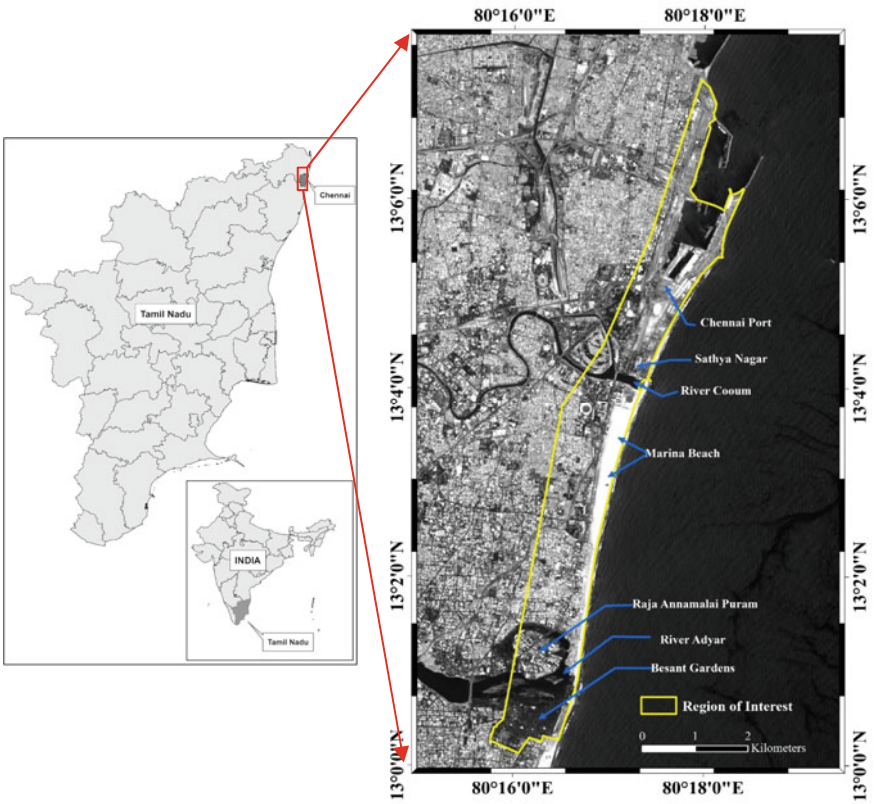

Fig. 1 Study area with important locations of interest (Background map courtesy of USGS)

2.3 Coastal Elevation, Slope and Rate of Shoreline Change

The coastal elevation is an important variable in determination of vulnerability; the higher the elevation, the lower the vulnerability and vice versa. The variables are categorized from very low to very high vulnerability according to Table 2 shown. The average coastal elevation of the study region is 3.16 m above the MSL with 68.5% and 29.9% being highly vulnerable zone and very highly vulnerable zone, respectively. The slope is derived from the DEM using the slope tool in ArcGIS software; 38.5% of the slope falls in the very low vulnerability category and 16% in the very high vulnerability category. The rate shoreline of change for the coastline [5] is being represented here as the linear regression rate (LRR) and is measured in m/year from 2000 to 2019. The study region experiences a shoreline erosion of −4.15 m/year north of river Adyar and an accretion rate of 7.32 m/year in the river Cooum mouth leading to stagnation of the water. The south of river Adyar mouth also experiences erosion of up to −1.88 m/year.

Table 1 Data sources

Category	Data	Data sources	Period
Physical parameter	Coastal elevation (m)	Digital elevation model (DEM) obtained by drone with a resolution of 10 m	2019
	Coastal slope (%)	Calculated from the DEM	2019
	Rate of shoreline change (m/year)	Data obtained from Gracy et al. [6]	2000–2019
	Sea level rise (mm/year)	Monthly mean sea level from Permanent Service for Mean Sea Level (PSMSL), Available at: http://www.psmsl.org/data/obtaining	1916–2015
	Storm surge (m)	ADCIRC model [16]	-
	Adyar flood simulation (m)	Data obtained from Sridharan et al. [12]	2015
	Tidal range (m)	WXTide32, Available at: http://www.wxtide32.com/	2021
Socioeconomic parameter	Land use and land cover	Sentinel 2 Satellite Available at: https://earthexplorer.usgs.gov/	2021

Table 2 Variable rankings

Category	Very low	Low	Moderate	High	Very high
Variables					
Coastal elevation (m)	>10	6 to 10	6 to 4	4 to 2	<2
Rate of shoreline change (m/year)	>+2	+1 to + 2	−1 to + 1	−1 to −2	<−2
Coastal slope (%)	>1.9	1.3 to 1.9	0.9 to 1.3	0.6 to 0.9	<0.6
Mean tidal range (m)	>6	4 to 6	2 to 4	1 to 2	<1
Sea level rise (mm/year)	<−1.21	−1.21 to 0.1	0.1 to 1.24	1.24 to 1.36	>1.36
Storm surge (m)	0	0 to 1.5	1.5 to 3	3 to 5	>5
Land use and land cover	Water bodies; marsh/bog; moor; sparsely vegetated areas; bare rocks	Natural grasslands; coastal areas	Forest	Agriculture	Urban or built-up and industrial infrastructure

2.4 Sea Level Rise and Tidal Range

The mean sea level rise of Chennai is estimated using the Permanent Service for Mean Sea Level data obtained from tide gauge station at 13.1, 80.3 from 1916 to 2016. The linear regression method estimates a sea level rise of 0.57 mm/year with a 95% confidence interval of ±0.31 mm/year based on the monthly mean sea level data. The tidal range is linked to permanent and episodic inundation hazards. The tidal range data have been obtained from WXTide32 software. For this study area, the historic maximum tidal range value has been adopted and is applied to the coastal boundary.

2.5 Storm Surge and River Adyar Flood

Storm surge is the abnormal rise in the water level due to a cyclone or any other hazard event. The storm surge is modeled in ADCIRC v12.3 [16]. ADCIRC is a finite element-based model that may be used to simulate storm surges and other coastal applications. Surface wind fields and atmospheric pressure fields are required for storm surge modeling. ADCIRC's versatility allows it to create unstructured grids with high resolution along the coast and coarser resolution further off. The storm surge extreme event model simulated is for the Very Severe Cyclonic Storm (VSCS) Vardah, the most intense tropical cyclone of 2016, and the cyclone made landfall over the eastern coast of India, close to Chennai, Tamil Nadu, with sustained wind speed up to 130 km/hr. The model grid covers the domain that covers the part of the east coast of India (78°E to 92°E and 2°N to 23°N). In the present work, inundation grid resolution varies from 100 m at the nearshore to 10 km in the deeper ocean with 157,390 grid points; the surge grid varies from 500 m at the nearshore to 40 km in the deeper ocean with 56,721 grid points. The grid covers an offshore length of 1500 km, which allows the model to predict and run even when the cyclone is located far off in the open ocean. The storm surge depth in this region is between 0 and 0.68 m with an inundation extent of up to 713 m. The storm surge vulnerability ranks have been considered as shown in Table 2. On December 1, extremely heavy rainfall (about 60 mm/hr) was recorded that was a one in hundred-year return period (i.e., 0.01 annual exceedance probability) event; because of such extreme event occurrence, most portions of the city were flooded, with the region adjacent to the Adyar River being the most severely damaged [12]. River Adyar flood simulation [12] has been used in the inundation vulnerability assessment for this study region.

2.6 Land Use and Land Cover

The LULC map shows the socioeconomic activities of the region. These maps help to assess the activities that shall be vulnerable to inundation. The urban and industrial infrastructures near the coast are highly vulnerable to inundation, while sparsely vegetated areas and bare rocky regions are less vulnerable. In this study, the LULC variable is given a weightage of 30% in the computation of CVI. The image data used are obtained from Sentinel 2A satellite with a spatial resolution of 10 m, and the LULC map is prepared using the maximum likelihood classifier methodology in ArcGIS software.

3 Results and Discussions

The vulnerability of the Chennai region to shoreline erosion and inundation due to extreme events has been studied in this paper. The vulnerability has been estimated as weighted sum of physical and socioeconomic parameters. The value of the CVI for the shoreline vulnerability presented in Fig. 2 ranges from 15 to 21 with a mean value of 18 and a standard deviation of 1.6, while the value of the CVI for the inundation vulnerability presented in Fig. 3 ranges from 4.1 to 12.7 with a mean value of 7.3 and a standard deviation of 1.4. The vulnerability index has been classified into five vulnerability zones based on a quantile classification method from very low vulnerability (1) to very high vulnerability (5).

Figure 2 shows the shoreline change vulnerability; the area north of Adyar River, Srinivasa Puram (13.018°, 80.278°) is highly vulnerable to erosion with CVI of 20, whereas in the region south of the Adyar River, the CVI ranges from 18 to 20, with mostly low-to-moderate vulnerability with a small region being highly vulnerable. The shoreline between the north of river Cooum and south of the Chennai Port (13.081472°, 80.292088°) has very low vulnerability with CVI ranging from 15 to 17. The Marina Beach stretching between rivers Adyar and Cooum has vulnerability index ranging between 18 and 21 that is from low to very high vulnerability; this substantial variation of the shoreline erosion CVI along Marina Beach coast is due to the consideration of additional variables like elevation, slope, sea level rise, tidal range and storm surge for a length 100 m across the coastal boundary, and this is done to capture the impact of extreme events on the shoreline erosion. Although the Marina Beach region experiences accretion rate of 0.2–2.69 m/year, the elevation of this region coupled with slope and storm surge of 0.65 m makes certain regions highly vulnerable. Both rivers Adyar and Cooum experience formation of sand bars which block the drainage of water to the sea, river Cooum has an average accretion rate (Linear regression rate) of 5.9 m/year and river Adyar has accretion rate of 1.32 m/year, formation of sand bars in the river mouth increases the likelihoods of

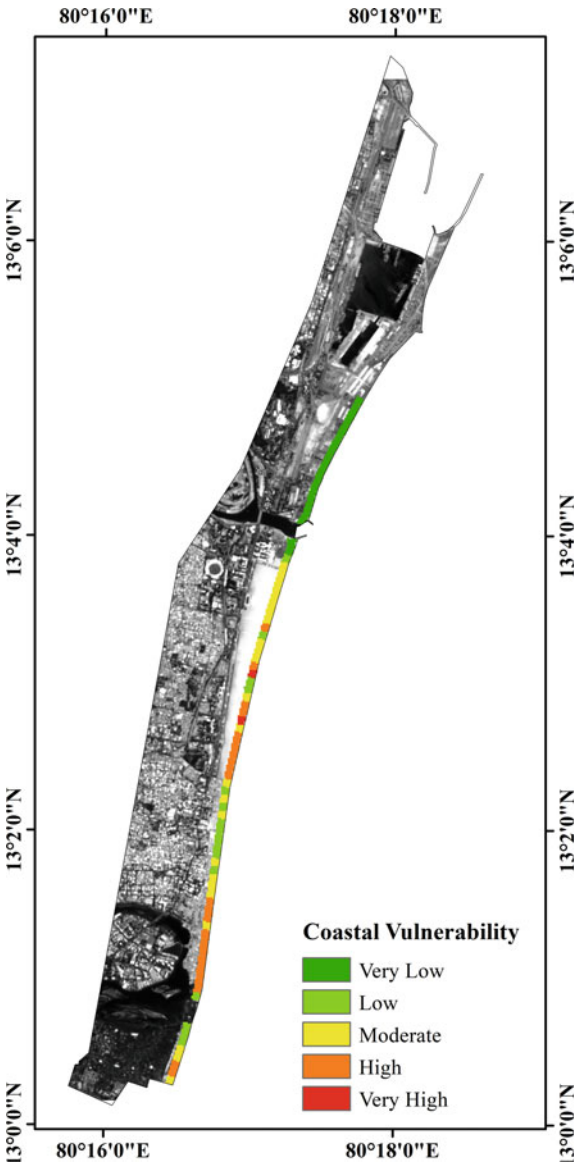

Fig. 2 Coastal Vulnerability Index map showing shoreline erosion (Background map courtesy of USGS)

flood hazards and although training walls have been constructed in the river Cooum mouth, it has not yielded the required outcome to reduce sand bar formation and floods.

Figure 3 shows the Coastal Vulnerability Index due to inundation for extreme events, and the CVI has been categorized into five classes: very low (4.1–6.2), low

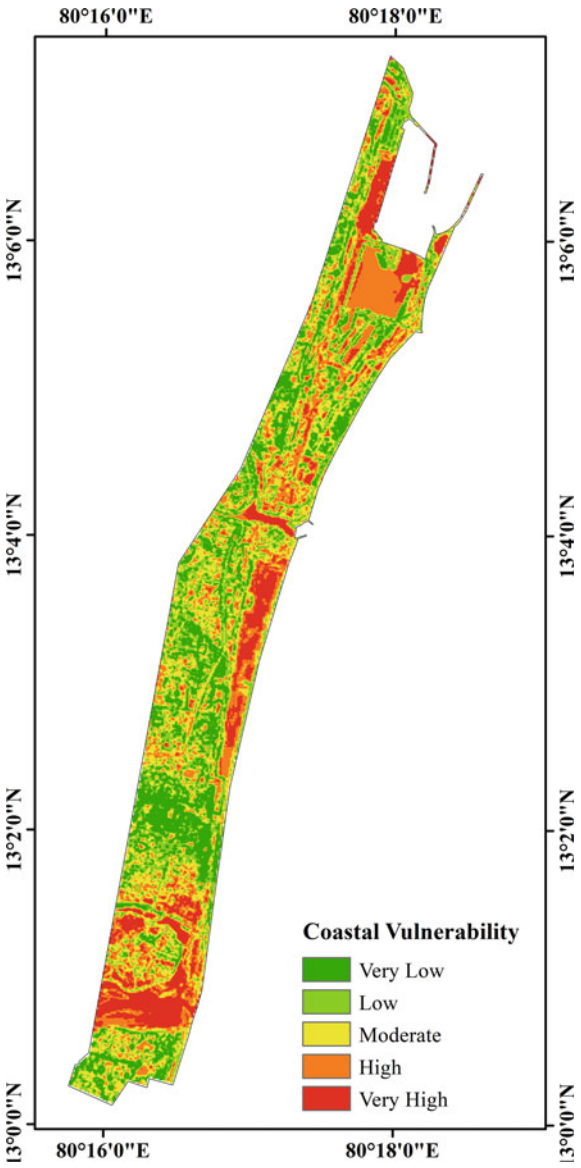

Fig. 3 Coastal Vulnerability Index map showing inundation for extreme events' hazard

(6.2–6.9), moderate (6.9–7.8), high (7.8–8.9) and very high (9.0–12.7). The parameters used in the assessment are coastal elevation, coastal slope, cyclone Vardah simulated storm surge, river Adyar flood, land use and land cover. The region around the Bharathi Dock in Chennai Port, particularly Chennai Container Terminal, is very highly vulnerable to inundation with CVI ranging from 9.2 to 9.9, and this region has relatively very low slope compared with other regions and therefore becomes

flooded in case of a storm. The Chennai Port trust area around Sathya Nagar, north of river Cooum, has a vulnerability index ranging from 7.6 to 9.2 with most of the region being highly vulnerable to inundation. The Navalar Nagar area south of river Cooum has CVI ranging from 5.5 to 7.8 with majority of the region being low to moderately vulnerable. The Marina Beach is highly vulnerable to inundation, and it has vulnerability index mostly ranging from 8.3 to 9; however, a small region south of river Cooum mouth and around Dr. MGR memorial is moderately vulnerable with CVI ranging from 6.9 to 7.6 because of the higher slope in this region. Marina Beach which is highly vulnerable to inundation is mostly contributed by the physical parameters like the elevation, slope and storm surge. The CVI assessment of region between the north of Adyar River and south of Marina Beach indicates low vulnerability to inundation; although this region is highly populated with the fisherman community and close to the coast, the elevation data collected indicate a predominantly higher elevation in this particular region and this is also evident with the low shoreline erosion vulnerability of the same region. It should be noted that presence of an urban or built-up regions close to the coast does not make a region highly vulnerable to a particular hazard; for this reason, the land use and land cover variable weightage considered in the CVI assessment is 30% to provide a better understanding and estimate of the CVI for flooding due to extreme events. Raja Annamalai Puram region surrounded by and around river Adyar has CVI ranging from 4.8 to 11.3; however, a significant portion of the area is very highly vulnerable to inundation and flooding due to extreme events such as storm surges and heavy rainfall. The Besant Gardens Forest area shown in Fig. 1 has vulnerability index ranging from 5.1 to 7.9, the region has very low-to-low vulnerability to inundation, and this is mainly due the higher elevation of this region.

4 Conclusions

The current study aims to address the impact of climate change-induced extreme events in the vulnerability of the coast to erosion and inundation. The CVI maps for shoreline erosion and inundation provide an insight to the regions that are highly vulnerable to extreme events. Although the extreme events are a reversible hazard, the increase in the frequency and intensity of these hazards as a result of climate change will cause continuous disruptions in these highly vulnerable regions; hence, it is necessary to plan and come up with suitable adaptation measures for safety of livelihood and coastal infrastructure. This study shows the long-term impact of sea level rise due to human-induced global warming and rapid infrastructure development on the Chennai coast. The regions depicted by the high vulnerability due to inundation are likely to result in loss of residential, industrial and farming lands, increase in saline water intrusion as a result of sea level rise and extreme events. The variables coastal elevation, slope, storm surge from extreme events are the main contributors

to the vulnerability of this region. The river Adyar flooding mainly affects region surrounding the river banks. The dredging of sand bars and construction of efficient training walls can help in reducing flood surrounding the rivers.

Acknowledgements The authors would like to thank the Department of Science and Technology, Government of India, for supporting through the grant number DST/CCP/CoE/141/2018(G), through the initiative Climate Change Impacts on Coastal Infrastructure and the Adaptation Strategies for development of hazard and risk maps along the east coast of India for coastal flooding.

References

1. Balica SF, Wright NG, Van der Meulen F (2012) A flood vulnerability index for coastal cities and its use in assessing climate change impacts. Nat Hazards 64(1):73–105
2. Change IC (2014) Synthesis report. Contribution of working groups I. II and III to the fifth assessment report of the intergovernmental panel on climate change, p 151(10.1017)
3. Church JA, Godfrey JS, Jackett DR, McDougall TJ (1991) A model of sea level rise caused by ocean thermal expansion. J Clim 4(4):438–456
4. Gornitz V (1990) Vulnerability of the U.S. to future sea-level rise. J Coast Res Spec Issue 9:201–237
5. Gornitz V, Kanciruk P (1989) Assessment of global coastal hazards from sea level rise (No. CONF-8907104-1). Oak Ridge National Lab (ORNL), Oak Ridge, TN (United States)
6. Gracy Margret Mary R, Sundar V, Sannasiraj SA (2022) Analysis of shoreline change between inlets along the coast of Chennai, India. Mar Georesources Geotechnol 40(1):26–35
7. Koroglu A, Ranasinghe R, Jiménez JA, Dastgheib A (2019) Comparison of coastal vulnerability index applications for Barcelona Province. Ocean Coast Manag 178:104799
8. Mahapatra M, Ratheesh R, Rajawat AS (2013) Sea level rise and coastal vulnerability assessment: a review. Int J Geol Earth Environ Sci 3(3):67–80
9. Nayak S, Bhaskaran PK (2014) Coastal vulnerability due to extreme waves at Kalpakkam based on historical tropical cyclones in the Bay of Bengal. Int J Climatol 34(5):1460–1471
10. Rajasree BR, Deo MC (2020) Assessment of coastal vulnerability considering the future climate: a case study along the central west coast of India. J Waterw Port Coast Ocean Eng 146(2):05019005
11. Ramieri E, Hartley A, Barbanti A, Santos FD, Gomes A, Hilden M, Laihonen P, Marinova, N, Santini M (2011) Methods for assessing coastal vulnerability to climate change. ETC CCA technical paper 1:1–93
12. Sridharan B, Gurivindapalli D, Kuiry SN, Mali VK, Nithila Devi N, Bates PD, Sen D (2020) Explicit expression of weighting factor for improved estimation of numerical flux in Local Inertial models. Water Resour Res 56(7):e2020WR027357
13. Thieler ER, Hammar-Klose ES (1999) National assessment of coastal vulnerability to sea-level rise: preliminary results for the US Atlantic coast (No. 99-593). US Geological survey
14. Thieler ER, Hammar-Klose ES (2000) National assessment of coastal vulnerability to sea-level rise; preliminary results for the US Gulf of Mexico Coast (No. 2000-179)
15. UN75 (2020) Shaping our future together. https://www.un.org/. Accessed 16 Sept 2021
16. Vyshnavi Y, Sriram V, Murali K (2021) Influence of coastal inundation on the east coast India for tropical cyclone Vardah based on future climate scenarios. Unpublished report
17. Zimmerman R, Faris C (2011) Climate change mitigation and adaptation in North American cities. Curr Opin Environ Sustain 3(3):181–187

Coastal Management Information System (CMIS) for South Indian Coastal States

J. Sriganesh, V. Sundar, S. A. Sannasiraj, and K. Murali

Abstract The coasts are exposed to hazards that are natural (global warming-induced sea-level-rise, river mouth closure by siltation, changing climate with the increased frequency of cyclonic storm surge, coastal flooding, tsunami, etc.) and due to anthropogenic activities (shoreline erosion, sewage treatment plants, desalination plants, etc.). There are several coastal protections that are in vogue for a specific (single) hazard around the world and different advanced techniques available to protect and preserve the coasts from such hazards. Apart from combating the hazards, there is rapid progress in coastal development. All of these might have provoked the thought of the necessity of the coastal management information to the scientific and engineering coastal working community. The Coastal Management Information System (CMIS) mainly focuses on the in situ data collection of environmental data for the planning, design of structures and schemes for sustainable coastal conservation and development. The monitoring parameters are wave, current, wind, tide, bathymetry, beach profile, shoreline, sediment characteristics in near-shore as well as offshore in case estuarine coasts the riverine data such as river current, discharge, conductivity, temperature along with the depth in a different location from sea to 2 km were measured. Although three coastal sites with different coastal features, Devaneri in Tamil Nadu, Ponnani in Kerala and Karaikal in Puducherry, were selected for this purpose, salient details only for the site along Karaikal are reported herein.

Keywords Shoreline · Beach profiles · Bathymetry · Current

J. Sriganesh (✉) · V. Sundar · S. A. Sannasiraj · K. Murali
Department of Ocean Engineering, Indian Institute of Technology Madras, Chennai 600 036, India
e-mail: sriganeshgeo@gmail.com

V. Sundar
e-mail: vsundar@iitm.ac.in

S. A. Sannasiraj
e-mail: sasraj@iitm.ac.in

K. Murali
e-mail: murali@iitm.ac.in

P. V. Timbadiya et al. (eds.), *Coastal, Harbour and Ocean Engineering*, Lecture Notes in Civil Engineering 321, https://doi.org/10.1007/978-981-19-9913-0_30

1 Introduction

There is an insufficient information on the characteristics of ocean waves and currents in the nearshore that are the essential driving parameters responsible for the stability of the shoreline in the presence or absence of structures. In addition, the local physical phenomenon depends on the local morphodynamics and coastal geomorphology. There are monitoring and warning systems in place to look at coastal extremes, such as waves, storm surges and associated coastal floods. However, along several stretches of the coast, the risk on the stability of the shoreline is poorly defined under assumed wave and current climate conditions because of sparse field networks and relatively limited historical records. This gives a poor baseline for decision makers in assessing the future changes, detecting changes in observed records or to plan and design mitigation measures if needed.

The assessment of coastal erosion or deposition like sand bar formations as well as the planning for the mitigation measures is directly on the driving parameters. Even though physical and numerical models are available to describe these phenomena, both do suffer as several parameters that dictate the driving forces are basically assumed. The ground truth of results from these simulation models is not easily verifiable against observations due to lack of high-quality observation data. Hence, prediction on coastal erosion/deposition close to reality is still a major issue. Beach erosion rates could be predicted based on the data obtained from monitoring campaigns and via coastal line observations obtained remotely. Both methods if combined produce the most accurate results closer to the nature.

The Coastal Management Information System (CMIS) deals with the monitoring (via onshore beach profiling through land surveying) to provide data needed for the planners, designers, decision makers and the validating numerical models that gained rapid momentum in understanding the behavior of waves, wave-induced sediment transport rates and a host other coastal and estuarine phenomenon. Three coastal sites with different coastal features: Devaneri in Tamil Nadu (Latitude: 12° 39′ 05″ N, Longitude: 80° 12′ 29″ E), Ponnani in Kerala (Latitude: 10° 44′ 50″ N, Longitude: 75° 55′ 46″ E) and Karaikal in Puducherry (Latitude: 10° 54′ 55″ N, Longitude: 79° 51′ 10″ E), were selected for this purpose. This paper reports salient details only for the site along Karaikal that experiences coastal flooding frequently.

2 Measured Parameters

For a monitoring campaign, the selection of site, parameters to measured, selection of necessary sensors and devices are of prime importance that requires a critical in-depth planning and decision making. The parameters that are usually considered for monitoring the coastal environment are provided in Table 1.

Table 1 Details of Parameters to be measured and respective instruments

S. No	Parameter	Characteristics	Instruments
1	Wave	Wave height	Directional Wave Recorder (DWR)
		Wave direction	
		Time period	
2	Current	Ocean current-velocity profile	Acoustic Doppler Current Profiler (ADCP)
		River current-point current	Current Meter (CM)
3	Tide	Tidal amplitude	Tide Gauge (TG)
4	Wind	Wind speed	Automatic Weather Station (AWS)
		Wind direction	
5	Bathymetry	Deep water (−5 m to −20 m)	Echo sounder with Differential Global Positioning System (DGPS)
		Shallow Water (−1 m to −5 m)	Water scooter
		Shoreline to −1 m contour	Real-Time Kinematic Global Positioning System (RTK GPS)
6	Shoreline and Beach profile changes	HTL & LTL mapping	RTK GPS
7	Coastal sediment		
	Shore sediments	Particle/grain size Specific gravity	Grab sampler NISKIN water sampler Sieve Shaker/hot air Owen
	Seabed sediments		
8	Riverine data	Salinity, conductivity, & temperature	Conductivity, Temperature and Depth (CTD)

3 Site Selection

3.1 Criteria for Site Selection

The criteria to be considered in the site selection are as follows:

- Degree of vulnerability.
- Planned development along the stretch of the coast.
- Need for reliable field data to effective planning of shore protection in the vicinity.
- Type of activities and density of the dwelling units along the coast.
- Accessibility to the site.
- Safety of equipment to be erected.
- Support from local public and concerned state government department in maintaining the equipment.
- Application of the data collected and scope for future projects.

4 Typical Instrument for the Designated Parameter

4.1 Waves

4.1.1 Sea Bottom Mounted Directional Wave Recorder

To measure the wave characteristics in the nearshore, a bottom-mounted Directional Wave Recorder (DWR) is usually proposed. To achieve good quality data all along the coast, the field data needs to be collected covering the coastal stretch under consideration and a few locations in relatively deeper waters (up to 15–30 m). This facilitates the validation of numerical model, for deriving the wave characteristics from wind characteristics at any location along the coast (for any extended use of measurements). The wave data in, say, 8–15 m water depth needs to be collected locations based on vulnerability of the location to extreme events.

A typical DWR instrument mounted and rigidly fixed to a frame to be deployed at the seabed is shown in Fig. 1. A wave rider buoy also could be deployed for this purpose. The DWR acquires the time history of water surface elevation in the ocean from which the height, period and direction of the waves are derived.

The DWR uses the proven Linear Wave Theory and wave analysis method of measurement for shallow water deployment (20 m maximum water depth). It uses Linear Wave Theory to analyze the pressure and current oscillations due to the waves. In near-shore environments (<20 m depth), it is not always possible to use a surface floating buoy to measure wave activity. In these circumstances, the most cost-effective solution is a bottom-mounted, pressure-based device. The DWR is fitted with a pressure sensor to measure the pressure variation and fitted with an electromagnetic current sensor to measure the current oscillations, with the direction referenced to an internal flux gate compass. The DWR is fitted with a choice of strain gauge or high-accuracy piezo-resistive pressure sensors, and a fast response PRT temperature sensor as standard. The piezo-resistive sensor offers a higher absolute accuracy, and the quality of wave data depends more on the deployment location and sampling pattern than to sensor performance.

4.1.2 Deployment of the DWR

The DWR needs to be fitted to a mooring frame which needs to be supported by the four bars counterweight of a minimum of about 20 kg each. This mooring frame should be connected to an anchor weight of about 50–80 kg. It is always advisable to deploy DWR with an anchor and counterweights, to avoid it to drift away particularly during severe weather conditions. The mooring frame with the DWR should be connected to a marker buoy for the identification of the location of the instrument and the anchor weight (see Fig. 1). After the arrangement of complete setup, DWR was deployed in 15 m water depth. The DWR, anchor for firmly anchoring the DWR to the seafloor, views of prior to and after deployment are projected in Fig. 1. The

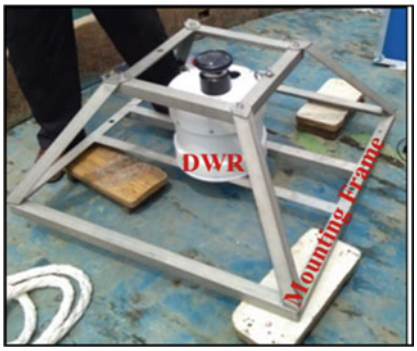

(a) DWR mounted on the frame

(b) Anchor Weight

(c) DWR Deployment from boat

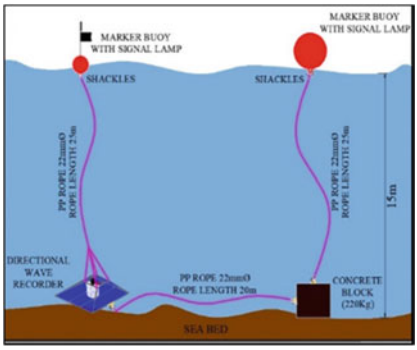

(d) Deployment Plan

Fig. 1 Deployment of DWR, **a–d**

DWR was set up with 2 Hz sampling rate of 2048 sample collection with a Wave Burst Interval of 60 min. The data along the Karaikal coast was measured from October 2017 to April 2018 and again from December 2020 to May 2021.

5 Ocean Currents

5.1 Acoustic Doppler Current Profiler (ADCP)

Acoustic Doppler Current Profiler (ADCP) is a hydro acoustic current meter similar to a sonar, used to measure water current velocities over a depth range using the Doppler effect of sound waves scattered back from particles within the water column It provides the velocity profile along the water column deployed to acquire the direction and magnitude of currents (ADCP). The coastal currents have its importance in shallow waters, so the data collection was done in less than 6 m water depth. A view of the deployed ACDP is shown in Fig. 2.

Fig. 2 Acoustic Doppler current profiler

An ADCP anchored to the boat vessel can measure current speed not just at the bottom, but also at equal intervals all the way up to the water surface. The instrument can also be mounted horizontally on seawalls or bridge pilings in rivers and canals to measure the current profile from shore to shore and to the bottoms of ships to take constant current measurements as the boats move. In very deep areas, they can be lowered through a cable from the surface.

5.1.1 Deployment of the Instrument

The ADCP powered up by batteries can be mounted as side-looking, downward-looking and upward-looking orientations. A bottom-mounted ADCP measures the speed and direction of currents at equal intervals all the way to the surface. The working frequencies range of ADCP range from 38 kHz to several megahertz. Since the ringing period of ADCP with 600 kHz frequency is 1.5 m, it is set with a frequency of 600 kHz. After configuring, it was connected with an external battery source and fixed on the boat with the sensors facing the seafloor which was deployed as shown in Fig. 3.

5.1.2 Typical Results of Ocean Current Observation by ADCP

The ADCP was deployed in the Ocean at 7 m water depth off the Karaikal coast during the period from October 14, 2018, to April 3, 2018. Typical directional distribution of the percentage of occurrence of magnitude of current at different depths (Bins) is projected in Fig. 4.

Fig. 3 ADCP mounted on the side of boat

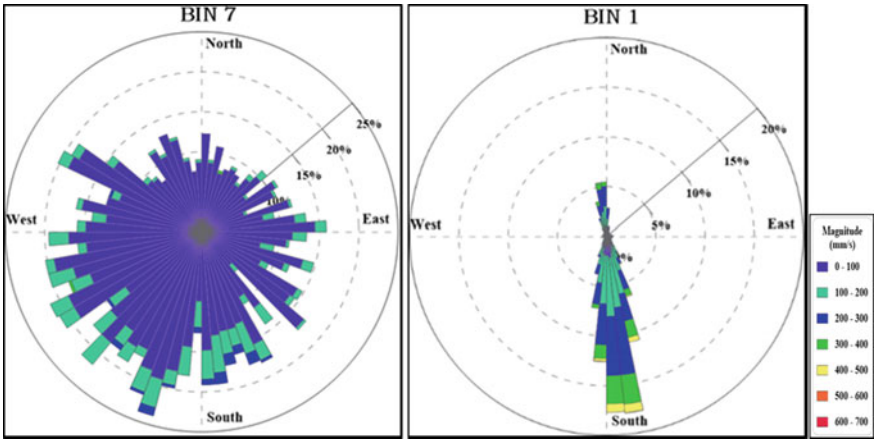

Fig. 4 Karaikal ADCP data—magnitude versus direction

6 Tides

6.1 Tide Gauge

A device for measuring the height (rise and fall) of the tide. Especially an instrument for automatically making a continuous graphic record of tide height versus time. In recent years, new technologies have developed allowing for real-time, remote tide

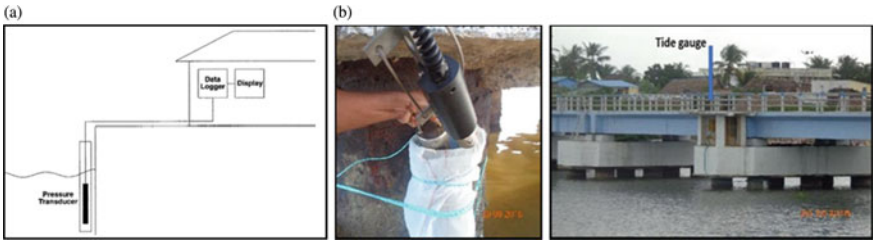

Fig. 5 **a** Measurement setup, **b** Tide gauge and its installation under the bridge

information to be published online via a solar-powered wireless connection to a tide sensor. Ultrasonic sensors have already been deployed to great effect and the data is regularly broadcast and displayed online. Tide gauges have a practical application in the shipping and fishing industries where low or high tide levels can hinder or prohibit access to shallow bays or locations with bridges. The principle of all pressure systems is to measure the hydrostatic pressure of the water column at a fixed point and convert that pressure into a level Direct Reading Systems (Tide Gauge with Pressure Sensor). The sea level may be measured by fixing a waterproof pressure transducer below the lowest expected tide level (Fig. 5a) with the power/signal cable connected to an onshore data logging unit. If a vented power/signal cable is used, a differential transducer may be fitted with the reference side of the transducer vented to atmosphere providing continuous correction for changes in atmospheric pressure. Most of these pressure sensors use strain gauge or ceramic technology. Changes in water pressure cause changes in resistance or capacitance in the pressure element. The signal is amplified and may be displayed and stored in shore-based data logging equipment. The maintenance and calibration of these transducers are more demanding than pneumatic bubbler systems as the transducer is fixed underwater where it is susceptible to temperature variation and fouling.

6.2 Deployment

The TideMaster is a small, cost-effective Water Level Recorder as shown in Fig. 5, specifically designed for applications where the user requires an accurate record of water height, but with an added option of meteorological data via an ultrasonic wind speed and direction sensor. The TideMaster was installed in the Arasalar River Railway Bridge Pier at Karaikal (Latitude 10° 54′ 42″ N, Longitude 79° 50′ 19.58″ E) (Fig. 5a and b) during the measurement period as mentioned earlier. A closer view of the tide gauge and a view of the bridge under which the tide gauge was installed are projected in Fig. 5b. A typical record from the tide gauge is shown in Fig. 6.

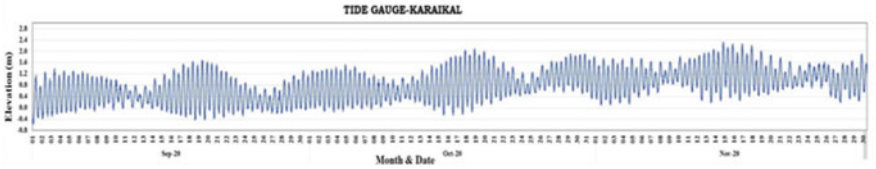

Fig. 6 Karaikal tide gauge data

7 River Current and Discharge (Near to River Mouth)

7.1 Current Meter

Reliable estimation of freshwater inflow to the ocean from large tidal rivers is vital for water resources management and climate analyses. Information on time-varying water levels, magnitude and direction of tidal currents is quite critical in coastal waterways and estuarine environment; real-time tide is measured by tide gauge nearer to the current meter location with respect to Chart Datum, and current meter shows velocity with the direction, and variation in the depth and direction of flow will be included in the discharge calculation. The most common method used for measuring discharge is the mechanical current meter method. In this method, the stream channel cross section is divided into numerous vertical subsections. In each subsection, the area is obtained by measuring the width and depth of the subsection, and the water velocity is determined using a current meter. The discharge in each subsection is computed by multiplying the subsection area which was corrected with respect to real-time tide by the measured velocity. The total discharge is then computed by summing the discharge of each subsection.

The instrument model 106 is an impeller-based meter, measuring speed and direction with optional temperature, and depth with respect to pressure at a rate of 1-s cycle. The 106 can be operated in self-recording mode or be operated in direct recording mode via a PC (Personal Computer). It can be self-recording mode meaning instrument set and data extraction can be carried out using the supplied 'y' lead from PC to external 10 ways subConn connector or direct recording mode: Over short cable lengths (up to 100 m), RS232 communication is possible via the external 10 Way SubConn and PC. Power to the model 106 may be taken from their internal battery, from a surface battery or power supply. When power is taken from the internal battery (1.5 V alkaline D cell), battery life is approximately 30 days at 10 s sampling rate. Using a 3.6 V lithium D cell, life is approximately 90 days at 10-s sample rate or 180 days at 5-min sample rate. The units are fitted with a 512 k byte memory. This equates to storage of over 8000 speed and direction.

7.2 Current Data Collection

Current meter observations are aimed at recording the data to analyze the magnitude and direction of flood/ebb stream. The tidal stream observations are to be carried out as per tidal cycle. The magnitude of flood/ebb stream is required to be correlated with the timings of high water (HW). To record and analyze the min. and max. rates, the observations are to be carried out during spring tides. The data may be collected at an hourly interval, six hours prior and after high water during spring tides. When the meter is lowered in water and when it faces the current of water in the channel, the wheel rotates. To keep the meter facing the direction of flow, a tail is attached. This tail aligns the meter in the direction of flow. The meter is also fitted with a streamlined weight (fish weight) which keeps the meter in a vertical position. The rate of rotation of the wheel depends on the velocity of flow. A dry battery is kept inside the current meter and an electric current is passed to the wheel from it. A commutator is fixed to the shaft of the revolving wheel.

It makes and breaks the contact in an electrical circuit at each revolution. An automatic revolution counter is kept in the current meter with the battery which registers the revolutions. The time taken for a required number of revolutions may be noted. The velocity of flow can be read from a rating table. The rating table is always provided with the meter. The velocity was measured at different elevations below the water surface.

The Valeport Rotan type current meter was deployed in the Arasalar River near Railway Bridge Pier at Karaikal and typical record of the current is projected in Fig. 7.

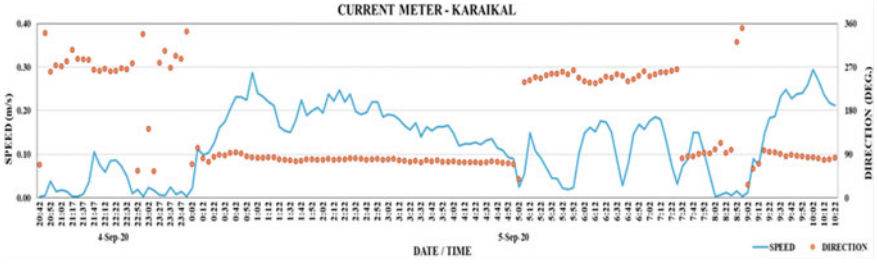

Fig. 7 Karaikal current meter data

8 Seabed Profile (Near Shore and Offshore)

8.1 Echo Sounder

In areas where detailed bathymetry is required, a precise echo sounder may be used for the work of hydrography. Most hydro graphic echo sounders are dual frequency, meaning that a low frequency pulse (typically around 20–24 kHz) can be transmitted at the same time as a high frequency pulse (typically around 200–250 kHz). Echo sounding is a more rapid method of measuring depth than the previous technique of lowering a sounding line until it touched bottom. An echo sounder measures the sea floor depth below sea surface. Echo sounder measures the depth of water by measuring the time for a pulse of energy to travel to the seabed and back and work on the principle of reflection of acoustic energy. Short pulse of sound energy is transmitted vertically down from the ship. This pulse having been reflected from the sea bottom returns to the boat/ship in the form of an echo. Two types of echo sounders, viz. single beam echo sounder and multi-beam echo sounders, are available for the measurement of bathymetry. For the nearshore survey, up to 1 m the beach profiling survey using RTK GPS at lowest low water spring is carried. In depths, 1–3 m, the ancient sounding rope technique with RTK positioning during calm weather was carried.

8.2 Setting up of the Instrument

To conduct a bathymetric survey effectively using Echo Sounder, it is necessary to obtain and load already existing map layers or background data. The line files should be created in navigational HYPACK Software in line file format.

The real-time data is displayed on the integral graphics LCD screen and output in a variety of industry standard formats, and all logged data may subsequently be uploaded to PC. The on-board microprocessor applies an accurate time stamp to each data point, ensuring that a complete time series record of each data input can be generated, together with interpolated position and depth information. Any corrective data received from a heave sensor or tide gauge can be applied in real time to the depth data, and the user may choose whether to log or output either the corrected or uncorrected data. A view of the echo sounder used, its installation and typical bathymetry record are projected in Fig.8a, b and c, respectively.

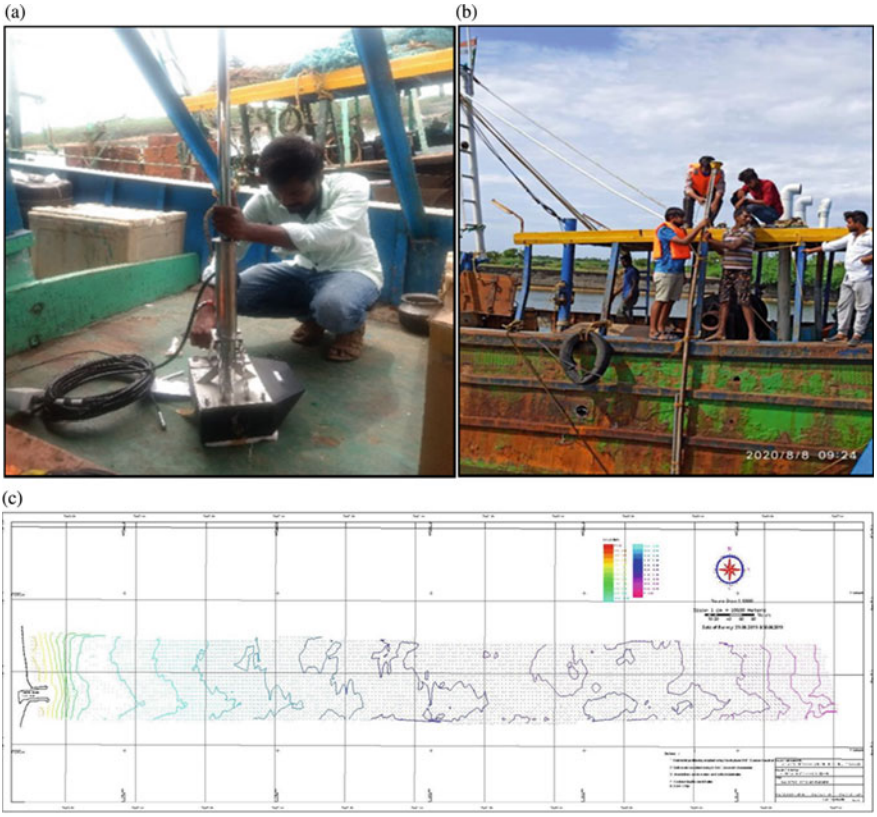

Fig. 8 **a** A view of the Echo sounder, **b** Echo sounder being installed, **c** Typical surveyed bathymetry chart of Karaikal

9 Wind

9.1 Anemometer/Windsonic Ultrasonic Wind Sensor

An anemometer is one of the tools used to measure wind speed. A device consisting of a vertical pillar and three or four concave cups, the anemometer captures the horizontal movement of air particles (wind speed). Another tool used to measure wind velocity includes a GPS combined with pitot. A fluid flow velocity tool, the Pitot tube, is primarily used to determine the air velocity of an aircraft. In CMIS, Wind Sonic Ultrasonic Wind Sensor was installed to measure wind parameters; Wind Sonic is a robust, low-cost ultrasonic wind sensor with no moving parts. This 2-axis ultrasonic wind sensor offers maintenance-free wind speed and direction monitoring for true 'fit and forget' wind sensing.

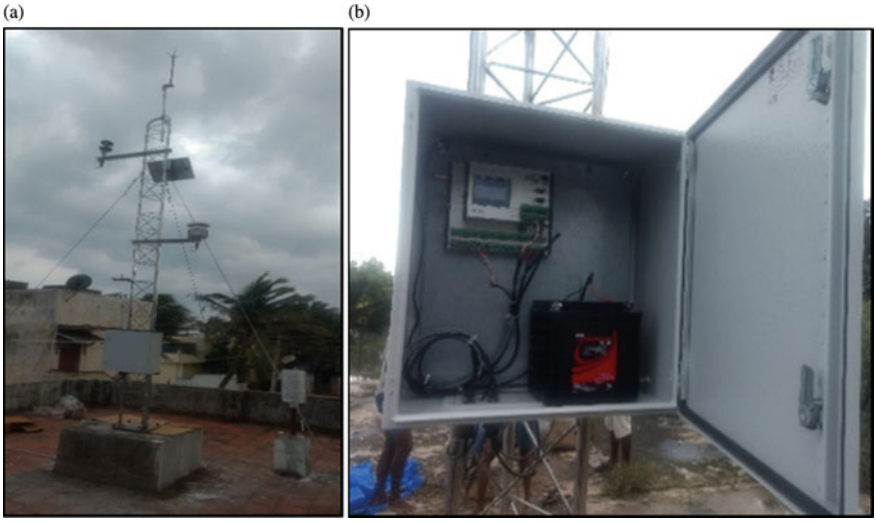

Fig. 9 **a** AWS installed in Karaikal, **b** AWS data logger

Automatic Weather Station, AWS, is a facility, either on land or on sea, with instruments and equipment for measuring atmospheric conditions to provide information for weather forecasts and to study the weather and climate. An AWS will typically consist of a weather-proof enclosure containing the data logger, rechargeable battery, telemetry (optional) and the meteorological sensors with an attached solar panel or wind turbine mounted upon a mast. The specific configuration may vary due to the purpose of the system. The system may report in near real time via the Argos System and the Global Telecommunications System or save the data for later recovery. The AWS include thermometer for measuring temperature, ultrasonic wind sensor for measuring wind speed and wind direction, hygrometer for measuring humidity and rain gauge for measuring rain. A view of the AWS installed in Karaikal and the data logger are shown in Fig. 9.

9.2 Typical Results of Wind Observation by AWS

The AWS data collection in Karaikal from January 1, 2018, to April 30, 2019, was acquired. Typical wind rose plots showing the percentage of occurrence of wind speed with respect to the direction for the individual months are shown in Fig. 10.

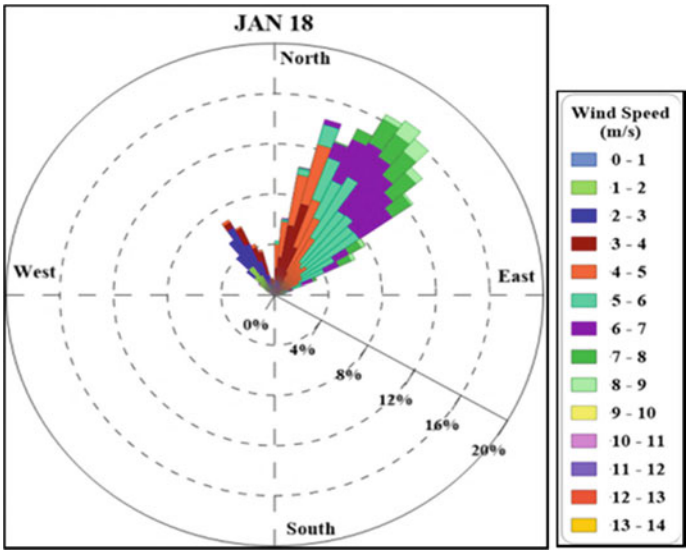

Fig. 10 Karaikal AWS-wind data—magnitude and direction

10 Beach Profile and Shoreline Changes

10.1 Profiling and Mapping

Beach profiling measurements are conducted along profile transects. The profile transect is a straight line running from the crest of the dune or other high point on the beach (such as a seawall) to the waterline. Along each of the transects, measurements are taken every five meters allowing observations of the beach to be made. Each monitoring coast has between two and ten profiles transect depending upon length of the coast. And each transect has a different number so that comparisons can be made between these various lines.

10.2 Instruments

The survey instruments used to conduct the beach profile survey and shoreline mapping are Total Station (Beach profile) and Real-Time Kinematic Global Positioning System (RTK GPS) (beach profile and shoreline). While the total station is an electronic/optical instrument used in modern surveying, the real-time kinematic (RTK) positioning is a satellite navigation technique used to enhance the precision of position data derived from satellite-based positioning systems (global navigation satellite systems, GNSS) such as GPS, GLONASS, Galileo and BeiDou. It uses

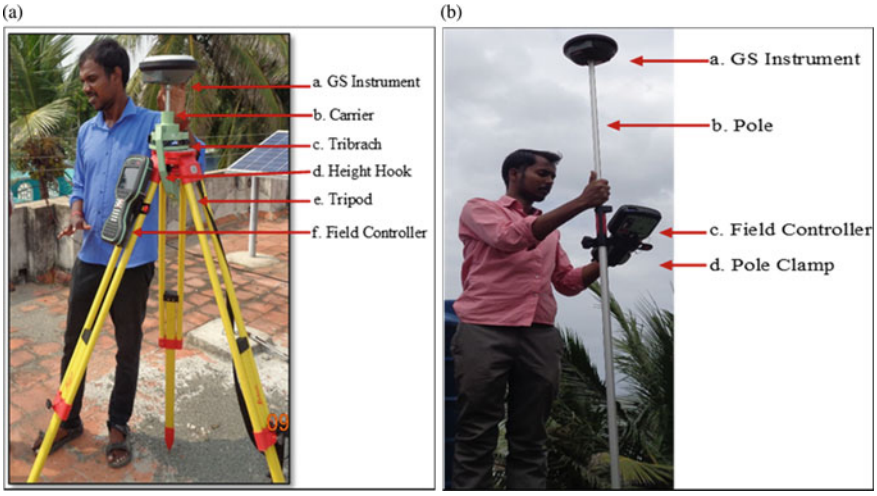

Fig. 11 **a** RTK GPS base setup**, b** RTK GPS Rover setup

measurements of the phase of the signal's carrier wave in addition to the information content of the signal and relies on a single reference station or interpolated virtual station to provide real-time corrections, providing up to centimeter-level accuracy. With reference to GPS in particular, the system is commonly referred to as carrier-phase enhancement or CPGPS. It has applications in land survey, hydrographic survey and consumer unmanned aerial vehicle navigation. The views of setup of RTK GPS adopted for the surveys are shown in Fig. 11. Typical plots of the beach profiles and shoreline surveys are shown in Fig. 12.

11 Coastal Sediment

Coastal sediments involve seabed sampling and near-shore sampling to determine the particle size distribution and its specific gravity. The sediment samples (onshore and offshore) at different locations along the stretch of the coast of the study area be collected monthly/seasonally. The seabed sediment samples collected using the grab sampler equipment by lowering it from the side of the sampling vessel/boat at every 2.5 m depth intervals from the shore to the −20 m depth (i.e., at every 2.5 m, 5.0 m, 7.5 m, 10.0 m, 12.5 m, 15.0 m, 17.5 m and 20.0 m depths) for a particular season. Shore sediments were collected at every month ten locations of five transects of which two samples at each transects of which three transects of samples along northern side of the Arasalar River of Karaikal and two transects of sample on southern side of the Arasalar River of Karaikal. The shore samples were taken along the shoreline

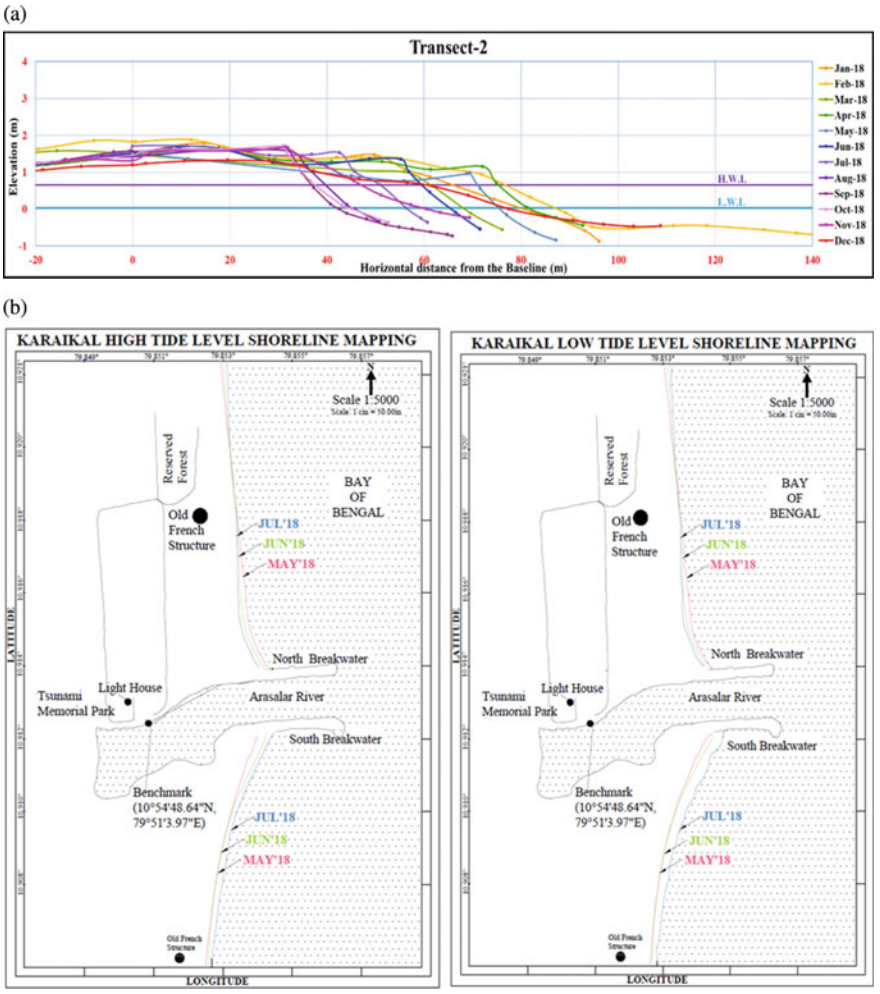

Fig. 12 **a** Karaikal-beach profile variations, **b** Karaikal-shoreline variations

(spring low tide) and on the berm (spring high tide) at every month and analyzed for the particle size distribution. The Karaikal sediments sampling and its location map details are shown in Fig. 13a–c.

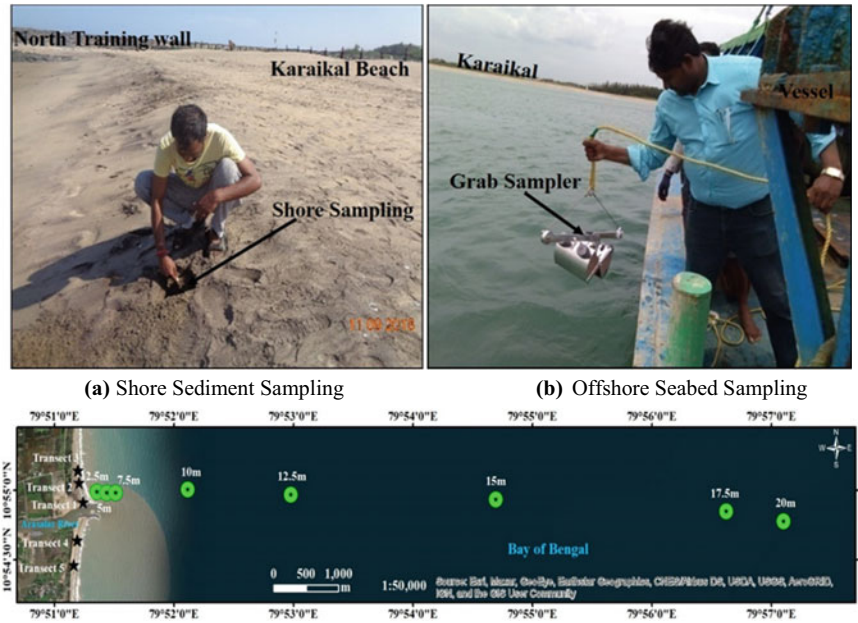

(a) Shore Sediment Sampling **(b)** Offshore Seabed Sampling

(c) Shore and Offshore Sediment Sampling Locations

Fig. 13 **a–c** Shore and offshore sediment samplings and its locations

12 Riverine Data—Conductivity, Temperature and Depth

12.1 CTD

The reason for measuring the conductivity is for determining the salinity. The other oceanographic parameters like Conductivity, Temperature and Depth (CTD) are measured, which is used for different kind of applications. CTD is a cluster of sensors fitted to probe which is attached to the cylindrical rosette and immersed into sea water. This instrument is one of the oceanographic instruments which helps in better understanding of the ocean.

12.2 Description of Instrument

The sensors are fitted to the instrument and take different measurements, these measurements are generally processed through computer software to create another set of parameters. For example, CTD will measure conductivity, temperature and pressure, and these parameters are processed for salinity. Temperature is measured through special temperature-sensing device called thermistor. It gives reading

through the thermal compression or expansion of liquid. Pressure is measured by pressure gauge. Pressure gauge operates on the principle that a small coil or tube of fluid will get compressed or changes in shape depending on external pressure exerted on the gauge.

12.3 Deployment of the Instrument

The CTD instrument can be deployed from the deck or jetty structure or even from the research vessel. The instrument is fully submerged into the water which is called the downcast to a determined depth or to a few meters above the ocean floor, generally at a rate of about 0.5 m/s. In general, a conducting wire cable is attached to the CTD instrument connecting the CTD to a computer or laptop and allows instantaneous uploading and real-time visualization of the collected data on the computer screen. The synoptic hour format is a standardized hour format used for CTD instrument deployment by all the marine organizations in the world. This system gives hour format (UTC: Universal Time Coordinated), determined by international agreement, at which meteorological observations are made simultaneously throughout the world. The interval between each time is 6 h.

The order of synoptic hour is 5:30, 11:30, 17:30 and 23:30. At this time, the CTD instrument is deployed in the river body in the vertical profile to collect the parameters. Deployment of CTD is shown in Fig. 14. Typical data obtained from the CTD is shown in Fig. 15.

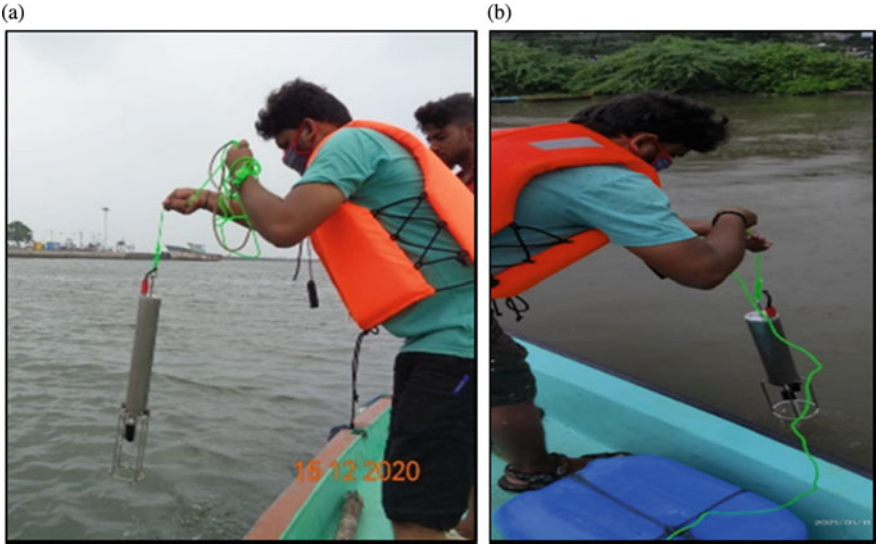

Fig. 14 **a** and **b** Deployment of CTD in Arasalar River, Karaikal

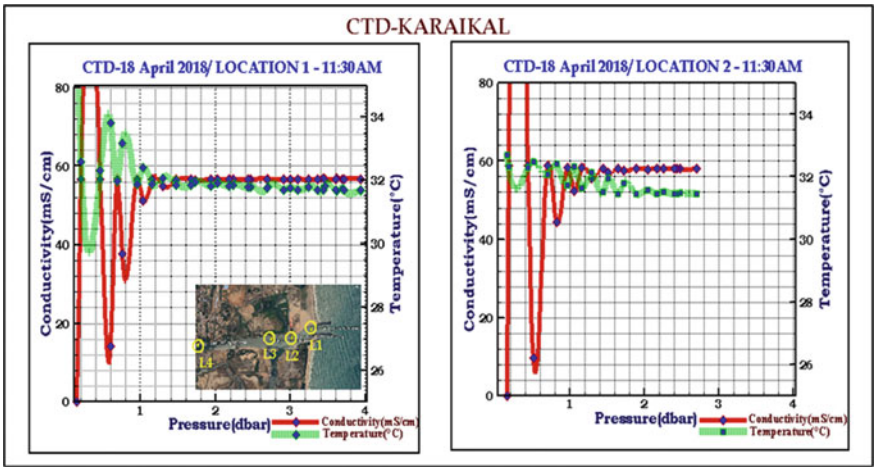

Fig. 15 Typical results from CTD in Karaikal

13 Summary

The first of its kind in India, a Coastal Management Information System (CMIS), has been established in 2017 and has been in operation till mid-2021 at the Department of Ocean Engineering, Indian Institute of Technology Madras for the three south India coastal states, namely, Tamil Nadu, Kerala and Union Territory of Puducherry. The host of parameters that dictate the driving parameters responsible for the stability of the coastline was identified along with the three sites for its implementation. The parameters measured, equipment used and typical results obtained are highlighted.

Acknowledgements The study was supported by the Central Water Commission (CWC), Ministry of Jal Shakti, Department of Water Resources, River Development & Ganga Rejuvenation, Government of India. The authors thank all the staff of the project who were involved in the installation, data acquisition and its transfer as well as its analysis. The authors also thank the members of Project Monitoring Committee for their valuable suggestions during the course of the installation of CMIS.

Strategies for Adaptation of Solid Waste Management Infrastructure in Coastal Areas to Climate Change

Anu Rachel Thomas, Mohammed Iqbal Thayyil, and Ligy Philip

Abstract Management of solid waste is one of the most pressing challenges faced by municipalities across the world. Increased consumption and improper disposal have led to the accumulation of solid waste in many urban areas, resulting in detrimental impacts on the atmosphere, hydrosphere and biosphere. In particular, coastal areas that accommodate over 60% of the global population face severe deficits in solid waste management, resulting in far-reaching impacts on water quality and the fragile marine ecosystem. The commonly adopted practices of uncontrolled burning, open dumping and unscientific landfilling contribute to significant emissions of greenhouse gases, leading to global warming and climate change. This article discusses the development and performance evaluation of a decentralized technology for management and resource recovery from solid waste generated in coastal areas, with increased resilience to climate change, by mitigating the greenhouse gas emission arising from the scenario of open dumping. The coastal village of Vichoor (Tamil Nadu, India) was selected as the study area, and the quantity and composition of waste generation were assessed. Baseline studies revealed an absence of systematic solid waste management in the study area. Organic fraction contributed to over 55% of the generated waste. An integrated municipal solid waste management scheme was devised, involving primary source segregation, collection, secondary segregation and resource recovery. Infrastructural provision for composting organic waste in a composting yard was adopted, which also doubled as a secondary segregation unit. Methane emission was assessed for scenarios involving open dumping of waste and windrow composting of the organic fraction. A reduction of 316.29 kg CO_2 eq/T of waste was observed by adopting the proposed practices over open dumping, thus proving to be a potential solution to combat climate change due to greenhouse gas emission from solid waste management. Long-term sustainability of the system was ensured by active community level participation and revenue generated from the sale of recyclable inorganic fraction and the generated compost.

Keywords Climate change · Solid waste management · Greenhouse gas · Adaptation

A. R. Thomas · M. I. Thayyil · L. Philip (✉)
Department of Civil Engineering, Indian Institute of Technology, Madras, Chennai 600036, India
e-mail: ligy@iitm.ac.in

P. V. Timbadiya et al. (eds.), *Coastal, Harbour and Ocean Engineering*, Lecture Notes in Civil Engineering 321, https://doi.org/10.1007/978-981-19-9913-0_31

1 Introduction

Globally, the trend of urbanization has witnessed a rapid increase in recent years. It has been estimated that over 68% of the global population will be residing in urban areas by 2050 [1]. Aided by industrialization and an increase in the standard of living, it is predicted that the consumption of consumer goods will increase 4 times by 2030 [2]. Coastal areas are particularly attractive hotspots for sprawling urban and peri-urban regions because of their additional benefits in ocean navigation, fisheries and tourism. They currently accommodate 60% of the global population and the coastal population is expected to be 71% by 2050 [3]. As a result, there has been an unprecedented increase in domestic, industrial, commercial and institutional waste in the coastal areas. Many municipalities across the world lack proper facilities for scientific management of the generated waste. Globally, over 2 billion people do not have access to facilities for waste collection [4]. Over 50% of the waste in low-income countries are dumped openly, and only 15% undergo recycling [5]. Improper solid waste management has taken its toll on the fragile coastal ecosystem in the form of bioaccumulation of pollutants [6] and disruption of marine biodiversity [7].

Municipal solid waste contributes to 5% of the Global Greenhouse Gas (GHG) emission, with the significant contribution from CH_4 released from landfills [8] and is projected to increase four times by 2050 [9]. CO_2 emission from the dumped waste is estimated as 1467 tons/day or 535.3 KT/year, equivalent to 114,000 vehicles emission per year [10]. According to CPCB, 135,198 T of solid waste is generated in India per day. While 82% of this is collected, 77% is left untreated without any segregation or attempts for resource recovery [11]. It is a common practice to dump solid waste in low-lying areas, roadsides and along the banks of water bodies. Most Class II and Class III cities dump waste in unscientifically designed landfills [12].

Even though landfilling lies towards the bottom of the waste management hierarchy [13], it is still the most commonly practised method, even in developed countries. Scientifically designed landfills are equipped with provisions for collection of landfill gases (LFG) arising from the anaerobic decomposition of waste. However, most landfills in developing countries operate as informal dumpsites either with dysfunctional or no facilities for collection of LFG. This results in fugitive emission of greenhouse gases like CH_4, N_2O and biogenic CO_2. Such emissions are predicted to increase from 1000 MT CO_2 eq in 2020 to 2900 MT CO_2 eq by 2050 [14], thus significantly contributing to climate change. If the status quo is maintained without mitigation measures, Manuja et al. [15] predict a compounded annual growth rate of 2.55% in the GHG emission from the solid waste management sector in India from 2011 to 2031. There is a huge potential to recover value-added products like compost and biogas from waste. Resource recovery from recyclable inorganics also plays a vital role in solid waste management. The Central Pollution Control Board in 2019 [16] estimated that 8 to 9 per cent of total MSW is plastic waste, and informal sectors recycle 60% of it. The recycling percentage of paper and cardboard in India is 27% which is much lower when compared to other industrialized countries, and

this can be attributed to poor waste segregation. Information on segregation at source is neither available nor reliable, even in large metropolitan cities.

Coastal communities represent a high degree of social and infrastructural vulnerability to the impacts of climate change in the form of extreme events like floods, tropical storms and prolonged changes like rising sea levels and sea surface temperature [17]. This can severely impair the functioning of solid waste management infrastructure. Extreme rainfall associated with climate change can result in water logging in waste storage facilities and reduce slope stability at landfills. An increase in seasonal temperature alters the waste decomposition rates [18]. Sea-level rise can inundate the facilities for collection/sorting and erodes dumpsites [19]. Solid waste that is improperly disposed chokes critical infrastructure such as storm drainage (both micro-drainage channels and macro-drainage channels) resulting in significant waterlogging and overflow of sewerage system. This was evident during the 2015 floods in Chennai [20]. Hence, there is an immediate need for a paradigm shift in waste management practices, predominantly in coastal areas. A sustainable system should have reduced dependence on capital intensive centralized treatment facilities. Also, it should involve active participation and collective ownership from the local communities to be sustainable in the long run.

Organic (biodegradable) fraction contributes 55–60% of the waste generated annually in Indian cities [21]. Segregation and separation of organic fraction from the mixed waste stream are an effective mitigation strategy to reduce GHG emission from landfills. Dehoust et al. [22] observed an approximate methane emission saving of 28.4 MT CO_2 eq in 2012 (Germany) by diverting untreated organic waste from landfill sites. 29.89% reduction in GHG can be achieved by 2031, by adopting suitable techniques to source segregate and prevent the entry of mixed organic waste into landfills [15].

In this context, composting of the organic fraction is widely considered an attractive solution for managing organic waste, not only due to their potential to reduce CH_4 emissions, but also the added benefits like improving soil fertility and water holding capacity [23]. Properly designed and operated composting practice does not contribute to inventory for national GHG as it emits only CO_2 which originates from biogenic sources [24]. Furthermore, application of compost for farming can cause temporary storage of carbon [25]. Boldrin et al. [26] estimates a net saving ranging from 2 to 79 kg CO_2 eq per Ton of compost applied to land. The use of compost can also bring about indirect savings in GHG emission by reducing the use of synthetic fertilizers, whose production is energy intensive [27].

The present study proposes a community-based decentralized strategy for solid waste management and resource recovery in a coastal village in India. A baseline survey was conducted to collect primary data on the quantity and composition of solid waste generated. A sustainable system involving localized collection and processing of wastes was adopted to minimize waste transport to dumping sites farther away. Value-added products like compost were obtained from source segregation of organic and inorganic fractions and by adopting good practices of composting. This model is

labour-intensive and provides employment opportunities to local inhabitants. Appropriate segregation of recyclable material leads to higher revenues. Furthermore, scientific management of solid waste inevitably leads to social benefits like better and healthier living conditions for the local residents.

2 Materials and Methods

2.1 Study Area

The village of Vichoor (Tamil Nadu, India) was selected to study the feasibility of integrated municipal solid waste management (Fig. 1). The study was conducted in two phases spanning from 2015 to 2020. During Phase I (2015–2019), Ezhil Nagar of Vichoor Panchayat was chosen as the study area, and it comprised 300 households. During Phase II (2019–2020), the study was further extended to 8 more nearby villages, namely Ganapathy Nagar, Sriram Nagar, Lakshmi Nagar, Velavan Nagar, Sivakumar Nagar, Srinivasa Nagar, Subramanya Nagar and Angallamman Nagar of Vichoor panchayat, comprising a total of 530 households.

Fig. 1 Location of the study area

2.2 Baseline Survey

A preliminary survey was conducted to assess the existing conditions of waste management practices at Ezhil Nagar. Two field visits were made, which involved direct interactions with the officials and the local community. A social survey was conducted to understand the demography, waste disposal trends and awareness about waste segregation among the local communities. The questions were asked based on issues identified in the literature review, participant observation and project objectives. The questionnaire used is given in Appendix 1. Interviews with market vendors and commercial and residential waste producers were semi-structured and left open-ended to generate quantitative data.

2.3 Infrastructural Provisions for Decentralized Municipal Solid Waste Management

Two bin system was adopted for primary source segregation of solid waste at the household level. Waste was categorized into three types—wet waste, dry waste (inorganic recyclable waste) and sanitary waste. Green-coloured bins were provided to collect wet waste, and blue-coloured bins were provided for dry waste. Sanitary waste was stored separately. A system for daily door-to-door collection of waste was established with the help of a team of sanitary workers comprising local women and members of self-help groups. The transportation of primary segregated waste was done using tricycles. A secondary segregation unit consisting of a composting facility for organic waste was constructed in the land procured from the Panchayat. The processing capacity of the yard was 150 kg/day. The dimensions of the compost pit were 10.5 ft length, 5 ft width and 1.6 ft height. Waste was segregated here into organic/vegetables, plastics, papers, cardboards, plastic bottles, glass bottles and other components. Inorganic waste was further segregated into different types and stored in the storage yard, later sold to recyclers. Organic waste was composted, processed and packaged for selling in the local market. Before project execution, awareness programmes were conducted with the help of Panchayat officials to imbibe a sense of collaborative partnership with the project among the local community. Villagers were informed about the importance of waste segregation at the source. Two local residents were identified, trained and employed to assist in implementing a community-based decentralized solid waste management scheme.

2.4 Composting of Organic Waste

The organic fraction of the segregated waste was subjected to windrow composting. Waste was air dried for 2 days to reduce moisture content and to prevent putrefaction.

It was then shredded to the size range of 2–5 cm using a shredder. Cow dung, which was collected from the locality, was added as the booster of biodegradation. Dried grass was added to organic waste in the ratio of 1:3 as a bulking agent. The windrow pile was turned periodically and was operated for 45 days. The temperature of the pile was monitored regularly. The compost thus obtained was dried, sieved through a 4 mm IS sieve and packaged for marketing. The quantity and quality of the compost produced were monitored.

2.5 Analysis of Methane Emissions

A comparative assessment of the methane emissions from the scenario of open dumping and windrow composting was done. Methane emission from open dumping of waste was calculated by the methodology propounded by UNFCCC [23]. To quantify the methane emission during composting, static chamber method was used for gas sampling. The detailed procedures for sampling and gas analysis were reported by Thomas et al. [28].

3 Results and Discussions

3.1 Existing Conditions in the Study Area Before the Project Execution

From the baseline survey, it was evident that the study area lacked any systematic facility to collect or manage solid waste. Even though the Panchayat had installed few public waste collection bins, it was unsuccessful, as evidenced by the spread of solid waste along the roadsides and open areas (Fig. 2). Waste segregation was not done, and the mixed waste was either dumped openly or burnt periodically. Institutional support in the form of grants from the government was also not in place.

The findings from the social survey are given in Fig. 3. It was observed that 80% of the households used bins for the collection of garbage and had knowledge about the need for segregation of waste. Food waste and kitchen waste contributed to 80% of the waste generated from households. 60% of the food waste was fed to animals, whereas 20% was dumped along the roadsides. 70% of the yard trimming waste was burnt, and 20% was disposed of along the roadsides. 50% of the households were willing to pay Rs 200 annually for waste collection systems.

Fig. 2 Unsanitary condition due to open disposal of waste

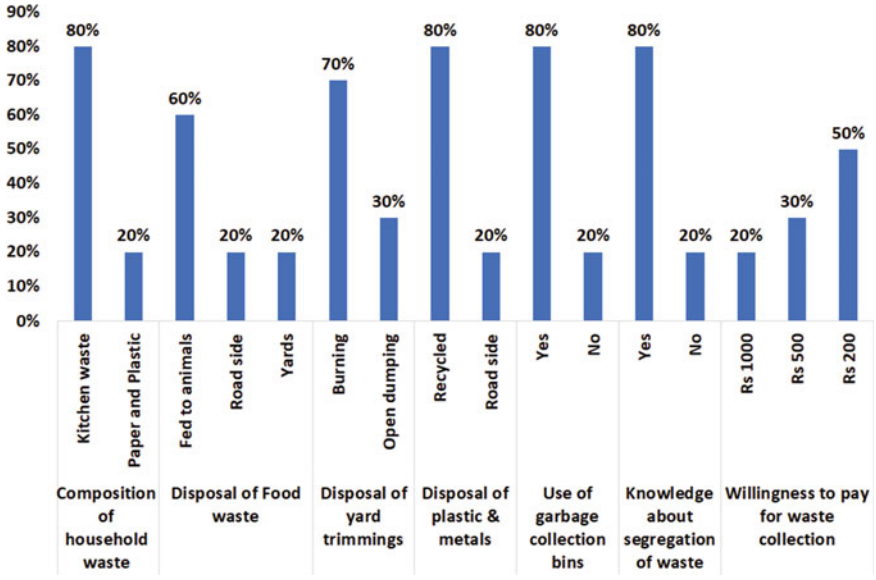

Fig. 3 Results of the social survey conducted at Ezhil Nagar

3.2 Quantity and Composition of Generated Waste

The composition of solid waste from January 2017 to December 2018 is given in Fig. 4a. The average pattern of waste generation is shown in Fig. 4b.

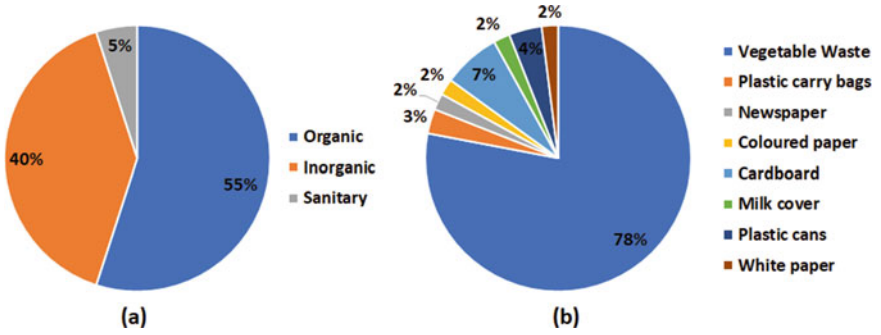

Fig. 4 **a** Overall composition of solid waste from January 2017 to December 2018; **b** Average composition of different constituents of municipal solid waste during Phase I and Phase II of the work

From January 2017 to December 2018, 62.9 tons of solid waste were collected from 250 households at Ezhil Nagar. On average, 2622 kg of waste was collected per month. It was observed that the majority of waste comprises organic/vegetable waste followed by cardboard, plastic cans. During the Second Phase of work, an average of 4565 kg /month of solid waste was collected from 530 households, and a similar trend in composition was observed. After the segregation of solid waste, resources such as plastics, papers, cardboards, and milk covers are sold to appropriate recycling vendors. In this connection, Rs. 39,552/- was earned from May 2017 to October 2018 (Phase I) and Rs.1,51,475 during June 2019 to October 2020 (Phase II) of the work.

3.3 Composting of Organic Waste Fraction

The results of compost sample analysis are given in Table 1.

Even though most of the parameters in Table 1 meet the City compost standard (FCO, 1985) [29], a few of them shows a variation. The main reason for this is that the compost sample used in the current study is a random grab sample analysed in triplicate. In the present data set, pathogen concentration of 157 MPN/100 mL was observed. As per a recent report by Hong Kong Organic Resource Centre (2021) [30], pathogen concentration $\leq$1000 MPN/g is permissible in compost. The same report proposes a pH range of 5.5–8.5 for use in organic farming. Hence, the compost produced in the present study can be used for farming purposes. From May 2017 to December 2018, 78% (1050 kg/ month) of total waste consisted of biodegradable organic matter. This organic waste was converted into compost through the windrow technique. 3058 kg of compost has been generated from 34,904 kg of organic waste collected (inclusive of organic waste collected from Phase II from June 2018 to December 2018), and 540 kg of compost has been sold in the marketplace from May 2017 to January 2019. An amount of Rs. 10,820/- has been earned from this.

Table 1 Compost sample analysis

Parameters	City compost standard (FCO, 1985)	Hong Kong Organic Resource Center Standard (2021)	Final compost sample
Moisture content (% by weight)	15.0–25.0	25.0–45.0	23 ± 1.0
Colour	Dark brown to black	–	Dark brown to black
Odour	Absence of foul odour	–	Absence of foul odour
Particle size	>90% material should pass through 4 mm IS sieve	Foreign matter >2 mm should be ≤0.5% dry weight	98% passed through 4 mm IS sieve
Bulk density (g/cc)	<1.0	–	1.05 ± 0.3
Total organic carbon (% by weight)	>12.0	≥ 20	29.5 ± 0.4
Total nitrogen (% by weight)	>0.8	–	1.6 ± 0.05
Total phosphates (% by weight)	>0.4	–	0.35 ± 0.02
Total potash (as K2O % by weight)	>0.4	–	2.0 ± 0.2
C:N ratio	<20	≤20	17.1 ± 0.5
pH	6.5–7.5	5.5–8.5	8.5 ± 0.1
Conductivity (dS/m)	<4.0	≤4.0	4.0 ± 0.05
Pathogens (MPN/100 mL)	Nil	≤1000 MPN/g	157
Tolerance limit (N + P + K) per cent	>1.5	≥4	3.95 ± 0.1
Seed germination index (per cent)	–	> 80	110

3.4 Quantification of Methane Emissions

The total quantity of waste generated, including Phase I and Phase II, was obtained as 344,976 kg over the duration from 2017 to 2020. The composition of biodegradable fraction consisting of vegetable/food waste, paper and yard trimmings was obtained from Fig. 4b. From the social survey results, the percentage of this waste which are openly dumped was obtained. The Degradable Organic Carbon (DOC, wet basis) fraction was obtained from USEPA (2010) [31]. The quantity of methane generated if this waste were openly dumped was calculated by the methodology given by UNFCCC [23]. It was assumed that 77% of the organic fraction undergoes anaerobic decomposition. A Methane Correction Factor (MCF) of 0.4 was taken, corresponding to shallow unmanned landfills [24]. The fraction of methane in the total emission

Table 2 Calculation of DOC of waste

Material	% Composition	% Openly dumped	DOC fraction	DOC in waste (kg)
Vegetable/food waste	0.78	0.4	0.15	16,144.88
Paper	0.13	0.2	0.4	3587.75
Garden	0.09	0.3	0.2	1862.87
Total DOC				21,595.50

Table 3 Estimation of methane emission

Total DOC (kg)	Decomposable DOC fraction	Fraction of methane	Correction factor	Global Warming Potential of methane	Methane correction factor (MCF)	CO_2 eq (kg)	kg CO_2 eq/Ton of waste
21,595.50	0.77	0.5	1.33	25	0.4	110,579.75	320.54

was taken as 50%. A correction factor of 1.33 was taken to account for model uncertainties. The result was reported as CO_2 equivalents by multiplying with 25, the global warming potential of methane, as shown in Tables 2 and 3.

Hence, open dumping can result in a methane emission corresponding to 320.54 kg CO_2 eq/Ton of waste. Methane emission calculated from the analysis of gas samples from the composting facility was 4.25 ± 0.1 kg CO_2 eq/Ton of waste. From this, it can be concluded that adopting good practices of waste segregation and composting of the organic fraction can result in an abatement of 316.29 kg CO_2 eq/Ton of waste.

4 Conclusions

From the present study, it can be concluded that a community-based decentralized approach is an attractive option to tackle waste management problems, particularly in coastal areas which are more vulnerable to the impacts of climate change. It can ensure long-term operability owing to the participation of local stakeholders. This study shows that revenue can be obtained by selling compost and recyclable inorganics and demonstrates the circular economy concept in the coastal village through a proper waste management approach. Adopting good composting practices by appropriate infrastructural provisions and constant monitoring of compost quality not only produces a value-added product but also ensures a significant reduction in methane emissions.

Acknowledgements The authors acknowledge the financial support received from India Additives Ltd. (IAL), Chennai, as part of the CSR Project. The authors are thankful to the Department of Science and Technology (DST), Ministry of Science and Technology, Government of India (Grant

Number: DST/CCP/CoE/141/2018(G)) for the financial support to carry out the present work. The authors also extend their gratitude to Prof. B.S. Murty (Project Coordinator); Mr. S. Yoganathan, Mr. R. Kaviyarasan, Mr. Varun Sridharan, Mr. Mohammad Dawood S, Mr. D. Kumaran, Mr. D. Kishore, Mr. G. Masanam (Project Associates); Dr C. Ramprasad, Mr. Manthiram Karthik, Mr. B. Sridharan (Research Scholars); Mr. B. Shivakumar, Mr. Aakash Dev (M. Tech. Students); Mrs. S. Poongodi, Mrs. G. Rekha, Mrs. M. Loganayagi, Mrs. P. Muthumaari, Mrs. M. Mythili, Mrs. Thamarai Selvi (Field Workers), for their constant support throughout the project.

Appendix 1: Survey Questionnaire

1. How do you dispose of the following garbage at home?

Types of garbage	Burn	Bury	Dump				Garbage Truck	Recycle	Reuse	Compost	Other (Specify)
			River/ Lake	In yard	On road	Dump site					
	1	2	3	4	5	6	7	8	9	10	11
Food waste											
Yard trimmings											
Paper/cardboard											
Plastic											
Metals											
Glass											
Sanitary napkins											
Other households											

2. Do you use a bin for the collection of garbage?

o Yes
o No

3. If yes, how many?

o One
o Two
o Three

4. If you use more than one bin, do you segregate and dispose of it?

o Yes
o No

5. If you are not using a bin, specify how you are disposing of it?

6. Do you compost yard trimming at home?

o Yes
o No

7. Do you compost food scraps at home?

o Yes
o No

8. Are you aware of any health issues relating to garbage?

o Yes
o No

9. Are you pay for waste collection services?

o Yes
o No

10. Do you know about the segregation of waste?

o Yes
o No

11. Do you know how to dispose of e-waste?

o Yes
o No

12. Where do you store your garbage?

o In a pile on the floor
o Big oil tin
o Iron bucket
o Plastic bucket
o Other (specify)

13. Approximate dimensions of container: Height ____ cm. Width ____ cm. 36 Volume ____ litres.

14. How much refuse do you collect in a day?

o Quarter container
o Half container
o Three-quarter container
o Full container Others (specify)

15. How much are you willing to pay for a proper solid waste collection system?

16. Did you sell scrap materials?

17. How much revenue do you generate from scrap materials?

18. How often is the waste from your house removed for disposal?

- o Once a day
- o Once in two days
- o Once in three days
- o Once in four days
- o Once a week
- o Other (specify)

19. Who removes the refuse from your house for disposal?

- o Householder sweepers
- o Other (specify)

20. How much do you pay your sweeper each month for removing refuse?

21. Where do you dump your refuse?

- o Open plot
- o Compost pile
- o Front of house
- o Roadside
- o Other (specify)

22. What happens to the dumped refuse?

- o Stays there
- o Removed by municipality
- o Burnt
- o Searched by scavengers
- o Other (specify)

23. Do you retain any material, either reusing it yourself or selling it; if so, which?

- o No
- o Paper
- o Coloured glass
- o Plastic
- o Clear glass bottles
- o Metals
- o Cardboard
- o Cloth

o Food wastes
o Other (specify)

24. For what price do you sell the articles mentioned above and in what quantity?

25. How often do you sell the above-mentioned quantities?

26. What articles would you store if they paid you for them? For what minimum value?

27. Have you heard about recycling & reuse?

28. Is there a difference between reuse and recycling?

o Yes
o No

29. Do you support the idea of recycling?

o Yes
o No

30. Are you interested in recycling?

31. What materials make up the majority of your household waste? (Tick those applicable)

o Wastepaper (e.g. newspaper)
o Cardboard
o Glass
o Plastics
o Kitchen waste
o Garden waste
o Fruit scraps
o Others Please Specify

References

1. United Nations Department of Economic and Social Affairs. (2018). 2018 revision of world urbanization prospects.
2. World Economic Forum (2019) Future of consumption in fast-growth consumer markets: India. World Economic Forum, Geneva
3. Merkens JL, Reimann L, Hinkel J, Vafeidis AT (2016) Gridded population projections for the coastal zone under the Shared Socioeconomic Pathways. Global Planet Change 145:57–66
4. UNEP, ISWA (2015) Global waste management outlook. UNEP, ISWA

5. Chandak S (2010) Community-based waste management and composting for climate/co-benefits–case of Bangladesh. In: International consultative meeting on expanding waste management services in developing countries, pp 18–19
6. Lestari P, Trihadiningrum Y (2019) The impact of improper solid waste management to plastic pollution in Indonesian coast and marine environment. Mar Pollut Bull 149:110505
7. Thushari GGN, Senevirathna JDM (2020) Plastic pollution in the marine environment. Heliyon 6(8):e04709
8. Jia X, Wang S, Li Z, Wang F, Tan RR, Qian Y (2018) Pinch analysis of GHG mitigation strategies for municipal solid waste management: a case study on Qingdao City. J Clean Prod 174:933–944
9. UNEP (2010) Waste and climate change- global trends and strategy framework. UN Environment Document Repository
10. Ahluwalia IJ, Patel U (2018) Solid waste management in india: an assessment of resource recovery and environmental impact.
11. Ministry of Environment, Forests and Climate Change (2017) Consolidated annual review report on implementation of solid waste management rules
12. Vij D (2012) Urbanization and solid waste management in India: present practices and future challenges. Procedia - Soc Behav Sci 37:437–447
13. USEPA (2012) Solid waste management pyramid. http://www.epa.gov/osw/nonhaz/municipal/hierarchy.html
14. Monni S, Pipatti R, Lehtilla A, Savolainen I, Syri S (2006) Global climate change mitigation scenarios for solid waste management. In: Technical research centre of Finland. VTT Publications, Espoo
15. Manuja S, Kumar A, Pandey S (2018) Greenhouse gas emissions and reduction stratagems from waste sector in India. Int J Latest Eng Res Appl 3(1):17–26
16. Central Pollution Control Board (2019) Annual report on implementation of plastic waste management rules. In: CPCB, Annual Report 2019–20 on Implementation of PWM Rules 2016
17. Mafi-Gholami D, Jaafari A, Zenner EK, Kamari AN, Bui DT (2020) Vulnerability of coastal communities to climate change: thirty-year trend analysis and prospective prediction for the coastal regions of the Persian Gulf and Gulf of Oman. Sci Total Environ 741:140305
18. Gichamo T, Gökçekuş H (2019) Interrelation between climate change and solid waste. J Environ Pollut Control 2:104
19. Christian EI (2010) Potential impacts of climate change on solid waste management in Nigeria. In: Abbreviation of institute of electrical and electronics engineers, pp 1–9
20. Narasimhan B, Bhallamudi SM, Mondal A, Ghosh S, Mujumdar P (2016). Chennai floods 2015: a rapid assessment. In: Interdisciplinary centre for water research, Indian Institute of Science, Bangalore
21. Ramachandra TV, Bharath HA, Kulkarni G, Han SS (2018) Municipal solid waste: generation, composition and GHG emissions in Bangalore, India. Renew Sustain Energy Rev 82:1122–1136
22. Dehoust et al (Oko-Institut e.V.) and Vogt and Giegrich (ifeu-Heidelberg GmbH), (2005) Status report on the waste sector's contribution to climate protection and possible potentials. In: Commissioned by the German federal environmental agency, August 2005
23. UNFCCC/CCNUCC (2008) Methodological tool. Tool to determine methane emissions avoided from disposal of waste at a solid waste disposal site. EB 41 Report, Annex 10. CDM Executive board, 9 pp.
24. Change IPOC (2006) 2006 IPCC guidelines for national greenhouse gas inventories. In: Institute for global environmental strategies, Hayama, Kanagawa, Japan
25. Favoino E, Hogg D (2008) The potential role of compost in reducing greenhouse gases. Waste Manag Res 2008(26):61–69
26. Boldrin A, Andersen JK, Moller J, Favoino E, Christensen TH (2009) Composting and compost utilization: accounting of greenhouse gases and global warming potentials. Waste Manag Res 2009(27):800–812

27. PROGNOS (2008) Resource savings and CO2 reduction potential in waste management in Europe and its possible contribution to the CO2 reduction target in 2020
28. Thomas AR, Arulraj PR, Kranert M, Philip L (2020) Investigation on greenhouse gas emissions and compost dynamics during in-vessel co-composting of septage and mixed organic wastes. Int J Environ Sci Technol 17(3):1675–1690
29. Ministry of Agriculture and Rural Development (1985) The fertiliser (Control) Order 1985. No.11-3/83-STU, G.S.R. 758 (E)
30. Hong Kong Organic Resource Centre (2021) Compost and soil conditioner quality standard. http://www.hkbu.edu.hk/~hkorc/
31. USEPA (2010) Greenhouse gas emissions estimation methodologies for biogenic emissions from selected source categories: Solid waste disposal, wastewater treatment, ethanol fermentation

Development of Index for Delineation of Potential Submarine Groundwater Discharge Zones Along the Coast

Chandrashekhar Bhagat, Anant Misra, Pranab Kumar Mohapatra, and Manish Kumar

Abstract Presently, there are limited techniques to identify submarine groundwater discharge (SGD) zones in the coastal regions due to the dynamic and invisible nature of the phenomenon driven by natural and anthropogenic factors. The driving factors for SGD include but are not limited to groundwater potential (hydraulic head), groundwater occurrence (type of aquifer: confined/unconfined), aquifer characteristics (hydraulic conductivity /transmissivity), aquifer thickness, the topography of the area, land use–land cover area, recharge–discharge pattern, sea level rise, dynamics of tides tidally driven oscillations, density-driven convection, and thermal convection. Considering some of the crucial factors, we have tried to develop an index that can help in indicating potential locations for SGD along the coastal regions based on easily accessible data. The most important factors which indicate the potential of SGD are groundwater level with respect to mean sea level (or hydraulic gradient (**S**)), **g**roundwater occurrence (G), **d**egree of pollution due to seawater intrusion in a coastal aquifer (D), **t**ransmissivity (T) or permeability of aquifer (K), and **a**quifer thickness (A). Based on this understanding of governing factors, the present work proposes SGDTA (highlighted acronym) index model to identify potential locations for SGD. The data required for this model are readily available with various agencies without any detailed investigation, so this index model is advantageous to delineate the potential location prior to a thorough investigation of SGD. Finally, we successfully demonstrate this model's first-hand application by identifying the SGD zones along the Bhavnagar district coast.

C. Bhagat (✉) · P. K. Mohapatra
Discipline of Civil Engineering, Indian Institute of Technology, Gandhinagar, Gandhinagar 382355, India
e-mail: chandrashekhar.b@iitgn.ac.in

P. K. Mohapatra
e-mail: pranabm@iitgn.ac.in

A. Misra
Discipline of Earth Science, Indian Institute of Technology, Gandhinagar, Gandhinagar 382355, India
e-mail: anant.misra@iitgn.ac.in

M. Kumar
School of Engineering, University of Petroleum and Energy Studies, Uttarakhand 248007, India

P. V. Timbadiya et al. (eds.), *Coastal, Harbour and Ocean Engineering*, Lecture Notes in Civil Engineering 321, https://doi.org/10.1007/978-981-19-9913-0_32

Keywords Potential SGD zones · Indices · SGDTA · Gujarat coastal regions

1 Introduction

Exchange of water between two hydrological masses, i.e., sea and coastal aquifers, happens along the coastal regions worldwide [1, 2]. This exchange of water at the interface of sea and aquifer is either defined as seawater intrusion (SWI) when seawater intrudes into the aquifer [3, 4] or submarine groundwater discharge (SGD) when fresh groundwater is discharged into the sea [5, 6]. Generally, SWI increases the solute concentration and sometimes escalates the trace metals' concentration in groundwater (Tadiboyina and Ptsrk, n.d.), subsequently deteriorating groundwater quality. Similarly, SGD, a complementary process to SWI, acts as a pathway to transfer the contaminants from the aquifer to sea along with fresh groundwater [7], leading to harmful impacts on the sensitive marine ecosystem [8]. Both the processes are complementary to each other and hence governed by the same multiple factors, which make that identification or delineation of SGD potential zones is complex. The delineation of SWI or SGD zones is crucial to understanding the exchange process in the coastal regions and curried out the further detailed investigation. Therefore, researchers use multiple techniques for the delineation of hotspots of SGD along coastal regions [6, 9]. Bhagat et al. [3] and Mannivannan and Elango, 2019) used the multitechniques' (GWL, In situ anomaly, and sea surface temperature anomaly) approach to identify the SGD and SWI potential zones along the Indian coast. Some studies [10, 11, 12, 13] employed a single tracer to identify the SGD potential zones, but to use these techniques, sophisticated instrument and expertise are required, which are rarely available; hence, a simple indicator or indices which can be efficiently used to delineate the probable SGD locations along the coast are required. The critical factors which govern SGD processes are as follows: (1) groundwater potential or level, (2) type of aquifers (unconfined/confined), (3) aquifer characteristics (hydraulic conductivity, porosity, and storativity), (4) tidal pumping, (5) recharge or extraction pattern of groundwater, etc. The present study attempts to develop an index using critical factors that can directly or indirectly be used as an indicator of SGD. Further, this study demonstrates the application of a developed index to delineate SGD zones in Gujarat's coastal (Bhavnagar) district. The developed index effectively helps to preliminary studies and delineation the SGD zones in the coastal regions around the world.

2 Material and Methods

2.1 Development of Index

The index developed in the present study has used the same approach as [14] used to develop the GALDIT index and Aller et al. [15], used to develop the DRASTIC index for the delineation of critical zones of seawater intrusion along the coastal region. The present index considered six critical factors which mainly govern and can be used as indicators of the SGD process in the coastal areas: (1) Groundwater level @ mean sea level (GWL@msl) or hydraulic gradient (**S**), (2) **G**roundwater occurrence or aquifer type (confined/unconfined), (3) Hydraulic conductivity (**K**) or transmissivity (**T**), (4) **A**quifer thickness from which GW flow as an SGD, (5) **D**egree of pollution due to seawater intrusion (SMI value with 5 km stretch from the coast). The acronym defined for the proposed modified index is SGDTA (all parameters defined are highlighted). We can add many more factors depending on the factor's sensitivity toward SGD according to local conditions and modify the acronyms accordingly. These considered factors, combined, can effectively delineate the potential location of SGD in the hydrogeological setting along the coastal regions. The factors considered for the SGDTA index are readily available from various sources without performing a detailed investigation at the site. A numerical ranking system approach is used to assess the SGD potential along the coastal regions. This ranking system includes the weights, ranges, and ratings assigned based on the relative importance of the factors. Each factor considers in SGDTA assigned a relative weightage ranging between 1 and4 (highest weight (4) for the high probable SGD zones and less probable zone for the lower weight (1)). The weightage assigned for the different factors is summarized in Table 1; the weights are adopted similarly to the GALDIT and DRASTIC indices. The maximum and minimum values of SGDTA are **120** and **12,** respectively; the maximum value is calculated for the maximum possible, probable SGD zones, whereas the minimum value is calculated when there is a least possible probability of SGD occurrence. The rating value varies from 1 to 10 depending on the sensitivity of factors on SGD process and depends on the local geological and hydrological conditions. The assigned weights and rating values for different factors and their possible hydro(geo)logical condition are attributed in Table 1. Finally, SGDTA index is calculated as a summation of the multiplication of relative weights and the corresponding rating of each considered factor for the given local conditions. The sensitivity and importance of five factors used as an indicator of the SGD process are explained in the following section.

(1) ***Groundwater level above the mean sea level (GWL@ MSL) or the hydraulic gradient*** (**S**): The groundwater level (GWL) is a vital tool to investigate the SGD and SWI processes along the coastal regions [4, 6]. This is a crucial factor for SGD occurrences, and therefore, a positive hydraulic gradient between the mean sea level and coastal groundwater level is essential for SGD to occur. If the GWL is relatively lower than MSL, seawater intrusion is highly likely to

Table 1 Summary of SGDTA parameter weights, rates, and ranges

Parameters	S: groundwater level (m) or hydraulic gradient	G: occurrence of groundwater (aquifer type)	D: degree of pollution due to seawater intrusion by SMI model	T: aquifer transmissivity or hydraulic conductivity ($m.d^{-1}$)	A: aquifer thickness (m)
Weights Rating	**4**	**1**	**2**	**3**	**2**
1	GWL $\leq$ 0	Leaky/confined aquifer not connected to seafloor	1.25 < SMI	**0 < K $\leq$ 4**	A $\leq$ 1
2	0 < GWL $\leq$ 1		1.2 < SMI $\leq$ 1.25	0 < K $\leq$ 4	1 < A $\leq$ 2
3	1 < GWL $\leq$ 2		1.1 < SMI $\leq$ 1.2	4 < K $\leq$ 8	2 < A $\leq$ 3
4	2 < GWL $\leq$ 3		1 < SMI $\leq$ 1.1	8 < K $\leq$ 12	3 < A $\leq$ 4
5	3 < GWL $\leq$ 4		0.9 < SMI $\leq$ 1	12 < K $\leq$ 20	4 < A $\leq$ 5
6	4 < GWL $\leq$ 5		0.8 < SMI $\leq$ 0.9	20 < K $\leq$ 28	5 < A $\leq$ 6
7	5 < GWL $\leq$ 7.5		0.7 < SMI $\leq$ 0.8	28 < K $\leq$ 41	6 < A $\leq$ 7
8	7.5 < GWL $\leq$ 10	Leaky confined connected seafloor	0.6 < SMI $\leq$ 0.7	41 < K $\leq$ 61	7 < A $\leq$ 8
9	10 < GWL $\leq$ 12.5	Unconfined	0.5 < SMI $\leq$ 0.6	61 < K $\leq$ 81	8 < A $\leq$ 10
10	GWL > 12.2	Confined connected seafloor	SMI $\leq$ 0.5	81 < K	10 < A

occur in the coastal region. To assign the rating for S, one must see the seasonal dynamics of GWL in the study area. In a general sense, groundwater potential (i.e., GWL) is higher in the post-monsoon season, which may result in a high probability of SGD occurrence. The index defined by Aller et al. [15], and Chachadi et al. [16], for assessment of SWI has been modified and adapted in the present index as the SWI and SGD phenomena are complementary to each other.

(2) ***Occurrence of Groundwater (aquifer type)*** (**G**): Generally, groundwater stored in geological formations composed of heterogeneous lithology such as confined, unconfined, and semi-confined (leaky). This groundwater reservoir loses water through underground seepage which reaches into the sea. This process is prevalent as the fresh/terrestrial submarine groundwater discharge [2, 5]. Unconfined aquifers are more prone to SGD compared to confined and leaky aquifers provided that they are not connected to the sea floor. If confined and leaky

aquifers are directly connected to the seafloor, then a considerable amount of groundwater is discharged as fresh SGD into the sea. Therefore, it is crucial to understand the nature of aquifers and their hydraulic connectivity to assign the ratings. For complex/multilayered aquifer, the maximum possible rating must be considered to accommodate the uncertainty of SGD occurrence in the study area.

(3) ***Hydraulic conductivity or transmissivity of the aquifer*** (**T**): The fundamental definition of hydraulic conductivity for aquifer strata is the ease or ability to transmit the groundwater. This parameter is used to quantify the magnitude of SGD flowing across the seafloor. Hence, with an increase in hydraulic conductivity, the magnitude of SGD increases and vice versa in the case of lower hydraulic conductivity. To assign the rating for this factor, the user must consider the hydraulic barriers which obstruct the flow in local aquifers' systems such as clay and basaltic formations, impervious dykes along the coast. In the present study, a rating is adopted from Aller et al. [15], and Chanchdi et al. (2003), as shown in Table 1.

(4) ***Aquifer thickness from which SGD is flowing*** (**A**): Thickness of aquifer/saturated unconfined aquifer thickness plays a vital role in determining the range and magnitude of SGD in the coastal regions. It is known that the larger the saturated aquifer thickness discharge, the huge amount of groundwater into the sea and vice versa. The rating for the factors is adopted from **Chachadi et al.** [16].

(5) ***Degree of pollution due to seawater intrusion*** (**D**): This factor serves as a proxy to SGD, as the seawater intrusion takes place when the GWL is relatively lower than MSL and results in the deterioration of groundwater quality along the coastal stretch, which indicates that there is least possibility of SGD occurrence. So this factor used the readily available hydrochemical dataset to investigate whether the coastal aquifer is influenced by seawater intrusion or not. The rating for this factor is decided based on the seawater mixing index (SMI) model value which is employed to investigate the mixing of seawater and groundwater and calculate using the following Eq. (1). The SMI is a semi-empirical model developed by [15] and used in many studies to investigate the degree of seawater intrusion along the coastal regions [3, 15, 16]. The assigned rating for this factor is as follows: If SIM < 0.5, the rating is 10; if 0.5 < SMI < 1, rating varies from 9 to 6; if 1 < SMI < 1.5, rating varies from 5 to 1; and if SMI > 1.5, then the rating assigned is 1. These ratings are based on the defined threshold value of SMI for the seawater intrusion, i.e., SMI > 1, which indicate the seawater intrusion [15].

$$\mathrm{SMI} = \mathrm{a} \times \frac{C_{Na}}{T_{Na}} + \mathrm{b} \times \frac{C_{Mg}}{T_{Mg}} + \mathrm{c} \times \frac{C_{Cl}}{T_{Cl}} + \mathrm{d} \times \frac{C_{SO^4}}{T_{SO^4}} \quad (1)$$

where *a*, *b*, *c*, and *d are the* coefficients denote the relative proportion of Na^+, Mg^{2+}, Cl^-, and $SO_4{}^{2-}$ ($a = 0.31$, $b = 0.04$, $c = 0.57$, and $d = 0.08$) in seawater. *C* is the concentration ($mg.L^{-1}$) of Na^+, Mg^{2+}, Cl^-, and $SO_4{}^{2-}$ in groundwater samples; T

Table 2 Categories of SGD potential zones' probability based on SGDTA index

Sr. No	Total SGDTA score	Probability of SGD zones
1	SGDTA > 90	High probability zones
2	60 < SGDTA ≤ 90	Moderate probability zones
3	30 < SGDTA ≤ 60	Low probability zones
4	SGDTA < 30	No probability

refers to the regional threshold concentration value in mg.L^{-} for the selected major ions in seawater composition. The quantification of the regional threshold value (T) (using inflection points (IP) of cumulative probability curves) was done based on Sinclair, 1974.

All the weights, ratings, and ranges of different factors are summarized in Table 1. The SGDTA index is calculated using the following Eq. 2.

$$\text{SGDTA} = \sum_{i=1}^{n} W_i R_i, \tag{2}$$

where W_i = weights of factor depending on the importance.

R_i = rating of the corresponding factor defined in Table 1.

For the application of SGDTA to delineate the probable SGD zones, the user can define all parameters depending on the local hydrogeological condition in the coastal area of interest. This index model can allow the user to quantify the numerical values to delineate the probable zones of SGD. It is an additive model; hence, the user can add some more factors/parameters depending on the local condition of the study area. Once the SGDTA index is estimated, it is possible to identify the different probable SGD zones; the classification of zones based on the SGDTA index values is given in Table 2. The index model estimates the probability of SGD zones, not absolute SGD zones; this is the limitation of the SGDTA model and hence works for the preliminary investigation of SGD zones in the coastal area.

Application of SGDTA Index: A Case Study of Bhavnagar, a Coastal District Gujarat

Study Area

The developed SGDTA index identifies the probable SGD zones along the Gujarat coast in the Bhavnagar districts, as shown in Fig. 1. The study is situated west of the Gulf of Khambhat region in the Saurashtra region; this area is classified as a semi-arid region in the country and receives less rainfall in the monsoon season. Therefore, facing the water crises and the community's dependency on groundwater is rising, so preserving groundwater resources is crucial work in the area. One side of available groundwater resources in the coastal aquifers is getting deteriorated due to seawater intrusion, and the other side is fresh groundwater getting discharged into the

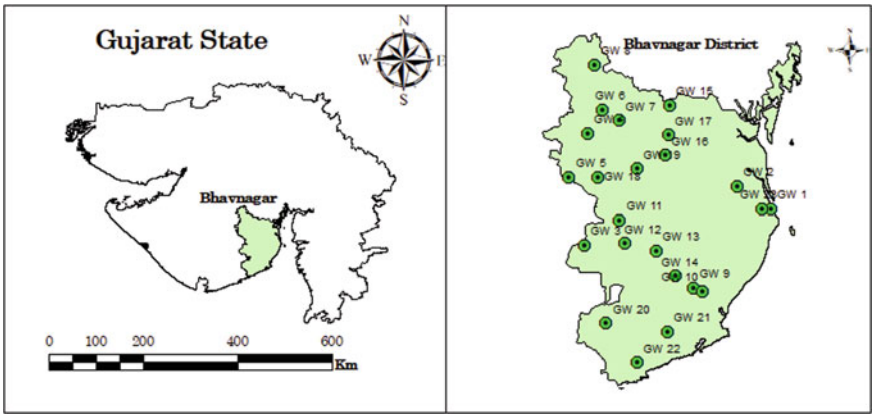

Fig. 1 Index map of a) Gujarat state and b) Bhavnagar district depicting the groundwater sample locations

sea, which increases the water stress in the coastal communities along the coast. The present case study tries to delineate the SGD zones so that the local community, local groundwater stakeholders, or local government or water managers must be aware of the aquifer's fresh groundwater losses. Once we identify the probable potential zones of SGD, further detailed investigation can be done to quantify the magnitude of groundwater loss.

Dataset used

The dataset used in the present study was collected from various agencies and published literature. The groundwater level data were collected from the Central Groundwater Board (CGWB) office Ahmedabad, Gujarat, aquifer properties like hydraulic conductivity and thickness were taken from [17], and groundwater quality data were also collected from CGWB regional office.

Groundwater level data are used to quantify the **S** parameter in the index; the GWL varies from 0 to 100 m throughout the districts, whereas in the post-monsoon period, the GWL was found to be raised in some parts of the district [6]. We speculated that SGD potential increases at few locations in the post-monsoon season compared to monsoon and pre-monsoon seasons.

3 Results and Discussion

Parameters of SGDTA index for the present case study groundwater level or hydraulic gradient (S): The potential of SGD mainly depends on the GWL, which means that the magnitude of SGD primarily depends on the GWL. Groundwater level (@MSL) in the study area varies from 2.5 to 114 m in May 2019 (pre-monsoon), whereas 3.5 to 116.5 m in November 2018 (post-monsoon). Maximum

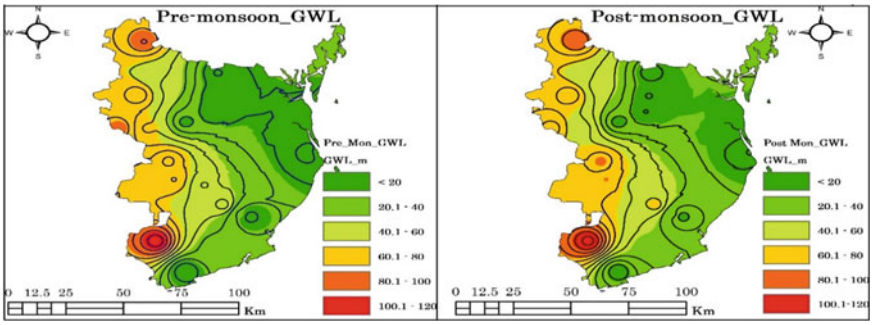

Fig. 2 Groundwater level with reference to mean sea level for pre-monsoon and post-monsoon seasons in the Bhavnagar district

GWL observed in the post-monsoon seasons was 116.5 m near Shantinagar, and the minimum GWL found near Ghogha Beach was 2.5 in the pre-monsoon season. Almost all the sampling locations show the declining groundwater in the pre-monsoon seasons in the Bhavnagar district. Coastal groundwater aquifer faces water stress.

due to GW's excessive water withdrawal and discharges into the sea as SGD in the study area. Generally, post-monsoon seasons have a high potential of SGD as the GWL was raised in the same seasons due to less dependence on GW, which leads to a decrease in the extraction of GW. Hence, the same scenario was observed in the study area. Groundwater level as shown in Fig. 2 and corresponding weightage and rating reported in the tables.

Groundwater occurrence (G), hydraulic conductivity (T), and aquifer thickness (A): The district's geology was covered with the basaltic formation with a certain thickness of soil and sand along the district's coastline. The entire district has the unconfined aquifer (Petliya et al., 2016), which stores the GW mainly and serves as the prime source of fresh GW throughout the year for the various water needs. The thickness of an unconfined aquifer varies from 10 to 36 m in the approximately entire area (Pateliya et al., 2016), and few locations, i.e., 1,2 and 23 thickness varies from 10 to 33.5 m [18]. Most of the GW wells are in the unconfined aquifer, consisting of an upper soil layer laying over the sand [18], and hydraulic conductivity value varies from 5 to 40 $m.d^{-1}$ [17]. These geological parameters indicate that the aquifers in the coastal districts have the colossal potential for the SGD [19, 20]. The values and ratings of corresponding factors are shown in Tables 1 and 3.

Degree of contamination (D): This factor indicates the influence of seawater intrusion in the coastal aquifer. To quantify the degree of contamination (D), we have used the seawater mixing index (SMI), defined above (Eq. 1) and estimated in the following section for the given case study. The estimated SMI value varies from 0.08 for GW 9 to 6.16 for GW 8, which depicts that a wide range of hydrochemical parameters indicates that GW in the study area influences seawater intrusion. Based

on the SMI value, more than 60% of samples sites indicate the high possibility of SGD and 40% of sites depict the seawater intrusion in the Bhavnagar district. The values, rating, and weights are summarized in Tables 1 and 3.

Estimation and Inference of Developed SGDTA Index

Once the weights, ranking, and values of different factors were assigned (Table 3), then using Eq. 2, we calculated the SGDTA index for the different sampling sites in the study area. The value of SGDTA index varies from 67.5 to 105.5 in the post-monsoon season, whereas it varies from 63.5 to 105.5 in the pre-monsoon season, and calculated values are summarized in Table 3. The probability of potential SGD zones, as defined in Table 2, depicts that SGDTA > 90 has the highest probability of SGD occurrence, whereas SGDTA < 30 indicates no probability of SGD and high chances of seawater intrusion. Out of 23 sample sites, 12 sites indicate the highest probability of SGD occurrence in the post-monsoon season and 10 sites in the pre-monsoon season. This decrease in the SGD sites is due to the decline of GWL in the study area for various reasons. Very high SGD potential was observed on the few sites, i.e., GW 2 (near Ghogha Beach), GW 11, GW 12 and GW 13 (surrounded by Palitana town), GW 19 (Umrala), and GW 20 (near Shantinagar). Remaining all the sites show a moderate probability of SGD occurrence in the study area. Sample site GW 10 (in Talaja) shows the sharp decline of GWL which depicted the high probability of SGD in the post-monsoon season and moderate portability in the pre-monsoon season, the same process observed at site GW 15 near Pavni.

Figure 3 depicts the spatial distribution of the SGDTA index calculated for the 23 sampling sites in the Bhavnagar district. The spatial distribution shows that the south part of the district has a high potential of SGD compared to the north part, which is aligned with the results of Bhagat et al. [3, 6], delineate the probable zones of SGD along the Gujarat coast, and the present study also depicted the approximately same results, which validate the applicability of the newly developed SGDTA index.

4 Conclusion

Presently developed SGDTA index for identifying probable potential SGD zones was successfully identified sites 10 and 12 as a potential SGD locations in pre- and post-monsoon seasons along the Bhavnagar district coastal stretch. The results are also aligned with Bhagat et al., 2021, where they have found probable SGD zones using three different approaches. The quantification of the SGDTA index was straightforward and used readily available data of GWL, GW quality, and aquifer characteristics, which makes the broad application of this index across the world. The developed index is robust and can be modified by the user to add different factors as per the sensitivity of parameters toward SGD processes. Moreover, the user can change the degree of influence that each variable of the SGDTA would assert, but the principle must be the same as adopted in the present study.

Table 3 Values, ranks, and weights of different factors for all sites of sampling

	Post-monsoon						Pre-monsoon					
ID	S	G	D	T	A	SGDTA	S	G	D	T	A	SGDTA
	=Ri × Wi					$= \sum Wi \times Ri$	=Ri × Wi					$= \sum Wi \times Ri$
GW 1	40	9	2	16.5	20	87.5	36	9	2	16.5	20	83.5
GW 2	40	9	20	16.5	20	105.5	40	9	20	16.5	20	105.5
GW 3	40	9	16	10.5	20	95.5	40	9	16	10.5	20	95.5
GW 4	40	9	2	16.5	20	87.5	40	9	2	16.5	20	87.5
GW 5	40	9	2	16.5	20	87.5	40	9	2	16.5	20	87.5
GW 6	40	9	2	16.5	20	87.5	40	9	2	16.5	20	87.5
GW 7	40	9	2	16.5	20	87.5	40	9	2	16.5	20	87.5
GW 8	40	9	2	16.5	20	87.5	40	9	2	16.5	20	87.5
GW 9	40	9	20	10.5	20	99.5	40	9	20	10.5	20	99.5
GW 10	40	9	20	10.5	20	99.5	24	9	20	10.5	20	83.5
GW 11	40	9	20	16.5	20	105.5	40	9	20	16.5	20	105.5
GW 12	40	9	20	16.5	20	105.5	40	9	20	16.5	20	105.5
GW 13	40	9	18	16.5	20	103.5	40	9	18	16.5	20	103.5
GW 14	40	9	20	10.5	20	99.5	40	9	20	10.5	20	99.5

(continued)

Table 3 (continued)

	Post-monsoon						Pre-monsoon					
ID	S	G	D	T	A	SGDTA	S	G	D	T	A	SGDTA
	=Ri × Wi					$= \sum Wi \times Ri$	=Ri × Wi					$= \sum Wi \times Ri$
GW 15	32	9	14	16.5	20	91.5	20	9	14	16.5	20	79.5
GW 16	36	9	2	16.5	20	83.5	32	9	2	16.5	20	79.5
GW 17	36	9	8	16.5	20	89.5	32	9	8	16.5	20	85.5
GW 18	40	9	4	16.5	20	89.5	40	9	4	16.5	20	89.5
GW 19	40	9	20	16.5	20	105.5	40	9	20	16.5	20	105.5
GW 20	40	9	20	16.5	20	105.5	40	9	20	16.5	20	105.5
GW 21	40	9	20	10.5	20	99.5	40	9	20	10.5	20	99.5
GW 22	36	9	10	10.5	20	85.5	20	9	10	10.5	20	69.5
GW 23	20	9	2	16.5	20	67.5	16	9	2	16.5	20	63.5

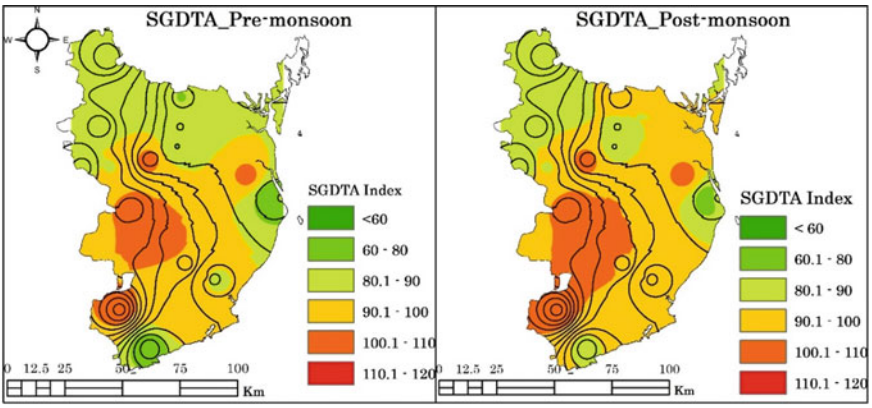

Fig. 3 Spatial distribution of SGDTA index for pre- and post-monsoon seasons

Acknowledgements We are thankful to the Central Groundwater Board, Regional office Ahmedabad, Gujarat, India, for providing groundwater data. We thank the Indian Institute of Technology (IIT), Gandhinagar, for their lab facilities and infrastructure.

References

1. McCoy CA, Corbett DR (2009) Review of submarine groundwater discharge (SGD) in coastal zones of the Southeast and Gulf Coast regions of the United States with management implications. Journal of Environmental Management 8
2. Taniguchi M, Dulai H, Burnett KM, Santos IR, Sugimoto R, Stieglitz T, Kim G, Moosdorf N, Burnett WC (2019) Submarine Groundwater Discharge: Updates on Its Measurement Techniques, Geophysical Drivers, Magnitudes, and Effects. Front Environ Sci 7:. https://doi.org/10.3389/fenvs.2019.00141
3. Bhagat C, Puri M, Mohapatra PK, Kumar M (2021) Imprints of seawater intrusion on groundwater quality and evolution in the coastal districts of south Gujarat, India. Case Studies in Chemical and Environmental Engineering 3:100101
4. Manivannan V, Elango L (2019) Seawater intrusion and submarine groundwater discharge along the Indian coast. Environ Sci Pollut Res 26:31592–31608. https://doi.org/10.1007/s11356-019-06103-z
5. Babu DSS, Khandekar A, Bhagat C, Singh A, Jain V, Verma M, Bansal BK, Kumar M (2021) Evaluation, effect and utilization of submarine groundwater discharge for coastal population and ecosystem: A special emphasis on Indian coastline. J Environ Manage 277:111362. https://doi.org/10.1016/j.jenvman.2020.111362
6. Bhagat C, Khandekar A, Singh A, Mohapatra PK, Kumar M (2021) Delineation of submarine groundwater discharge and seawater intrusion zones using anomalies in the field water quality parameters, groundwater level fluctuation and sea surface temperature along the Gujarat coast of India. J Environ Manage 296:113176
7. George ME, Akhil T, Remya R, Rafeeque MK, Babu DS (2021) Submarine groundwater discharge and associated nutrient flux from southwest coast of India. Mar Pollut Bull 162:111767

8. Oehler T, Ramasamy M, George ME, Babu SD, Dähnke K, Ankele M, Böttcher ME, Santos IR, Moosdorf N (2021) Tropical Beaches Attenuate Groundwater Nitrogen Pollution Flowing to the Ocean. Environmental Science & Technology
9. Tirado-Conde J, Engesgaard P, Karan S, Müller S, Duque C (2019) Evaluation of Temperature Profiling and Seepage Meter Methods for Quantifying Submarine Groundwater Discharge to Coastal Lagoons: Impacts of Saltwater Intrusion and the Associated Thermal Regime. Water 11:1648. https://doi.org/10.3390/w11081648
10. Garcia-Orellana J, Cochran JK, Bokuniewicz H, Daniel JWR, Rodellas V, Heilbrun C (2014) Evaluation of 224Ra as a tracer for submarine groundwater discharge in Long Island Sound (NY). Geochim Cosmochim Acta 141:314–330
11. Jacob N, Babu DSS, Shivanna K (2009) Radon as an indicator of submarine groundwater discharge in coastal regions. Curr Sci 97:8
12. Oehler T, Tamborski J, Rahman S, Moosdorf N, Ahrens J, Mori C, Neuholz R, Schnetger B, Beck M (2019) DSi as a tracer for submarine groundwater discharge. Front Mar Sci 6:563
13. Peterson RN, Burnett WC, Taniguchi M, Chen J, Santos IR, Ishitobi T (2008) Radon and radium isotope assessment of submarine groundwater discharge in the Yellow River delta, China. Journal of Geophysical Research: Oceans 113:. https://doi.org/10.1029/2008JC004776
14. Chachadi AG, Lobo Ferreira JP, Noronha L, Choudri BS (2002) Assessing the impact of sea-level rise on salt water intrusion in coastal aquifers using GALDIT model. Coastin—A Coastal Policy Res Newsl 7:27–32
15. Aller L, Bennet T, Lehr JH, Petty RJ, Hackett G (1987) DRASTIC: A standardized system for evaluating ground water pollution potential using hydro- geologic settings. EPA/600/2-85-018, United states environmental protection agency, Washington, DC, USA
16. Chachadi AG (2005) Seawater intrusion mapping using modified GALDIT indicator model: A case study in Goa
17. Pateliya P, Singh NP, Mahmood K, Prakash I (2016) Impact of seawater intrusion on coastal aquifer of Bhavnagar, Gujarat, India using GALDIT method. Int J Adv Res Eng Sci Technol 3:477–484
18. Singh AP, Gupta PK, Khandelwal M (2013) Prediction of sea water intrusion for mining activity in close precincts of sea shore. Springer Plus 2:1–10
19. Misra A, Bhagat C, Kumar M (2022) Geochemical ratios mediated understanding of estuarine dynamics in submarine groundwater discharge prevalent basaltic aquifer. Mar Pollut Bull 181:113812
20. Bhagat C, Kumar M (2022) Muddy (silty-sand) beaches in semi-arid regions attenuate the contaminants flowing into the sea as a submarine groundwater discharge. Sci Total Environ 833:155111
21. Park S-C, Yun S-T, Chae G-T, Yoo I-S, Shin K-S, Heo C-H, Lee S-K (2005) Regional hydrochemical study on salinization of coastal aquifers, western coastal area of South Korea. J Hydrol 313:182–194
22. Kumar PS (2016) Deciphering the groundwater–saline water interaction in a complex coastal aquifer in South India using statistical and hydrochemical mixing models. Modeling Earth Systems and Environment 2:1–11
23. Sinclair AJ (1974) Selection of threshold values in geochemical data using probability graphs. J Geochem Explor 3:129–149
24. Bhagat C, Mohapatra PK, Kumar M (2021) Unveiling the extent of salinization to delineate the potential submarine groundwater discharge zones along the North-western coast of India. Mar Pollut Bull 172:112773

Assessment of Submarine Groundwater Discharge (SGD) Zones Along the Coastal Tract of Odisha

Y. R. Satyaji Rao, Soumya Kanta Nayak, Girish Yenagimath, Vijay Teeparthi, and Sudhir Kumar

Abstract Submarine Groundwater Discharge (SGD) is the continuous flow of groundwater under favourable hydrogeological and hydrological settings, which carries nutrients, traces metals and other contaminants to the sea coast and influences the coastal ecosystem. Therefore, integrated site-specific field investigations are necessary for identifying the SGD zones and its magnitude assessment for sustainable development of the coastal ecosystem. An attempt has been made to identify the potential SGD zones along the 485 km long coastline of Odisha using the groundwater level data and physico-chemical analysis of groundwater, pore water and sea water samples. The areas having an occurrence of groundwater level above mean sea level (more than tidal amplitude) together with the absence of any significant seasonal/diurnal variation in groundwater levels were identified as probable SGD zones. In situ measurement of basic water quality parameters (temperature, pH, salinity, EC, DO, etc.) was carried out at every 3–5 km intervals along the coastline for sea water (44), pore water (43) and groundwater (36) samples using portable multiparameter water quality kit during the field investigation. The pore water samples, indicating low salinity (<25 ppt) and low EC values (<35 mS/cm), were considered to be suspected SGD. A total number of seven such suspected zones were identified along the coastal tract of Odisha. The pore water salinity in these seven locations is found to be 14.6 ppm (Chaumukh–Balasore), 3.05 ppt (Chandipur–Balasore), 3.71 ppt (Madanpur–Balasore), 19.79 ppt (Pentha–Kendrapara), 18.9 ppt (Beleshwar–Puri), 12.59 ppt (Golden Beach, Puri) and 0.46 ppt (Nolia Nuagaon, Ganjam) in the proximity of sea coast between low tide and high tide. The nutrients (Nitrate, Phosphate and Silica) analysed in the pore water samples also have shown elevated signatures for the identified zones, thus support possible SGD and need further conformation using stable isotopes, sea surface temperature and radon measurements.

Y. R. Satyaji Rao (✉) · S. K. Nayak · G. Yenagimath · V. Teeparthi
Deltaic Regional Centre, National Institute of Hydrology, Kakinada, Andhra Pradesh, India
e-mail: yrsrao.nihr@gov.in

S. Kumar
National Institute of Hydrology, Roorkee, Uttarakhand, India
e-mail: skumar.nihr@gov.in

P. V. Timbadiya et al. (eds.), *Coastal, Harbour and Ocean Engineering*, Lecture Notes in Civil Engineering 321, https://doi.org/10.1007/978-981-19-9913-0_33

Keywords Ubmarine groundwater discharge · Groundwater level · Pore water · Odisha coast

1 Introduction

Submarine Groundwater Discharge (SGD) is the continuous flows of groundwater under favourable hydrogeological and hydrological settings, which carries nutrients, trace metals and other contaminants to the sea coast and influences the coastal ecosystem. It was recognised by hydrologists for many years [6], but SGD drew little attention from the oceanographic community until after [2]. However, SGD has received increased attention during the last few decades since it was recognised that it may be both volumetrically and chemically important [5, 7]. Although SGD is generally small compared to riverine flow into oceans, it contributes high concentrations of nutrients, trace metals and other land-derived contaminants [8, 10]. So, identifying and quantifying the SGD are essential to understand this component of the water cycle. The discharge of groundwater into the sea through coastal aquifers has been recognised as small by volumetrically, but quite significant ecologically because SGD offers an important pathway of nutrients, carbon and other geochemical constituents to the ocean [11]. Knowledge of the nature of SGD in any region allows estimating optimum extraction levels of potable groundwater and also provides information on feasible waste disposal sites in coastal zones [1]. SGD is temporally and spatially variable [9], as the interaction between multiple forcing mechanisms varies at any given location and time. Thus, site-specific investigation is necessary to evaluate comprehensively the timing, magnitude and importance of SGD in any interface zone between salt water and fresh water [3]. In this study, an attempt has been made to identify the potential SGD zones along the 485 km long coastline of Odisha using the groundwater level data and physico-chemical analysis of groundwater, pore water and sea water samples collected during the field investigation.

2 Study Area

Odisha is one of the coastal states of India located on the eastern side and has 485 km of coastline along the Bay of Bengal, extended from the Balasore district in the north to Ganjam district in the south. The climate is tropical, and it receives a decent annual rainfall of about 2000 mm. There are six coastal districts in the Odisha coast, namely Balasore, Bhadrak, Kendrapara, Jagatsinghpur, Puri and Ganjam. Out of these six districts, the main focus is on 22 coastal blocks as classified by Odisha government bordering the Bay of Bengal, and the same is shown in Fig. 1.

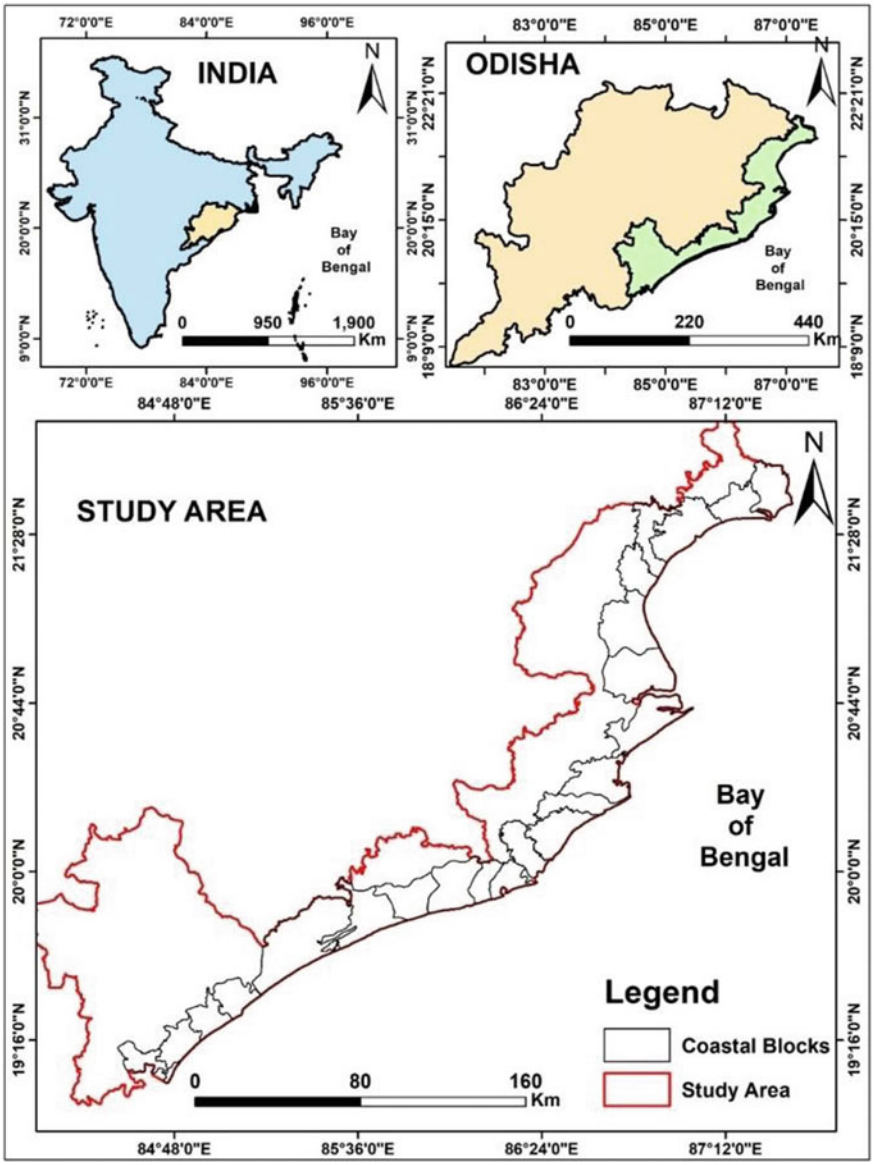

Fig. 1 Study area showing coastal districts and coastal blocks of Odisha state

3 Methodology

3.1 Use of Archival/Secondary Groundwater Level Data

Open accessible latest groundwater level data from the India-WRIS portal [4] were collected, and by using the locations of piezometers, map of piezometer network for the coastal districts was prepared for the study area as shown in Fig. 2.

A total number of 203 piezometers were taken into consideration for coastal Odisha, and from the groundwater level data (pre-monsoon data of May 2018) of the above shown piezometer network, groundwater level 'bgl' is converted to 'amsl' and groundwater level map (amsl) for the coastal districts of Odisha and groundwater contour of +2 m were prepared as shown in Fig. 3a and b, respectively. Field investigations are focused mainly between coastline and +2 m groundwater level.

3.2 Field Investigation

3.2.1 In Situ Measurement of Water Quality Parameters

In situ water quality data collected during field visits help for spot verification of water quality variation at onshore as well as offshore locations. In order to assess the SGD

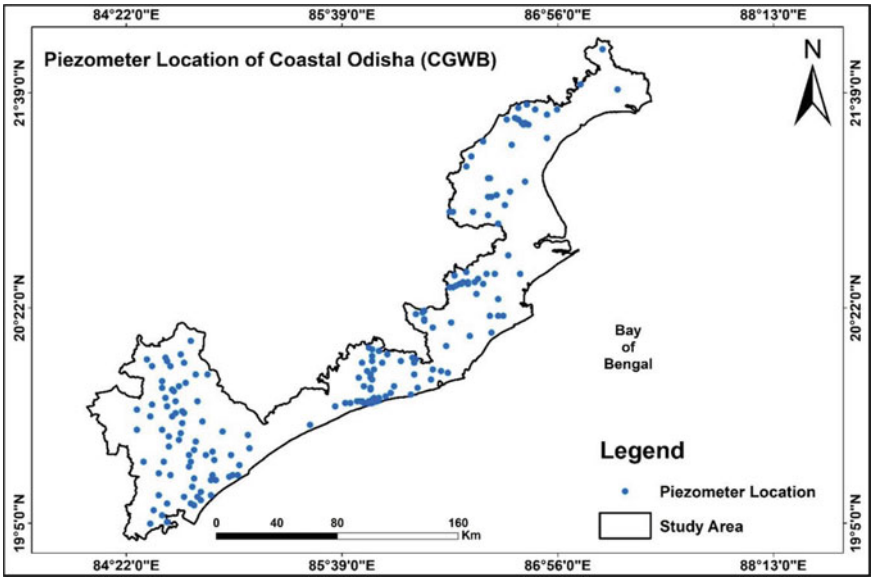

Fig. 2 Location map of piezometers in the coastal districts of Odisha

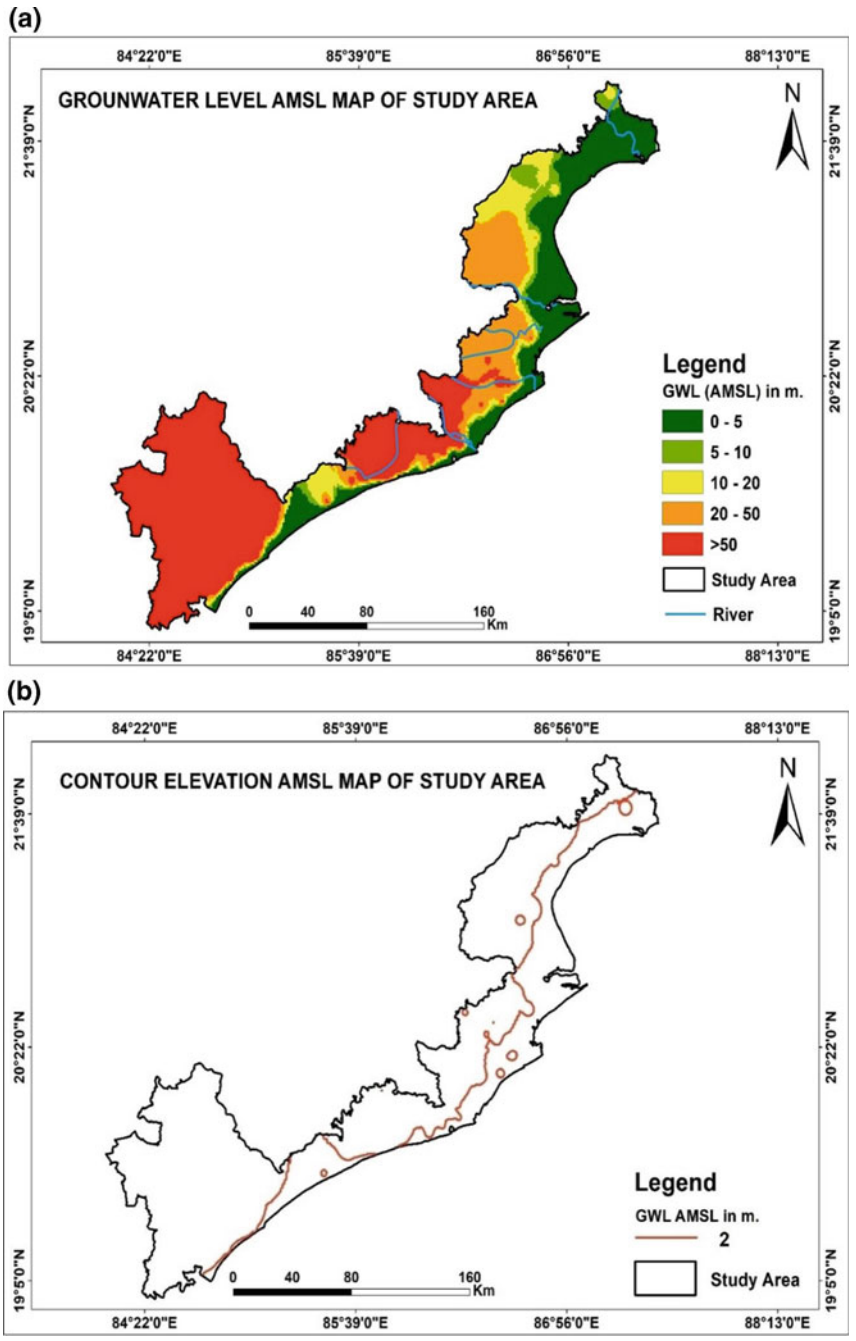

Fig. 3 **a** Groundwater level (amsl) in the coastal districts of Odisha. **b** Groundwater level contour of +2 m in the coastal districts of Odisha

and water quality variations, in situ measurement of basic water quality parameters, namely, temperature, pH, salinity, EC, dissolved oxygen, etc., was carried out using portable multiparameter water quality kit for sea water, pore water and groundwater samples, respectively, during the field investigation in the study area, and the same samples were brought to the water quality laboratory for further analysis.

3.2.2 Sample Collection

Water samples were collected from piezometric wells, pore water and from sea surfaces at every 3–5 km interval along the shoreline (parallel to the coast). Push point sampler equipped with 50 ml polyethylene syringes was used to collect pore water samples from a depth of 1 m during low tide periods from the intertidal zone. At the location where the pore water salinity was <25 ppt within the intertidal zone, one more verification of pore water sample was done at a distance of 100 m from the first pore water sample location towards the land. Sea water samples were also collected from the sea at a distance of 100 m from the shoreline towards the sea, and fresh water samples were collected from the coastal groundwater wells available within 1 km distance or +2 m groundwater level from the shoreline. All the water samples were filtered through 0.22 μm syringe-driven membrane filters and were transferred into polyethylene bottles. All samples were collected following the standard sampling procedure during the field visit and were transported to the laboratory with utmost care for further analysis of nutrients. The total number of 44 sea water samples, 43 pore water samples and 36 groundwater samples were collected covering all the six coastal districts, and the sample locations were plotted in GIS framework and the same is shown in Fig. 4.

4 Results and Discussion

After analysing all groundwater level data, hydrogeological characteristics, field investigation of the study area, a number of suspected SGD zones were identified as described below.

4.1 Analysis of Groundwater Level Data

Groundwater level maps were generated using archival data and used to identify the signatures of SGD. Occurrence of groundwater levels near or below to mean sea level (within the tidal amplitude) together with observation of seasonal/diurnal variation in groundwater levels and chemistry are indications of the possible salt water intrusion zone. On the other hand, occurrence of groundwater levels above mean seal level (more than tidal amplitude) together with the absence of any significant

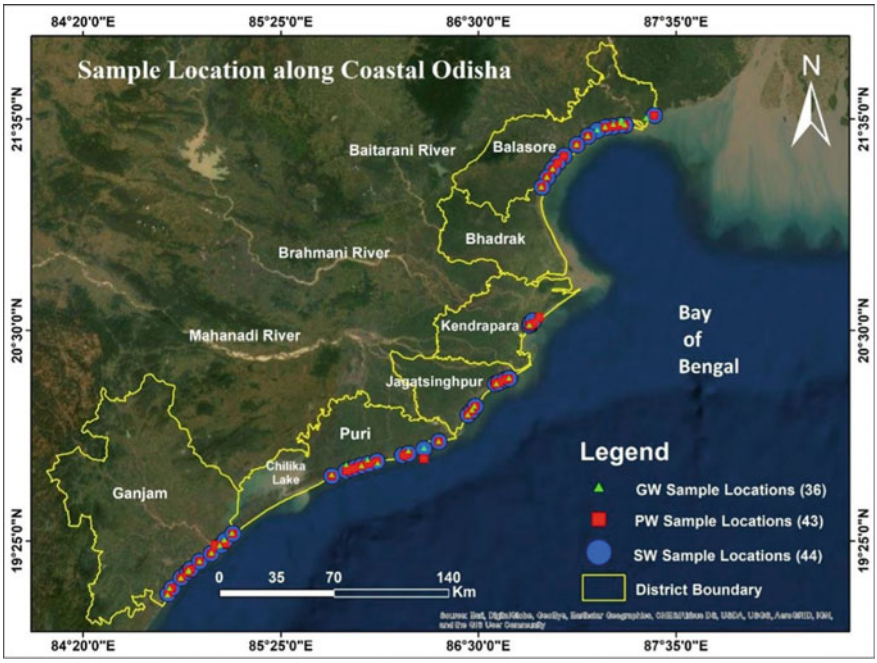

Fig. 4 Water sample locations along coastal Odisha

seasonal/diurnal variation in groundwater levels and chemistry are indicators of the possible SGD zone. Two suspected SGD zones were identified as a preliminary indication of SGD by using groundwater table (amsl) data in the Odisha coast as shown in Fig. 5. Therefore, inferences about probable SGD or SWI zone should be drawn holistically and should be treated only as a preliminary, indication to guide subsequent field campaigns for further investigations involving detailed geochemical and geophysical investigations.

4.2 In Situ Physio-chemical Parameters

In situ measured basic physical parameter values, namely temperature, pH, ORP, salinity, Electrical Conductivity (EC) and dissolved oxygen (DO), for all the pore water, sea water and ground water samples (collected during post-monsoon of 2019) were measured, and salinity and EC were mainly used to identify the suspected SGD zones along the study area. The EC and salinity of collected groundwater, pore water and sea water samples were analysed, and it was found that these two parameters are highly correlated. So, this signature is used to identify the suspected zones along the coast. As parameters of pore water sample play a major role in this SGD context, an attempt has been made to identify the suspected SGD zones along the study area

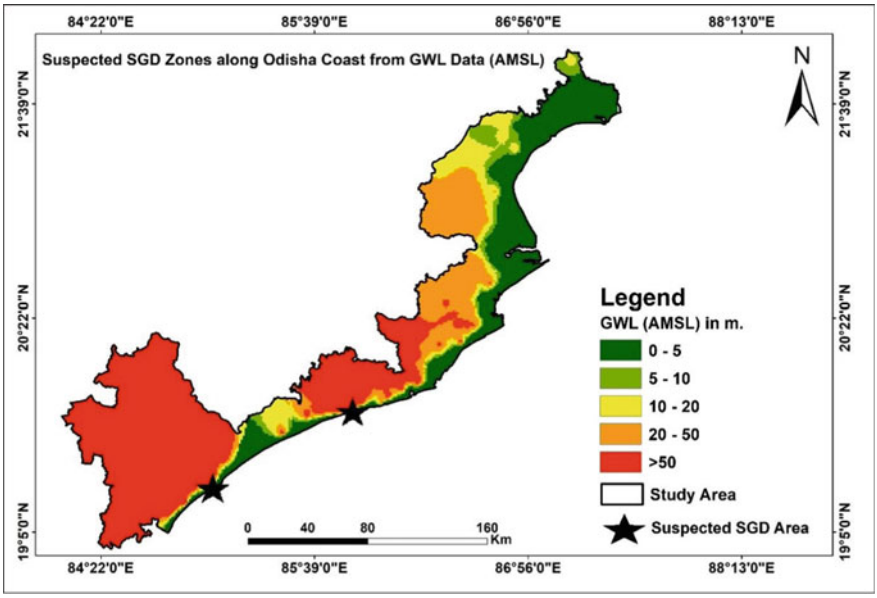

Fig. 5 Suspected SGD zones along Odisha coast using GWL (amsl) data

by using pore water salinity and EC values of the water samples. The pore water samples, indicating low salinity (<25 ppt) and low EC values (<35 mS/cm), were considered to be suspected SGD areas along the coastal tract. A total number of seven such suspected zones were identified on the basis of low salinity and low EC values along the Odisha coast as shown in Fig. 6a and b, respectively.

4.3 Results from Nutrient Analysis

Nutrients like Nitrate ($NO3^-$), Phosphate ($PO4^{3-}$) and dissolved Silica (SiO2) were analysed in the lab using Spectrophotometer for all the sea water, pore water and ground water samples. After comparison, it was observed that the nutrient values of pore water samples are showing elevated signatures for the suspected SGD zones than their natural values, thus supporting the possibility of SGD along the Odisha coast. The salinity and EC values for both the pore water samples (PW—pore water sample at intertidal zone and PW*—pore water samples taken at 100 m distance from PW sample towards inland) of suspected SGD zones along with the analysed nutrient values and their location are shown in Table 1.

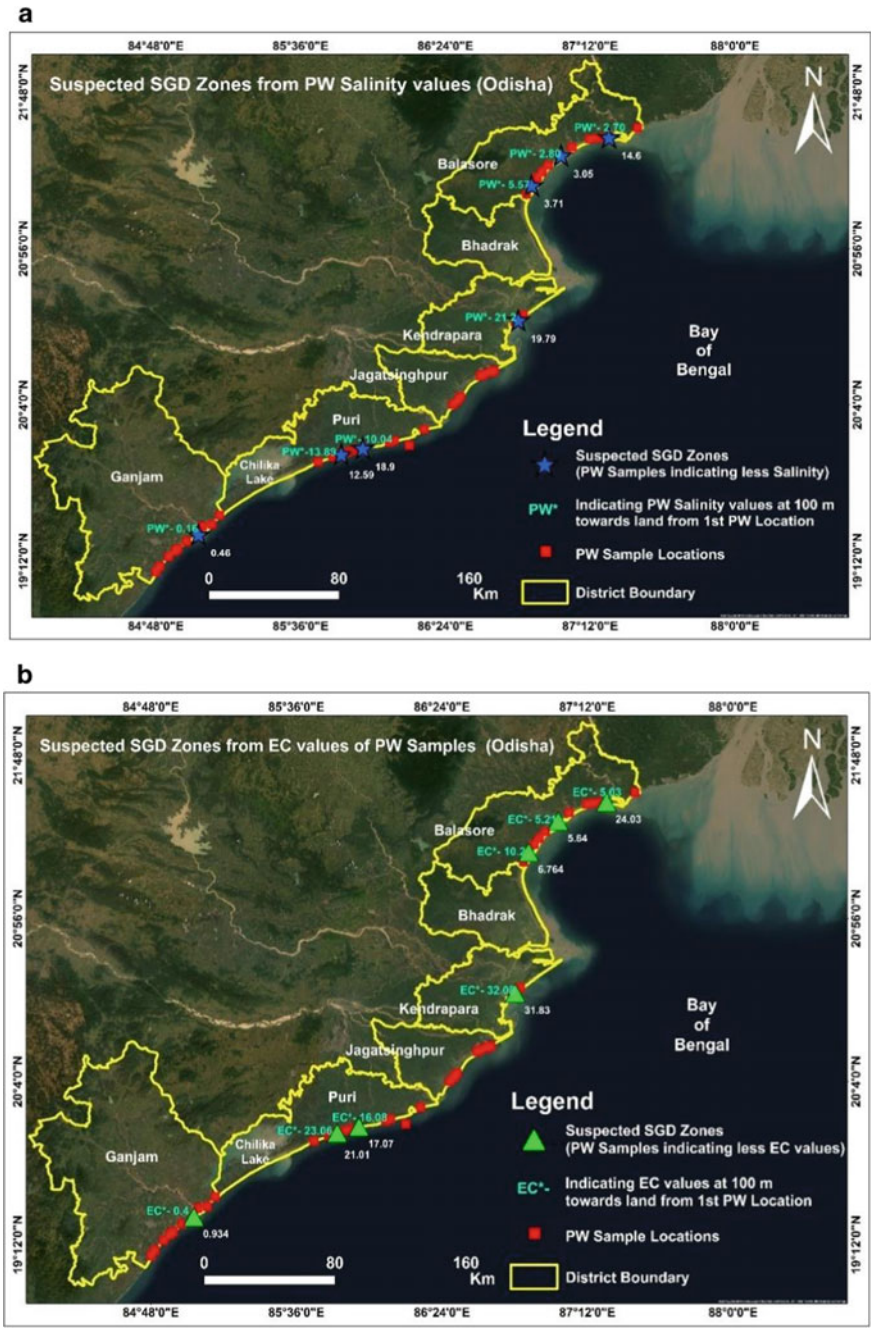

Fig. 6 **a** Suspected SGD zones using salinity values (ppt) of PW samples. **b** Suspected SGD zones using EC values (mS/cm) of PW samples

Table 1 Showing the details of suspected SGD zones along Odisha coast

Suspected	PW parameters		PW* parameters		PW nutrient values			Location
SGD zones	Salinity in ppt	EC in mS/cm	Salinity in ppt	EC in mS/cm	Nitrate in ppm	Phosphate in ppm	Silica in ppm	
1	14.6	24.03	2.70	5.03	3.27	0.1	6.5	Chaumukh–Balasore
2	3.05	5.64	2.80	5.21	15.52	0.26	21.3	Chandipur–Balasore
3	3.71	6.764	5.57	10.2	5.77	1.59	30	Madanpur–Balasore
4	19.79	31.83	21.2	32.08	6.89	0.03	4	Pentha–Kendrapara
5	18.9	17.07	10.04	16.08	8.23	0.04	2.2	Beleshwar–Puri
6	12.59	21.01	13.89	23.06	3.01	0.04	1.9	Golden Beach, Puri
7	0.46	0.934	0.16	0.4	2.44	0.04	7.9	Nolia Nuagaon, Ganjam

5 Conclusion

i. The Odisha coast, having a total coastal length of 480 km, was successfully covered for in situ measurement of physico-chemical parameters of pore water.
ii. Identified two probable SGD zones using groundwater level data. These zones, helped subsequent field campaigns for further investigations involving detailed geochemical investigations.
iii. Pore water salinity and EC indicated that seven suspected SGD zones along the coastal tract of Odisha.
iv. The nutrients (Nitrate, Phosphate and Silica) analysis of pore water samples have shown elevated values than natural for the identified SGD zones, thus supports possible SGD zones and needs further conformation using stable isotopes, sea surface temperature and radon measurements.

Acknowledgements This work is funded by National Centre for Earth Sciences Studies, Earth System Science Organisation, Ministry of Earth Sciences, Government of India (Grant No. NCESS/MOES/402/GIA, dt.29.03.2019). The authors are thankful to Dr. D.S. Suresh Babu, NCESS, Thiruvananthapuram, for his constant support for the project and South Eastern Regional office of the Central Ground Water Board is duly acknowledged for sharing the hydrological data.

References

1. Babu DS, Anish M, Vivekanandan KL, Ramanujam N, Murugan KN, Ravindran AA (2009) An account of submarine groundwater discharge from the SW Indian coastal zone. J Coastal Res 25(1):91–10
2. Burnett B (1999). Offshore springs and seeps are focus of working group. Eos Trans Am Geophys Union 12;80(2):13–15

3. George ME, Babu DS, Akhil T, Rafeeque MK (2018) Investigation on submarine groundwater discharge at Kozhikkode coastal aquifer, SW western Ghats. J Geol Soc India 92(5):626–633
4. https://indiawris.gov.in/wris/
5. Johannes RE (1980) The ecological significance of the submarine discharge of groundwater. Mar Ecol Prog Ser 15:365–373
6. Kohout FA (1966) Submarine springs: a neglected phenomenon of coastal hydrology. Hydrology 26:391–413
7. Moore WS (1996) Large groundwater inputs to coastal waters revealed by 226Ra enrichments. Nature 380(6575):612–614
8. Moore WS (2010) The effect of submarine groundwater discharge on the ocean. Annu Rev Mar Sci 2(1):59–88
9. Mulligan AE, Charette MA (2006) Intercomparison of submarine groundwater discharge estimates from a sandy unconfined aquifer. J Hydrol 327(3–4):411–425
10. Szymczycha B, Vogler S, Pempkowiak J (2012) Nutrient fluxes via submarine groundwater discharge to the Bay of Puck, southern Baltic Sea. Sci Total Environ 438:86–93
11. Taniguchi M, Dulai H, Burnett KM, Santos IR, Sugimoto R, Stieglitz T, Kim G, Moosdorf N, Burnett WC (2019) Submarine groundwater discharge: updates on its measurement techniques, geophysical drivers, magnitudes, and effects. Front Environ Sci 7:141